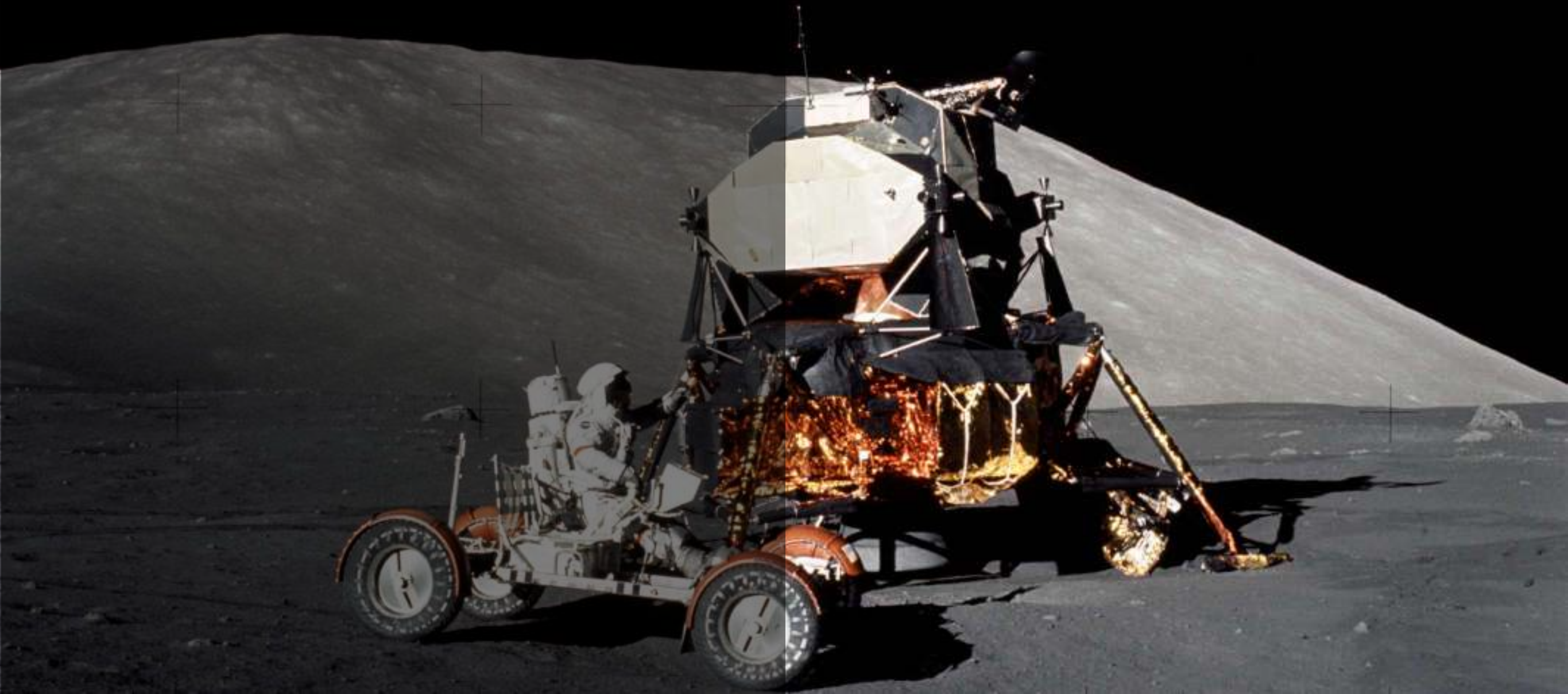


Moon Minerals

a visual guide

A.G. Tindle and M. Anand

Preliminaries



Preface

Virtual microscope work at the Open University began in 1993 and has culminated in the on-line collection of over 1000 samples available via the virtual microscope website ([here](#)).

Early days were spent using LEGO robots to automate a rotating microscope stage thanks to the efforts of our colleague Peter Whalley (now deceased). This automation speeded up image capture and allowed us to take the thousands of photographs needed to make sizeable (Earth-based) virtual microscope collections.

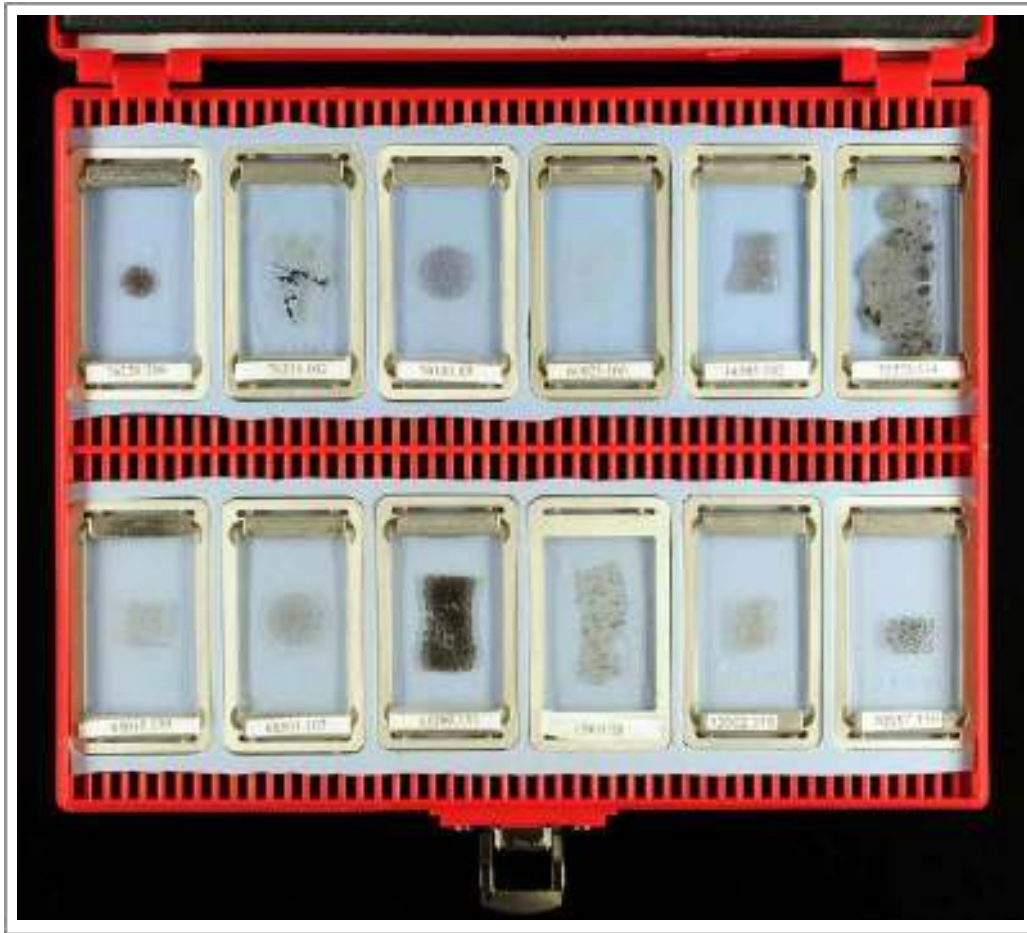
Virtual microscope methods are ideal for bringing rare and often unique samples to a wide audience so we were not surprised when 10 years ago we were approached by the UK Science and Technology Facilities Council who asked us to prepare a virtual collection of the 12 Moon rocks they loaned out to schools and universities. This would turn out to be one of many collections built using extra-terrestrial material.

The major part of our extra-terrestrial work is web-based and we have build collections of Europlanet meteorites, UK and Irish

meteorites, Martian meteorites and most recently over 500 virtual microscopes of Apollo samples.



The authors - Mahesh Anand (left) and Andy Tindle (middle) with colleague Peter Whalley (right). Thank you Peter for your pioneering contribution to the Virtual Microscope project. We could not have produced this book without your earlier efforts.



Apollo Thin Section Set once available for loan to schools from the UK Science and Technology Facilities Council. Now available to universities.

However, our output has not been exclusively web-based and three interactive books have also been published (on the Apple Bookstore) - **Minerals Under the Microscope**, **Fossil Guide** and **Moon Rocks**. The latter has been by far the most successful, not least because of the contribution of our friend and co-author Simon Kelley.

Moon Minerals is our latest output. We see it as a companion volume to **Moon Rocks**.

Members of staff who over the years have contributed to the virtual microscope project include:

Tom Vincent, Peter Whalley, Ben Hawkrige, Chris Valentine, Kevin Quick, Paul Hogan, Trevor Collins (Knowledge Media Institute)

Dave Williams, Dee Edwards, Simon Kelley, Susanne Schwenzer, Michelle Higgins, Kay Green (Department of Earth Sciences - now School of Environment, Earth and Ecosystem Sciences)

Colin Pillinger, Judith Pillinger (School of Physical Sciences)

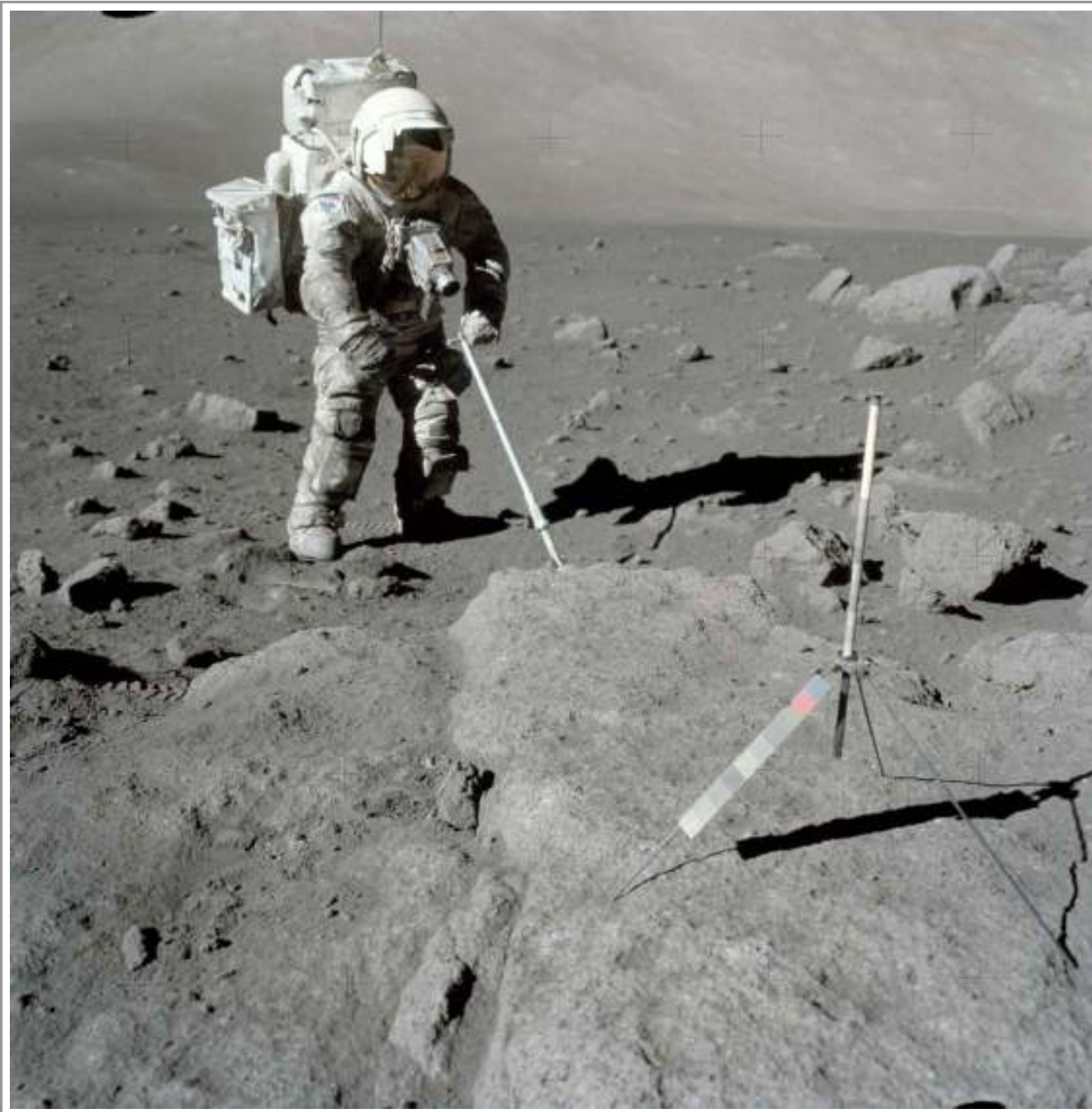
Also: Everett Gibson of the Astromaterials Research and Exploration Science Division, NASA

We also thank NASA CAPTEM for allocation of Apollo samples.

All are thanked for their part in helping to create such a wonderful teaching tool from which this book is derived.

Finally the greatest thanks of all should be to the Apollo astronauts who risked their lives to collect and return to Earth a great many of the samples described in this book.

We hope you enjoy dipping into the different sections of this book and welcome any feedback on new or otherwise interesting discoveries that we could include in future versions.



Harrison (Jack) Schmitt collecting a sample at Station 5 (Camelot Crater) during the second extra-vehicular activity (EVA) of the Apollo 17 mission.

Quotes from Station 5:

Schmitt: "Here I am, folks, in the middle of a boulder field. Just minding my own business".

Schmitt: I don't know whether I mentioned it. The mineral texture appears to be sub-ophitic to...(sort of) like a good diabase, although a little coarser. But it's unquestionably organized with that variation in vesicle concentration.

Schmitt: Okay, I got it. Okay, that looks like our old friend, the gabbro, all right.

Cernan: By golly, your geology training is coming in handy.

Schmitt: Whoops, oh, yeah; I got some soil.

Cernan: (Singing) Hippity-hoppity, hippity-hoppity, hippity-hopping over hill and dale.

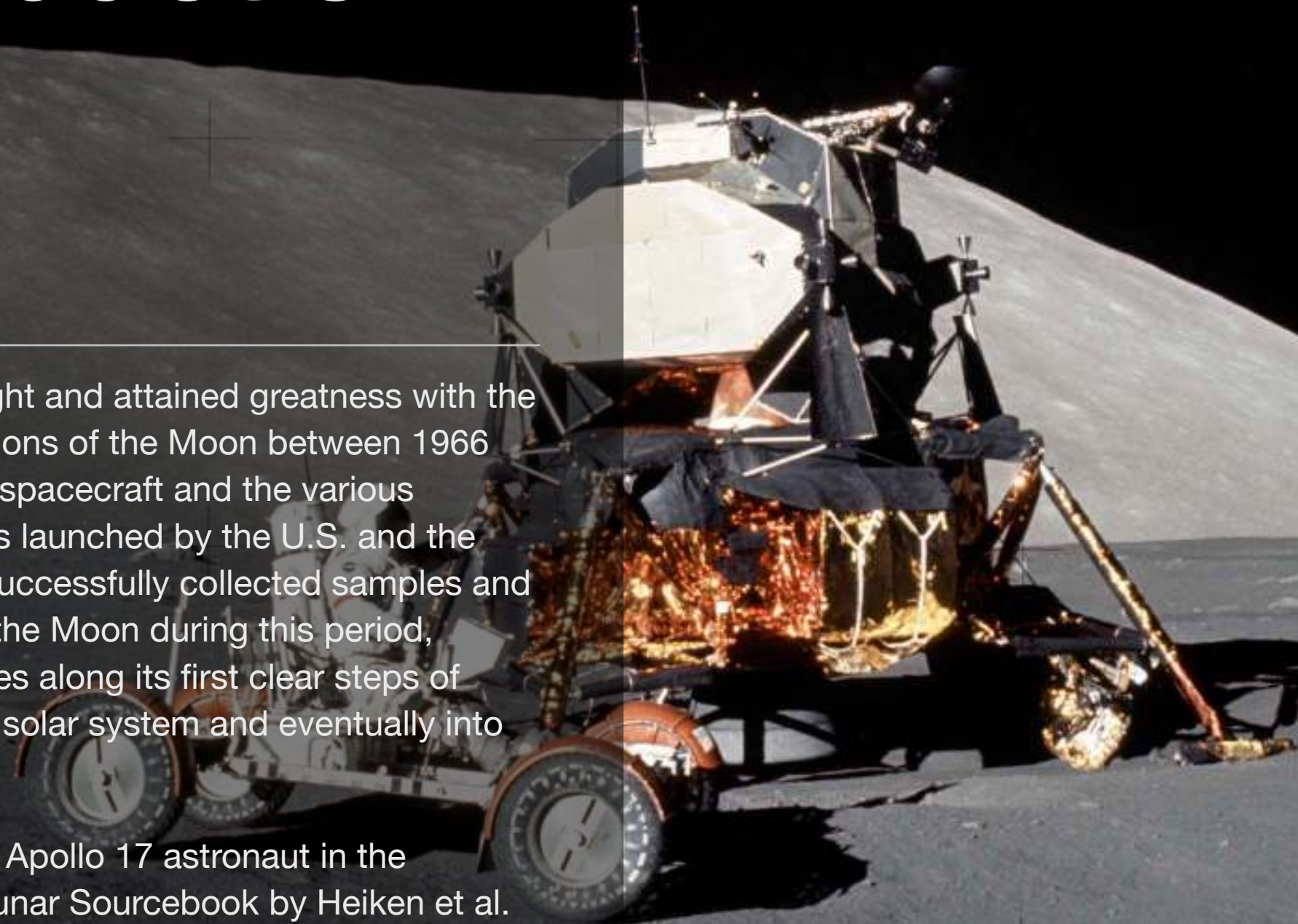
Cernan: Okay. My golly, this time goes fast!

(Courtesy of NASA).

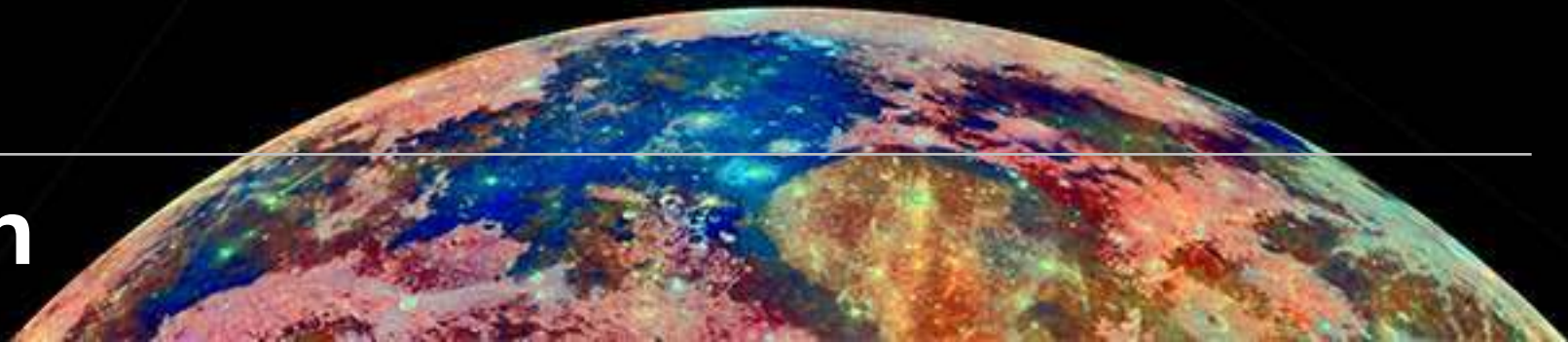
Introduction

“Humankind sought and attained greatness with the first field explorations of the Moon between 1966 and 1976. Apollo spacecraft and the various automated probes launched by the U.S. and the U.S.S.R., which successfully collected samples and information from the Moon during this period, pushed the species along its first clear steps of evolution into the solar system and eventually into the galaxy.”

Harrison Schmitt, Apollo 17 astronaut in the foreward to the Lunar Sourcebook by Heiken et al. (1991).

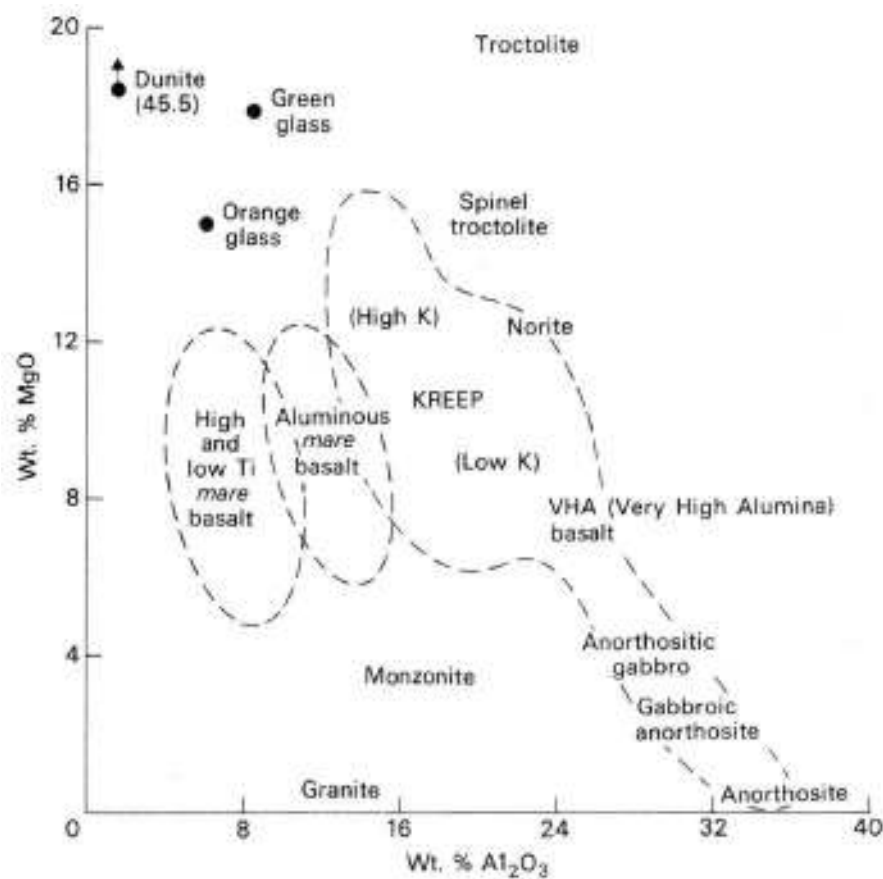


Mineral Introduction



MAJOR ROCK TYPES ON THE MOON

1. Highland Rocks
2. Mare Basalt
3. Regolith Breccia
4. Impact Melts



Lunar rock compositions (taken from Cadogan, 1981)

Why this book is needed?

To answer a few basic questions like:

What are the minerals found in Moon rocks?

What do they look like and what are their sizes and abundances?

What does analysis of those minerals tell us?

This book aims to provide a summary based on many published works together with providing examples of some of these species in mineral virtual microscopes (many more lunar virtual microscopes are available [here](#)).

Since the major books on lunar mineralogy (e.g. Levinson and Taylor, 1971 & Frondel, 1975) were written before the discovery of lunar meteorites, this book also covers a wider range of source rocks and hence mineral species.

This book does not try to provide a comprehensive treatise on the origin of the Moon, nor does it try to describe the lunar rock types. They are outside of its scope, although an insight is provided in our earlier iBook “Moon Rocks: an Introduction to the Geology of the Moon” (for further details: UK, US, Canada and Australia [go here](#) - Other Regions [go here](#)).

Format of this book

Moon Minerals has two substantive chapters - Chapter 2 “Major Minerals” and Chapter 3 “Accessory Minerals”. They both have the same format although Chapter 3 has significantly fewer interactive virtual microscopes. This is because most accessory minerals form very small crystals and these cannot be clearly resolved with a conventional petrological microscope.

Putting this difference aside, the two chapters both begin with short descriptions of a mineral species or mineral group mostly based on the published scientific literature. Typically each reference is condensed down to one or two paragraphs detailing the mineral being described, plus wherever possible the scientific conclusion that analysis of the mineral has provided.

For many species, key geochemical diagrams are provided next. They show various aspects of how minerals inter-relate with one another (for example the diagram on page 11 shows the proportions of four of the major minerals depicted in a way that also shows how minerals and rock types are intimately related). Other diagrams show how mineral chemistry changes between individual samples.

Usually virtual microscopes come next (if they are available) and these are followed by photographs of the minerals. These take the form of transmitted or reflected light images collected with a petrological microscope, and backscattered electron images and X-ray maps collected with a scanning electron microscope (SEM) or electron microprobe. Some of the most complex images are composite X-ray maps where three single element images are merged into the red, green and blue channels of a colour image

resulting in images that clearly separate individual minerals on the basis of their combined colours. In the search for elusive accessory minerals these combination maps are invaluable.

Note that some images are not referred to in the text. They are simply there to illustrate some of the variations within species.

Chapter 4 is an interactive reference list from which it is possible to view the actual research publications on which this book is based. These usually open up as pdf files which can be read directly. Some publications are not freely available, hence the lack of a link. We obtained copies through our university library.

The book concludes with an Appendix listing additional “mineral species” that we have encountered during our research for this book. Many are described in Russian literature which we have not interrogated fully. For this reason we placed these species outside the main content of the book.

List of Minerals

Olivine Group & Related Species

Forsterite - Mg_2SiO_4

Fayalite - Fe_2SiO_4

and related species:

Ringwoodite - $(\text{Mg},\text{Fe}^{2+})_2\text{SiO}_4$

Wadsleyite - $(\text{Mg},\text{Fe}^{2+})_2\text{SiO}_4$

Pyroxene Group

Enstatite - $\text{Mg}_2\text{Si}_2\text{O}_6$

Pigeonite - $(\text{Mg},\text{Fe}^{2+},\text{Ca})(\text{Mg},\text{Fe}^{2+})\text{Si}_2\text{O}_6$

Augite - $(\text{Ca},\text{Mg},\text{Fe}^{2+})\text{Si}_2\text{O}_6$

Diopside - $\text{CaMgSi}_2\text{O}_6$

Hedenbergite - $\text{CaFe}^{2+}\text{Si}_2\text{O}_6$

Feldspar Group

A solid solution series between anorthite ($\text{CaAl}_2\text{Si}_2\text{O}_8$) and albite ($\text{NaAl}_2\text{Si}_3\text{O}_8$) [lunar samples are nearer the anorthite end-member]. Note: maskelynite is the solid state transformation of plagioclase to glass.

K-Feldspar - KAlSi_3O_8 [see Chap 3 Accessory Minerals - Sect 11]

Hyalophane or Barian Sanidine - $(\text{K},\text{Ba})\text{AlSi}_3\text{O}_8$

Iron-Titanium Oxide

Ilmenite - $\text{Fe}^{2+}\text{TiO}_3$

Glass - not a mineral, but a major constituent of impact melts

Metals

Iron-Nickel (taenite and kamacite)

Copper

Silicon

Tin

Alloys

Hapkeite - Fe_2Si

Linzhiite - FeSi_2

Naquite - FeSi

Awaruite - Ni_3Fe

Sulphides

Troilite - FeS

Pyrrhotite - Fe_{1-x}S (where $x = 0.1 - 0.2$)

Mackinawite - FeS

Pentlandite - $(\text{Fe},\text{Ni})_9\text{S}_8$

Chalcopyrite - CuFeS_2

Cubanite - $\text{Cu,Fe}_2\text{S}_3$

Sphalerite - ZnS

Greigite - FeFe_2S_4

Chalcocite? - Cu_2S

Bornite? - Cu_5FeS_4

Molybdenite? - MoS_2

Ninningerite? - $(\text{Mg,Fe,Mn})\text{S}$

Carbides & Phosphides

Graphite - C

Cohenite - $(\text{Fe,Ni,Co})_3\text{C}$

Moissanite - SiC

Schreibersite - $(\text{Fe,Ni})_3\text{P}$

Barringerite - $(\text{Fe,Ni})_2\text{P}$

Spinel Group

Spinel - MgAl_2O_4 (inc. pleonaste)

Ulvöspinel - Fe_2TiO_4

Chromite - FeCr_2O_4

Phosphates

Fluorapatite - $\text{Ca}_5(\text{PO}_4)_3\text{F}$

Chlorapatite - $\text{Ca}_5(\text{PO}_4)_3\text{Cl}$

Merrillite - $\text{Ca}_9\text{NaMg}(\text{PO}_4)_7$

Whitlockite - $\text{Ca}_9\text{Mg}(\text{PO}_4)_6[\text{PO}_3(\text{OH})]$

Stanfieldite - $\text{Ca}_4(\text{Mg,Fe}^{2+})_5(\text{PO}_4)_6$

Farringtonite - $\text{Mg}_3(\text{PO}_4)_2$

Monazite - $\text{REE}(\text{PO}_4)_2$

and related species Britholite - $(\text{Ce,Ca})_5(\text{SiO}_4)_3\text{OH}$

Chlorides

Akaganéite - $\text{Fe}_{7.6}\text{Ni}_{0.4}\text{O}_{6.35}(\text{OH})_{9.65}\text{Cl}_{1.25}$

Halite - NaCl

Lawrencite? - $\text{Fe}^{2+}\text{Cl}_2$

Titanium Minerals

Armalcolite - $(\text{Mg,Fe}^{2+})\text{Ti}_2\text{O}_5$

Rutile (& Anatase) - TiO_2

Titanite - CaTiO_5

Yttrobetafite-(Y) (renamed oxycalciobetafite) - $\text{Y}(\text{Ti,Nb})_2\text{O}_6$

“Pyrochlore” - $(\text{Ca,Pb,Y,Th})_2(\text{Ti,Nb})_2\text{O}_6$

Chevkinite - $(\text{Ce,Ca,Na,Th})_4(\text{Fe}^{2+},\text{Mg})_2(\text{Ti, Fe}^{3+})_3\text{Si}_4\text{O}_{22}$

Perovskite (variety dysanalyte)? - $(\text{Ca,Fe})(\text{Ti,REE})\text{O}_3$

Zirconium Minerals

Tranquillityite - $\text{Fe}_8(\text{Zr,Y})_2\text{Ti}_3\text{Si}_3\text{O}_{24}$

Baddeleyite - ZrO_2

Zircon - ZrSiO_4

Zirconolite - $\text{CaZrTi}_2\text{O}_7$ / Zirkelite - $(\text{Ti,Zr,Ca})\text{O}_{2-x}$ (where $x \sim 0.3$)

Silica Minerals

Quartz - SiO_2

Cristobalite - SiO_2

Tridymite - SiO_2

Coesite - SiO_2

Stishovite - SiO_2

Moganite - SiO_2

Seifertite - SiO_2

Other Species

Pyroxferroite - $(\text{Ca,Fe})(\text{Fe}^{2+}\text{Mn})_6(\text{Si}_7\text{O}_{21})$

Cordierite - $\text{Mg}_2\text{Al}_4\text{Si}_5\text{O}_{18}$

Almandine - $\text{Fe}_3\text{Al}_2\text{Si}_3\text{O}_{12}$

Yoshiokaite - $\text{Ca}(\text{Al,Si})_2\text{O}_4$

Rhönite - $\text{Ca}_2(\text{Mg,Fe}^{2+},\text{Fe}^{3+},\text{Ti})_6(\text{Si,Al})_6\text{O}_{20}$

Keiviite-(Y) - $(\text{Y,REE})_2\text{Si}_2\text{O}_7$

Thorite - ThSiO_4

Corundum - Al_2O_3

Magnetite - $\text{Fe}^{2+}\text{Fe}^{3+}_2\text{O}_4$

Calcite - CaCO_3

Siderite - FeCO_3

Goethite? - αFeOOH

Nepheline Group

Nepheline? - $(\text{Na,K})\text{AlSiO}_4$

Amphibole Group

Arfvedsonite? - $\text{NaNa}_2(\text{Mg}_4\text{Fe}^{3+})\text{Si}_8\text{O}_{22}(\text{OH})_2$

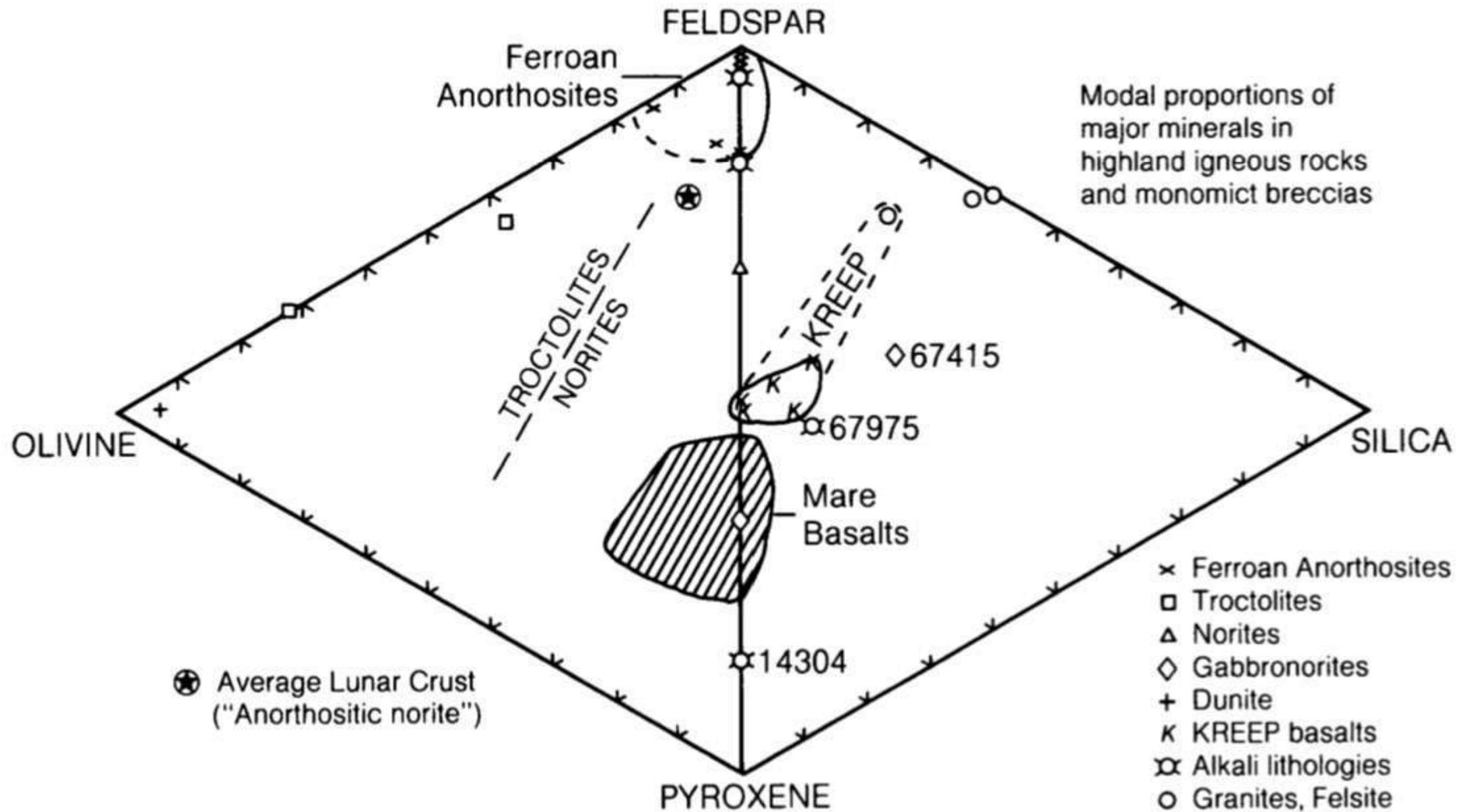
Tschermakite? - $\text{Ca}_2(\text{Mg}_3\text{Al}_2)(\text{Si}_6\text{Al}_2)\text{O}_{22}(\text{OH})_2$

Richterite? - $\text{Na}(\text{NaCa})\text{Mg}_5\text{Si}_8\text{O}_{22}(\text{OH})_2$

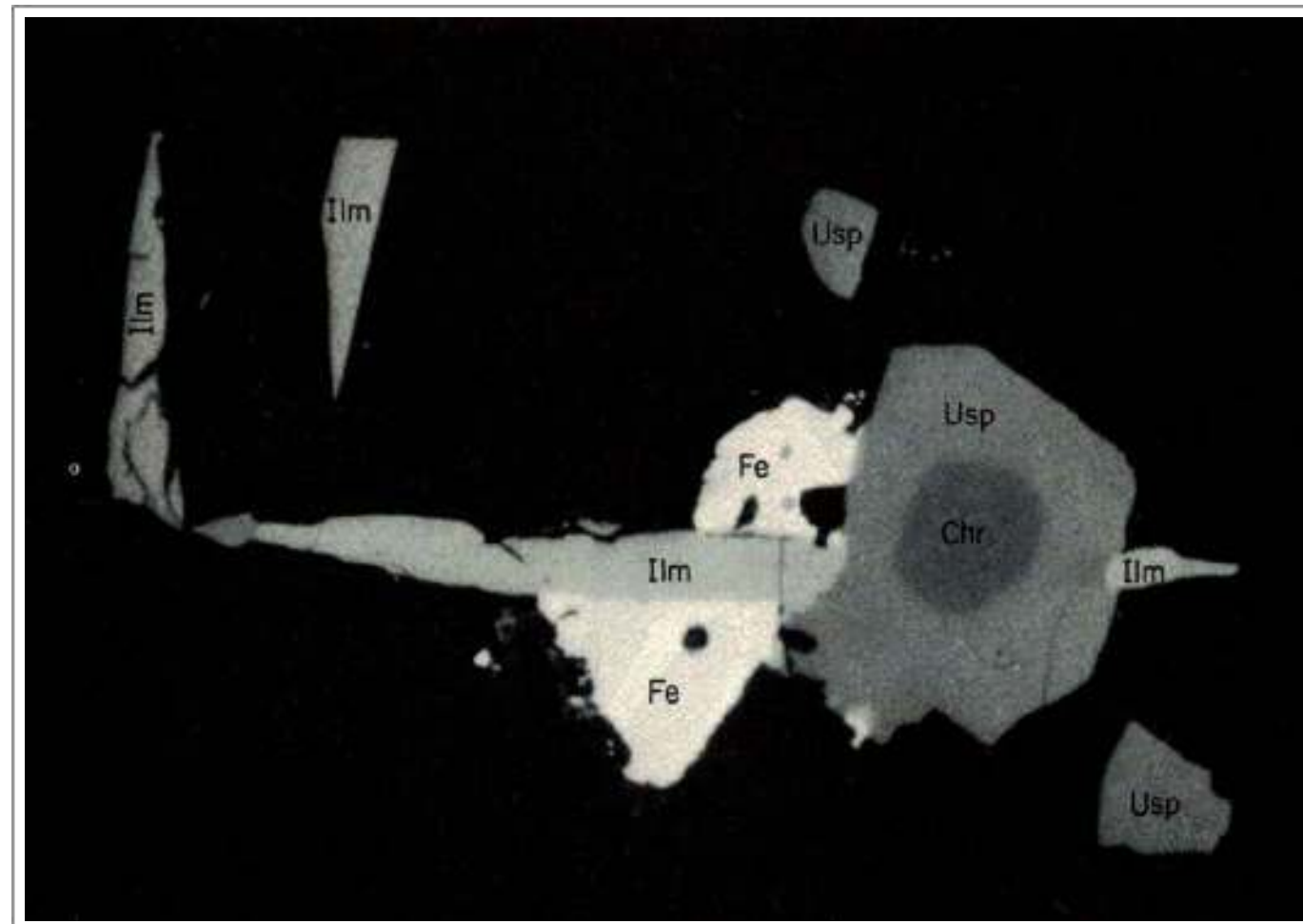
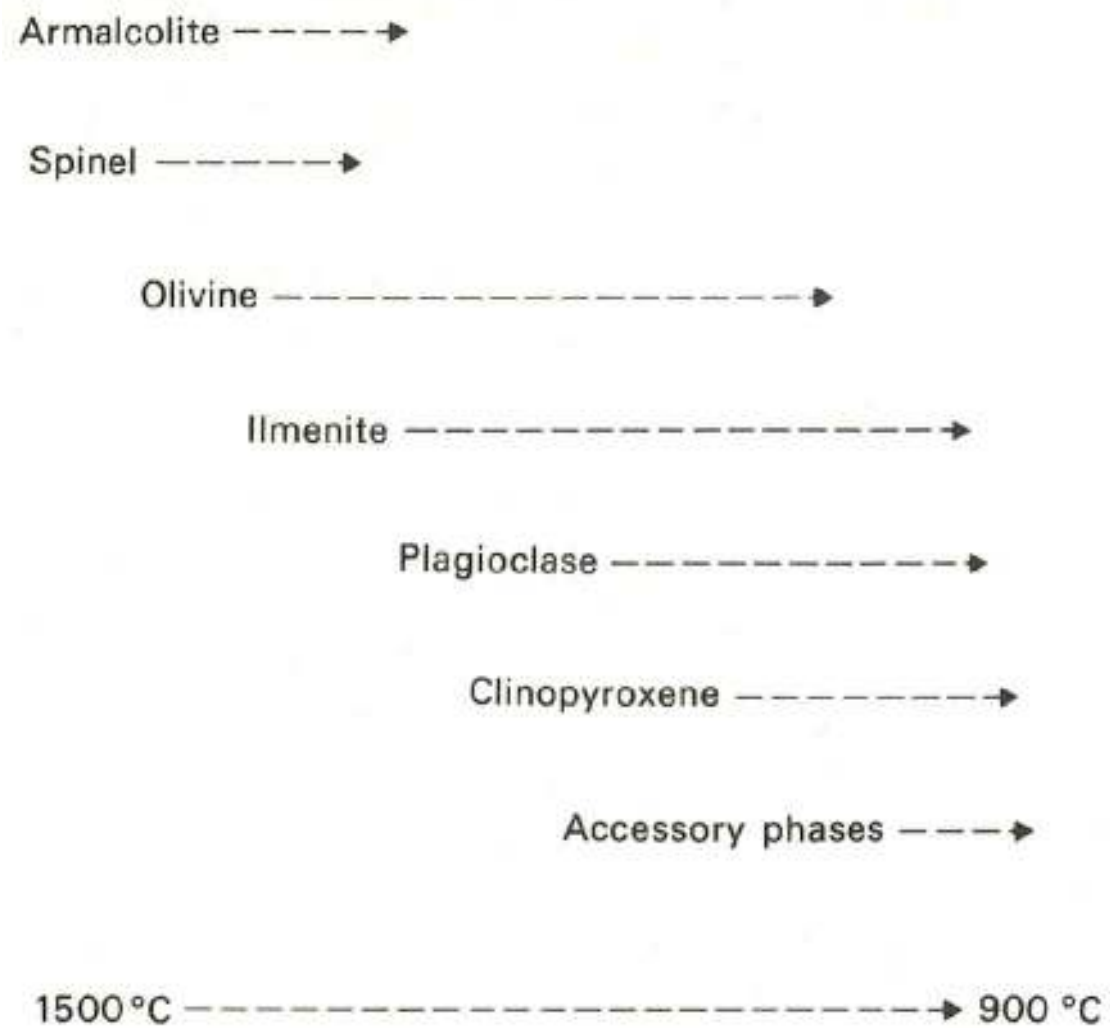
Kaersutite? - $\text{NaCa}_2(\text{Mg}_3\text{Ti}^{4+}\text{Al})\text{Si}_8\text{O}_{22}(\text{OH})_2$

? = further confirmation is desirable

See Appendix for additional minerals noted in the literature

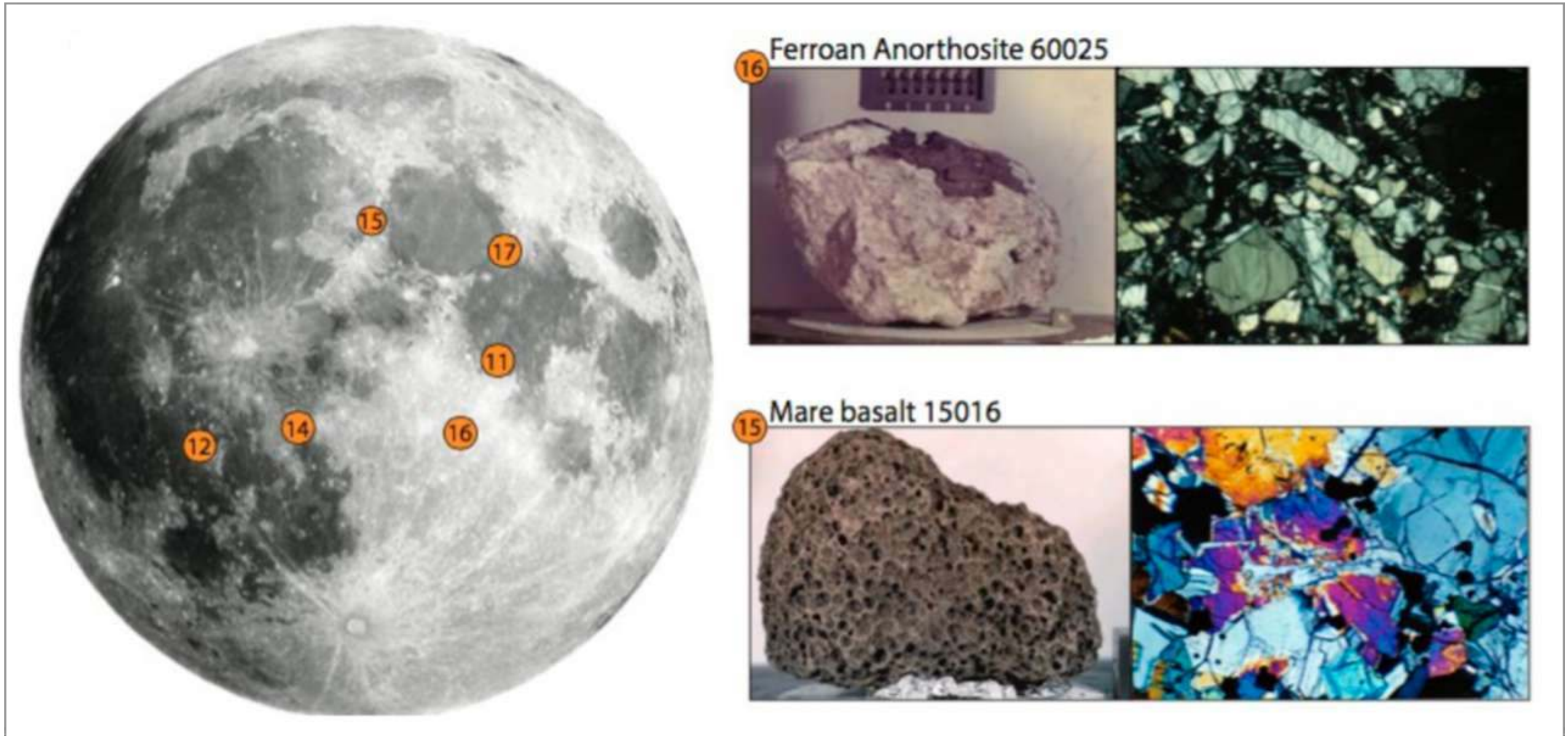


Modal (volume) proportions of the four major minerals in highland pristine igneous rocks and monomict breccias. Gabbronorites include the sodic ferrogabbro 67415; alkali lithologies include two alkali anorthosites (with abundant feldspar), alkali norite 14304 and alkali granite 67975. The general area of mare basalt composition is shown for comparison (ruled area). The KREEP basalts have higher amounts of feldspar and silica minerals. The boundary between norite and troctolite is defined by the line representing a 1:1 olivine-to-pyroxene ratio (Stöffler et al., 1980; Heiken, 1991).



Taken From Cadogan (1981)

Order typical of mineral crystallization in a mare basalt. The reflected light image shows the order of crystallization of some of these species. Chromite (Chr) followed by ulvöspinel (Usp), followed by ilmenite (Ilm), and finally metallic iron (Fe).

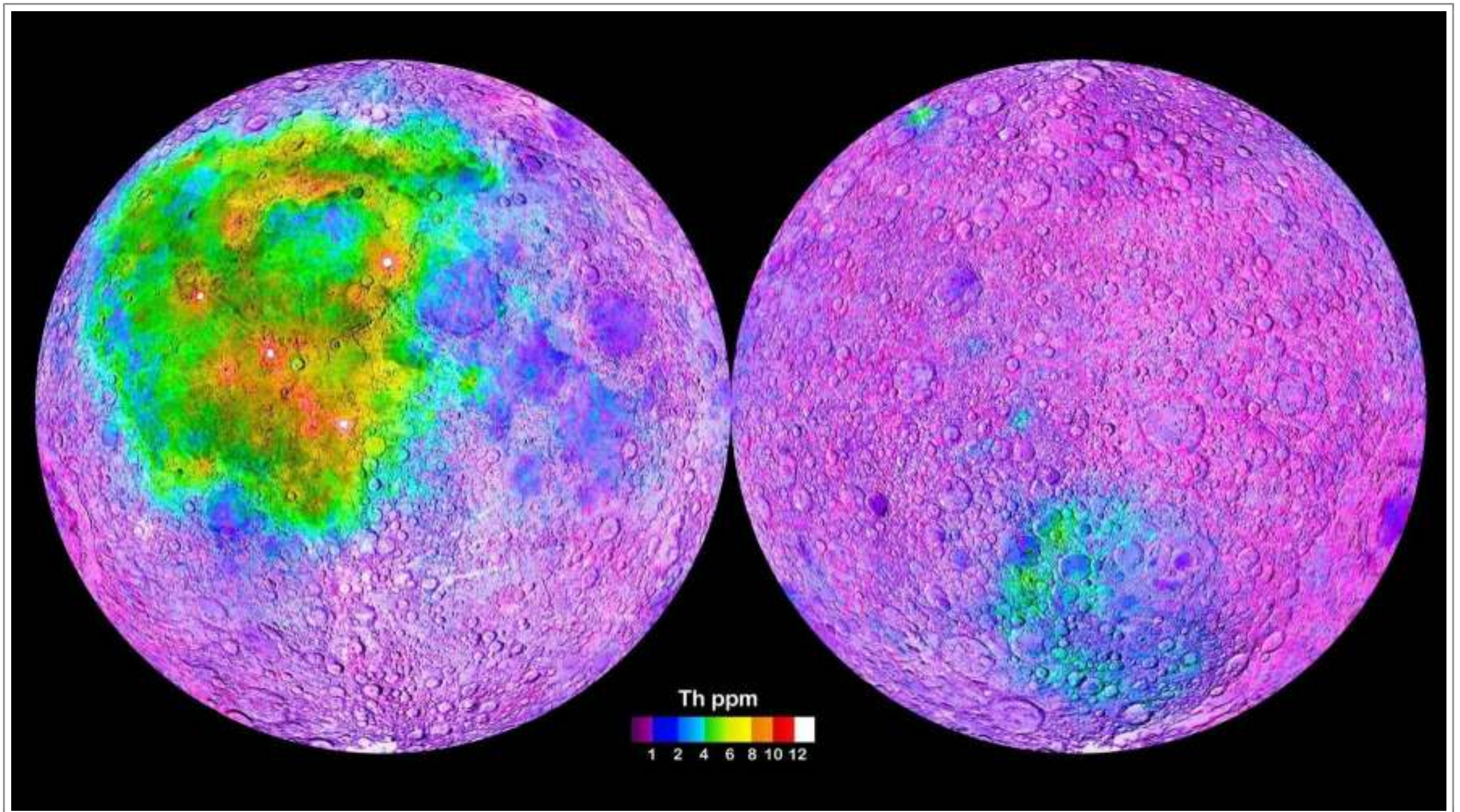


Taken From McLeod and Krekeler (2017)

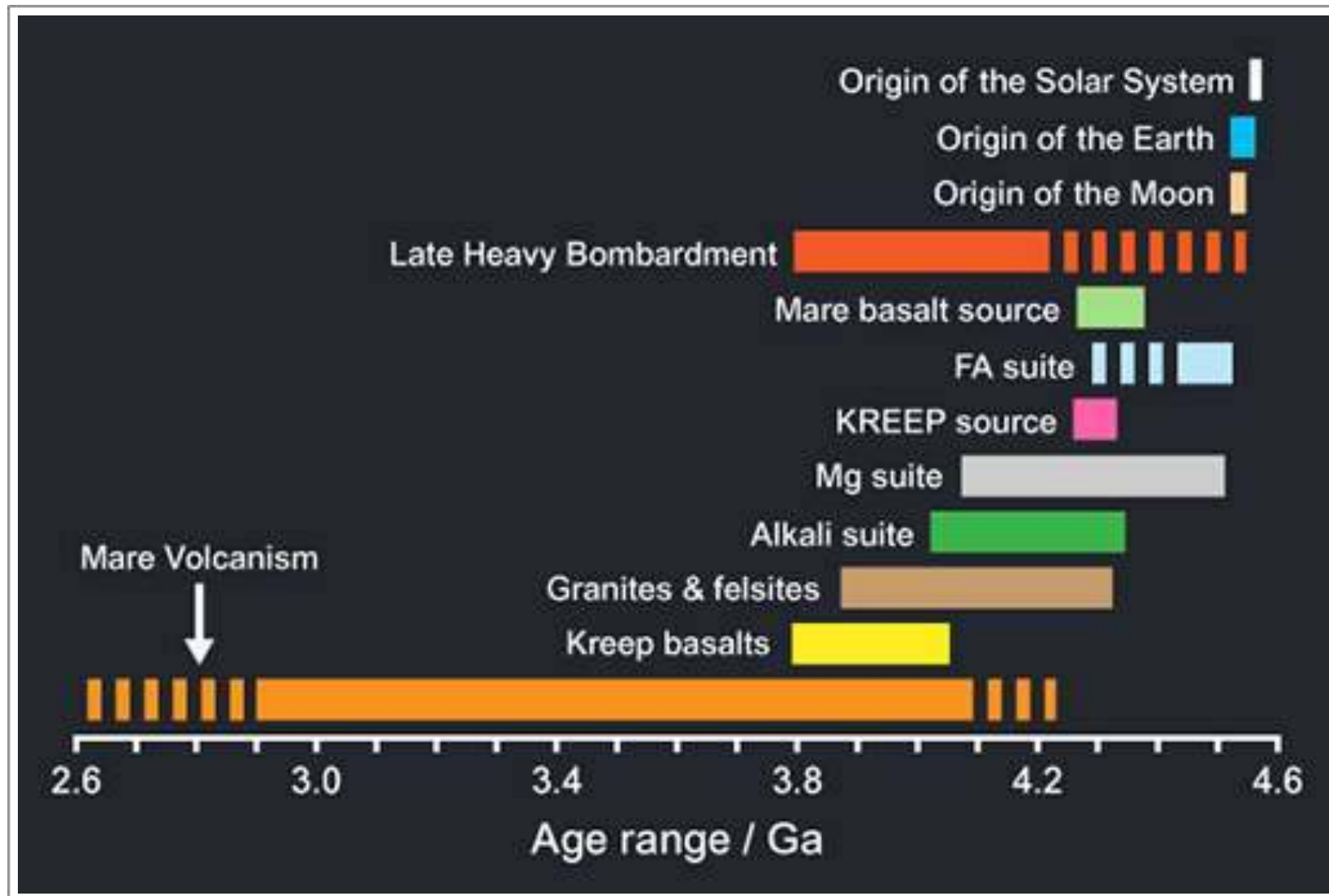
Near side of the Earth's Moon with Apollo landing sites shown. The majority of landing sites targeted the lunar mare (dark regions).

Top Right: Image on left shows a hand specimen of 60025, a ferroan anorthosite. Image on right shows a thin section view of 60025, characterized by 70-98% plagioclase feldspar.

Bottom Right: Image on left shows a hand sample of 15016, a vesiculated basalt. Image on right shows a thin section view of 15016, characterized by olivine (6-10%), pyroxene (59-67%), plagioclase (21-27%), ilmenite (6%), and <1% of chromite, ulvöspinel and mesostasis.



KREEP terrane on the Moon (green-blue-orange). A distribution map of thorium concentration shows a large area of KREEP on the Near Side (left) corresponds to the Procellarum KREEP Terrane, and the smaller area on the Far Side (right) to the South Pole-Aitken Terrane. KREEP is an acronym built from the letters K (the atomic symbol for potassium), REE (Rare Earth Elements) and P (for phosphorus). Source [NASA](#).



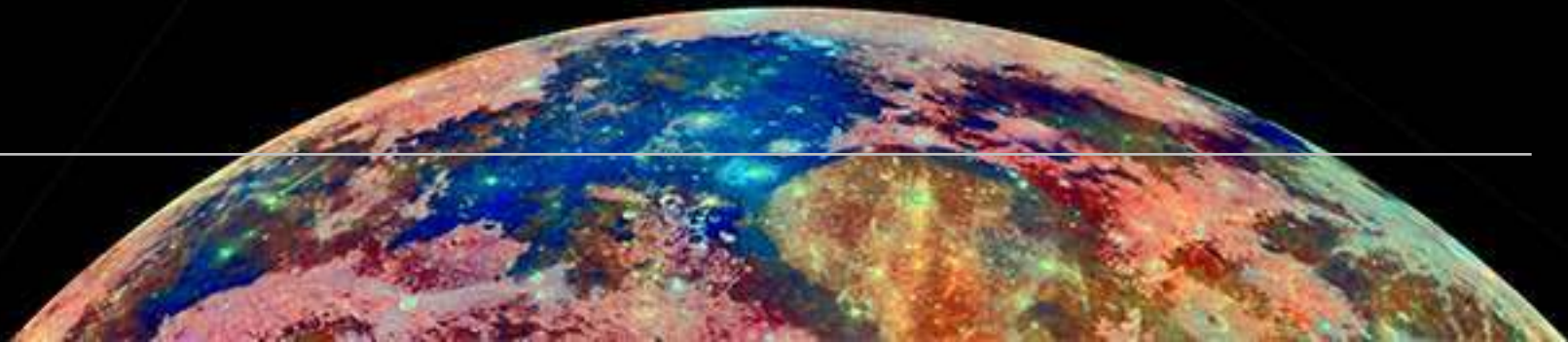
Summary of the chronology of the formation of the lunar crust. Ga (Giga-annum) is 1 billion years. Source Open University on-line Open Learn - "Moons" course, Week 5 ([link to website](#)).

Major Minerals

These are the minerals that make up over 95% of all Moon rocks.



Olivine Group



SPECIES

1. Forsterite - Mg_2SiO_4
2. Fayalite - Fe_2SiO_4
3. and related species
4. Ringwoodite - $(\text{Mg},\text{Fe}^{2+})_2\text{SiO}_4$
5. Wadsleyite - $(\text{Mg},\text{Fe}^{2+})_2\text{SiO}_4$

Forsterite-Fayalite Series

The major compositional variation within olivine is caused by exchange of Fe for Mg; this variation in composition is represented by the ratio $\text{Fe}/(\text{Fe} + \text{Mg})$. The Mg end member is forsterite and the Fe end member is fayalite. The most magnesian mare basalt olivine grains contain only 20% fayalite (Fa), but most olivine in mare basalt has a compositional range of $\text{Fa}_{20}\text{-Fa}_{70}$. However, a few mare basalts contain end-member fayalite ($\text{Fa}_{90}\text{-Fa}_{100}$). This olivine is part of an equilibrium three-phase assemblage (Ca,Fe pyroxene - Fe olivine - silica) that crystallized stably from the late-stage iron-enriched portions of mare basalt melts. Overall the olivine composition of clast-poor highland melt rocks and coarse-crystalline highland igneous rocks is more magnesian than in the mare basalts.

Compared to terrestrial olivine compositions, lunar olivine is more Fe-rich - a reflection that the Earth's mantle is more magnesian than that of the Moon (Heiken et al., 1991).

Apollo 17 basalt 71597 is the sole high-titanium mare basalt showing evidence for olivine accumulation during crystallization. The majority of cumulates are low-titanium ($\text{TiO}_2 < 6 \text{ wt}\%$) composition comprising Apollo 12 ilmenite basalts 12005 and 12036 (Dungan et al., 1977; Rhodes et al., 1977), several members of the Apollo 12 olivine basalt suite (Neal et al., 1994), Apollo 15 basalts 15385 and

15387 (Ryder 1985), Apollo 14 clast 14305,122 (Taylor et al., 1983), and six fragments in lunar meteorite NWA 773 (Jolliff et al., 2003). Quantitative textural analysis and major- and trace-element mineral geochemistry allowed Donohue and Neal (2018) to suggest an origin for 71597 by fractionation from the Type B2 chemical suite of Apollo 17 high-Ti basalts.

Lunar meteorite NWA 773 is essentially a dimict breccia consisting of two main lithologies, including a prominent igneous clast lithology. The clast lithology is an olivine-gabbro cumulate exhibiting cumulus textures and includes 48% olivine (Fo_{67.5}), 27% pigeonite, 11% augite, 2% orthopyroxene, 11% plagioclase, and trace amounts of barian K-feldspar, ilmenite, Cr-spinel, merrillite, troilite, and metallic iron (Jolliff et al., 2003).

Burger et al. (2009) note that in lunar meteorite NWA 032 (an unbrecciated mare basalt) the olivine is compositionally zoned and entirely forsteritic (Fo₆₄ to Fo₅₁).

The most Mg-rich olivine found in Apollo samples (spinel troctolite) has a composition of Fa₈, however, lunar meteorite breccia NWA 8001, is unique among lunar highlands rocks in containing sparse grains of even more Mg-rich forsterite (Fa_{5.7-9.0}) (Kuehner et al., 2014).

Forsteritic olivine is the major mineral (95.3% by volume) of a dunite clast found in lunar meteorite NWA 11421 - an impact-melt breccia. Dunite is a rare rock type on the Moon having only been

found in Apollo 17 sample 72415, and as a few clasts in polymict breccias. The dunite clast in NWA 11421 is interpreted to be a highly tectonized and recrystallized fragment of the Moon's upper mantle (Treiman and Semprich, 2019).

Working on lunar meteorite NWA 8632, a porphyritic, low-Ti, low-Al, low-K lunar basalt containing large olivine phenocrysts (up to ~2 mm in length) Fagan et al. (2018) were able to show evidence of unique oscillatory zoning of P in the phenocrysts. Because P diffuses slowly in olivine the individual grains retain remnant P zoning more efficiently than with other elements, leading P to be a useful indicator of magmatic processes.

Further evidence of oscillatory zoning of P (and Ti) is also described in olivine (Fo₈₂₋₈₃ interiors with narrow Fo₆₈ rims) within dunite xenoliths in Apollo 17 high-Ti mare basalt 74275(96,97) by Shearer et al. (2015a). X-ray maps of the xenoliths illustrate that these slow diffusing elements preserve primary cumulate zoning textures.

Provincio et al. (2015) studied olivine alteration in Apollo 16 feldspathic polymict breccia 67915 and found sulphide replacement textures present in Mg-suite clasts. Textures typically consist of secondary low-Ca pyroxene, troilite, ilmenite and metallic iron pseudomorphically replacing primary igneous olivine - most notably "myrmekite-like" intergrowths of low Ca-pyroxene and troilite. These formed by the interaction of the Mg-suite clasts with a sulphur-bearing metasomatic fluid.

Fayalite

Trace amounts of fayalite occur as narrow borders between ilmenite and pyroxferroite in Apollo 11 ilmenite basalt 10044 (Fuchs 1970). A possible reaction relationship of pyroxferroite and ulvöspinel to form fayalite and ilmenite was proposed.

Apollo 14 sample 14053 is a fine-grained, holocrystalline, equigranular hi-Al mare-type basalt containing mostly pyroxene (~50%), plagioclase (~40%) and olivine (4%). In late-stage mesostasis areas it contains fayalite, silica, K-Ba-rich glass, K-feldspar, F-Cl-bearing apatite, merrillite, baddeleyite and opaque minerals. In this mesostasis there is evidence for a reduction reaction - the breakdown texture of fayalite to metallic iron and silica: $\text{Fe}_2\text{SiO}_4 \rightarrow 2\text{Fe} + \text{SiO}_2 + \text{O}_2$. This rock also displays extreme reduction of Cr-ulvöspinel to ilmenite. The reduction is thought to have occurred when solar wind H_2 permeated the sample during a re-heating event (Patchen, 2004; Boyce et al., 2010).

Olivine in basaltic lunar meteorite MIL 05035 is exclusively fayalitic, unlike in the majority of Apollo mare basalts. Large (~1 mm) fayalite grains have uniform compositions of Fa_{98} and are associated with late-stage phases (SiO_2 droplets, K-Si-rich glass with K-Ba-feldspar [hyalophane], apatite, and baddeleyite) in a “swiss-chess” texture, which suggests that these fayalite grains formed at the extreme end-stage of crystallization, most likely during silicate-liquid immiscibility. Small fayalitic olivines (Fa_{90} ,

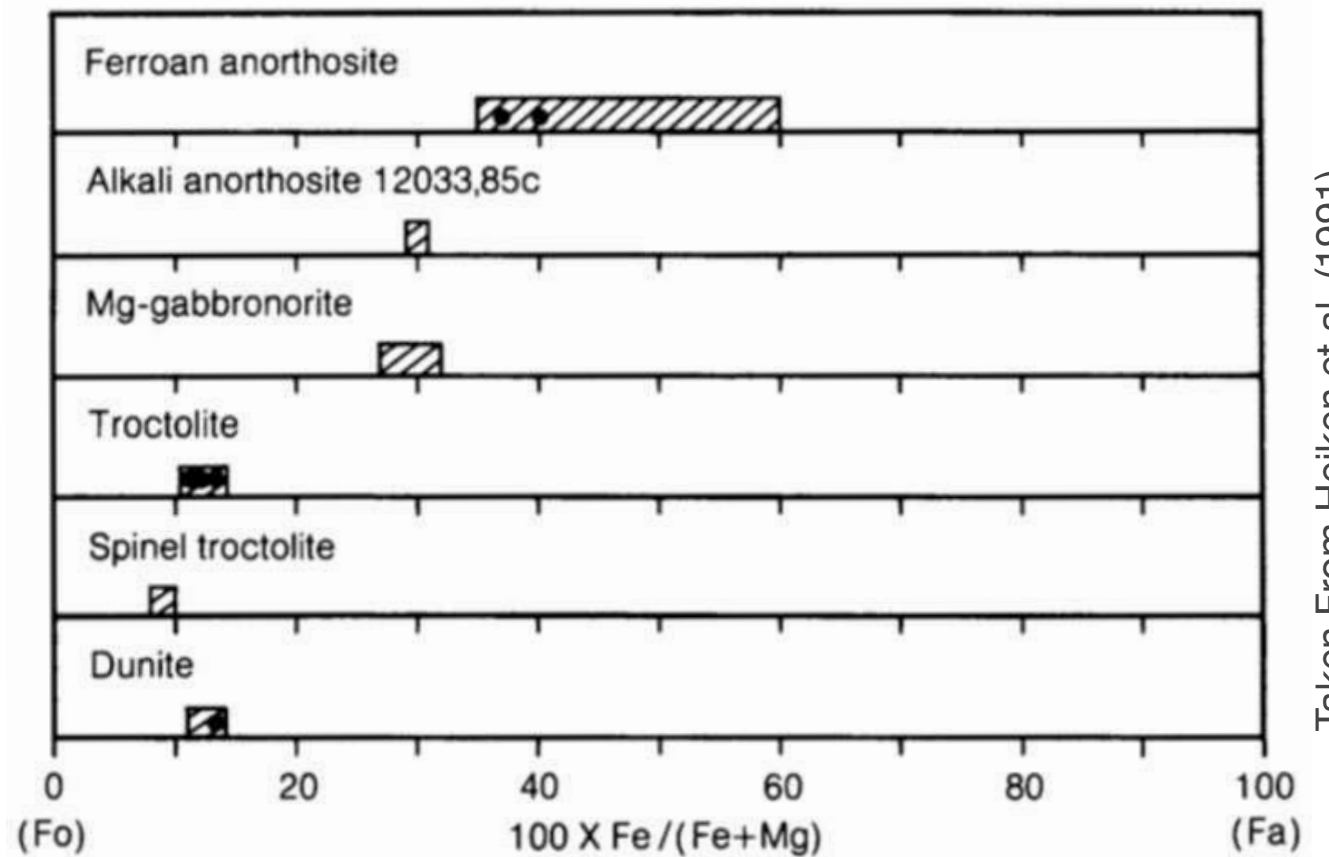
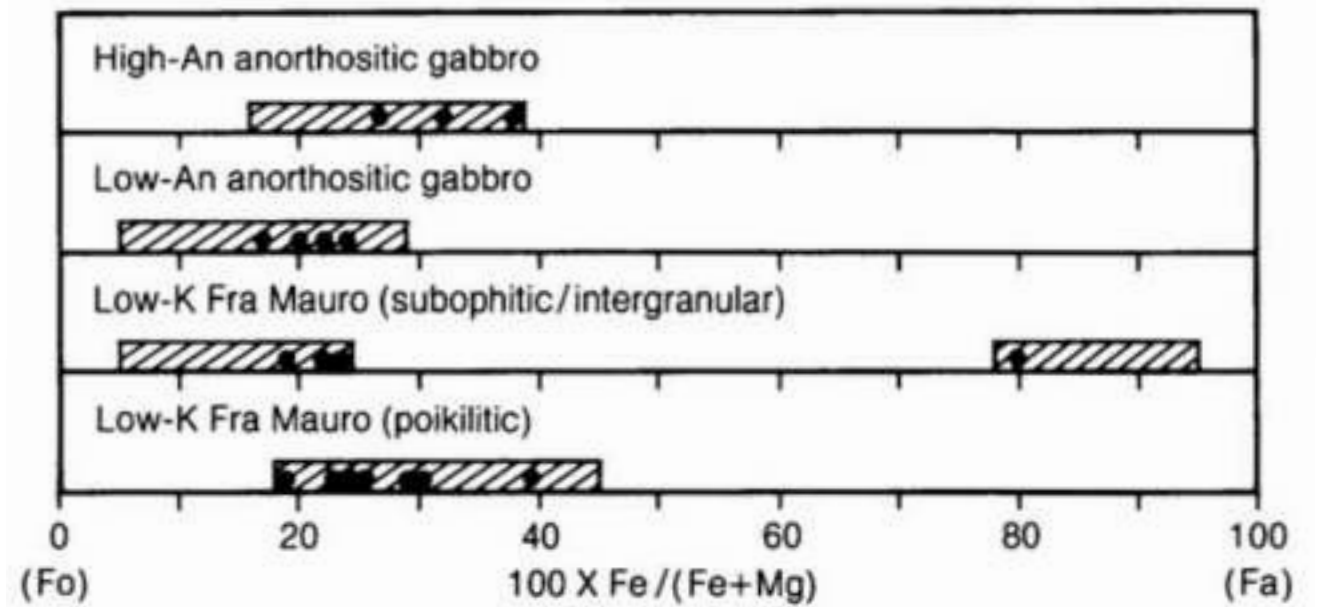
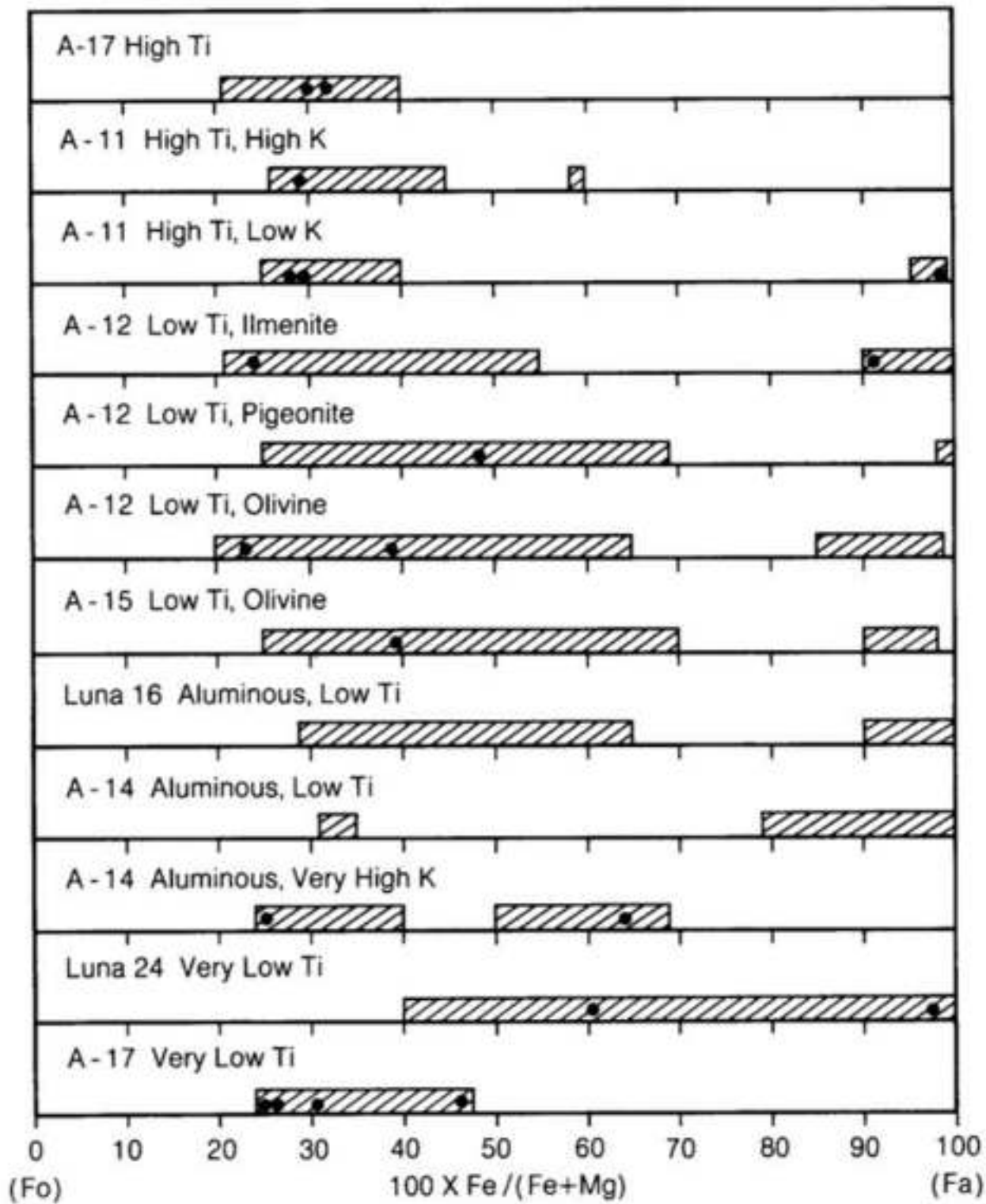
<50 μm) are also found in the mesostasis. Enriched REE contents in large olivine grains suggest they formed during late-stage crystallization of the MIL 05035 parental liquid (Liu et al., 2009).

in lunar meteorite Sayh al Uhaymir (SaU) 169 (a regolith breccia) one anhedral (>200 μm) unzoned fayalitic olivine (Fo_{88}) grain has been reported. A second (fayalite + tridymite) clast is more complex and could represent a breakdown assemblage after pyroxferroite (Al-Kathiri et al., 2007). This is the same origin proposed by Zeigler et al. (2005b) for silica and fayalite-hedenbergite symplectite grains found in lunar meteorite MET 01210 - a basaltic regolith breccia.

Fayalite grains are common in lunar mare basalt meteorites LaPaz Icefield (LAP) 02205, 02224, and 02226, and all are associated with the mesostasis regions of the samples. These masses are anhedral and form a groundmass containing Al, K-enriched glass, silica, troilite, plagioclase, Fe-rich pyroxene and ilmenite. The fayalite could be formed by the breakdown of pyroxferroite at low pressure into a stable of assemblage of hedenbergite-fayalite- SiO_2 (Joy et al., 2006).

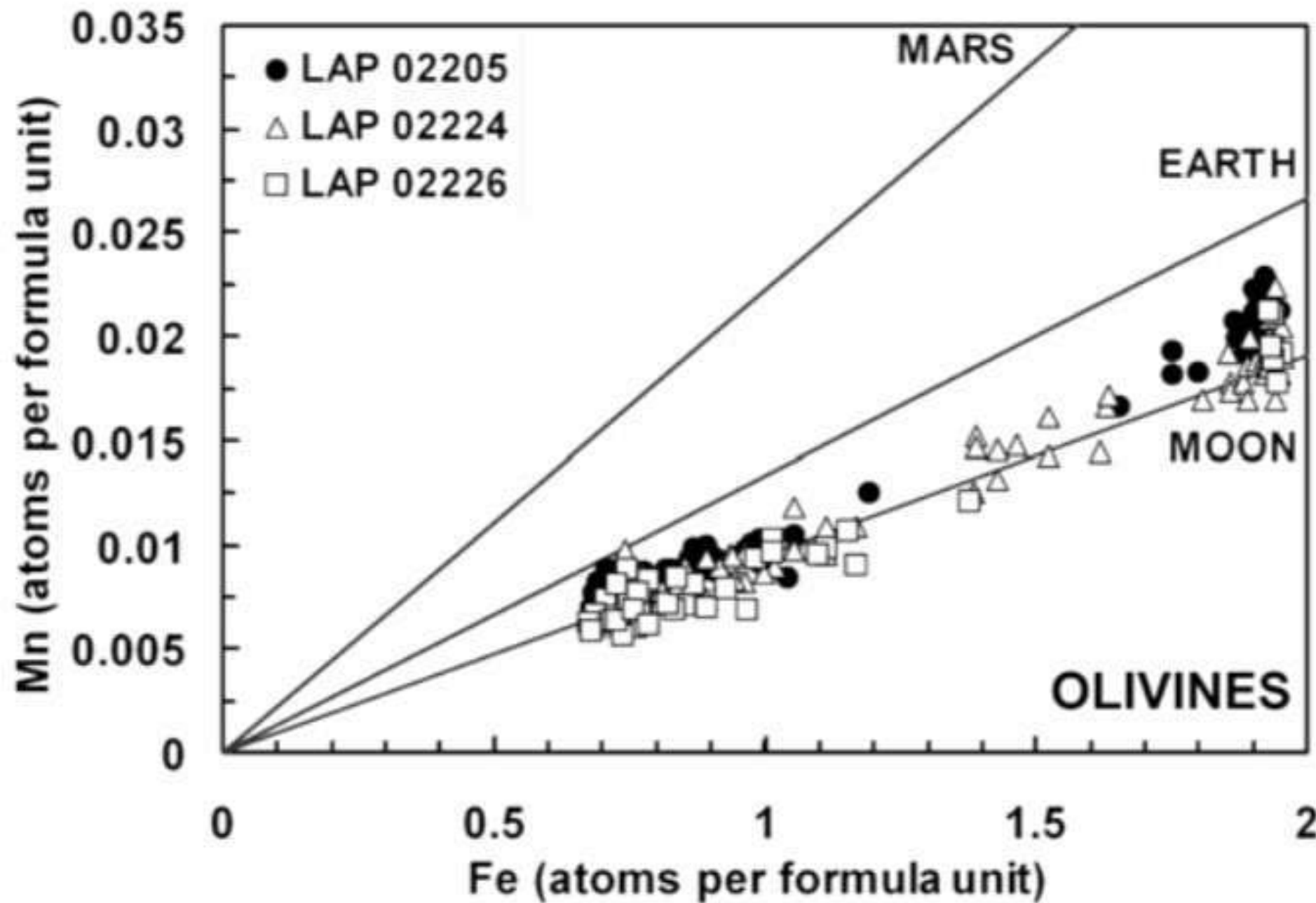
Ringwoodite and Wadsleyite

The high-pressure polymorphs of olivine (ringwoodite and wadsleyite) are reported from shock-melt veins in the unbrecciated low-Ti basalt lunar meteorite NWA 479. They indicate shock-pressures of at least 20 GPa. The most obvious shock features observed in thin section consist of microfaults, dispersed melt pockets and veins, $\sim 100 \mu\text{m}$ in width, running throughout the sample and produced by rapid shear movements. They enclose rounded fragments of the host rock, or individual matrix minerals or grains, which have been entrained and transformed by a solid-state reaction to polycrystalline high-pressure phases. Raman spectra confirm these phases are ringwoodite and wadsleyite (Barrat et al., 2005).



Taken From Heiken et al. (1991)

Compositional ranges of olivine in mare basalts (left); highland clast-poor melt rocks (top right); and highland coarse-crystalline igneous rocks (bottom right).

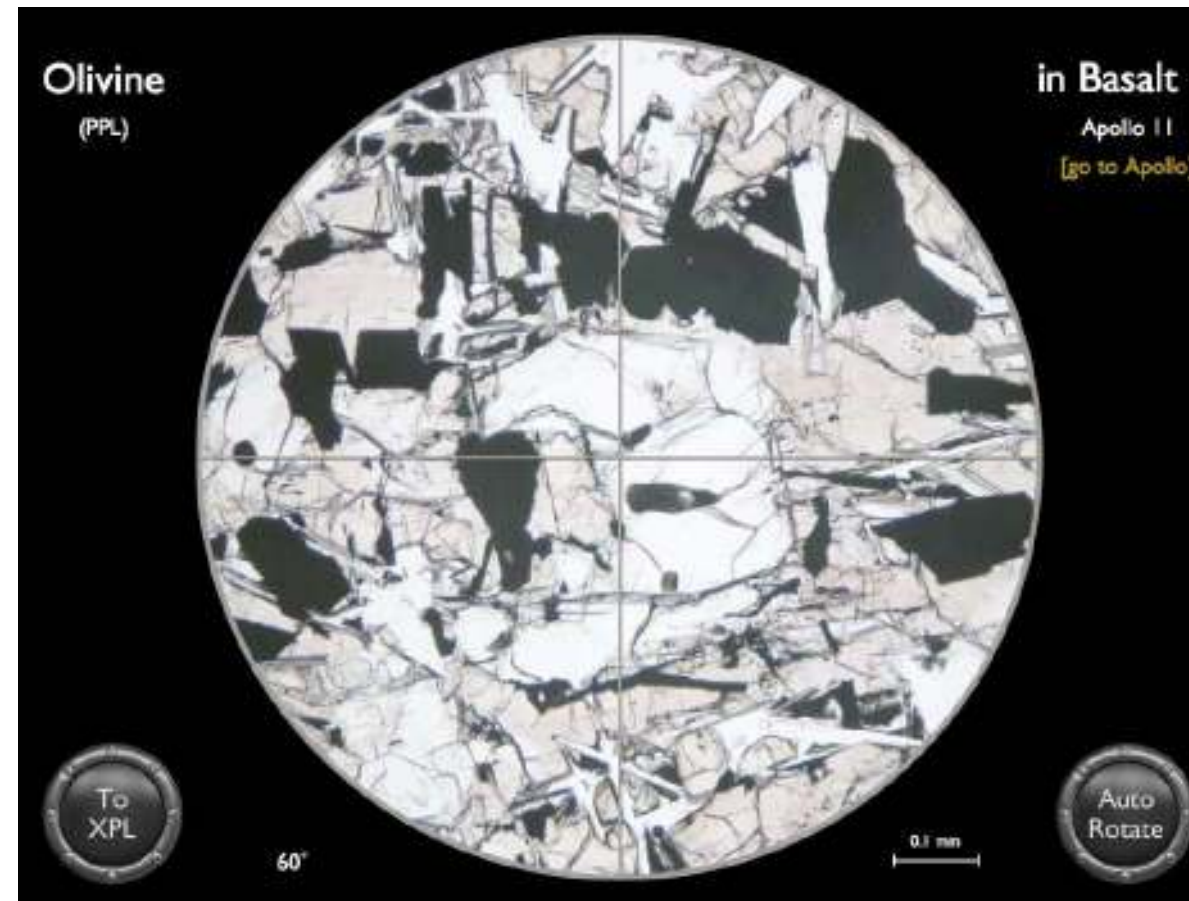


Taken From Joy et al. (2006)

The Fe/Mn ratio in olivine is an indicator of planetary origin. Lunar olivine exhibits a diagnostic Fe/Mn ratio compared to the Earth, Mars, Vesta and chondritic meteorites - probably as the result of volatile loss in an early Moon-forming event (Papike et al. 2003). Here data from lunar meteorites LAP 02205, 02224 and 02226 are superimposed over the typical planetary fractionation trends. Atoms per formula unit are based on 4 oxygen atoms.

Moon Minerals: Olivine Group

Mineral Virtual Microscope: Olivine



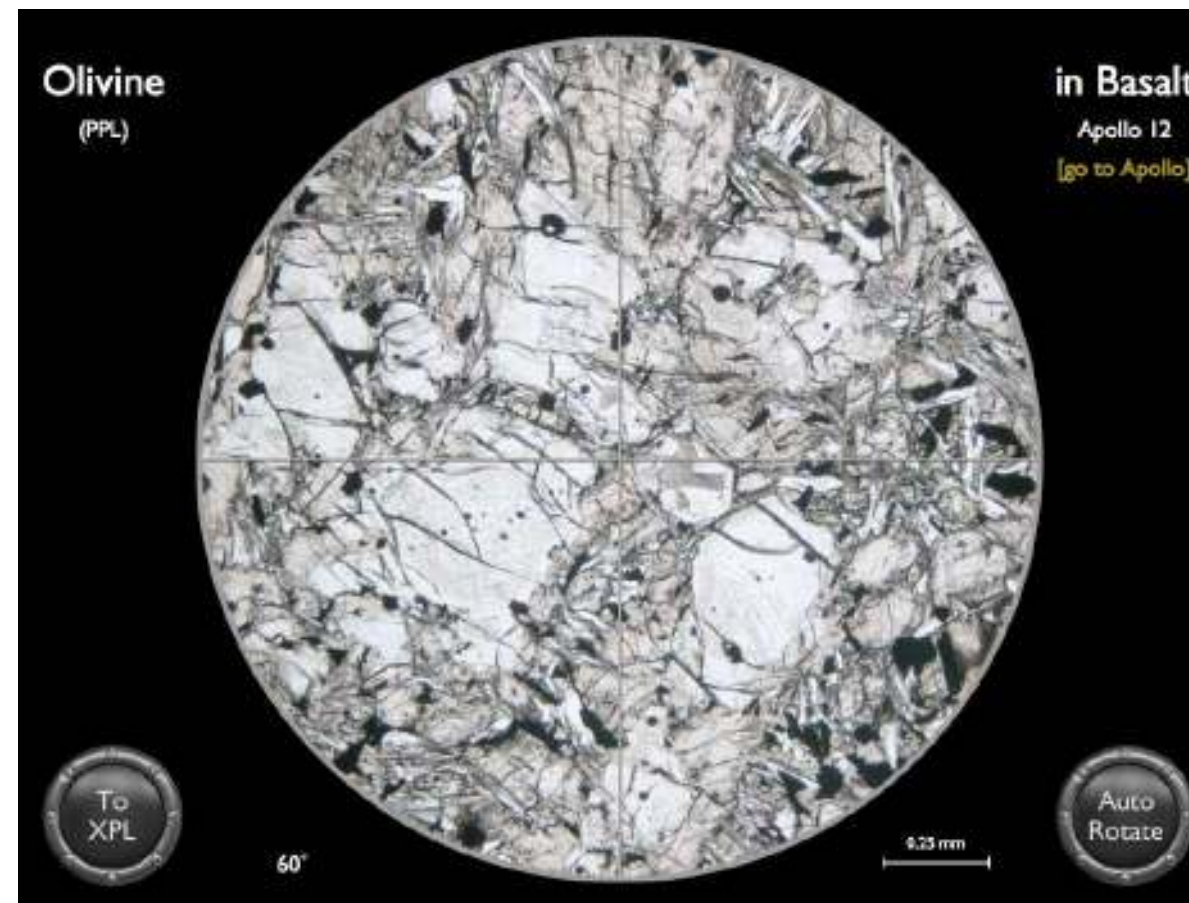
10092 is a fine-grained vesicular basalt, in which plagioclase feldspar, pyroxene and ilmenite are the three main constituents. Olivine occurs less commonly as anhedral crystals, some containing dark brown melt inclusions.

Apollo 11, Sample 10092.

Credit: NASA (AGT Photographer)

Moon Minerals: Olivine Group

Mineral Virtual Microscope: Olivine



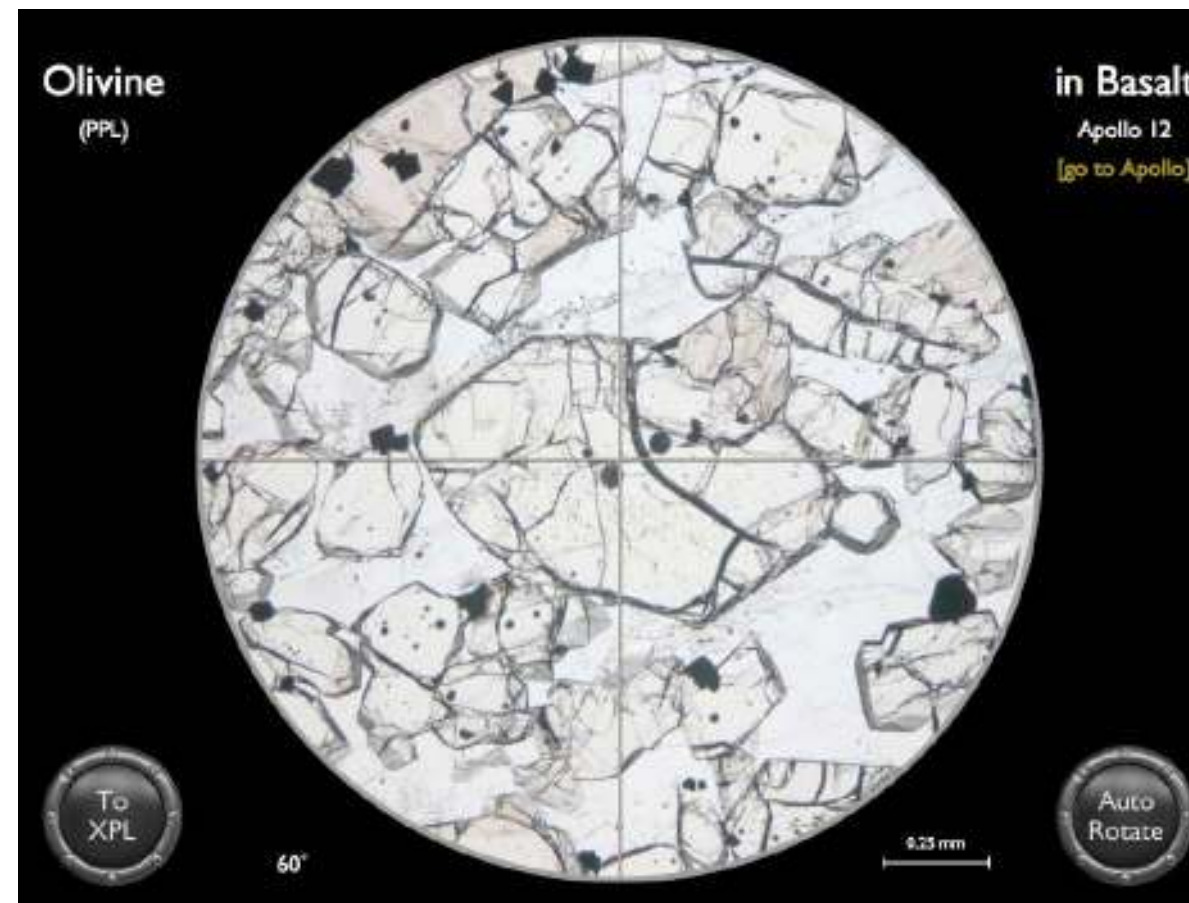
Sample 12004 is a porphyritic olivine basalt with small olivine and pyroxene phenocrysts set in a fine-grained variolitic groundmass.

Apollo 17, Sample 12004.

Credit: NASA (AGT Photographer)

Moon Minerals: Olivine Group

Mineral Virtual Microscope: Olivine



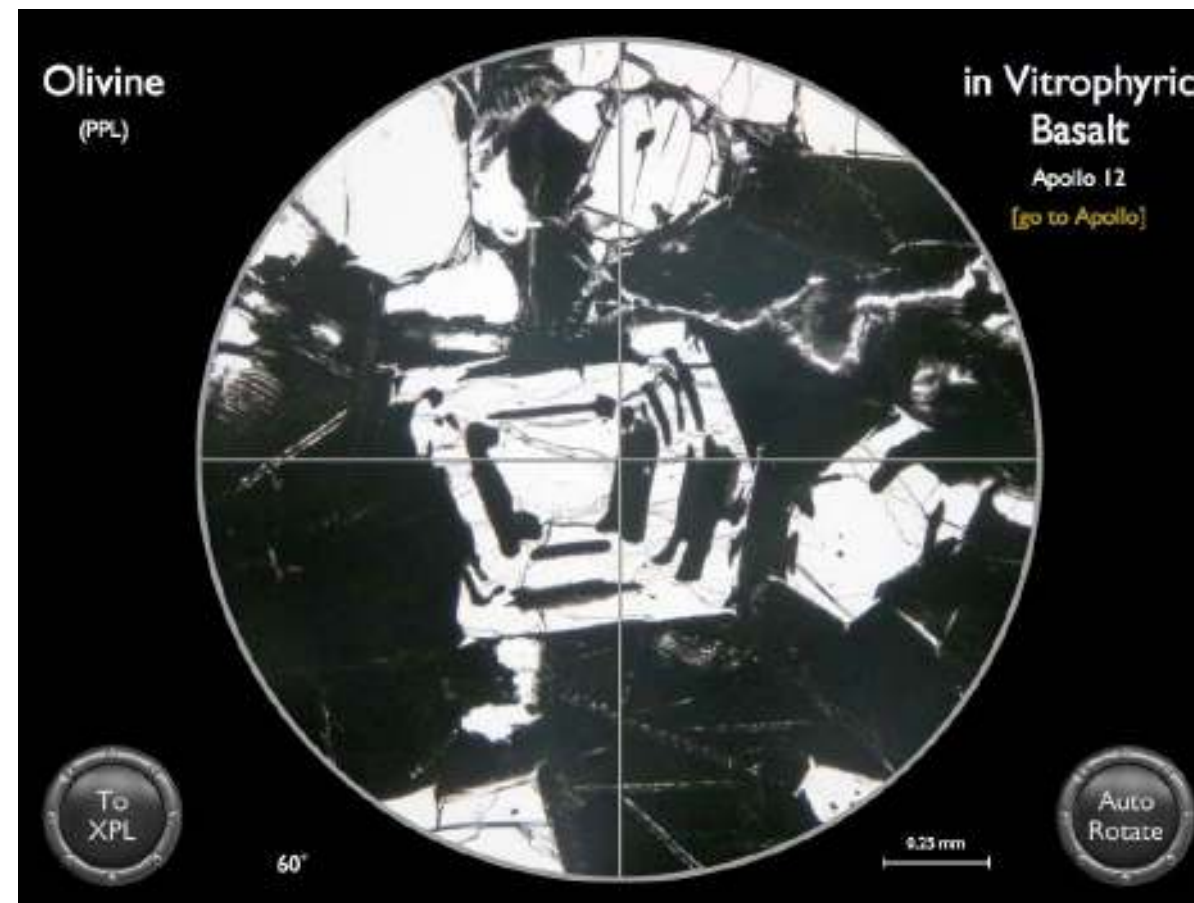
12005 is a mare basalt which contains the highest magnesium content of all lunar basalts and is similar to primitive picritic basalts on Earth. The thin section of this sample exhibits a cumulate texture, formed when dense crystals settled within a partially crystallized magma.

Apollo 17, Sample 12005.

Credit: NASA (AGT Photographer)

Moon Minerals: Olivine Group

Mineral Virtual Microscope: Olivine



12015 is an olivine vitrophyre with skeletal and dendritic olivine and pyroxene phenocrysts. Microphenocrysts of chromite are also an early phase. These phenocrysts are set in a nearly opaque fine-grained matrix of dendritic pyroxene, plagioclase, filamental ilmenite, chromite, cristobalite, troilite, metallic iron and glass.

Apollo 17, Sample 12015.

Credit: NASA (AGT Photographer)

Moon Minerals: Olivine Group

Mineral Virtual Microscope: Olivine



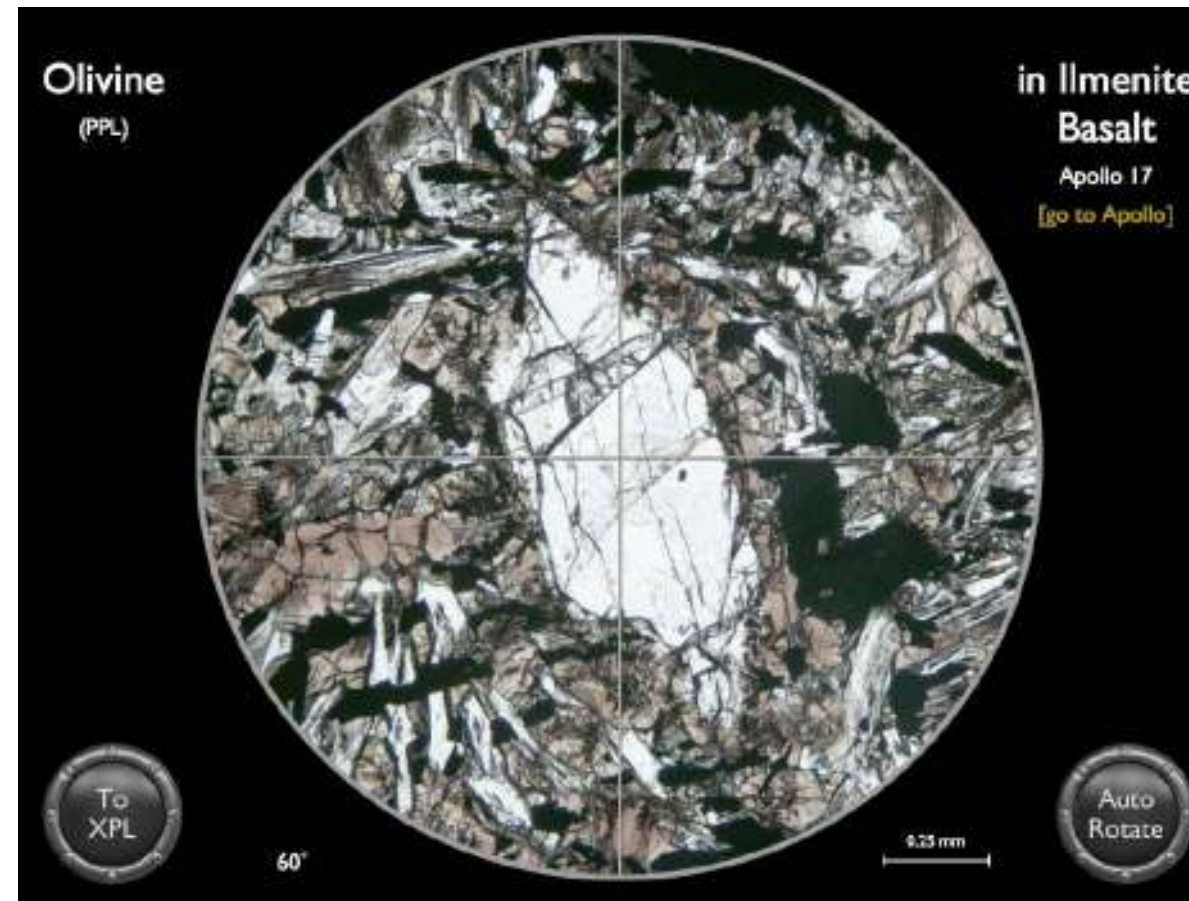
14235 is an olivine vitrophyre containing ~20% equant subhedral to euhedral phenocrysts of olivine (0.2-0.4 mm). The fine-grained opaque matrix is made of microlites of aluminous titanite, ilmenite and plagioclase feldspar. In this example the euhedral olivine contains a large melt inclusion.

Apollo 14, Sample 14235.

Credit: NASA (AGT Photographer)

Moon Minerals: Olivine Group

Mineral Virtual Microscope: Olivine



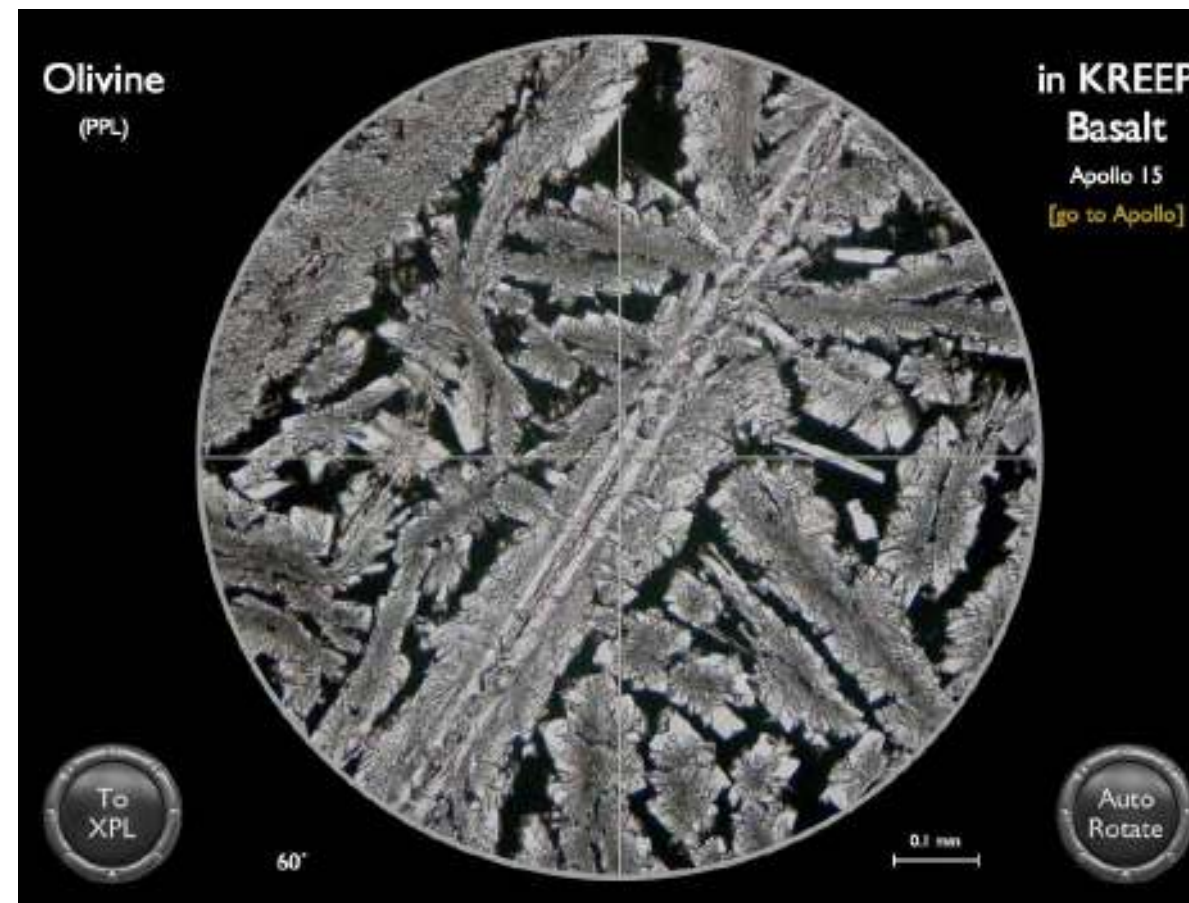
70275 is an olivine porphyritic ilmenite basalt with olivine and ilmenite phenocrysts set in a variolitic matrix of pyroxene and plagioclase feldspar. In this example the euhedral olivine is rimmed by pyroxene.

Apollo 17, Sample 70275.

Credit: NASA (AGT Photographer)

Moon Minerals: Olivine Group

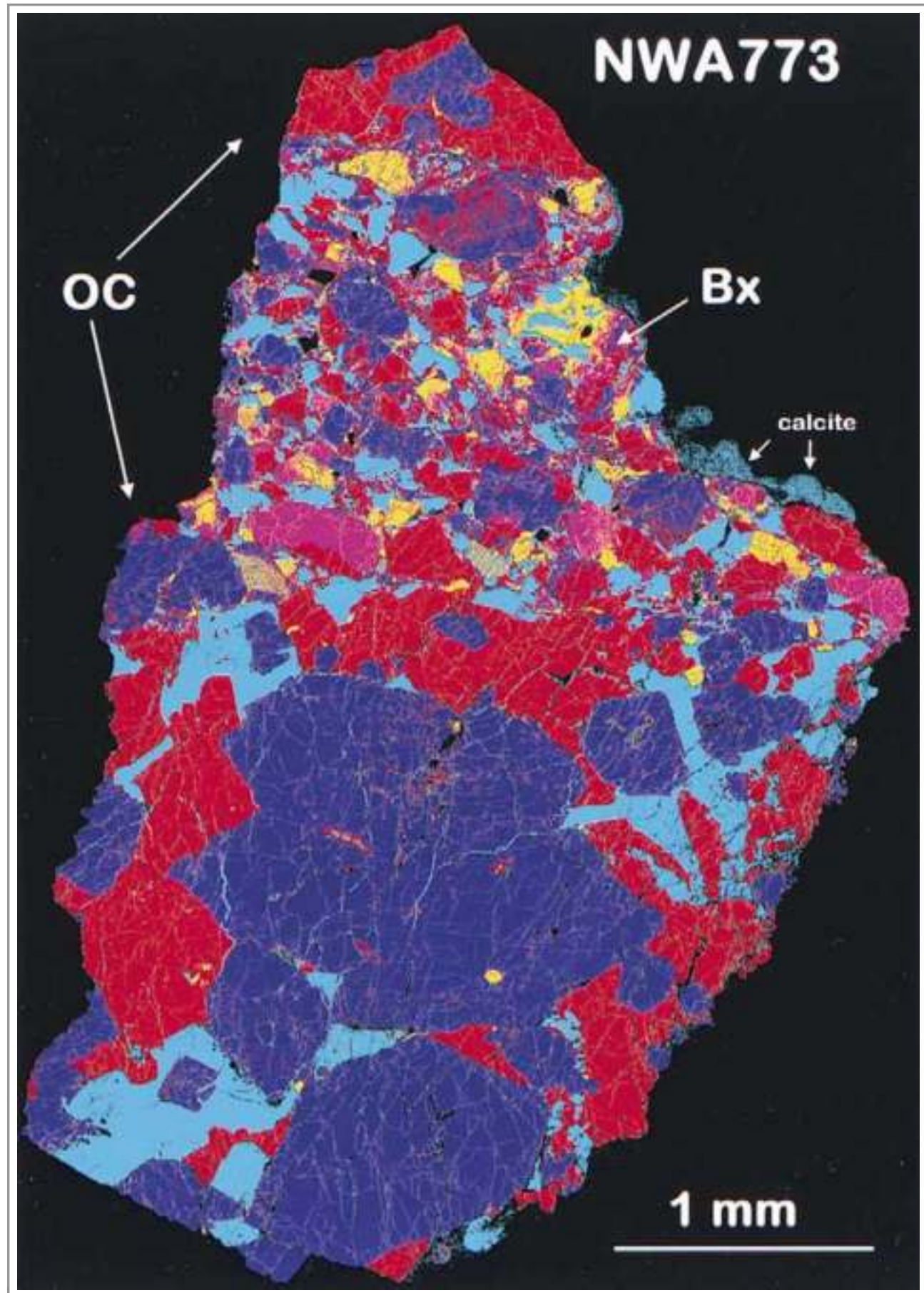
Mineral Virtual Microscope: Olivine



15434 is one of many sand-sized basaltic particles collected during the Apollo 15 mission. This olivine-rich grain exhibits a very distinctive spinifex texture consisting of elongate feathery crystallites. Similar textures are reported in komatiite lava flows on Earth where rapid crystallisation of extremely hot lava flows has occurred.

Apollo 15, Sample 15434.

Credit: NASA (AGT Photographer)

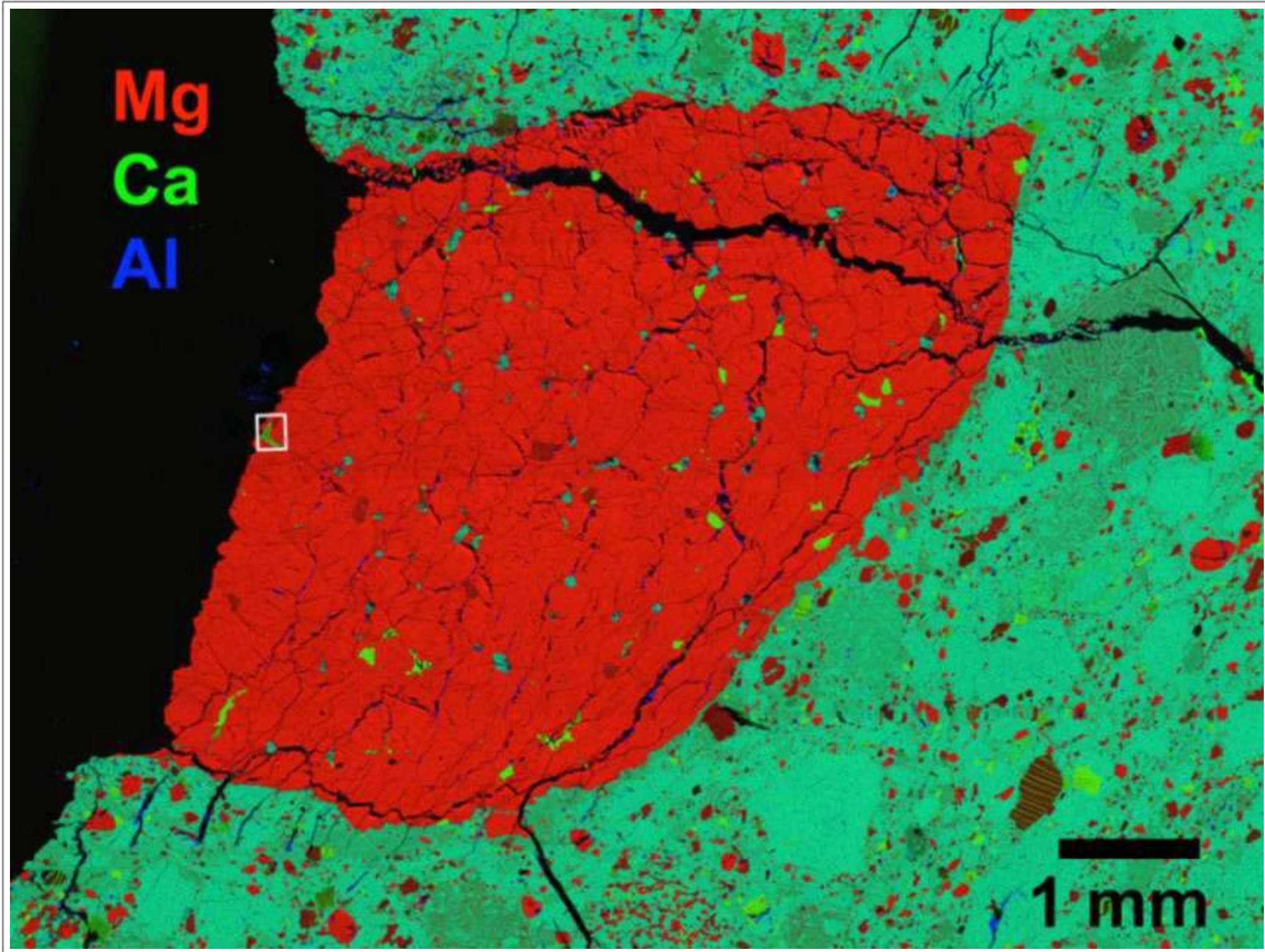


Northwest Africa (NWA) 773, a lunar mare breccia meteorite with a shallow-formed olivine-cumulate component.

False-coloured backscattered electron image showing coarse-grained cumulus texture, with pyroxene and plagioclase filling interstices between subhedral to euhedral olivine phenocrysts.

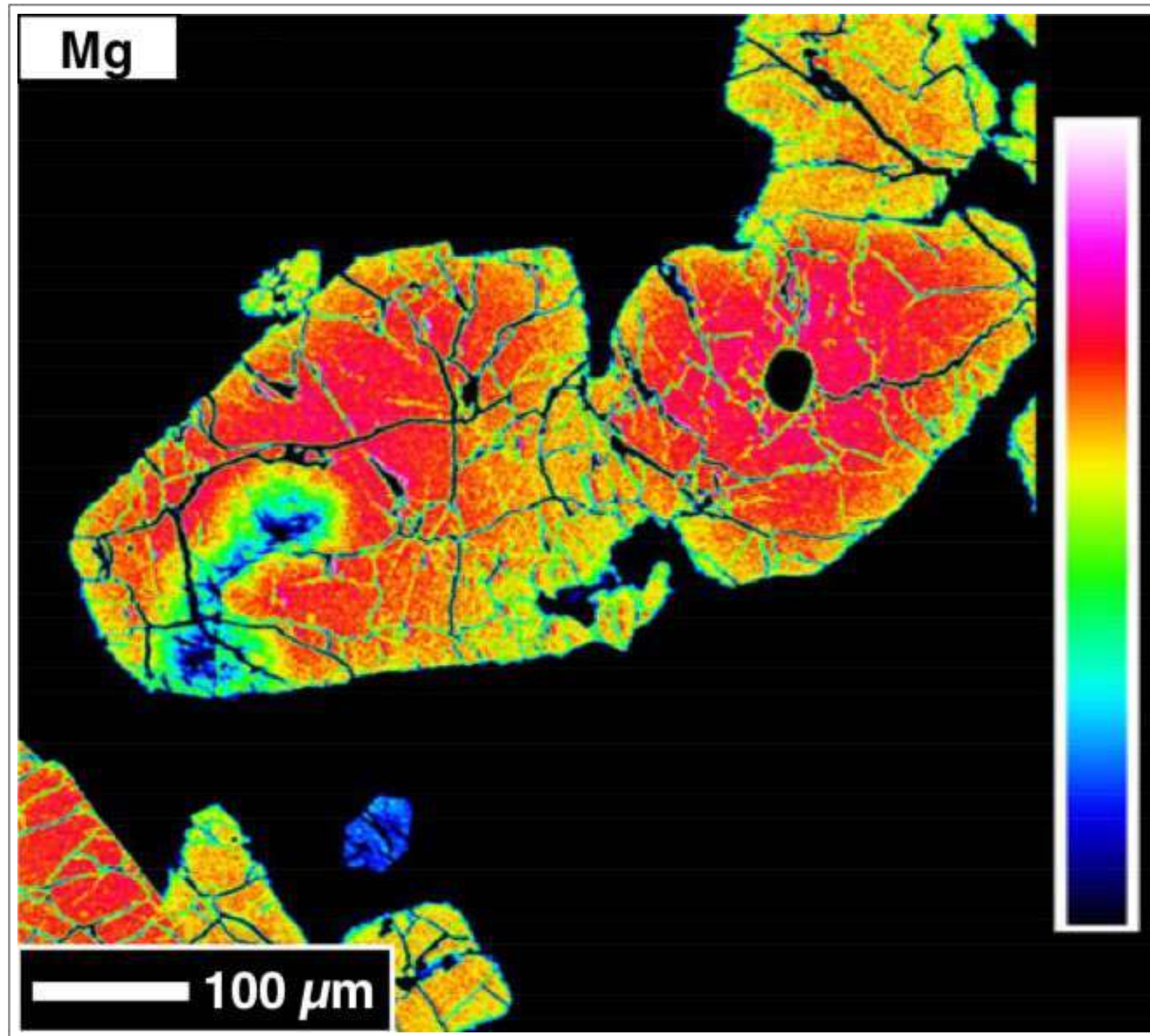
Within the olivine cumulate (OC), dark blue = olivine, red = pyroxene, cyan = plagioclase, and yellow = high atomic number phases (spinel, ilmenite, troilite, etc.).

At upper right, on the edge of Bx, delicate (terrestrial) calcite deposits, which survived the thin sectioning process, are present.

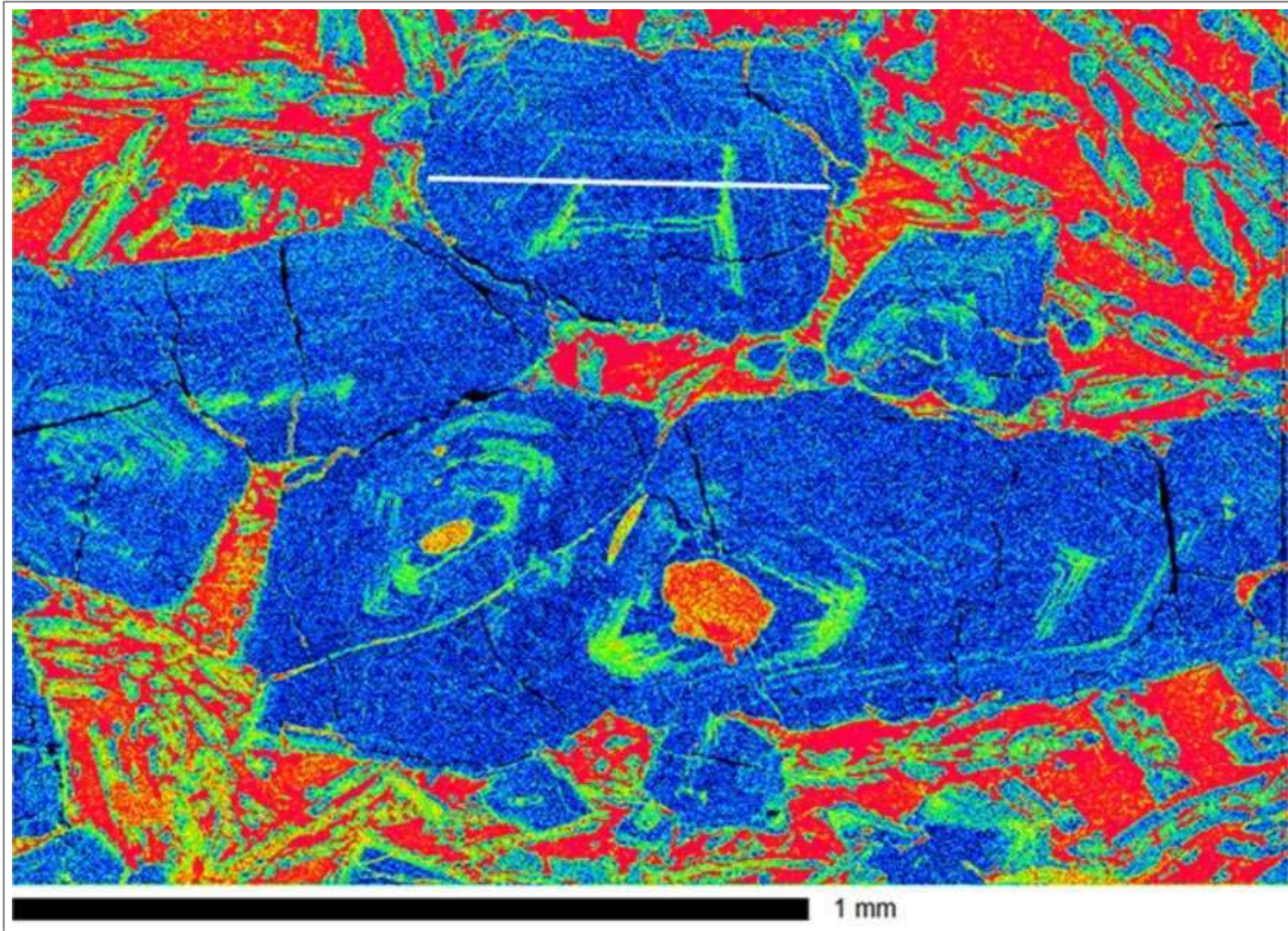


Taken From Treiman and Semprich (2019)

False colour composite X-ray map of the dunite clast in lunar meteorite NWA 11421 - an impact melt breccia. Olivine is bright red; low-Ca pyroxene is dull red; augite is bright green; plagioclase is bluish green, chromite is black. Epoxy to left (black); impact melt breccia (light green with multicoloured spots) surrounds the dunite.



Magnesium X-ray map of phenocrystic olivine in lunar meteorite NWA 032 (an unbrecciated mare basalt), illustrating normal zoning from Mg-rich cores to Fe-rich rims. The Mg anomaly in the lower left of the grain is the result of previous SIMS work. Warmer colours indicate increasing X-ray intensity.



Taken From Fagan et al. (2018)

Phosphorus zoning X-ray map of olivine phenocrysts in lunar meteorite NWA 8632 - a low-Ti, low-Al, low-K lunar basalt. Red indicates the highest P abundance (corresponds to the matrix), green is intermediate, and blue is the lowest (below detection limit of the electron microprobe technique).

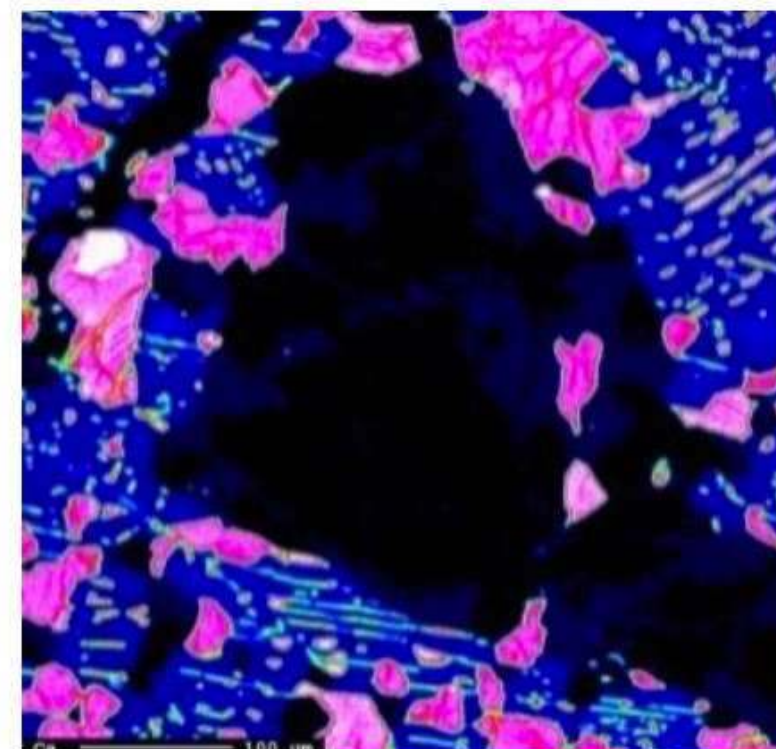
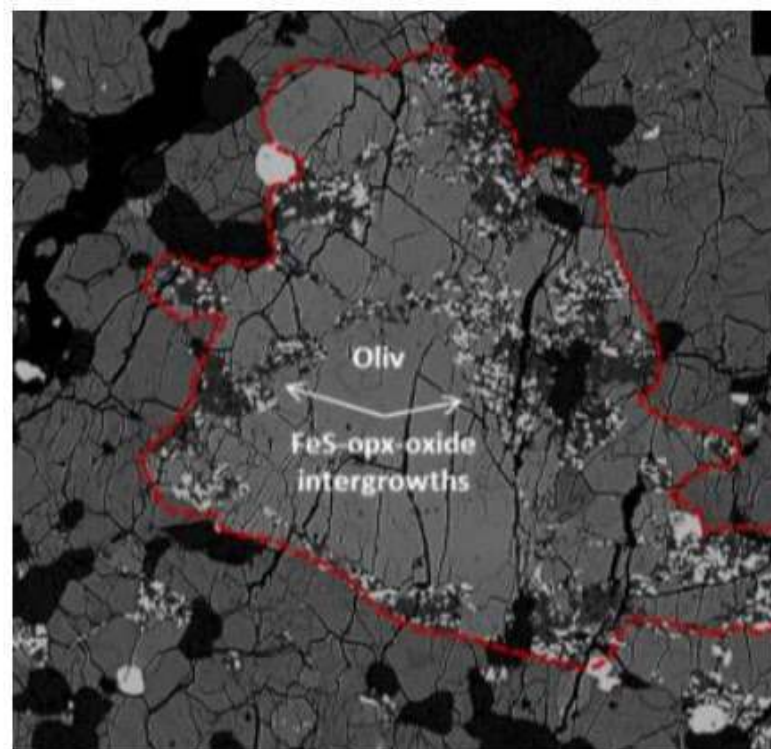
Olivine alteration in Apollo 16 feldspathic polymict breccia 67915.

Top left: a macro-scale backscattered electron image of an olivine phenocryst that that has been partially pseudomorphed by troilite-orthopyroxene-oxide intergrowths. The grain boundary of the olivine phenocryst is indicated with a red dashed line.

Top right: a Ca X-ray map of the same area. In this image, distribution of the orthopyroxene intergrowths within the host olivine phenocrysts can just be distinguished (dark blue). pink = augite; blue = pigeonite (with augite exsolution lamellae); white = apatite.

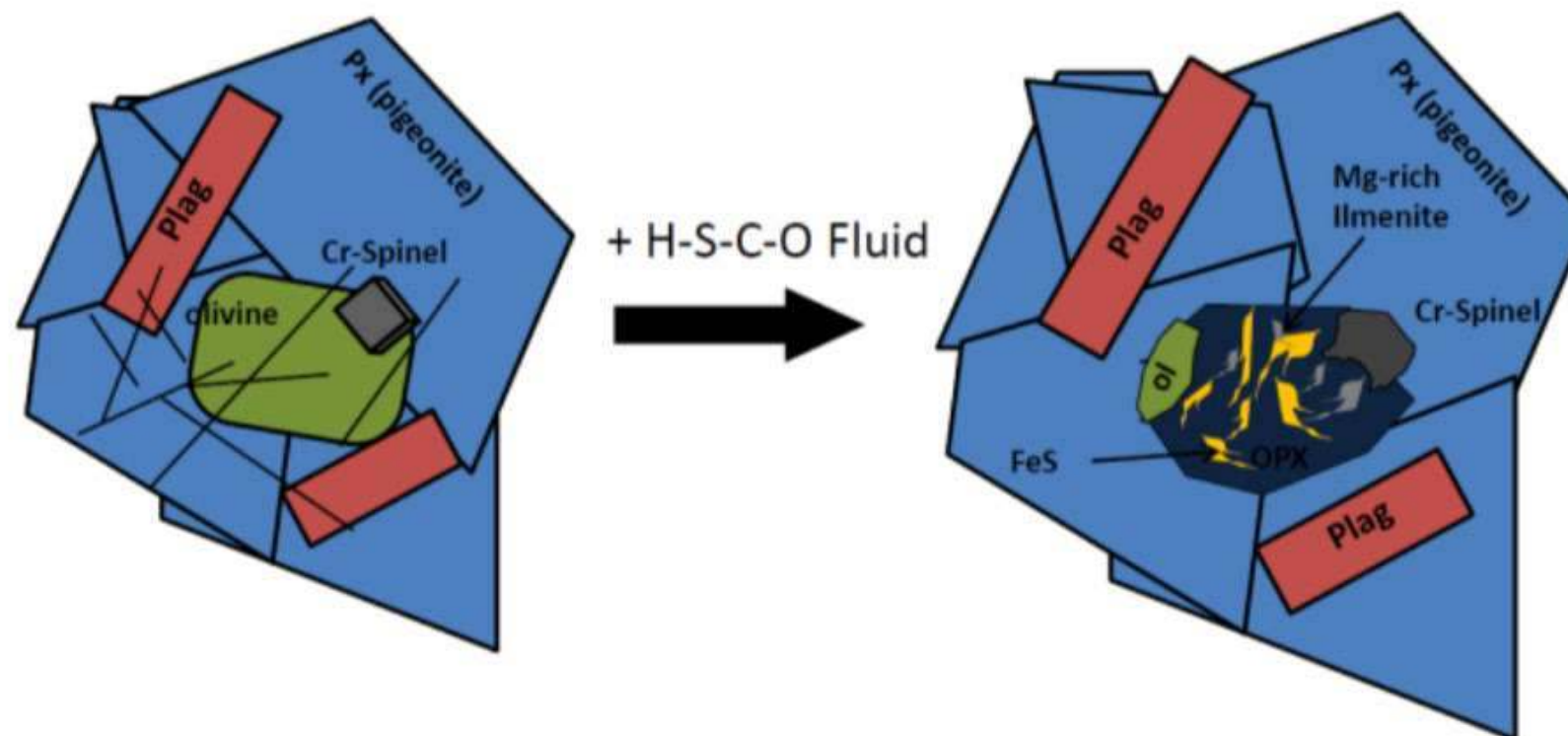
The field of view in each image is approximately 300 μm in width.

Bottom: A cartoon of the fluid mineral-reaction responsible for the development of the sulphide reactants and products in the metasomatic phase replacement textures.

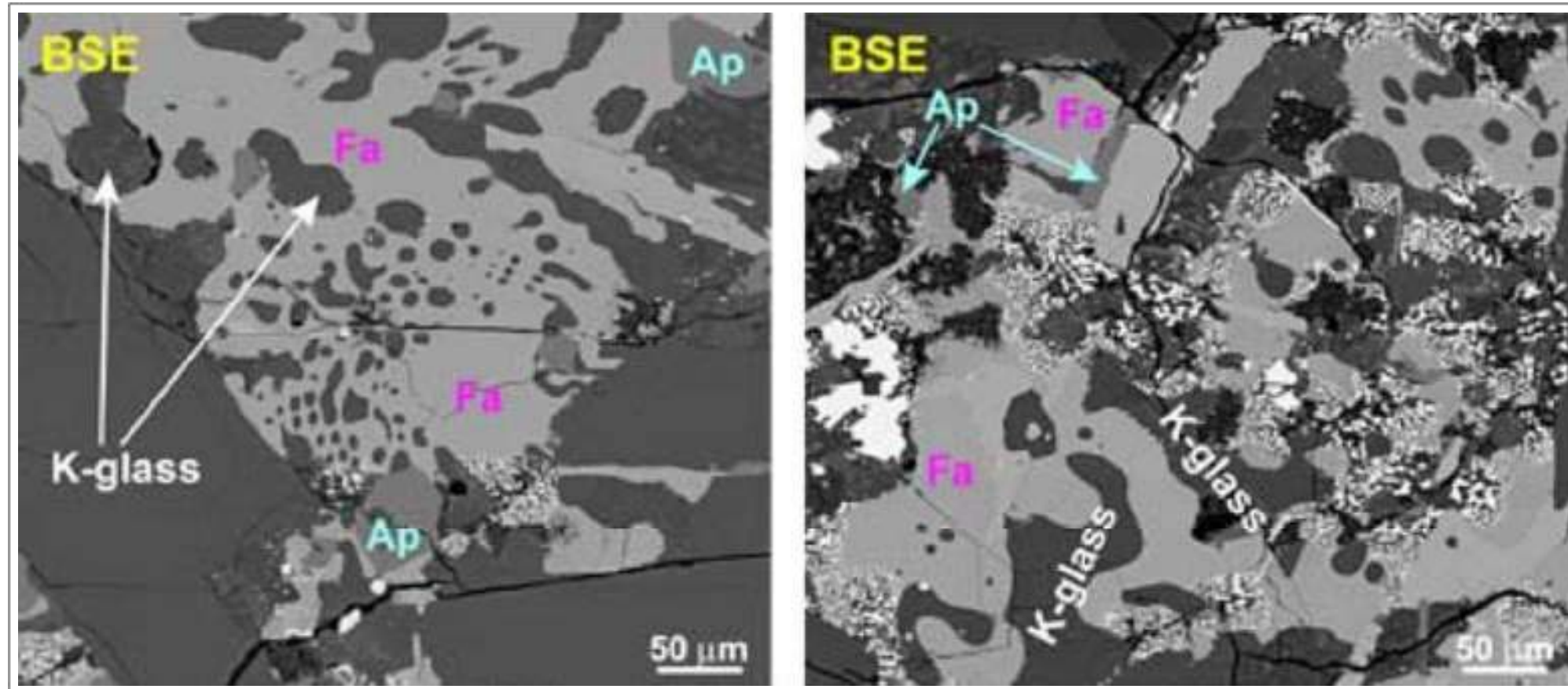


Pristine Magmatic Phase Assemblage

Alteration Assemblage

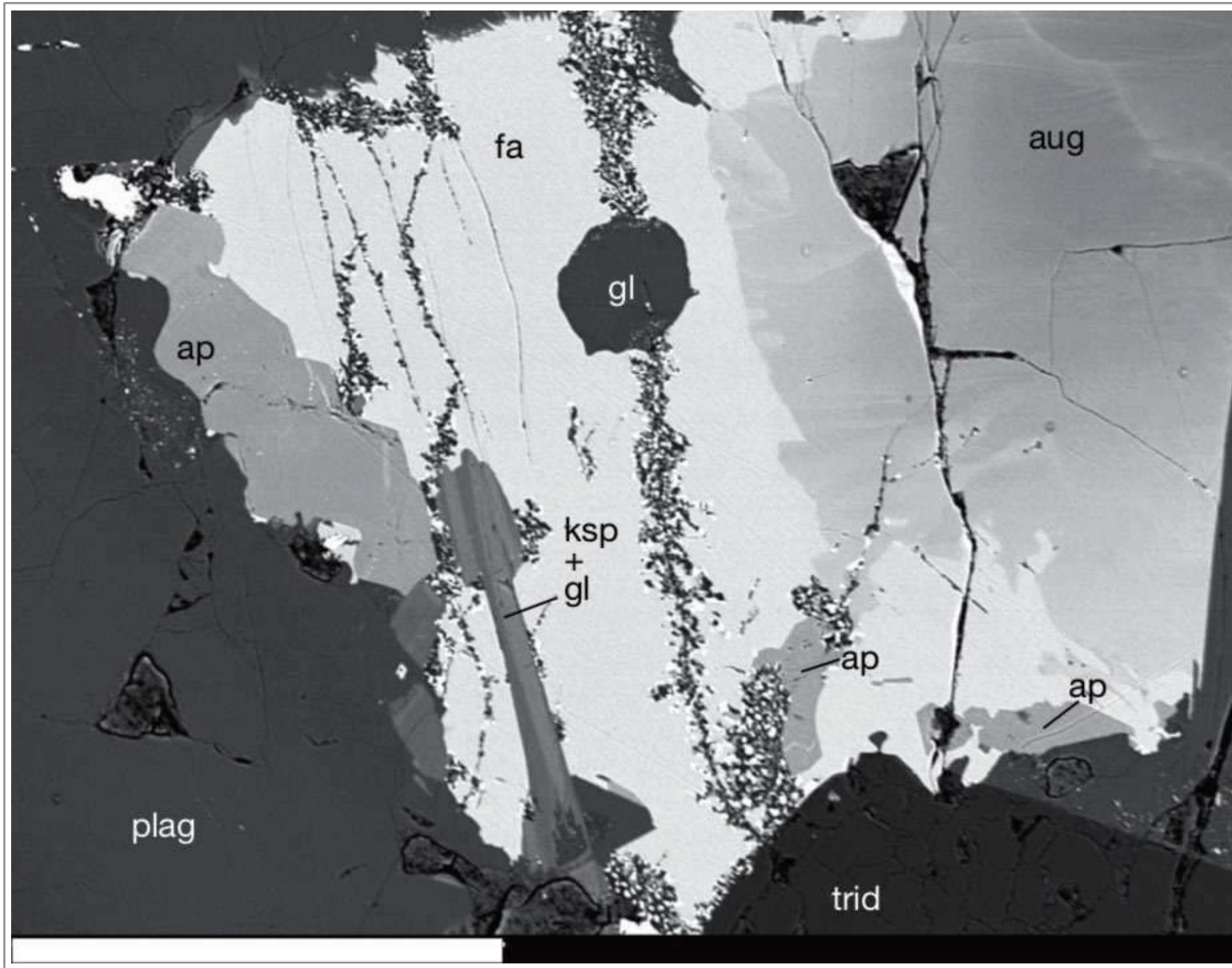


C-O-H-S volatile phase percolates through existing fracture network



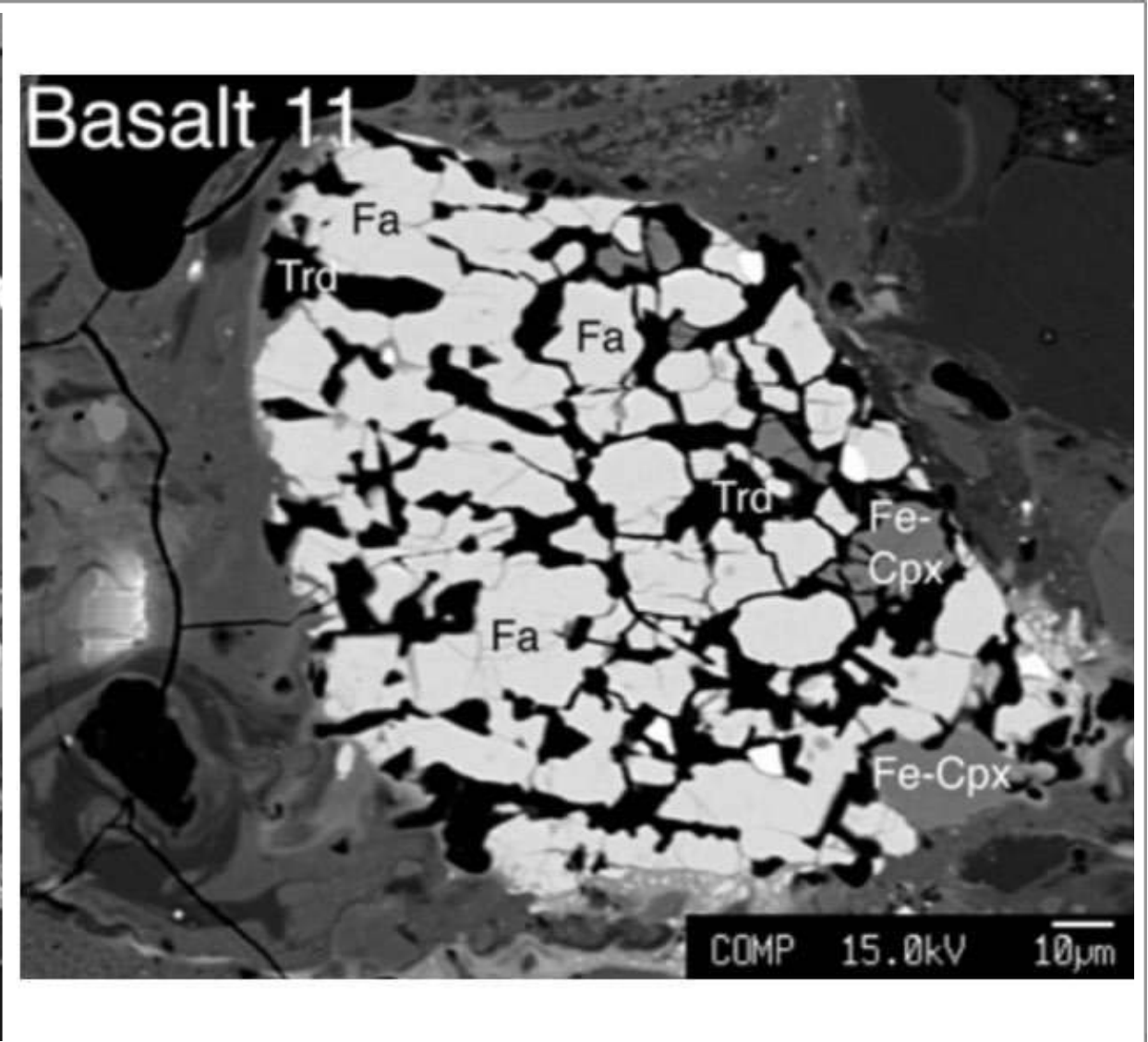
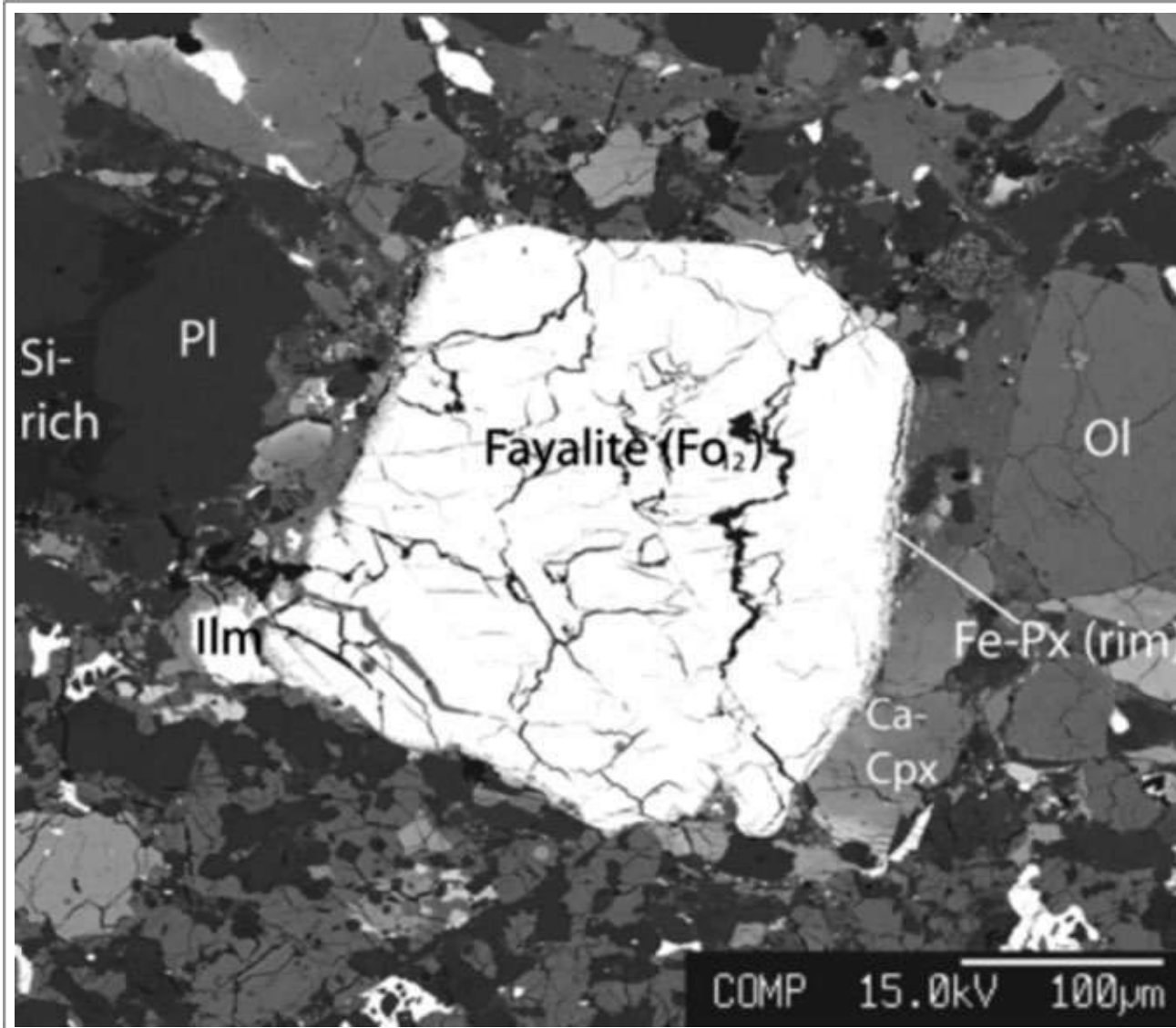
Taken From Patchen (2004)

Backscattered electron images from Apollo 14 high-Al mare basalt 14053, showing the late stage reduction of fayalite (Fa) to metallic iron and silica in the mesostasis. K-glass and apatite (Ap) are associated phases.



Taken From Boyce et al. (2010)

Backscattered electron image of Apollo 14 high-Al basalt 14053,241 showing partial reduction of fayalite along fractures to $\text{SiO}_2 + \text{Fe}$ metal by a subsolidus metamorphic reaction developed under highly reducing conditions. Scale bar is $200 \mu\text{m}$. Minerals are labelled as: ap (apatite), fa (fayalite), gl (glass), aug (augite), trid (tridymite), ksp (K-feldspar) and plag (plagioclase).



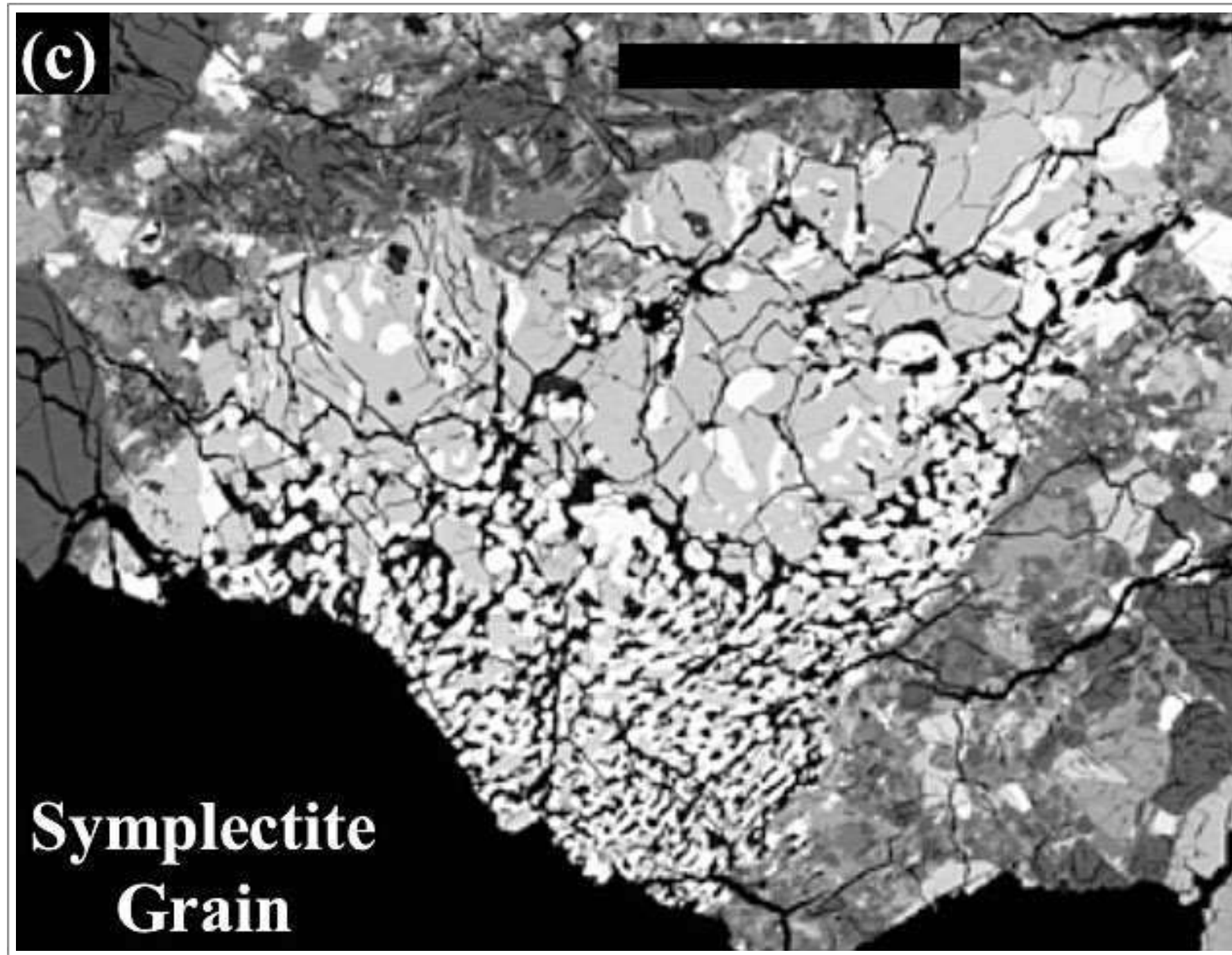
Taken From Al-Kathiri et al. (2007)

Backscattered electron images of fayalite in lunar meteorite Sayh al Uhaymir (SaU) 169 - a regolith breccia.

Left: anhedral (>200 μm) unzoned fayalitic olivine grain in the younger regolith breccia portion of SaU 169.

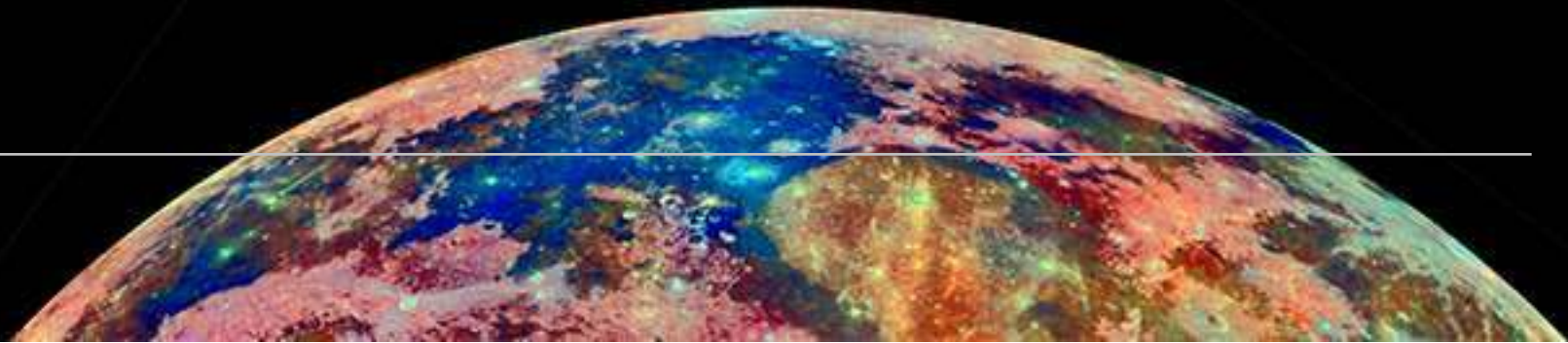
Right: intergrowth of fayalite and tridymite in the younger regolith breccia portion of SaU 169. This clast could represent a breakdown assemblage after pyroxferroite.

Fa = fayalite; Trd = tridymite; Ca-Cpx = Ca-rich clinopyroxene; Fe-Cpx = Fe-rich clinopyroxene; Pl = plagioclase; Ilm = ilmenite; Ol = olivine.



Backscattered electron image of symplectite grain in basaltic regolith breccia lunar meteorite MET 01210. Brightest phase is fayalite, middle brightness is pyroxene, and silica is the darkest phase. The symplectite represents a breakdown assemblage after pyroxferroite. Scale bar = 300 μm .

Pyroxene Group



SPECIES

1. Enstatite - $Mg_2Si_2O_6$
2. Pigeonite - $(Mg,Fe^{2+},Ca)(Mg,Fe^{2+})Si_2O_6$
3. Augite - $(Ca,Mg,Fe^{2+})Si_2O_6$
4. Diopside - $CaMgSi_2O_6$
5. Hedenbergite - $CaFe^{2+}Si_2O_6$

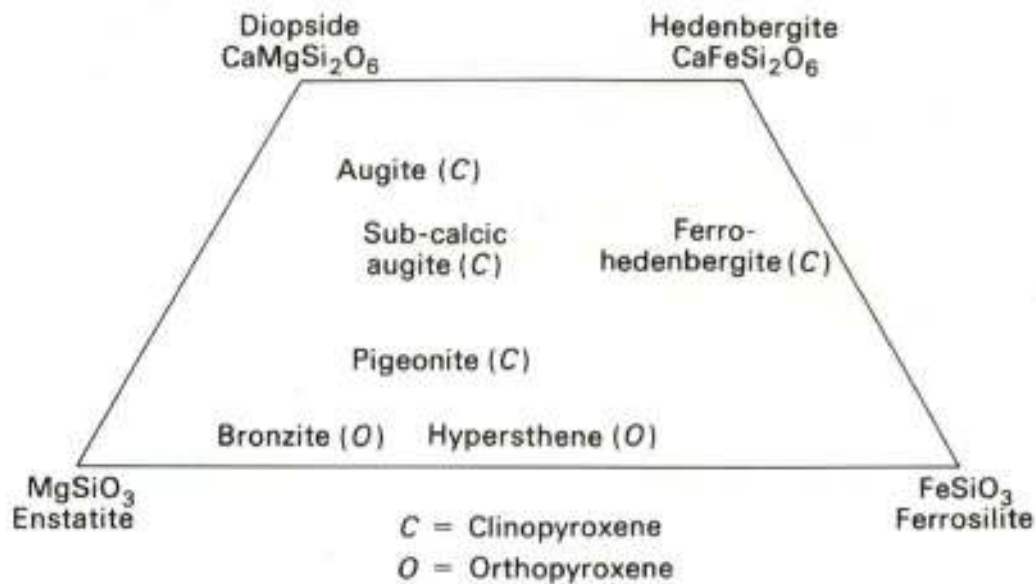
Pyroxene Compositions

Pyroxenes are the most chemically complex of the major silicates in lunar rocks. They are compositionally variable solid solutions, that are best summarised in a pyroxene quadrilateral. In many cases two or more species of pyroxene occur in the same rock (e.g. enstatite and augite in highland rock types).

Pyroxenes also hold a signature of the Moon as they have a distinctive Fe/Mn ratio unlike rocks from Earth and Mars. This ratio can also be used to discriminate lunar meteorites from chondritic meteorites as shown by Joy et al. (2006) and Morland et al. (2019).

Lunar pyroxenes also show substantial subsolidus reactions (i.e., recrystallization and other changes that take place below melting temperatures). These include submicroscopic, subsolidus separation (exsolution) of two distinct pyroxenes - augite (high-Ca clinopyroxene) and pigeonite (low-Ca clinopyroxene) from an originally uniform pyroxene. This process produced distinctive exsolution lamellae, i.e., thin layers of pigeonite in augite (or vice versa) that are related to the relative cooling histories of mare basalts. Shock lamellae can also be produced in pyroxenes - by shock waves caused by meteoroid impact (Heiken et al., 1991).

Exsolution lamellae in pyroxenes from an Apollo 17 gabbro clast in impact-melt breccia 76255 suggest that most samples of Mg-suite highland rocks formed



Pyroxene compositions (from Cadogan, 1981)

in relatively shallow level plutons. Coexisting pyroxenes indicate an initial temperature of formation for 76255 of $\sim 1100^{\circ}\text{C}$. The mineral and lithic fragments seen in thin sections of 76255 have been cataclased, but they form a monomict assemblage derived from a relatively coarse-grained gabbroic source rock. The most abundant mineral clasts are unshocked plagioclase with oscillatory zoning, clear crystals of augite with lamellae of pigeonite on (001) and (100), and clear crystals of orthopyroxene formed by the inversion of primary pigeonite. The orthopyroxene grains contain relict exsolution lamellae of augite and post inversion lamellae of augite (McCallum et al., 2006).

Diopside is one of the least common of the pyroxene species found in lunar rocks, but a ferroan variety is reported from Apollo 14 crystalline breccia 14171. It forms separate monomineralic fragments within breccia clasts and is described as “unusual” (non-mare?) (Walter et al., 1972). Diopside (and enstatite) are also present in an anorthositic norite clast in Apollo 15 impact-melt breccia 15455 (Ryder and Bower, 1977; Heiken, 1991).

As part of a study of mesostasis areas in mare basalts from Apollo 11, 12 and 15 (samples 10044, 12064 & 15058) Griffiths et al. (2014) reported extreme Fe-enrichment in Ca-rich and Ca-poor pyroxenes. The continuum of compositions fall between hedenbergite-ferrosilite end-members. Such mesostasis areas essentially represent pockets of residual melt, evolved from

basaltic melts that underwent fractional crystallization, resulting in melt compositions similar to lunar granites.

Pyroxene is the most abundant mineral in lunar meteorite MIL 05035 - a lunar mare basalt. It occurs mainly as primary grains, as well as secondary grains in symplectite. Individual primary grains possess edges that are generally intergrown with maskelynitized plagioclase and symplectite, and most are twinned. Compositions of primary pyroxenes (up to 5 mm long) show extensive variations in terms of Ca-Mg-Fe contents, from relatively Fe-poor cores that grade toward ferroaugite rims. Compared to nearly all other lunar basalts and basaltic meteorites, MIL 05035 pyroxene cores are more Fe-rich, and rims lack enrichment toward pyroxferroite, with only a single grain discovered to have this composition. The compositions of the ferroaugite rims of MIL 05035 pyroxenes are located in the “forbidden zone” of pyroxenes and are, therefore, metastable (Liu et al., 2009).

Burger et al. (2009) note that in lunar meteorite NWA 032 (an unbrecciated mare basalt) the pyroxene is oscillatory zoned and varies between zones of enriched Fe+Mg (pigeonite), and those enriched in Ca (augite).

A prominent gabbro lithology within lunar meteorite NWA 10985 (a fragmental breccia) has been studied by Chen et al. (2019). They report a very diverse range of pyroxenes which includes large-scale core to rim normal magmatic zoning from pigeonite and augite to pyroxferroite compositions. Oscillatory zoning in a

few pyroxene crystals indicate complex formation suggesting there was convection or replenishment occurring in the primitive magma.

A wide spectrum of pyroxene compositions are reported by Joy et al. (2014) from clasts in three brecciated lunar meteorites - Dhofar 925 (a glassy impact melt breccia), Dhofar 961 and Sayh al Uhaymir 449 (both lithic polymict breccias). Basaltic clasts are dominated by zoned pigeonite comparable to pyroxene in Apollo 17 very low-Ti (VLT) mare basalts. Granulitic clasts contain unzoned low-Ca and high-Ca pyroxene grains that interstitially infill the spaces between plagioclase grains; and impact melt clasts contain zoned pigeonitic pyroxene enclosing plagioclase crystals. Also present in impact melt clasts are a few low-Ca pyroxene and high-Ca pyroxene grains with REE concentrations and element ratios more akin to lunar highland lithologies than mare basalts.

Yamato 983885 is a lunar polymict breccia meteorite containing clasts of KREEP basalt, high-Al basalt, low-Ti basalt, Mg-rich rocks and Si, Na-rich impact spherules. The KREEP basalt is mineralogically distinct from Apollo KREEP basalts due to the lack of typical Ca zoning from orthopyroxene to pigeonite - instead, it hosts co-existing pigeonite/augite with chemical zonings and micron-scale exsolution (Arai et al., 2005).

Cohen et al. (2019) studied lunar meteorite NWA 12008 (a mare basalt) and recorded a wide range of pyroxene compositions

which show extensive compositional zoning from pigeonite, to subcalcic augite, to augite, to ferropigeonite at the rim. They also reported crystallized melt inclusions within olivine containing skeletal pyroxene (Al-Ti-bearing augite) and Cr-Ti-Fe spinel.

Enstatite

Aluminous enstatite has been found in lunar meteorites of highland origin where it occurs in impact breccias of troctolitic composition. Aluminous enstatite is distinctly different from common orthopyroxene of lunar rocks and is associated with spinel (pleonaste), olivine, anorthitic plagioclase feldspar and the accessory minerals: rutile, Ti-Zr oxides, troilite, and metallic iron. The same assemblage was described in rare fragments of spinel cataclasites from the samples of the Apollo missions. Rocks hosting aluminous enstatite are of deep origin and occur at depths from 25 km to 130-200 km at a temperature of 800 to 1300°C, i.e., at least in the lower crust and, possibly, in the upper mantle of the Moon. These rocks could form individual plutons or dominate the composition of the lower crust. The most probable source of aluminous enstatite is troctolitic magnesian rocks and, especially, spinel troctolite. The transport of deep-seated materials to the lunar surface was probably related to impact events during the intense meteorite bombardments >3.9 Ga ago. (Nazarov et al., 2011).

Pigeonite

Twelve samples of pigeonite basalt were collected during the Apollo 12 mission. They are porphyritic and have a variable groundmass ranging from a fine-grained variolitic to coarse-grained microgabbroic with ophitic to graphic textures. Studying samples 12007, 12011, and 12043, Baldrige et al. (1979) were able to show all the chemical data could be explained by fractionation of olivine, pigeonite and Cr-spinel within the upper portions of a single, initially homogeneous magma chamber.

Inverted pigeonite has been found in the deep-seated Mg-suite norite returned by the Apollo missions, such as in Apollo 17 breccia 76255 (Takeda and Miyamoto, 1977). Inverted pigeonite was also found in clasts in Apollo 14 polymict breccia 14083 (Papike and Bence, 1972).

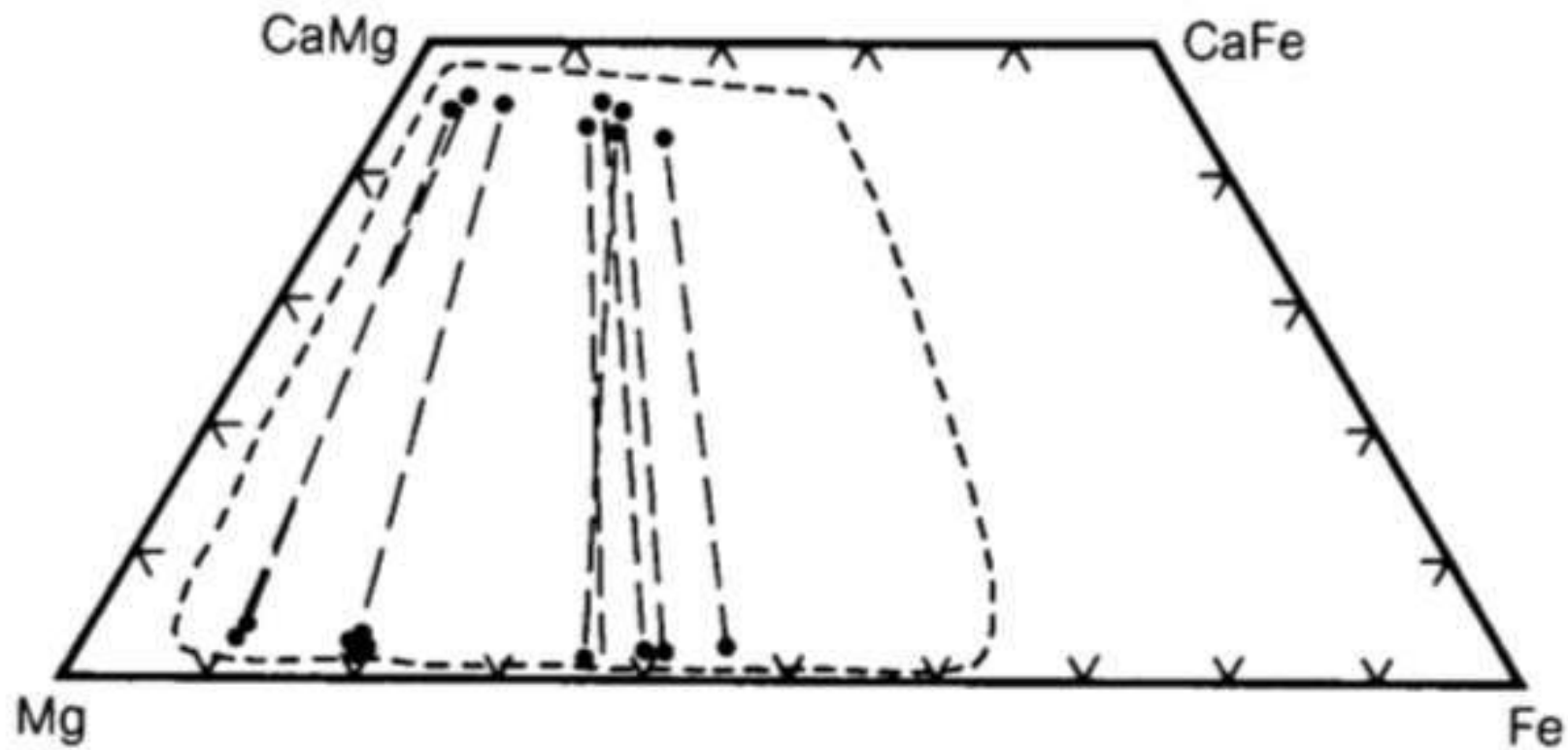
Some of the orthopyroxene in lunar meteorite NWA 2977 (a cumulate olivine gabbro) has abundant augite lamellae with compositions indicating formation by inversion of pigeonite. The pigeonite was inverted at 1140°C and required a relatively slow cooling rate (Nagaoka et al., 2015).

Hedenbergite

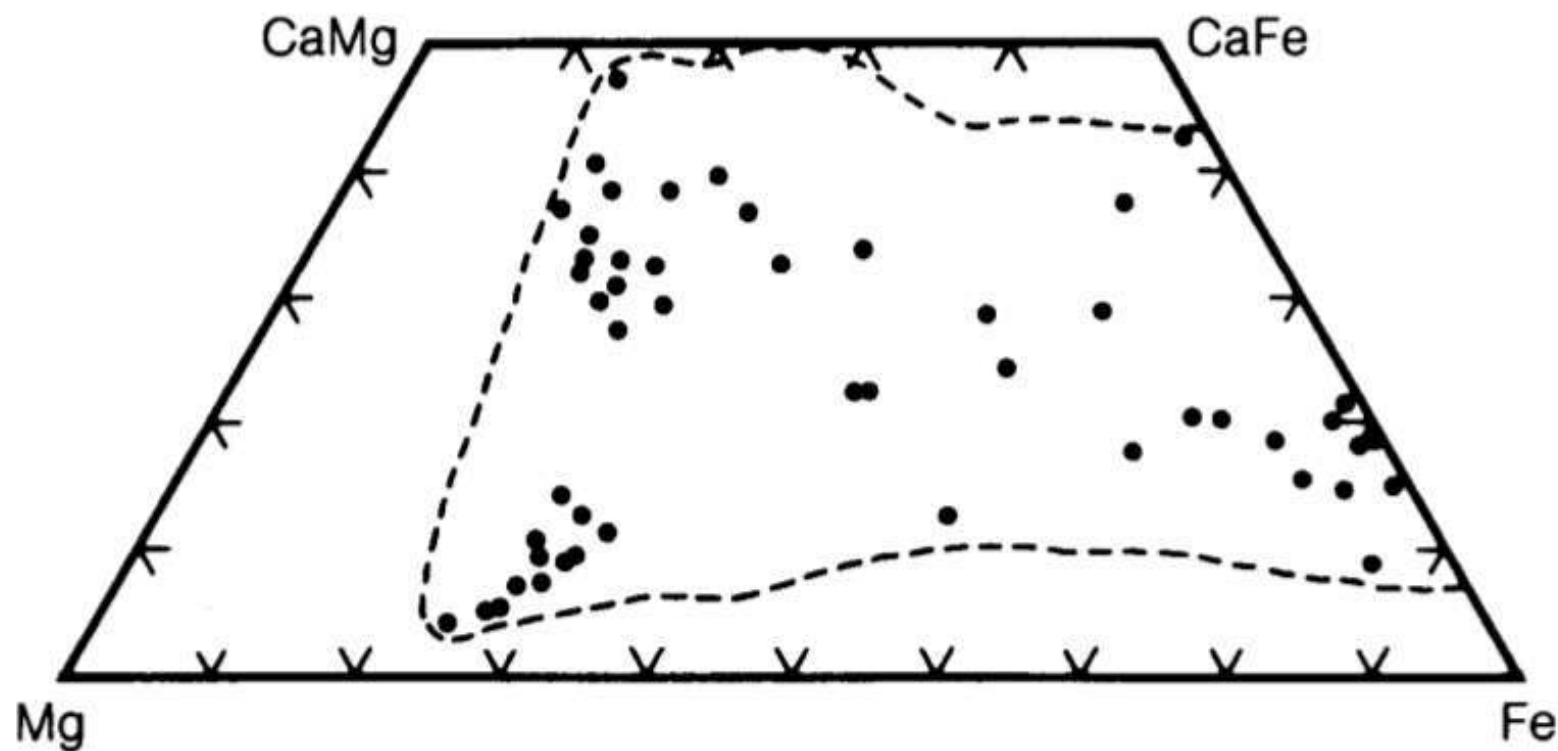
Seddio et al. (2012a) examined two granitic lithic fragments from the Apollo 12 regolith. In sample 12023,147-10 they found minor

hedenbergite (modally 2.3%) in a fragment consisting mainly of ~80% granophyric intergrowths of silica with of K-feldspar and with plagioclase. In sample 12001,909-14 they also found a zoned high-Ca pyroxene (0.3 mm across) that has a hedenbergite core and an augite rim. Puzzlingly this is the opposite trend to the zoned pyroxene crystals found in basaltic lunar meteorite MIL 05035 reported by Joy et al. (2008) and Liu et al. (2009).

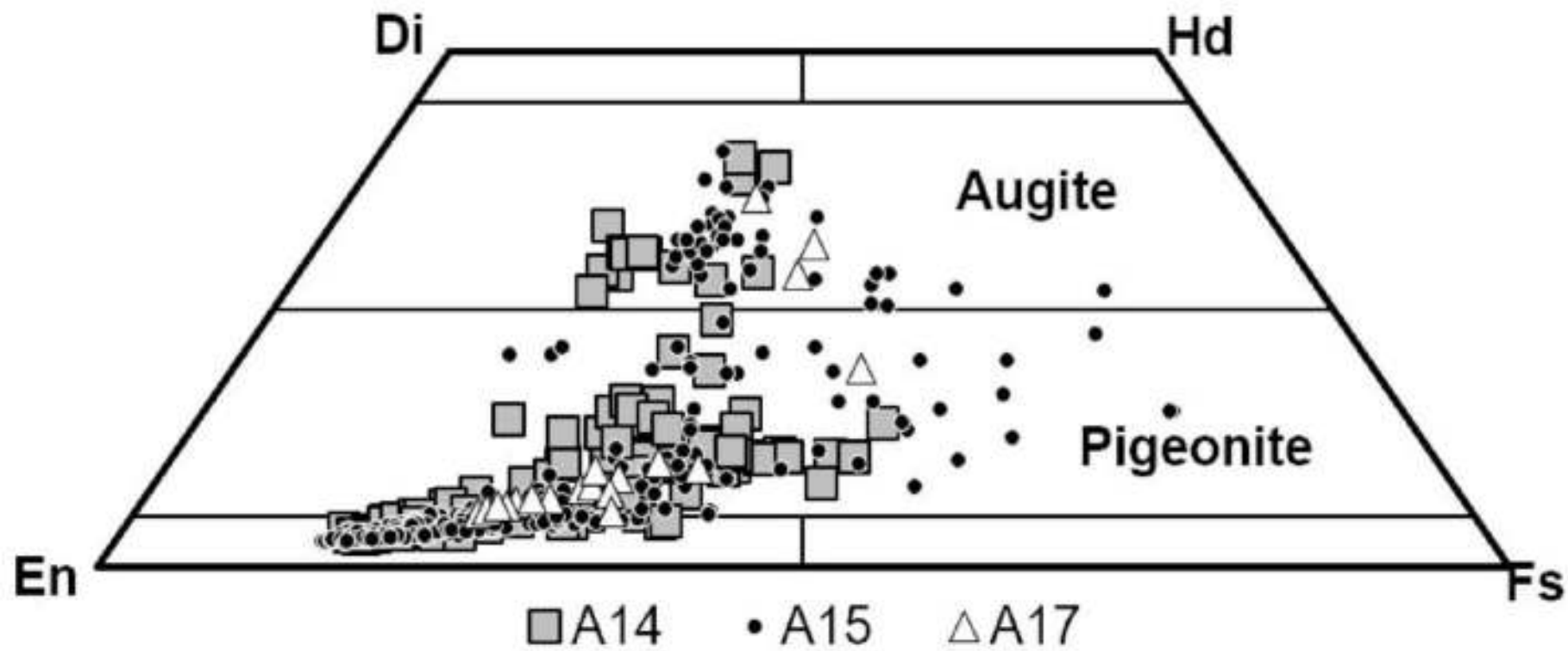
Seddio et al. (2013b) also report hedenbergite - in a granite fragment found in Apollo 12 soil sample 12032,366-19. The sample is mainly a micrographic intergrowth of K-feldspar and quartz and, to a lesser extent, plagioclase and quartz. Fayalite, ilmenite, apatite, merrillite, baddeleyite and zirconolite are also present.



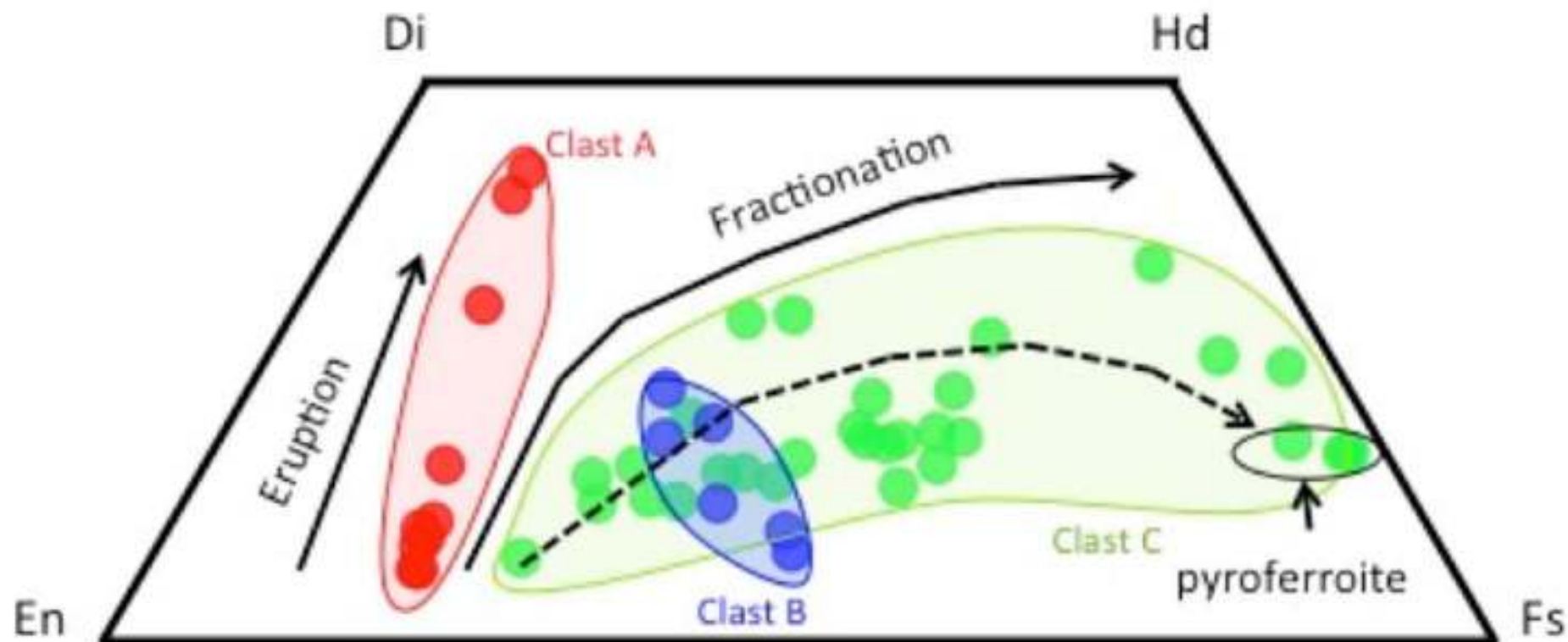
Pyroxene compositions from highland coarse-crystalline igneous rocks (ferroan anorthosites and Mg-rich rocks), in the pyroxene quadrilateral. Dots represent analyses in Heiken et al. (1991). Dashed line encloses the total range of pyroxene compositions reported in the literature for these highland rock types. Straight dashed lines connect compositions of high-Ca and low-Ca pyroxenes that coexist in the same rock.



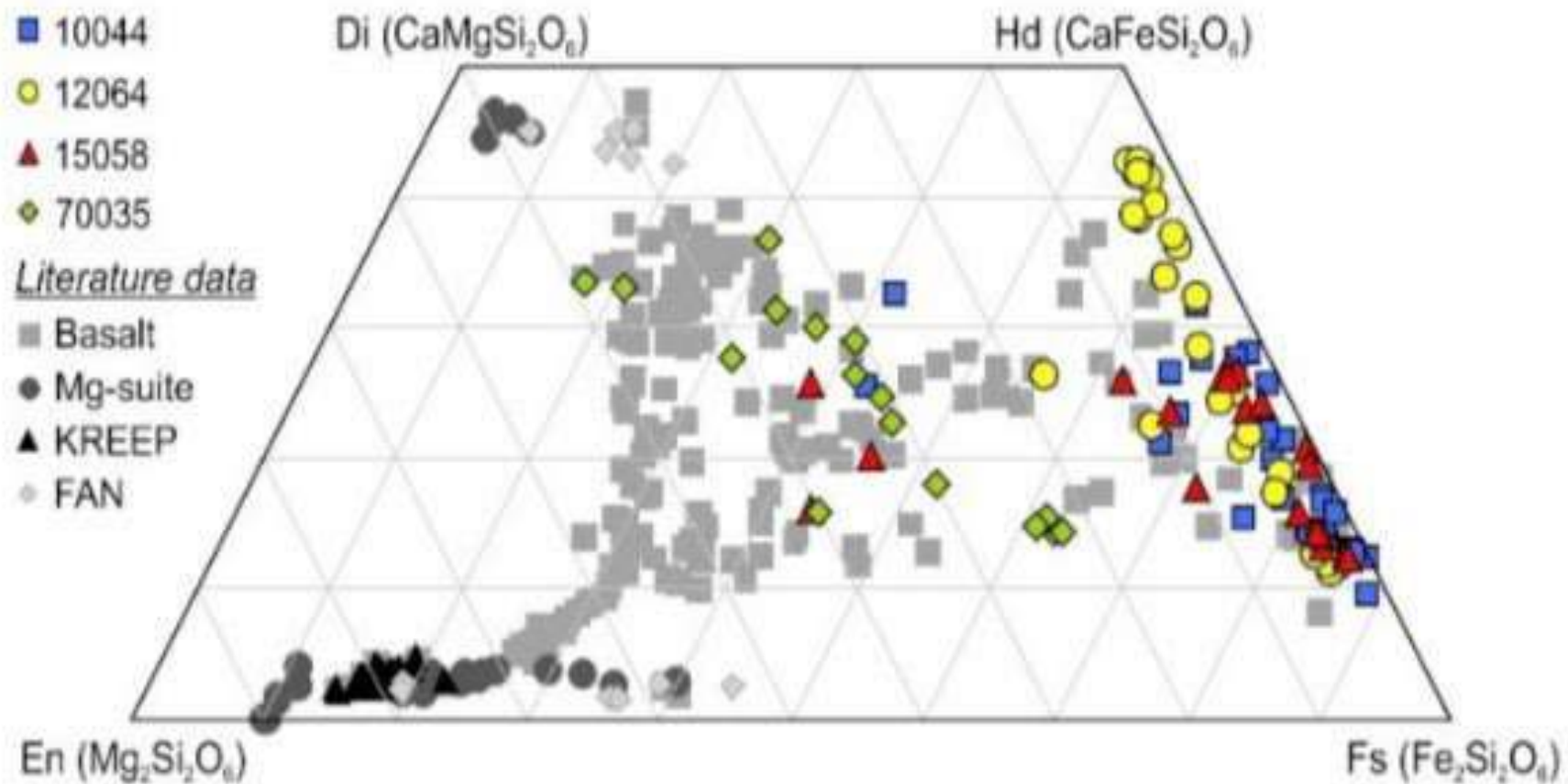
Pyroxene compositions from mare basalts, shown in the pyroxene quadrilateral. Dots represent analyses in Heiken et al. (1991). Dashed line encloses the total range of mare basalt pyroxene compositions.



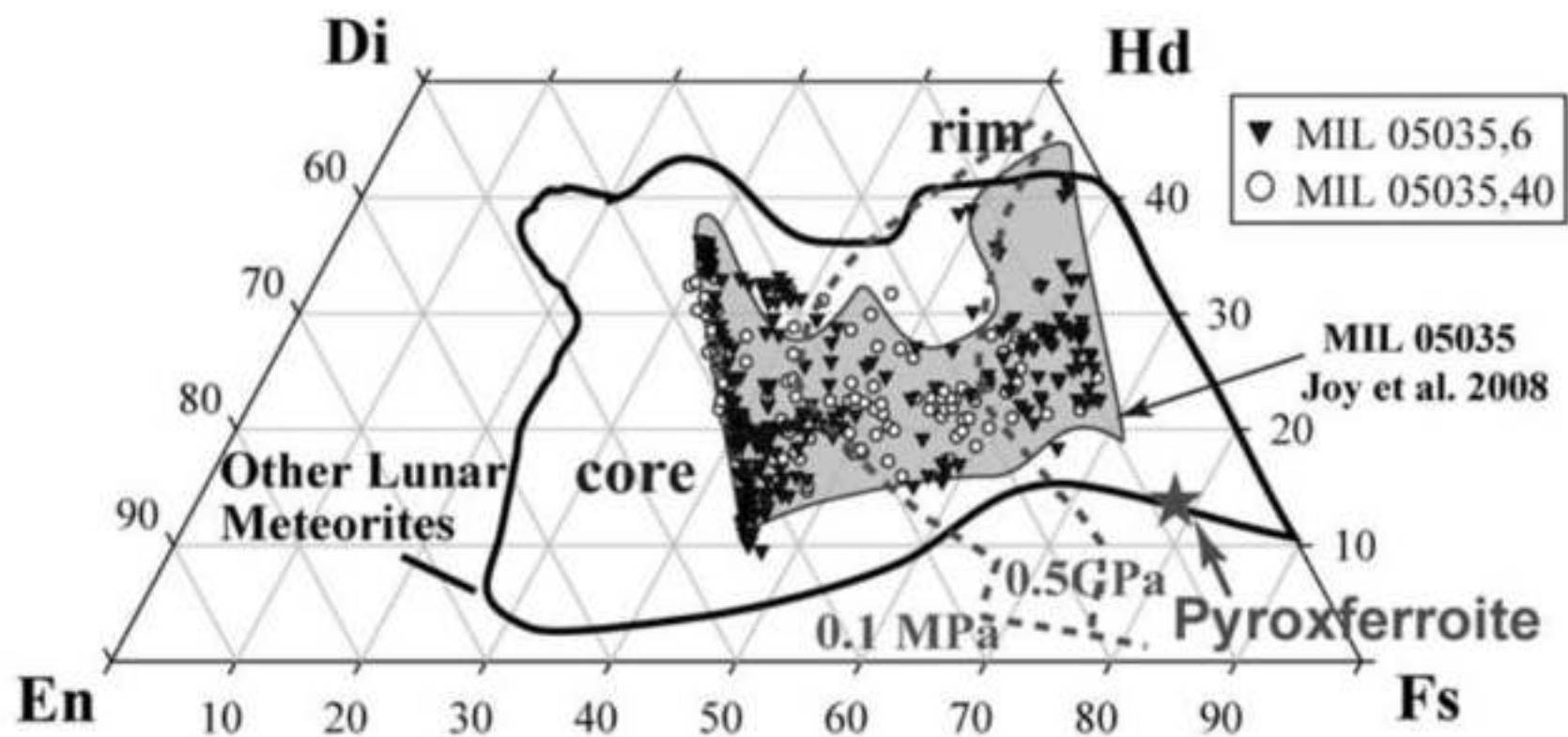
Pyroxene compositions from Apollo 14, 15 and 17 KREEP basalts. They are derived from the last dregs of liquid from the lunar magma ocean. KREEP basalts are distinct from mare basalts by having a lower Ca/Al ratio reflected in a paucity of high-Ca pyroxene and are the result of endogenous melting of the lunar interior. Pyroxenes from the Apollo 15 KREEP basalts trend from enstatite, to Mg-rich pigeonite to augite and Fe-rich pigeonite (Cronberger and Neal, 2018).



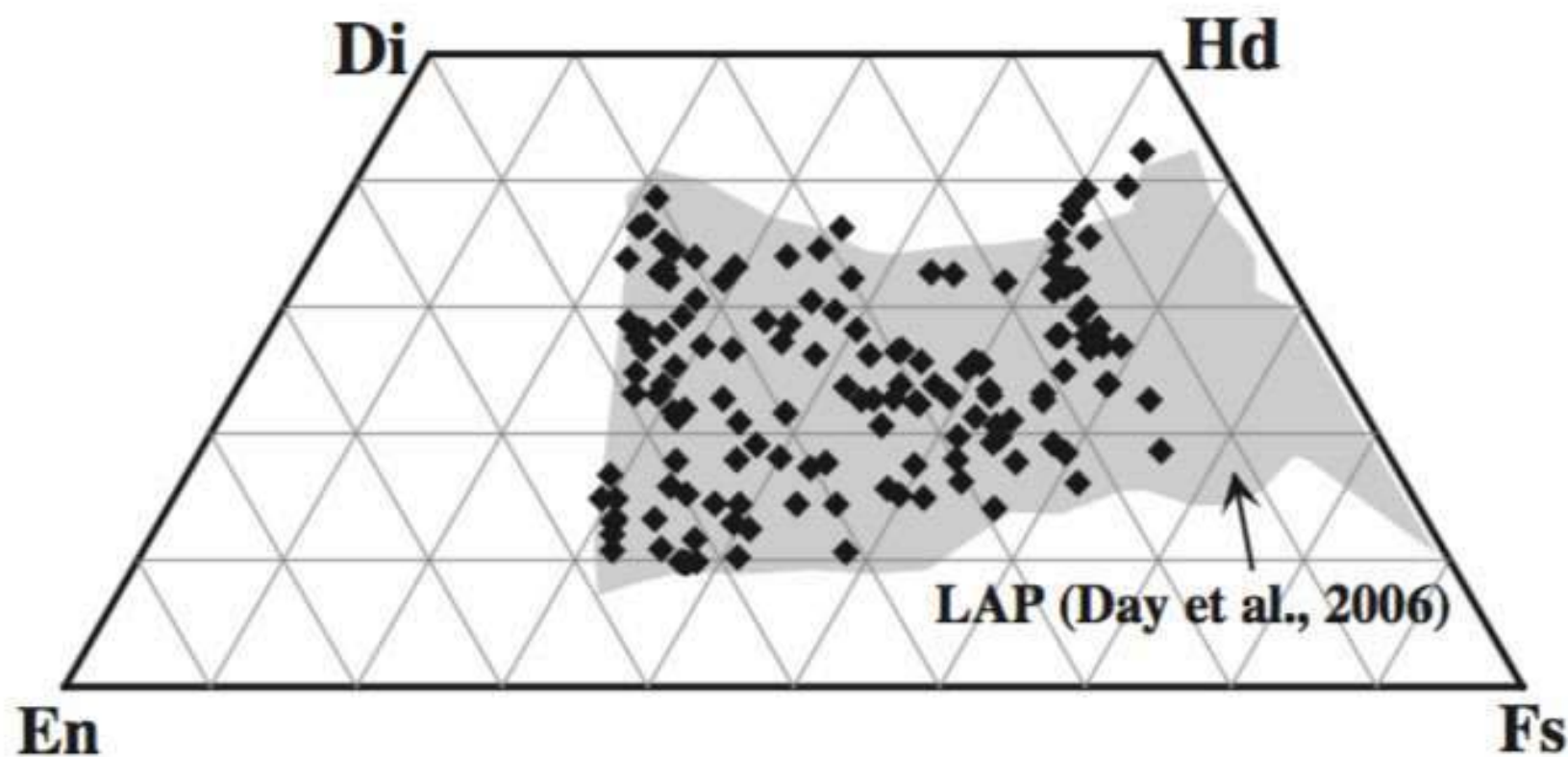
Pyroxene compositions from a range of clast types within lunar impact-melt breccia meteorite NWA 10986 - a rock from the lunar highlands. The least evolved pyroxenes from Clast A show a linear trend from pigeonite to augite, which are indicative of primitive parent melts. Whereas the highly evolved pyroxenes, including pyroxferroite, found in Clast C, suggest extensive fractionation (Roberts et al., 2017).



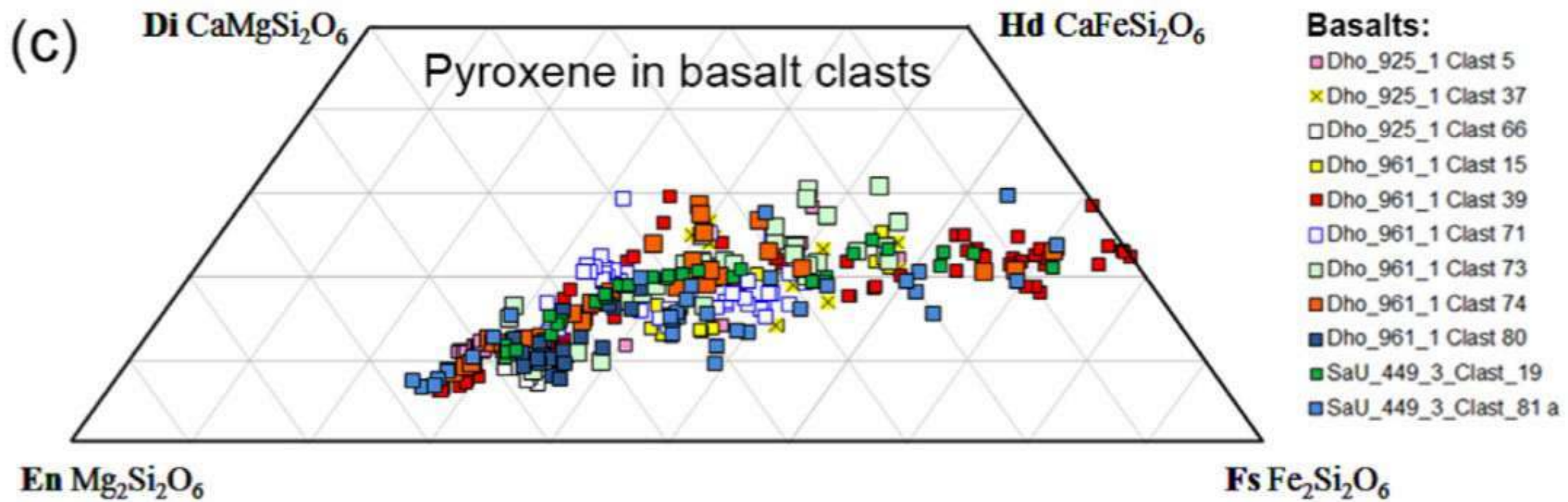
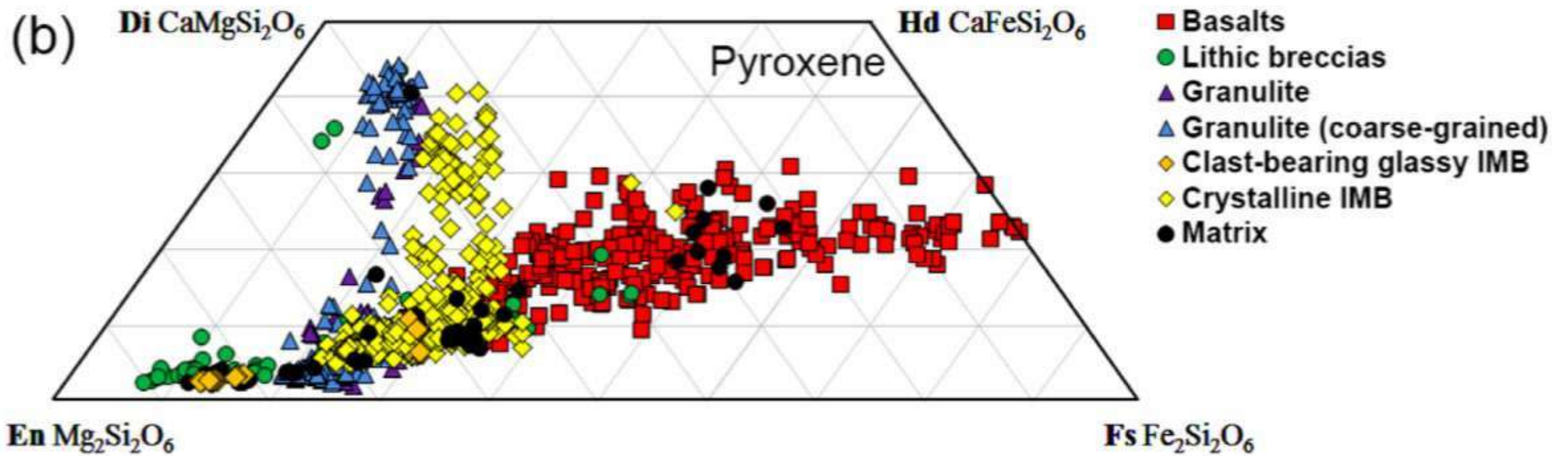
Pyroxene quadrilateral showing compositions of pyroxene in the mesostasis areas of four mare basalts studied by Griffiths et al. (2014). For comparison, the compositions of pyroxene in mare basalts, Mg-suite highland rocks, KREEP, and ferroan anorthosites are also plotted [compilation of pyroxene compositions courtesy of K. H. Joy]. Note the Mg-enrichment of Mg-suite highland rocks (black circles) and the Fe-enrichment of the mesostasis areas of the Apollo 11, 12 and 15 samples (red, blue and yellow symbols). Pyroxene from mesostasis areas of Apollo 17 sample 70035 appear anomalous possibly because “true” mesostasis areas were not analysed or that conditions of crystallization were different between it and the other samples. FAN = ferroan anorthosite.



Pyroxene compositions from basaltic lunar meteorite MIL 05035 (Liu et al., 2009). Only primary pyroxene data are plotted (excludes pyroxene in symplectites). The shaded field encircles data also from MIL 05035 (Joy et al., 2008). The outlined field corresponds to pyroxene compositions measured in other lunar meteorites (e.g. EETA 96008, MET 01210, LaPaz 02205, A-881757 and Y-793169).

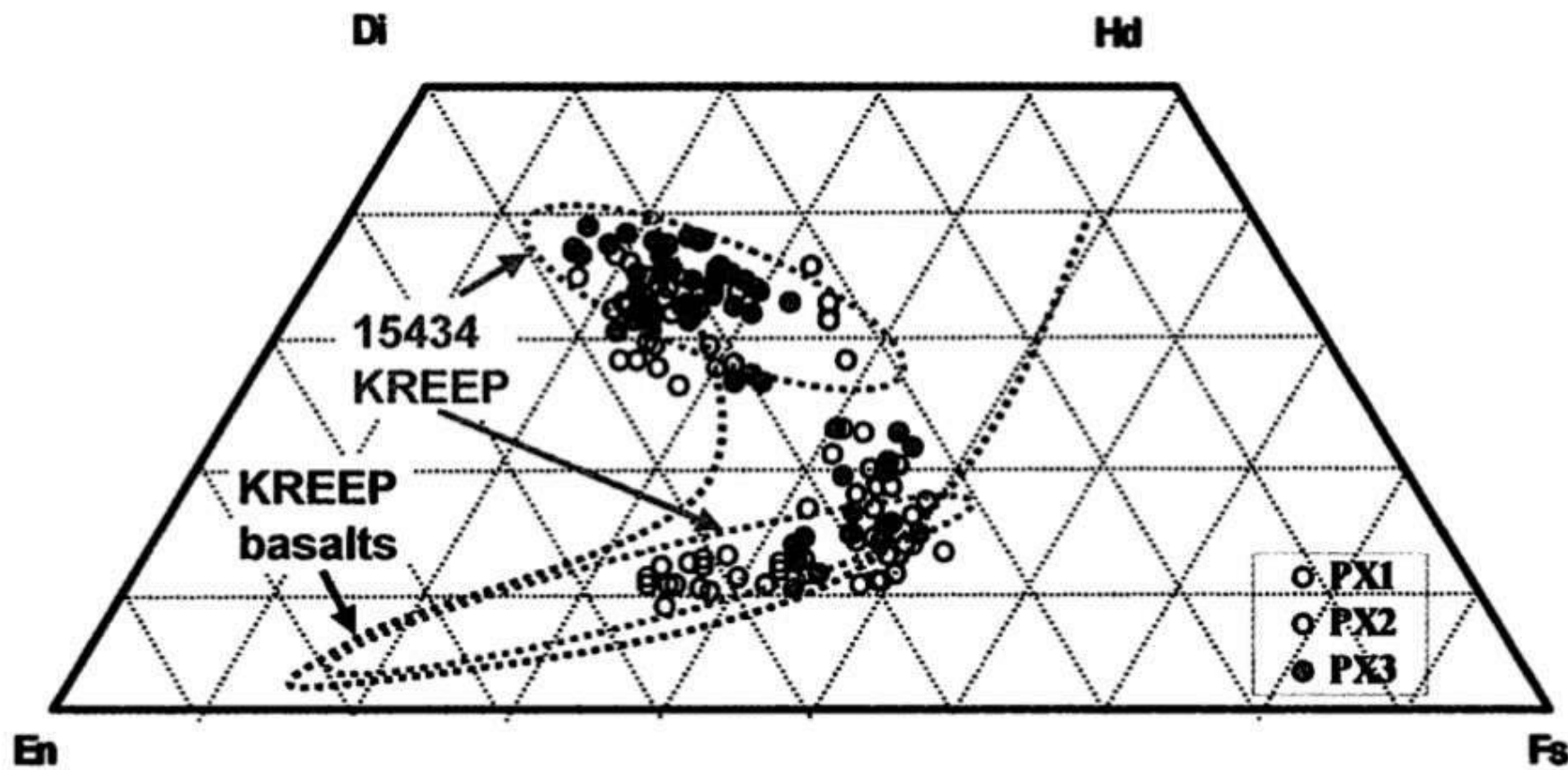


Pyroxene compositions from basaltic lunar meteorite NWA 4734 (Wang et al., 2012a). The shaded region represents the compositional range of pyroxenes in the LaPaz lunar meteorites (Day et al., 2006). Pyroxenes in NWA 4734 and the LaPaz lunar meteorites show similar compositional trends.

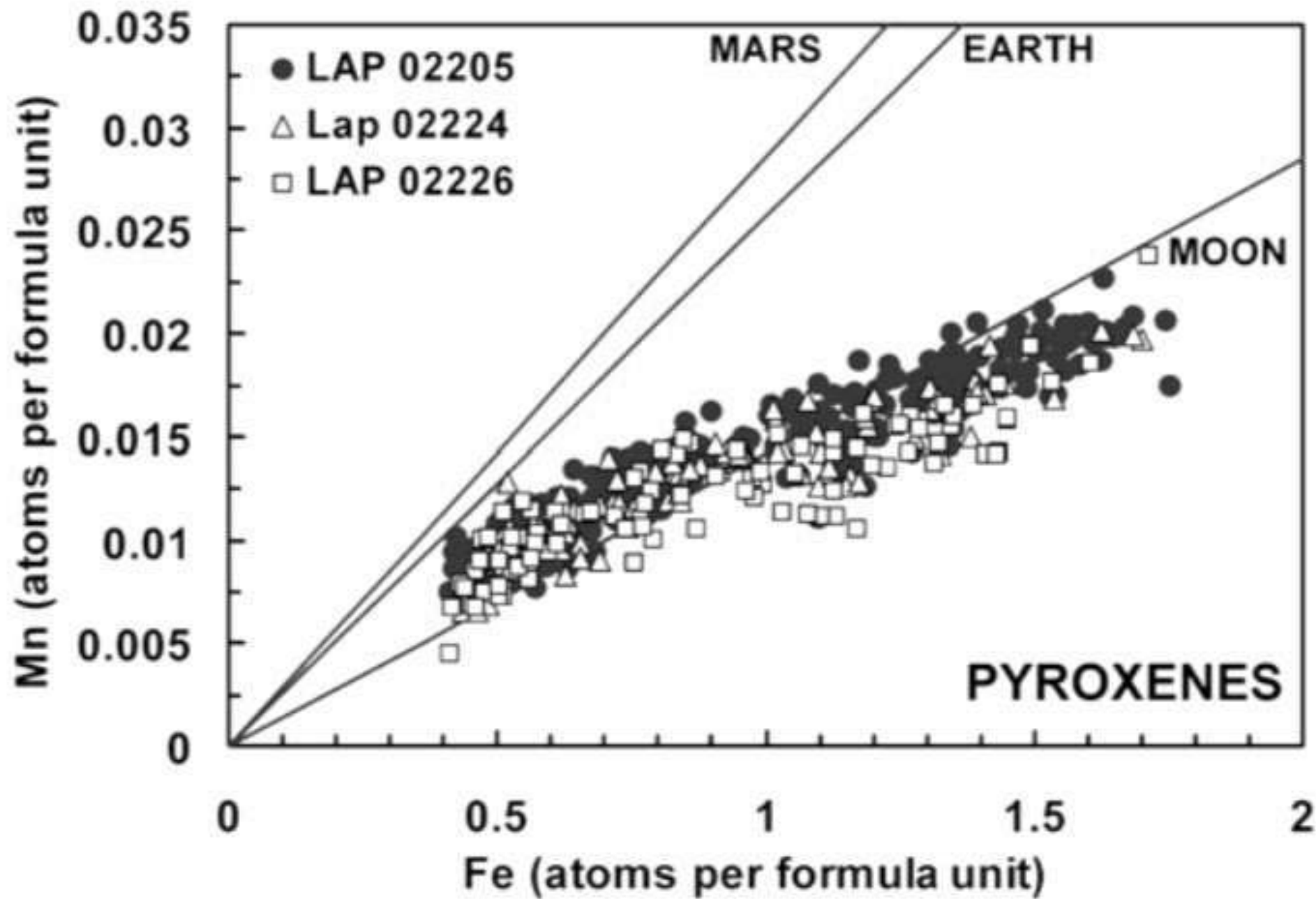


Pyroxene data from brecciated lunar meteorites Dhofar 925,1; 961,1 and SaU 449,3.

(b) all clasts and (c) detail from basaltic clasts only. IMB = impact melt breccia (Joy et al, 2014).

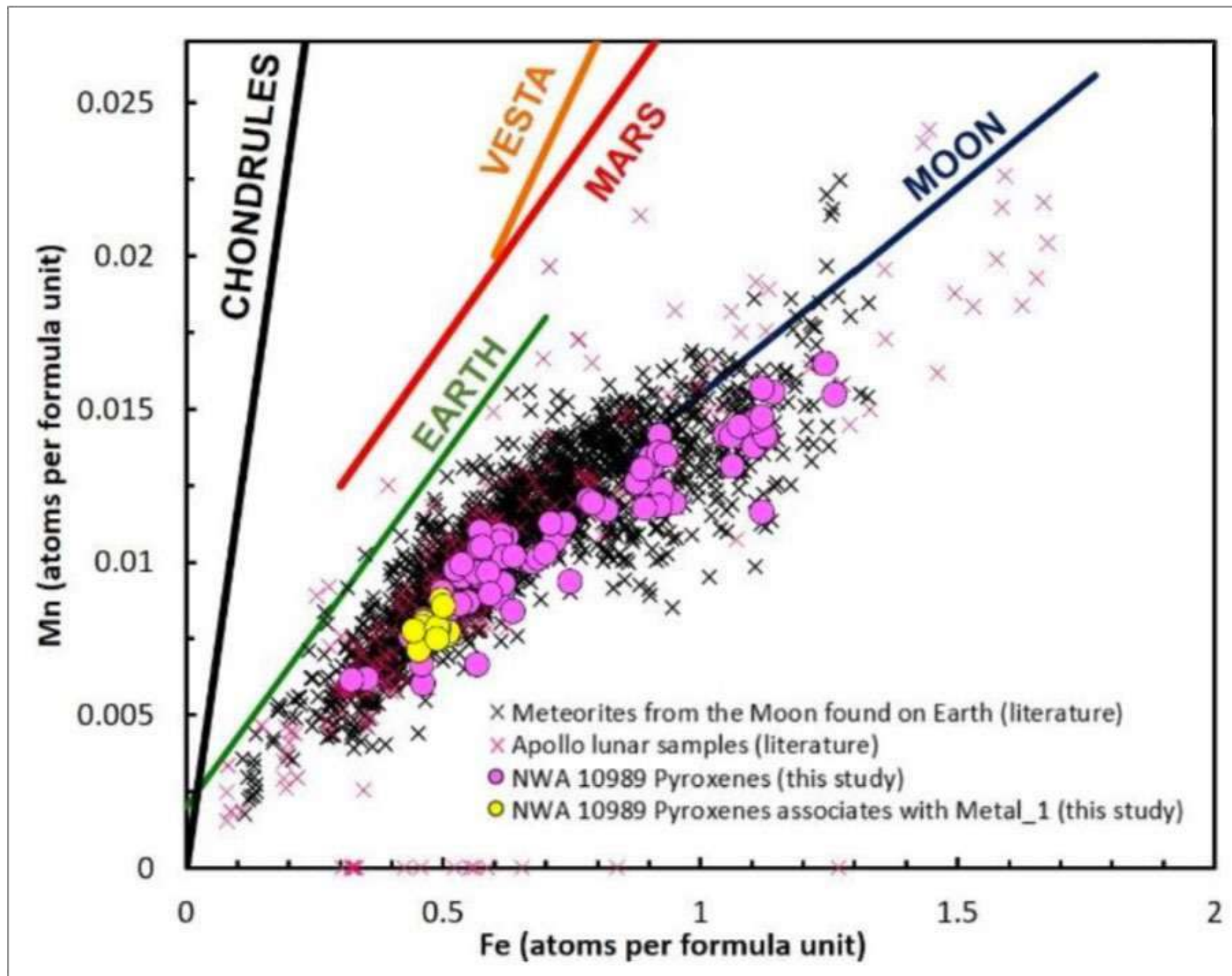


Pyroxene compositions from a KREEP basalt clast in basaltic lunar polymict breccia meteorite Yamato 983885 (Arai et al., 2005). The dotted areas represents the compositional range of pyroxenes in KREEP basalts including Apollo 15 sample 15434. The largest pyroxene grain is 200 μm across and consists of augite mantled by a low-Ca pyroxene, coexisting with whitlockite, plagioclase and Si, Al, K-rich glass.



Taken From Joy et al. (2006)

The Fe/Mn ratio in pyroxene is an indicator of planetary origin. Lunar pyroxene exhibits a diagnostic Fe/Mn ratio compared to the Earth, Mars, Vesta and chondritic meteorites - probably as the result of volatile loss in an early Moon-forming event (Papike et al. 2003). Here data from lunar meteorites LAP 02205, 02224 and 02226 are superimposed over the typical planetary fractionation trends. Atoms per formula unit are based on 6 oxygen atoms.

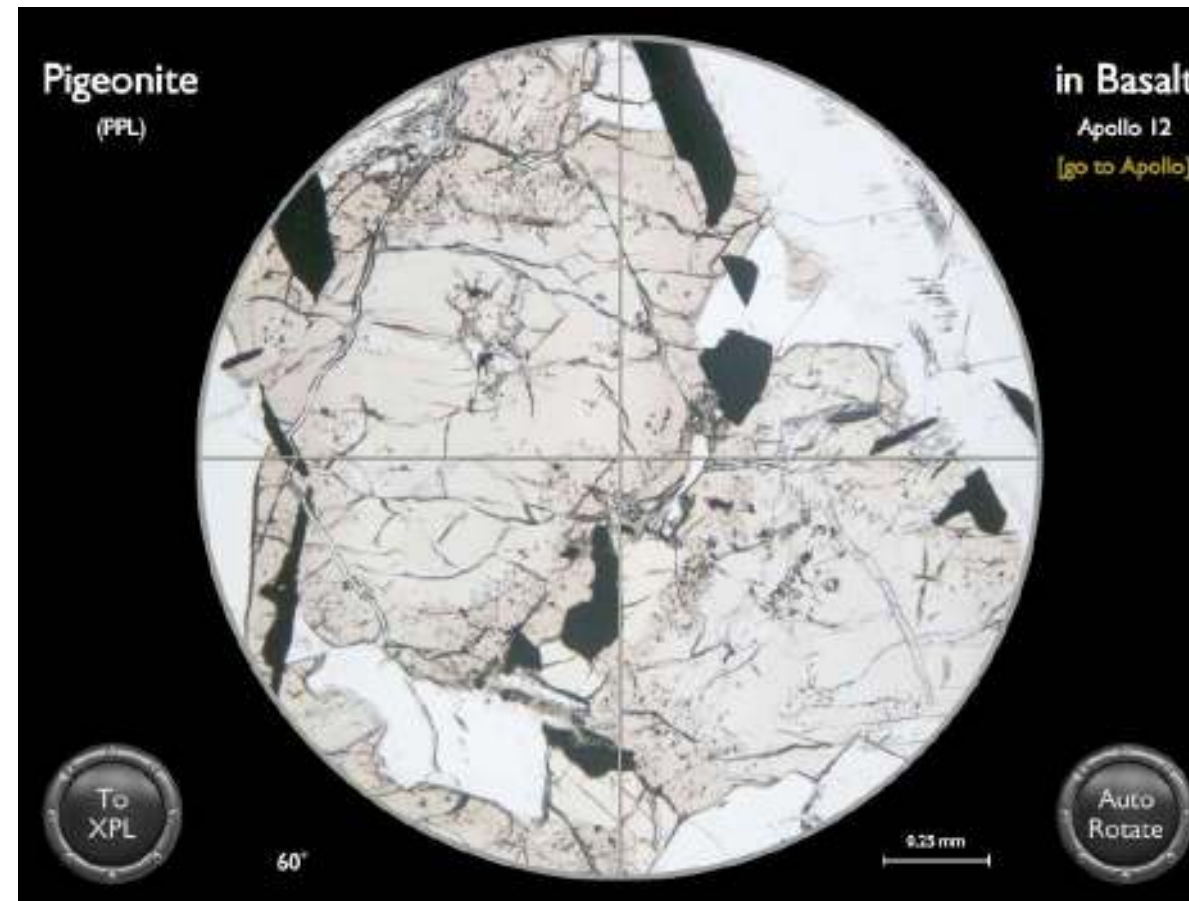


Taken From Morland et al. (2019)

Pyroxene data from lunar regolith breccia meteorite NWA 10989 (purple circles) plotting alongside data from other meteorites from the Moon. Pyroxene data collected adjacent to a large metallic iron grain (yellow circles) plot along the same line. Trend lines for pyroxenes found on Earth, Mars, Vesta and in chondrules are shown for comparison.

Moon Minerals: Pyroxene Group

Mineral Virtual Microscope: Pigeonite

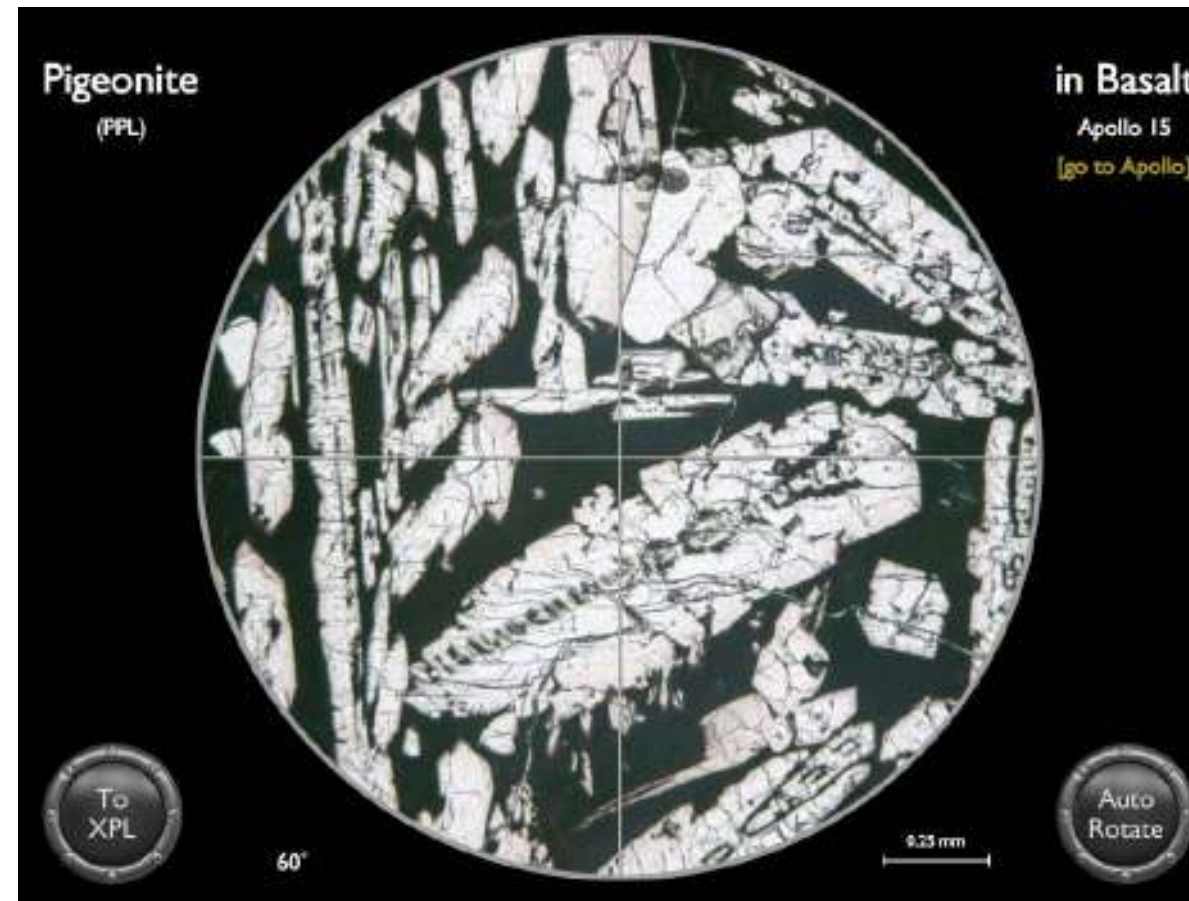


12039 is a coarse-grained porphyritic basalt which consists of pyroxene phenocrysts, some of which are mantled by pyroxferroite, set in a matrix of intergrown plagioclase crystals, anhedral pyroxene, rounded laths of ilmenite and euhedral laths of tridymite. Many of the clinopyroxene crystals show optical zonation from very light tan interiors (augite) to dark tan (ferroaugite) to reddish-brown (ferrohedenbergite) with an abrupt change to light yellow-green borders (pyroxferroite).

Apollo 15, Sample 12039.

Moon Minerals: Pyroxene Group

Mineral Virtual Microscope: Pigeonite

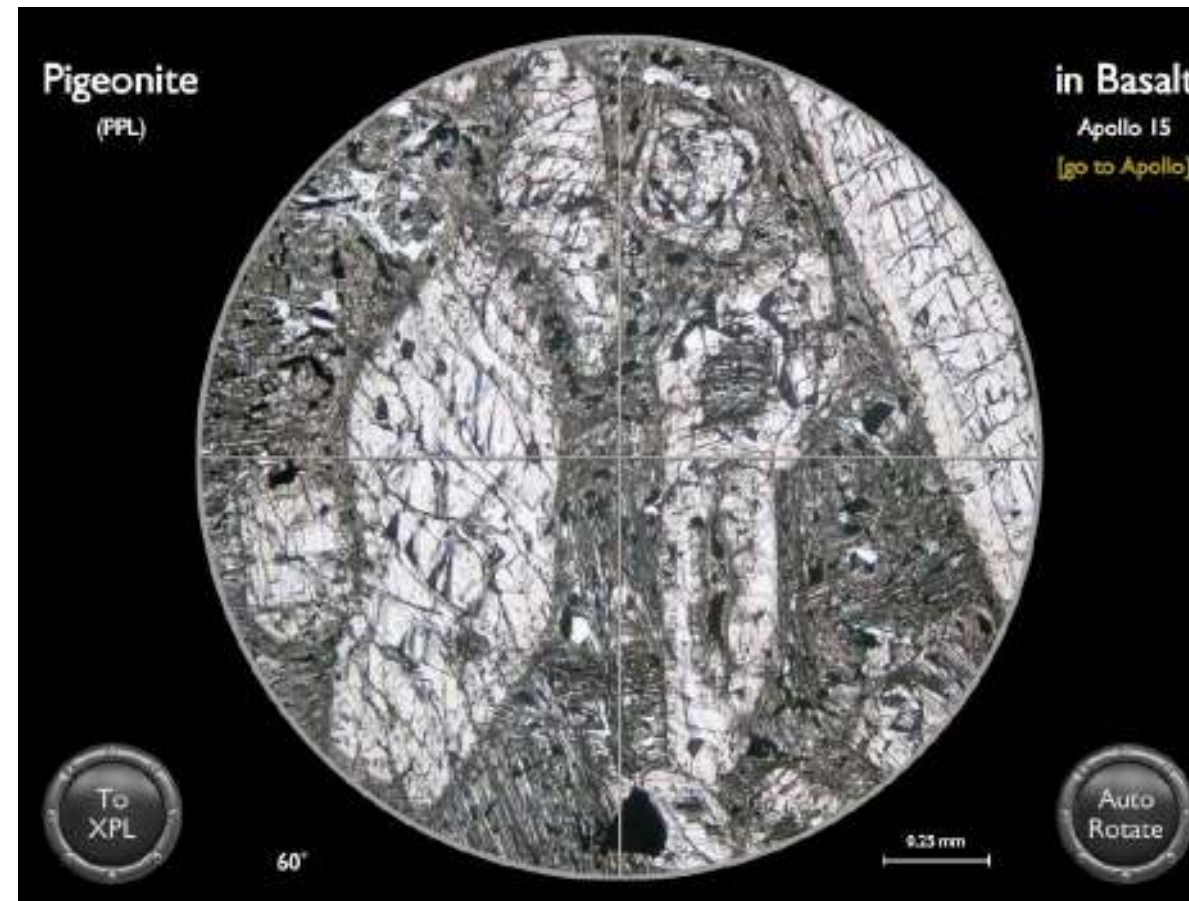


15485 is a rapidly cooled vitrophyric pigeonite basalt with a porphyritic, diktytaxitic texture. The vitrophyre is composed of elongate pyroxene prisms in a matrix of opaque devitrified glass with 3% globulose vugs. Pyroxene crystals are highly zoned. The main accessory minerals are ilmenite, troilite and metallic iron.

Apollo 15, Sample 15485.

Moon Minerals: Pyroxene Group

Mineral Virtual Microscope: Pigeonite

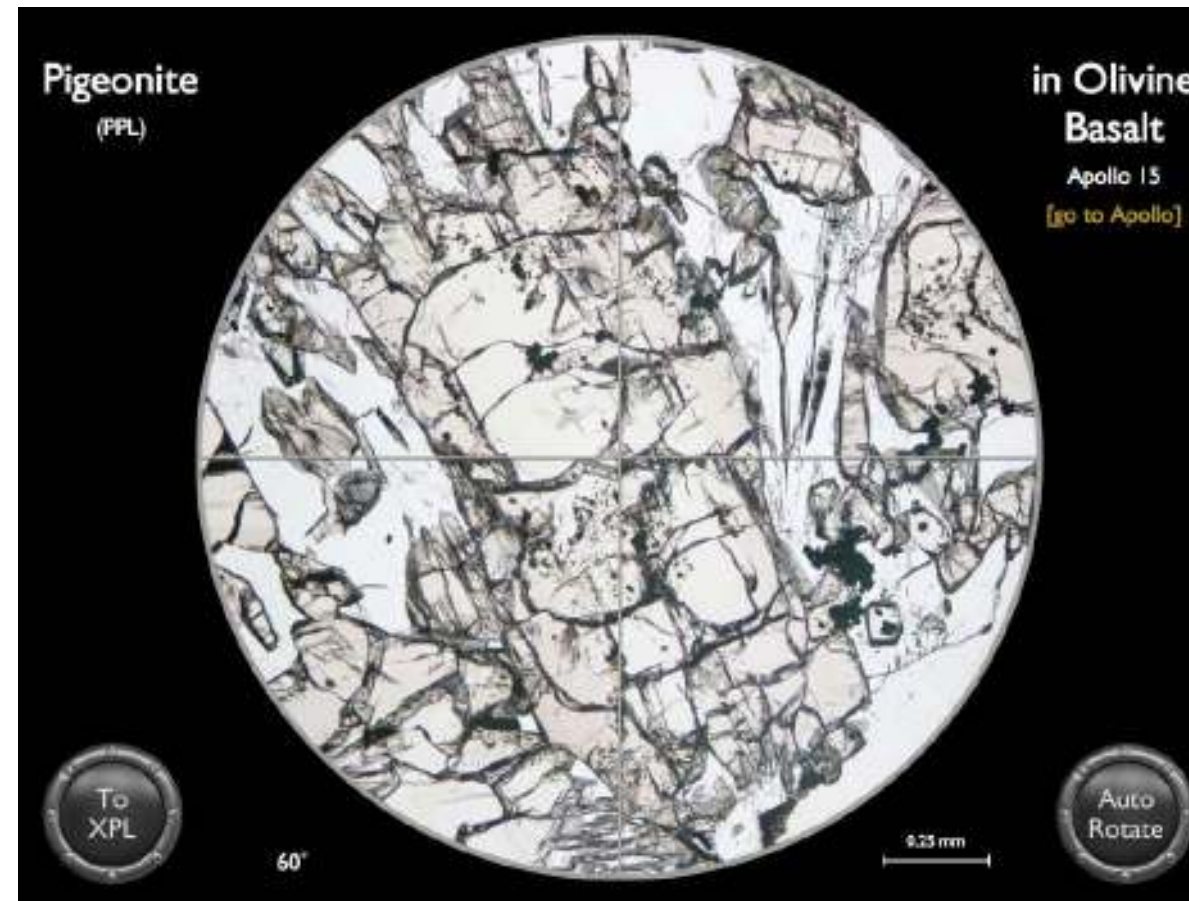


15596 is a fine-grained, porphyritic Mare basalt containing pigeonite phenocrysts in a spherulitic, almost vitrophyric groundmass. The groundmass is made up of clinopyroxene, plagioclase and opaque minerals, with occasional rare zoned olivine and Cr-spinel microphenocrysts. The larger pyroxene phenocrysts have homogeneous pigeonite cores, with a sharp transition to sub-calcic augite rims.

Apollo 15, Sample 15596.

Moon Minerals: Pyroxene Group

Mineral Virtual Microscope: Pigeonite

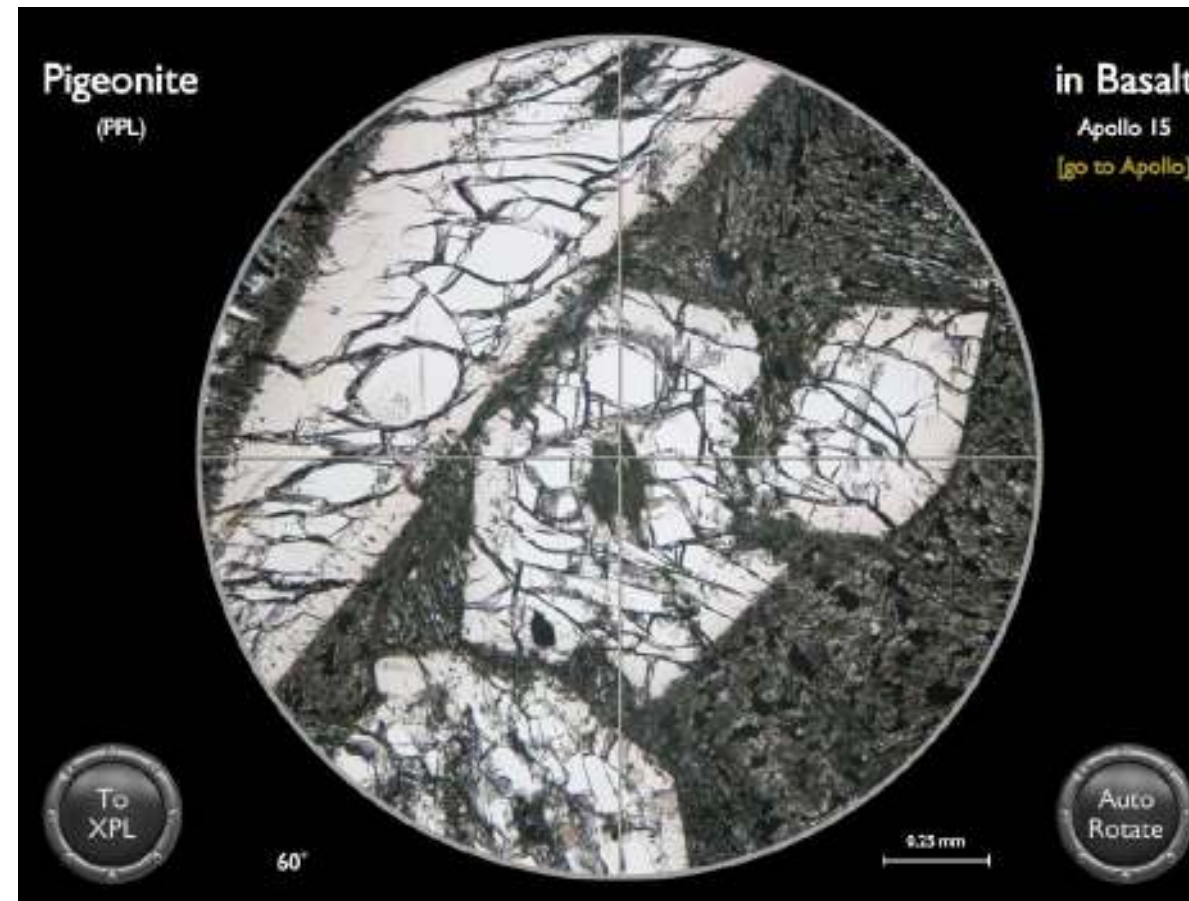


15643 is a relatively coarse-grained basalt of the abundant olivine normative Apollo 15 basalt clan. Pyroxene grains are up to 2 mm across and somewhat elongate. They are chemically zoned from pigeonite to Fe-rich augite and sometimes twinned (as in this example).

Apollo 15, Sample 15643.

Moon Minerals: Pyroxene Group

Mineral Virtual Microscope: Pigeonite

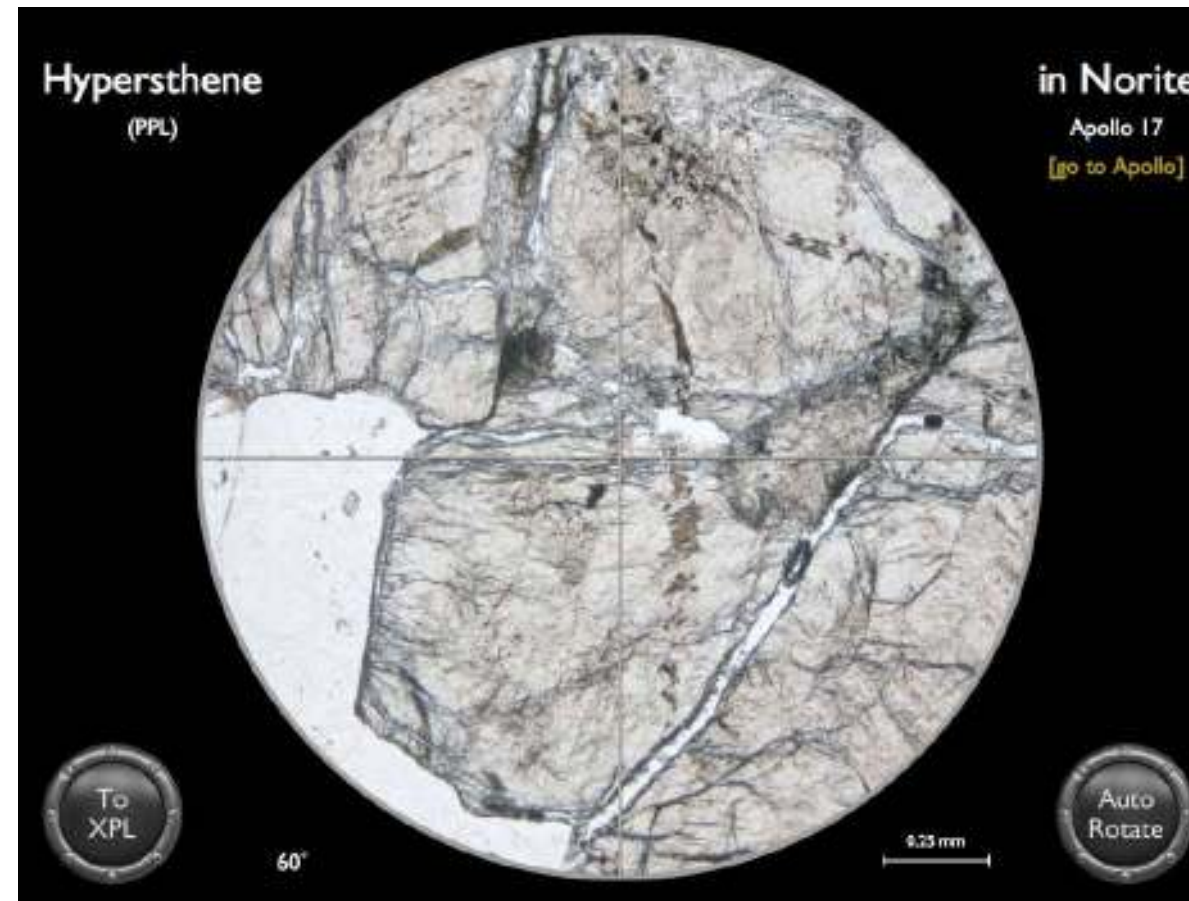


Pigeonite phenocrysts dominate the mineral assemblage in this porphyritic basalt. They are euhedral, elongate and chemically zoned, with distinct boundaries. Vesicles, ilmenite, metallic iron and tiny troilite grains are also present. The groundmass is finely crystalline and consists of elongate crystals of pyroxene and plagioclase with minor olivine. 15666 was rapidly cooled.

Apollo 15, Sample 15666.

Moon Minerals: Pyroxene Group

Mineral Virtual Microscope: Hypersthene

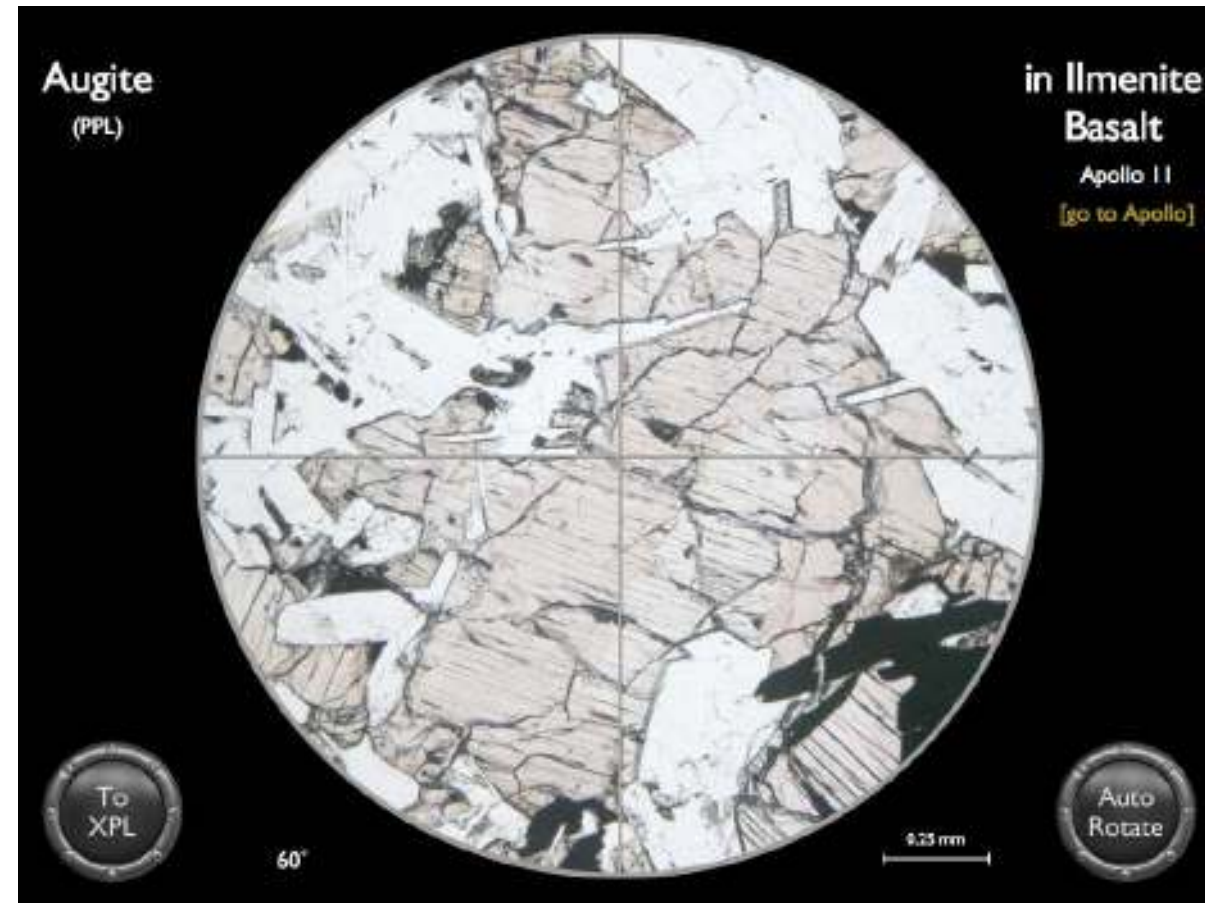


78235 consists of tabular orthopyroxene (hypersthene) and plagioclase feldspar. Both minerals are partially shattered, and maskelynite (formed by cold transformation from crystal to glass by shock) replaces some of the feldspar.

Apollo 17, Sample 78235.

Moon Minerals: Pyroxene Group

Mineral Virtual Microscope: Augite

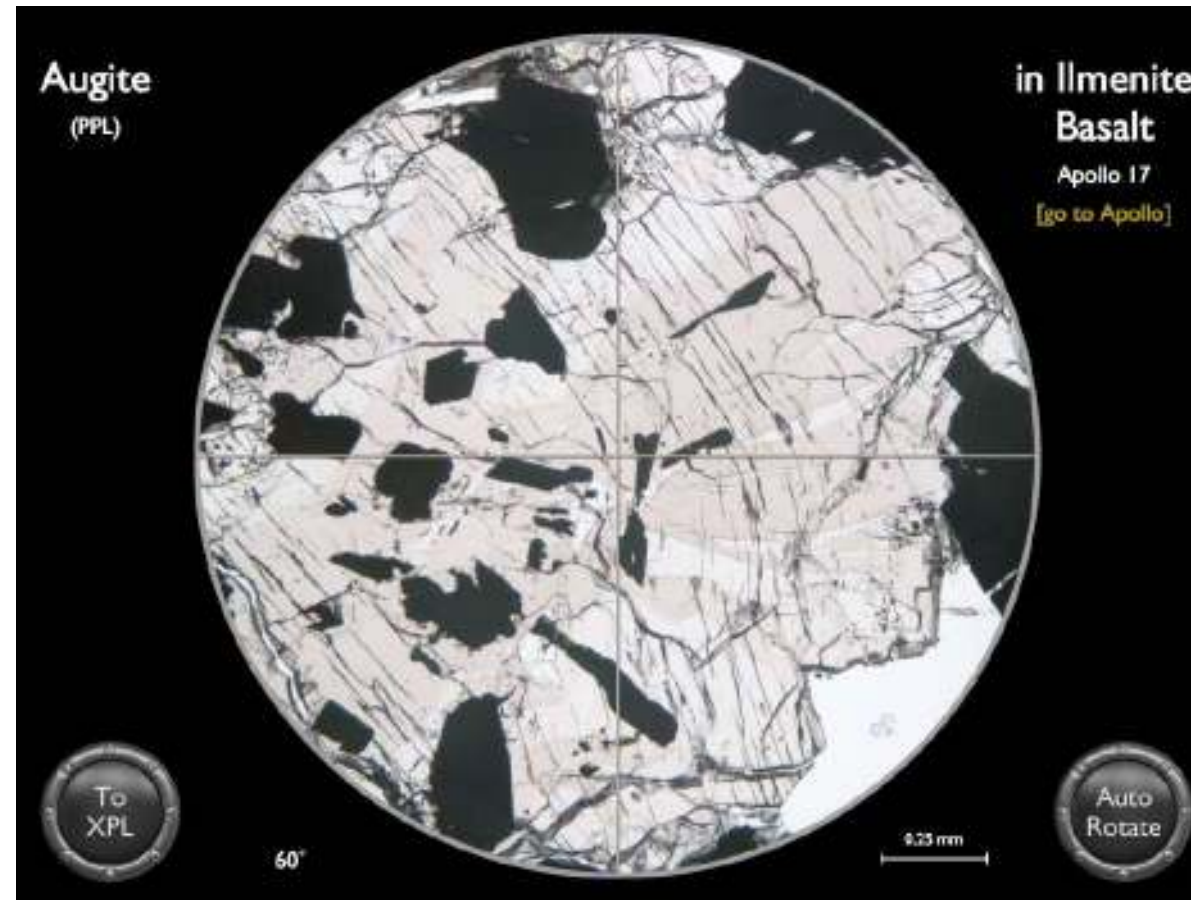


10044 consists of anhedral phenocrysts of pyroxene in a partially enclosing matrix of plagioclase feldspar and ilmenite. The pyroxene composition is variable with core to rim zoning from augite to the rare species pyroxferroite.

Apollo 11, Sample 10044.

Moon Minerals: Pyroxene Group

Mineral Virtual Microscope: Augite

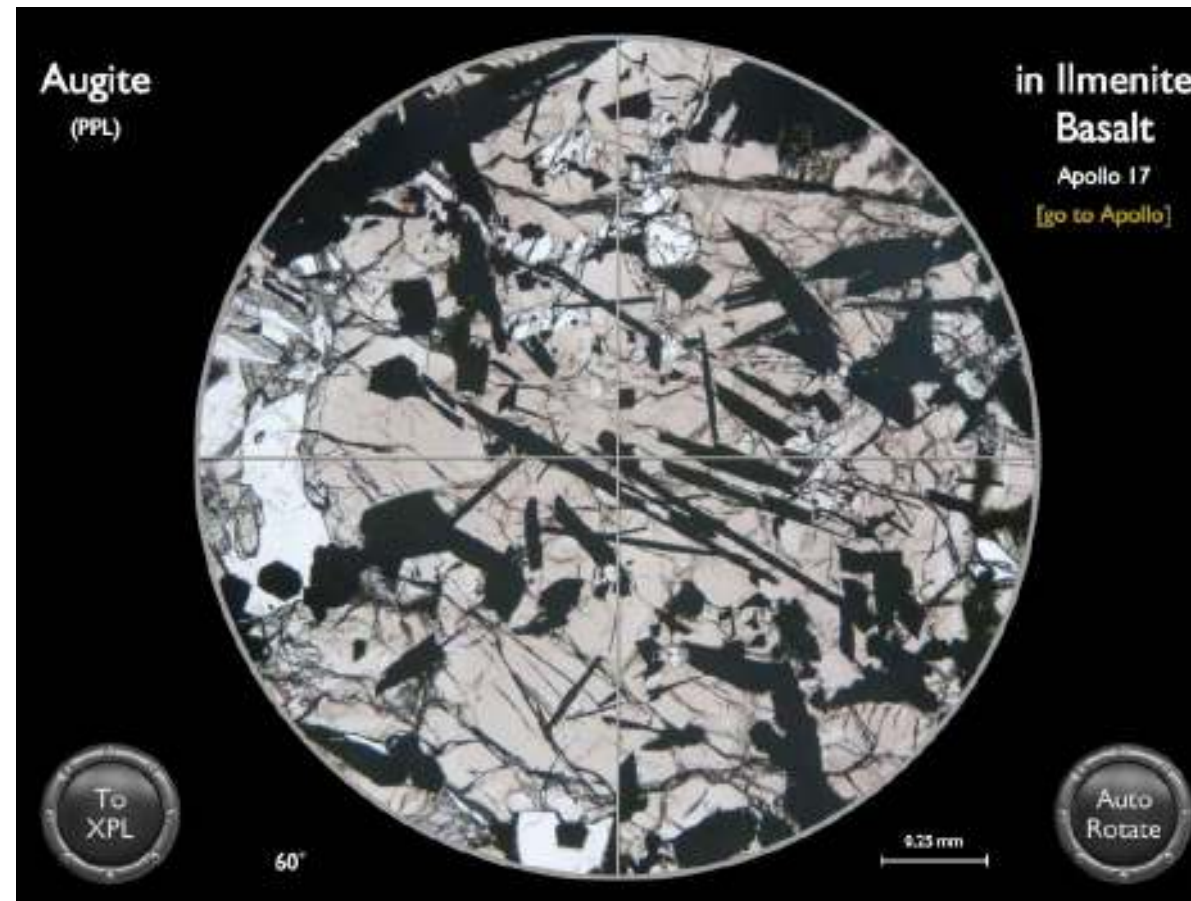


71175 is an equigranular ilmenite basalt with a sub-ophitic texture. It contains compositionally zoned and twinned pyroxene containing many ilmenite inclusions. This particular crystal of augite shows strain features indicating it was subjected to a later impact event.

Apollo 17, Sample 71175.

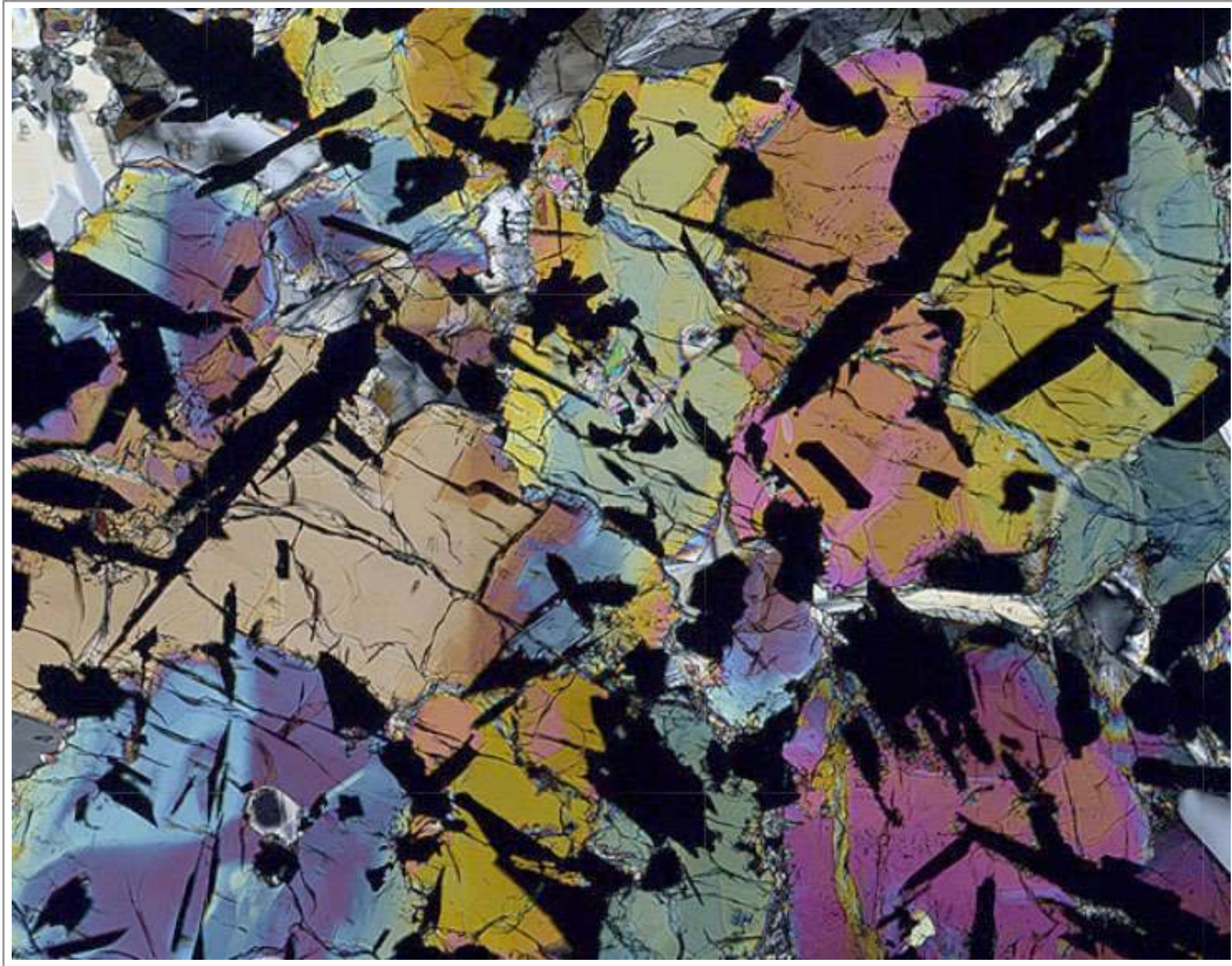
Moon Minerals: Pyroxene Group

Mineral Virtual Microscope: Augite



The crystallization sequence for this sample starts with armalcolite and Cr-spinel, which are found as unreacted inclusions in both olivine and pyroxene cores. Olivine crystallized next, reacting with the melt to form augite before armalcolite ceased crystallization. Ilmenite was next and is included in the augite phenocrysts as they zone to become more Fe-rich, followed by plagioclase feldspar and pigeonite. Fe-rich pyroxene, silica, Na plagioclase and potassic mesostasis formed last.

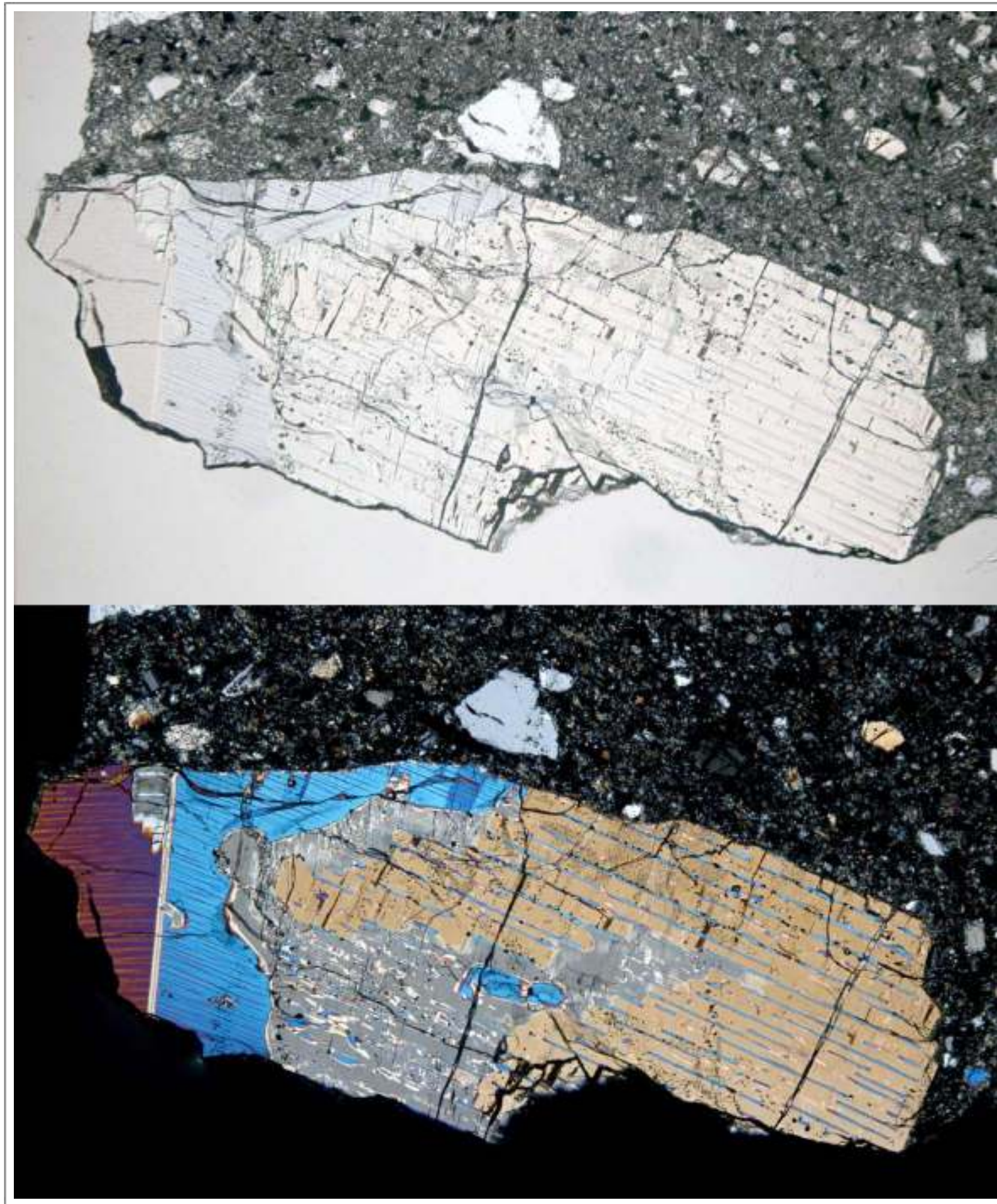
Apollo 17, Sample 74255.

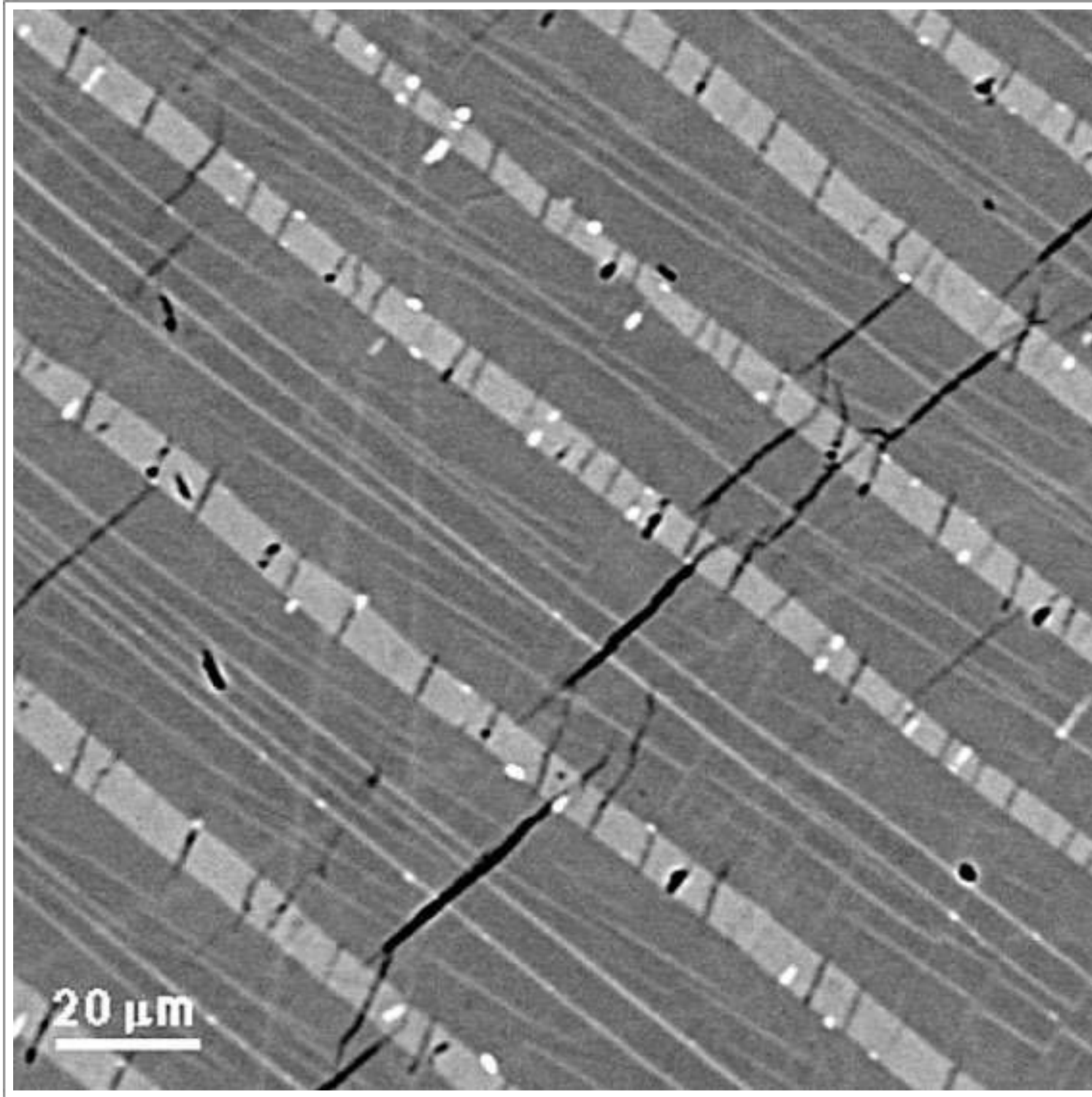


Cluster of chemically zoned and shocked pyroxene crystals in Apollo 17 ilmenite basalt 74255,52.
Note the sector zoning in the bottom left crystal. Transmitted light image (between crossed polars). Width 2.2 mm.

Transmitted light images (ppl top, xpl bottom) of a pyroxene clast in Apollo 17 impact-melt breccia 73218,26.

The larger part of the clast is pigeonite (cream) containing augite exsolution lamellae (blue rods) that has been subjected to a degree of replacement (grey). Mantling the left edge of the pigeonite is a twinned crystal of augite (purple-blue) which also displays exsolution (probably fine laths of pigeonite). Width 2.8 mm.





Taken From McCallum et al. (2006)

Backscattered electron image of Apollo 17 Mg-suite gabbro-norite 76255,69 (a clast in impact-melt breccia). Augite grain showing exsolution of pigeonite lamellae on (001) of the host augite. Small bright spots are oxide grains. The rock formed in the lunar crust (~2 km), most likely during the Serenitatis basin-forming impact event.

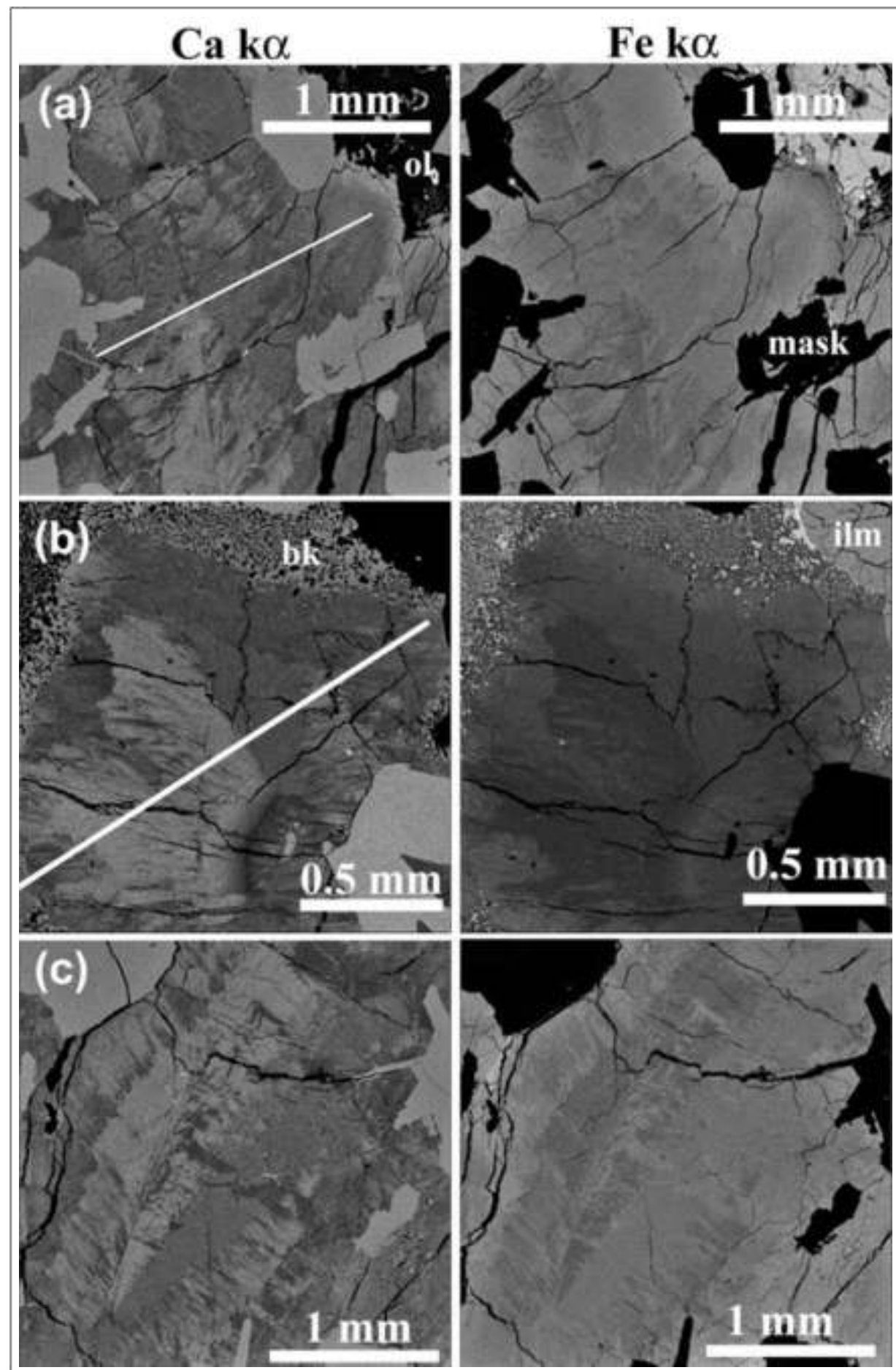
Complex zoning patterns of pyroxenes in lunar meteorite MIL 05035 - a low-Ti mare basalt.

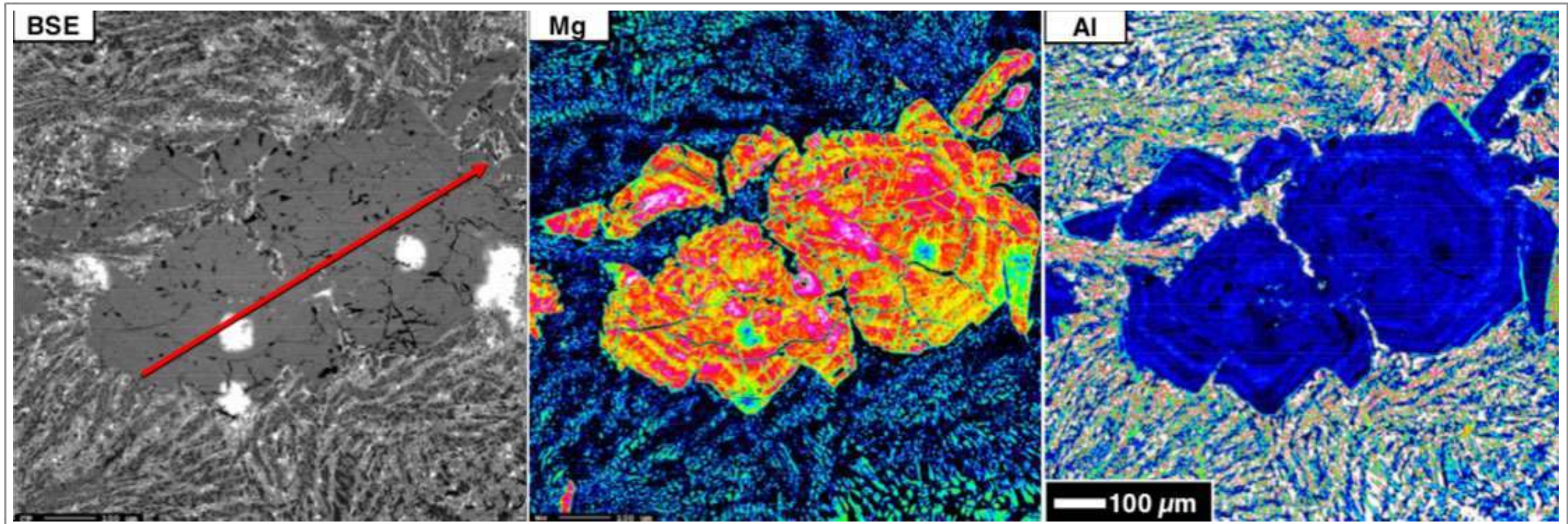
Ca and Fe X-ray maps.

(a) pyroxene grain in MIL 05035,60 with sector zoning accentuated by Ca-poor veinlets.

(b) pyroxene grain in MIL 05035,40 with sector zones and twins, containing thin veins of lower Ca, higher Fe pyroxene. White lines in (a) and (b) mark EMPA traverse shown in the original publication.

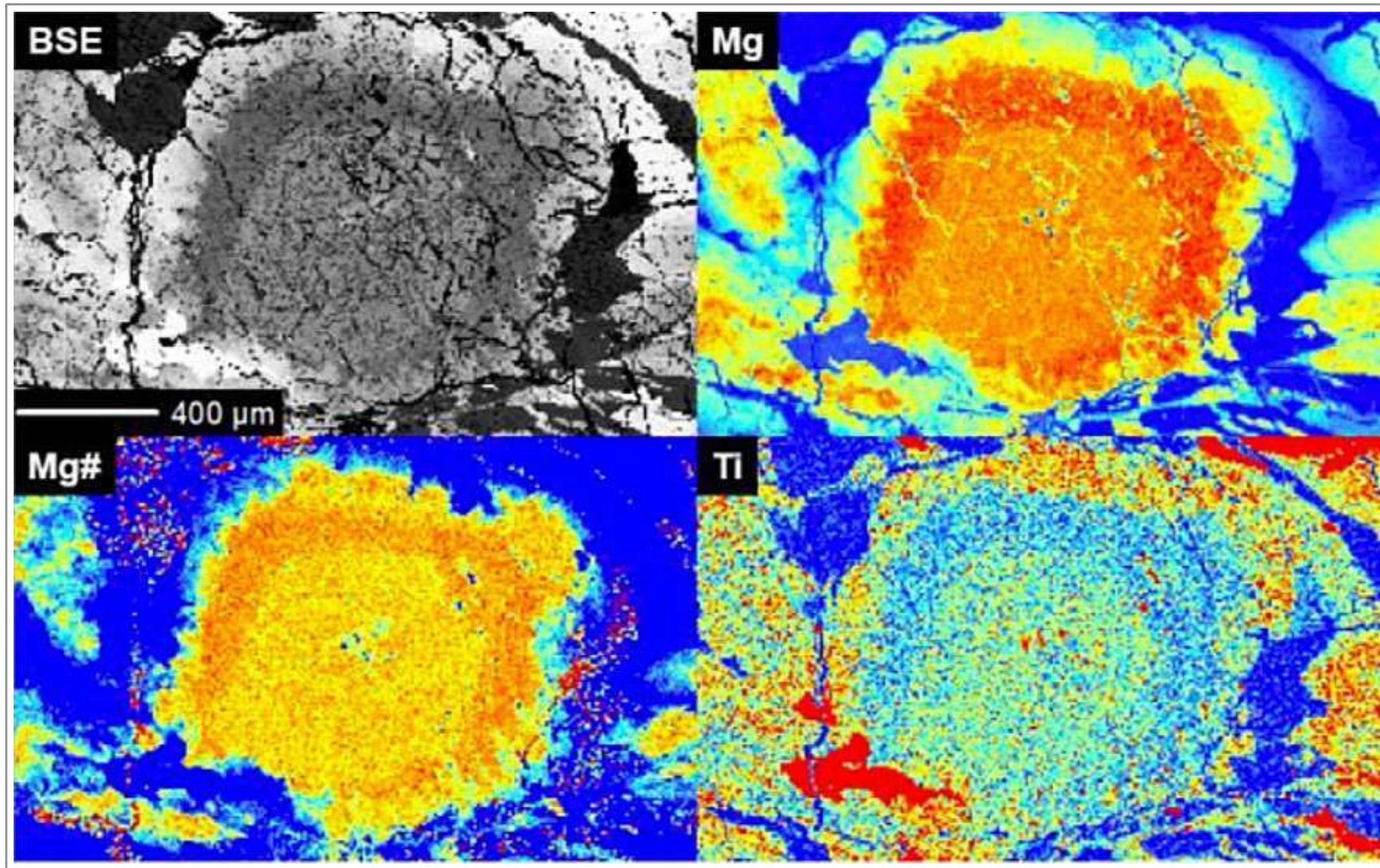
(c) complex zoning in a pyroxene grain in MIL 05035,6 with no clear indication for sector zoning but clear evidence for twinning.





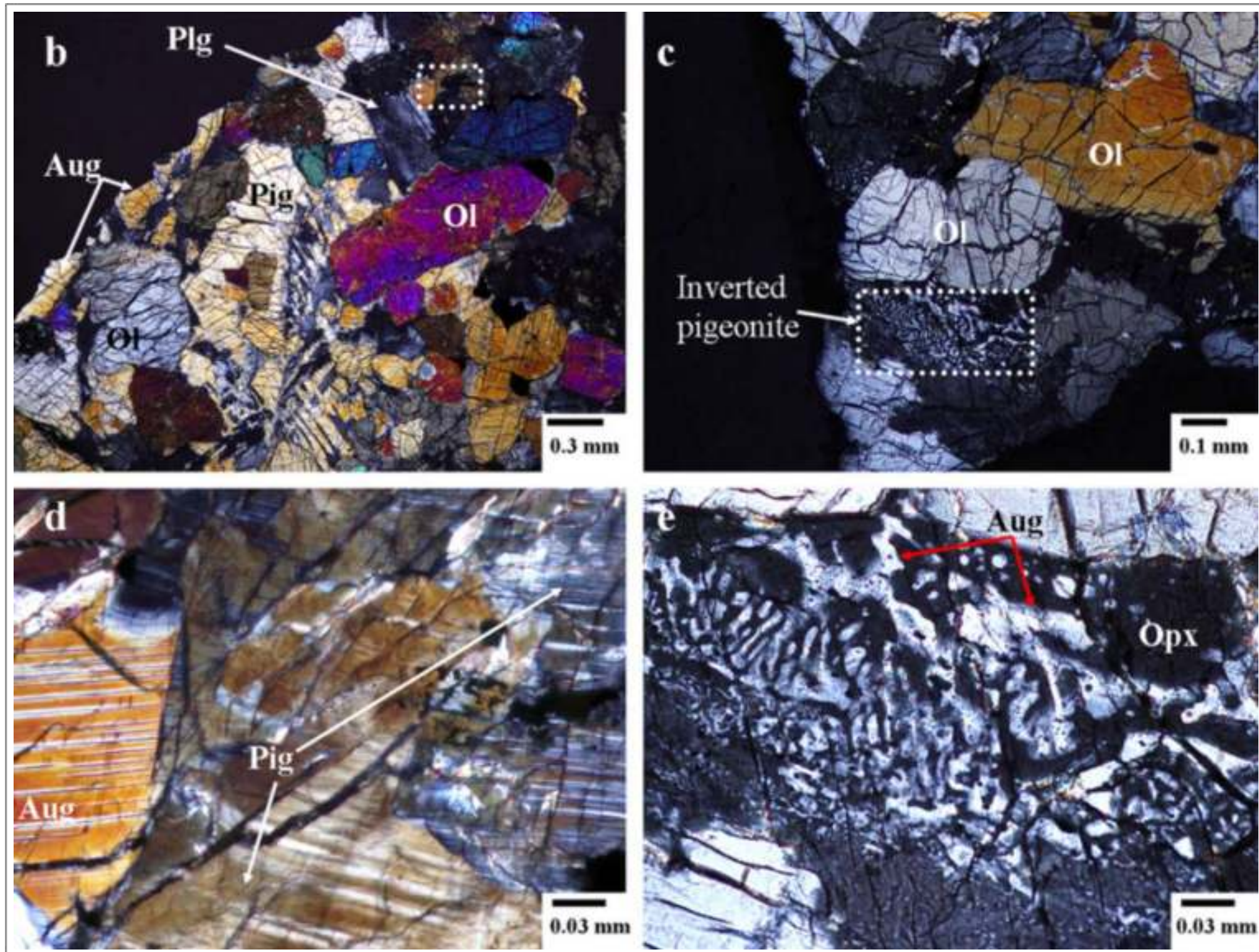
Taken From Burger et al. (2009)

Backscattered electron image (BSE) and X-ray maps (Mg & Al) of pyroxene phenocrysts in lunar meteorite NWA 032 (an the unbrecciated mare basalt).The red arrow on the BSE image marks the line of a quantitative microprobe traverse (not shown).



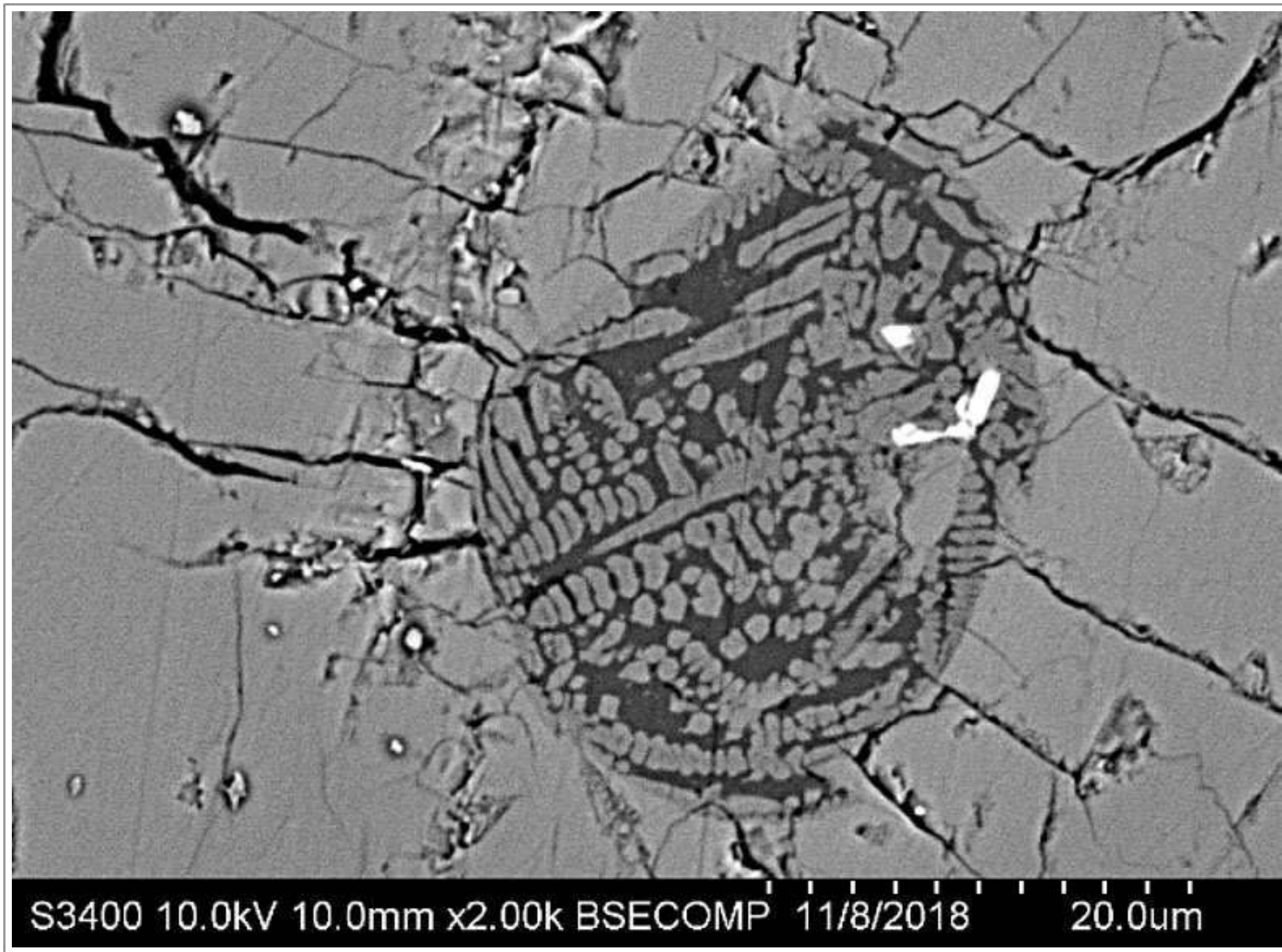
Taken From Chen et al. (2019)

Backscattered electron image and X-ray maps of Mg, Mg# (molar $\text{Mg}/[\text{Mg}+\text{Fe}]\times 100$), and Ti of a pyroxene phenocryst in a gabbroic clast within lunar meteorite NWA 10985.



Taken From Nagaoka et al. (2015)

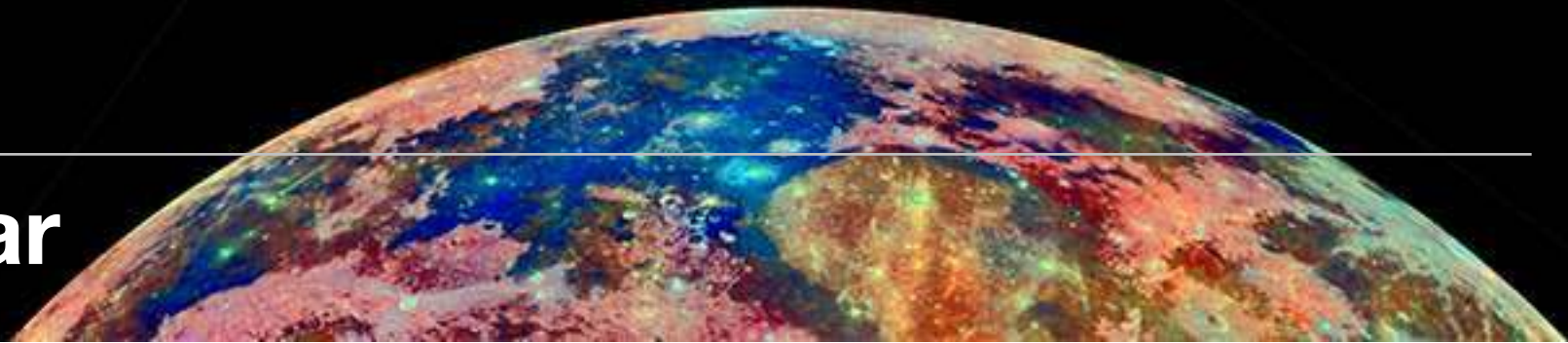
Lunar meteorite NWA 2977 - a cumulate olivine gabbro. Transmitted light images (between crossed polars) showing: b&c) detailed textures of minerals. d) photograph of exsolution lamellae occurring in pyroxene which shows the detailed textures surrounded by the white dotted line box in b. e) photograph of blebby textures of augite in an orthopyroxene (inverted pigeonite) which shows the detailed textures surrounded by the white dotted line box in c. Ol olivine, Pig pigeonite, Opx orthopyroxene, Aug augite, Plg plagioclase.



Taken From Cohen et al. (2019)

Lunar meteorite NWA 12008 - a mare basalt. Backscattered electron image of a crystallized melt inclusion within olivine containing skeletal pyroxene (Al-Ti-bearing augite) and Cr-Ti-Fe spinel (small white crystals). The dark phase is a K-bearing glass.

Plagioclase Feldspar



SPECIES

1. A solid solution series between end-members anorthite ($\text{CaAl}_2\text{Si}_2\text{O}_8$) and albite ($\text{NaAl}_2\text{Si}_3\text{O}_8$)
2. Maskelynite - shock-melted glass after plagioclase feldspar

See Section 11 for details of accessory potassium feldspar compositions

Plagioclase Series

Aside from rare potassium- and barium-enriched feldspars (discussed in the Accessory Minerals chapter, Section 11), most lunar feldspars belong to the plagioclase series, which consists of solid crystalline solutions between albite and anorthite. Because of the alkali-depleted nature of the Moon, lunar plagioclase is also depleted in Na (the albite component) relative to terrestrial plagioclase.

Plagioclase from highland impact melts, from breccias, and from KREEP rocks have more Na-rich compositions (i.e., less anorthite) than mare basalts.

Plagioclase from highland coarse-crystalline igneous rocks have more restricted compositions (Heiken et al., 1991). Shock effects in plagioclase are particularly noticeable in Apollo 16 fragmental polymict breccia 67215 (Norman, 2003).

Plagioclase (anorthite An_{94-97}) is the dominant species in the first lunar meteorite (ALHA81005) ever discovered. It was found on January 18th, 1982 in the Allan Hills region of Victoria Land, Antarctica and is a polymict anorthositic breccia. The breccia contains anorthositic clasts displaying shock textures and plagioclase grains dispersed in the matrix (Marvin, 1983; Simon et al., 1983).

Lunar meteorite Dhofar 911 is a recrystallized melt breccia containing a large white anorthositic clast (2.4×1.8 mm in size) embedded in a dark fine-grained crystalline matrix. Many smaller plagioclase feldspar fragments are distributed in

the matrix but their numbers are small. The chemical composition of plagioclase is very uniform at An₉₆ (Takeda et al., 2012).

Pure anorthosite clasts in another lunar meteorite (Dhofar 489) contain >99 area% plagioclase (An₉₅₋₉₆) associated with traces of olivine, orthopyroxene and troilite. Because of its very low Th and Fe contents it has been suggested that Dhofar 489 came from the far side of the Moon (Nagaoka et al., 2014).

Lunar meteorite NWA 2200 is a feldspathic regolith breccia containing a diverse mixture of mineral fragments, lithic clasts, glassy clasts, and impact glass spherules embedded in a brown glassy matrix. The most abundant discrete mineral fragments embedded in the matrix are Ca-rich plagioclase (An₉₅₋₉₈).

Nagaoka et al. (2013) suggest it may have originated from the ferroan KREEP-poor highlands.

Plagioclase fragments in lunar meteorite SaU 300 (an impact-melt breccia) show a wide variety of shock effects, including undulose extinction, mechanical deformation, and kink bands, in addition to local transformation to maskelynite in areas adjacent to localized melt features (veins and pockets). Severely fractured grains (mineral and lithic) show internal brecciation (Hudgins et al., 2007).

According to Haloda et al. (2009), of the 10 unbrecciated mare-basalt meteorites only NEA 003-A, Dhofar 287-A and Asuka 881757 show complete plagioclase to maskelynite conversion.

Martin et al. (2017) used data from Miller Range (Antarctica) lunar meteorites MIL 090034, MIL 090070, and MIL 090075 to note that Fourier transform infrared (FTIR) spectroscopy can be employed to identify shocked feldspathic phases in lunar samples; estimate peak shock pressures; and when compared with chemical data, can be used to investigate their shock histories. These authors identify six categories of shock-modified feldspar:

Type (1): Crystalline anorthite

Type (2): Partially shock-modified anorthite

Type (3): Maskelynite

Type (4) Polycrystalline impact-melt

Type (5) Devitrified feldspathic glass

Type (6) Homogenous feldspathic glass

Pernet-Fisher et al. (2016) also investigated the shock history of lunar samples - using anorthosite clasts in Apollo 16 and lunar meteorite regolith breccias. They used cathodoluminescence imaging and FTIR spectroscopy to show that meteorite impact had distorted and disordered plagioclase lattice structures in these rocks. They further noted that some regolith breccias that have been classified as being 'pristine' (e.g., 66035), do display some evidence for shock damage.

Maskelynite - shock-transformed diaplectic glass

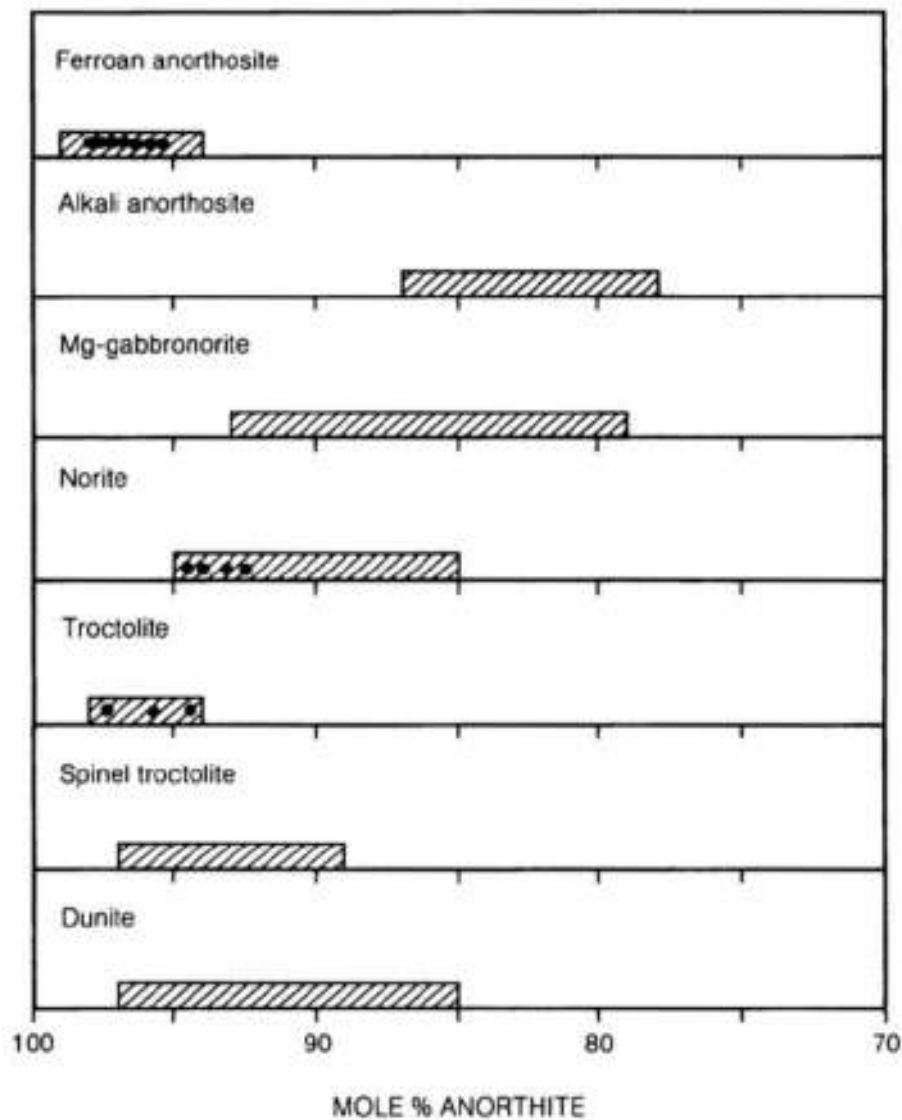
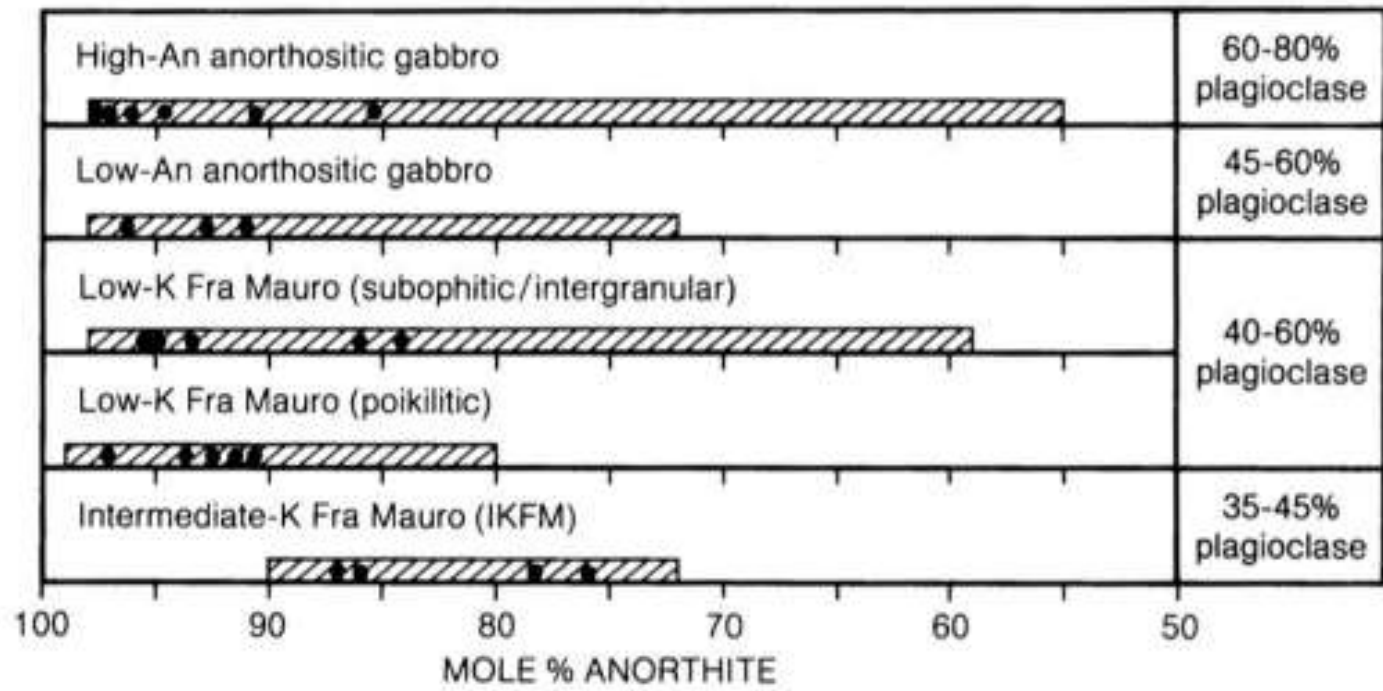
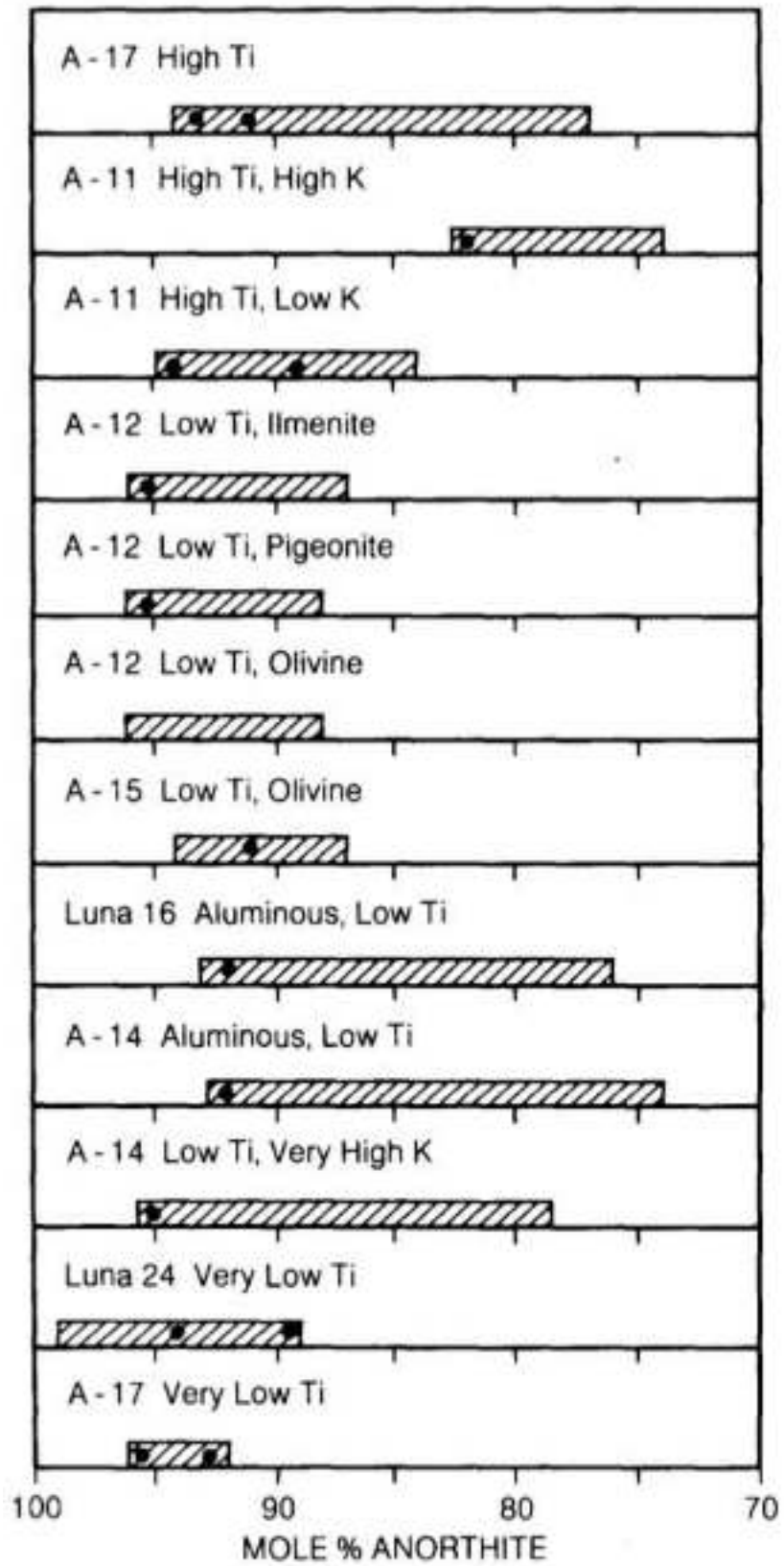
On the Moon, meteoroid impact and shock-metamorphic processes play a major role in altering rocks. Maskelynite is formed when shock damage leads to the formation of shock glasses (sometimes described as diaplectic glasses) from original plagioclase feldspar. It is rare (~1%) among mare basalts and basaltic fragments in Apollo 11, 12, 15 and 17 soils, but about 30% of lunar basaltic meteorites are maskelynite rich. Most notable of these basaltic meteorites are:

(1) Dhofar 287, a basalt in which plagioclase was totally converted into maskelynite; (2) NEA 003, a basaltic breccia in which plagioclase was totally converted into maskelynite; (3) MIL 05035, a basalt containing maskelynite; (4) NWA 2727, a basaltic-gabbroic breccia in which plagioclase was partially converted into maskelynite; (5) NWA 2977, a gabbro in which plagioclase was partially converted into maskelynite; (6) NWA 4734, an extensively shocked rock with a “shergottite-like” texture that contains plagioclase laths partly transformed into maskelynite; and (7) NWA 4898, a basalt with plagioclase laths completely transformed into maskelynite (Rubin, 2015).

Maskelynite has been reported in only three non-basaltic lunar meteorites: (1) NWA 3163, a feldspathic granulitic impactite in which plagioclase has been almost entirely converted into maskelynite; (2) NWA 4483, a granulitic breccia in which plagioclase has been mainly converted into maskelynite; and (3)

NWA 4881, a granulitic breccia in which plagioclase has been partially converted into maskelynite (Rubin, 2015).

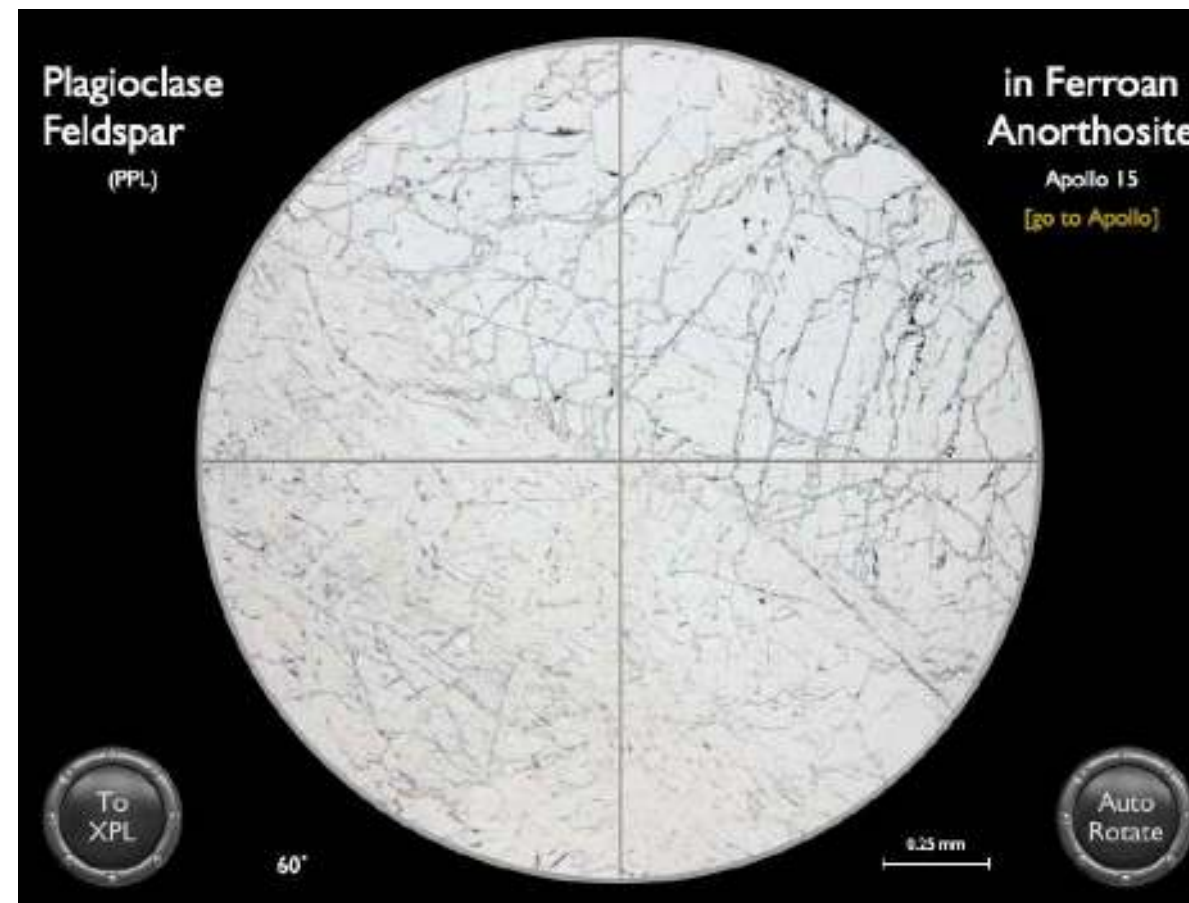
Lunar meteorite Dhofar 026 is a strongly shocked granulitic breccia (or a fragmental breccia consisting almost entirely of granulitic breccia clasts) that experienced considerable post-shock heating, probably as a result of diffusion of heat into the rock from an external, hotter source. Maskelynite in this sample indicates that the shock pressure was between 30 and 45 GPa. The post-shock heating raised the rock’s temperature to about 1200°C; as a result, the maskelynite devitrified, and extensive partial melting took place. The melting was concentrated in pyroxene-rich areas; all pyroxene melted. As the rock cooled, the partial melts crystallized with fine-grained, subophitic-poikilitic textures (Cohen et al., 2004).



Plagioclase mole% anorthite variation $[100 \cdot Ca / (Ca + Na)]$ in lunar mare basalts (left); in highland breccias, clast-poor melt rocks, and KREEP rocks (top right); in highland coarse-crystalline igneous rocks - i.e. ferroan anorthosite, alkali anorthosite, and five types of Mg-rich rocks (bottom right). Dots represent analyses presented in Heiken et al. (1991).

Moon Minerals: Plagioclase Feldspar

Mineral Virtual Microscope: Plagioclase Feldspar



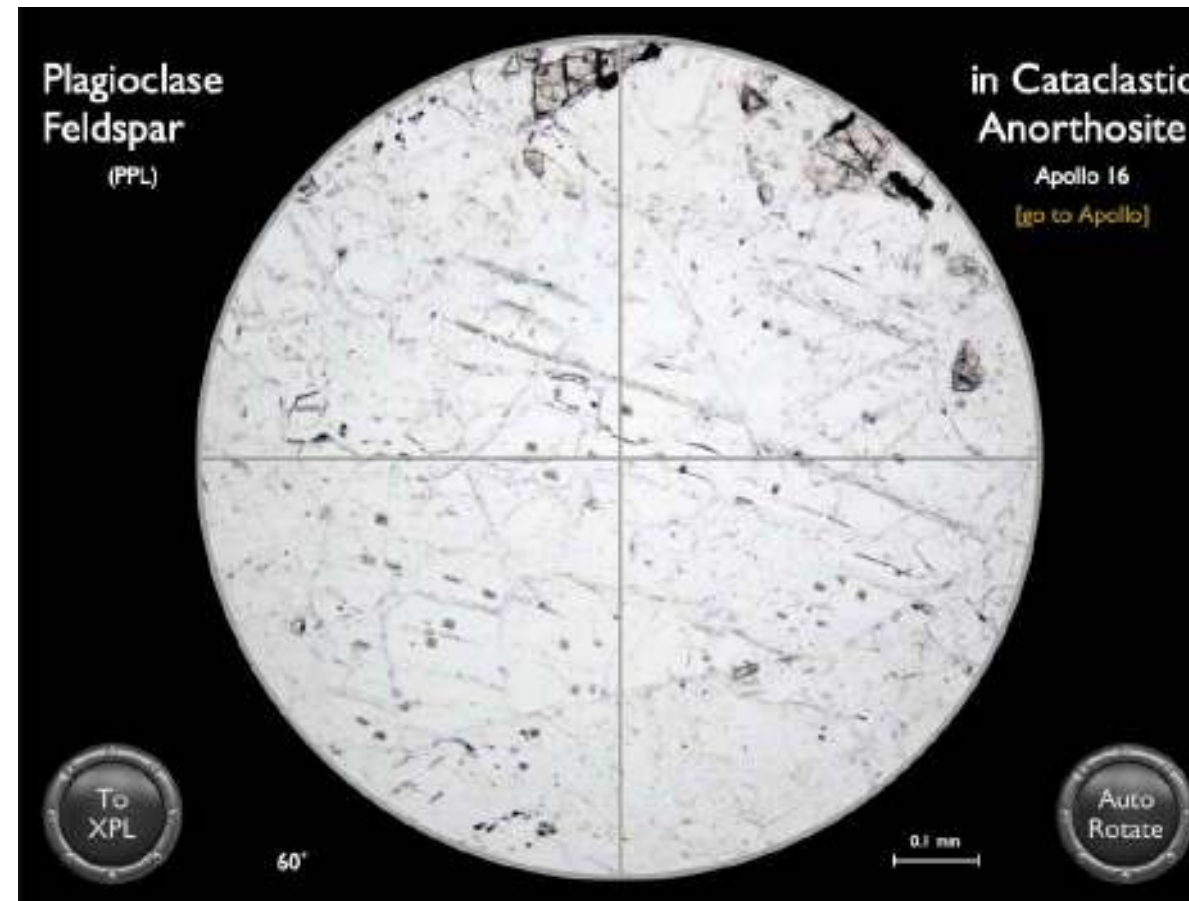
15415 is a ferroan anorthosite - a coarse-grained plagioclase-rich rock containing 98% of plagioclase feldspar and minor pyroxene, ilmenite and silica. The grain size of the plagioclase reaches 1.8 cm. The grains show evidence of shock cracking and fracturing.

Apollo 15, Sample 15415.

Credit: NASA (AGT Photographer)

Moon Minerals: Plagioclase Feldspar

Mineral Virtual Microscope: Plagioclase Feldspar



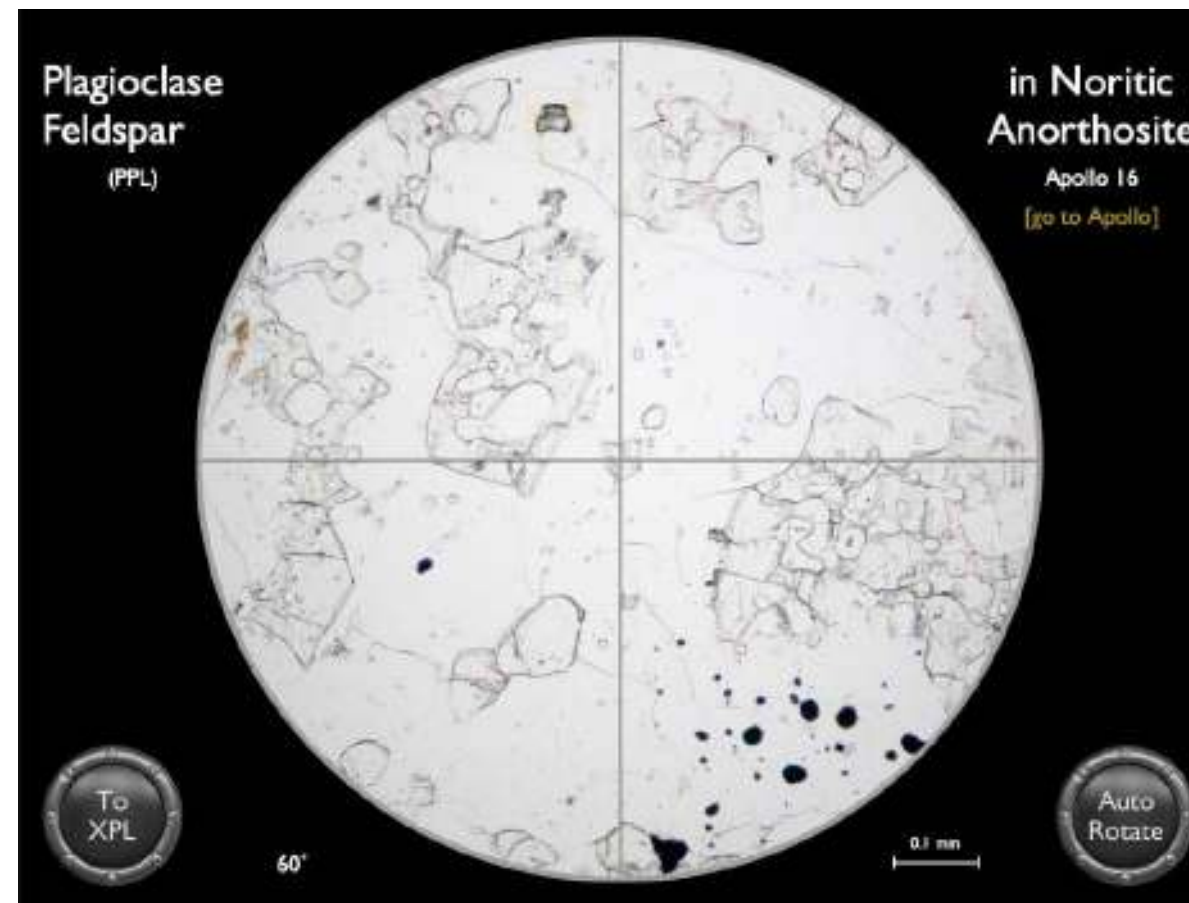
60519 is a small rake sample from the lunar module site at Apollo 16. It is a cataclastic anorthosite – of the ferroan variety. The virtual microscope shows an angular plagioclase feldspar clast containing shock deformation features.

Apollo 16, Sample 60518.

Credit: NASA (AGT Photographer)

Moon Minerals: Plagioclase Feldspar

Mineral Virtual Microscope: Plagioclase Feldspar



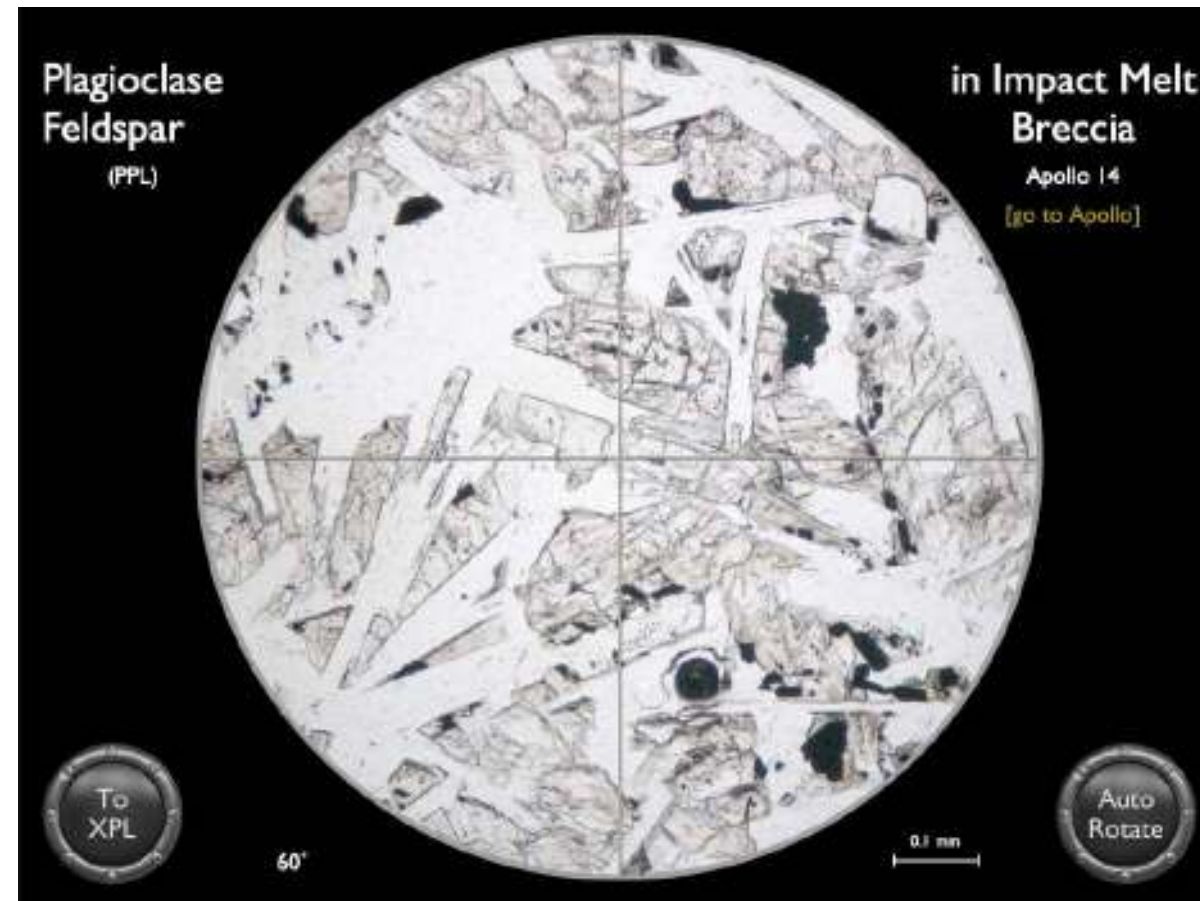
67746 is a small rake sample with an unusual granoblastic texture and unusual rare earth element pattern. Modally it has a granulitic poikilitic texture consisting of > 75 % plagioclase feldspar associated with pyroxene.

Apollo 16, Sample 67746.

Credit: NASA (AGT Photographer)

Moon Minerals: Plagioclase Feldspar

Mineral Virtual Microscope: Plagioclase Feldspar



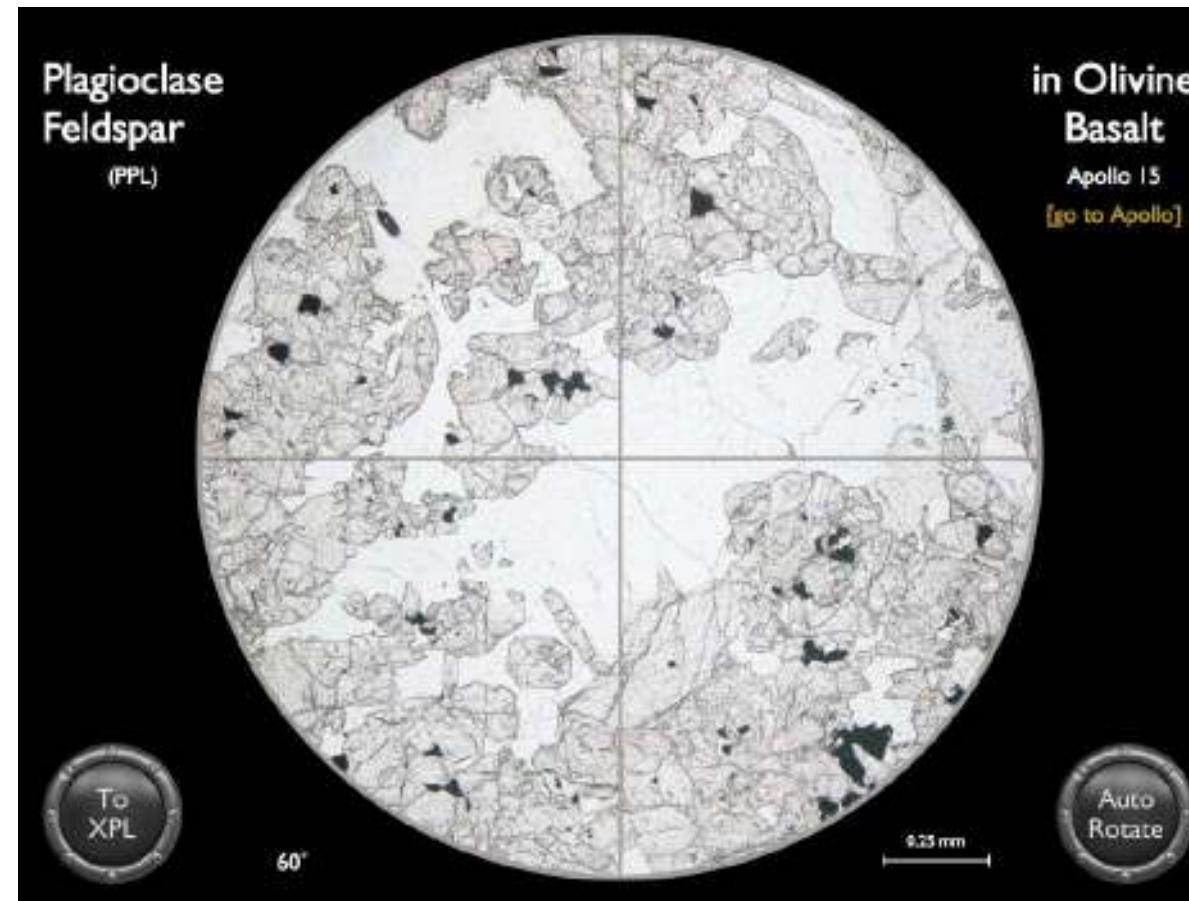
14310 appears to be a fine grained crystalline igneous basalt but its chemistry reveals it to be derived from a lunar soil that has been welded into a rock by shock melting during a meteorite impact. It is a fine-grained feldspathic basalt with intersertal texture consisting of lath-like plagioclase and anhedral pyroxene.

Apollo 14, Sample 14310.

Credit: NASA (AGT Photographer)

Moon Minerals: Plagioclase Feldspar

Mineral Virtual Microscope: Plagioclase Feldspar



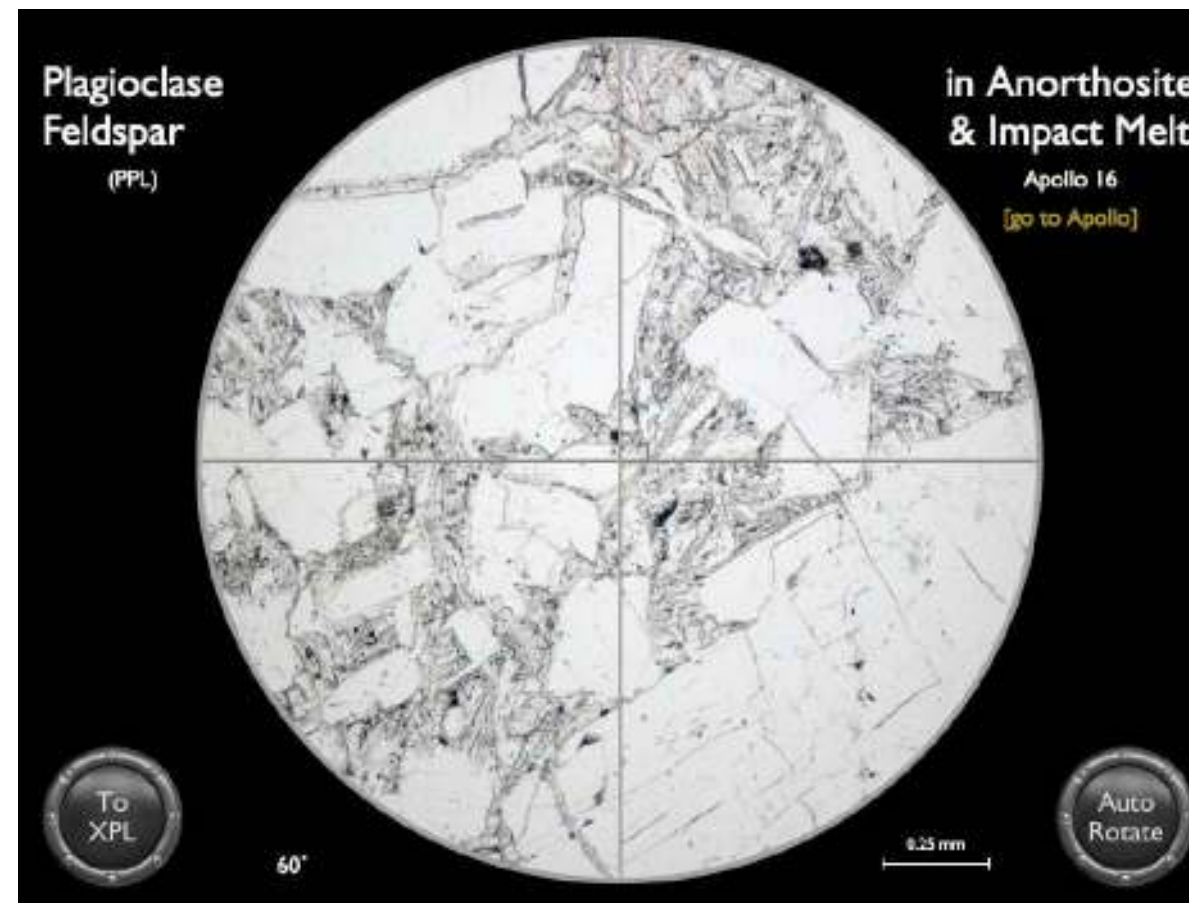
15607 is a Mare basalt with an intergranular texture consisting of numerous small olivine and pyroxene grains embedded in larger plagioclase crystals. Plagioclase crystals are lath-shaped and up to 2mm long. In the example here the twin lamellae are slightly curved. Interstitial phases include fayalite, cristobalite, chromite, ilmenite, spinel, troilite and K-rich glass.

Apollo 15, Sample 15607.

Credit: NASA (AGT Photographer)

Moon Minerals: Plagioclase Feldspar

Mineral Virtual Microscope: Plagioclase Feldspar



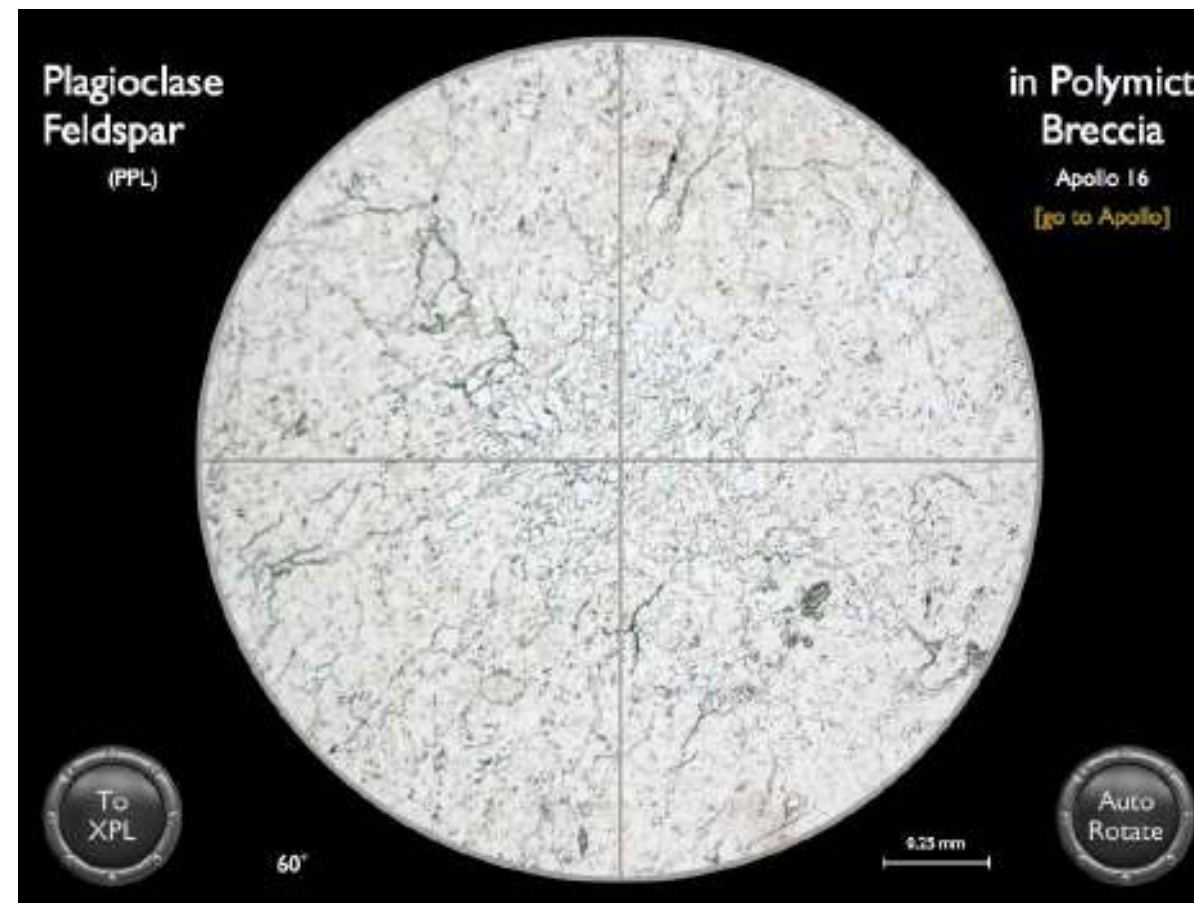
60618 is composed of two lithologies - anorthosite and impact-melt rock. The impact-melt rock portion contains many relatively large equant (0.5 mm) plagioclase grains (which are relicts) and plagioclase needles (up to 0.5 mm) which crystallized from the melt.

Apollo 16, Sample 60618.

Credit: NASA (AGT Photographer)

Moon Minerals: Plagioclase Feldspar

Mineral Virtual Microscope: Plagioclase Feldspar



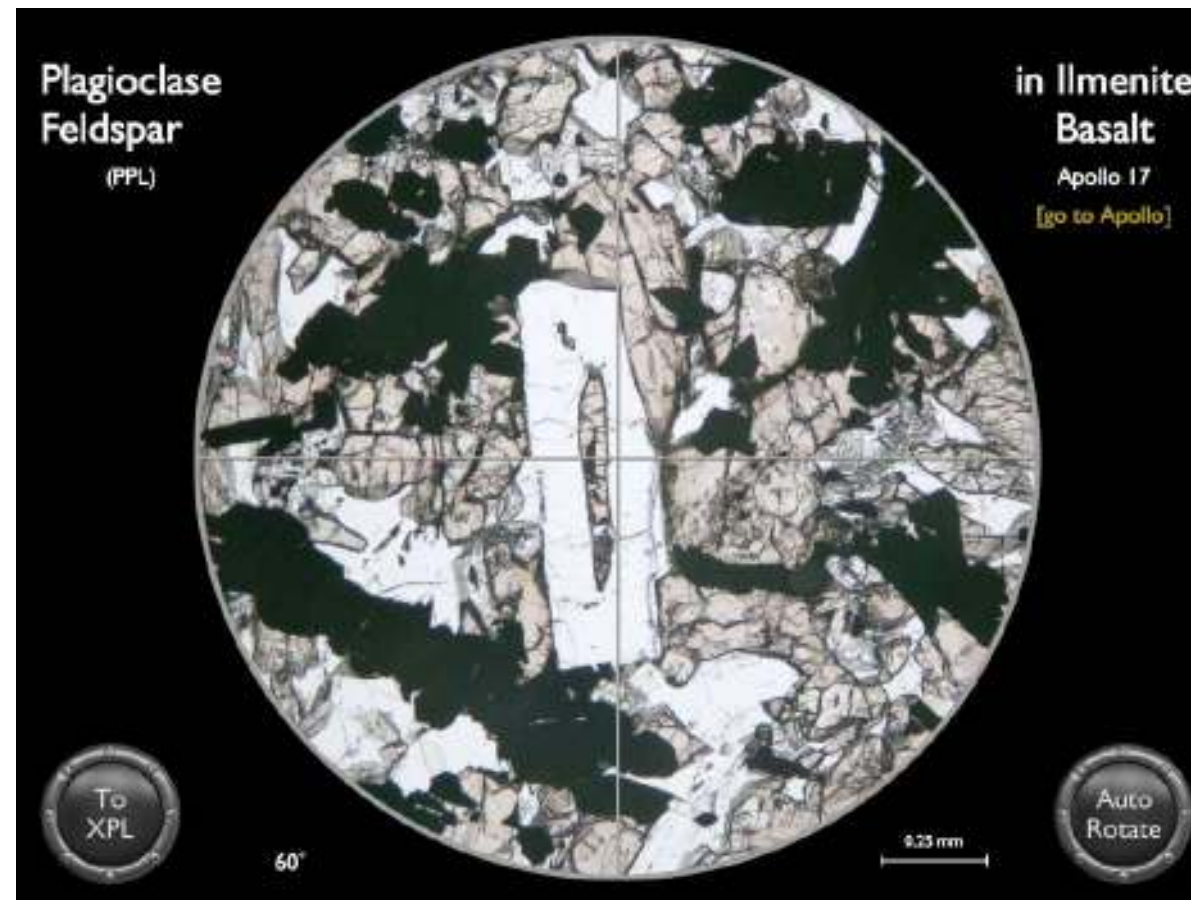
60659 contains two distinct lithologies dominated by cataclastic anorthosite. Shocked plagioclase feldspar is abundant in both lithologies, and in this field of view shows distorted lamellar twinning in the central crystal.

Apollo 16, Sample 60618.

Credit: NASA (AGT Photographer)

Moon Minerals: Plagioclase Feldspar

Mineral Virtual Microscope: Plagioclase Feldspar



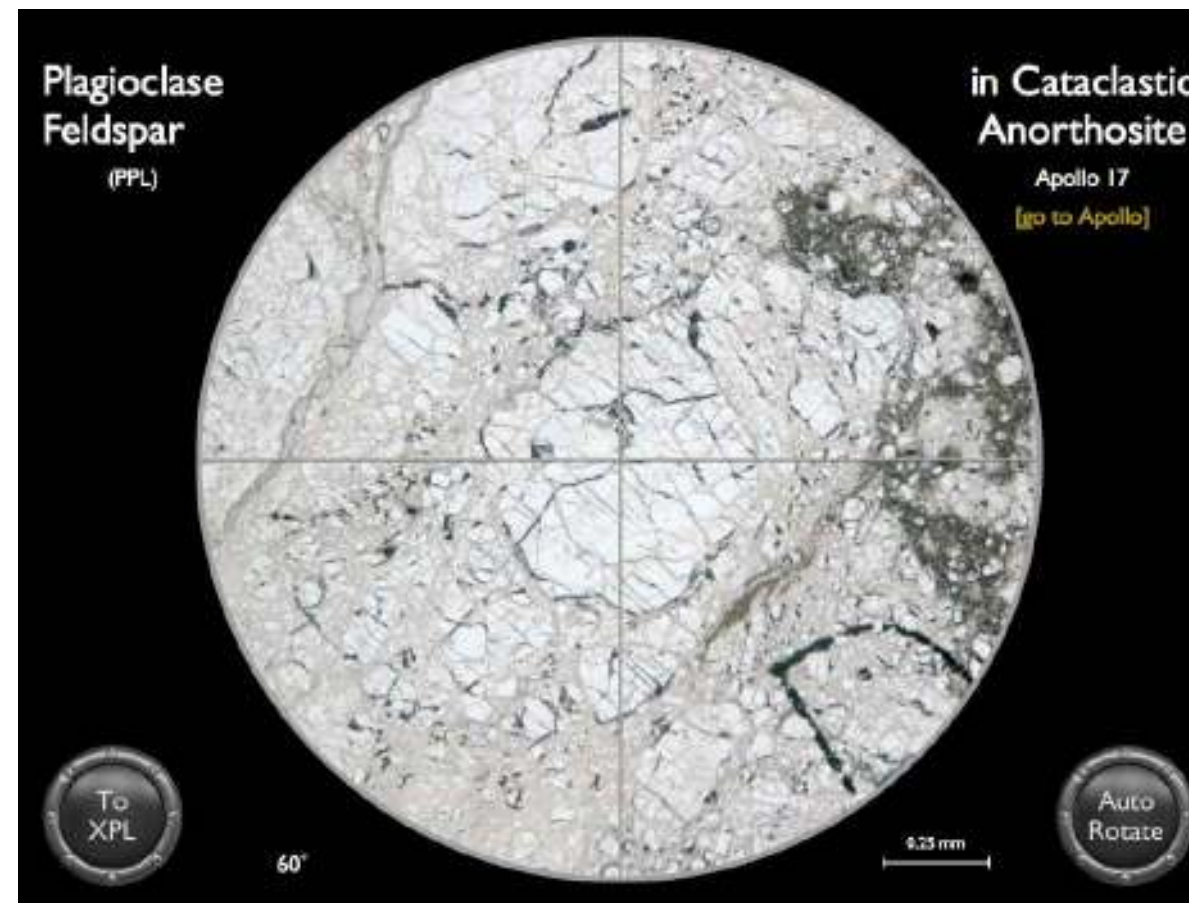
71055 is an ilmenite basalt with an intrafasciculate texture consisting of plagioclase feldspar laths containing early crystallized pyroxene.

Apollo 17, Sample 71055.

Credit: NASA (AGT Photographer)

Moon Minerals: Plagioclase Feldspar

Mineral Virtual Microscope: Plagioclase Feldspar



76335 is a highly shocked anorthosite. It contains an orthopyroxene dominated assemblage which includes orthopyroxene, olivine, and as shown here - highly crushed plagioclase feldspar. These crystals are heavily fractured and display anomalous wavy extinction.

Apollo 17, Sample 76335.

Credit: NASA (AGT Photographer)

Moon Minerals: Plagioclase Feldspar

Mineral Virtual Microscope: Plagioclase Feldspar

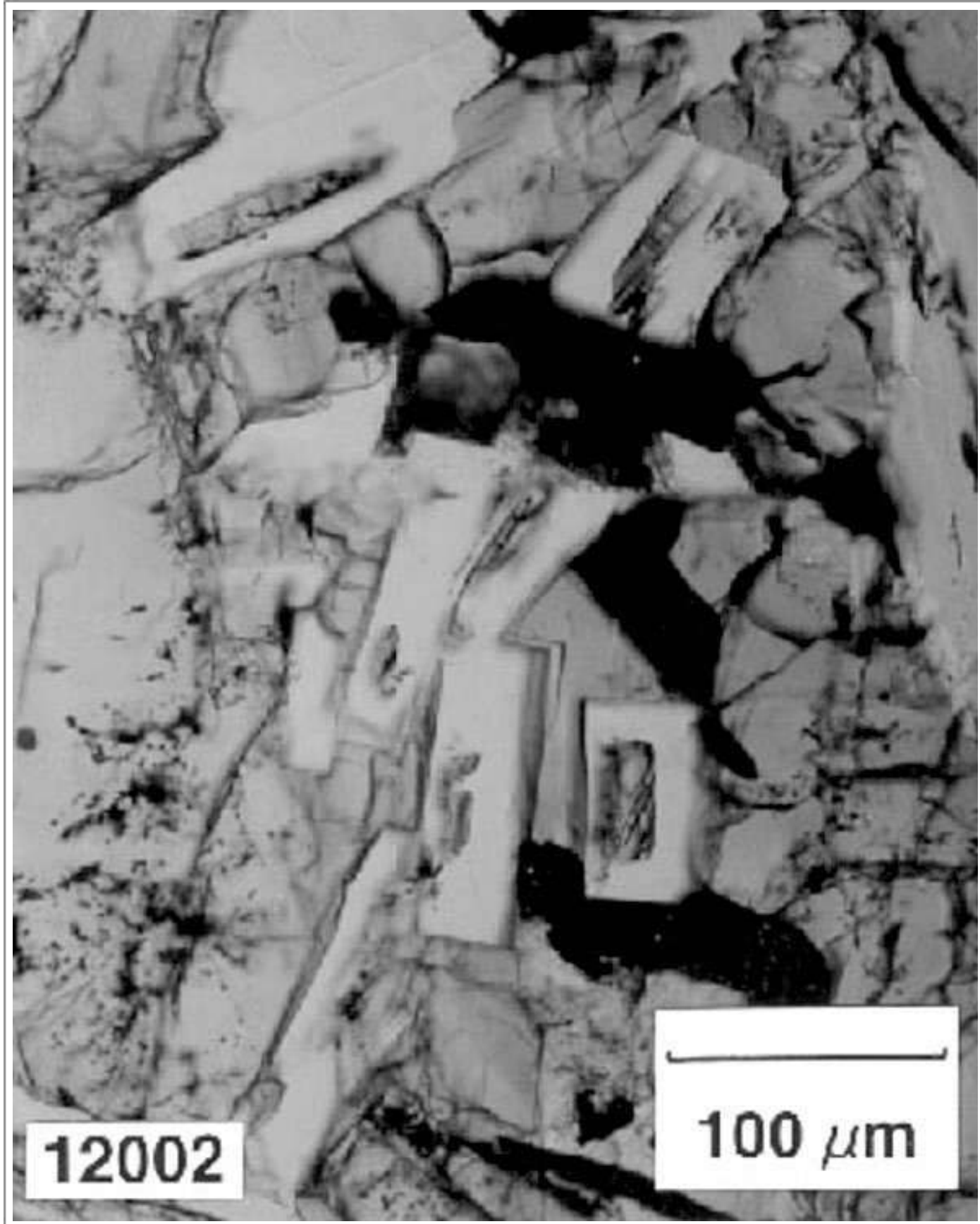


78238 is a heavily-shocked norite of cumulate origin with a glass coating and glass veins. Cumulus orthopyroxene and plagioclase feldspar are the main species present. Both minerals are partially shattered and display anomalous wavy extinction. Elsewhere in this thin section much of the plagioclase is converted to maskelynite. The elongate dark feature is partially devitrified impact melt.

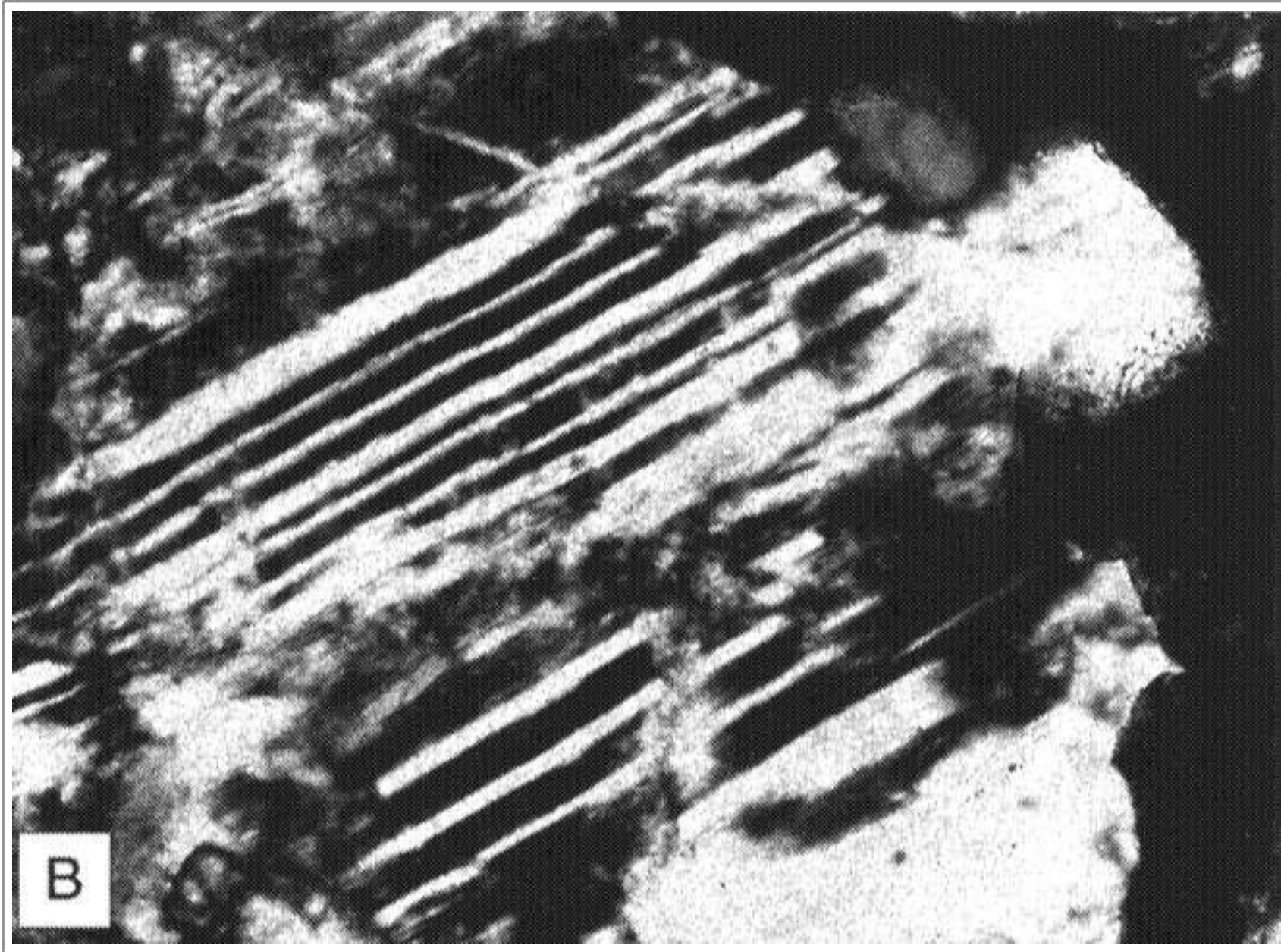
Apollo 17, Sample 78238.

Credit: NASA (AGT Photographer)

Transmitted light image (ppl) of Apollo 12 low-Ti basalt 12002 showing intrafasciculate texture of plagioclase laths. Bundles of hollow plagioclase crystals are intergrown with pyroxene (medium grey), ilmenite (black) and mesostasis.

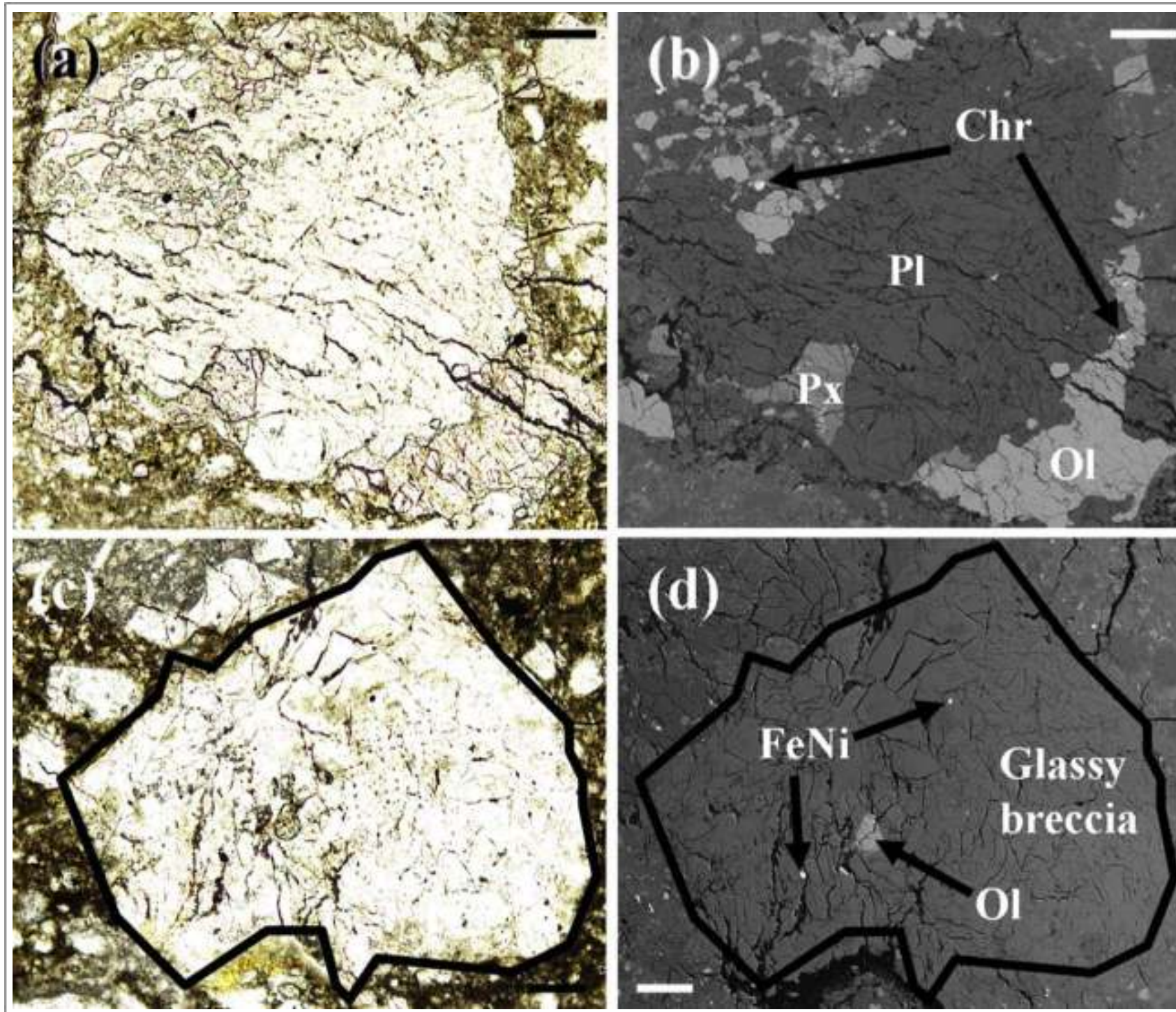


Taken From Meyer (2003)



Taken From Norman et al. (2003)

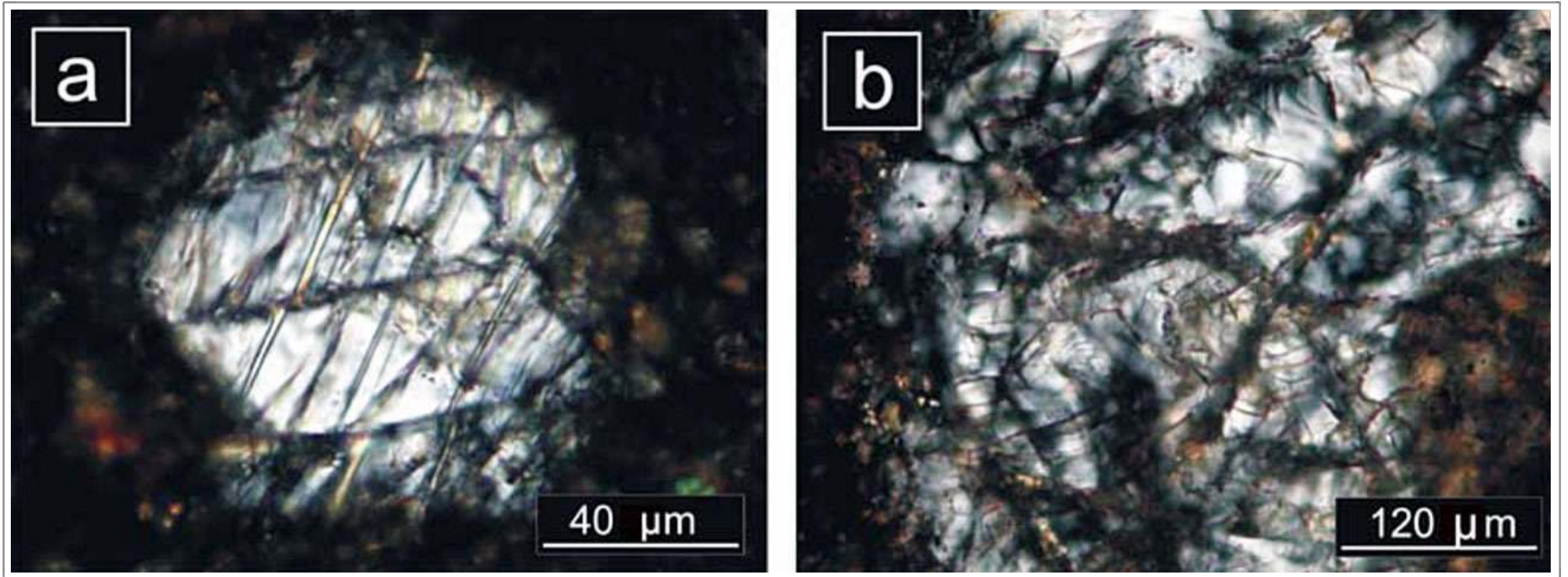
Plagioclase feldspar in Apollo 16 fragmental polymict breccia 67215 showing shock features and igneous twinning (between crossed polars).



Taken From Nagaoka et al. (2013)

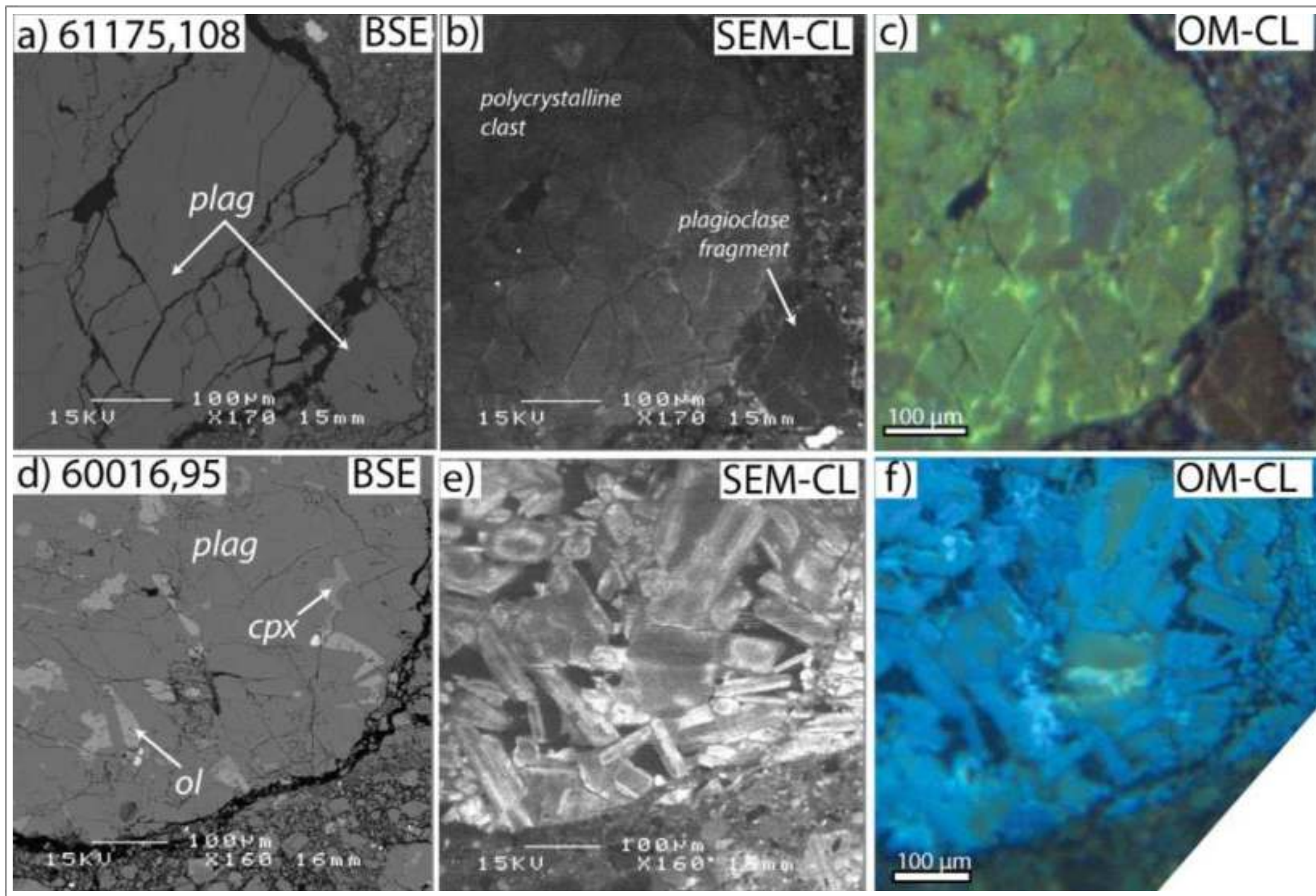
Images of plagioclase feldspar-rich clasts in lunar meteorite NWA 2200. (a, b) plane polarised light and backscattered electron image of a ferroan anorthositic granulitic breccia. (c, d) plane polarised light and backscattered electron image of the poikiloblastic granulitic breccia.

Scale bar is 0.1 mm. Pl = plagioclase, Px = pyroxene, Ol = olivine, Chr = chromite, FeNi = metallic iron.



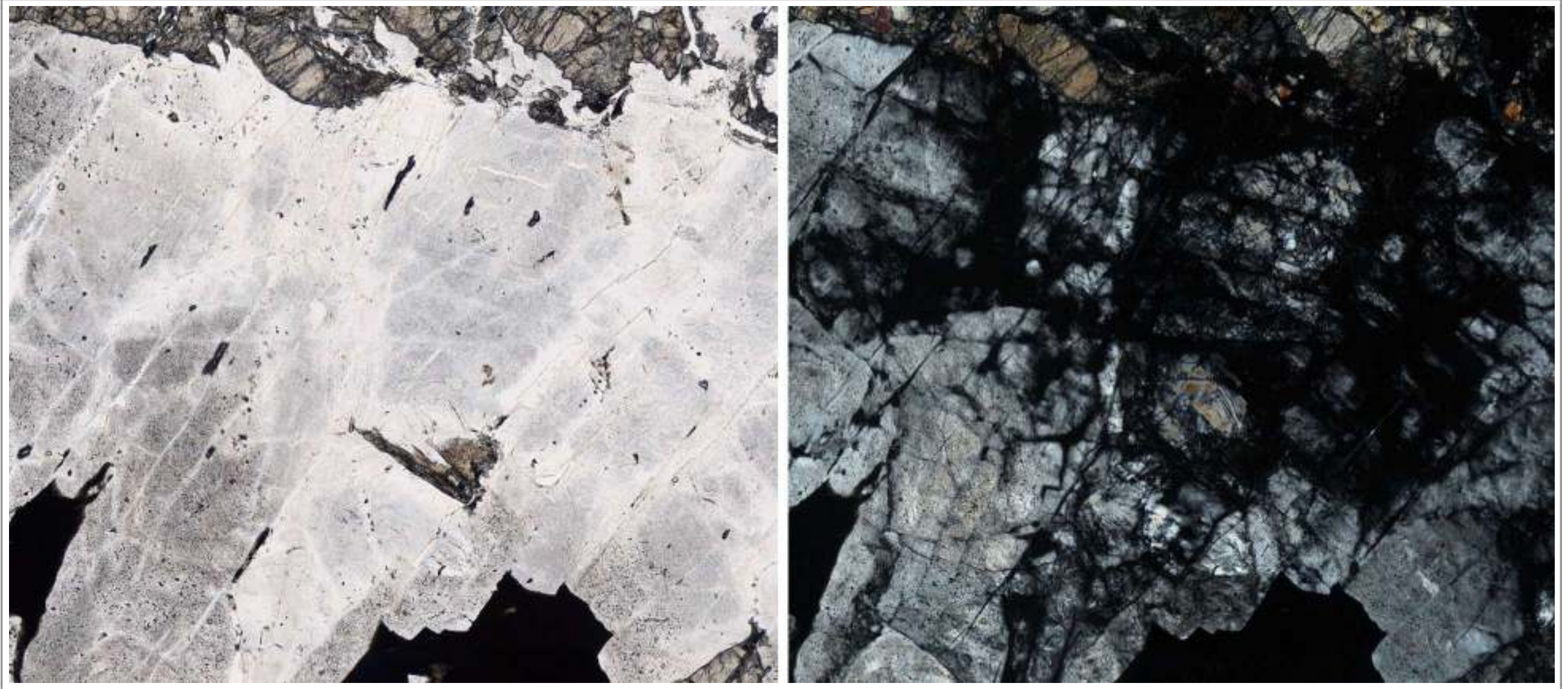
Taken From Hudgins et al. (2007)

Transmitted light images of plagioclase feldspar in lunar meteorite SaU 300 - an impact-melt breccia. a) anorthite mineral fragment showing mechanical deformation (offsetting of twin planes). b) internally brecciated anorthite clast with patchy maskelynitization.

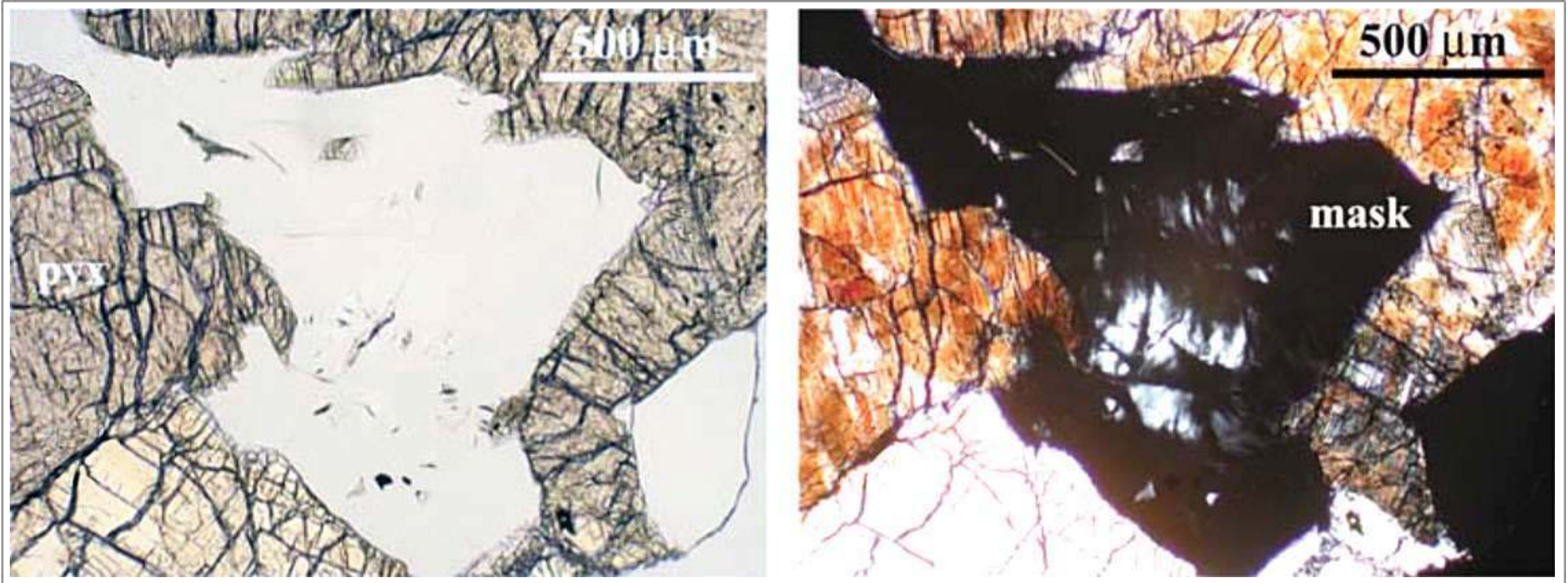


Taken From Pernet-Fisher et al. (2016)

Backscattered electron (BSE), Scanning electron microscope cathodoluminescence (SEM-CL), and optical microscope cathodoluminescence (OM-CL) images of polycrystalline clasts within Apollo 16 breccia 61175,108 and 60016,95. Mafic minerals (bright intensities in BSE) do not luminesce due to their high-Fe content. The complex crystalline nature of these clasts are clear in the CL images. Clast in sample 61175,108 displays predominantly green/yellow emission characteristic of an unshocked plagioclase. Sample 60016,95 clast displays predominantly blue emission characteristic of highly shocked plagioclase.



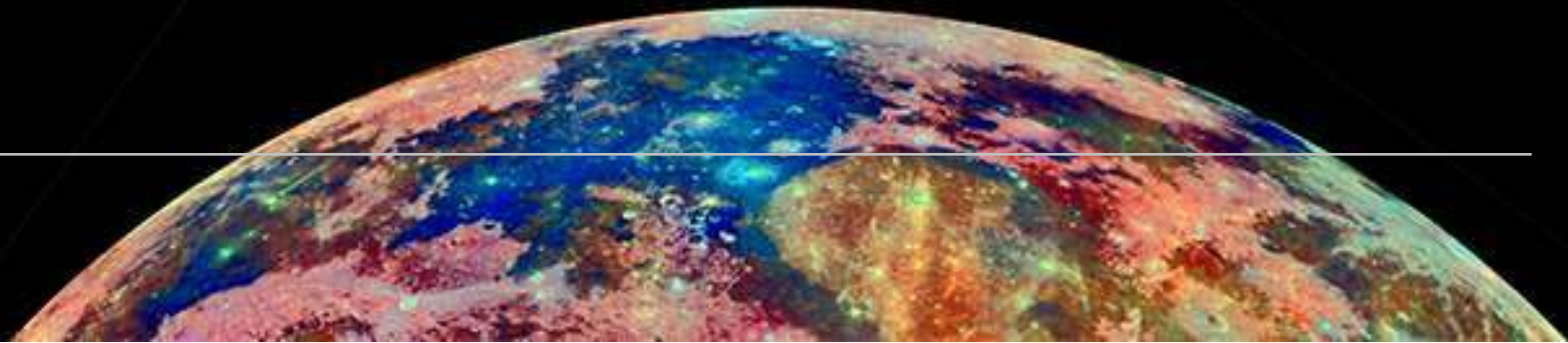
Transmitted light images (ppl and xpl) of plagioclase feldspar partially altered to maskelynite in Apollo 17 norite 78235. The black material just visible at the bottom of the image is a glassy melt vein formed due to shock during meteorite impact. Field of view 4.4 mm across. Credit: NASA (AGT Photographer).



Taken From Liu et al. (2009)

Transmitted light images (ppl and xpl) of partially recrystallized maskelynite grains surrounded by pyroxene in basaltic lunar meteorite MIL 05035.

Ilmenite



SPECIES

1. Ilmenite - $\text{Fe}^{2+}\text{TiO}_3$

Ilmenite is the most abundant oxide mineral in lunar rocks. The amount of ilmenite in these rocks is a function of the bulk composition of the magma from which the ilmenite crystallized; the higher the TiO_2 content of the original magma, the higher the ilmenite content of the rock. Ilmenite forms as much as 15-20% by volume of many Apollo 11 and 17 mare basalts (McKay and Williams, 1979). However, the volume percentages of ilmenite in mare basalts vary widely across the Moon as indicated by the range of TiO_2 contents in samples from different lunar missions.

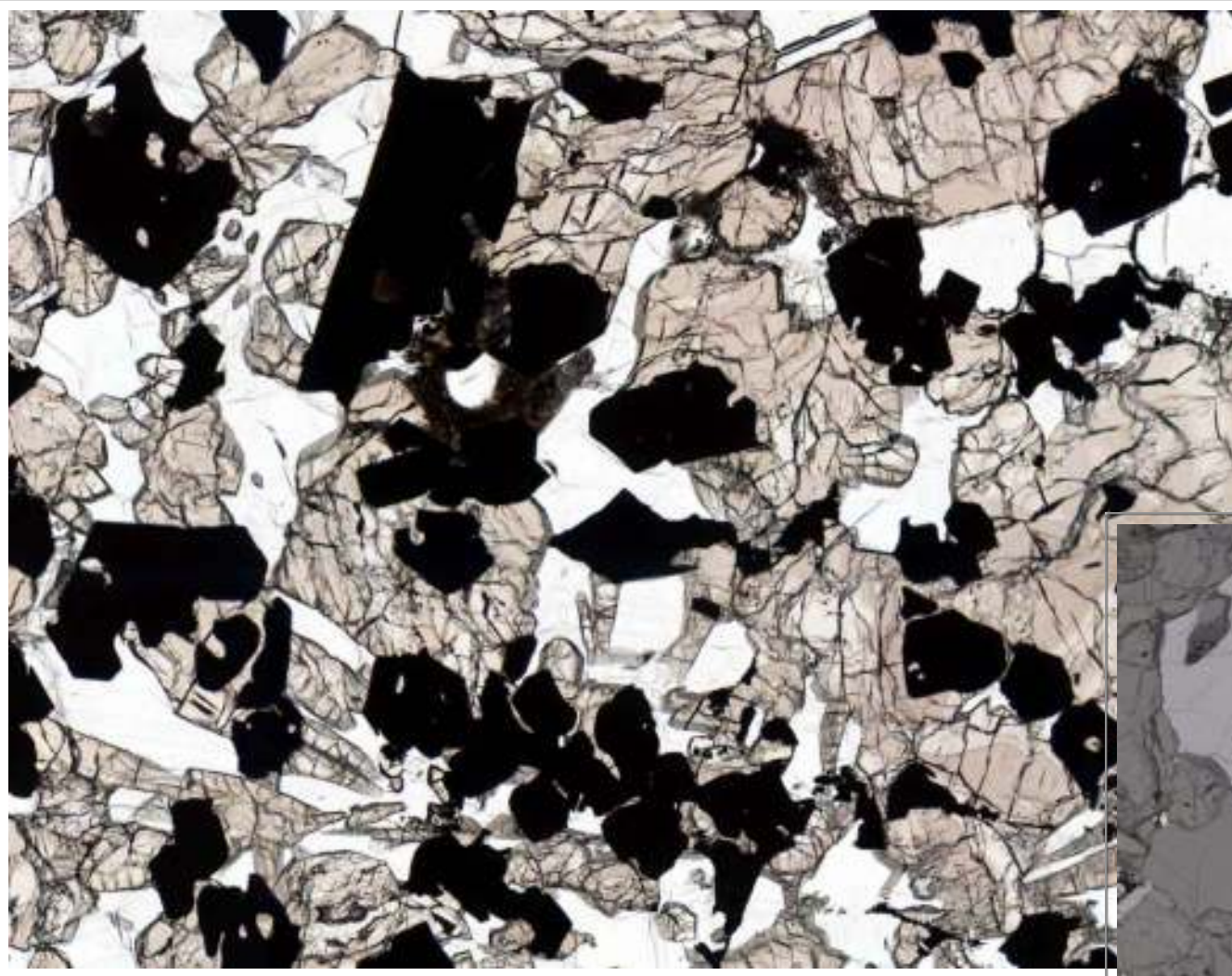
Lunar petrologists have argued that high-Ti basalts can be produced by partial melting of an ilmenite-bearing cumulate lunar mantle or partial melting of the lunar mantle followed by assimilation of ilmenite as the melt migrated to the lunar surface. In either scenario, ilmenite is an important component of the lunar basalt source region (Dygert et al., 2015).

Ilmenite in Apollo 17 ilmenite basalt 75035 has been studied in some detail. Ilmenite is the third most abundant species in this rock (at 17%) and occurs as medium to coarse tabular, subhedral laths comparable in size to plagioclase feldspar (Meyer and Boctor, 1974).

Ilmenite commonly occurs in mare basalts as bladed crystals up to a few millimeters long. It typically forms near the middle of the crystallization sequence, where it is closely associated with pyroxene. It also forms later in the sequence

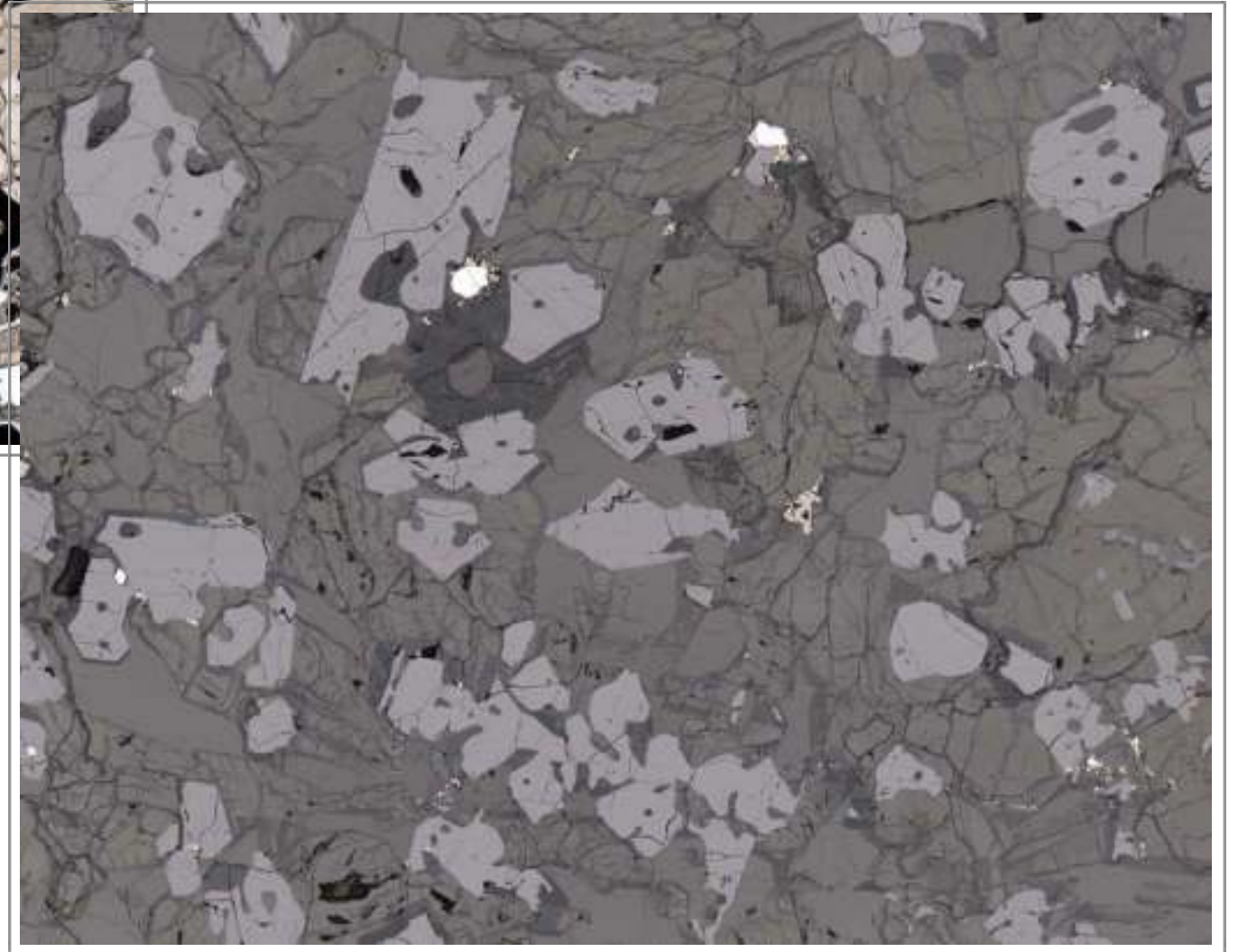
and at lower temperatures, where it is associated with native iron and troilite. In Apollo 17 rocks, ilmenite often mantles armalcolite crystals (Haggerty, 1973a; Williams and Taylor, 1974). In these instances, ilmenite has possibly formed by the reaction of earlier armalcolite with the melt during crystallization (Heiken et al., 1991).

Although terrestrial ilmenite almost always contains some Fe³⁺, lunar ilmenite contains none because magmatic conditions are more reducing on the Moon (Heiken et al., 1991).

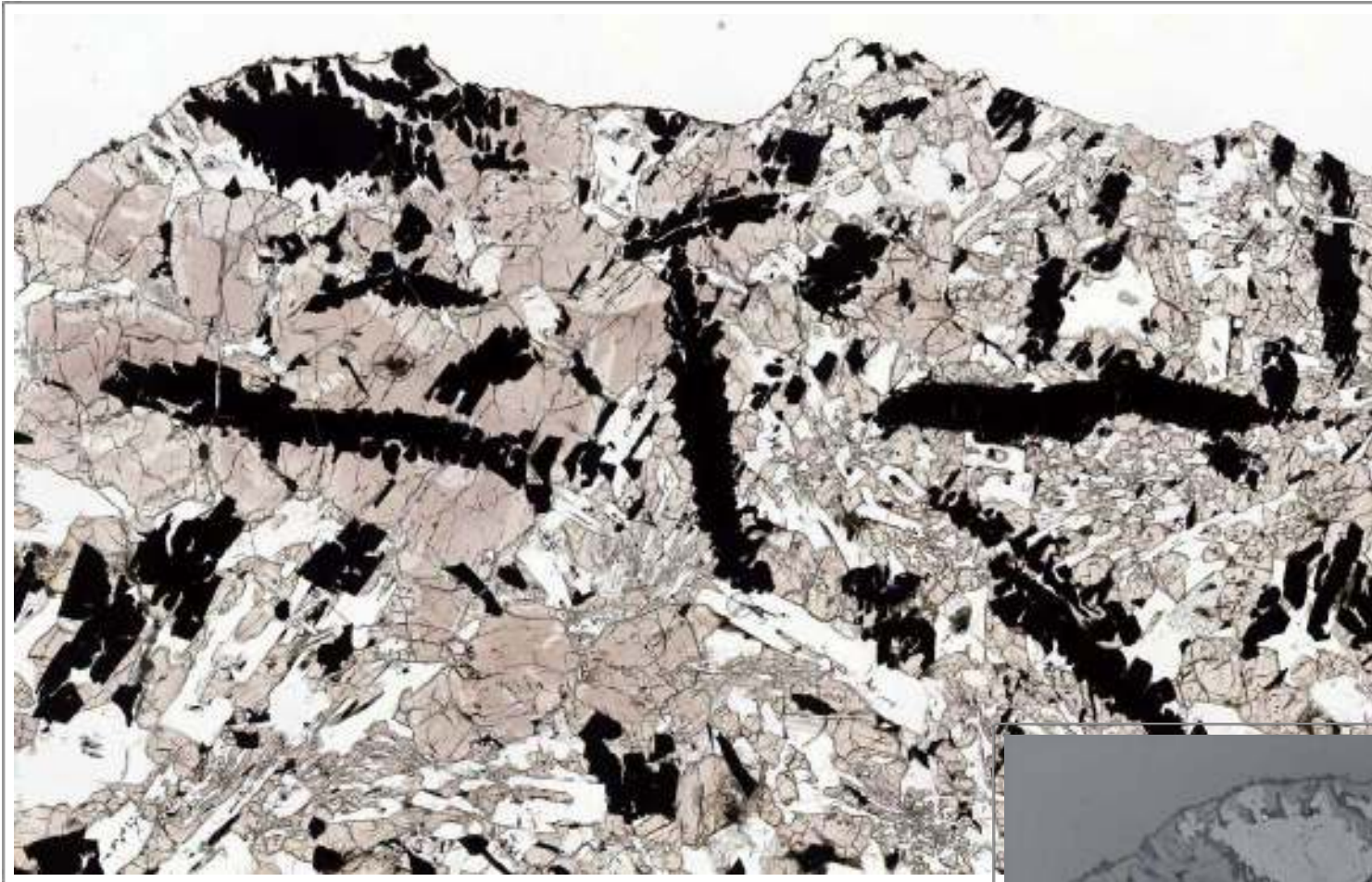


Plane polarised light

Apollo 17: 70017 is a high-titanium mare basalt with a relatively coarse grain size indicating that this basalt cooled relatively slowly. Ilmenite forms prismatic to sub-rounded crystals (light grey in reflected light) and is associated with large poikilitic pyroxene (brown) and plagioclase feldspar (colourless in PPL). Cristobalite, the high temperature form of quartz is present in interstices between pyroxene, plagioclase and ilmenite. Minor amounts of olivine, troilite (yellow in reflected light), metallic iron (white in reflected light) and chromite are also present.

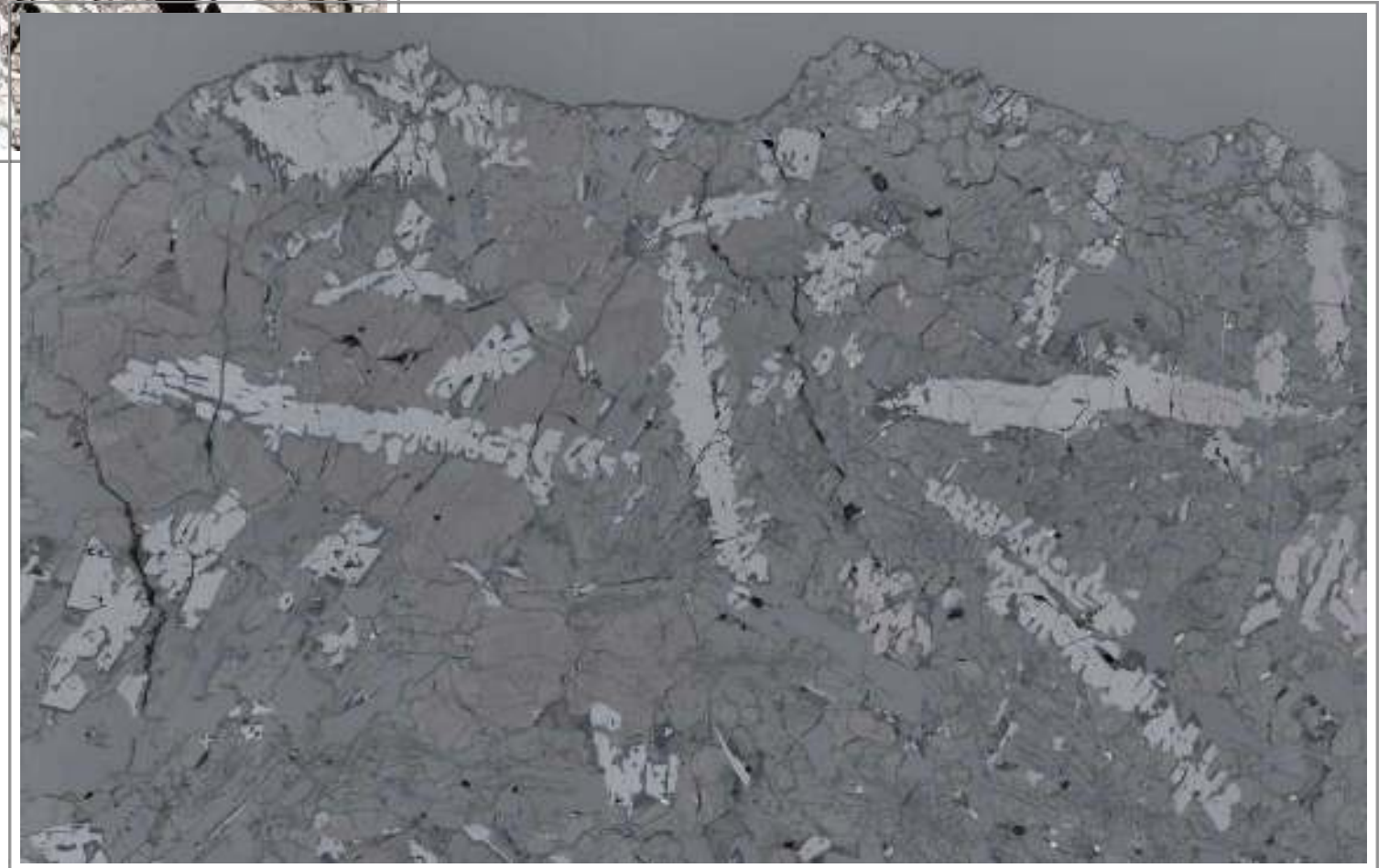


Reflected light



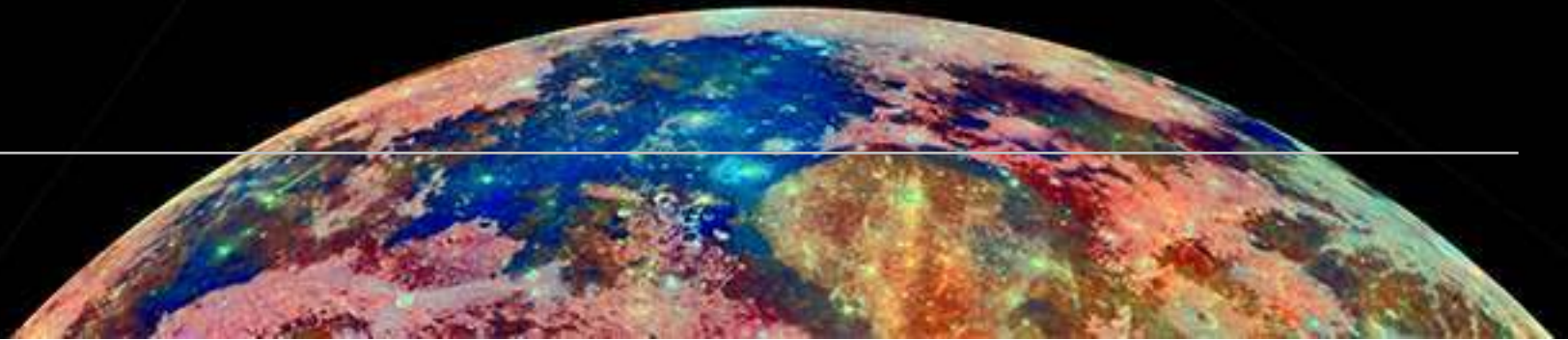
Plane polarised light

Apollo 17: 71035 is a high-titanium mare basalt containing pyroxene, plagioclase feldspar and skeletal ilmenite (light grey in reflected light).



Reflected light

Glass



1. Impact-melt Glass

2. Volcanic (fire-fountain) Glass

In an investigation of melt rocks from Apollo 16, Dowty et al. (1974) concluded that samples 60666, 65779, 60615, 60618, 65795 and 60635 all crystallized very rapidly from liquids derived from heterogeneous highland rocks - either from partial melting in the lunar interior or from shock melting due to impact on or near the surface. Petrographic features consistent with shock melting include: the presence of relict crystals or xenoliths; small-scale textural homogeneities; presence of schreibersite-sulphide blebs. The evidence for such an origin is, however, not conclusive.

A similar origin has been proposed for the Apollo 17 green glass vitrophyre 78526 although the bulk composition suggests impact melting of at least two different varieties of mare basalt (Warner et al., 1978).

A very different origin for Apollo 15 green glass 15410 and related beads has been proposed by Keppta et al. (2014). These authors show the glass was formed in gas-rich fire fountains. As the magmatic fluid became super-saturated in volatile gas, bubbles or vesicles formed within the magma. These exsolved gases became trapped within vesicles as the glasses were ejected from the fire-fountain and subsequently quenched.

Petrogenetic modelling of similar green glass beads, some of picritic composition, from Apollo 15 sample 15426,72 revealed they could not be formed by a

continuous assimilation and fractional crystallization process. After an initial intrusive event, a picritic magma crystallized and provided heat to melt magma ocean cumulates. In a later replenishment event, the picritic magma incrementally mixed with the melted cumulate, ascended to the lunar surface and erupted as a fire fountain (Elkins-Tanton et al., 2003).

Perhaps the best example of a lunar fire-fountain deposit is the pyroclastic soil of Apollo 17 sample 74220. Orange volcanic glass spherules from this sample represent primary magma from the lunar mantle (Delano, 1996). If devitrified these spherules change colour to black and contain skeletal olivine crystals mantled by ilmenite. Some spherules contain fragments and euhedral crystals of endogenous olivine. Cooling rates of the orange melt droplets indicate they were erupted together with a large mass of hot gas and/or formed a dense cloud of heat-radiating droplets (Arndt and von Engelhardt, 1987).

Advances in secondary ion mass spectrometry (SIMS) techniques allowed Saal et al. (2008) to examine the CO₂, H₂O, F, S and Cl contents of lunar volcanic glasses and confirm the presence of indigenous water in the lunar interior. Their work was based on three main compositional groups of glasses: very low-Ti and low-Ti glasses (Apollo 15 - 15427,41), and high-Ti glasses (Apollo 17 - 74220,864). Radial concentration profiles of these elements within a single very-low-Ti glass bead show that volatile contents decrease from core to rim, and indicate such glasses were

affected by degassing upon eruption. It was suggested that the beads lost approximately 19% S, 45% F, 57% Cl and 98% H₂O and that the pre-degassing H₂O content was at least 260 ppm - the best fit being obtained for an initial H₂O content of 745 ppm.

Further work by these authors (Saal et al., 2013, Hauri et al., 2017) show that lunar magmatic water has an isotopic composition that is indistinguishable from that of the bulk water in carbonaceous chondrites and similar to that of terrestrial water, implying a common origin for the water contained in the interiors of the Earth and the Moon.

Picritic glass beads, including those from Apollo 17 sample 74220, were analysed for Fe³⁺ by McCanta et al. (2016) using X-ray Absorption Spectroscopy. Values ranged from 1 to 60% Fe³⁺. No correlation with melt chemical properties, such as Mg# or weight % TiO₂, or physical properties, such as bead diameter, was observed. The presence of low % Fe³⁺ values and beads zoned in redox concentrations may result from a combination of post-eruptive oxidation followed by subsequent reduction either in the lunar vacuum or in the dissipating gas cloud that may have been fairly reducing due to the addition of H from the degassing melt.

Glassy melt inclusions in olivine also occur in Apollo 17 sample 74220. These have been investigated by Ni et al. (2017) to constrain the model of Moon formation. Recently, the earlier understanding of a “dry” Moon has shifted to a fairly “wet” Moon

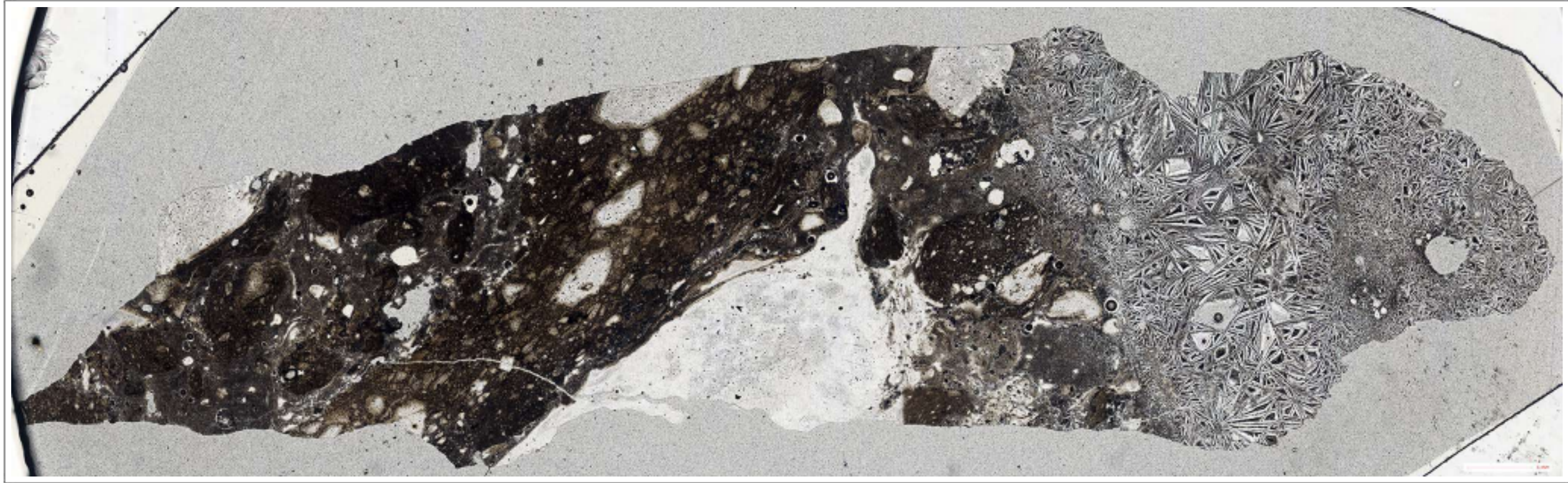
due to the detection of measurable amount of H₂O in lunar volcanic glass beads, apatite, olivine-hosted melt inclusions and plagioclase in lunar highland anorthosites.

Melt inclusions have also provided clear evidence for liquid immiscibility on the Moon - in minerals that crystallized from mare basalts, within mesostasis in mare basalts and in one sample of a lunar plutonic rock. These inclusions are blade-like in shape and range in length from 2 to 150 µm. They consist of two coexisting glasses separated by a sharp meniscus. The colourless, low-index glass (felsite) is spherical and immersed in a dark-brown, high-index glass (high-Fe basalt). It is most likely that lunar felsites are a product of extensive fractionation followed by whitlockite fractionation and silicate liquid immiscibility (Shearer et al., 2001).

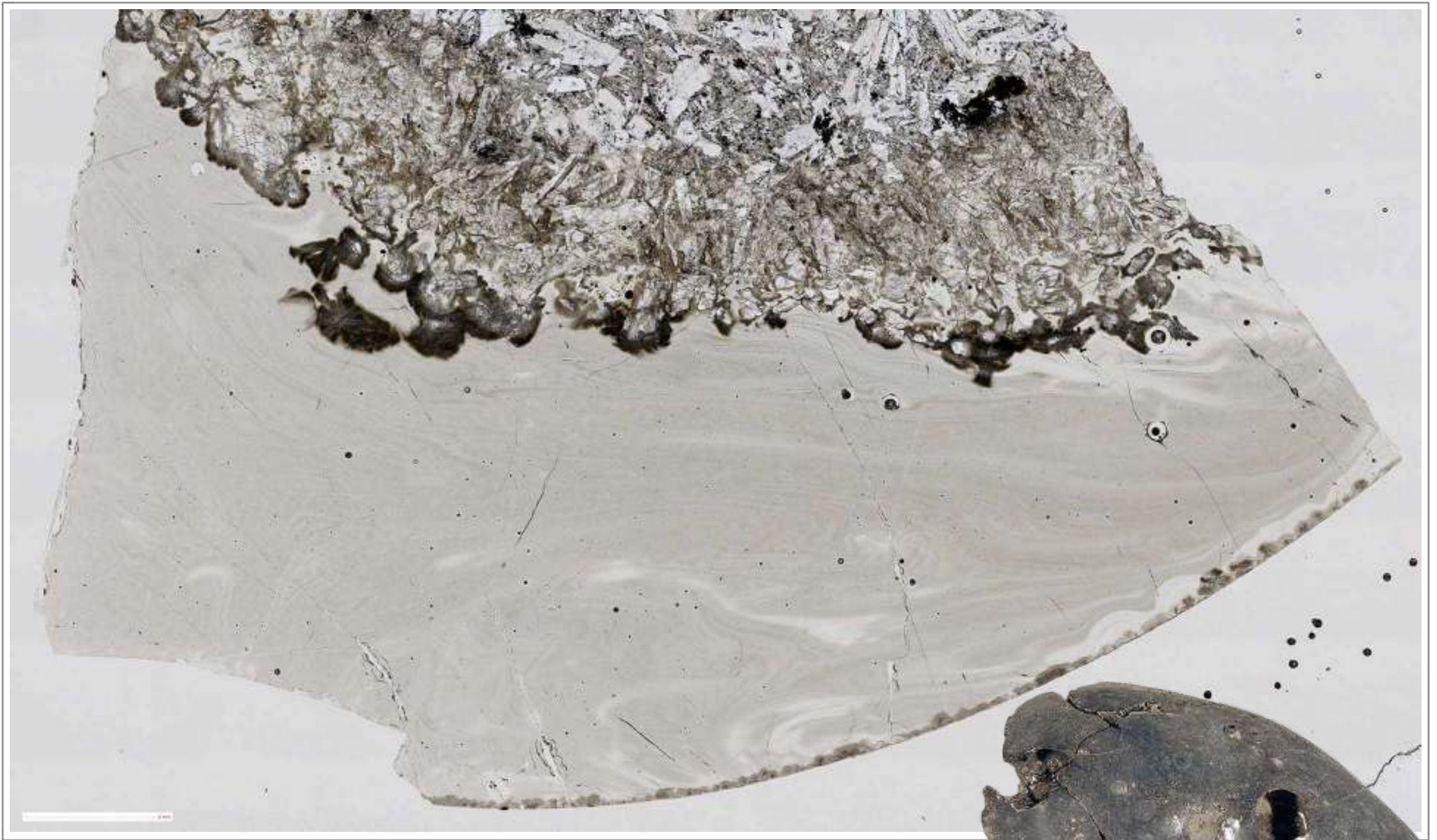
Lunar meteorite NWA 10404 is a feldspathic regolith breccia with a remarkable content of partly devitrified glass clasts. These clasts range from translucent to brown to green, with shapes from angular to round. All glass clasts are holohyaline with isotropic cores and 0.1-0.3 mm thick concentric rims of spherulitic crystallites, implying reactions with the matrix. Semi-quantitative analyses of the glasses show highly variable contents of Si, Al, Ca, Fe and Cr, which are thought to signify impact-triggered melting of various mixtures of the major minerals present during breccia formation (Kuehner et al., 2016).

Fragments of clear to pale green glass spherules are abundant in lunar meteorite Yamato 981031 - a polymict regolith breccia. The chemical composition of the glass implies mixing of mafic mare and feldspathic highland material. These are thought to be of impact origin and pyroclastic-origin, but they are intimately mixed, suggesting mixing of debris by impact ejecta from highland to mare regions and disturbance of highland and mare soils by small impacts in the mare region (Arai et al., 2002, Sugihara et al. 2004).

Lunar mare basalt meteorite LaPaz Icefield (LAP) 02224 has a glassy vesicular fusion crust caused by ablation melting and degassing of the rock's surface as it passed through the Earth's atmosphere. It provides evidence that the sample accumulated solar-wind-implanted volatiles in the lunar near-surface environment that have exsolved upon remelting and suggests that it must have been part of a lava flow that was exposed at or near the lunar surface for a significant proportion of its history (Joy et al. 2006).

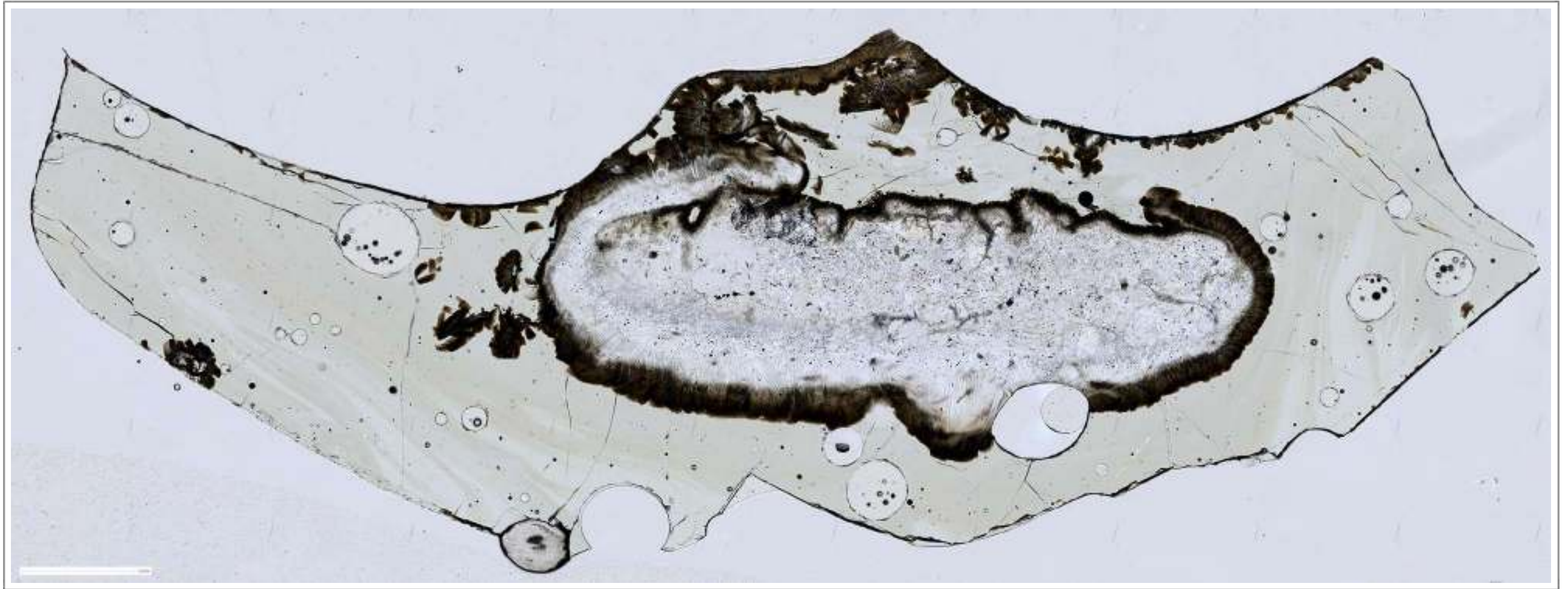


Apollo 16: 60017 is a microbreccia impact-melt composed primarily of well-rounded clasts of anorthositic gabbro, mosaically recrystallized anorthosite and large crystals of olivine set in a cryptocrystalline groundmass. The clasts frequently have a fine-grained rim due to reaction of the clast with the groundmass. The rock contains two dominant lithologies ~70% variolitic melt (on right) and ~30% (mostly) dark aphanitic clasts (on left). The variolitic melt consists of plagioclase clasts with interstitial mafic minerals, minor ilmenite, metallic iron, rare troilite, rare spinel and cryptocrystalline material. Credit: NASA (AGT Photographer).



Apollo 16: 64455 is an egg-shaped object about 5 cm long and 3 cm across, almost completely covered with thick black glass. The inside “yoke” is a fragment of basaltic melt rock (top). It is a basaltic impact-melt with a very thick glass coat. In thin section a swirling glassy pattern can be seen in this coat. Hand specimen photo courtesy of NASA. Credit: NASA (AGT Photographer)





Apollo 16: 65016 is a hollow, broken sphere or glass bubble. It is about 3-4 cm across. The glass surface is smooth and without zap pits. The glass has a green colour and is notable for its flow structures and prominent vesicles. 65016 is all glass except where some microlites/crystallites are growing adjacent to nucleation centres around included feldspar. Credit: NASA (AGT Photographer). Hand specimen photo courtesy of NASA.





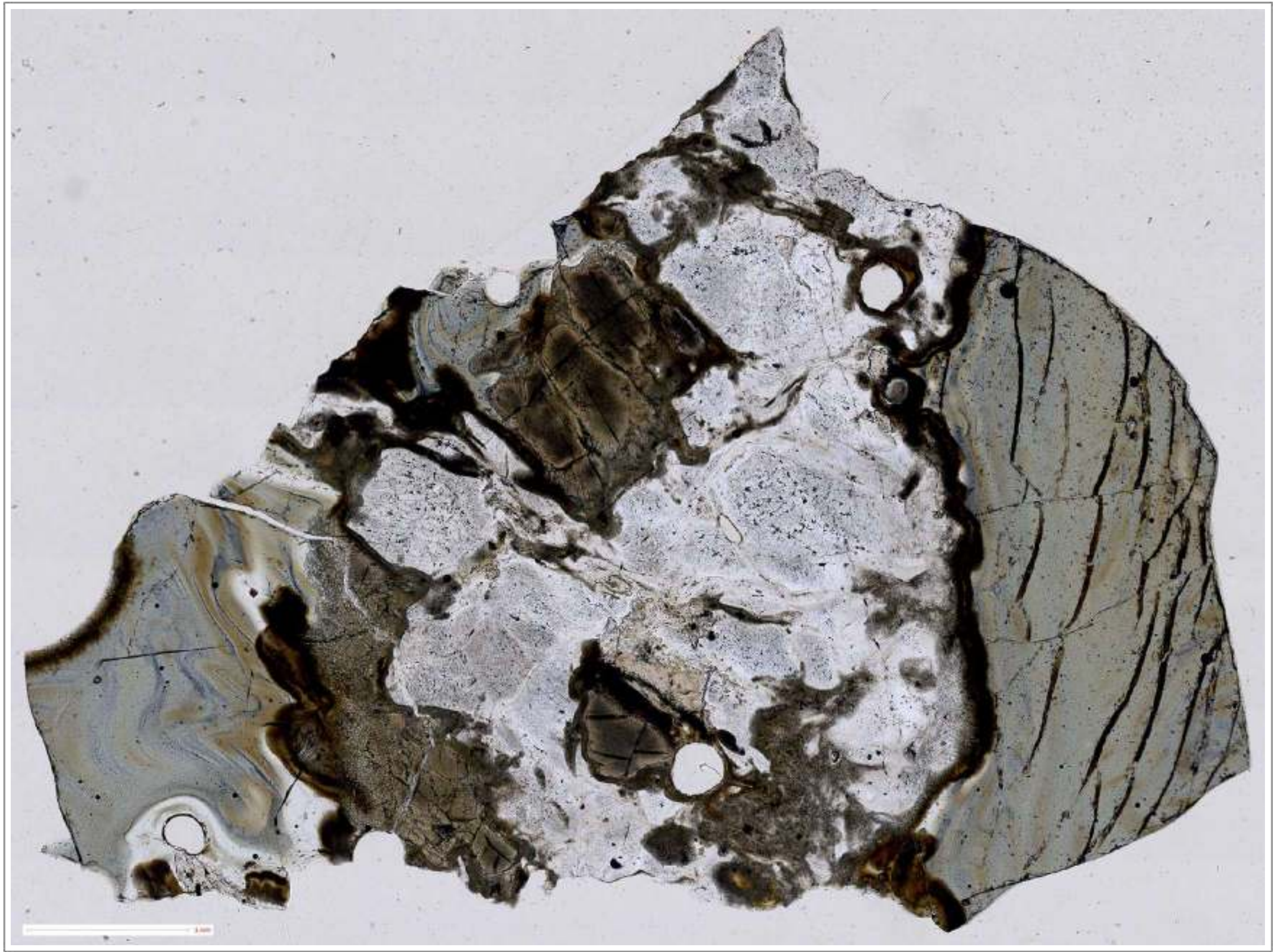
Apollo 16: 65035 is a breccia with large clasts of cataclastic anorthosite intermixed with basaltic impact-melt. It was a glass coated bomb that landed on the regolith while the glass was apparently still molten, allowing welding of fine regolith material. The glass coating is in parts flow-banded and in other parts devitrified (the darker portion). Credit: NASA (AGT Photographer).



Apollo 16: 67728 is a devitrified glass particle that was collected in a rake sample. It is vesicular and contains lithic clasts - mainly plagioclase feldspar. The thin section shows the contact of the glass particle with a plagioclase-rich breccia. At the contact the glass is dark brown and has developed coarse crystallites mostly at right angles to the contact. Away from the contact crystallites are smaller. Credit: NASA (AGT Photographer).



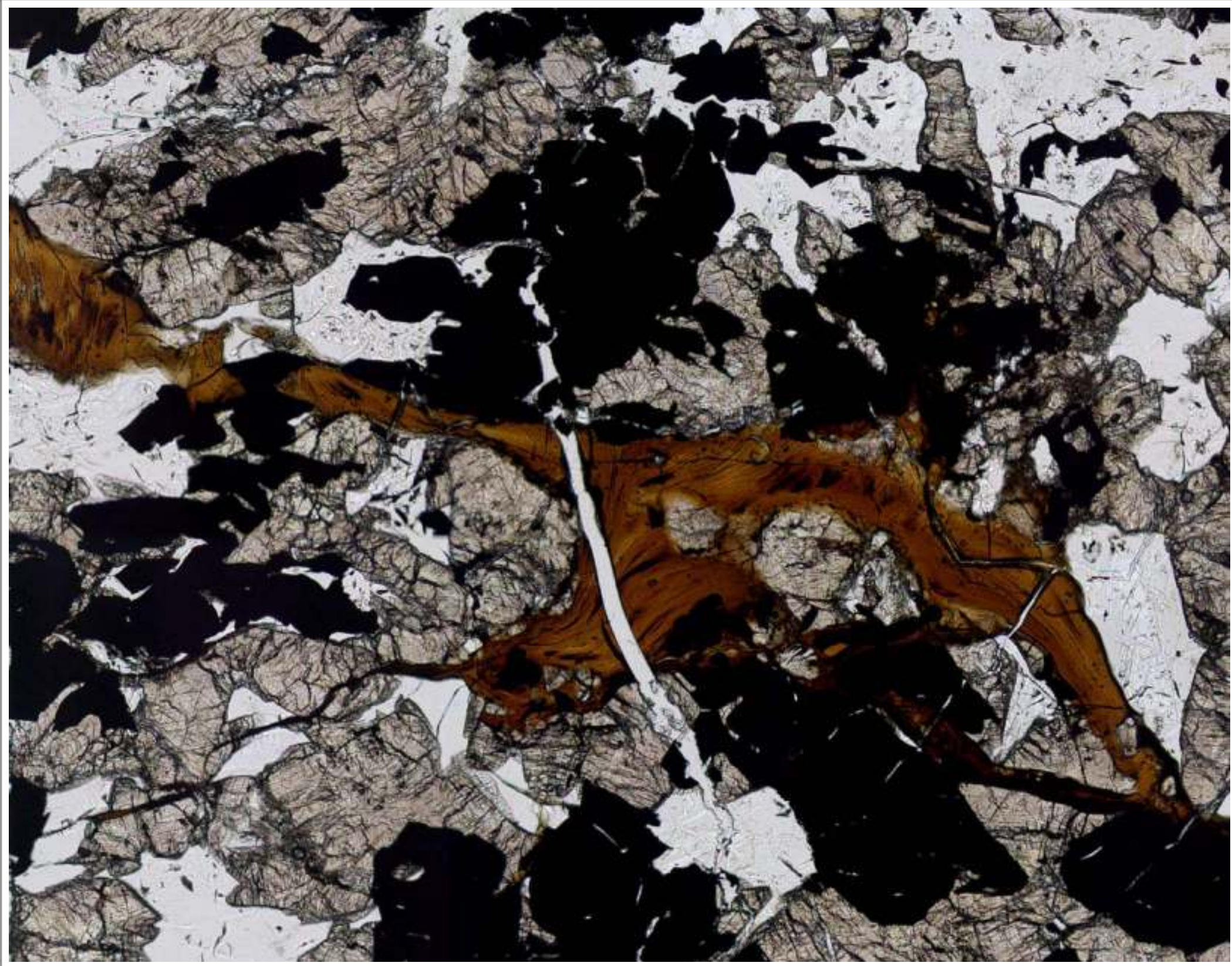
Apollo 17: 78235 was chipped off the top of a small glass-covered boulder (~ 0.5 m) which was found perched on top of the lunar regolith. It is a heavily-shocked norite of cumulate origin with a glass coating and glass veins. The glassy melt formed during a meteorite impact event. Credit: NASA (AGT Photographer). Note 1 mm scale bar at bottom left (large fragment is 7.5 mm across).



Apollo 17: 78255 was chipped from the bottom of the same boulder as 78235 and is also described as a shocked norite. Our thin section consists of shocked pyroxene and plagioclase feldspar with a distinct glassy exterior. The glass is banded and folded. Credit: NASA (AGT Photographer).



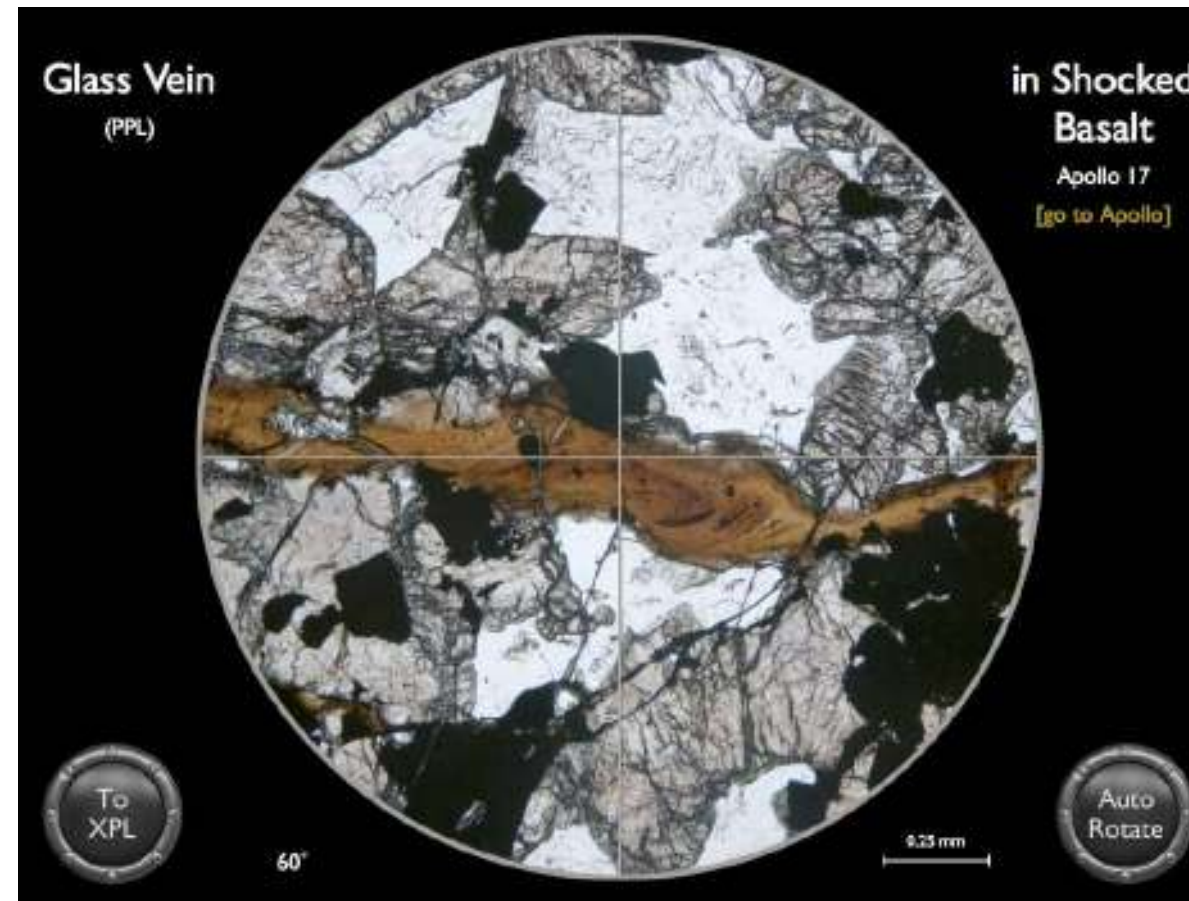
Apollo 17: 78526 is a green glass impact-melt vitrophyre containing feathery pyroxene and acicular, chain olivine and pyroxene. The impact-melt supercooled to produce the vitrophyre, with contrasting textural domains resulting from differences in nucleation kinetics and degrees of supercooling in various portions of the sample. Circular features are most likely laser-ablation holes created during analysis of the glass. Credit: NASA (AGT Photographer).



Apollo 17: 79155 is a mildly-shocked coarse basalt (or gabbro) with large grain size (2 mm). Both pyroxene and plagioclase have undulose extinction and there are stringers of brown glass throughout the thin section indicating shock melting.
Credit: NASA (AGT Photographer).

Moon Minerals: Impact-Melt Glass

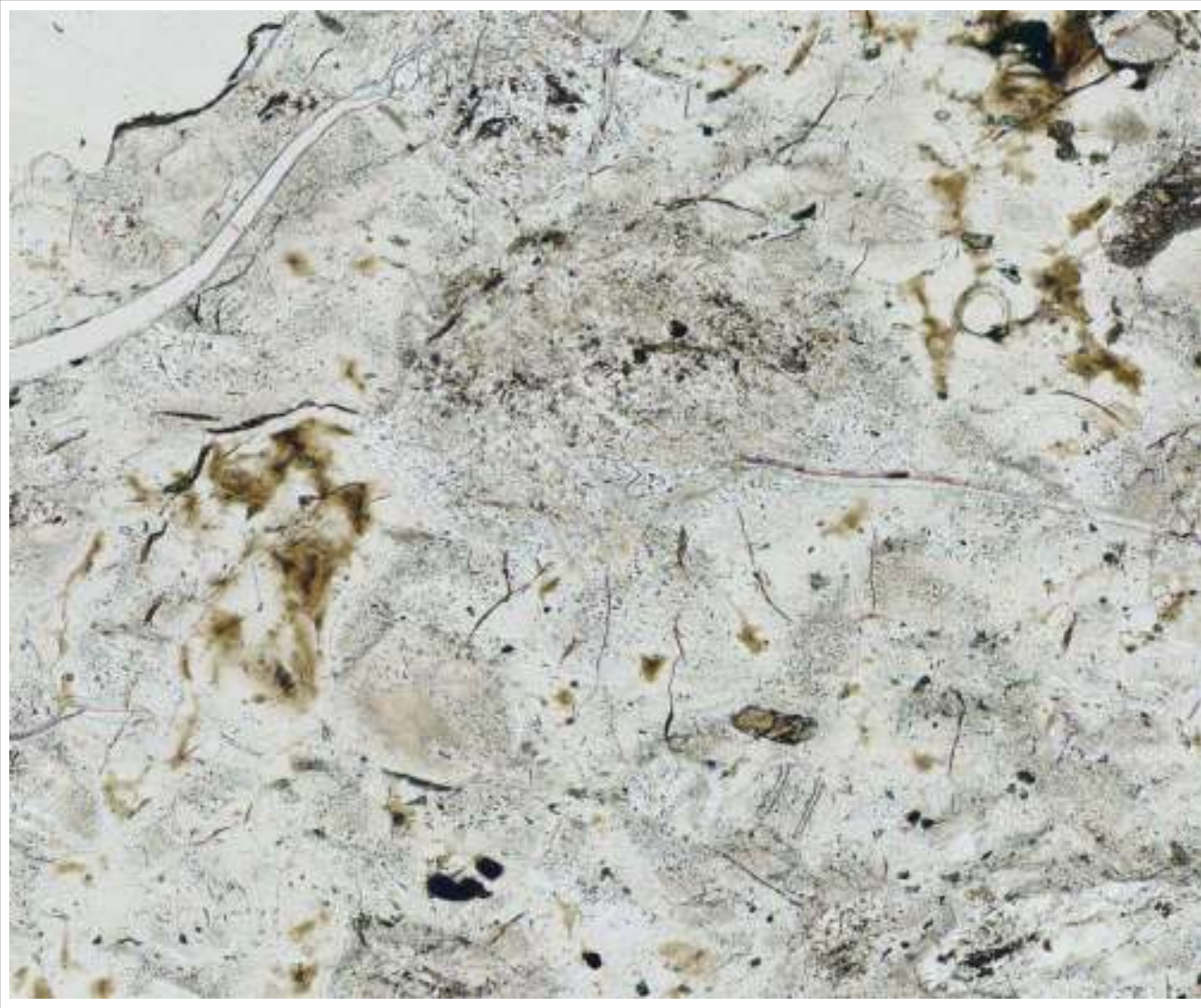
Mineral Virtual Microscope: Impact-Melt Glass



This sample is a mildly-shocked coarse basalt (or gabbro). Both pyroxene and plagioclase display undulose extinction and there are stringers of brown glass throughout the thin section indicating shock melting.

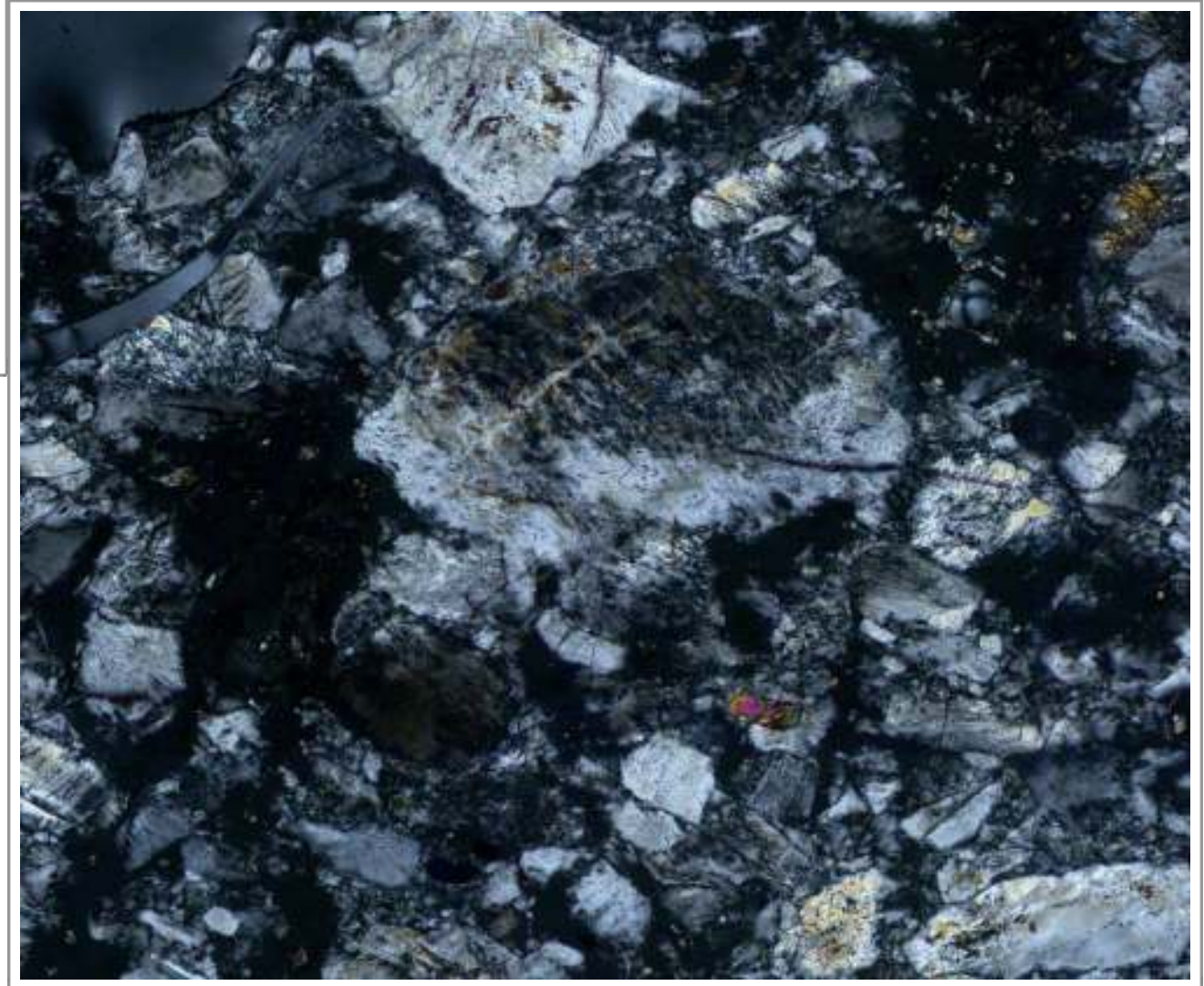
Apollo 17, Sample 79155.

Credit: NASA (AGT Photographer)



Plane polarised light

Apollo 16: 69955 is a cataclastic anorthosite, predominantly consisting of plagioclase feldspar, which has been partially converted into glassy maskelynite. Maskelynite is thought to be formed by the quenching of dense mineral melts produced by higher-pressure shock waves during an impact event. Width 3.6 mm. Credit: NASA (AGT Photographer).



Between crossed polars

Backscattered electron images of glasses in lunar breccia meteorite Dhofar 1180.

a) A mafic glass including some anhedral-subhedral pigeonite grains.

b) A mafic glass with a near-circular outline. This glass includes a relict augite grain and plagioclase glass. The glass portion shows devitrification.

Some very fine-grained metal grains exist in this glass.

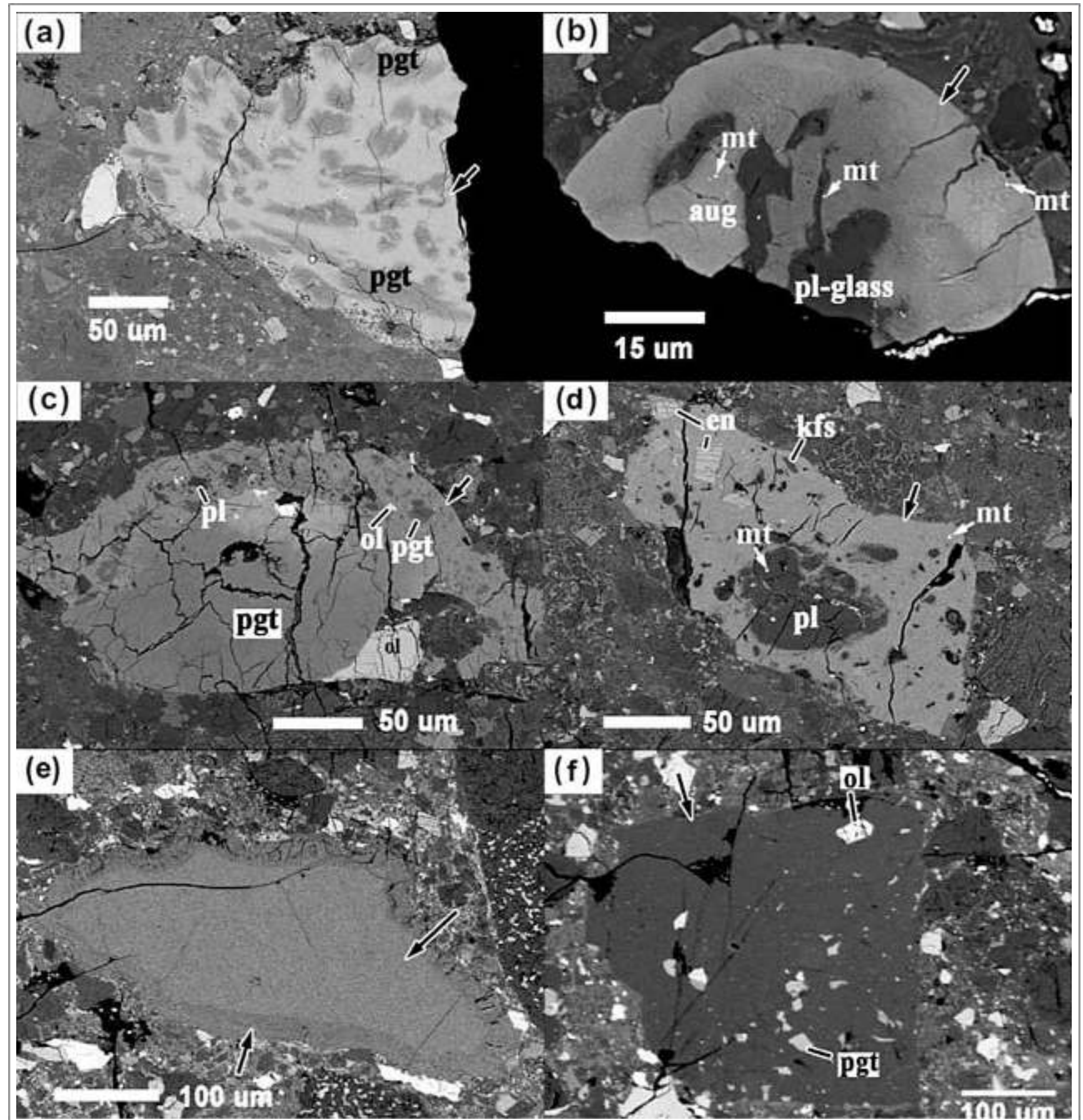
c) A mafic glass that is attached to a pyroxene grain.

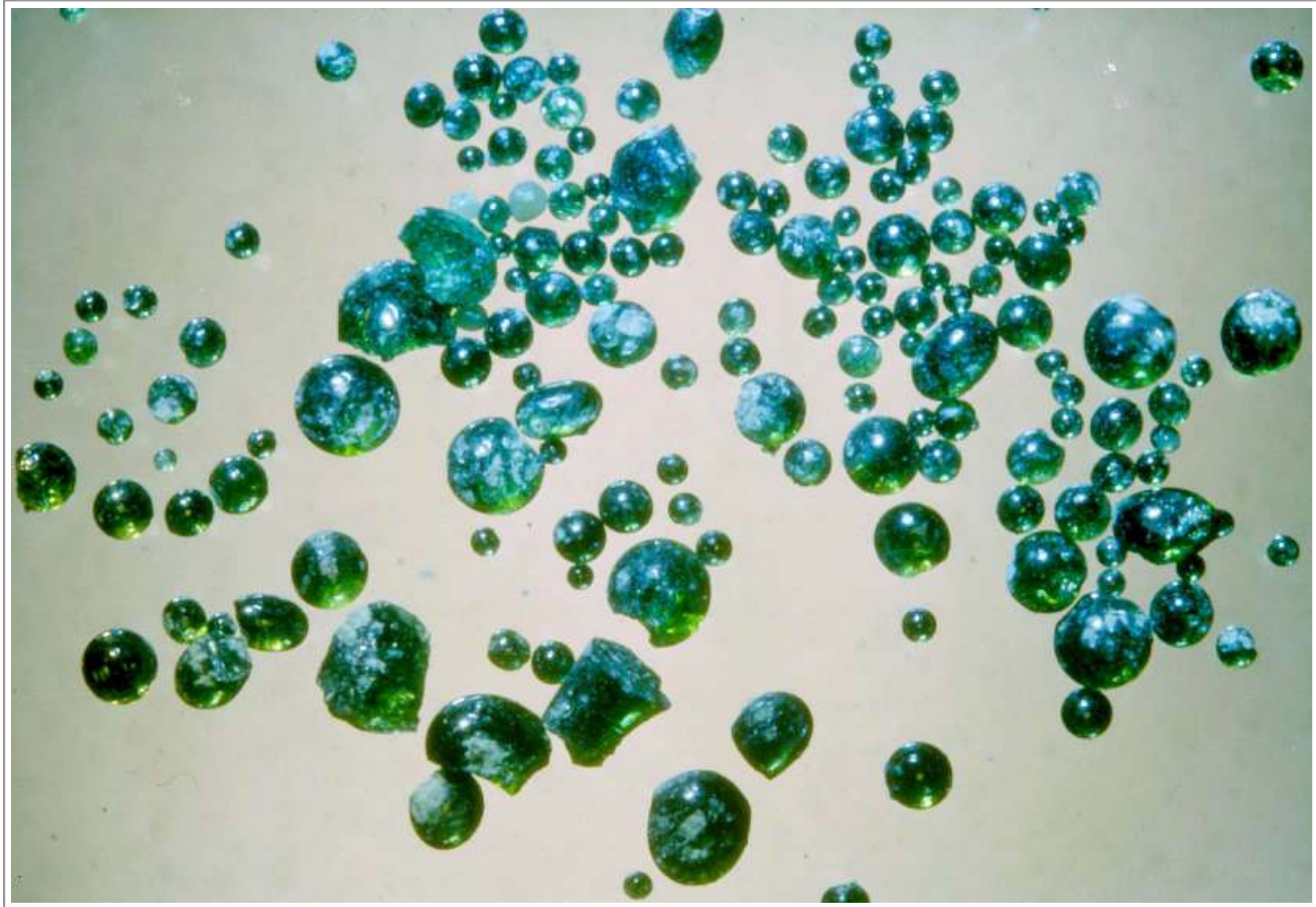
d) A mafic glass containing some plagioclase grains, and fragments of exsolved enstatite and K-rich feldspar. Some very fine-grained metal grains exist in this glass.

e) A feldspathic glass showing devitrification at the margin. Arrows indicate glass regions.

f) Not described.

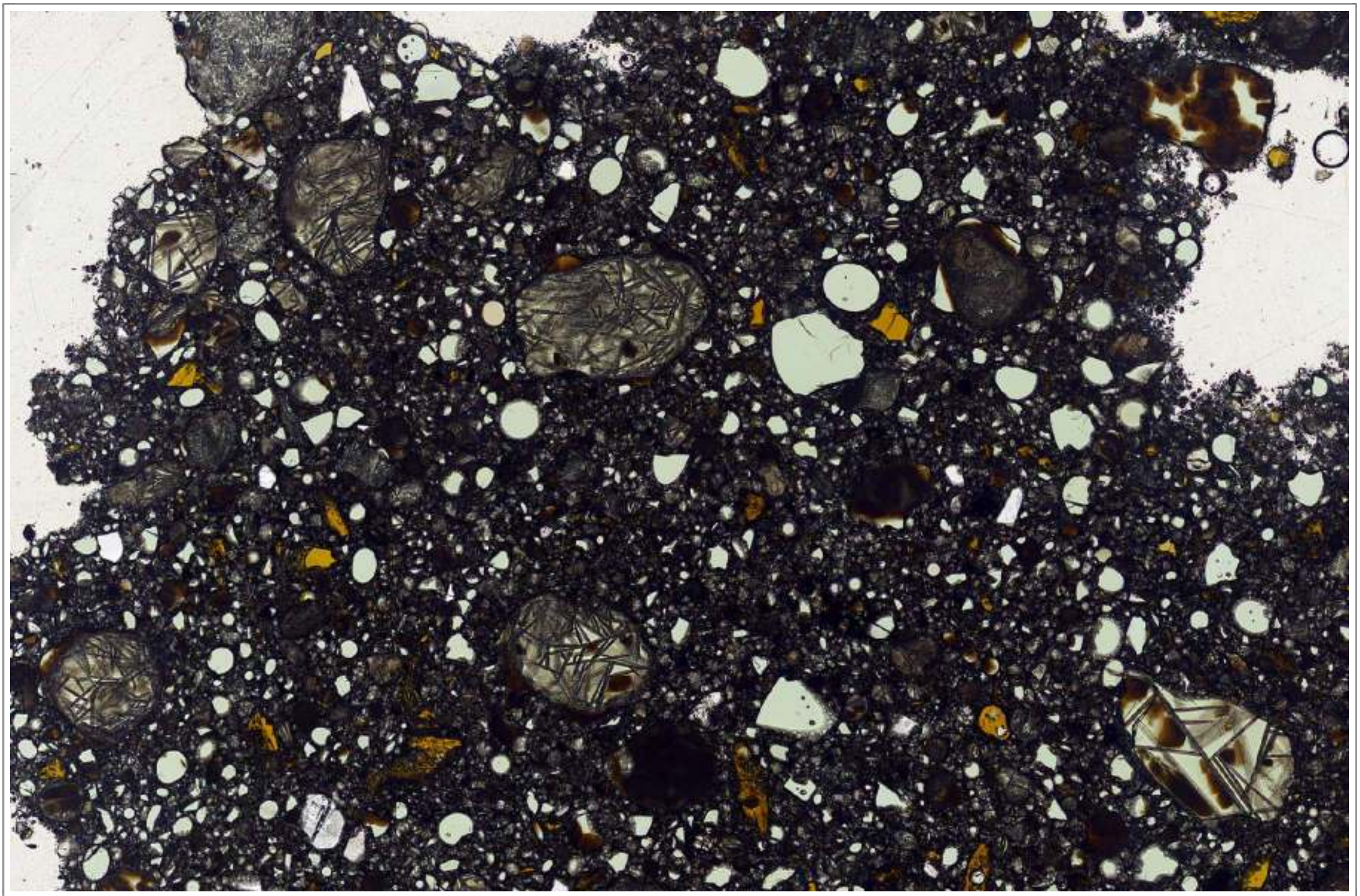
pgt=pigeonite; aug=augite; ol=olivine; pl=plagioclase; kfs=K-rich feldspar; en=enstatite; mt=metallic iron.



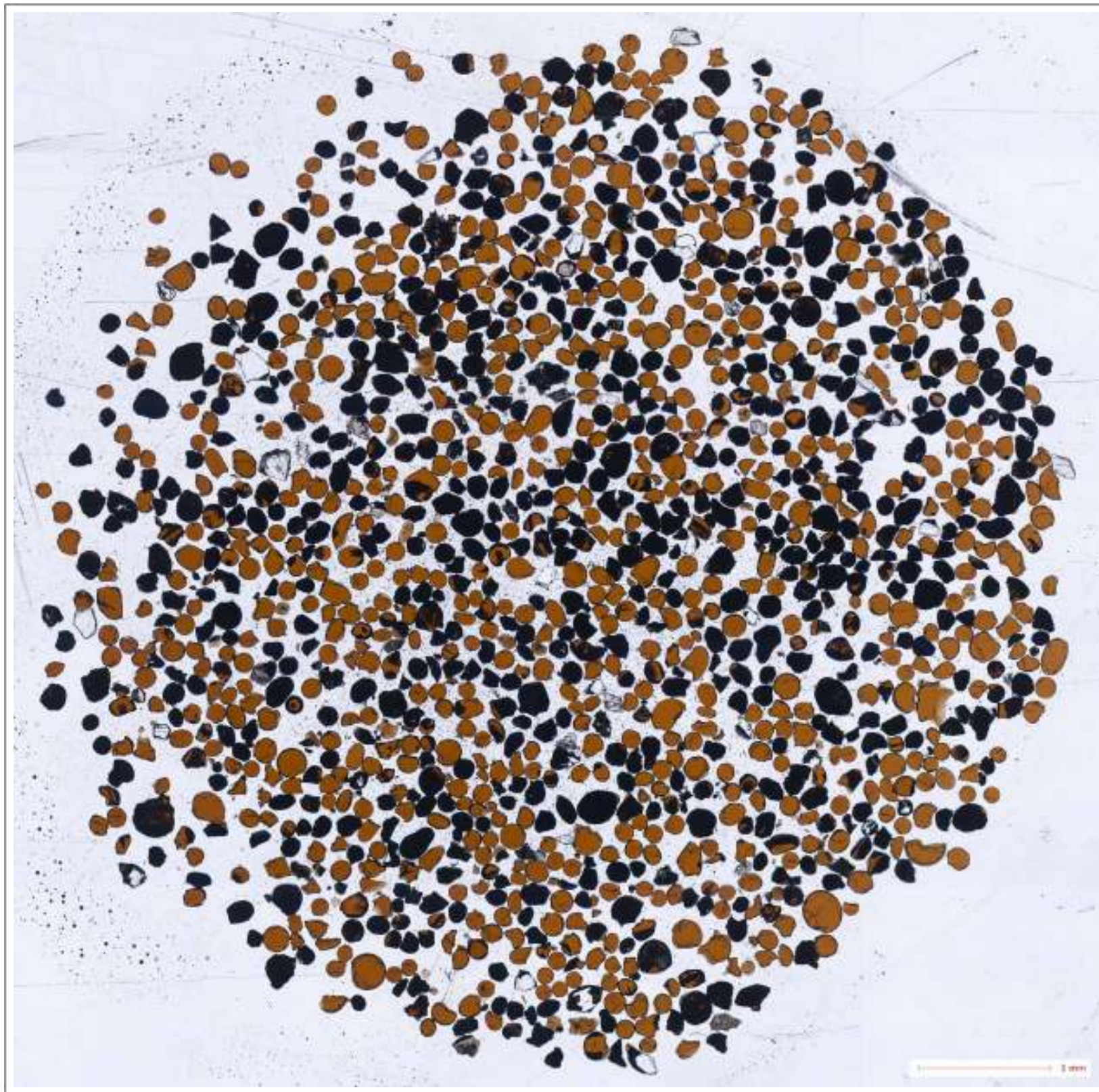


Green glass spheres in Apollo 15 sample 15426, 51.

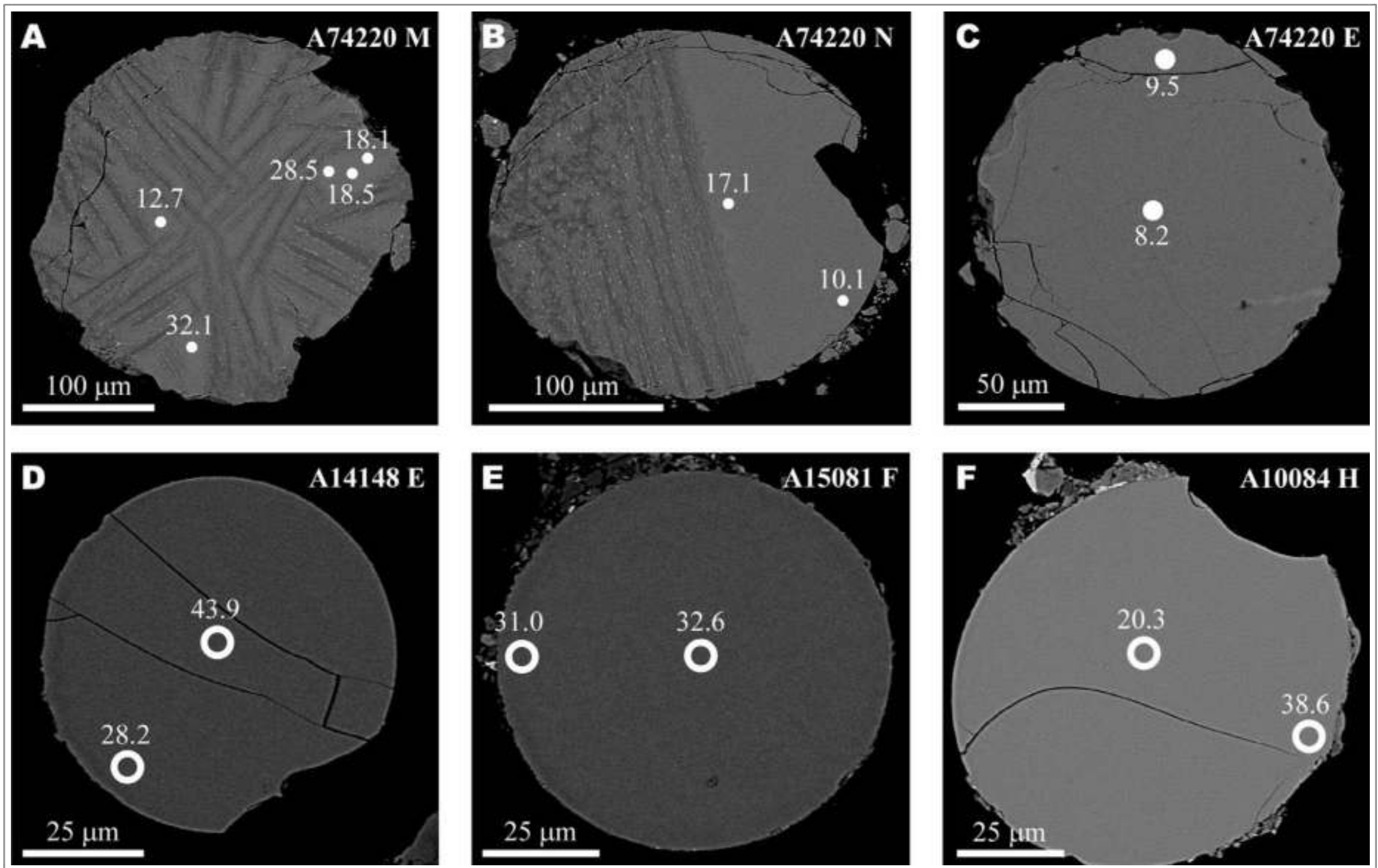
Source [NASA](#). Photo no. S79-32189.



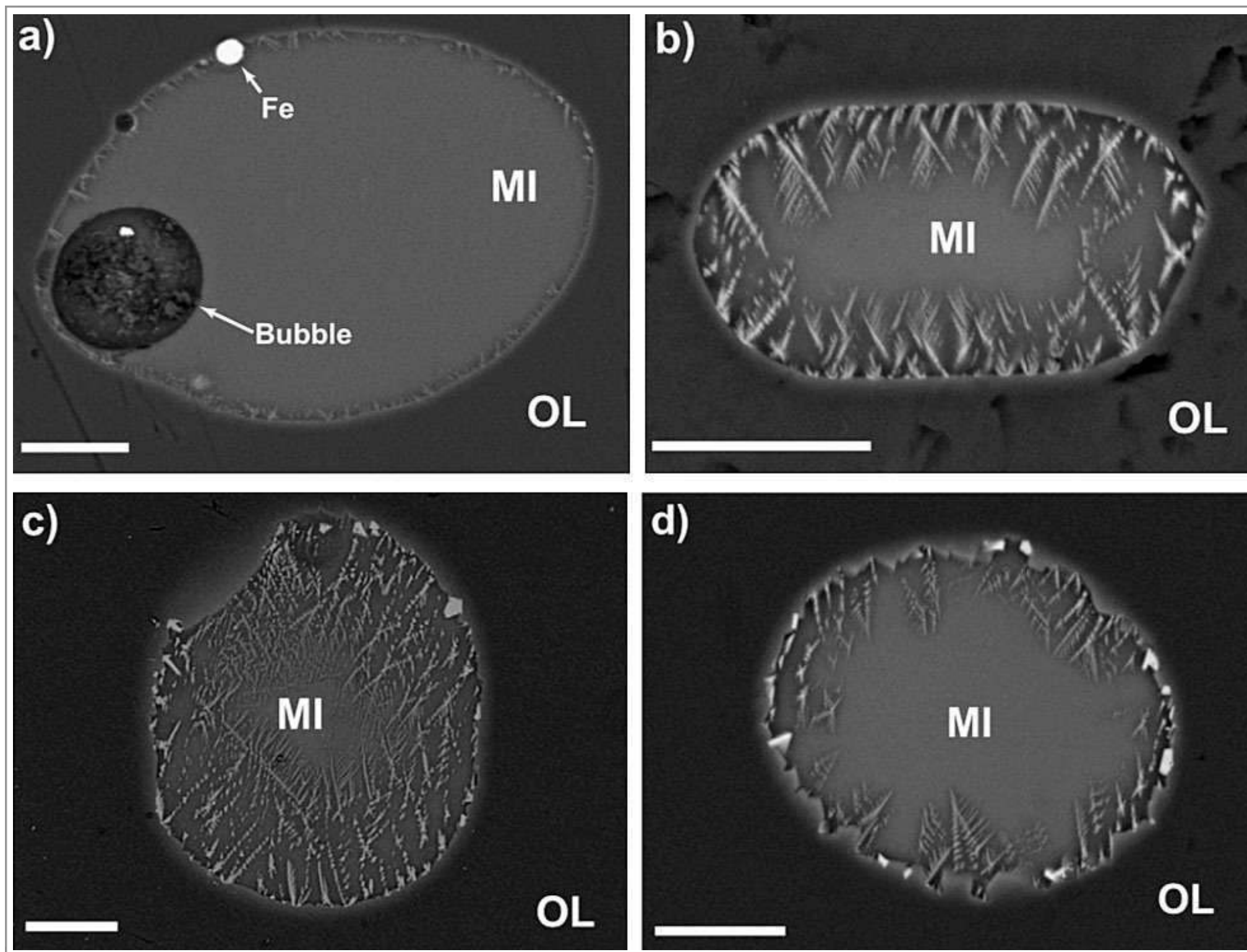
Apollo 15: 15427 is a green glass clod - partially light-greenish-grey and partly greyish-brown. It is blocky and very friable, with average particle size less than 0.1 mm. The grey portions appear to be regolith breccia, with admixed basalt fragments. Some glass beads form composite aggregates, indicating collision while molten in the volcanic plume. Fine-featured olivine microlites criss-cross many of the beads - they formed during quenching. Red and yellow-brown volcanic glass is also present. Width 7.8 mm. Credit: NASA (AGT Photographer).



Apollo 17: 74220 is an unusual soil sample. It is part of the splatter from a volcanic eruption that formed a pyroclastic deposit. Most of the sample consists of orange glass spheres, although a proportion of the glass has devitrified and is now black where fine olivine needles and ilmenite feathers have grown. Compositionally the black 'glass' is identical to the orange glass. The glass is enriched in Ti (~9.3% TiO_2).
Credit: NASA (AGT Photographer).

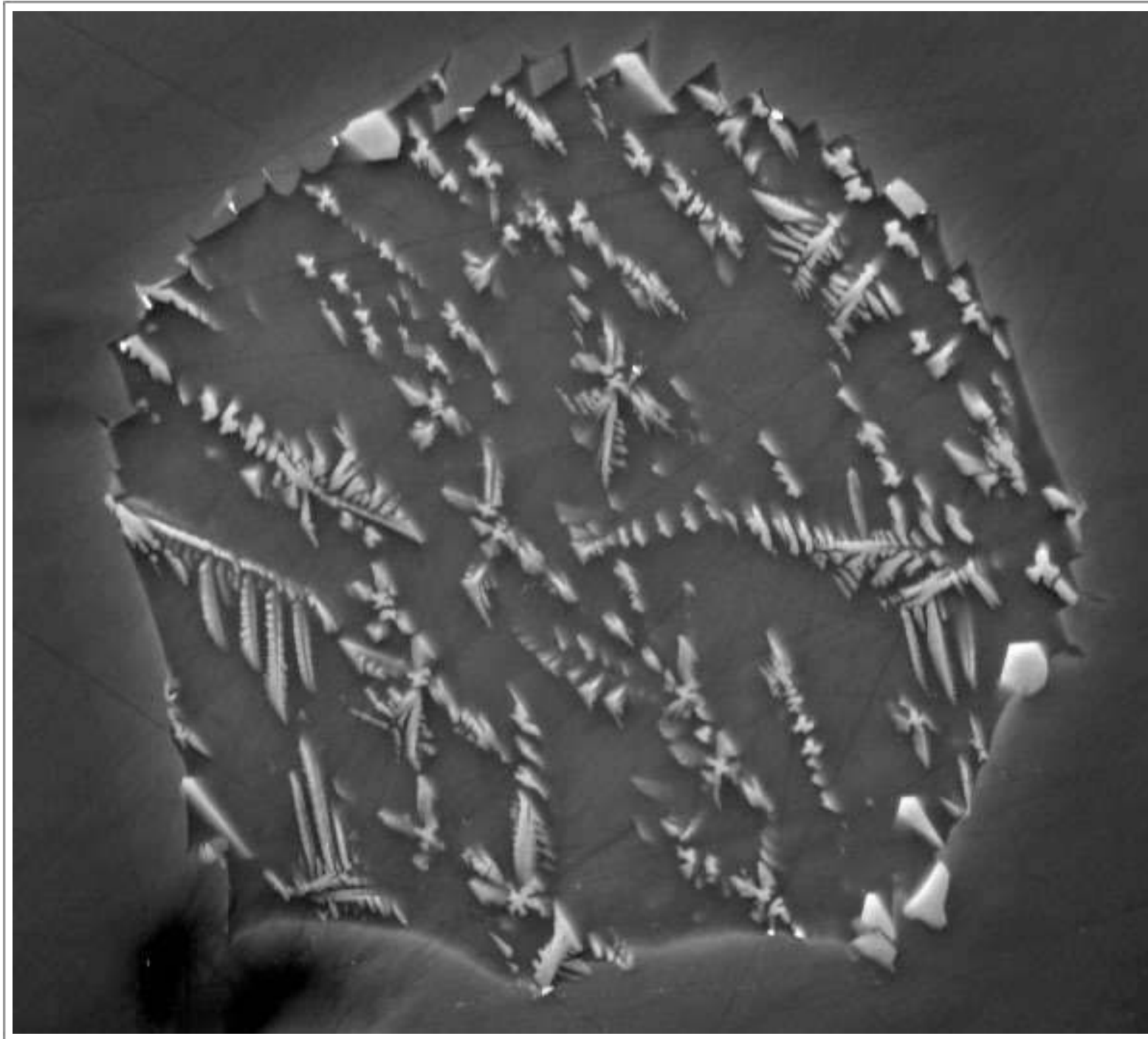


Backscattered electron images of lunar picritic glass beads. A) Apollo 17, 74220 highly crystalline bead. B) Apollo 17, 74220 half crystalline bead. C) Apollo 17, 74220 holohyaline bead. D) Apollo 14, 14148 holohyaline bead. E) Apollo 15, 15081 holohyaline bead. F) Apollo 11, 10084 holohyaline bead. The relative X-ray absorption spectroscopy spot sizes and ferric iron concentrations are overlain.



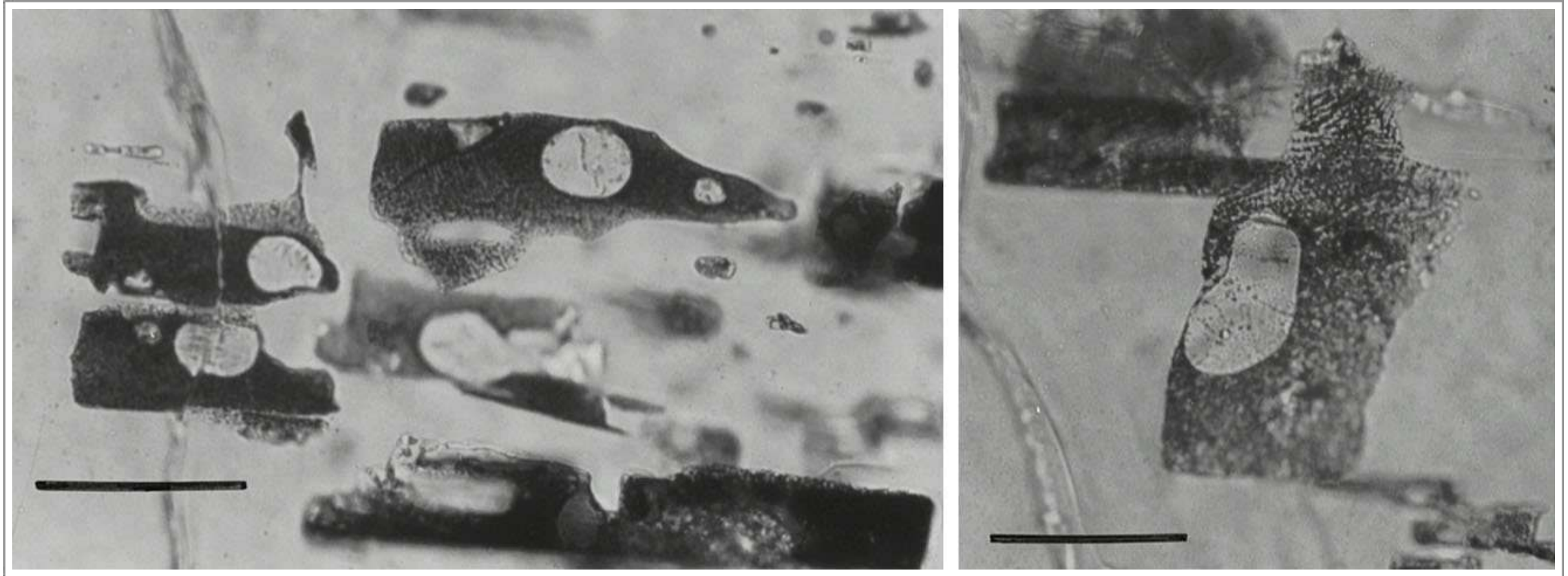
Taken From Ni et al. (2017)

Backscattered electron images of olivine-hosted melt inclusions in Apollo 17 orange spherule regolith 74220. a) Homogenized melt inclusion contains a bubble and a spherical Fe metal after homogenization; b) Homogenized melt inclusion shows more dendritic olivine growth, which might be due to the thick-wall crucible used for its homogenization; c) Natural unheated melt inclusion showing extensive dendritic olivine growth almost across the entire inclusion; d) Natural unheated melt inclusion showing less dendritic olivine growth compared to c). Scale bars in the images represent 10 μm .



Taken From Hauri et al. (2017)

Apollo 17: 74220 orange pyroclastic soil sample. Backscattered electron image of a lunar melt inclusion, enclosed within an olivine crystal. The inclusion is 30 μm in diameter. Skeletal crystals within the melt inclusion are a fine mixture of olivine and ilmenite. Dark area in the lower-left is an ion microprobe sputter crater. Credit: John Armstrong, Geophysical Laboratory, Carnegie Institution of Washington.

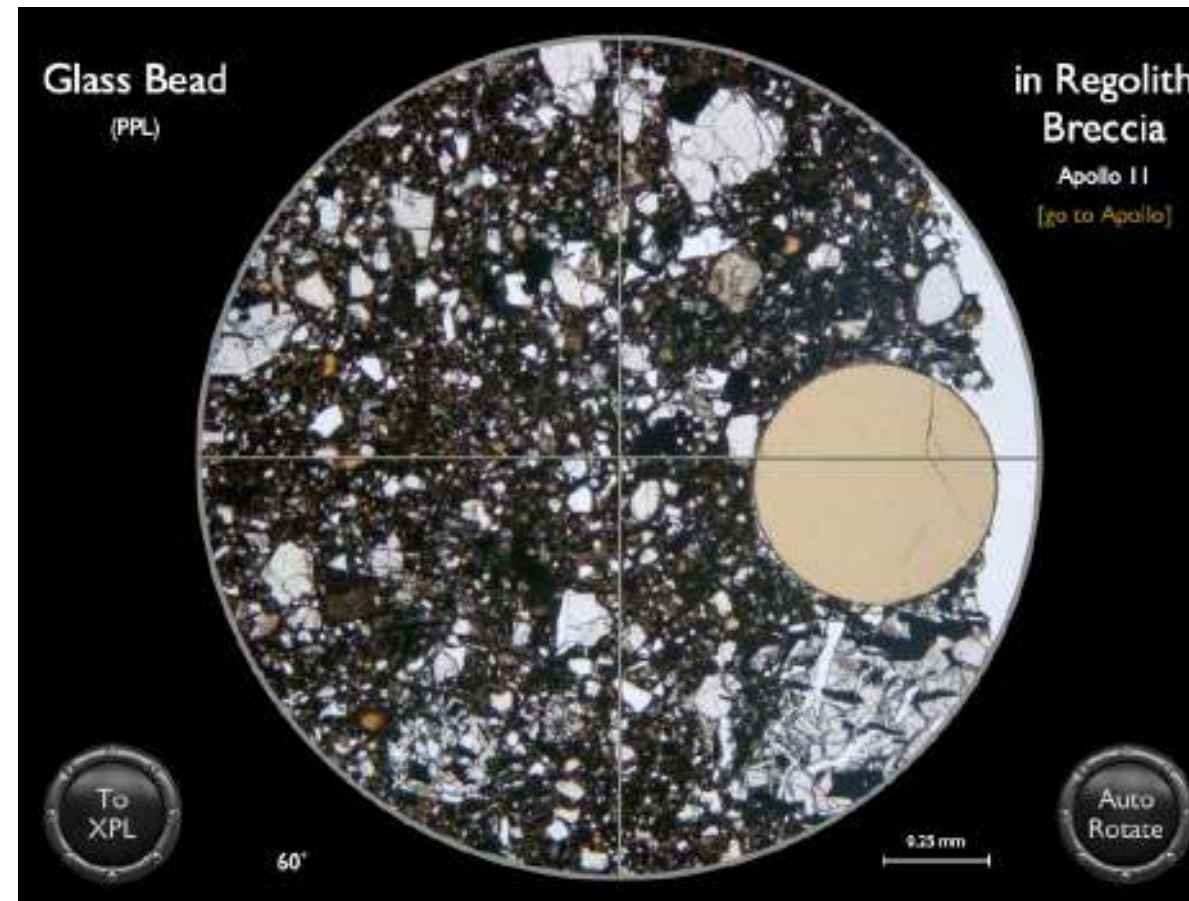


Taken From Shearer et al. (2001)

Photomicrographs of immiscible melt inclusions in plagioclase from lunar mare basalts. Left- close-up image of several melt inclusions with the felsic component forming spherical bodies immersed in dark basaltic matrix. Right- large single inclusion illustrating the feathery texture of the basaltic component. (Both images - scale bar = 75 μ m).

Moon Minerals: Regolith Breccia

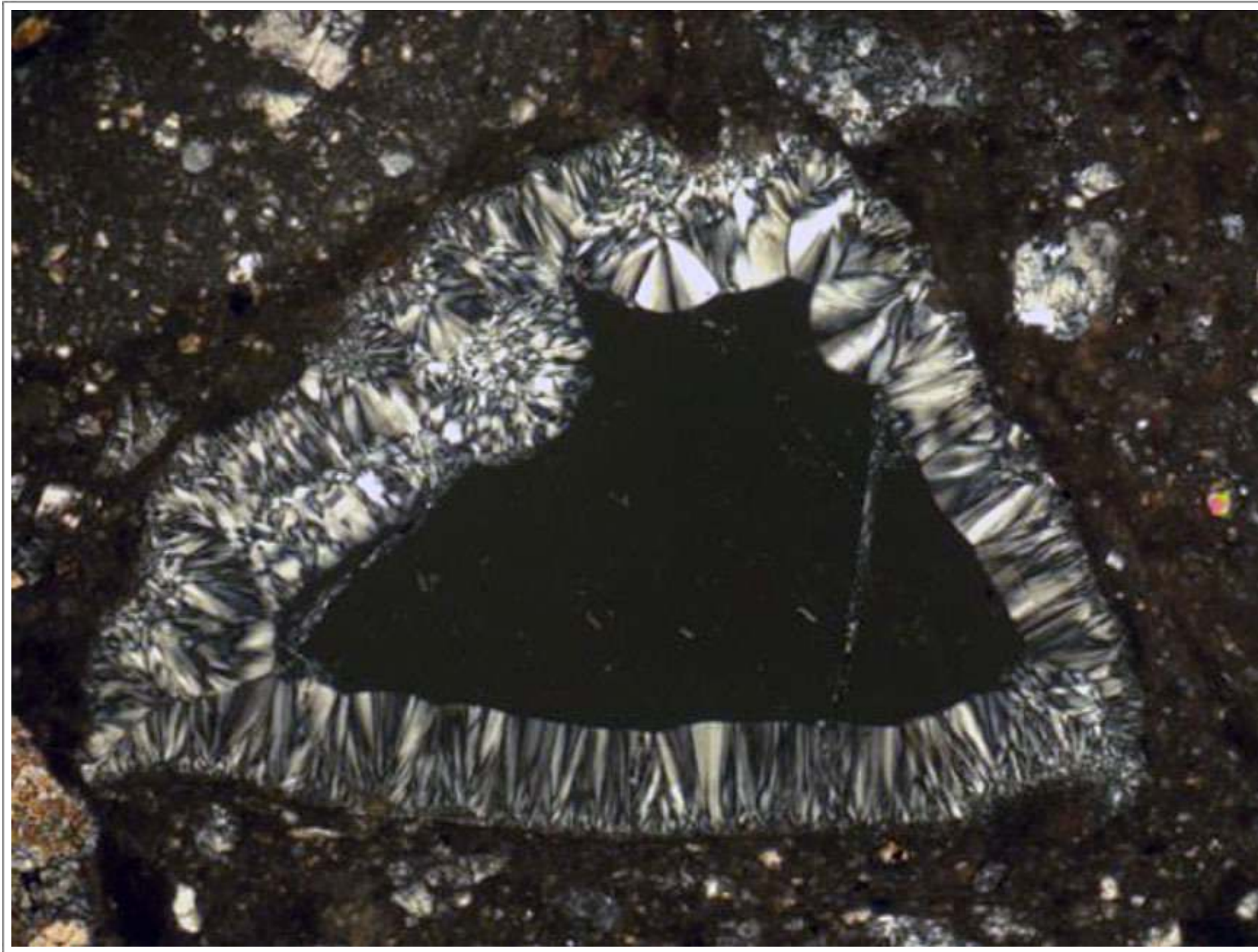
Mineral Virtual Microscope: Glass Bead in Regolith Breccia



10026 was collected as part of the contingency sample from the area immediately in front of the Lunar Module. At least two generations of orange glass are found in the sample, including one relatively large, perfectly spherical glass bead (probably of volcanic origin). Note the glass is isotropic between crossed polars.

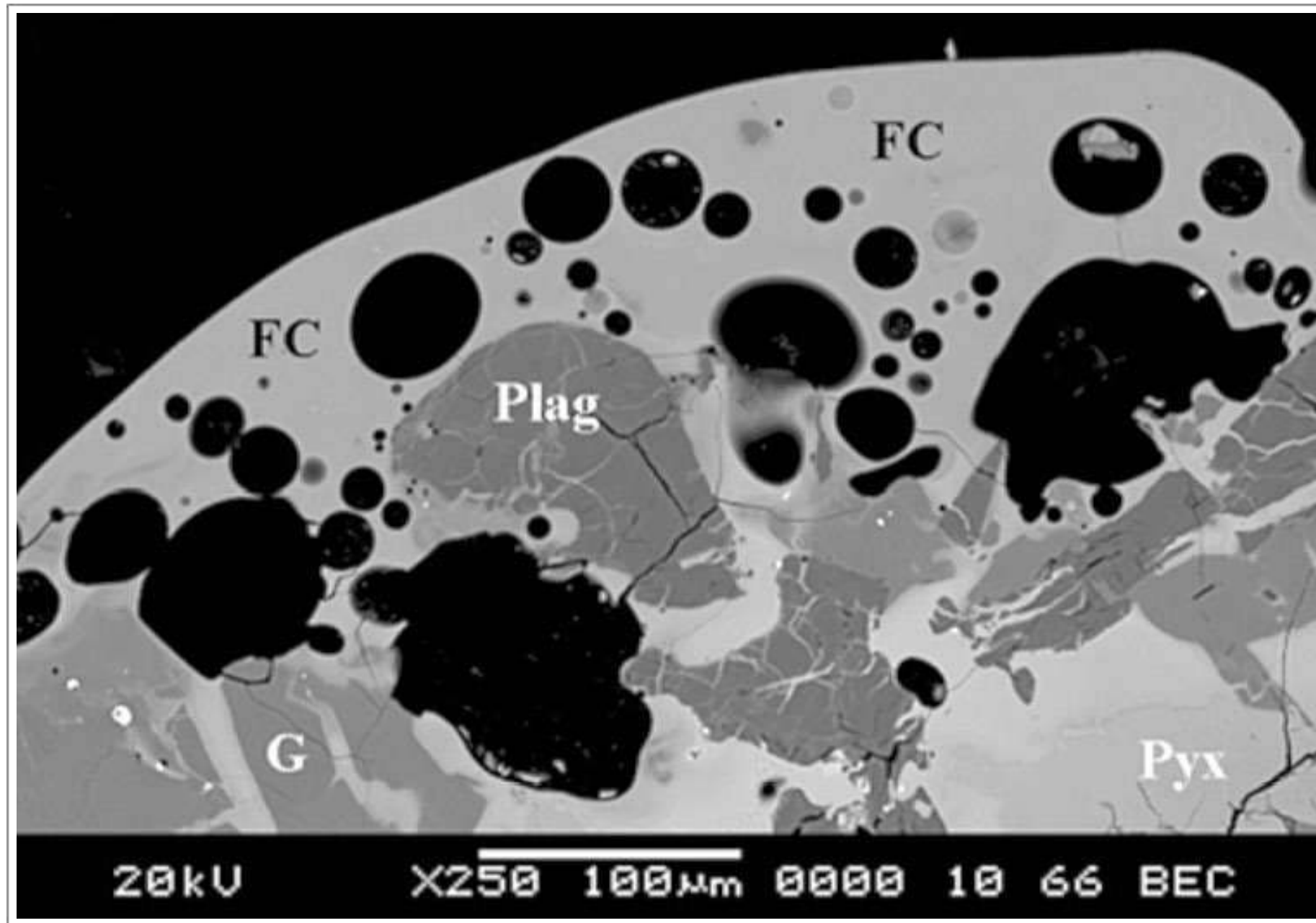
Apollo 11, Sample 10026.

Credit: NASA (AGT Photographer)



Taken From Kuehner et al. (2016)

Transmitted light (XPL) image of partly devitrified glass clast in lunar meteorite NWA 10404 - a feldspathic regolith breccia. Width of field = 2.37 mm.



Taken From Joy et al. (2006)

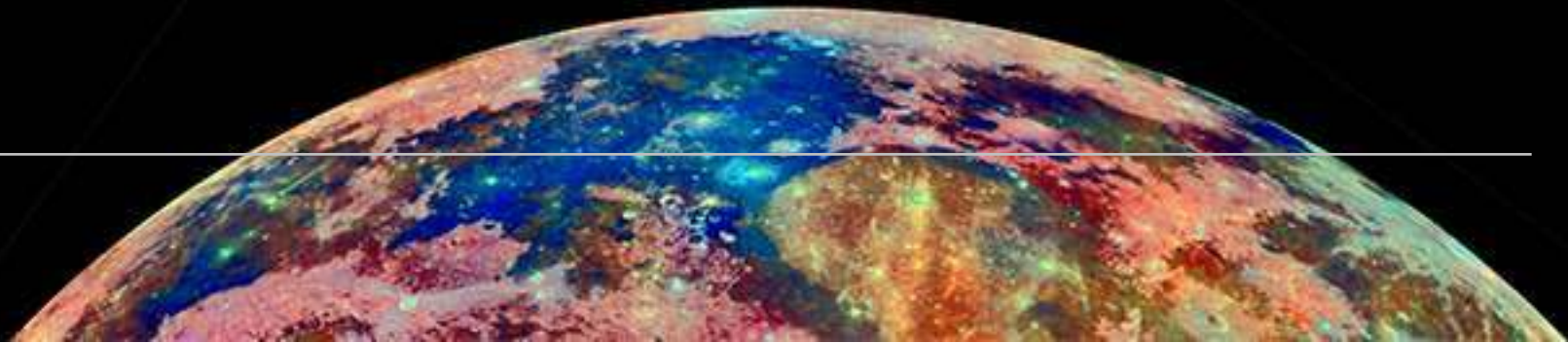
Backscattered electron image of the fusion crust of lunar mare basalt meteorite LAP 02224. The vesicular grey area at the top of the image is the fusion crust; minerals being melted into this zone can be seen at the bottom of the image. Vesicles (black circular regions) are heterogeneously distributed throughout the melted/melting area. Dark grey crystals are plagioclase, pale grey at the base of the image is pyroxene, and the small bright white blebs are troilite. G = glass, Plag = plagioclase, Pyx = pyroxene, and FC = fusion crust.

Accessory Minerals

These are the relatively rare minerals that are found in Moon rocks. Their abundance is less than 5%.

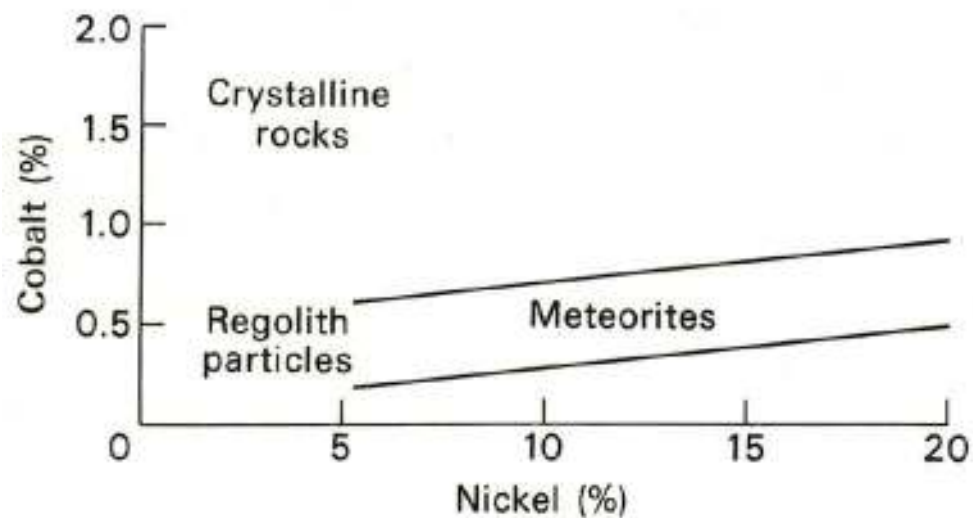


Metals



SPECIES

1. Iron-Nickel (kamacite, taenite & tetrataenite)
2. Copper
3. Silicon
4. Tin



Metallic iron - the nickel and cobalt contents of lunar metal can be used to establish whether or not the metal is extralunar or not (from Cadogan, 1981).

Metallic Iron-Nickel

Native iron metal, is only rarely found in terrestrial rocks. However, in lunar rocks it is a ubiquitous minor phase, largely because of the low oxygen partial pressures (reducing conditions) during original crystallization of lunar magmas and during subsequent meteoroid impacts. Metallic iron has now been identified in all returned lunar rocks. The amount of metal varies between samples as well as between sites, but is always less than 1% by volume (Heiken et al., 1991).

Metallic iron occurs in lunar rocks as three different minerals. They occur in various proportions and form intricate textures, either from exsolution during cooling or from later subsolidus re-equilibration. The three minerals also have different chemical compositions, involving varying amounts of solid solution between Fe and Ni.

Kamacite contains 0-6 wt.% Ni.

Taenite contains 6- 50% Ni.

Tetrataenite is essentially FeNi, with $50 \pm 2\%$ Ni.

(metallic iron can also contain up to 8 wt.% Co)

In lunar samples, kamacite is the most abundant metal phase and taenite the second most abundant. Tetrataenite is only rarely observed, and that which occurs is most likely due to meteoritic contamination. These minerals are apparently formed by four different processes:

- (1) normal igneous crystallization;
- (2) subsolidus reduction of oxides, or of troilite and olivine (e.g. Apollo 14 basalts 14053 and 14072);
- (3) reduction of the FeO component in impact-produced silicate melts in the soil;
- (4) meteoroid contamination.

The best means of determining the meteoroid contribution to the metal contents of lunar soils and breccias is through use of the rarer siderophile (i.e., readily soluble in molten iron) elements, other than Ni. These elements, which tend to concentrate in Fe-metal minerals, especially during melting processes, include Au, Pt, Ir, Os, Mo and Ge. Because lunar rocks contain relatively small amounts of these elements compared to meteoroid FeNi metal, estimates can be made about the quantity of meteoroid material in a soil or breccia. It has been determined, for example, that the average Apollo 16 soil contains about 2% input from chondritic meteoroids (Heiken et al., 1991).

In Apollo 17 ilmenite basalt 75035 metallic iron with a low Ni content occurs; (i) as iron-troilite intergrowths in the form of blebs, or occasionally as crystals with distinct outlines, (ii) as droplets in ilmenite or silicate minerals, (iii) as discrete grains of iron with thin discontinuous rims of troilite. The iron seems to have crystallized continuously during the formation of this rock as suggested by the immiscible droplets in early formed silicates and ilmenite, and in later cristobalite (Meyer and Boctor, 1974).

Troilite-iron assemblages in lunar rocks suggest immiscible Fe-FeS liquids formed at 988°C (Skinner, 1970).

One of the most striking features of the Antarctic LaPaz mare basalt meteorites is that they possess metallic iron grains with anomalously high Ni and Co abundances similar to those found in Apollo 12 basalts. Metallic iron grains in Apollo 12 basalts have previously been considered as the result of reduction of the melt through fractional crystallization of silicate and oxide phases. However, Day et al. (2006) suggest re-evaluation may be required for the origin of such grains in mare basalts. These authors also present an excellent mineral dataset for a wide range of major and accessory species found in the meteorites.

Morland et al. (2019) studied a 1 cm² fragment of lunar meteorite NWA 10989 (a regolith breccia) and reported a large metallic iron grain (1.90 × 0.85 mm) composed of predominantly kamacite (low-Ni) with minor amounts of taenitic (high-Ni) material and K-rich schreibersite. Using an electron backscatter diffraction

technique they were able to study the crystallographic structure of the metal components and show it to be an aggregate of variably orientated grains 50-150 μm in size. They concluded that the large metal fragment represents material delivered to the Moon as a projectile during an impact event - i.e. it has a meteoritic origin rather than being lunar.

Metallic Copper

The lunar compendium entry for Apollo 11 ilmenite basalt 10045 suggest metallic copper is present but no further details are given (Simpson and Bowie, 1970). Frondel (1975) report on a few occurrences of native copper including 10045 (microscopic grains in a small segregation in troilite). Copper has also been found in Apollo 12 porphyritic basalts 12018 and 12063 (minute $\sim 2 \mu\text{m}$ veins within ulvöspinel and ilmenite), in Apollo 12 ophitic basalt 12040, and in Apollo 14 High-Al basalt 14053.

El Goresy et al. (1971b) report metallic copper in Apollo 12 basalts 12018 and 12063, where it occurs in $2 \mu\text{m}$ veins within ulvöspinel and ilmenite.

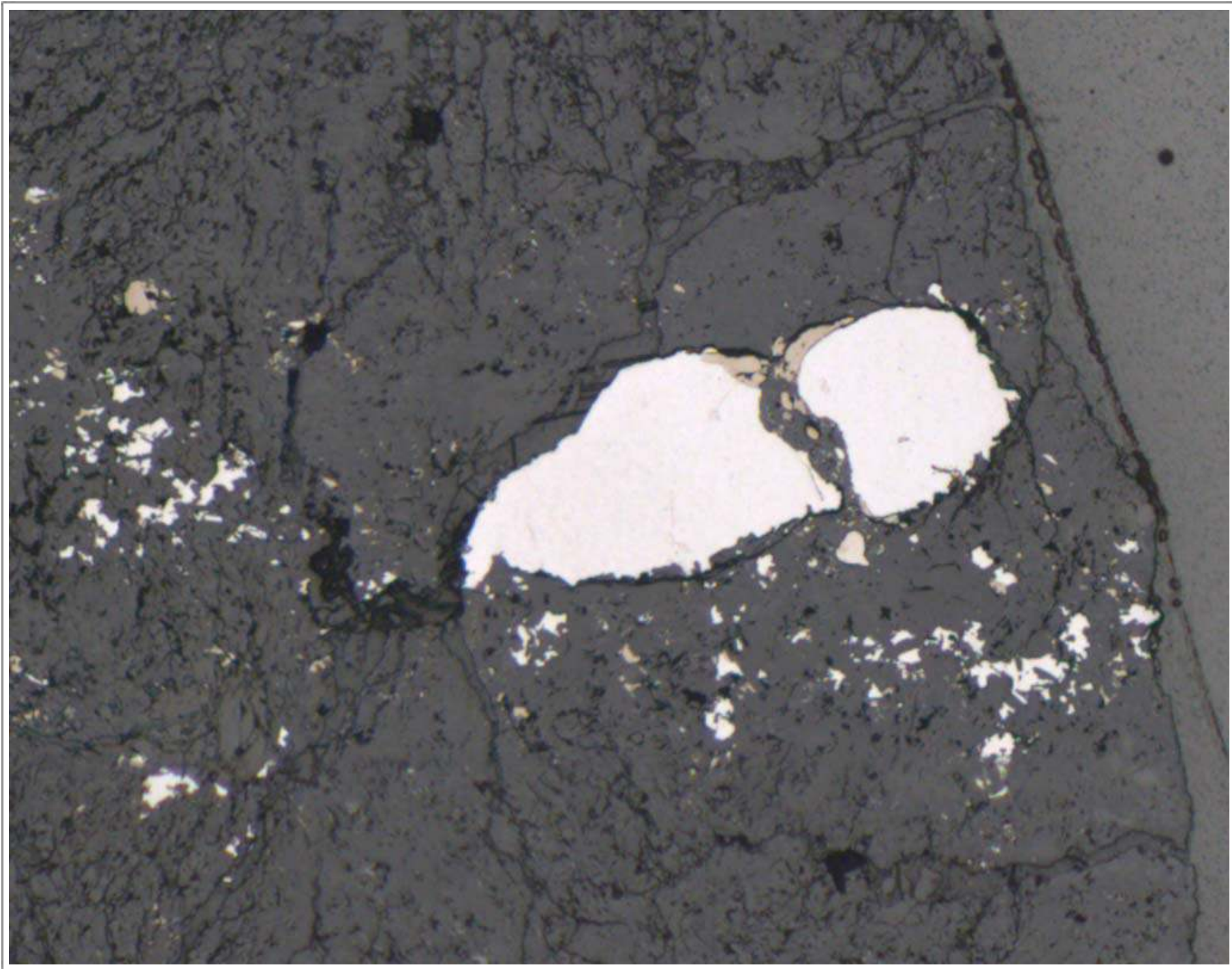
Metallic Silicon

Silicon associated with Fe-silicides has been found in anorthositic fragments from the Apollo 16 regolith. Textures suggest that these materials formed as the result of silicate-metal immiscibility driven by high temperature shock melting on the Moon (Spicuzza et al., 2011).

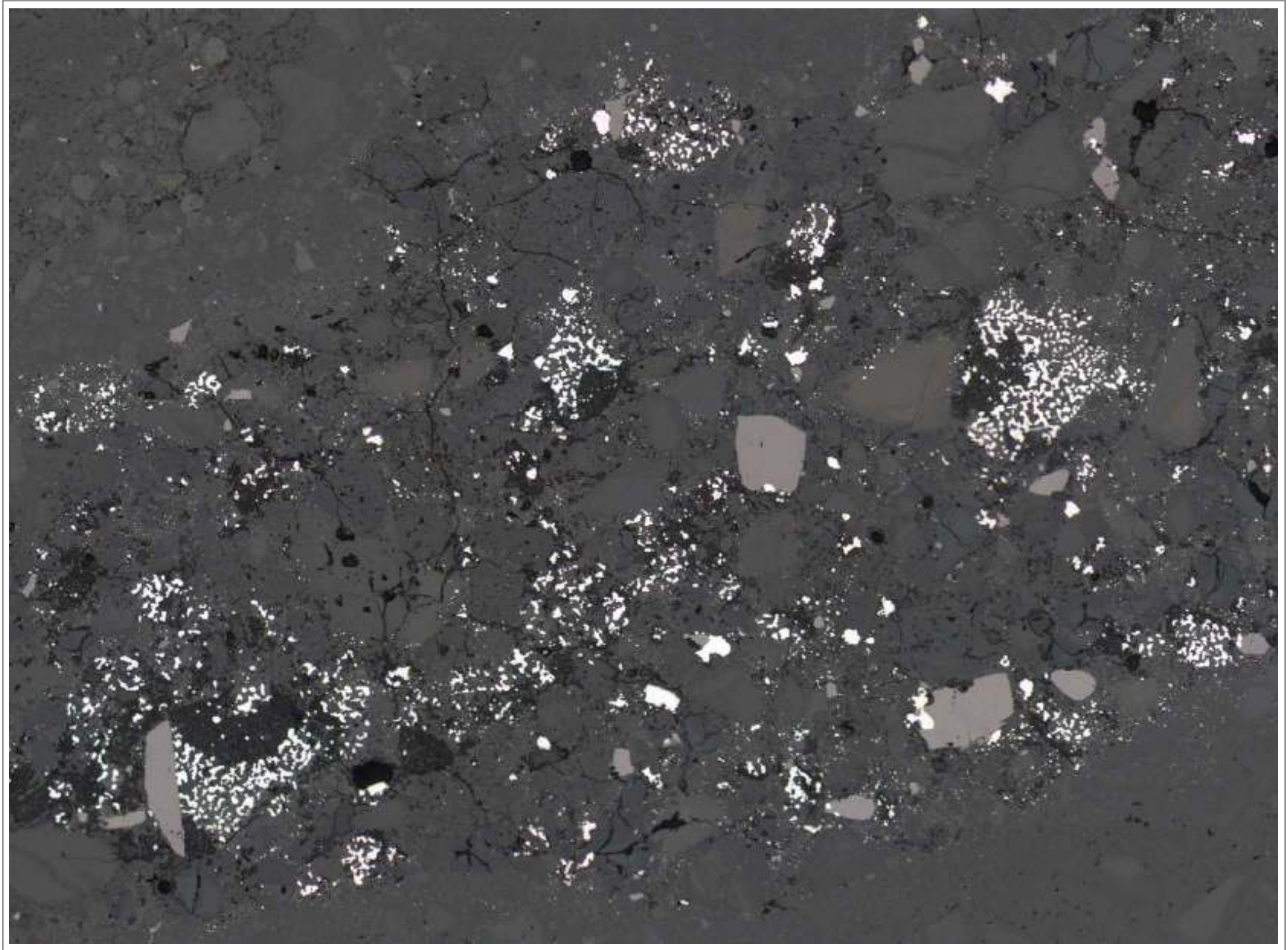
Silicon has also been found in lunar meteorite Dhofar 280 - a typical lunar breccia with an abundant anorthositic impact-melt component. It contains rare schlieren and spot inclusions with native silicon and Fe silicides in the impact melt. The inclusions consist of aggregates of very tiny silicon grains and droplets of Fe-silicides. It is suggested that the Si-rich association of Dhofar 280 was formed by condensation of an impact-induced vapour, remelted and mixed with the Dhofar 280 host rock. Experimental data show that metallic silicon can be obtained under lunar conditions by distillation of anorthositic melts (Nazarov et al., 2012a and 2015).

Metallic Tin

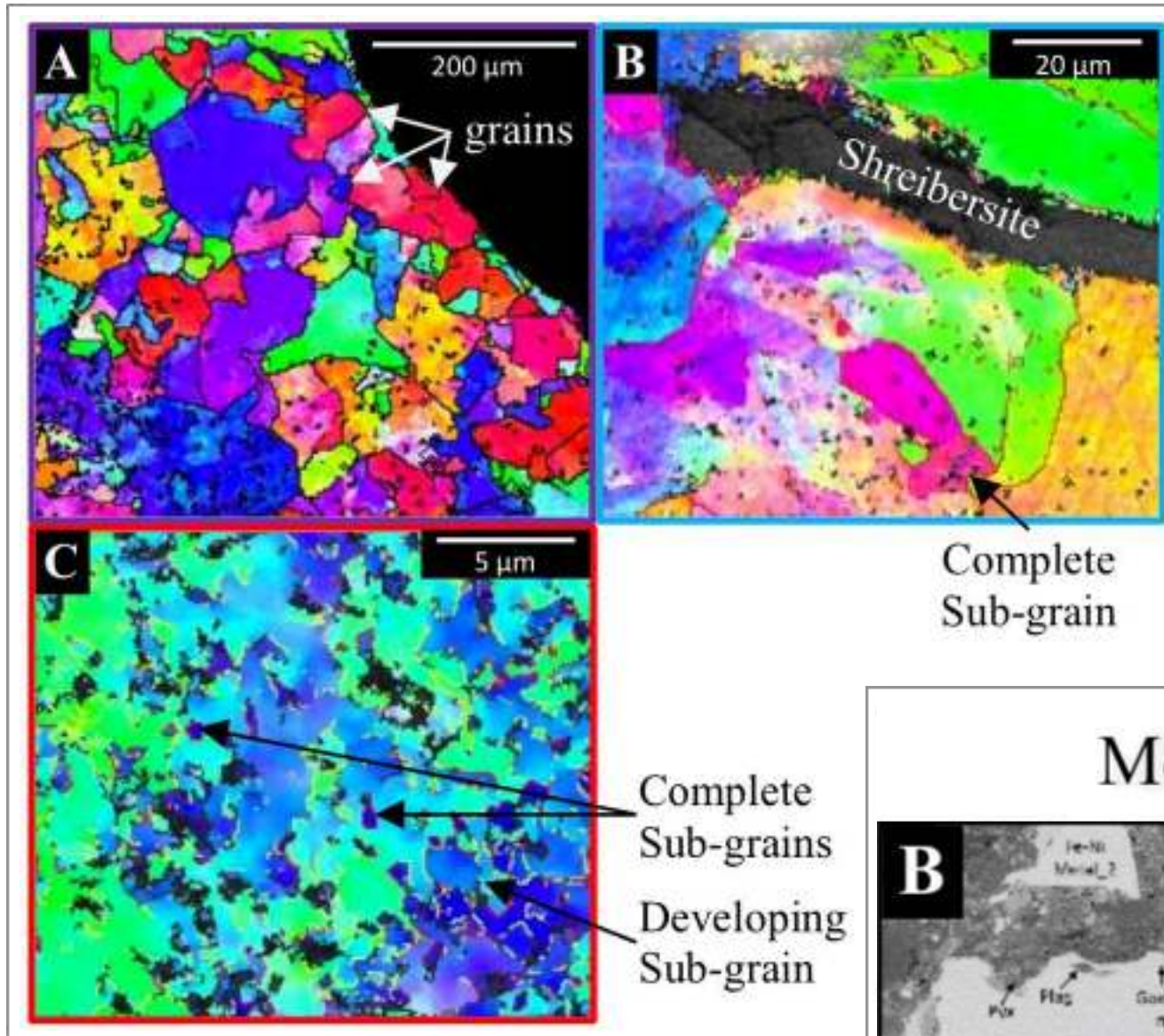
Frondel (1975) reports tin in a small metallic iron fragment from the Apollo 11 fines sample 10084. Tin in lunar rocks is mentioned (but not described) in Wenkui (1995). The species is also mentioned in Mokhov et al. (2008) from the Luna 16 (Mare Fecunditatis) and Luna 24 (Mare Crisium) sites.



Metallic Iron: Apollo 16: 60625 is an impact-melt breccia with a high plagioclase feldspar content, and an enriched rare earth element content (i.e. it is unusual for a breccia or impact-melt rock). Texturally it contains irregular pyroxene oikocrysts, enclosing euhedral plagioclase chadocrysts. Some plagioclase is shocked. The mineralogy is 65% plagioclase feldspar, 17% olivine and 16% pyroxene with minor ilmenite, armalcolite and a K-rich phase. In reflected light (above), metallic iron can be seen to form rounded crystals partially mantled by yellowish troilite. Width 1.8 mm. Credit: NASA (AGT Photographer).

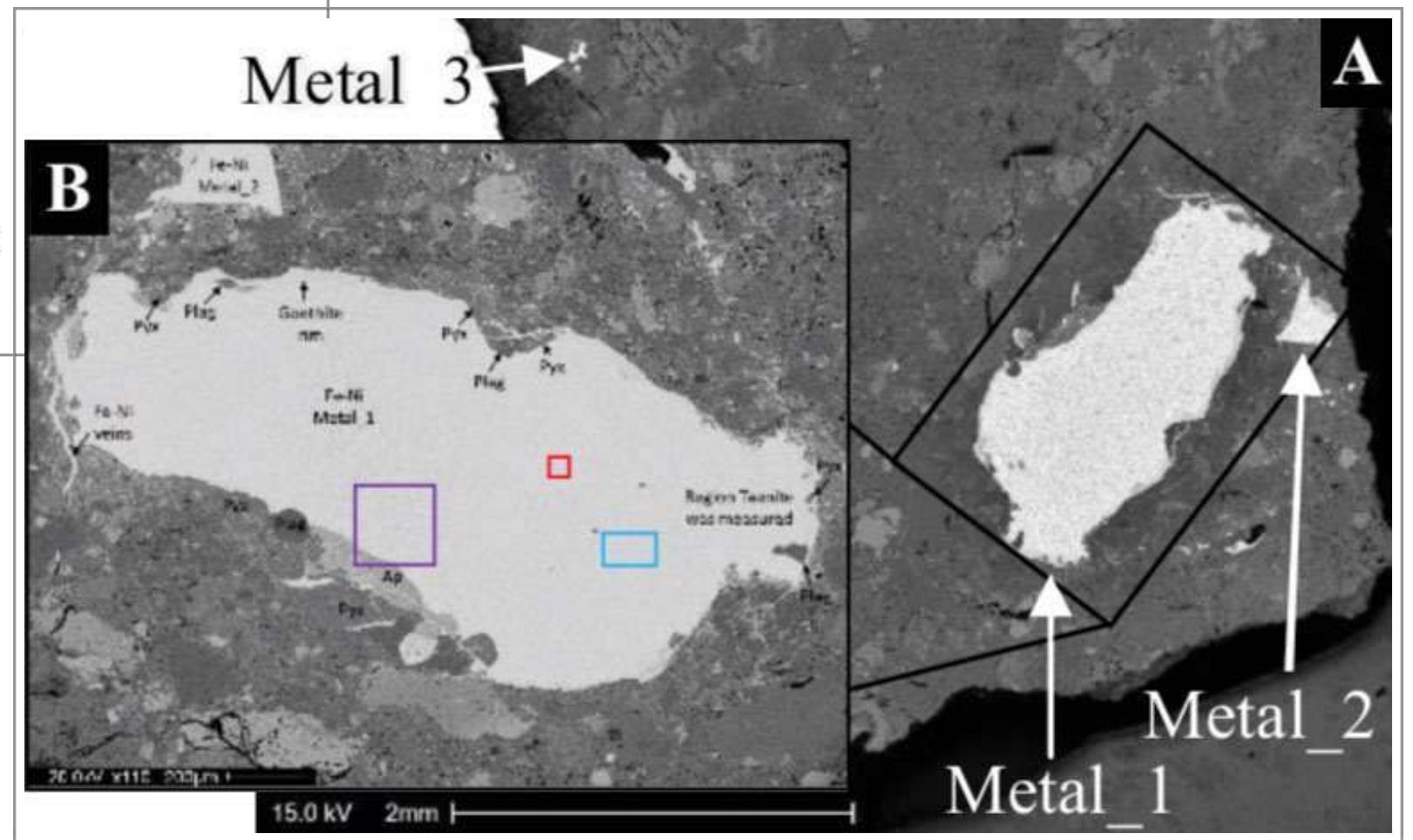


Metallic Iron: Apollo 16: 67475 is an impact-melt breccia containing unusual clasts. There are two major clast types - a dark clast rich in metallic iron (white crystals above associated with light grey ilmenite) and a light clast with a high percentage of olivine. Clasts of devitrified glass are also present in this sample. Other clasts are rich in troilite. Width 2.5 mm. Credit: NASA (AGT Photographer).

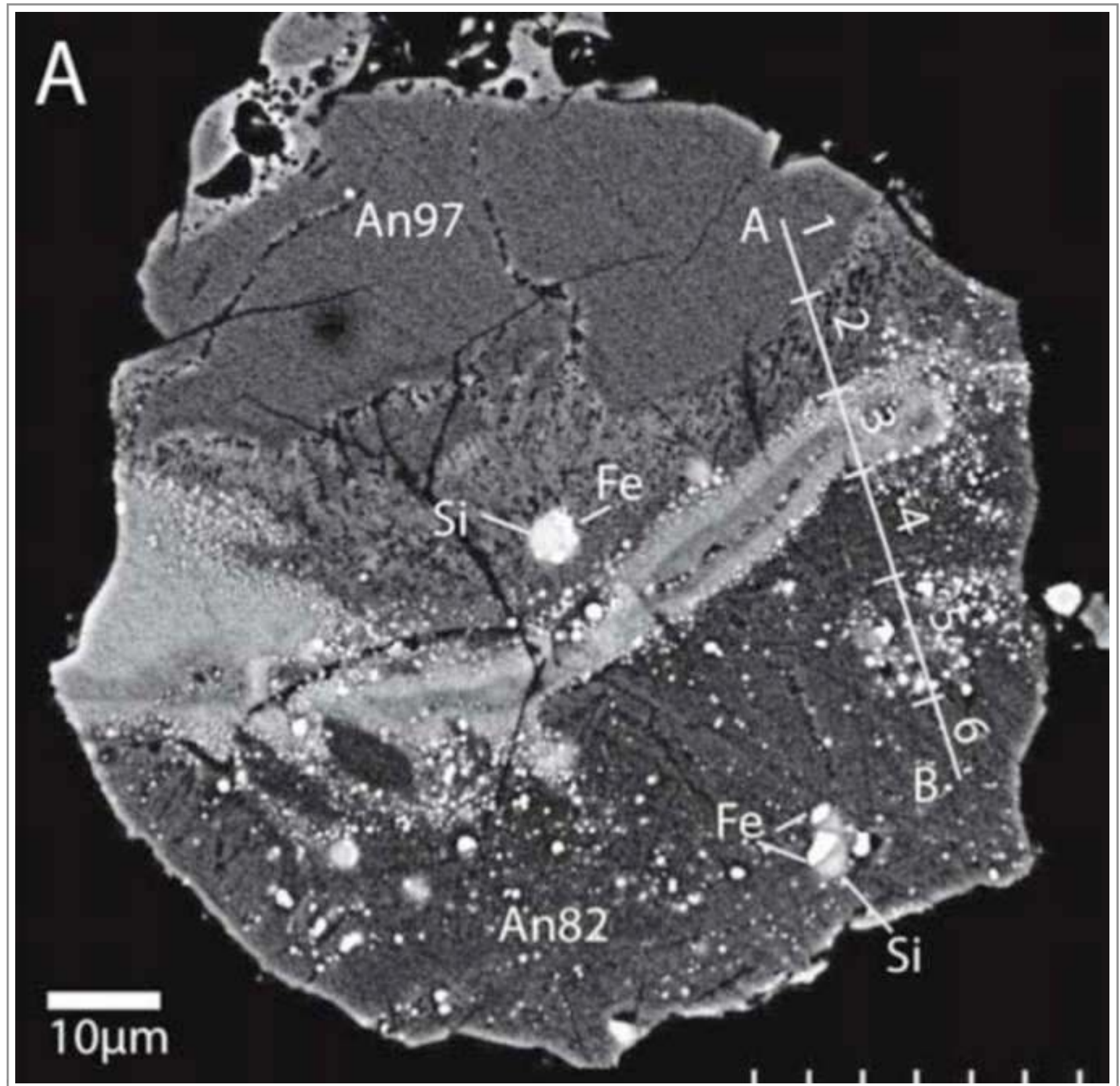


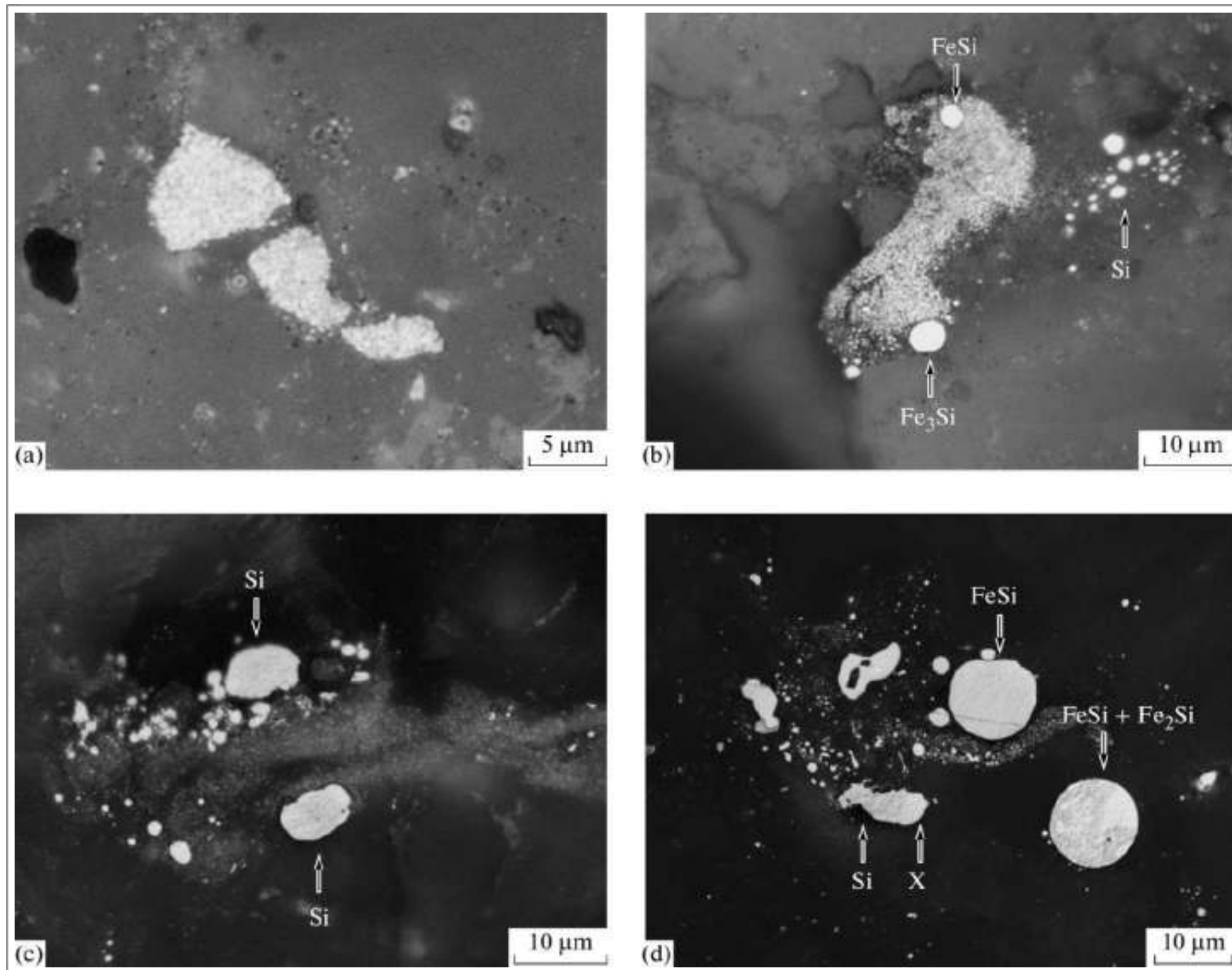
Below: Metallic iron in lunar regolith breccia meteorite NWA 10989. The metallic grain is composed of predominantly kamacite (low-Ni) with minor amounts of taenitic (high-Ni) material and K-rich schreibersite. Greyscale - backscattered electron images of metallic iron (light grey). The small coloured squares indicate where EBSD was used.

Above: Electron Backscatter Diffraction (EBSD) reveals the metal's internal microstructure to be an aggregate of variably orientated grains 50-150 μm in size cut by a vein of schreibersite. Colour gradients indicate gradual variations in lattice orientation, suggesting crystal lattice bending.



Silicon: backscattered electron image of a complex plagioclase feldspar fragment from Apollo 16: A6-8 anorthosite in the lunar regolith. It shows the entire grain and the locations of the largest native silicon (Si) grains associated with Fe-silicides (Fe). (An) is anorthite.





Taken From Nazarov et al. (2015)

Reflected light images (c–d = oil immersion) of native silicon and iron silicides in lunar anorthositic meteorite Dhofar 280. (a) A cryptocrystalline Si^0 object. (b) A cryptocrystalline Si^0 object of irregular shape with droplets of Fe silicides. Droplets of native silicon are nearby. (c) Droplets of native silicon on the periphery of a schlieren-like segregation. The opalescent matrix is enriched in SiO_2 . (d) Large droplets of Fe silicides spatially associated with numerous droplets of native silicon. The largest silicon grain has an irregular shape and occurs in intergrowth with a silicide (phase X), which probably has a Fe_3Si_7 composition.

Alloys

SPECIES

1. Hapkeite - Fe_2Si

1. Linzhiite - FeSi_2

1. Naquite - FeSi

2. Awaruite - Ni_3Fe

Hapkeite-Linzhiite-Naquite

Grains of three new Fe-Si phases from 2 to 30 μm in size were discovered in a regolith-breccia clast in Dhofar 280 - a lunar meteorite. This clast also contains numerous small (0.5-10 μm) FeNi metal grains, similar to an agglutinitic-glass-rich soil. X-ray maps of the Fe_2Si grain revealed hotspots of Ti- and P-rich areas in this grain (4.6 and 15 wt%, resp.). In general, more than 95 wt% of this mineral is composed of Fe and Si with only minor amounts of Ni, P, and Cr.

Synchrotron energy dispersive single-crystal X-ray diffraction was used to determine the crystal structure of one of the largest Fe-Si phase (Fe_2Si). Cell parameters obtained by this technique match well with those of synthetic Fe_2Si and confirm the first natural occurrence of this mineral.

The presence of these Fe-Si minerals in Dhofar 280 indicates extreme reducing conditions, whether on the Moon or on an asteroid. However, as hapkeite occurs in a fragmental lunar breccia, an extra-lunar origin is also possible (Anand et al., 2003a, 2004).

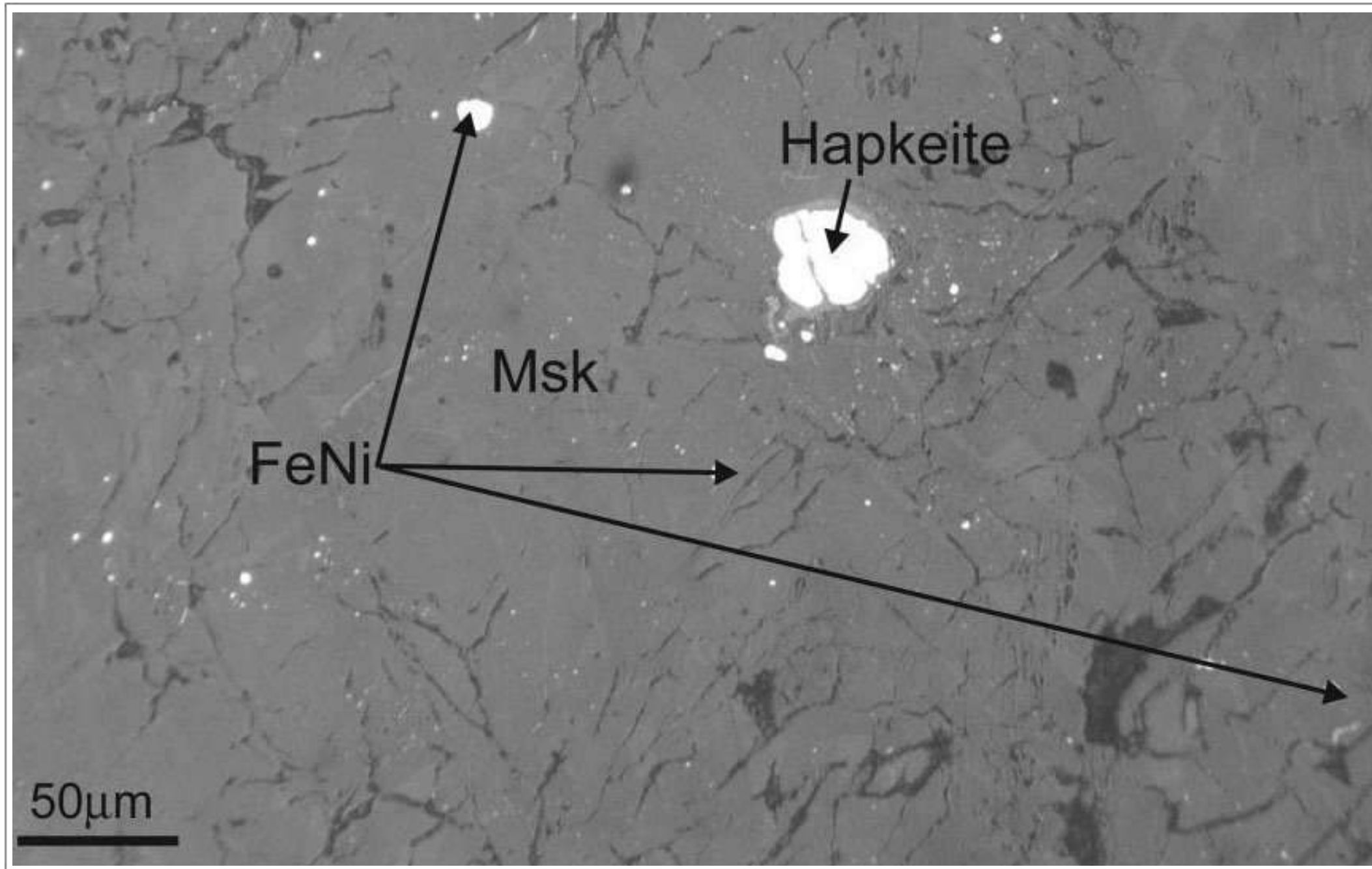
It was later suggested that the Si-rich association of Dhofar 280 has an impact origin and was formed by condensation of an impact-induced vapour, then remelted and mixed with the Dhofar 280 host rock. The formation of iron silicides

occurred when native silicon reacted with the FeO that was present in the impact melt (Nazarov et al., 2012b and 2015).

Later work suggests the two other Fe-Si phases are linzhiite (FeSi₂) and naquite (FeS). Both were named in 2012 by Shi et al. and Li et al. respectively, who describe terrestrial occurrences of these minerals.

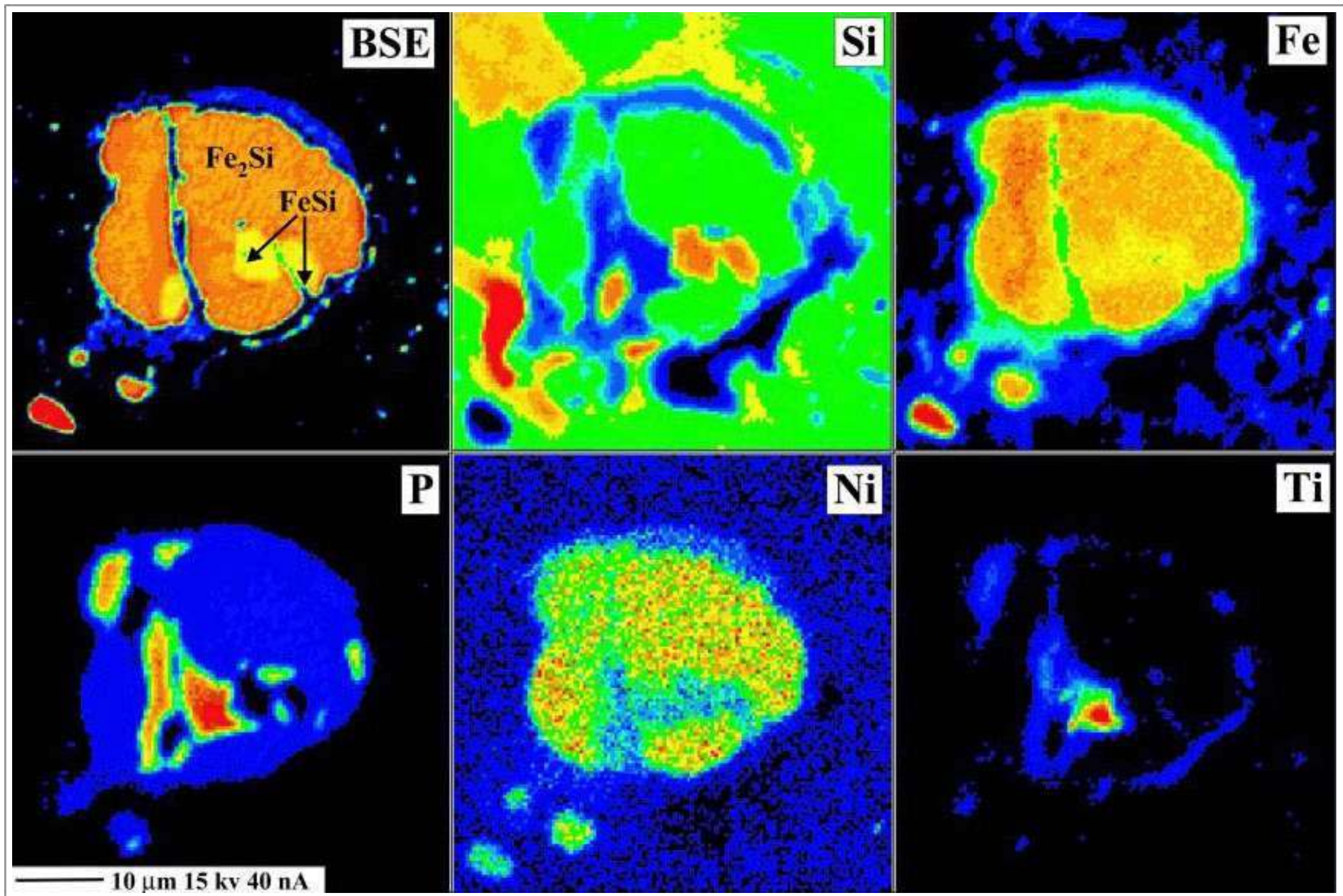
Awaruite

The Meteoritical Society report that rare awaruite has been found in the lunar feldspathic breccia NWA 8022 - a sample purchased in Morocco in 2013. This highly recrystallized breccia contains large anorthite grains (up to 2 mm), associated with extremely fine grained (~10 μm) anorthite, pigeonite, olivine, Cr-ulvöspinel, ilmenite, fayalite, kamacite and pentlandite. This discovery was later reported by Kuehner et al. (2014).



Taken From Anand et al. (2003a)

Hapkeite in lunar fragmental breccia Dhofar 280.
Metallic iron = FeNi; maskelynite = Msk



Taken From Anand et al. (2003a)

Backscattered electron (BSE) and elemental X-ray images of hapkeite in lunar fragmental breccia Dhofar 280. Intergrowths of an FeSi phase are seen in the lower part of the hapkeite. Elemental maps also reveal “hotspots” of Ti- and P-rich areas in this grain.

Sulphides

SPECIES

1. Troilite - FeS
2. Pyrrhotite - Fe_{1-x}S (where $x = 0.1 - 0.2$)
3. Mackinawite - FeS
4. Pentlandite - $(\text{Fe,Ni})_9\text{S}_8$
5. Chalcopyrite - CuFeS_2
6. Cubanite (chalcopyrrhotite) - $\text{Cu,Fe}_2\text{S}_3$
7. Sphalerite - ZnS
8. Greigite - FeFe_2S_4
9. Chalcocite? - Cu_2S
10. Bornite? - Cu_5FeS_4
11. Molybdenite? - MoS_2
12. Ninningerite? - $(\text{Mg,Fe,Mn})\text{S}$

Troilite

The most abundant sulphide mineral in lunar rocks is troilite. It commonly occurs with metallic iron in a eutectic texture and probably results from crystallization of an immiscible sulphide liquid.

In lunar crustal rocks, sulphides (dominantly troilite) occur as either primary magmatic crystallization products or as products of vapour/fluid interaction with existing crustal rocks. Magmatic troilite is typically found as discrete grains or in late-stage mesostasis pockets, sometimes intergrown with metallic iron. Vapour or fluid deposited troilite is often found to fill cracks or as intergrowths with olivine and/or pyroxene. These textures have been observed in clasts within Apollo 16 fragmental breccias 67915, 67016, and 66095 (known as the “Rusty Rock”), in Mg-suite troctolite 76535, and in Mg-suite gabbro-norite 76255 (McCubbin et al., 2015).

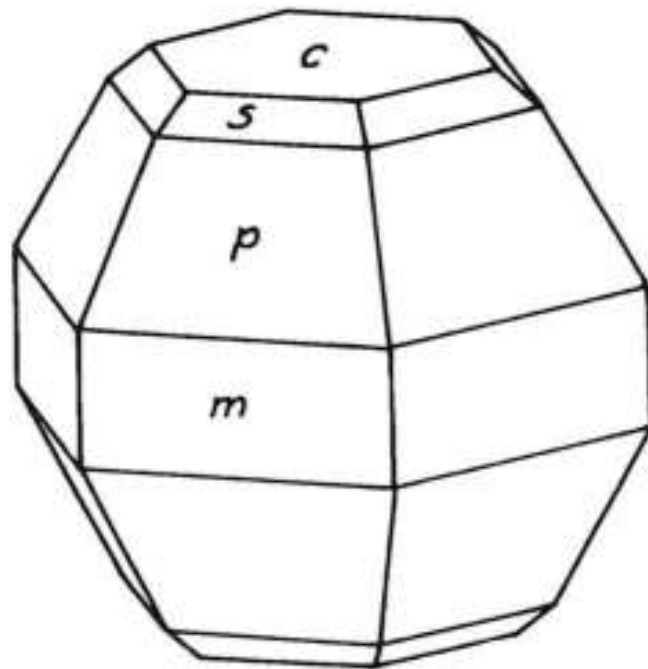
In Apollo 11 samples, troilite is always associated with metallic iron and this has been considered to indicate formation from an Fe-FeS liquid. However, troilite in Apollo 12 and 14 samples is more often found in an association with ilmenite and spinel (Fron del, 1975).

In Apollo 17 ilmenite basalt 75035 it is next in abundance to ilmenite with respect to the opaque minerals. It is represented by troilite-iron intergrowths, and less commonly by discrete isolated grains. Often large crystals of troilite or troilite-iron

intergrowths occur on the borders of tabular ilmenite crystals. Troilite also occurs with the zirconium-bearing phases and is present as inclusions in cristobalite (Meyer and Boctor, 1974).

Evans (1970) reports euhedral crystals of troilite in Apollo 11 10050 - a coarse-grained ilmenite basalt. They were found implanted on pyroxene crystals lining a vug.

Euhedral troilite in ilmenite basalt 10050 (Evans 1970).



Apart from troilite the remaining sulphides reported from the Moon appear to be mainly condensates from the vapour phase inside vugs (holes) within lunar breccias. They often form tiny well-formed crystals of mackinawite, pentlandite, chalcopyrite, chalcocite, cubanite (chalcopyrrhotite) or sphalerite (Cadogan, 1981).

Apollo 16 samples 67016,294, 67915,150, and 67016,297 represent clasts of Mg-suite and ferroan anorthosite lithologies that have interacted with a S-rich vapour to produce extensive troilite veins and replacement textures in these breccias. The replacement reaction consists of olivine being replaced by troilite + low-Ca pyroxene. “Wormy” shaped troilite also occurs adjacent to composite metallic iron grains (Shearer et al., 2012).

Pyrrhotite is reported with ilmenite, ulvöspinel, chromite, K-feldspar, glass, apatite, merrillite, tranquillityite, kamacite, taenite, troilite and mackinawite as part of the accessory mineral assemblage in basaltic lunar meteorite NWA 4734. Pyrrhotite is sparsely present as a eutectic intergrowth with ilmenite and was likely formed from mackinawite by re-condensation of shock-evaporated sulphur (Wang et al., 2012a; Wang and Hsu, 2016). Both pyrrhotite and pentlandite are reported from the Jiddat al Harasis 838 lunar meteorite - a fragmental breccia composed of a variety of lithic clasts and mineral fragments (Bouvier et al., 2017).

Mackinawite is tentatively identified from its strong bireflectance as tiny spots associated with troilite from porphyritic basalts 12018 and 12063 (Taylor and Williams, 1973). Frondel (1975) describes mackinawite occurring with troilite in Apollo 12 ophitic basalt 12038.

Mackinawite is also reported as a large bleb in a shock induced melt pocket within lunar meteorite NWA 4734 where it is considered to have formed when troilite was transformed to

mackinawite due to sulphur evaporation. The rounded morphology of mackinawite suggests that it was once melted spherules suspending in silicate melt due to immiscibility (Wang et al., 2012a; Wang and Hsu, 2016).

Chalcopyrite and cubanite are reported along cracks and grain boundaries of troilite from Apollo 12 pigeonite basalt 12021,134 (Taylor and Williams, 1973).

Chalcopyrite is also reported on the outside of native Cu rims around metallic iron grains in Apollo 15 pigeonite basalt 15475 (Taylor and Williams, 1973).

Chalcopyrite in association with pentlandite and troilite has been observed in vugs within Apollo 17 breccias 76016 and 76215 (Carter et al., 1975).

Pentlandite is reported from Apollo 14 regolith breccia 14315 (Ramdohr, 1972) and from lunar feldspathic breccia NWA 8022 - a highly recrystallized breccia that also contains anorthite, pigeonite, olivine, Cr-ulvöspinel, ilmenite, fayalite, kamacite and awaruite (Kuehner et al., 2014).

Sphalerite with 28 mol% troilite in solution has been documented in Apollo 16 anorthositic breccia impact melt 66095 (El Goresy et al., 1973b; Taylor et al., 1973). Textural relationships between sphalerite and the Cl-rich phases akaganéite and lawrencite in this sample suggest that they were produced during the same episode of low-temperature alteration. The exterior of troilite

grains have been unevenly modified to sphalerite and griegite (Shearer et al., 2014).

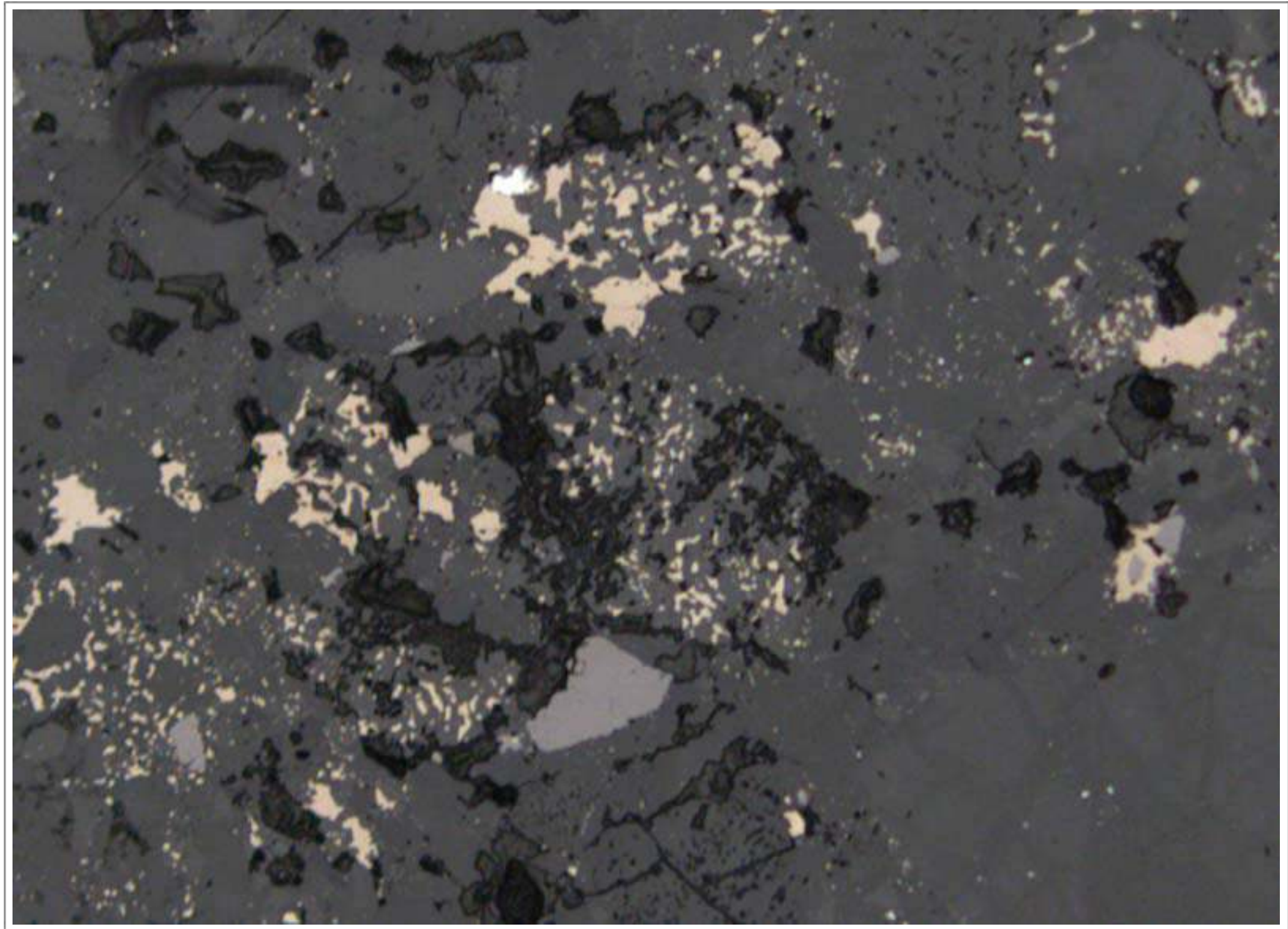
The rare sulphides often condensed from the vapour phase inside holes (vugs) in lunar breccias (Cadogan, 1981).

Chalcocite is reported from Apollo 12 rocks without supporting data (Fron del, 1975).

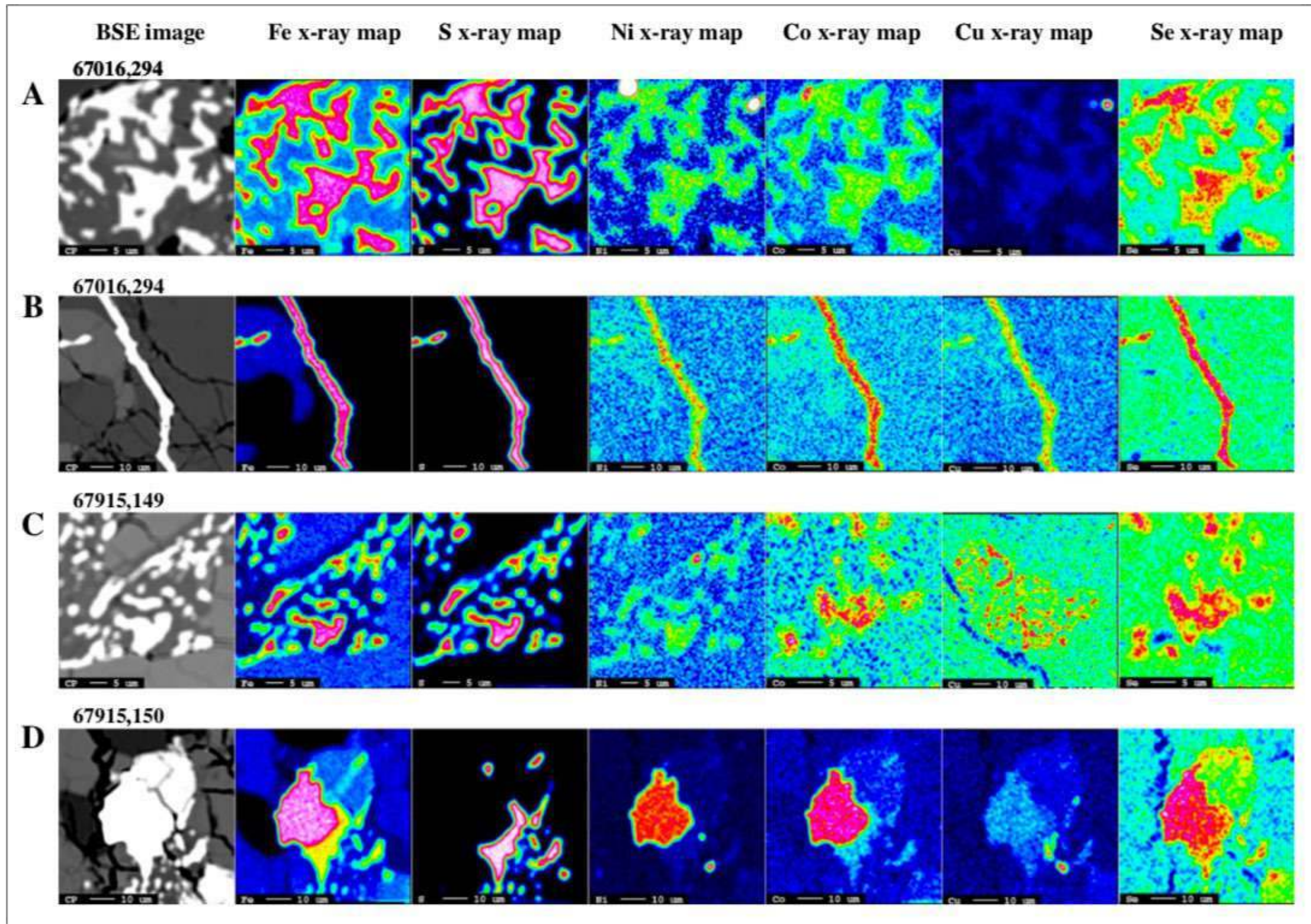
Bornite is tentatively reported from Apollo 16 soil 68841 where it is said to occur with minor troilite coating a metallic spherule (Smith and Steele, 1976).

Molybdenite is reported in lunar samples but almost certainly is not of lunar origin. It was commonly used on the Apollo missions as a lubricant (Cadogan, 1981).

Ninningerite, largely of meteoritic origin is a very rare lunar mineral found in regolith samples. It is a characteristic mineral component of enstatite chondrites (Cadogan, 1981; Heiken et al., 1991). Fifteen grains of niningerite are reported from Apollo 15 soil sample 15602,29 (Fron del, 1975).

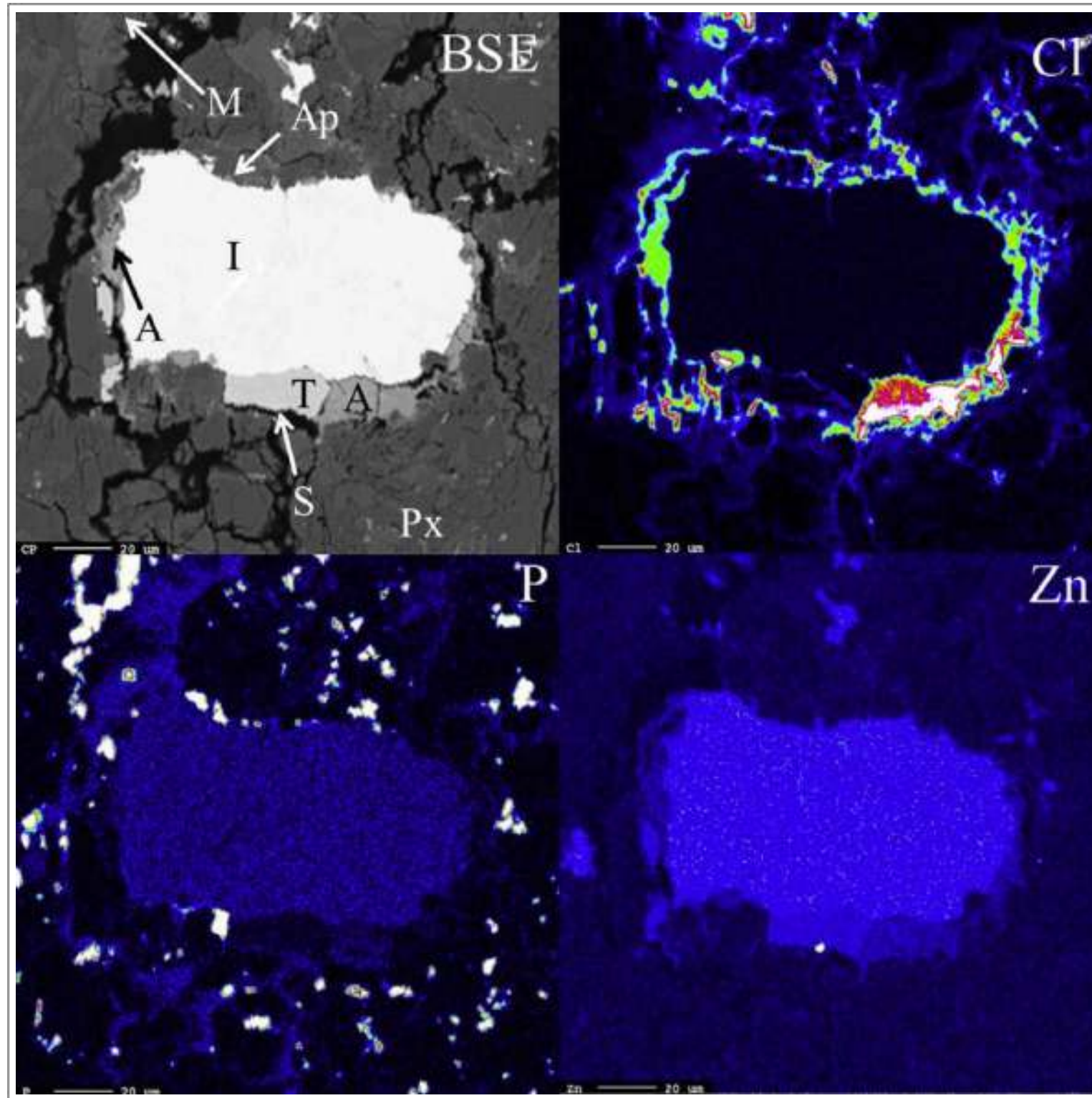


Troilite: Apollo 16: 67475 is an impact-melt breccia containing unusual clasts. There are two major clast types - a dark clast rich in metallic iron and a light clast with a high percentage of olivine. Clasts of devitrified glass are also present. Other clasts such as the one illustrated in the reflected light image above are rich in troilite (yellow). Width 0.75 mm. Credit: NASA (AGT Photographer).



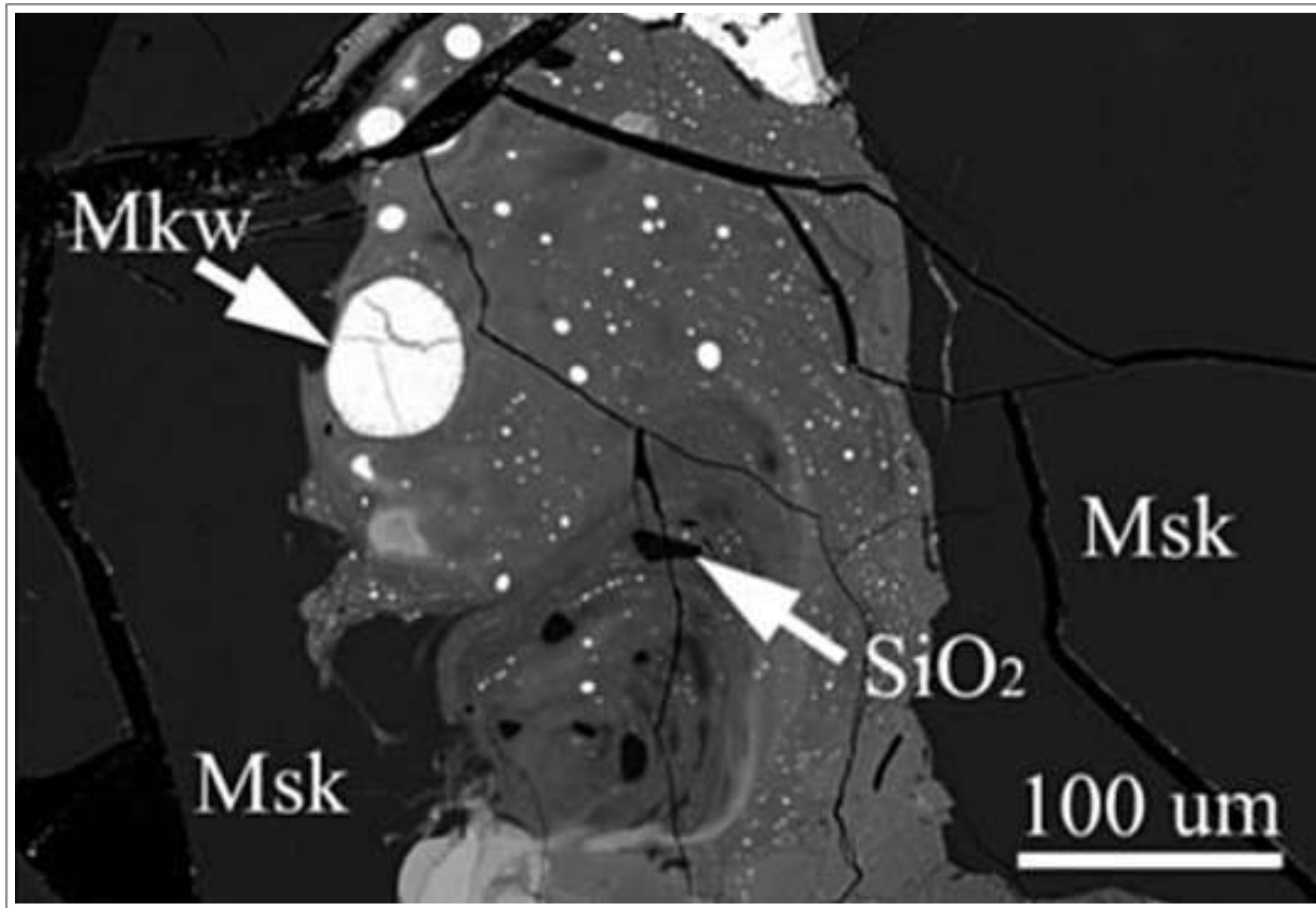
Taken From Shearer et al. (2012)

Apollo 16 samples 67016,294, 67915,150, and 67016,297 represent clasts of Mg-suite and ferroan anorthosite lithologies that have interacted with a S-rich vapour to produce extensive troilite veins and replacement textures in these breccias. The replacement reaction consists of olivine being replaced by troilite + low-Ca pyroxene.



Taken From Shearer et al. (2014)

Apollo 16 “rusty rock” impact-melt 66095. Backscattered electron (BSE) and X-ray maps (Cl, P, Zn) illustrating low-temperature alteration surrounding a metallic iron grain (I). Minerals in the BSE image include apatite (Ap), merrillite (M), pyroxene (Px), troilite (T), sphalerite (S) and akaganéite, in addition to other Fe-bearing phases (A).



Taken From Wang et al. (2012a)

Backscattered electron image of basaltic lunar meteorite NWA 4734 - image shows a shock-induced melt pocket with numerous Fe-sulphide globules. The biggest globule is mackinawite (Mkw). Maskelynite (Msk) surrounds the melt pocket.

Carbides and Phosphides

SPECIES

1. Graphite - C
2. Cohenite - $(\text{Fe,Ni,Co})_3\text{C}$
3. Moissanite - SiC
4. Schreibersite - $(\text{Fe,Ni})_3\text{P}$
5. Barringerite - $(\text{Fe,Ni})_2\text{P}$

Graphite

Graphite has been found with FeS - as a nodule in an α -iron fragment of Apollo 14 soil 14003 (Goldstein et al., 1972). It is thought that diamond has not been found on the Moon because instead its potential source (meteoritic carbon) was vapourised during impact (Cadogan, 1981).

Graphite was also found by Dikov et al. (2002) who used electron diffraction studies to examine the surface layers of lunar orange glass spherules from Apollo 17 sample 74220. Precipitation via a chemical vapour deposition process on the spherule surface from a carbon-rich vapour cloud was proposed.

Moissanite

The carbide moissanite has been briefly described as a terrestrial contaminant on the Moon (Cadogan, 1981). The author does not mention the rock type in which moissanite was found.

Moissanite was also found by Dikov et al. (2002) on the surface layers of lunar orange glass spherules from Apollo 17 sample 74220.

Regolith particles from the Luna 16 drill-core are also inferred to contain moissanite (Dikov et al., 1998 & 1999) and an origin for the carbon from the impact of a comet or a carbonaceous chondrite-like body was proposed.

Cohenite

The carbide cohenite has been found as a separate phase in a few metal particles from Apollo 11, 14, 16 and 17 soils. It has also been observed in melt rock 66095, in mesostasis-rich melt rock 64559 and in poikilitic rock 73275. Identification of cohenite has been made on the basis of its greater hardness and slightly yellow colour when compared to kamacite, and by its weak reflection anisotropism (Taylor et al., 1973).

Cohenite occurs in an aggregate with ilmenite, troilite, crystalline SiO₂, apatite and metallic iron in Apollo 11 ilmenite basalt 10017 (Adler et al., 1970).

Carbide forms by precipitation of carbon from the γ -taenite phase on cooling of lunar metal particles in their host rocks or soil fragments. Carbide-metal assemblages are found in anorthositic hornfels, melt rock, dark matrix breccia and agglutinate, but not in any primary igneous rocks (Goldstein et al., 1976).

Schreibersite

Apollo 16 impact-melt rock 66095 contains metallic iron with a characteristic intergrowth of schreibersite and to a lesser extent, cohenite (Taylor et al., 1973). Melt rocks 60615, 60666 and 65779 also contain schreibersite. Accessory amounts of ilmenite, armalcolite, metallic iron, spinel, chromite, rutile and troilite are common associates (Dowty et al., 1974).

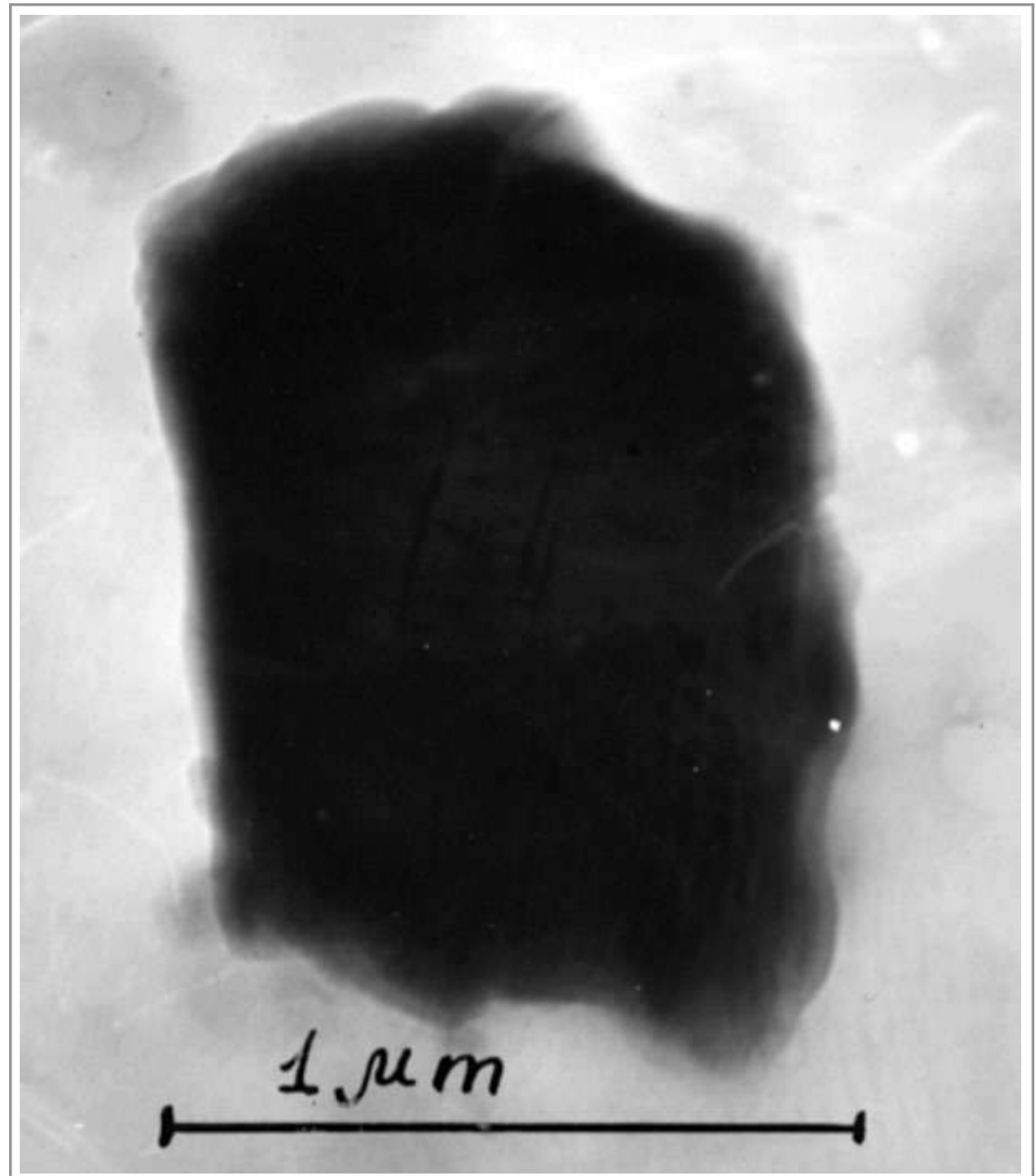
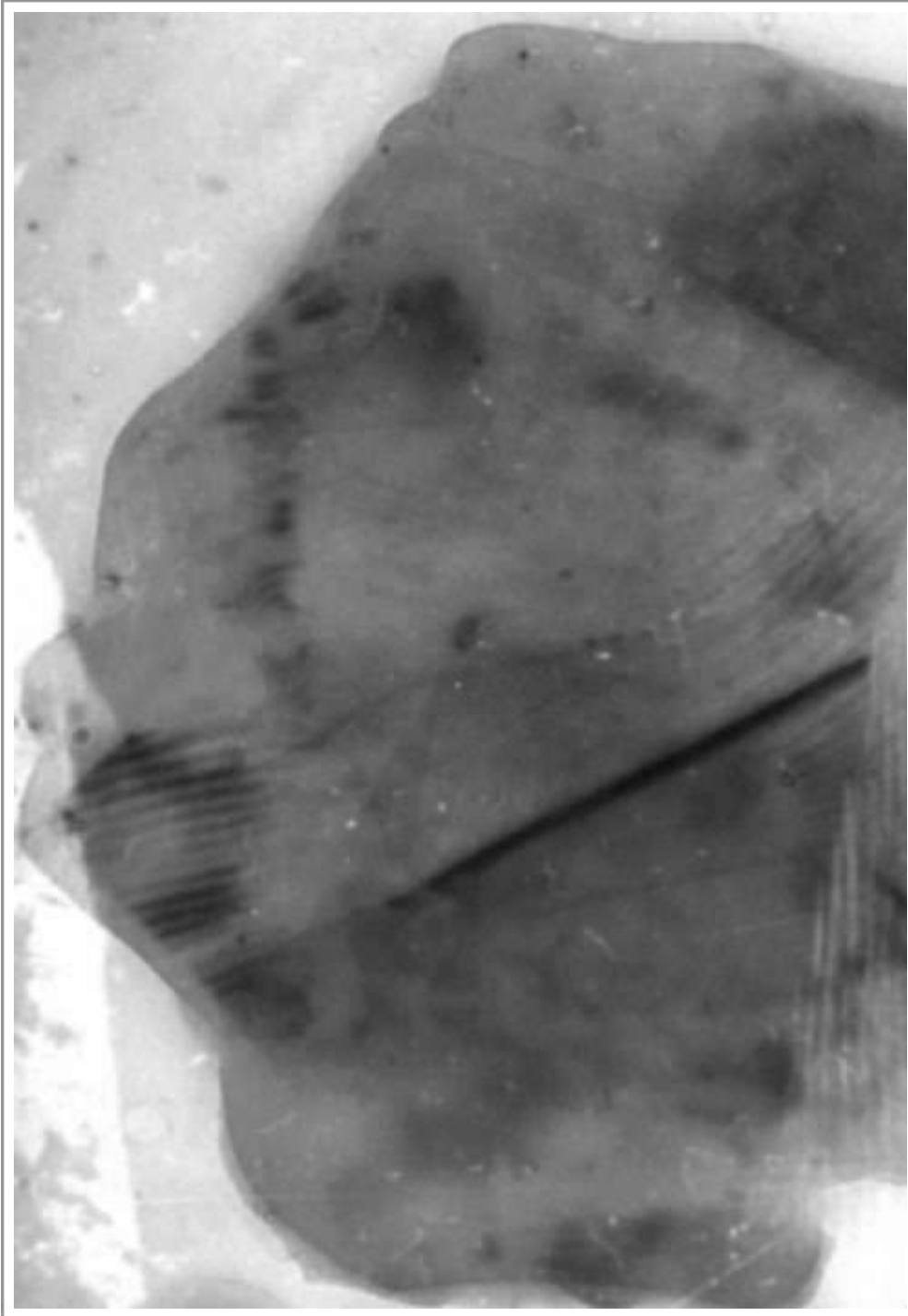
In a study of alteration assemblages in Apollo 16 “rusty rocks”, Jean et al. (2016) noted cohenite and schreibersite as intergrowths within many of the FeNi metal grains. Their samples included 60016, 63585, 65359, 66036, 68505, 60255, 64455, 65759, 66055, 68841, 60625, 64567, 65766, 66095, 69935, 61135, 65095, 65779, 67455, 69941, 62241, 65326, 66035, 68501, 69961.

When occurring as needles and elongate crystals, schreibersite has been given the varietal name of rhabdite. Gooley et al. (1973) studied Apollo 16 soil and reported 4 μ m wide rhabdite lamellae in sample 64657.

Schreibersite is also reported from feldspathic breccia NWA 5000 - the largest (11.528 kg) lunar meteorite yet found (Connelly et al., 2007).

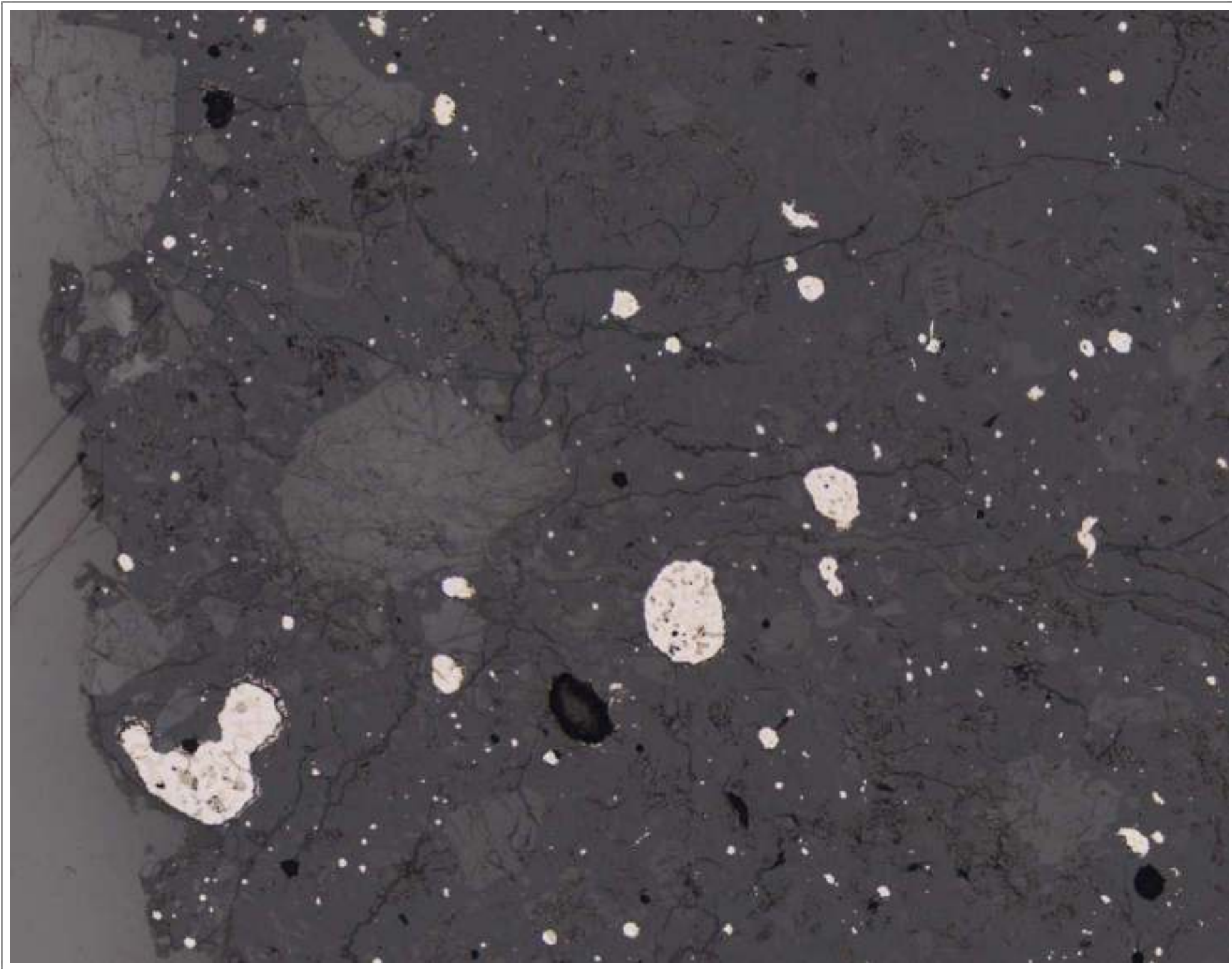
Barringerite

One grain of the phosphide barringerite has been found in lunar meteorite Yamato 793274 (Koeberl et al., 1991). The sample is a shock lithified fragmental breccia containing a minor regolith component and numerous mafic mineral fragments and glasses. It is a mixture of about two thirds mare material and one third highland component.

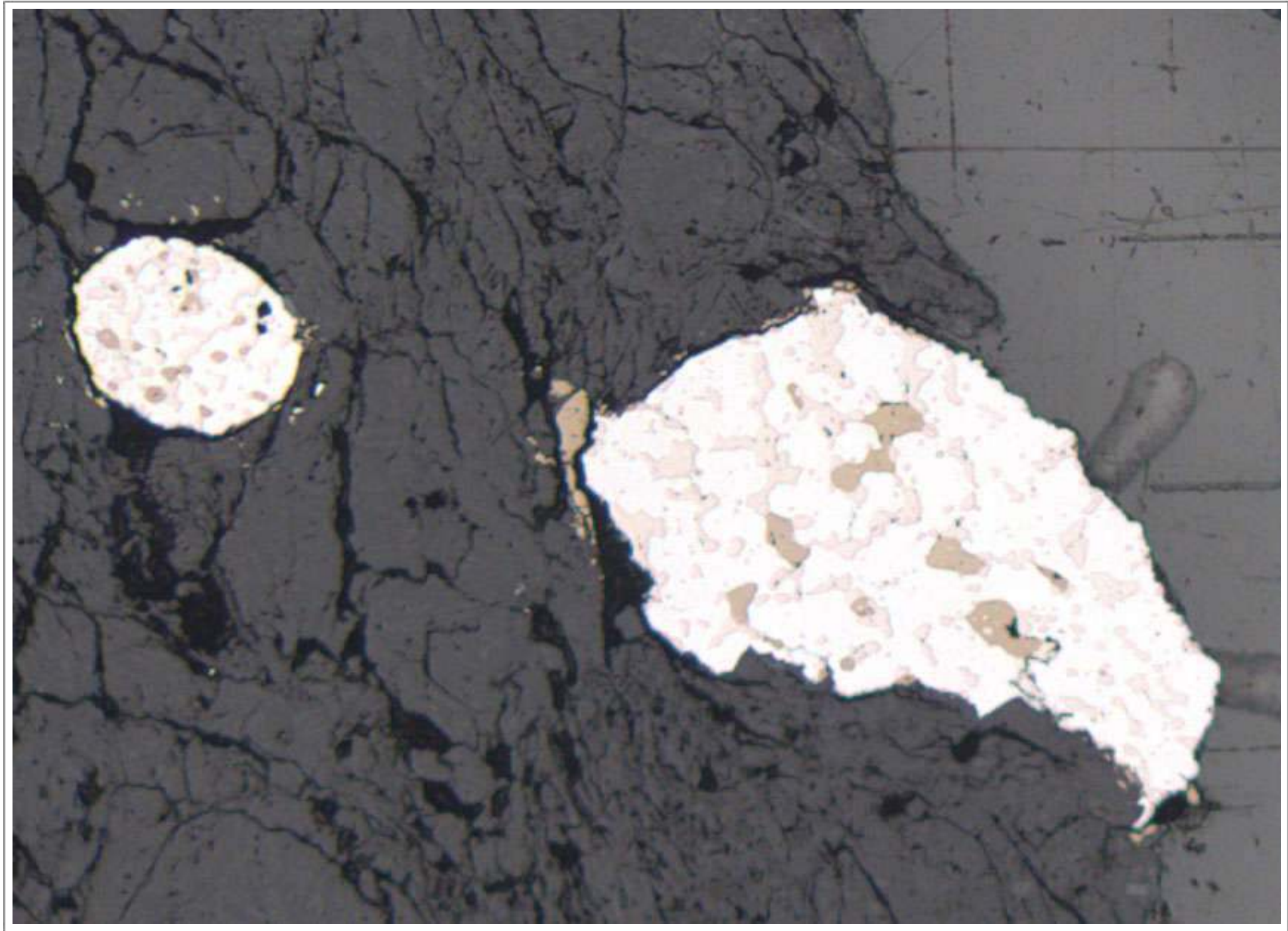


Taken From Dikov et al. (2002)

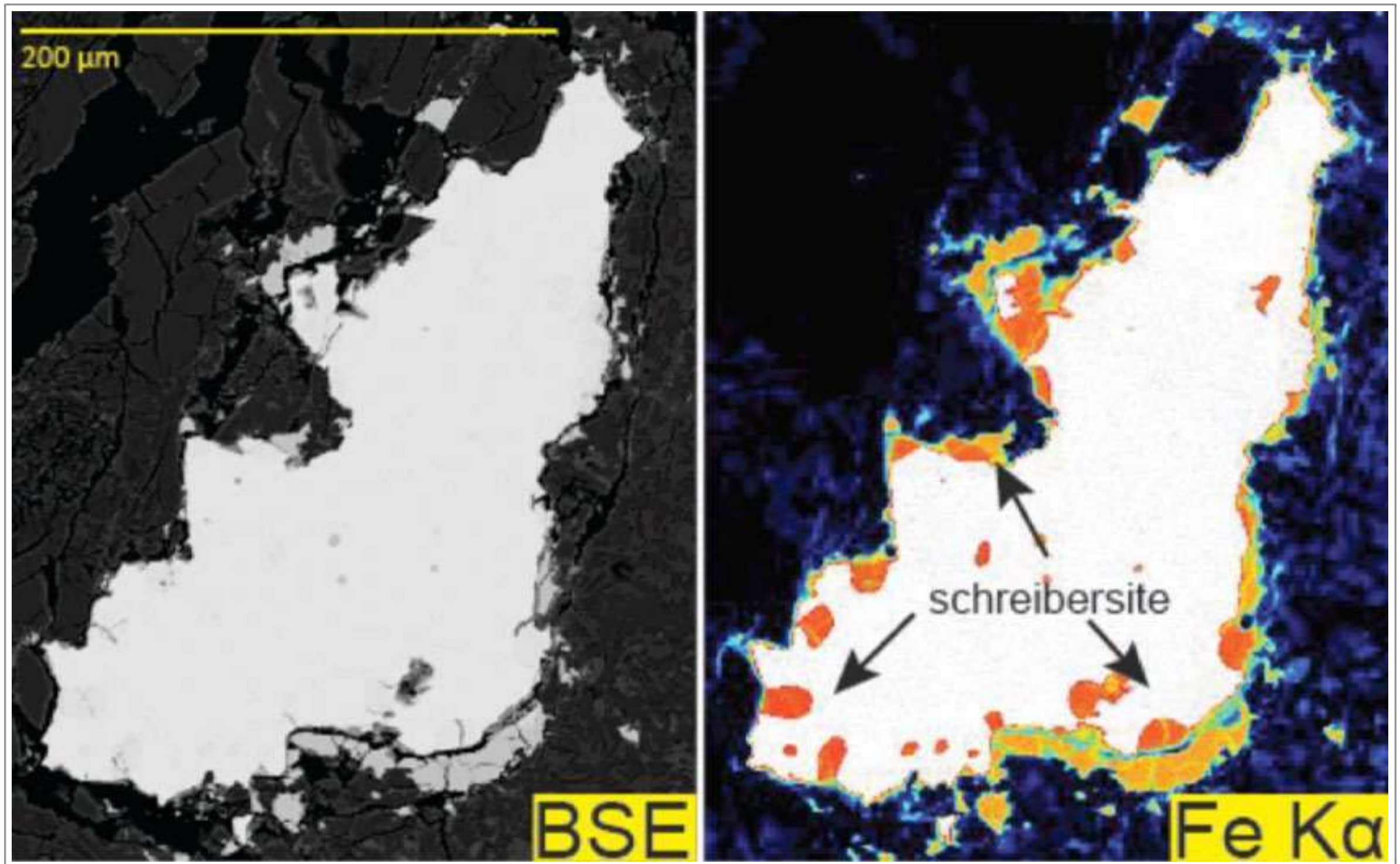
Graphite (left - 1 μm across) and moissanite (right) from the surface layers of orange glass spherules in Apollo 17 sample 74220.



Schreibersite: Apollo 16: 68115 is a heterogeneous breccia which is welded together by flow-banded glass. The sample appears to be made up of a wide variety of impact melts, with a variety of recrystallized textures. The generally aluminous composition and frequent large plagioclase inclusions indicate that the precursor material was ferroan anorthosite. The sample contains abundant schreibersite (deeper yellow) as inclusions in metallic iron. Reflected light image; width 3.5 mm.



Schreibersite: Apollo 16: 66055 is a polymict breccia with a composition intermediate between fragmental breccias and glassy melt breccias. The sample contains schreibersite (deeper yellow) inclusions within grains of metallic iron. The iron includes nickel-rich taenite and nickel-poor kamacite. Troilite forms elongate crystals and tiny blebs around the metallic iron. Reflected light image; width 1.6 mm.



Taken From Jean et al. (2016)

Schreibersite inclusions (orange) in a metallic iron grain in Apollo 16 “rusty rock” impact-melt 66055. Troilite (yellow) partially rims the grain.



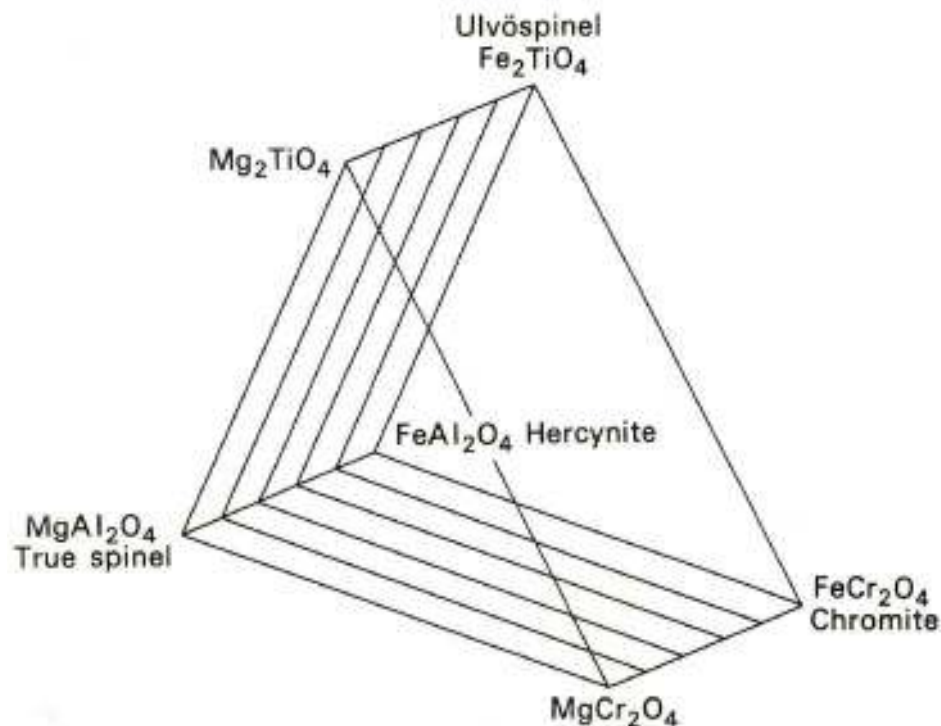
Taken From Koeberl et al. (1991)

Backscattered electron image of barringerite in lunar meteorite Yamato793274,94 - a fragmental breccia.

Spinel Group

SPECIES

1. Spinel - $MgAl_2O_4$
2. Pleonaste - an intermediate variety of the Hercynite-Spinel Series (iron-rich spinel or magnesium-rich hercynite)
3. Ulvöspinel - Fe_2TiO_4
4. Chromite - $FeCr_2O_4$



In lunar samples, members of the spinel group tend to be intermediate between chromite and ulvöspinel, but like pyroxene, spinel may be strongly chemically zoned (from Cadogan, 1981).

Spinel group minerals are the second most abundant oxide minerals found on the Moon. This group, has a widely varying composition and actually consists of a complex series of solid solutions. Members of this group include: chromite, $FeCr_2O_4$; ulvöspinel, Fe_2TiO_4 ; hercynite, $FeAl_2O_4$; and spinel (sensu stricto), $MgAl_2O_4$.

Brett et al. (1973) published data on oxide minerals found in lithic fragments collected during the Soviet Luna 20 un-manned mission to the Moon (February 1972). Oxide minerals occur as discrete grains, as rounded to angular grains in micro-breccia and agglutinates, and as rare euhedral to anhedral grains in crystalline fragments. Spinel has the best developed crystals. Chromite occurs in all lithic types, with the exception of spinel troctolite, whereas ulvöspinel occurs rarely in fragments of non-mare origin but is more abundant in mare basalt.

Further subdivision of the Luna 20 fragments gives rise to the following compositional groups:

(1) spinel; (2) spinel-pleonaste; (3) chromian-pleonaste; (4) Mg-Al-chromite; (5) Al-titanian-chromite; and (6) Al-titanian spinel. Groups 1-4 and group 6 are primary crystallization products whereas two modes of occurrence of group 5 are present. The first are primary chromites and the second a chromite exsolved from ilmenite in association with an iron-bearing rutile (Haggerty, 1973b).

Spinel/Pleonaste

The magnesium spinel found in many Fra Mauro breccias is slightly chromiferous pleonaste. Light to bright pink in thin section, examples are abundant in Apollo 14 breccia sample 14063 and have also been reported in samples 14321 and 14318. A red example is present in sample 14066. Other examples include breccia samples 14049, 14055, 14066, 14171, 14303, 14305, 14312, 14314, 14319 and 14320 (Christophe-Michel-Levy and Levy, 1972).

The presence of several vol% Mg-rich pleonaste, or “pink spinel” differentiates the spinel troctolites from the troctolites, the latter of which never contain Mg-rich spinel. Spinel troctolite samples include Apollo 12 12071, Apollo 14 14304, Apollo 15 15295, 15445; Apollo 16 65785, 67435; Apollo 17 73263, 76503, 77517. The spinel troctolites all occur as clasts within polymict breccias and have been heavily shocked, which led to them sometimes being referred to as spinel cataclasites. Two spinel troctolite clasts from Apollo 11 (72425,8 and 72425,30) contain olivine and plagioclase along with Mg-rich spinel grains, and one sample (72435,8) contains a single grain of cordierite. Up to 11 modal % ispinel is reported from Apollo 17 spinel cataclasite 72435 (Baker and Herzberg, 1980).

Apollo 16 spinel troctolite 65785 is also notable, as it is the only lunar sample to host the rare Mg phosphate farringtonite. One

small (< 4 μm) grain was found included in spinel (Dowty et al., 1974).

A spinel troctolite clast in Apollo 15 breccia 15295 contains cordierite along with olivine, plagioclase and pink Mg-rich spinel (Shearer et al., 2015b; Treiman et al., 2019) and another spinel troctolite clast in Apollo 16 sample 67435 retains a cumulate texture (Prinz et al., 1973; Ma et al., 1981; Marvin et al., 1989; Treiman et al., 2019). In both cases, pink spinel occurs as rounded equant grains enclosed in olivine, plagioclase, or cordierite. In the partially melted troctolite fragment in Apollo 12 12033,618 spinel forms perfectly euhedral crystals and is the first solid phase to form from melted olivine + plagioclase (Marvin and Walker, 1985).

Prissel et al. (2016) note spinel is commonly observed in the lunar troctolites as anhedral to euhedral mineral grains and also inclusions within both olivine and plagioclase indicating it is a primary crystallization product of a Mg-suite parent magma.

Lunar meteorite ALHA 81005,9 - a polymict, anorthositic regolith breccia from the lunar highlands, contains a spinel anorthositic troctolite clast with ~30% of a pale purple (Mg,Fe)Al spinel. The spinel forms euhedral crystals and is in contact with olivine and plagioclase, but not pyroxene. It could have formed as a spinel cumulate from an impact melt of troctolitic composition or from a picritic magma body that assimilated crustal anorthosite on its

margins. All of the critical petrologic inferences suggest the latter (Gross and Treiman, 2011).

A large (1.1 mm across) euhedral pink spinel grain has been found in lunar meteorite NWA 10401 - an anorthositic troctolite with a granulitic texture. The spinel displays a symplectite intergrowth zone of Cr-rich spinel and plagioclase around its entire rim followed by a plagioclase-zone and an olivine-zone. Both zones re-trace the original euhedral spinel crystal faces. Each corona represents different diffusion fronts or gradients and indicate that although the spinel originated from a slowly cooled parental melt was not in equilibrium at the end of the crystallization process (Gross et al., 2017).

Similar spinel grains with coronas have also been noted in NWA 5744 (a KREEP-poor, troctolitic lunar meteorite) by Robinson and Kring (2018). These authors also report a large pleonaste grain in a similar lunar meteorite - NWA 8687. The spinel has a deep red colour in plane polarised light and a unique reaction texture with plagioclase and olivine coronas, associated with opaque minerals including ilmenite.

Remotely sensed high-resolution compositional data from NASA's Moon Mineralogy Mapper suggest that "pink spinel anorthosite" (PSA) represents a new member of the plutonic Mg-suite. It has an unusually low modal abundance of mafic silicates, distinguishing it from known lunar spinel-bearing samples (Pieters

et al., 2011; Prissel et al., 2014) and is inferred to contain 20-30% Mg-Al spinel (Gross et al., 2014).

Magnesium-rich spinel assemblages occur in two vitric breccia lunar meteorites - Dhofar 1528 and Graves Nunataks (GRA) 06157. Dhofar 1528 contains troctolitic and gabbroic clasts in which cumulate Mg-rich spinel crystals are associated with Mg-rich olivine, Mg- and Al- rich pyroxene, plagioclase and rare cordierite. GRA 06157 contains a troctolitic clast hosting anhedral spinel associated with olivine, plagioclase feldspar and minor skeletal clinopyroxene. These spinel assemblages resulted from the impact melting of Mg-rich rocks and do not represent remotely sensed "pink spinel anorthosite". Thermodynamic equilibrium calculations indicate that some of these cumulate spinel assemblages could have originally crystallized at depths of 42 to 100 km or deeper, making them plausible representatives of lunar upper mantle rocks (Wittmann et al., 2018).

Treiman et al. (2019) examined the formation of lunar spinel, by considering the enthalpy (i.e., heat) required to produce spinel anorthosite by assimilation or dissolution of anorthite (from lunar anorthosite) into basaltic and picritic magmas. They concluded that near the lunar surface, the most likely process of spinel formation is rapid crystallization of impact melts of anorthosite + picrite or peridotite compositions. The presence of spinel anorthosite on the walls and central peaks of impact craters results from rapid cooling and partial crystallization of

superliquidus melts produced in the impacts, and not from uplift of deep material to the Moon's surface.

Ulvöspinel

Cameron (1970) studied the opaque mineral assemblages in four Apollo 11 samples - two ilmenite basalts (10044,50 & 10058,32), a fragmental breccia (10060,32), and a sample of regolith fines (10084,64). He found ulvöspinel always intergrown with ilmenite and commonly associated with metallic iron. The Cr content of ulvöspinel in these samples is low and approaches end-member composition.

Ulvöspinel is the dominant spinel group species found in three Antarctic meteorites: two are crystalline mare basalts - Asuka-881757 and MIL 05035; and the third a polymict regolith breccia with a large basaltic clast - MET 01210 (Arai et al., 2010).

Other Antarctic lunar mare meteorites were studied by Arai et al. (1996). Two are unbrecciated igneous basalts (Y-793169 and A-881757). In A-881757 the spinel is very Fe-rich chromian ulvöspinel. In Y-793169 titanian chromite and chromian ulvöspinel were both found - as accessory minerals in late-formed mesostasis regions of the sample. In common with Apollo 12 mare basalt 12064 there is a marked compositional gap between the two spinel group species. Petrographic studies of vitrophyric

mare basalts indicate that Cr-rich spinel tends to be almost entirely crystallized at a very early stage.

Anand et al. (2006) studied lunar meteorite La Paz (LAP) Icefield 02205 - (a low-Ti mare basalt) and note that spinels are the second most abundant of the opaque minerals and occur as aluminous chromite rimmed by ulvöspinel, with the latter being more abundant. Cr-rich spinel generally occurs in or near forsteritic olivine. The LAP spinel compositions follow fractionation trends similar to spinels in Apollo 12 and Apollo 15 mare basalts.

Similar ulvöspinel-chromite compositions are reported by Joy et al. (2014) from clasts in three brecciated lunar meteorites - Dhofar 925 (a glassy impact melt breccia), Dhofar 961 and Sayh al Uhaymir 449 (both lithic polymict breccias). Additionally, a spinel-pleonaste composition is reported from a clast-bearing impact melt.

A unique spinel crystallization assemblage is noted for lunar mare basalt meteorite Asuka 881757. The absence of titanian chromite and the variations in composition and texture of the chromian ulvöspinel are atypical, compared to the co-existing chromite and ulvöspinel in the majority of Apollo and Luna basalts. Results from cooling experiments by Arai et al. (2006) suggest that chromian ulvöspinel crystallized solely from highly-fractionated interstitial melts in the late stage of crystallization of the parent basalt.

Chromite

Chromian spinel is a useful and important petrogenetic indicator because of systematic relationships among spinel chemistry, bulk-rock composition, cooling history, mineral assemblage and geological processes (Sack and Ghiorso, 1991). For low-Ti mare basalts, Arai et al. (2006) note the principal cationic substitution is represented by $\text{Fe}^{2+} + \text{Ti}^{4+} \leftrightarrow 2(\text{Cr}^{3+}, \text{Al}^{3+})$ with substantial

substitution of Mg and Fe. Most spinels tend to occur as titanian chromite mantled by chromian ulvöspinel, although some show discontinuous compositional variations between the two with a sharp boundary, indicating that later chromian ulvöspinel discontinuously precipitated onto the earlier titanian chromite without subsequent subsolidus equilibration.

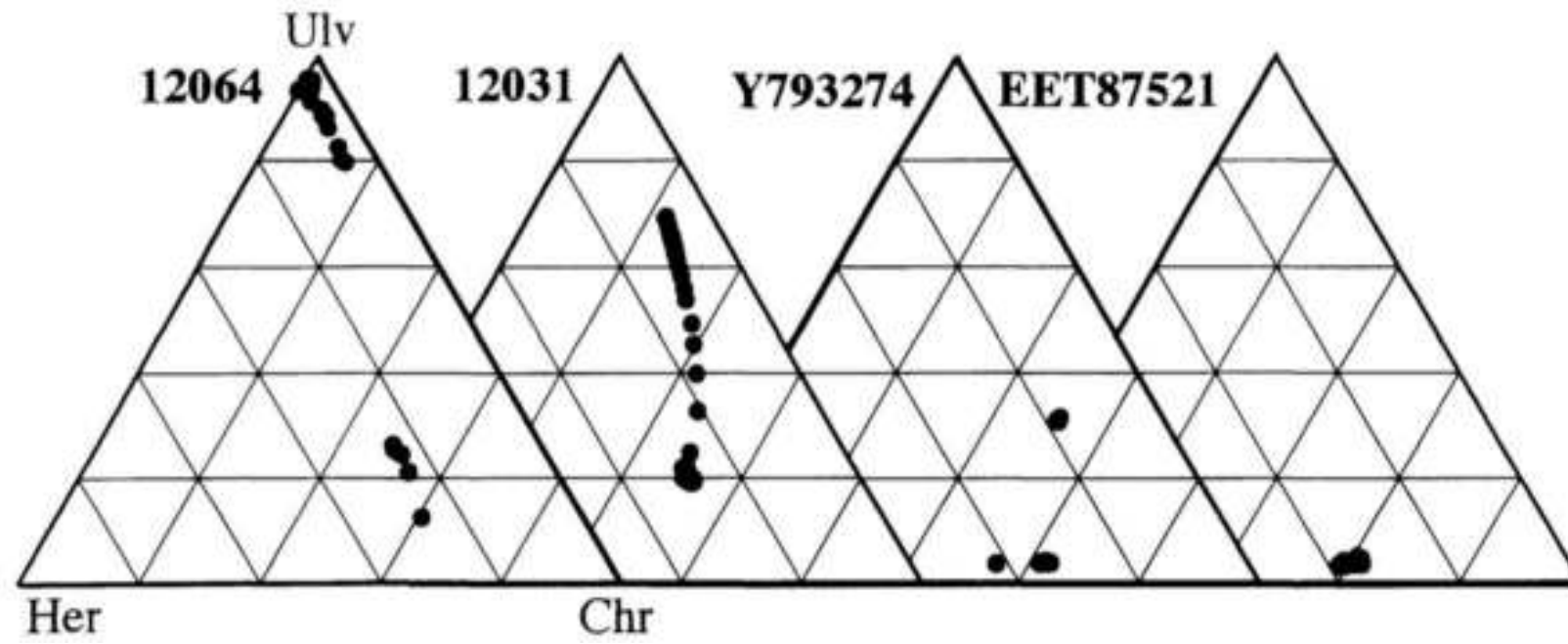
Zoned chromite-ulvöspinel crystals are reported in Apollo 15 olivine basalt 15555,171 by Dalton et al. (1974). The marked transition of ulvöspinel to chromite corresponds with the onset of plagioclase crystallization.

Chrome-spinel forming symplectite with pyroxene was the focus of a study of Apollo 17 troctolite 76535. The most common symplectite type has a fine, wormy intergrowth of clinopyroxene and chrome-spinel at an olivine-plagioclase contact. McCallum & Schwartz (2001) were able to show that 76535 and other lunar troctolites are igneous cumulates and it appears likely that some

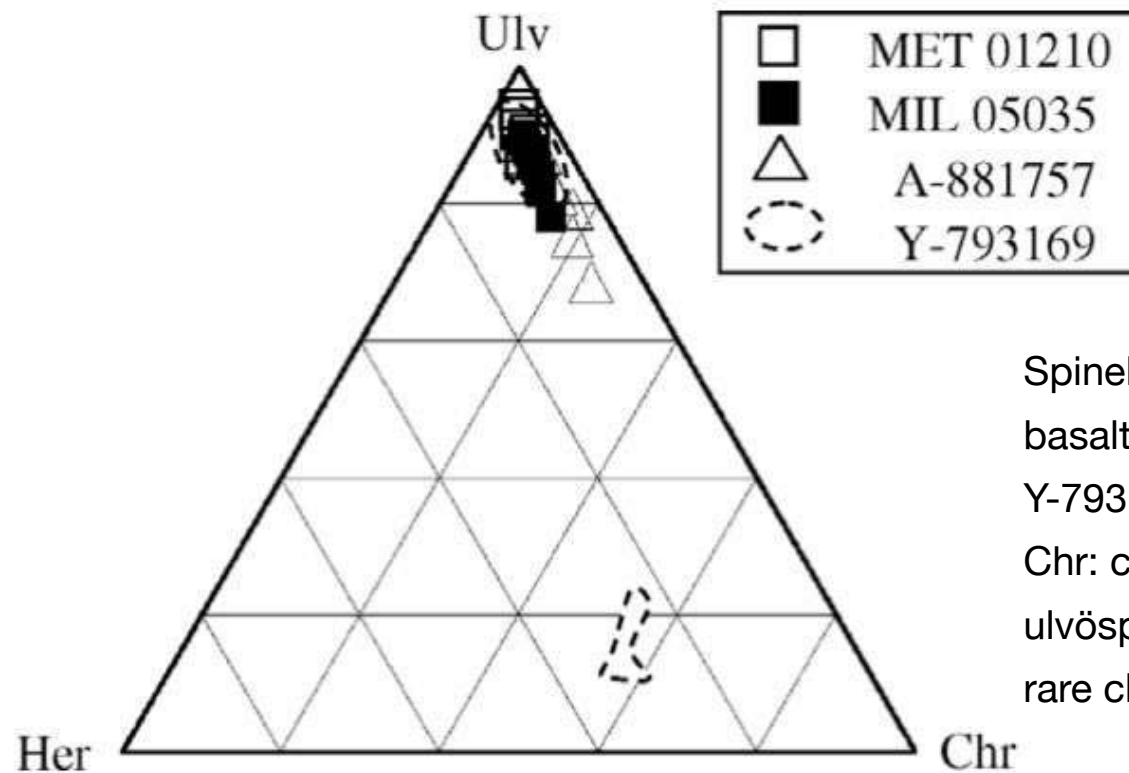
are residues from crustal melting processes at a depth of 30-50 km.

However, Elardo et al. (2012) reinterpreted troctolite 76535. They confirm it contains large amounts of Cr in symplectite assemblages consisting of Mg-Al-chromite and two pyroxenes and suggest proposed symplectite formation mechanisms including crystallization of trapped interstitial melt, diffusion of Cr from cumulus olivine, and/or remobilization of cumulus chromite grains is in doubt. Multiple textural observations, melt inclusion chemistry, and modelling of chromite-olivine equilibrium rule out previously proposed symplectite formation mechanisms, and strongly suggest that chromite was not a primary crystallization product of the 76535 parental magma. Accordingly, the post-cumulus addition of Cr and Fe is required to produce the symplectites. After considering multiple models, the addition of Cr and Fe to 76535 via infiltration metasomatism by an exogenous chromite-saturated melt is the model most consistent with multiple textural and geochemical observations.

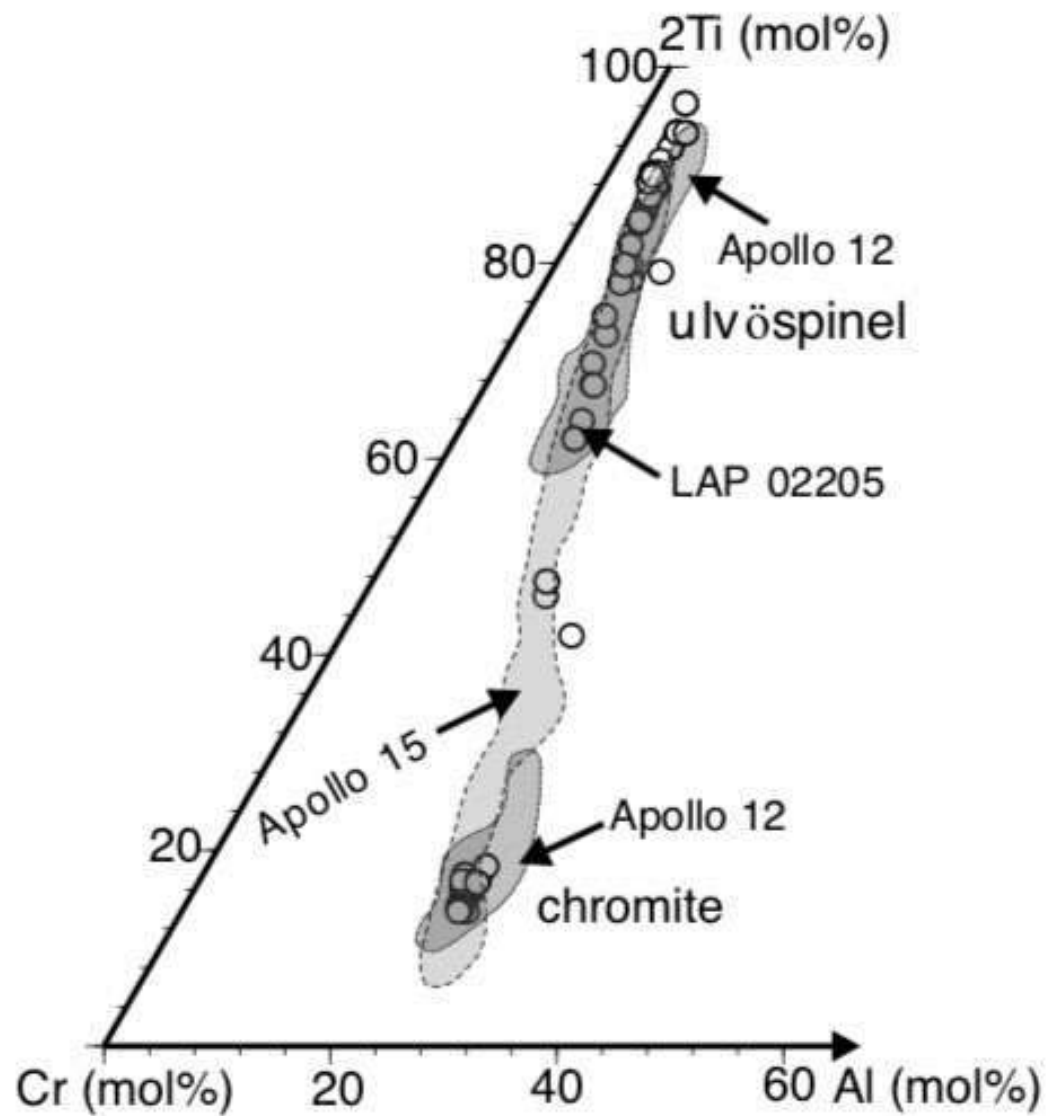
The impact melted granulitic breccia lunar meteorite Dhofar 1766 hosts chromian spinel. Crystals are granular and 30 to 250 μm across. Variable degrees of decomposition and recrystallization has produced zoned, variably Mg, Fe, Cr and Ti-rich clusters of micro-crystals (to $<1-10 \mu\text{m}$) with interstitial spaces empty or filled with feldspathic material (Wittmann et al. 2014).



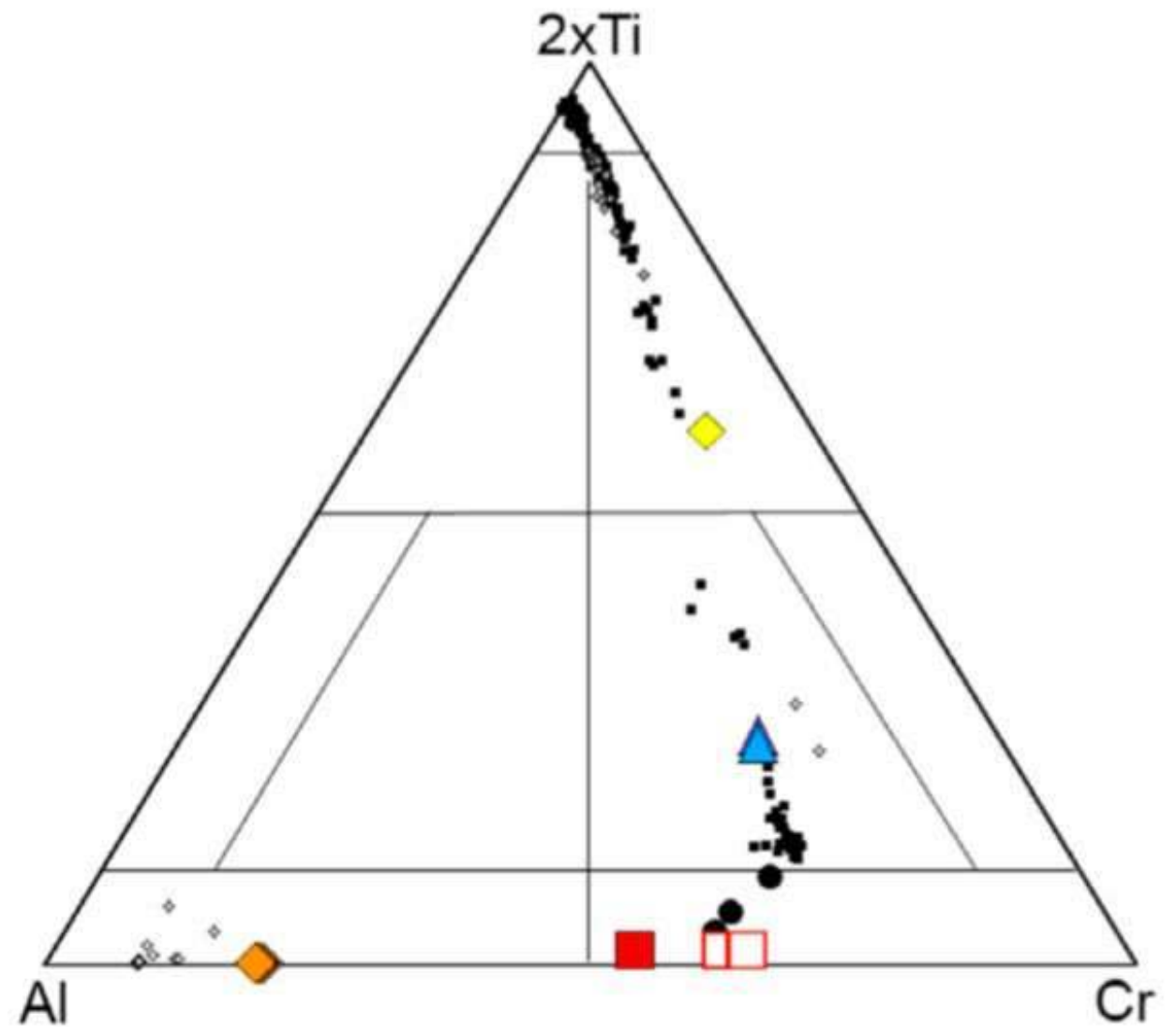
Spinel compositions in two Apollo 12 samples - 12064 (ilmenite basalt) and 12031 (pigeonite basalt) compared to two Antarctic lunar meteorites Y793274 (regolith breccia) and EET87521 (fragmental breccia). Chr: chromite, Her: hercynite, ulv: ulvöspinel (Arai et al., 1996).



Spinel compositions in Antarctic basaltic lunar meteorites MET 01210, Y-793169, A-881757 and MIL 05035. Chr: chromite, Her: hercynite, ulv: ulvöspinel. Y-793169 includes one rare chromite grain (Arai et al., 2010).



Spinel compositions in lunar meteorite LaPaz Icefield (LAP) 02205 (a low-Ti mare basalt) plotted on a ternary plot of 2Ti–Cr–Al (in mol %). Compositions follow the lunar trend defined by Apollo 12 and 15 samples (Anand et al., 2006).



Lunar meteorites

- LAP basalts
- ◇ MIL 05035 basalt
- ◇ NWA 4472

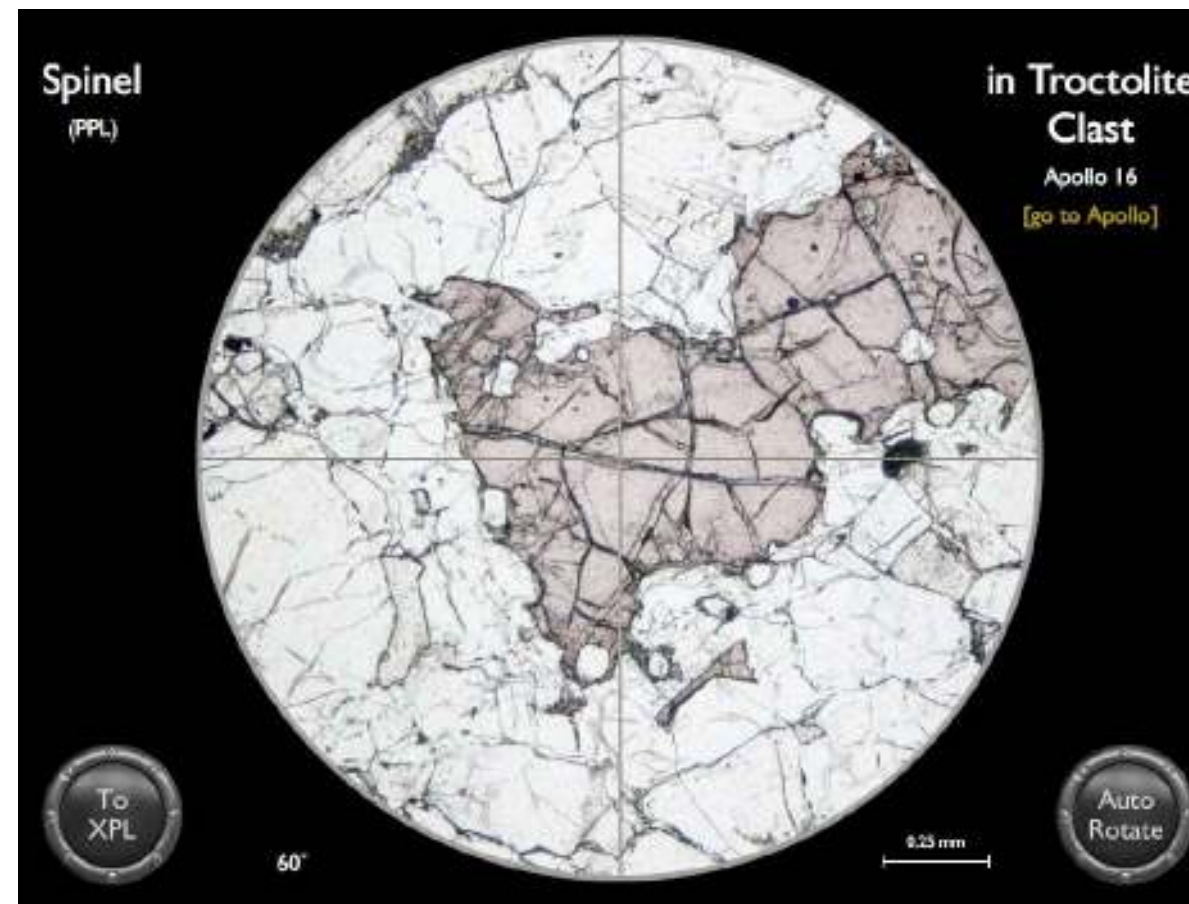
Dhofar group meteorites

- Matrix
- Basalt (Dho_961_1_Clast 15)
- Basalt (SaU_449_3_Clast 81)
- ◆ Type 1 crystalline IMB
- ◆ Clast-bearing glassy IMB
- ▲ Granulite (coarse-grained)

Spinel data from brecciated lunar meteorites Dhofar 925,1; 961,1 and SaU 449,3 compared with other lunar meteorites (Joy et al, 2014). Note this diagram is in reverse when compared with the previous figure.

Moon Minerals: Spinel

Mineral Virtual Microscope: Spinel (Pleonaste)



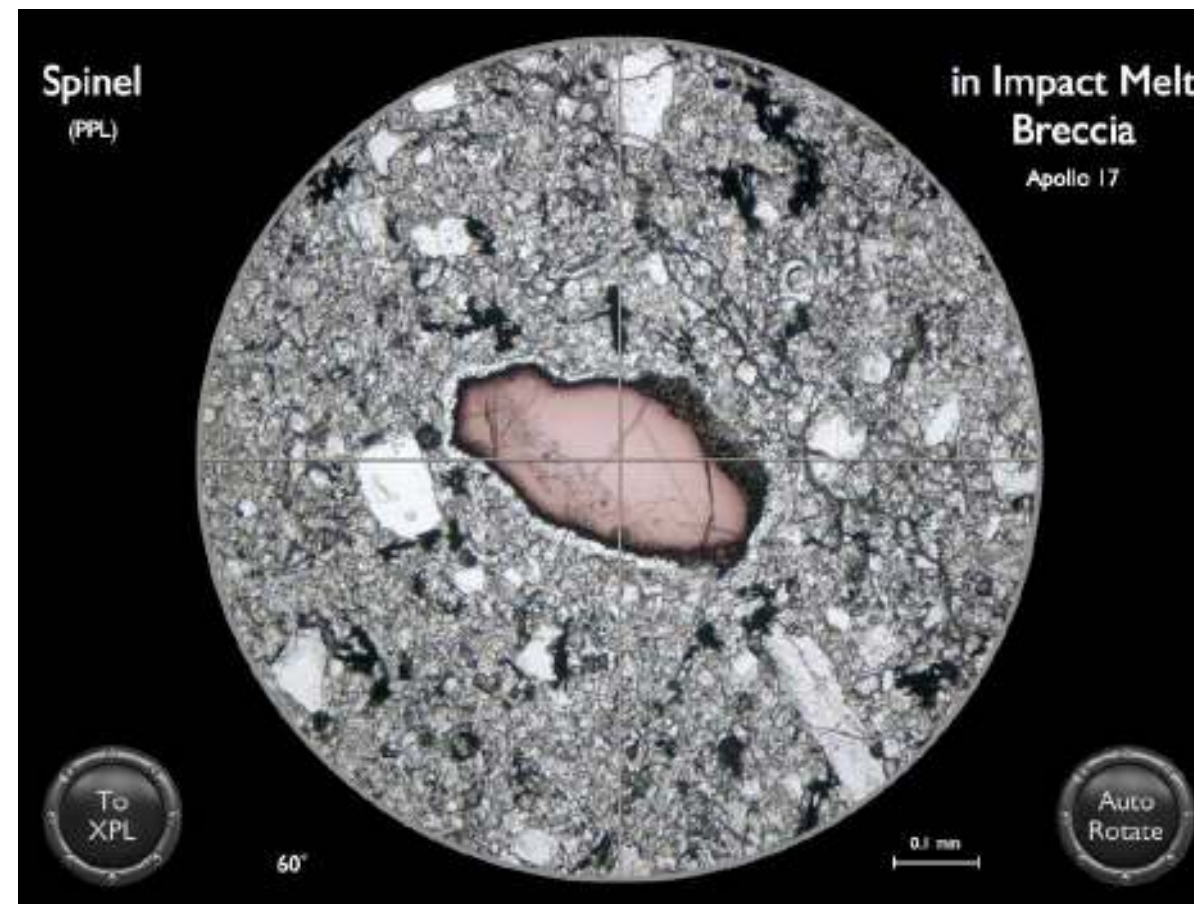
Pink spinel (pleonaste) in a troctolite clast within an impact melt. Plagioclase feldspar is the associated species.

Apollo 16, Sample 65785.

Credit: NASA (AGT Photographer)

Moon Minerals: Spinel

Mineral Virtual Microscope: Spinel (Pleonaste)



Pink spinel (pleonaste) in impact-melt breccia. Plagioclase feldspar is the main associated species.

Apollo 17, Sample 77518.

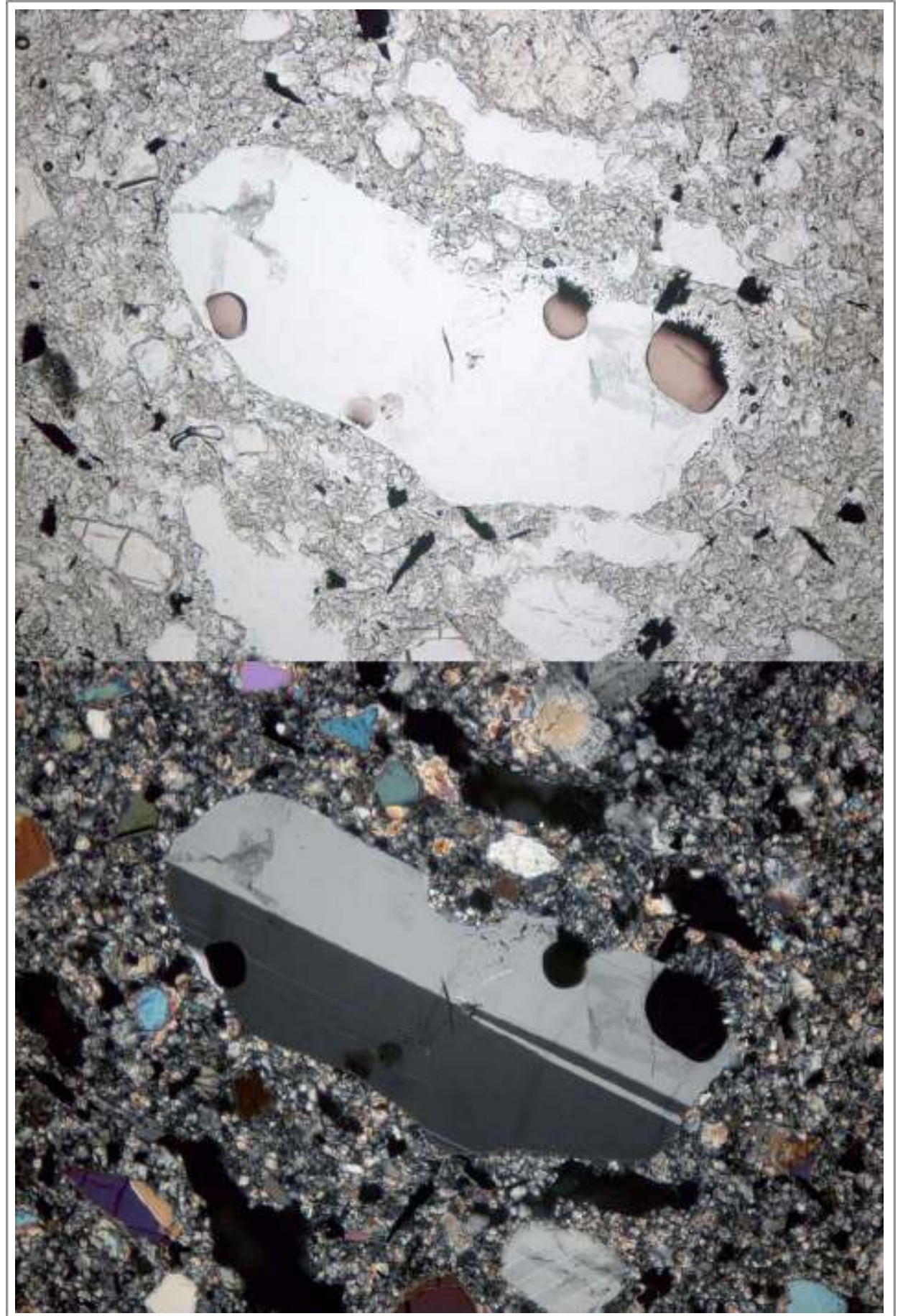
Credit: NASA (AGT Photographer)

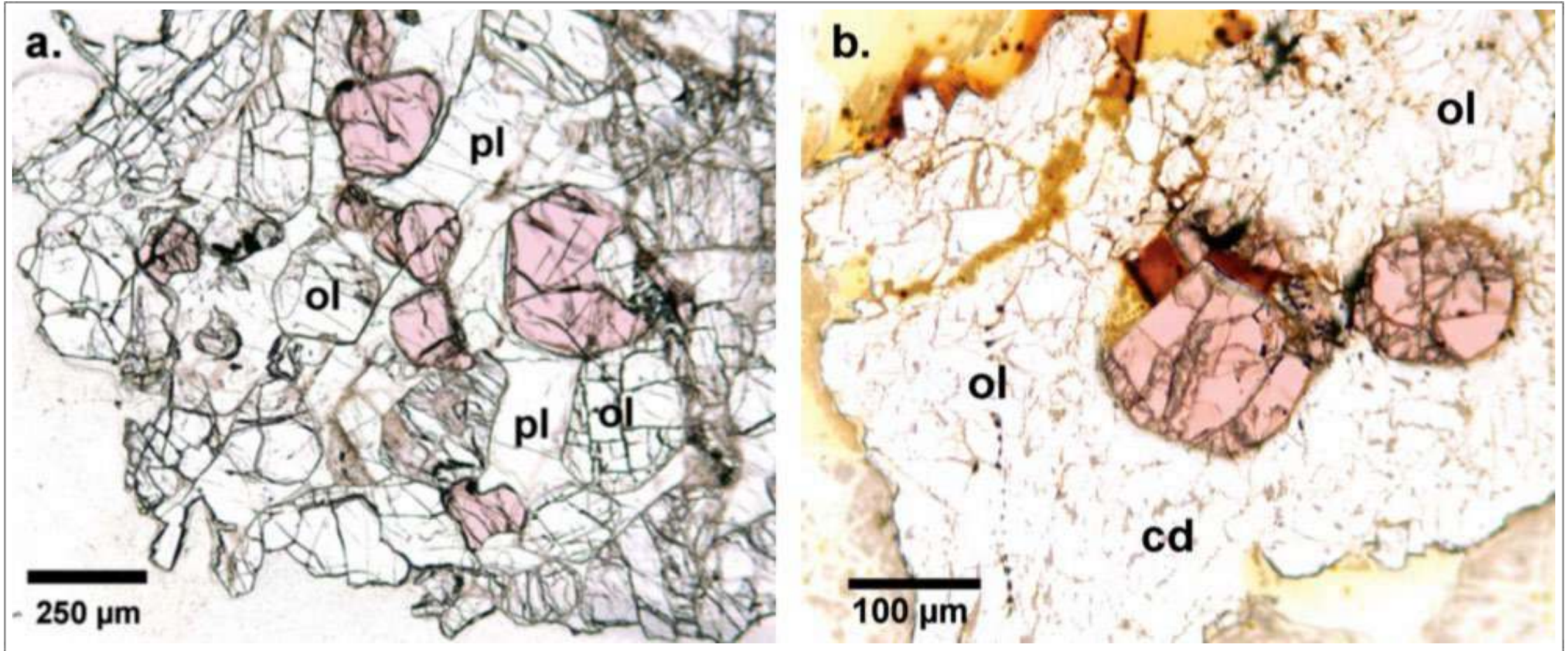
Transmitted light images of a rounded plagioclase clast in Apollo 17 impact-melt breccia 76055 (top ppl, bottom xpl).

Pink pleonaste spinel occurs as rounded blebs in the plagioclase and where it has been in contact with the breccia matrix a complex corrosive reaction has occurred.

Width 1.4 mm.

Credit: NASA (AGT Photographer).





Taken From Treiman et al. (2019)

Lunar spinel in thin section, transmitted light (PPL). (a) Cumulate Apollo 16 troctolite 67435. Pink spinel and clear olivine (Ol, higher relief) enclosed poikilitically by plagioclase (Pl). (b) Apollo 15 cordierite-spinel troctolite 15295,100. Pink spinel euhedra embedded in olivine (Ol, clear) and cordierite (Cd, also clear). Yellow and brown colours are burned epoxy, caused by exposure to electron beams.

Lunar meteorite ALHA 81005 - a polymict, anorthositic regolith breccia from the lunar highlands, containing a spinel anorthositic troctolite clast.

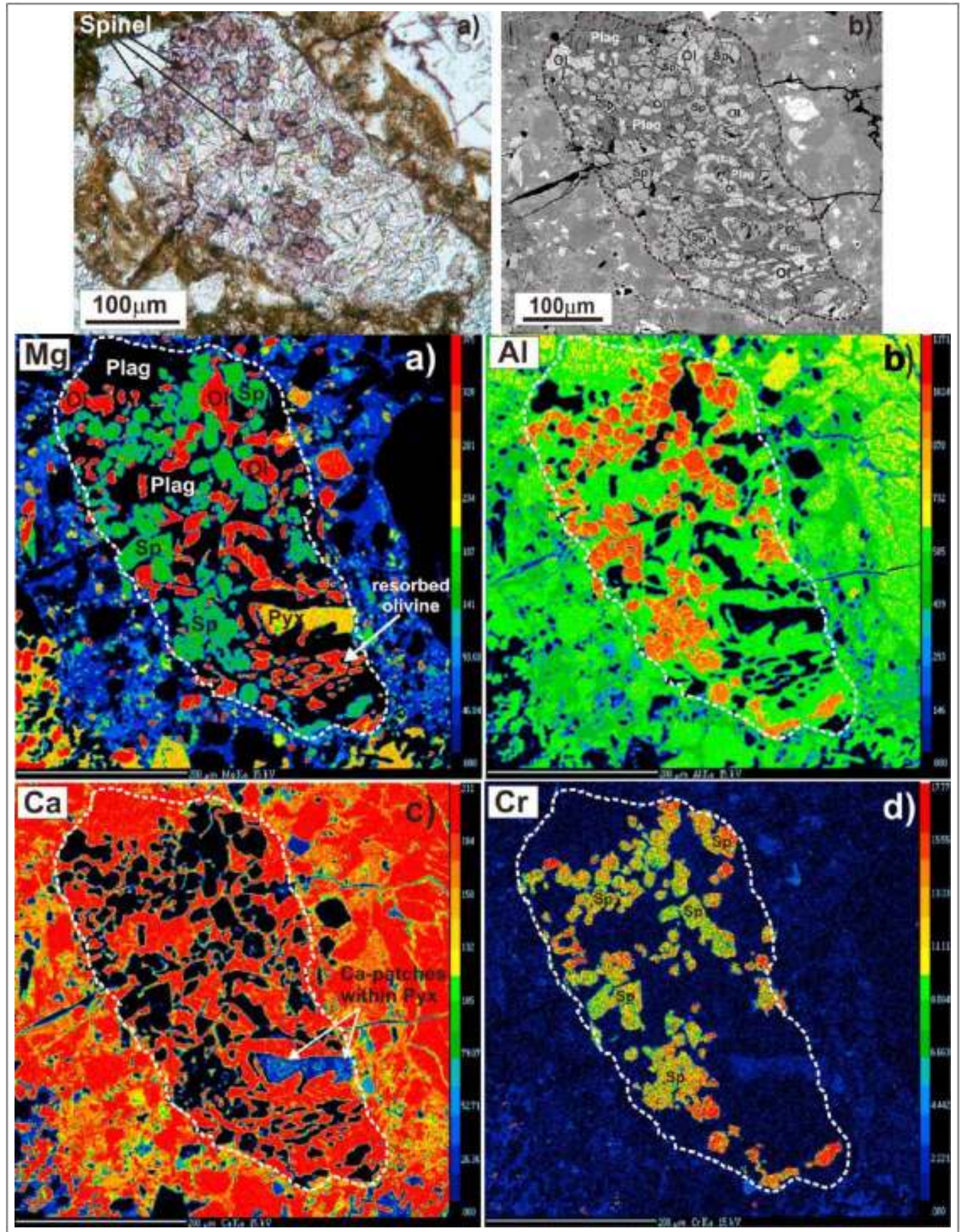
Top:

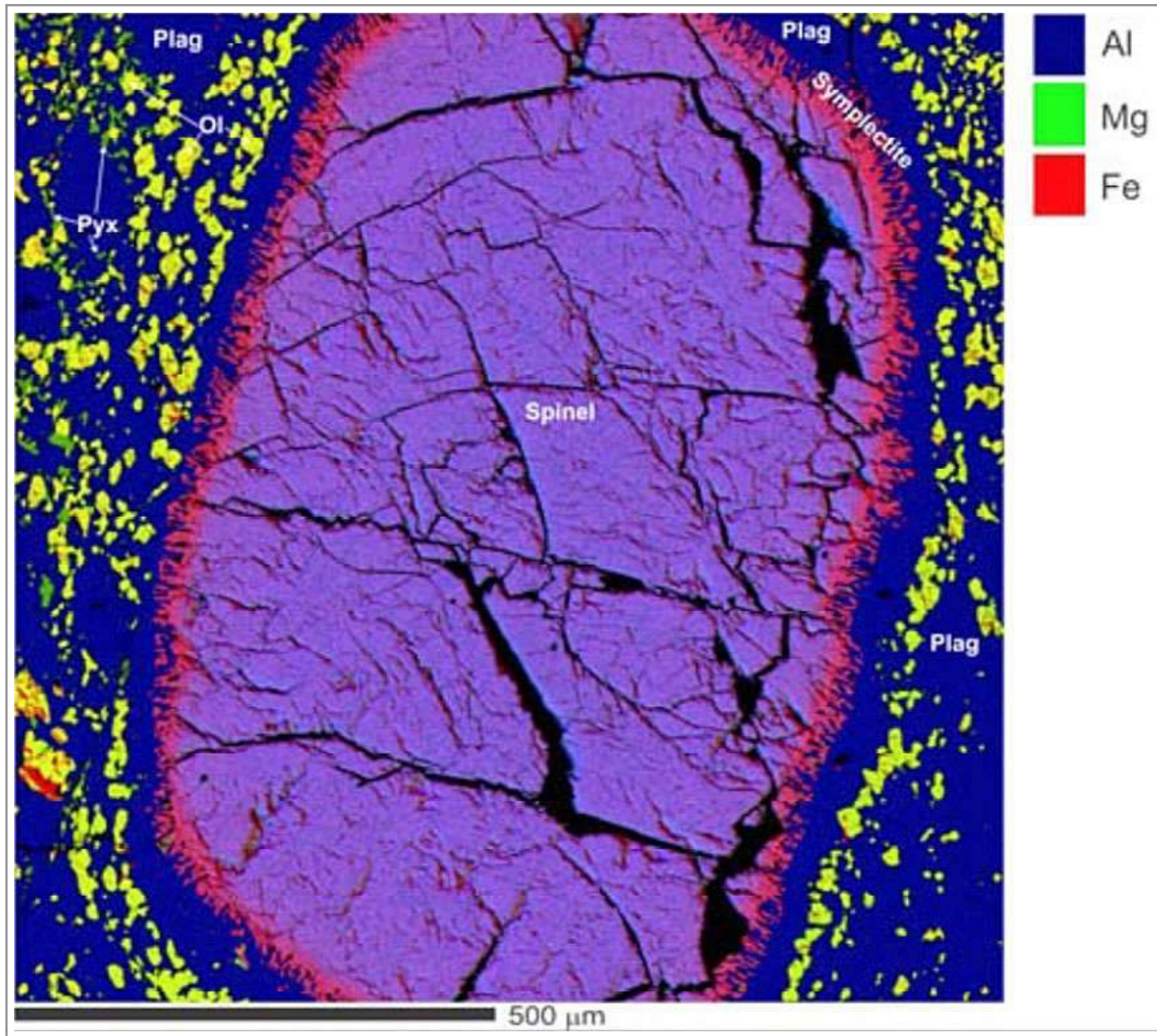
(a) Transmitted light image of the spinel-rich clast. The euhedral to subhedral spinels grains are pale purple.

(b) Backscattered electron image of the spinel-rich clast. Spinel grains (Sp, grey) are surrounded by olivine (Ol, light grey) and plagioclase (Plag, darkest grey). Pyroxene (Pyx, slightly darker grey than spinel).

Bottom:

(a-d) X-ray maps of the spinel-rich clast showing relative enrichment in Mg, Al and Cr and absence of Ca within the spinel.





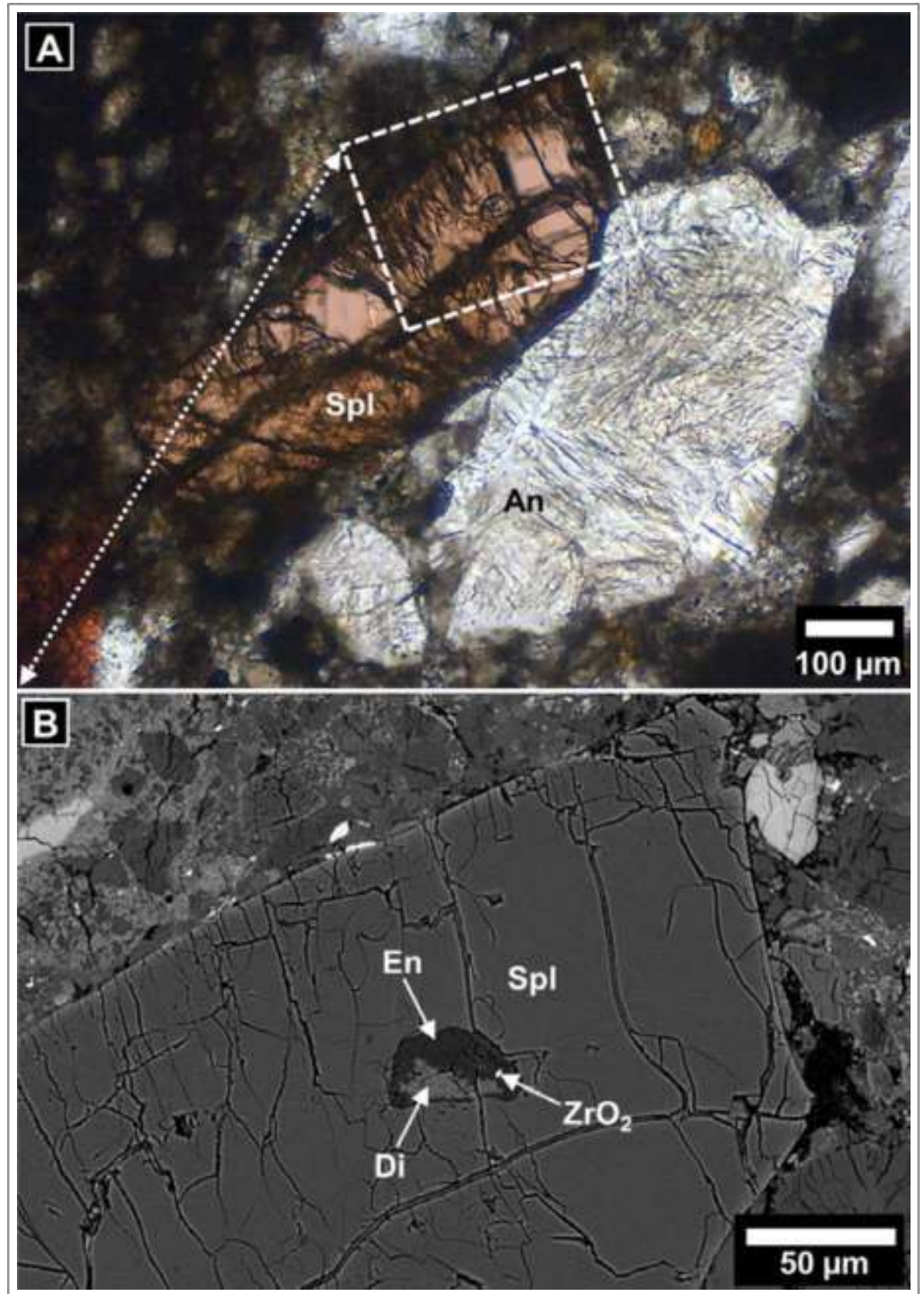
Taken From Gross et al. (2017)

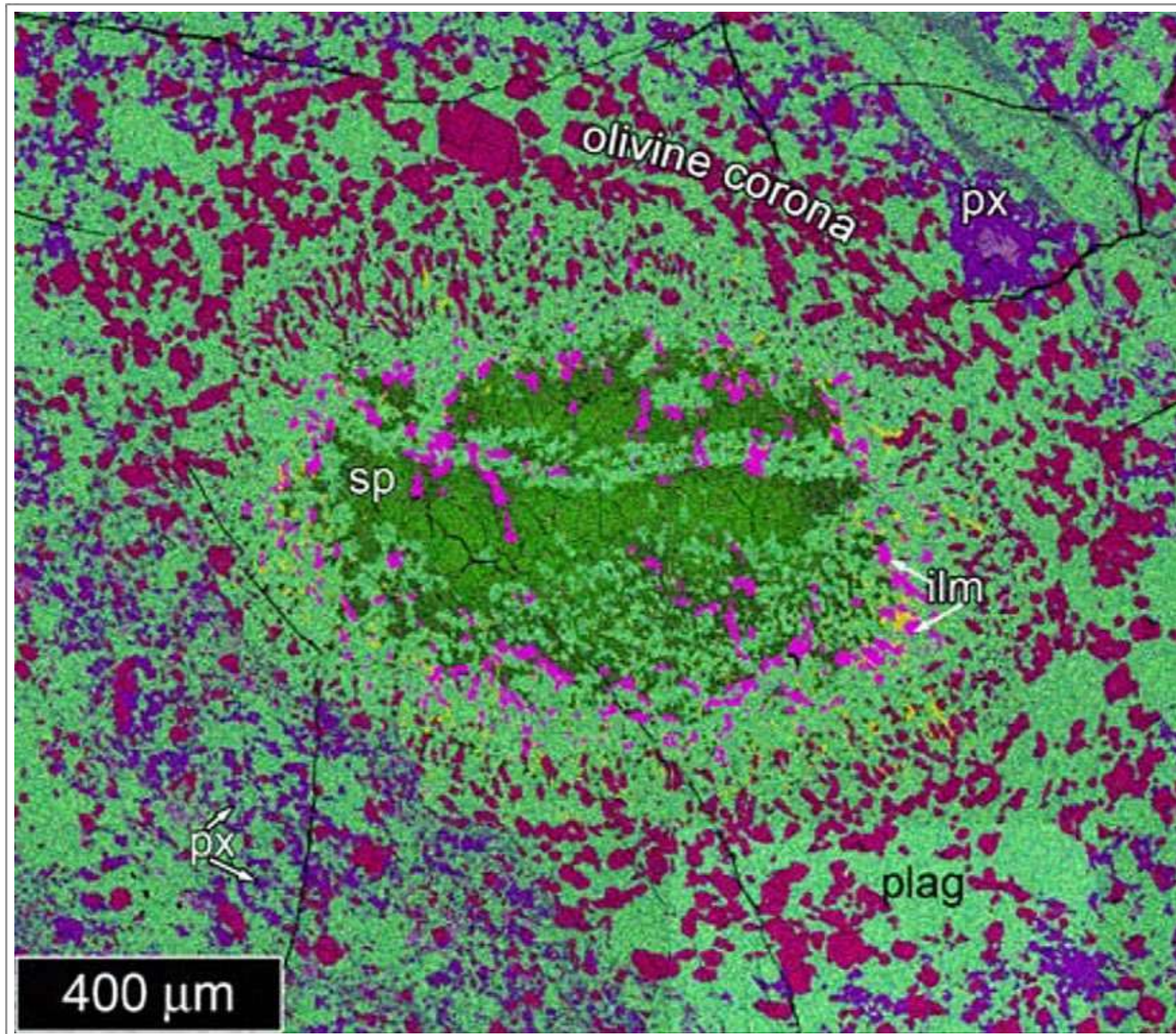
False colour composite X-ray map of a large spinel crystal in lunar meteorite NWA 10401 - an anorthositic troctolite with a granulitic texture. The spinel has a symplectite intergrowth zone of Cr-rich spinel and plagioclase around its entire rim followed by a plagioclase-zone and an olivine-zone. Al = blue; Mg = green; Fe = red. The symplectitic rim of the spinel grain is enriched in Fe and Cr.

Spinel assemblages in vitric breccia lunar meteorite Dhofar 1528.

A) Transmitted light image of a 680 μm pink spinel (Spl) clast intergrown with anorthite (An) and embedded in impact melt-rich polymict breccia.

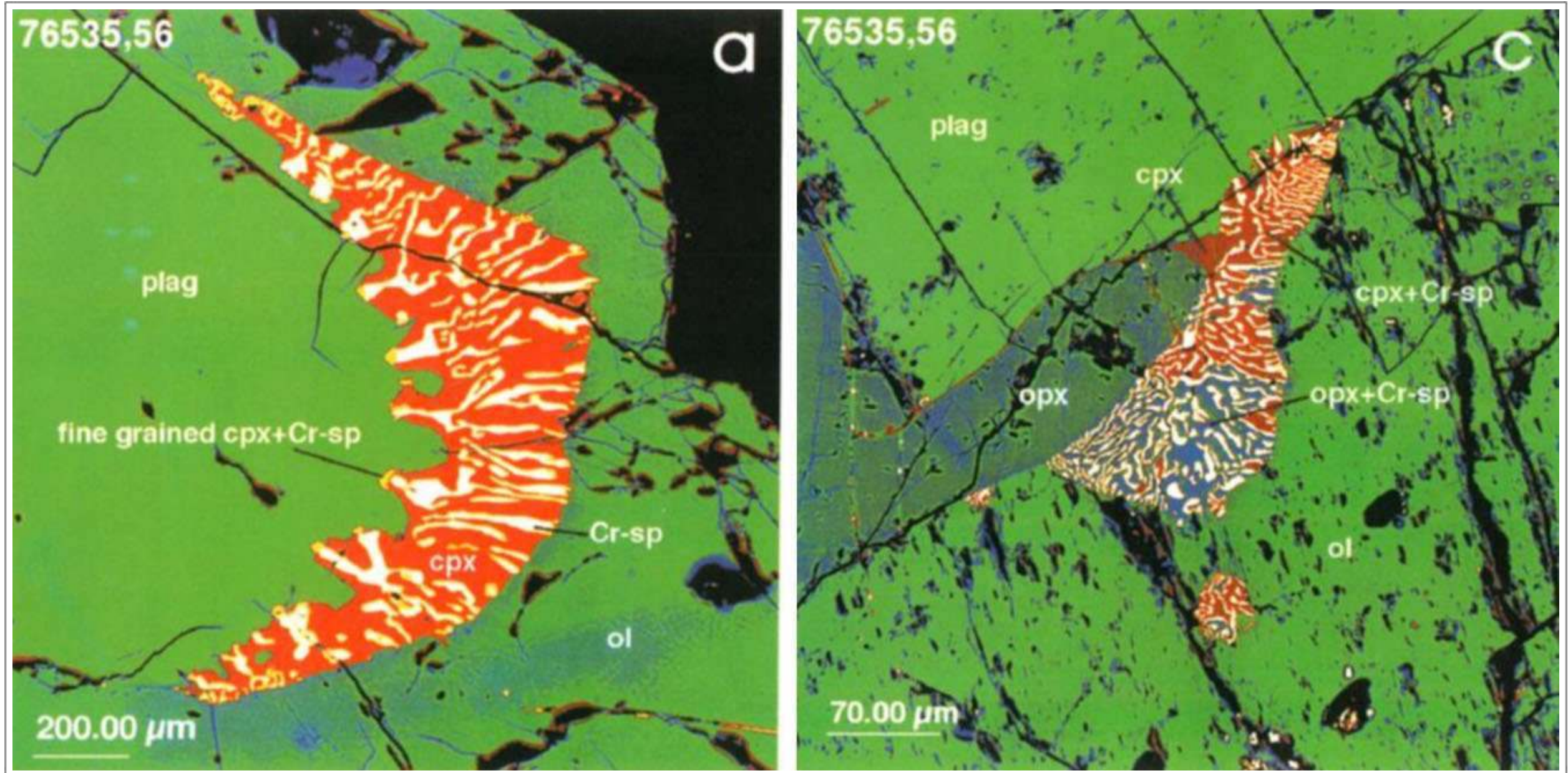
B) Backscattered electron image of (A) showing a composite inclusion of Al-rich enstatite (En), diopside (Di), and a minute baddeleyite (ZrO_2) crystal enclosed in spinel (Spl).





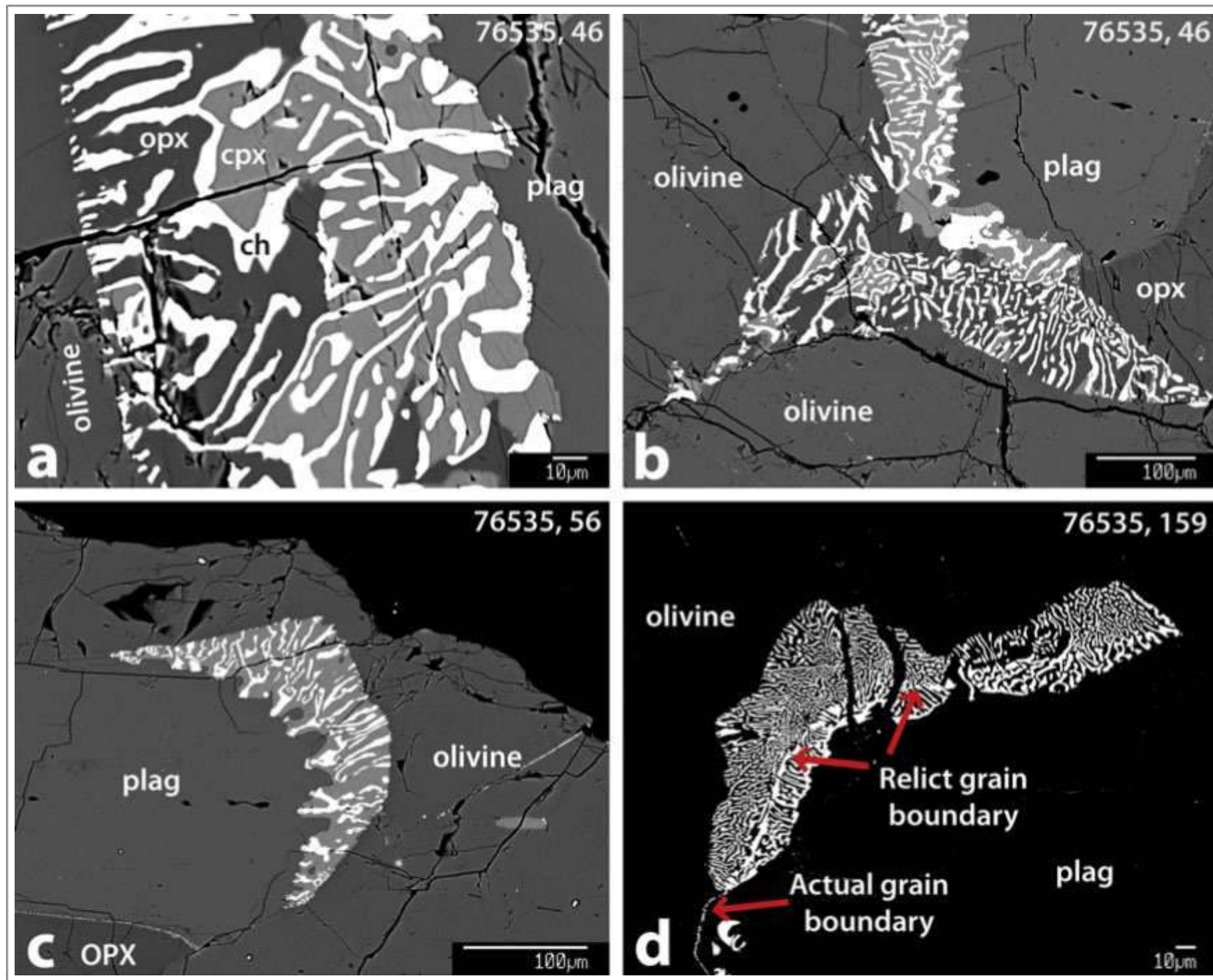
Taken From Robinson and Kring (2018)

False colour composite X-ray map of a pleonaste spinel phenocryst with a dramatic reaction corona in lunar meteorite NWA 8687 - a KREEP-poor, spinel troctolite. Plagioclase is pale green, pyroxene is purple, olivine is red, ilmenite is pink, phosphate is yellow, and spinel is dark green. The darker areas of the spinel contain more Cr.



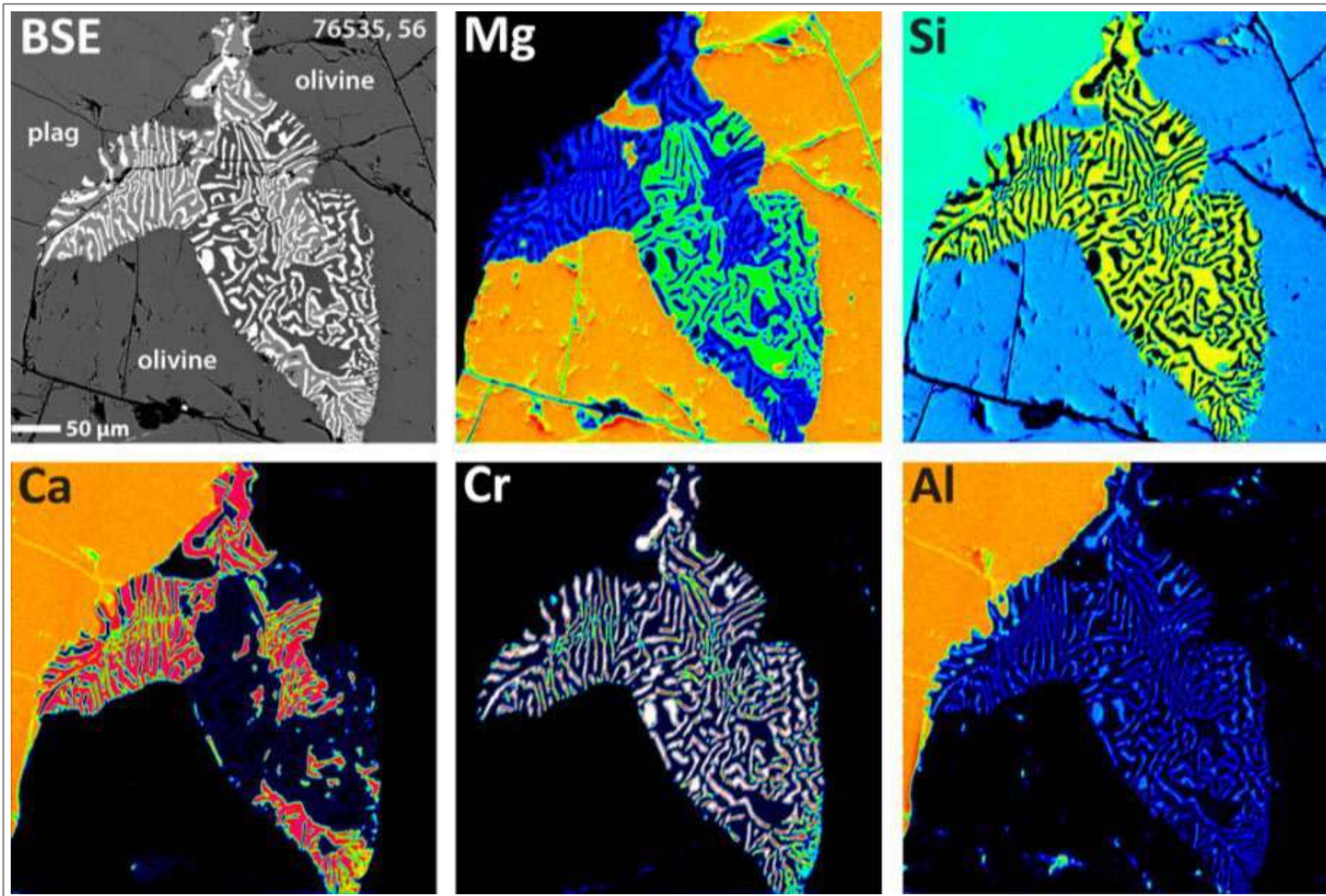
Taken From McCallum and Schwartz (2001)

False colour backscattered electron images of symplectites in Apollo 17 troctolite 76535. (a) Clinopyroxene-chromiite symplectite at a plagioclase-olivine contact. Note the fingers of symplectite with chromite at their tips extending into the plagioclase. Orthopyroxene is noticeably absent from this symplectite. (c) Symplectite developed at a plagioclase-olivine-orthopyroxene triple junction. Note also the small symplectite enclosed within olivine.



Taken From Elardo et al. (2012)

Backscattered electron images of various symplectites and chromite veining in Apollo 17 troctolite 76535. (a) Typical symplectite at an olivine-plagioclase boundary. (b) Symplectite in contact with olivine, plagioclase and an intercumulus opx grain. (c) Symplectite consisting of only chromite and cpx. Note how the symplectite seems to be “digesting” the plagioclase grain. (d) Symplectite darkened to better show a relict grain boundary preserved by chromite.

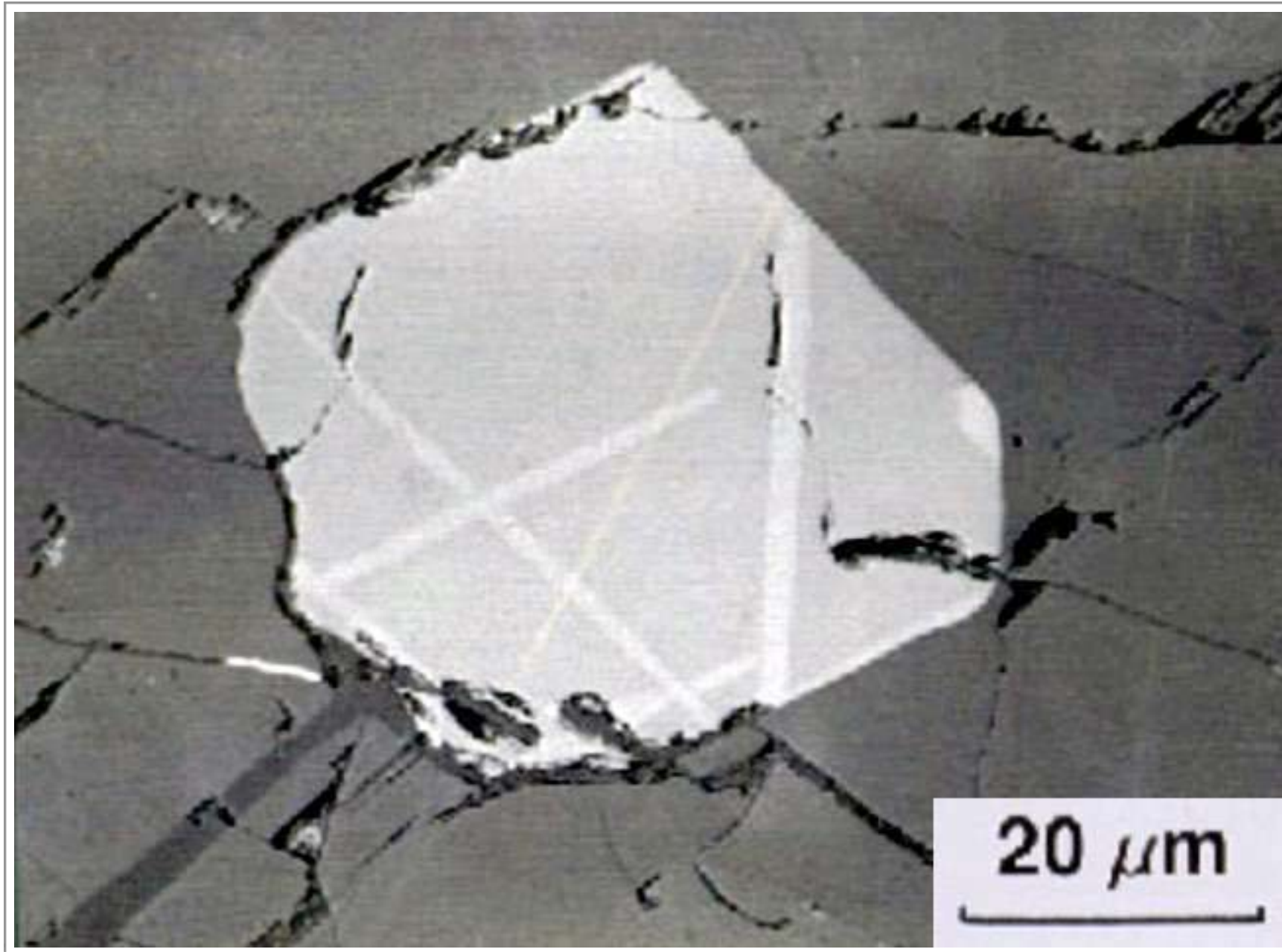


Taken From Elardo et al. (2012)

Backscattered electron image and X-ray maps of an opx-xpx-chromite symplectite at an olivine-plagioclase boundary in Apollo 17 troctolite 76535. X-ray maps show the distribution of opx, cpx and chromite within this typical symplectite. “Hot” colours indicate a higher concentration of a particular element. The apparent zoning in Cr in the chromite is due to beam overlap with surrounding phases during the mapping process.

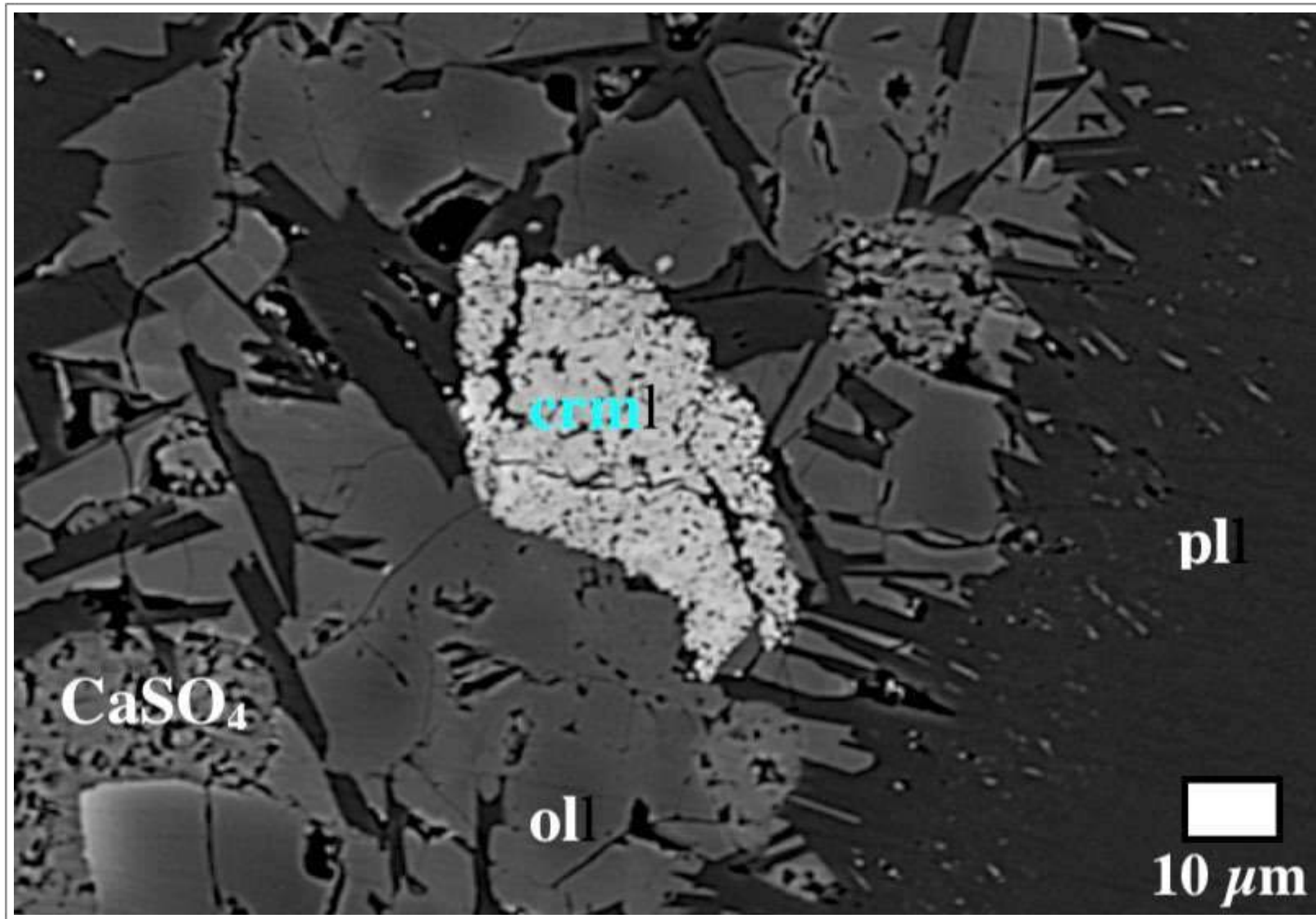


Reflected light image of chromite mantled by ulvöspinel in Apollo 12 low-Ti basalt. The large bright white grain, and the small specks of iron in the triangular troilite grain toward the lower right are metallic iron. Field of view is 0.32 mm across. From the website of Kurt Hollocher, Geology Department, Union College, Schenectady, NY, U.S.A. ([link to website](#)).



Taken From Meyer (2003)

Reflected light image of a euhedral ulvöspinel crystal with exsolution lamellae of ilmenite in Apollo 12 magnesium-rich basalt 12005.

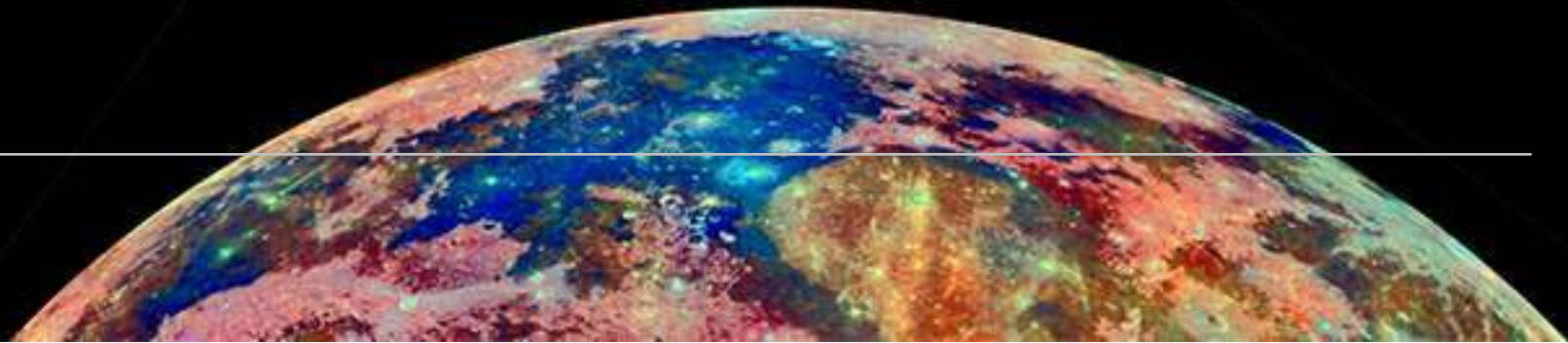


Taken From Wittmann et al. (2014)

Backscattered electron image of granular chromian spinel (crm) in impact melted granulitic breccia lunar meteorite Dhofar 1776. Abundant vesicles occur in the impact melt, typically filled by secondary CaSO₄.

crm - chromian spinel, ol - olivine, pl - plagioclase feldspar

Phosphates



SPECIES

1. Fluorapatite - $\text{Ca}_5(\text{PO}_4)_3\text{F}$
2. Chlorapatite - $\text{Ca}_5(\text{PO}_4)_3\text{Cl}$
3. Merrillite - $\text{Ca}_9\text{NaMg}(\text{PO}_4)_7$
4. Whitlockite - $\text{Ca}_9\text{Mg}(\text{PO}_4)_6[\text{PO}_3(\text{OH})]$
5. Stanfieldite - $\text{Ca}_4(\text{Mg},\text{Fe}^{2+})_5(\text{PO}_4)_6$
6. Farringtonite - $\text{Mg}_3(\text{PO}_4)_2$
7. Monazite - $\text{REE}(\text{PO}_4)_2$
8. and related species:
9. Britholite - $(\text{Ce},\text{Ca})_5(\text{SiO}_4)_3\text{OH}$

Fluorapatite

Apatite is a useful tracer for investigating the history of volatiles in the Moon as it is the only hydrous species found in lunar rocks. Hydrogen (typically reported in terms of equivalent H_2O or OH and referred to as “water”) in apatite has been measured in most major lunar rock types and seems to vary both in terms of abundance (e.g. “wet” and “dry” reservoirs) and isotopic composition in the lunar interior (Robinson et al., 2016). However, current models for the Moon’s formation have yet to fully account for its thermal evolution in the presence of H_2O and other volatiles.

Apatite in lunar samples ranges in crystal habit from anhedral to euhedral and range in size from sub-micrometer to 2 mm (McCubbin et al., 2011; Treiman et al., 2014; Hauri et al., 2017). Many anhedral apatite crystals are clearly late-crystallizing phases that fill the available space interstitial to the earlier formed phases. The smallest crystals typically occur in mare basalts, and the larger crystals occur in plutonic rocks and impactites (e.g., troctolite 76535 and granulite 79215) (McCubbin et al., 2015).

The first extra-terrestrial discovery of fluorapatite was made by Fuchs (1970) in Apollo 11 ilmenite basalt 10044. Euhedral crystals containing unusually high Y_2O_3 (1.2 wt.%) and REEs ($\text{RE}_2\text{O}_3=2.54$ wt.%) were found as inclusions in pyroxferroite.

A SIMS study of apatite and zircon in Apollo 14 breccias (14306,60; 14066,47; 14303,52 and 14321,16) by Nemchin et al. (2009) showed that unlike the zircons, the apatite grains have been isotopically reset during an event at 3926 ± 3 Ma. Zircons gave ages ranging from 4023 ± 24 Ma to 4342 ± 5 Ma. The apatite age corresponds to the formation of the Fra Mauro Formation and also determines the timing of the Imbrium impact.

Studying apatite in the mesostasis areas of mare basalts from Apollo 11, 12, 15 and 17 (samples 10044, 12064, 15058 and 70035) enabled Potts et al. (2016) to ascertain the compositions of the melts from which apatite crystallized. They concluded that the development of individual melt pockets, combined with the occurrence of silicate liquid immiscibility, exerts control on the composition and texture of mesostasis regions and modelled late-stage lunar melts have roughly andesitic to dacitic compositions with low alkali contents.

Some of the highest REE contents reported for lunar apatite and the lowest for lunar whitlockite occur in lunar meteorite EET 96008 (a fragmental breccia that predominantly consists of basaltic mineral clasts, along with minor lithic fragments and breccia clasts). It is thought to be derived from a mare-basalt precursor (Anand et al., 2003b).

In lunar meteorite NWA4472, a KREEP-rich breccia, one basaltic clast is particularly enriched in fluorapatite. It forms an intergrowth with coarse grained zoned ilmenite, large (up to $250 \mu\text{m}$) zoned

fluorapatite (2.8-4 wt% F) and hedenbergitic pyroxene. Apatite was analyzed in both discrete mineral grains within the NWA 4472 matrix, and in polymict mare basalt clasts (Joy et al., 2009, 2011). Despite lacking plagioclase, olivine and pigeonite it is thought to have originated from a highly fractionated KREEP basalt source.

McCubbin et al. (2008) note large elongate crystals of apatite in Apollo soil samples 14161 and 12033 and lunar meteorite NWA 2977, and small anhedral apatite patches in lunar meteorites LAP 02205, LAP 03632 and SaU 169.

Secondary ion mass spectrometry (SIMS) analysis of apatite in: Apollo 14 high-Al basalt 14053, an alkali-rich clast in Apollo 15 soil grain 15404,51, and lunar meteorite sample NWA 2977 has confirmed that hundreds to thousands of ppm water (in the structural form hydroxyl) is present in apatite from the Moon. Moreover, the first two of the studied samples likely had water preserved from magmatic processes, which would qualify the water as being indigenous to the Moon. The identification of water from multiple types of lunar rocks that display a range of incompatible trace element signatures indicates that water may be ubiquitous within the lunar interior, potentially as early as the time of lunar formation and magma ocean crystallization (Boyce et al., 2010; McCubbin et al., 2010).

The analysis of some of the most primordial samples from the Moon (such as Apollo 14 granite clast in 14303, and Apollo 17 troctolite 76535 and norites 77215 and 78235) show that the

water they contain, locked in the crystalline structure of apatite, is characterised by a H isotopic composition similar to that of the Earth and strongly argues for a common origin for water in the Earth-Moon system (Barnes et al., 2014).

Anand et al. (2014) presented a compiled dataset of D/H and hydroxyl content in lunar apatite from a wide range of lunar rock types using NanoSIMs: low-Ti basalt (12039, 12064); high-Ti basalt (10044, 10058, 74246, 75055, 79195); KREEP basalt (15386); Mg-suite norite (77215, 78235); Mg-suite troctolite (76535); alkali granite (14303); and lunar meteorites (LAP 04841, MIL 05035, NWA 773). See also Barnes et al. (2013) and Tartèse et al. (2013c). This work unambiguously detected and quantified water in lunar apatite. Furthermore, the H isotopic composition of this measured water points to a common origin for the water in the Earth-Moon system.

Petrogenetic processes such as crystallization and degassing can modify characteristics of indigenous water in primary mantle melts. Tartèse et al. (2014b) analysed apatite in phosphorus-rich KREEP basalts to try and establish more reliable estimates for the water content of lunar magmas, as some apatite likely crystallized before substantial degassing occurred. On the basis of H isotope data from Apollo 15 lunar KREEP basalt 15386 they concluded that degassing occurred during apatite crystallization. However, similar data from apatite in Apollo 17 KREEP basalt 72275 and lunar meteorite NWA 773 indicate crystallization before degassing

and H isotope fractionation, and their D/H ratios thus directly reflect those of their source regions. Data from these apatites suggest the presence of a water reservoir in the Moon characterized by moderate H₂O contents similar to that of the Earth's interior. These findings imply that significant amounts of water in the Moon were inherited from the proto-Earth, surviving the purported Moon-forming impact event.

Tartèse et al. (2013c) used the NanoSIMs technique to show that in low-Ti mare basalts, apatite crystallisation occurred after degassing of H-bearing species and the OH variations reflect different degrees of fractional crystallization. In high-Ti mare basalts, large δD variations with a relatively restricted range in OH content implies that apatite crystallization and degassing of H-bearing species were mostly coeval. They interpreted the large variations of apatite δD values in mare basalts between ~200‰ and 1000‰ as a result of different amounts of degassing of H-bearing species initially dissolved in the basaltic parental melts.

Barnes et al. (2016a,b) investigated apatite in Apollo basalts 10044, 10058, 14304, 15386, 15555, 70035, 76535, 78235 and 79215. Twenty nine grains were suitable for chlorine isotope analysis by ion probe. Their dataset included low-Ti, high-Ti, KREEP and very high potassium (VHK) basalts, and selected plutonic highlands rocks from the magnesian suite. The data supports a mechanism of differentiation of the Moon via a lunar magma ocean (LMO). In order to account for the Cl-isotopic

composition of KREEP, residual melt had to degas following enrichment at relatively low pressures. To do this, puncturing of the lunar crust by one or several large impact events, prior to the solidification of the KREEP liquid in the lunar magma ocean (LMO) must have occurred.

As part of a chlorine isotope study of apatite, Barnes et al. (2019) summarise all previously published data and show that fluorapatite is clearly the dominant species in lunar rocks - the exception being in low-Ti basalts where hydroxylapatite is commonly found.

Cernok et al. (2019) examined the shock-induced microtextures in apatite and merrillite from a set of well-studied Apollo 17 highlands samples - the Mg-suite rocks 76535, 76335, 72255, 78235, and 78236 - listed here in order of increasing shock deformation. Using electron backscatter diffraction (EBSD) and other techniques they were able to show subgrain formation and granularization of grains caused by recrystallization. As differently shocked domains can yield significantly different ages and volatile contents EBSD can be used to evaluate stages of shock deformation it should be taken into account when interpreting in-situ analyses of phosphates.

Three lunar meteorites (feldspathic breccia Dhofar 458, mare basalt Miller Range MIL 05035 and the KREEP-assimilated gabbro Northwest Africa NWA 2977) were examined by Wang et al. (2019) in an investigation of the Cl reservoir of the Moon. They

were able to show that the H₂O and Cl contents and $\delta^{37}\text{Cl}$ and δD values of lunar apatite exhibit distinct inter- and/or intra-sample variations and that water and Cl are heterogeneously distributed in the Moon. The heterogeneous distribution of lunar Cl isotopes probably resulted from complex lunar formation and differentiation processes.

Chlorapatite

Although there has been one report of chlorapatite in sample 14161 (McCubbin et al., 2011), and hydroxylapatite has been reported in the brecciated matrix of lunar meteorite NWA 773 (Tartèse et al., 2014a), nearly all of the apatite that has been analyzed in lunar samples is fluorapatite (McCubbin et al., 2011).

Chlorapatite, however, does occur in the low-Ti mare-basalt lunar meteorite NEA003A, where it is found in a late-stage assemblage of consisting of plagioclase, ilmenite, troilite, fayalite, Si-K-rich glass, and a rare SiO₂ phase. Other accessory minerals include ulvöspinel, chromite, and trace metallic iron (Haloda et al., 2009).

Chlorapatite is also reported in Apollo 17 troctolite 76535, where it is associated with whitlockite, orthopyroxene, clinopyroxene, chromite, baddeleyite and metallic iron within olivine and plagioclase crystals. Such clusters of minerals are interpreted as evidence of trapped melt (McCallum and Schwartz, 2001).

An exceptional apatite (chlorapatite?) crystal in lunar impact melt breccia Dhofar 458 is reported by Wang et al. (2012b). They measured extremely high $\delta^{37}\text{Cl}$ of 67.2 ± 2.0 to 81.1 ± 2.0 ‰, and a relatively low water content averaging 240 ± 40 ppm in the breccia indicating it sampled a reservoir of extremely heavy Cl isotopes on the lunar surface, possibly produced by repeated ^{35}Cl loss during multiple shocks events or gardening processes.

Merrillite

Merrillite, also known as “whitlockite” is one of the main phosphate minerals, along with apatite, that occur in lunar rocks. The name “whitlockite” was still being used by some lunar researchers until quite recently (Jolliff et al., 1999) and some authors refer to merrillite-whitlockite (Shearer et al. (2011).

Merrillite can be synthesized from the mineral whitlockite by heating it to >1000 °C. Whitlockite and merrillite form a solid-solution, with whitlockite being the H-bearing end-member and merrillite being H-free (Adcock and Hausrath, 2017). Lunar merrillite, ideally contains high concentrations of Y+REE (merrillite often carries greater than 90% of a rocks total REE content). Intrinsically low Na concentrations in lunar rocks, combined with the typical formation of merrillite in late-stage basaltic mesostasis or residual, intercumulus melt pockets, produce these high REE concentrations.

A crystallochemical study of merrillite used the following lunar samples: shocked Ti-rich basaltic rock 10085, KREEP-rich granite bearing breccia 12013, basalts (12036, 12039 and 15475), impact melt, breccia, monzogabbro and anorthosite (all 14161), impact melt breccias (65903, 73216 and 76503) and an Antarctic lunar meteorite. Extraterrestrial merrillite differs from terrestrial whitlockite by enrichments in Ca^{2+} , Na^+ , or $\text{Y}+\text{REE}^{3+}$, and the lack of H^+ (Jolliff et al., 2006). These features set lunar merrillite apart from its martian and meteoritic counterparts, and from terrestrial whitlockite. Merrillite is therefore a good indicator of Moon-Mars parentage (Papike et al., 2014).

Wang et al. (2012a) report merrillite grains in basaltic lunar meteorite NWA4734 that are highly enriched in rare earth elements (5.5 wt% in total). Their REE content is comparable to that in the LaPaz lunar meteorites (Zeigler et al., 2005a).

Pb/Pb dating of merrillite (and apatite) in lunar meteorite Dhofar 1442 (a glassy-matrix regolith breccia containing basaltic, granulitic, and felsic lithic clasts) produced variable ages from ~ 3.2 to ~ 4.3 Ga, with a major peak age around 3.8 Ga. Cogenetic zircon gave a date of ~ 4.3 Ga suggest a resetting of the U/Pb phosphate system due to a later impact event (Zhou et al., 2015).

Whitlockite

Early work on lunar samples suggested that “lunar whitlockite” is similar in structure to meteoritic merrillite (Gay et al., 1970b; Fuchs, 1971). Dowty (1977) refined the structure of whitlockite from the Angra Dos Reis meteorite and recommended the use of merrillite for the extraterrestrial variety on the basis that the lack of H led to a fundamental structural difference between the extraterrestrial and terrestrial varieties. Extraterrestrial whitlockite has the anhydrous β -Ca₃(PO₄)₂ structure, which is different from that of hydrous terrestrial whitlockite.

Whitlockite is apparently more abundant than apatite in lunar rocks. Both phosphates occur in the high-KREEP rocks or in KREEP-rich areas of low-KREEP rocks, sometimes as intergrowths readily characterized by cathodoluminescence. Many breccias and lunar rocks contain veins and vugs lined with phosphates, silicates, ilmenite and metallic iron; these testify to ubiquitous vapours penetrating the surface rocks of the Moon (Smith and Steele, 1976).

The U distribution in Apollo 12 polymict breccia 12013 was studied by fission track and elemental mapping techniques by Haines et al. (1971). They found composite apatite-whitlockite crystals with higher Y content in whitlockite and higher Cl content in apatite.

Warren et al. (1983b) report two Apollo 14 whitlockite-rich lithologies - an anorthositic troctolite clast in polymict breccia 14305,301 and alkali anorthosite? clast in regolith breccia 14313,70. The mode of 14313,70 is roughly 40% plagioclase, 35% whitlockite and 25% low-Ca pyroxene.

Neal and Taylor (1991) describe REE-rich whitlockite in alkali anorthosites, ferroan anorthosites, Mg-suite anorthosites, the alkali gabbro suite from Apollo 16, the Apollo 15 quartz-monzodiorite, and in the mesostasis of mare basalts.

The presence of whitlockite in the basaltic mesostases suggests that extreme fractional crystallization of a basaltic magma is responsible. In these basalts, whitlockite and/or apatite is commonly found in association with ilmenite, fayalite, silica (cristobalite), and K-rich glass.

Apollo 14 olivine basalt 14256,40 contains 2-3% modal whitlockite - crystals of which are blocky to “puzzle-piece” in shape and 0.03 to 0.08 mm in size. They are associated with sieve-textured zircon, apatite and K-feldspar in a late-stage interstitial assemblage (Snyder and Taylor, 1991).

Neal and Taylor (1991) suggest that whitlockite found in lunar highlands rocks is a post-cumulus metasomatic phase precipitated from a melt formed when urKREEP underwent silicate liquid immiscibility. The basic immiscible melt thus produced was able

to percolate through the lunar highlands due to its low viscosity and act as a metasomatising agent.

Apollo 14 whitlockite gabbronorite 14161 is the first analysed lunar intrusive rock to show textural evidence for the formation of granitic material by silicate liquid immiscibility and geochemical evidence for separation of that material, at least on a small scale, from mafic residua. It has REE concentrations that are ~5-6x KREEP levels (Jolliff et al., 1993 and 1999). The assemblage contains ~47 vol% pyroxene, 26% plagioclase, and some 27% minor and accessory minerals, including apatite, potassium feldspar, silica, ilmenite, zircon, troilite and an unusually high proportion of whitlockite (~8%).

Apollo 14 polymict breccia 14321 contains fragments of microrite in which whitlockite typically occurs as poikiloblastic intergrowths with plagioclase feldspar (Greive et al., 1975).

Apollo 14 basaltic impact-melt breccia 14310,123 contains interstitial intergrowths of whitlockite, apatite, ilmenite and fayalite? The whitlockite is enriched in REE's relative to the associated apatite (Griffin et al., 1972).

Yamato 983885 is a lunar polymict breccia meteorite containing clasts of KREEP basalt and modally 2.8% of REE-rich whitlockite. In places, the whitlockite occurs within droplets of Si, Al, K-rich glass and in other places glass is included within whitlockite.

Fractional crystallization and liquid immiscibility are proposed to explain this phenomena (Arai et al., 2005).

Whitlockite is a significant accessory mineral in a quartz monzogabbro clast within the highly shocked lunar meteorite Dhofar 1428 - a regolith breccia. It constitutes approximately 5 vol% and is associated with a Ca, Ti, Zr-bearing phase (described as zirconolite-like), K-feldspar, ilmenite and a Si, Al, K-rich phase (Hidaka et al., 2014).

Stanfieldite

Stanfieldite occurs with merrillite and apatite in the so called "rusty rock" (66095) from Apollo 16 - a fine-grained, sub-ophitic to ophitic polymict melt breccia that has suffered low-temperature alteration. Merrillite is the dominant phosphate in this sample followed by stanfieldite and apatite. They are associated with schreibersite, metallic iron, FeOOH, and the chlorides akaganéite and lawrencite (Shearer et al., 2014).

However, Shearer et al. (2014) suggest the volatile enrichment in 66095 is due to degassing of an ejecta blanket or far less likely degassing of a shallow basaltic intrusion. An ejecta-forming process and initial degassing may have been responsible for the formation of stanfieldite at high temperatures (>850°C).

Stanfieldite is also reported from a gabbro clast in aphanitic impact-melt breccia 73255. The major minerals are plagioclase feldspar, orthopyroxene, augite and ilmenite. Other minor mineral phases include apatite, whitlockite, chromite, troilite, metallic iron, armalcolite and rutile. Minute grains of K-feldspar and K-Si glass are also present (Meyer, Lunar Compendium).

Farringtonite

Farringtonite occurs in Apollo 16 spinel troctolite 65785. The rock is heterogeneous and consists of a coarse-grained central portion surrounded by a fine-grained, feldspar rich melt rock. In the troctolite, farringtonite is accompanied by accessory amounts of ilmenite, metallic iron, troilite, rutile, whitlockite, armalcolite, K-feldspar and chromite. Only one small ($< 4 \mu\text{m}$) grain of farringtonite included in spinel was found (Dowty et al., 1974).

Monazite

A phosphate-rich clast in a pigeonite-plagioclase mineral assemblage occurs in Apollo 17 impact-melt breccia 76503,7025. The clast, measuring 0.9 x 0.4 mm in thin section, contains 3.3% (volume) apatite, 0.8% whitlockite and trace monazite. Monazite is intergrown with whitlockite as small masses of maximum dimension $\sim 8 \mu\text{m}$. Textures suggest the following phosphate

crystallization sequence: apatite-whitlockite-monazite-whitlockite (Jolliff, 1993).

Monazite has been found in a small, monomict rock granitic fragment in Apollo 12 sample 12023. The rock comprises graphic intergrowths of K-feldspar and quartz, and plagioclase and quartz, along with minor or accessory hedenbergite, fayalite, ilmenite, zircon, yttrrobetafite, thorite, monazite and metallic iron (Seddio et al., 2014).

Barnes et al. (2018) found monazite associated with apatite and merrillite in Apollo 11 high-Ti basalt 10029. The monazite forms a symplectite with apatite, suggesting it exsolved from the apatite, possibly during cooling.

Monazite has been identified as small ($10 \mu\text{m} \times 3 \mu\text{m}$) inclusions in pyroxene from Apollo 11 basalt sample 10047 (FrondeL, 1975).

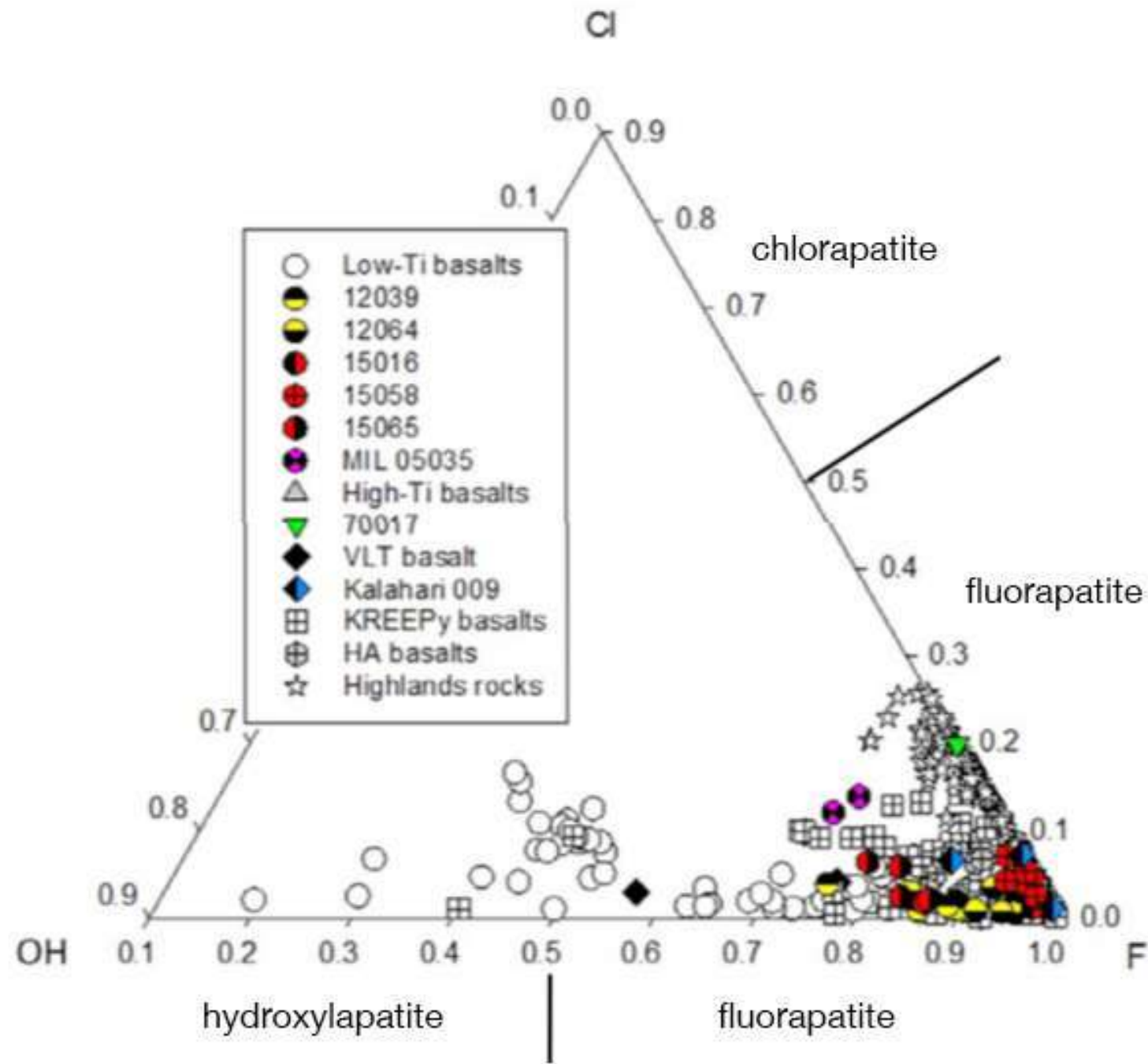
Further tiny particles of monazite were found among K-feldspar particles in regolith from Mare Crisium (A/S Luna 24) (Kartashov et al., 2006), in a granitic lithic fragment (12023,147-10) from the Apollo 12 regolith (Seddio et al., 2012a), and in basaltic lunar meteorite NWA 4734 (Wang et al., 2012a).

Monazite is one of many accessory species identified in granitic fragments within lunar meteorites Dhofar 925, 960 and 961 - all impact-melt breccias. It is associated with ilmenite, silica, K-Ba feldspar, whitlockite, apatite, baddeleyite, zircon and tranquillityite (Demidova et al., 2005).

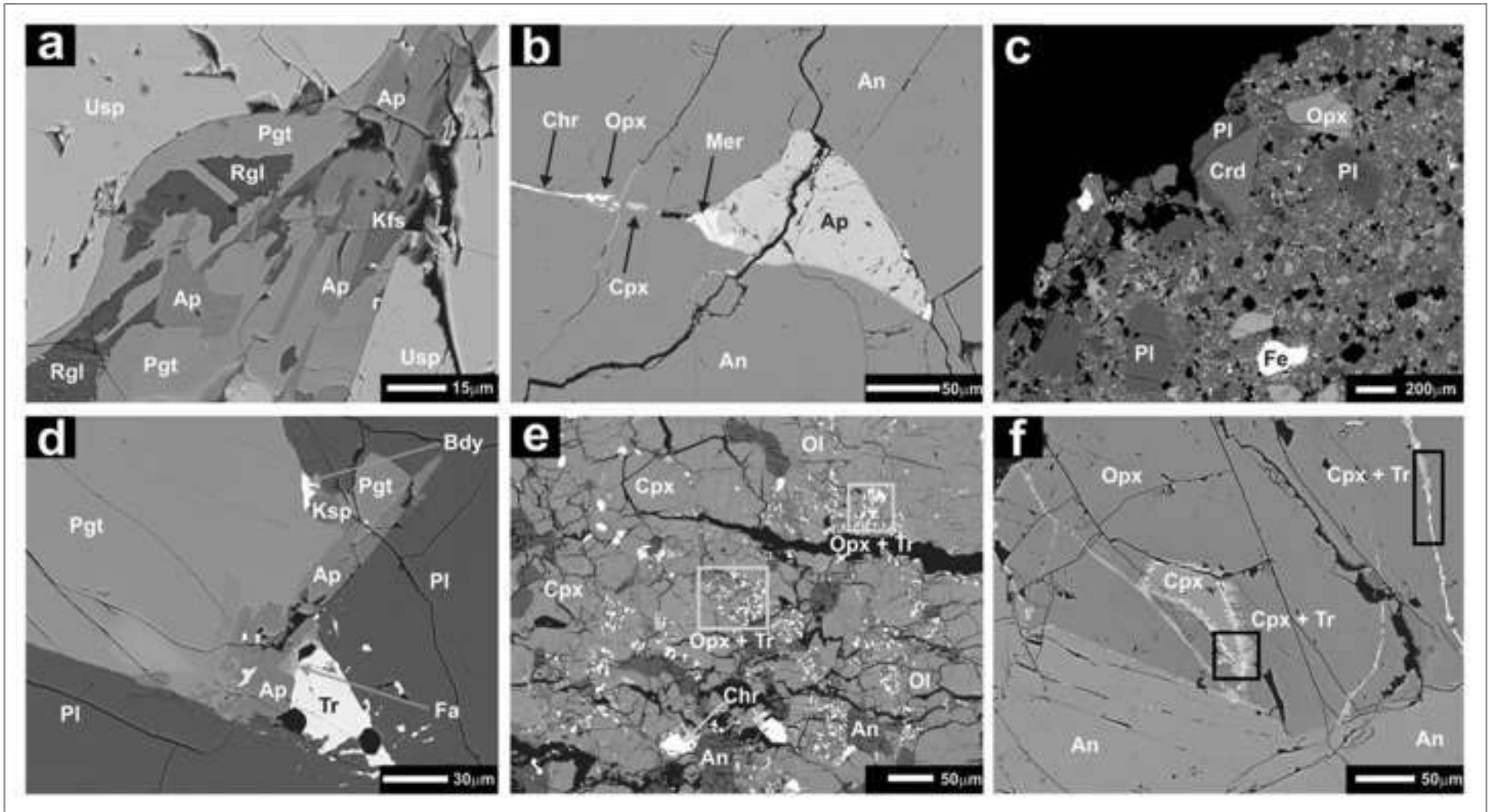
Britholite

Rare britholite has been found in Apollo 11 lunar mare basalt 10047 within angular pockets of late-stage mesostasis containing Si-Al-K glass and minerals rich in K, Ba, U, Th, Zr, REE, Nb, P, and Fe, including barian-potassium feldspar, fayalite, pyroxferroite, troilite, metallic iron, apatite, monazite, chevkinite-(Ce), zirconolite, tranquillityite, and baddeleyite (Muhling et al., 2014).

In a study of lunar phosphates, Lowe et al. (2016) found Cl-rich britholite substitution in apatite from Apollo 17 basalt 75055,50. They suggest F, Cl- bearing and REE-enriched phosphate in high-titanium basalts indicate that substantial REE-replacement of Ca^{2+} was occurring in combination with silica and chlorine enrichment. This zonation and replacement of silica for phosphate and the increasing quantities of rare earth elements show that there was extreme fractional crystallization in the high titanium mare basalts and that even in late stages of crystallization, volatiles were incompletely degassed.

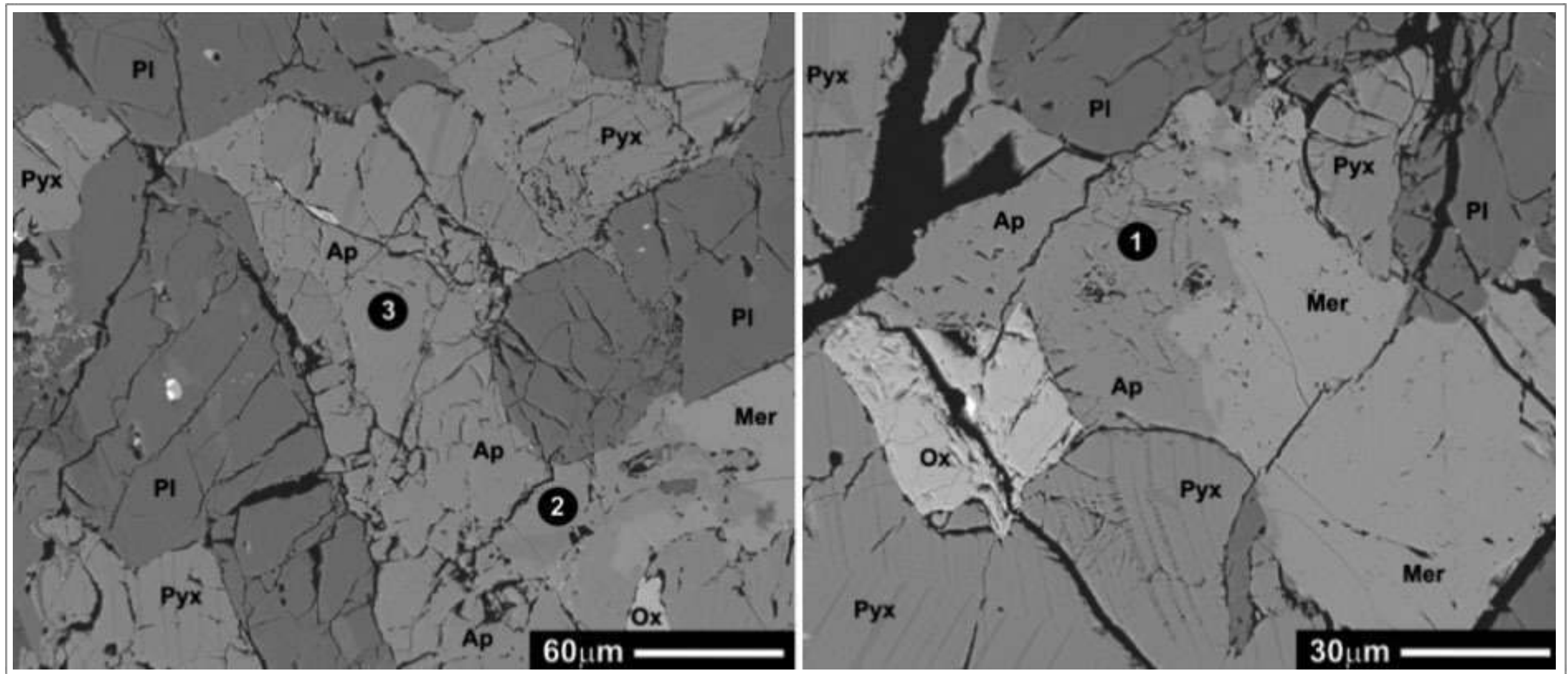


F, Cl, and OH chemistry of lunar apatite from (mainly) basaltic rocks compiled by Barnes et al. (2019). The plot includes NanoSIMS data (coloured symbols) and earlier data collected by other authors, either by SIMS or electron microprobe techniques. For F and Cl data collected by electron microprobe the data were summed, and full X-site occupancy assumed ($X = 1$), the missing component was assigned to OH. All data were normalized so that $X = 1$ and F was assigned as the missing component.



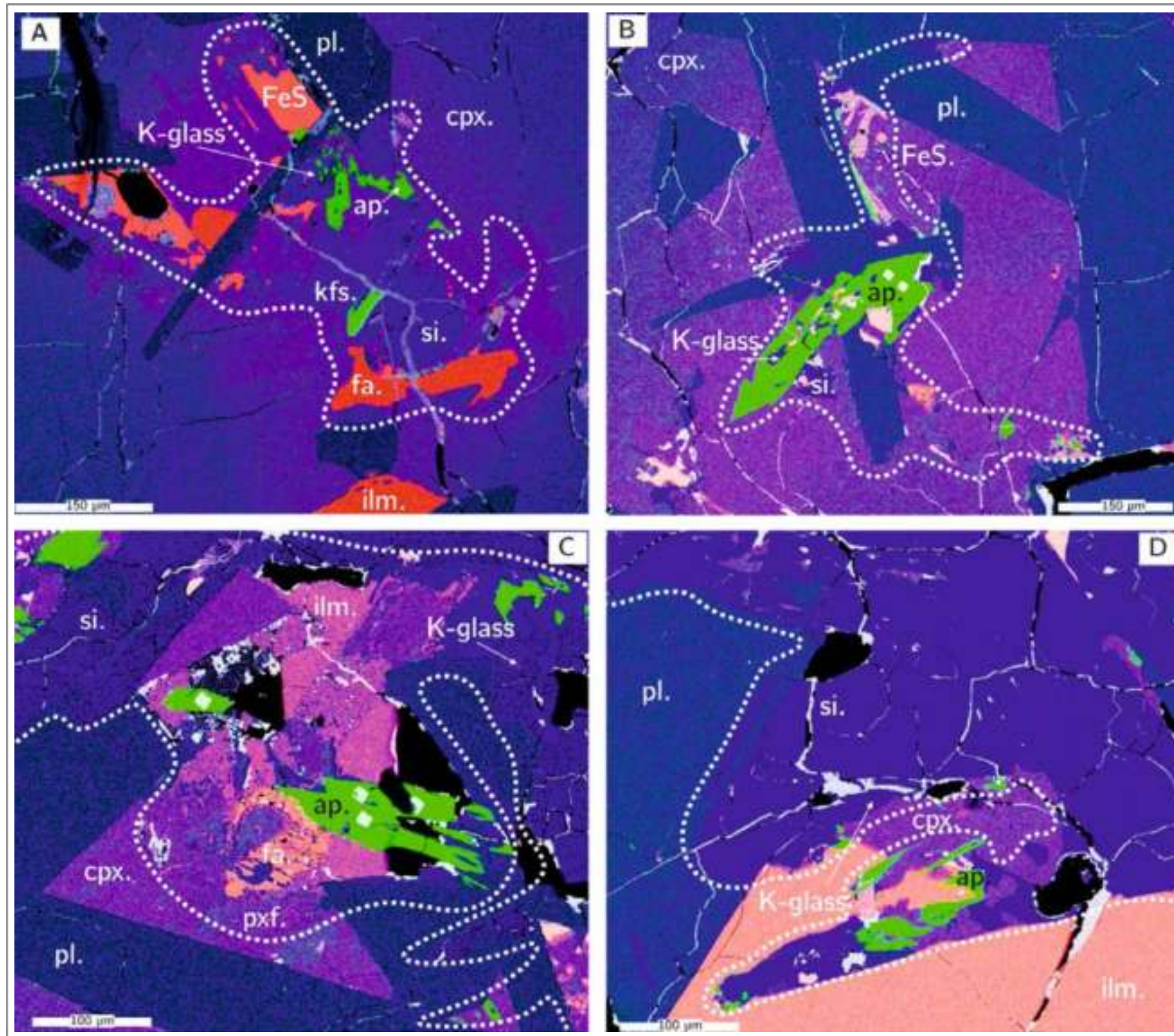
Taken From McCubbin et al. (2015)

Backscattered electron images of regions within lunar samples containing volatile-bearing minerals. (a) Low-Ti mare basalt 15058, (b) Troctolite 76535, (c) Spinel troctolite 72435, (d) Low-Ti mare basalt 15058, (e) Gabbro clast in 67915, and (f) Troctolite 76535. Phase abbreviations are as follows: An = anorthitic plagioclase, Ap = apatite, Bdy = baddeleyite, Chr = chromite, Cpx = clinopyroxene, Crd = cordierite, Fa = fayalite, Fe = iron metal, Kfs = potassium-rich alkali feldspar, Mer = merrillite, Opx = orthopyroxene, Pgt = pigeonite, Pl = plagioclase, Rgl = residual glass, Tr = troilite, Usp = ulvöspinel. Inset boxes both highlight examples of secondary alteration of silicates to sulphides.



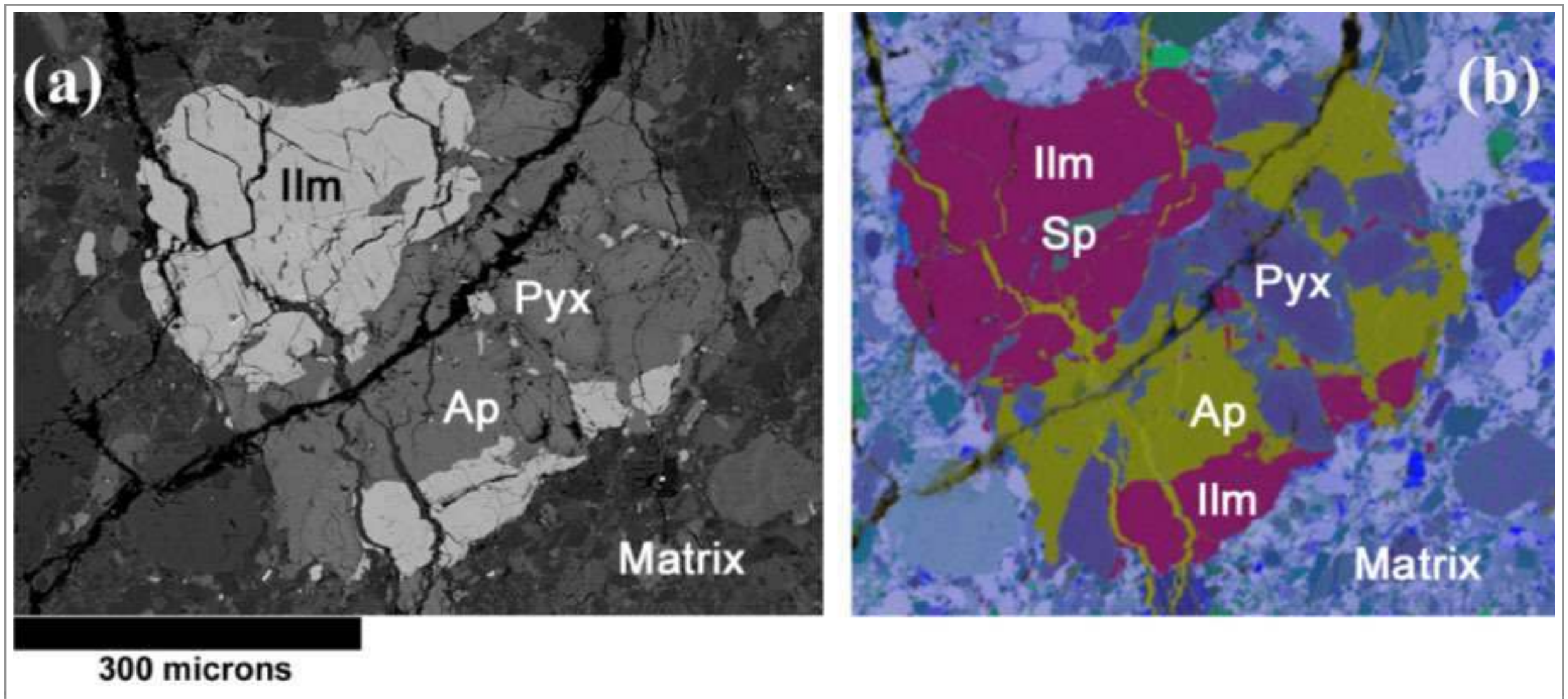
Taken From McCubbin et al. (2010)

Backscattered electron images of phosphate-rich regions in Apollo 15 soil grain 15404,51. Phase abbreviations are as follows: Ap, apatite; Pyx, pyroxene; Ox, Fe-Ti oxide; Pl, plagioclase; Mer, merrillite. The black circles with the white numbers indicate the positions where SIMS data was collected.



Taken From Potts et al. (2016)

False-colour composite X-ray maps (Si = blue, Ca = green, Fe = red) of mesostasis regions in Apollo 11 ilmenite basalt 10044,645. Mesostasis regions are outlined with a white dashed line. ap. = apatite, cpx. = clinopyroxene, fa. = fayalite, ilm. = ilmenite, pl. = plagioclase, pxf. = pyroxferroite, si. = silica, FeS = troilite.

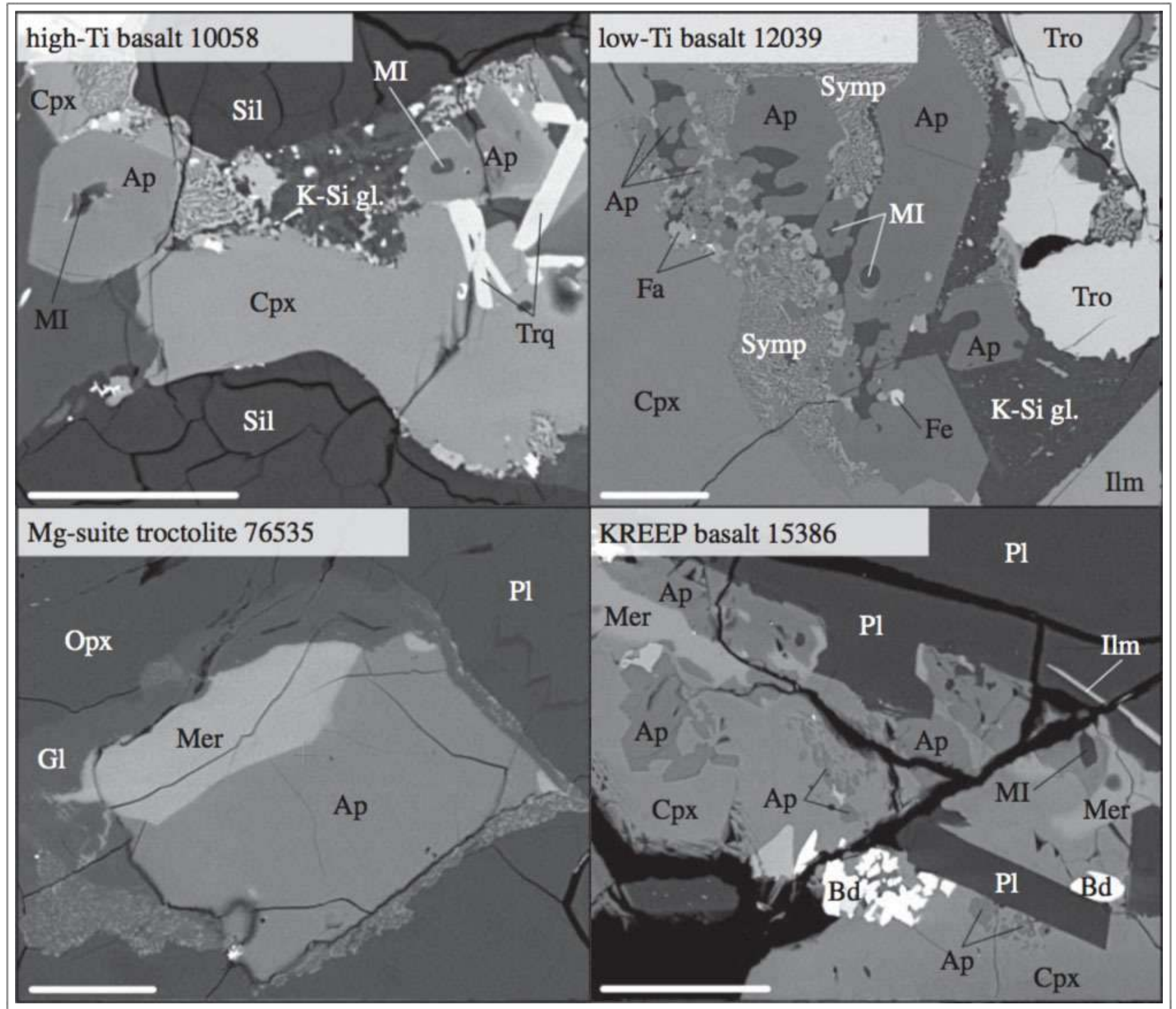


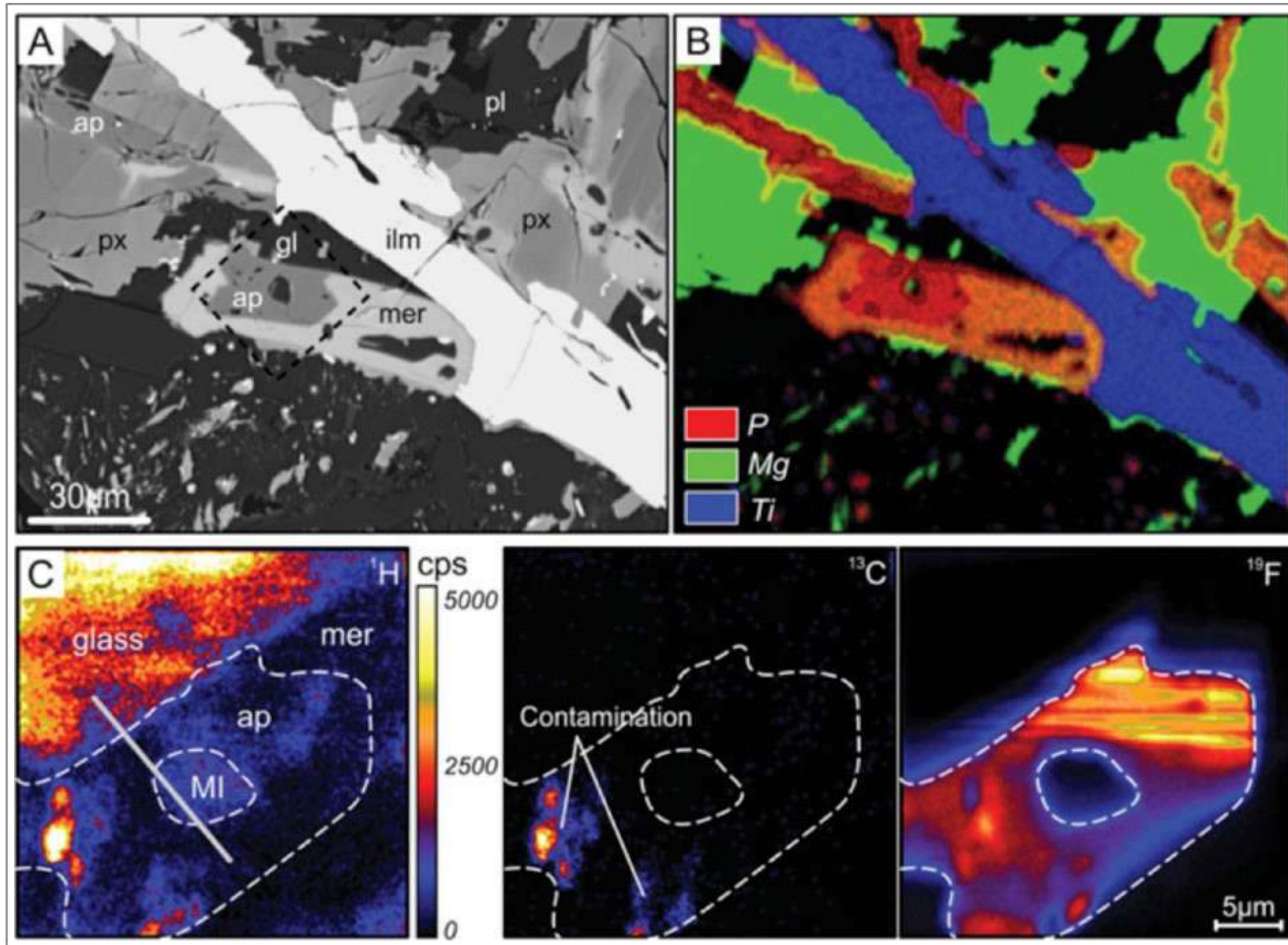
Taken From Joy et al. (2009)

North West Africa (NWA 4472) is a KREEPy lunar meteorite regolith breccia. (a) Backscattered electron image of evolved basalt clast containing large apatite phases and zoned clinopyroxene. (b) X-ray element map of the same clast coloured so that Si = blue, Al = white, Mg = green, Fe = red, Ca = yellow (apatite and terrestrial contamination occurring in fractures) and Ti = pink (ilmenite). Scale bar = 300 μm .

Backscattered electron images illustrating the textural context for apatite occurrences in diverse lunar lithologies.

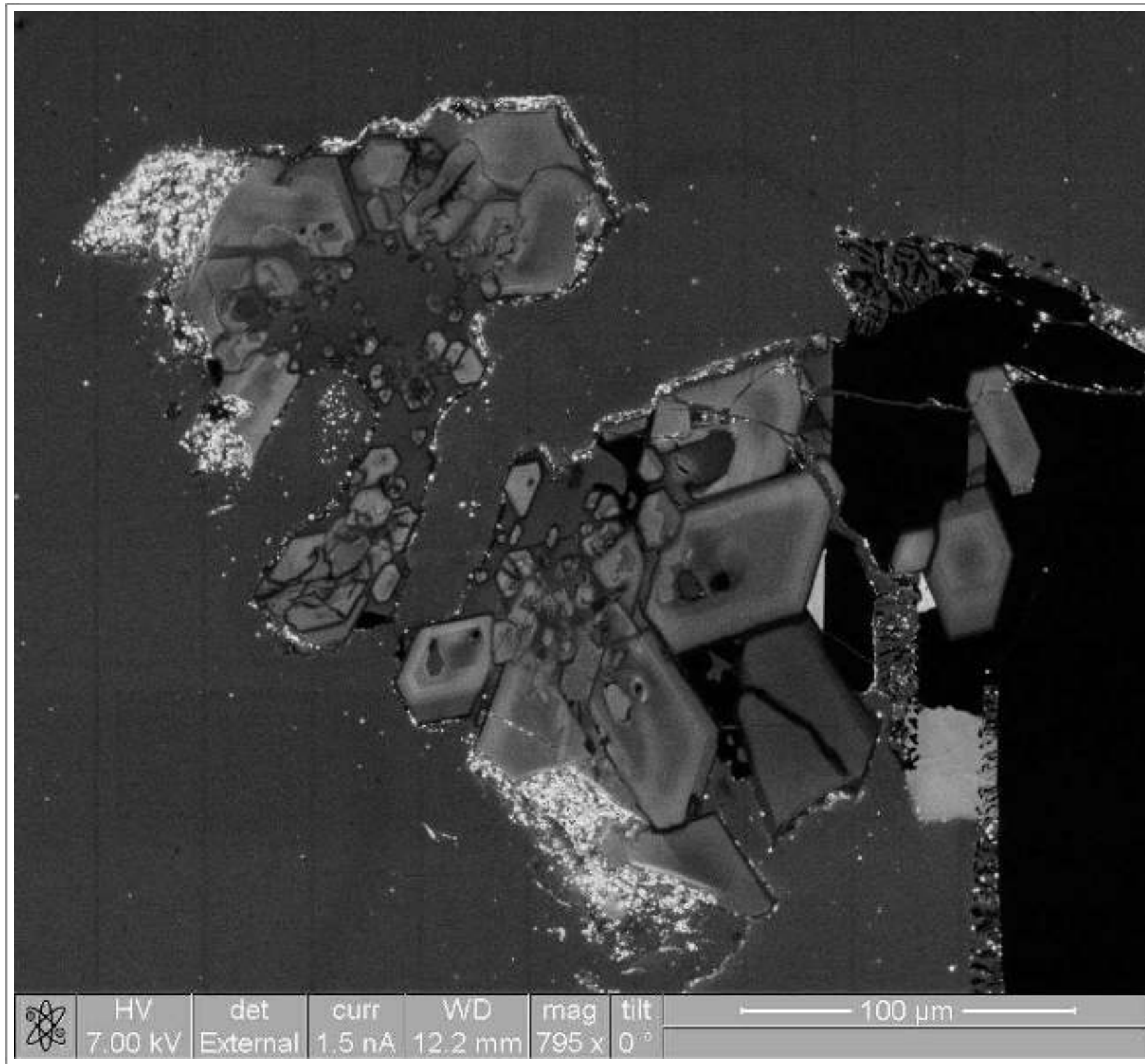
- Ap - apatite
- Bd - baddeleyite
- Cpx - clinopyroxene
- Fe - metallic iron
- Gl - glass
- Ilm - ilmenite
- Mer - merrillite
- MI - melt inclusion
- Pl - plagioclase feldspar
- Si - silica (cristobalite?)
- Symp - symplectite
- Tra - tranquillityite
- Tro - troilite





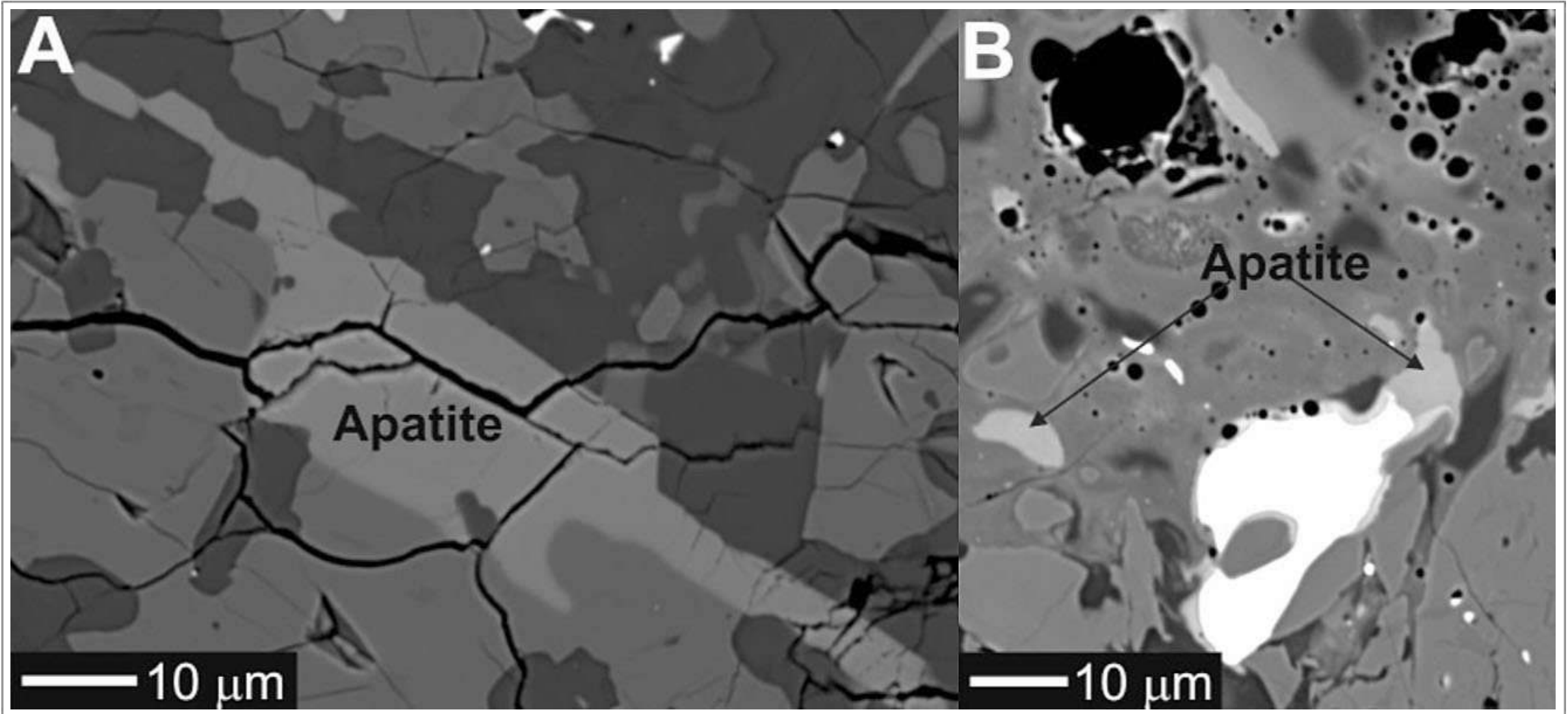
Taken From Tartèse et al. (2014b)

A: Backscattered electron image of area enclosing a glass + melt inclusion + apatite assemblage in Apollo 15 KREEP basalt 15386. ap=apatite; gl=glass; ilm=ilmenite; mer=merrillite; pl=plagioclase; px=pyroxene. B: Corresponding combined X-ray map; red=P, green=Mg, and blue=Ti. C: Secondary ion images showing distribution of ^1H , ^{13}C , and ^{19}F in an apatite and the melt inclusion (MI) it hosts (cps=counts per second). Corresponding area is depicted in A by dashed black square.



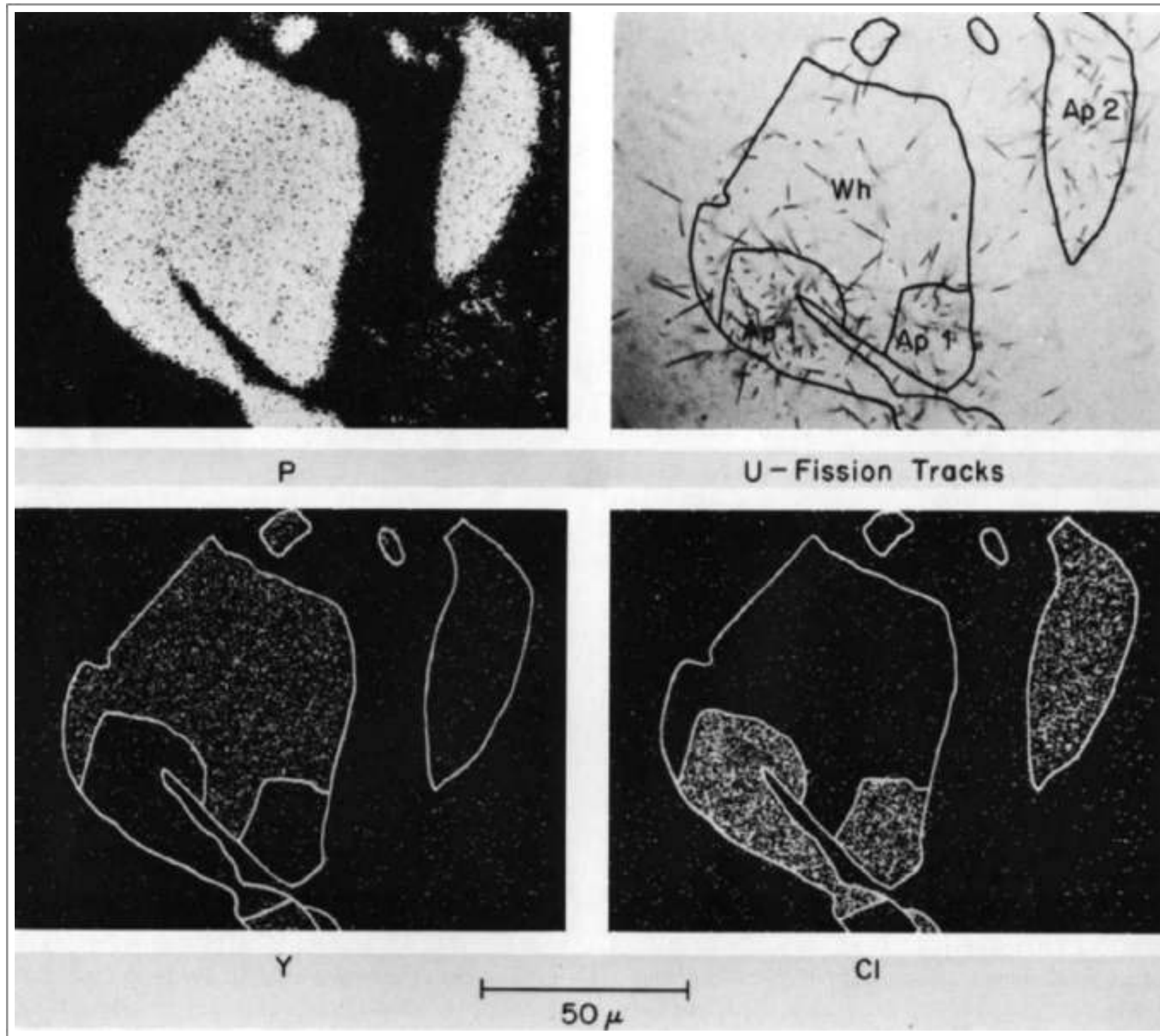
Courtesy of S. Faircloth (Open University)

Cathodoluminescence image of compositionally zoned euhedral apatite crystals within vugs in Apollo 15 pigeonite basalt 12039.



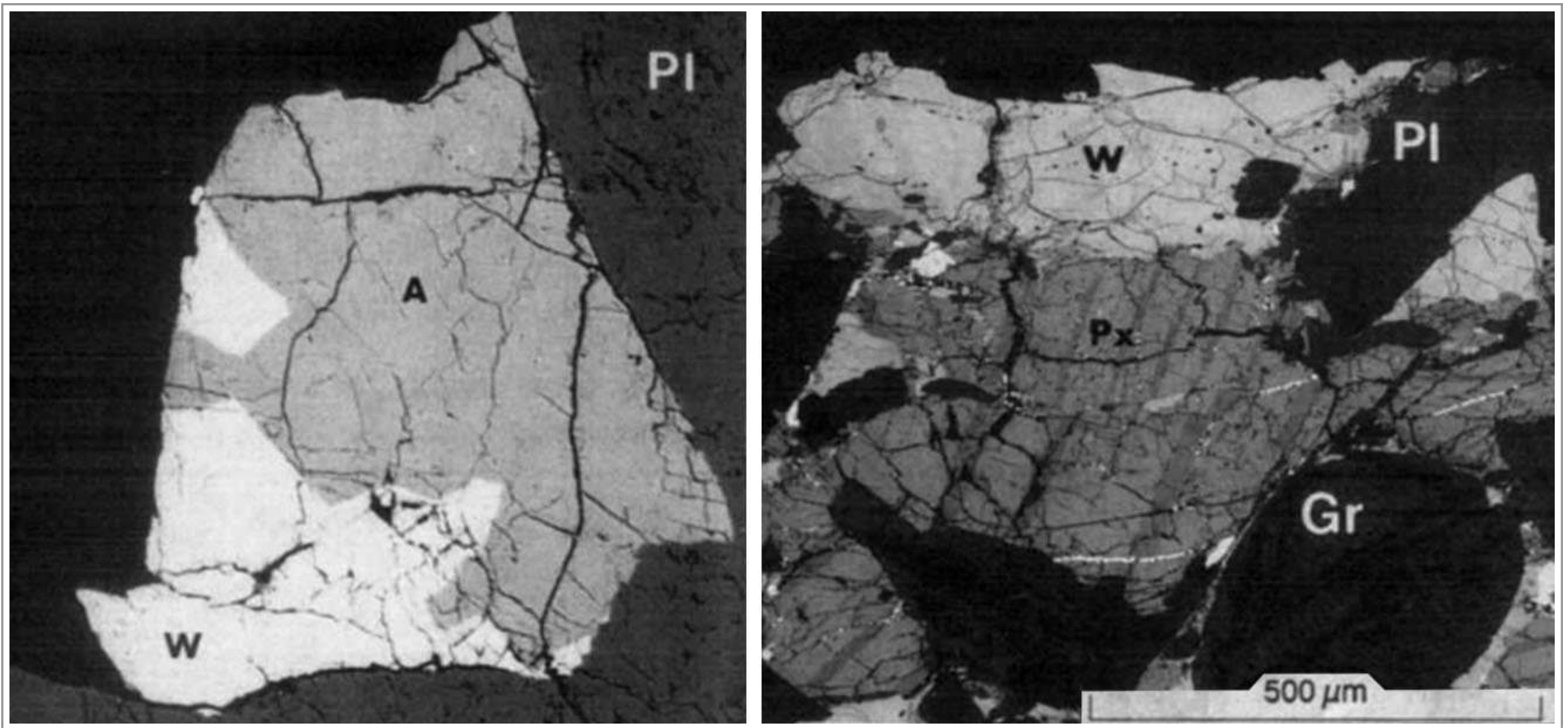
Taken From McCubbin et al. (2008)

Backscattered electron images of (A) elongate subhedral apatite in Apollo 14 soil sample 14161. (B) anhedral apatite patches in lunar meteorite SaU 169.



Taken From Haines et al. (1971)

Elemental maps of apatite-whitlockite cluster in Apollo 12 polymict breccia 12013, 10. The P map indicates the area occupied by phosphates. Whitlockite is indicated by the Y-rich portion. The presence of chlorine in the portion labelled Ap indicates chloro-fluorapatite. Outlines delineated by the Y and Cl maps were graphically superimposed on the U-fission track map.



Taken From Jolliff et al. (1993)

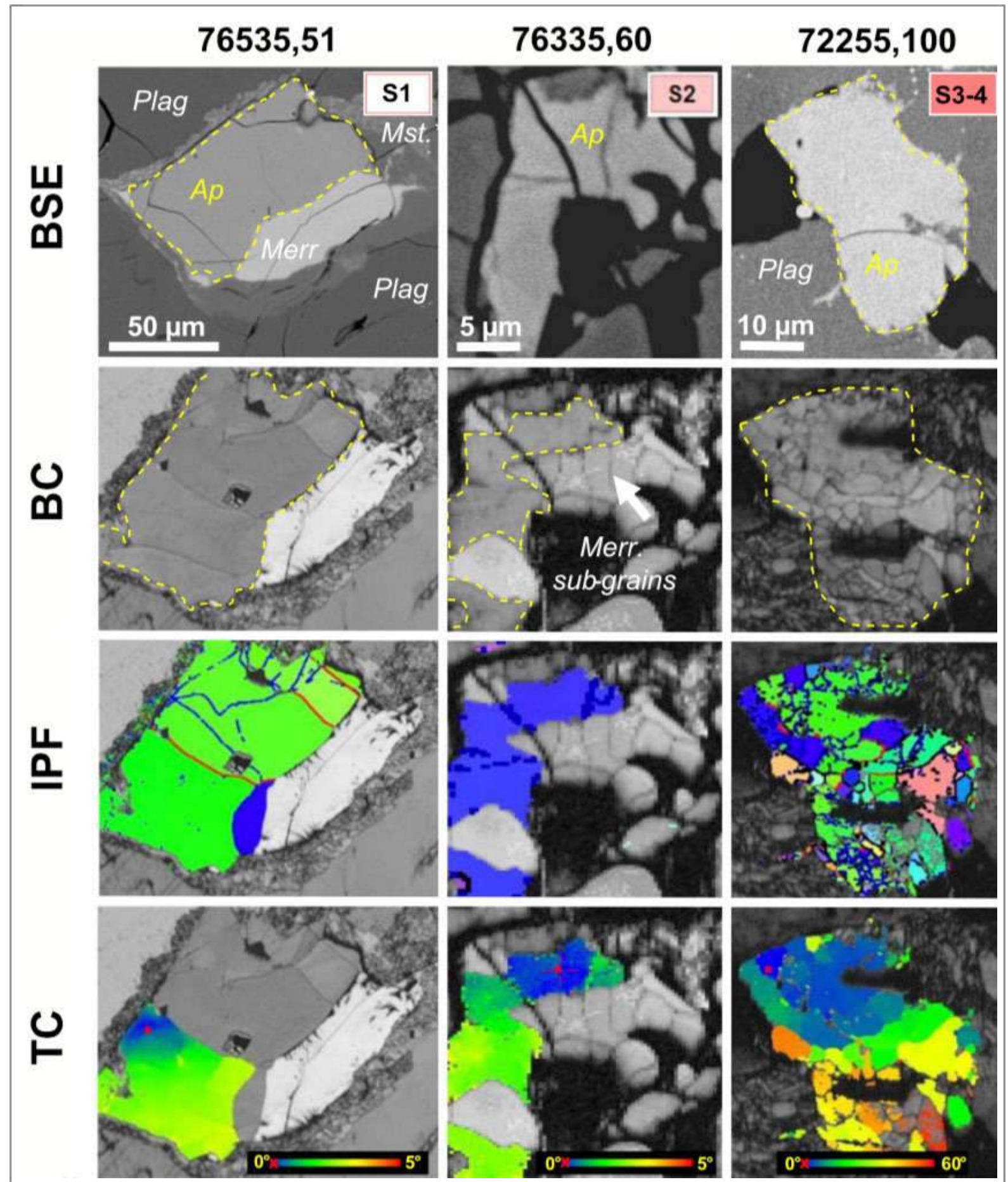
Backscattered electron images of Apollo 14 soil fragments. Left: composite apatite-whitlockite grain in magnesian anorthosite 14161, 7350; light grey is apatite (A), bright grey is whitlockite (W), dark grey is anorthitic plagioclase (PI). Width 300 μm . Right: quartz monzogabbro 14161, 7373. Pyroxene (Px) is coarsely exsolved; silica and K-feldspar form granophyric segregations (Gr).

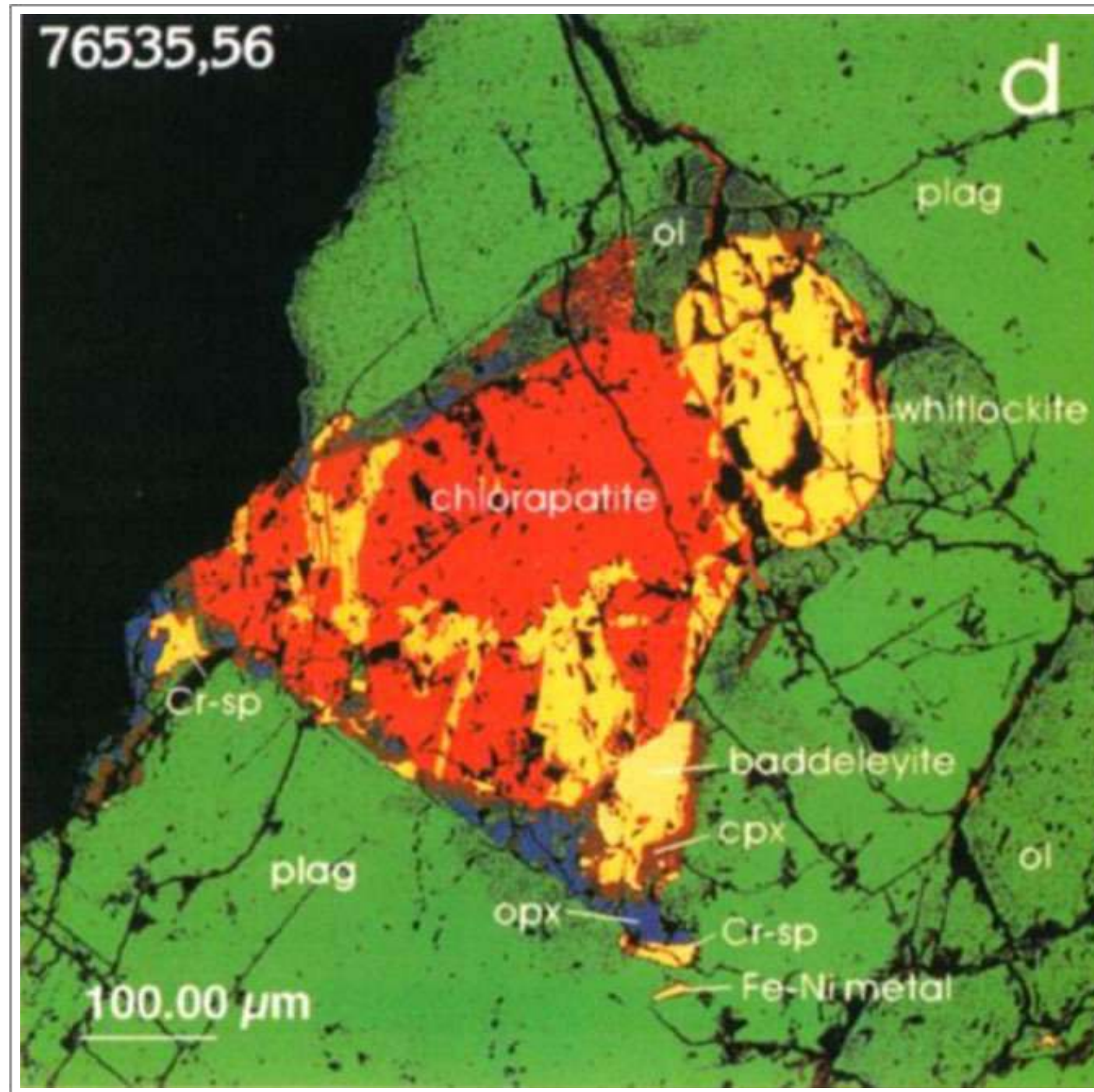
Apatite in Apollo 17 rocks; troctolite 76535, cataclastic magnesian anorthosite 76335 and aphanitic impact melt breccia 72255.

Backscattered electron (BSE), band contrast (BC), inverse pole figures (IPF) including grain boundaries, and texture component (TC) maps of apatite grains that have experienced deformation from S1 to S4 stages. Yellow dashed lines in BSE and BC panels outlines the studied apatite grains.

BSE images clearly indicate individual fragments of apatite but do not reveal any internal complexities of the apatite structure that occur in response to increasing shock-loading.

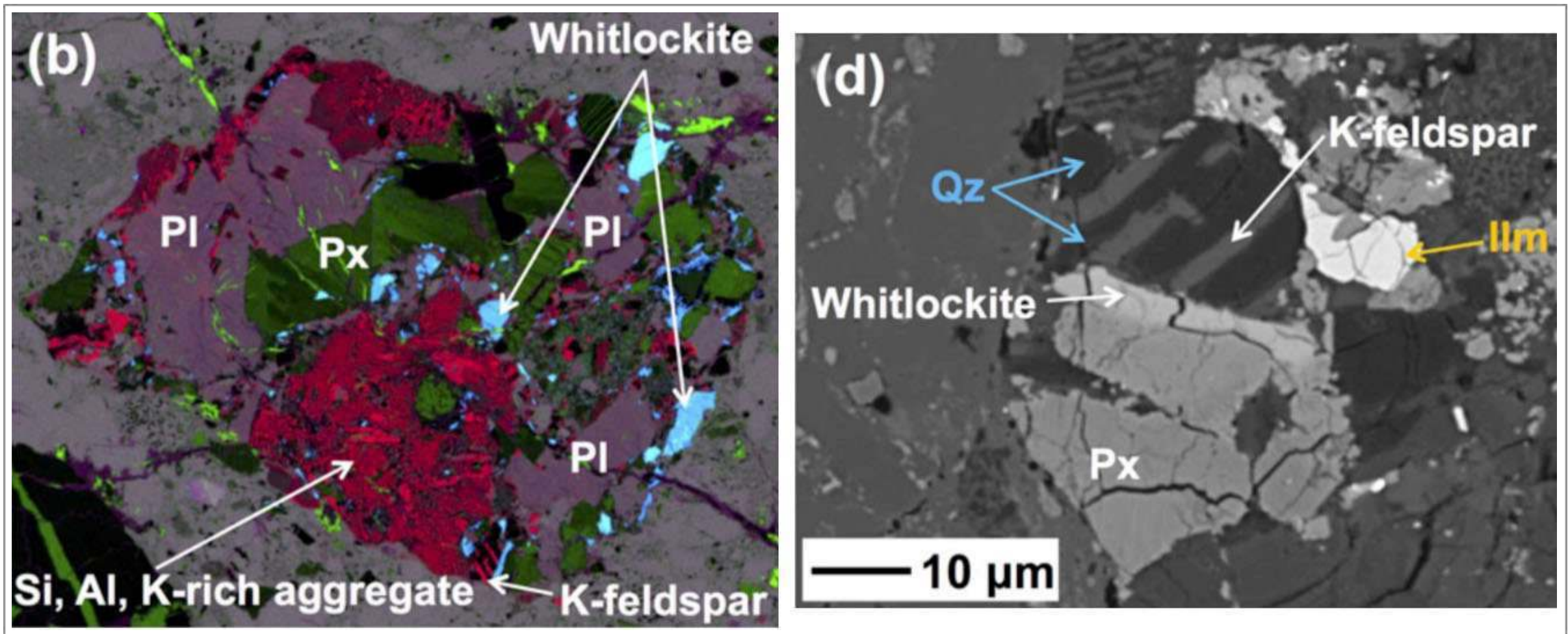
BC maps show that subgrain formation becomes more prominent with increasing shock-loading.





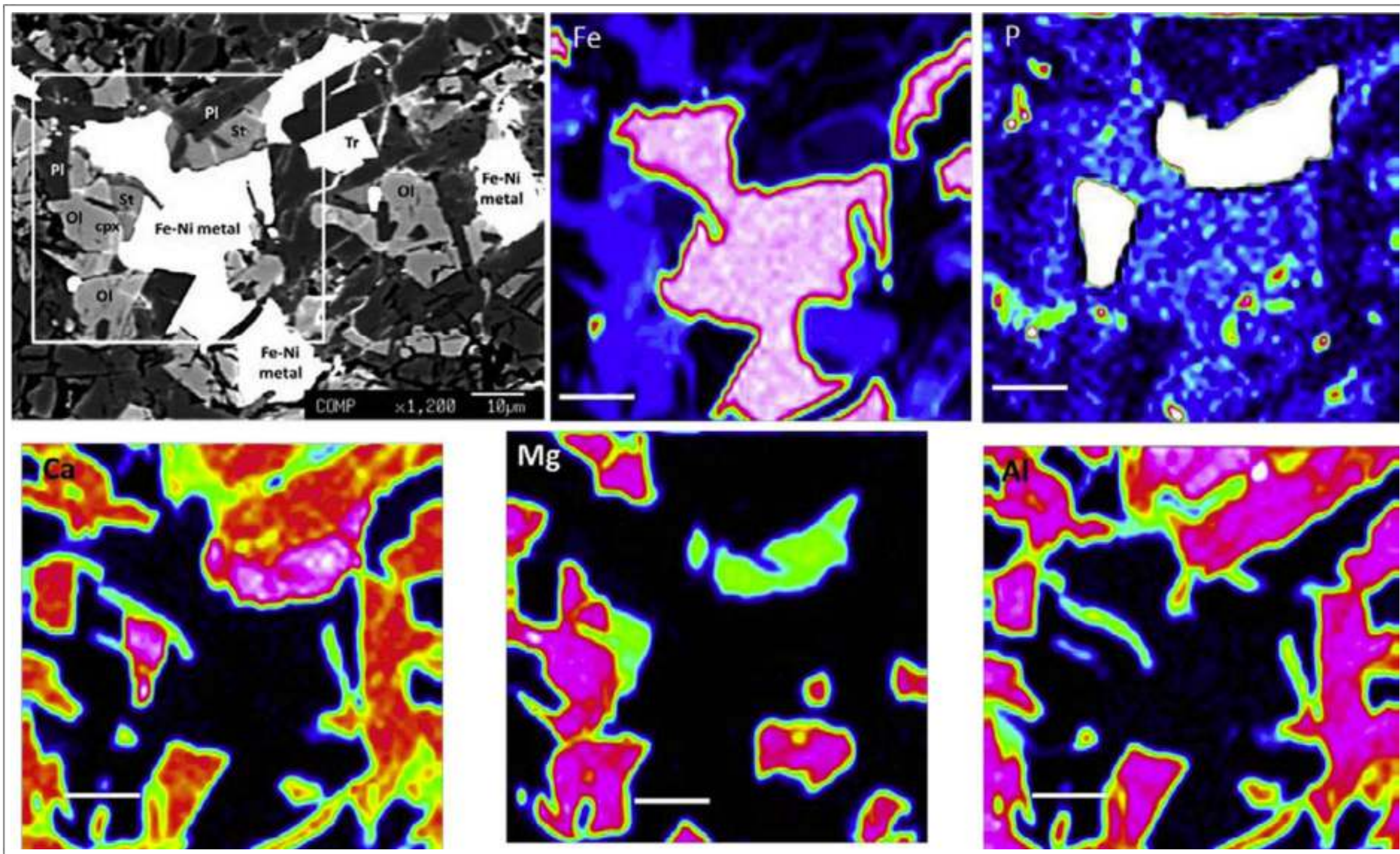
Taken From McCallum and Schwartz (2001)

False colour backscattered electron image of chlorapatite in Apollo 17 troctolite 76535. It is associated with whitlockite, orthopyroxene, clinopyroxene, chromite, baddeleyite and metallic iron within plagioclase feldspar. Such clusters of minerals are interpreted as evidence of trapped melt.



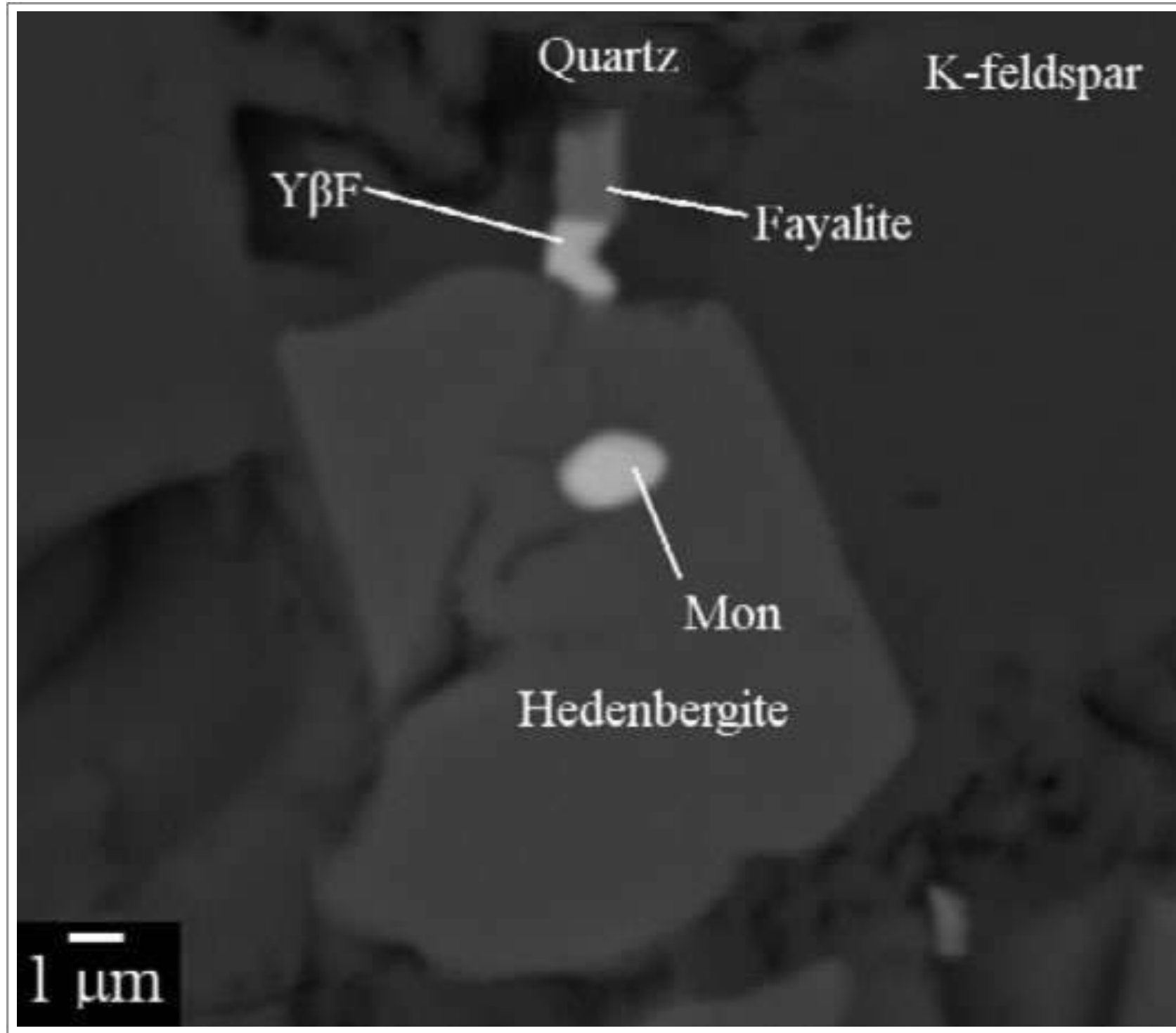
Taken From Hidaka et al. (2014)

Backscattered electron images of a quartz monzogabbro clast in lunar meteorite Dhofar 1428. b) The elemental map of Si, Al, K-rich aggregate. Al = magenta, K = red, Ca = green, P = blue. d) The enlarged view of quartz-rich region. Ilm = ilmenite, Qz = quartz, Pl = plagioclase, Px = pyroxene.



Taken From Shearer et al. (2014)

Stanfieldite associated with metallic iron in Apollo 16 “rusty rock” impact-melt 66095. Backscattered electron image and associated X-ray maps for Fe, P, Ca, Mg and Al, illustrating the textural relationship between stanfieldite (St) and other phases. These phases include metallic iron, olivine (Ol), troilite (Tr), plagioclase (Pl), and clinopyroxene (cpx). Note that stanfieldite occurs adjacent to phosphorous-bearing Fe-Ni metal and Ca-bearing silicates.



Taken From Seddio et al. (2014)

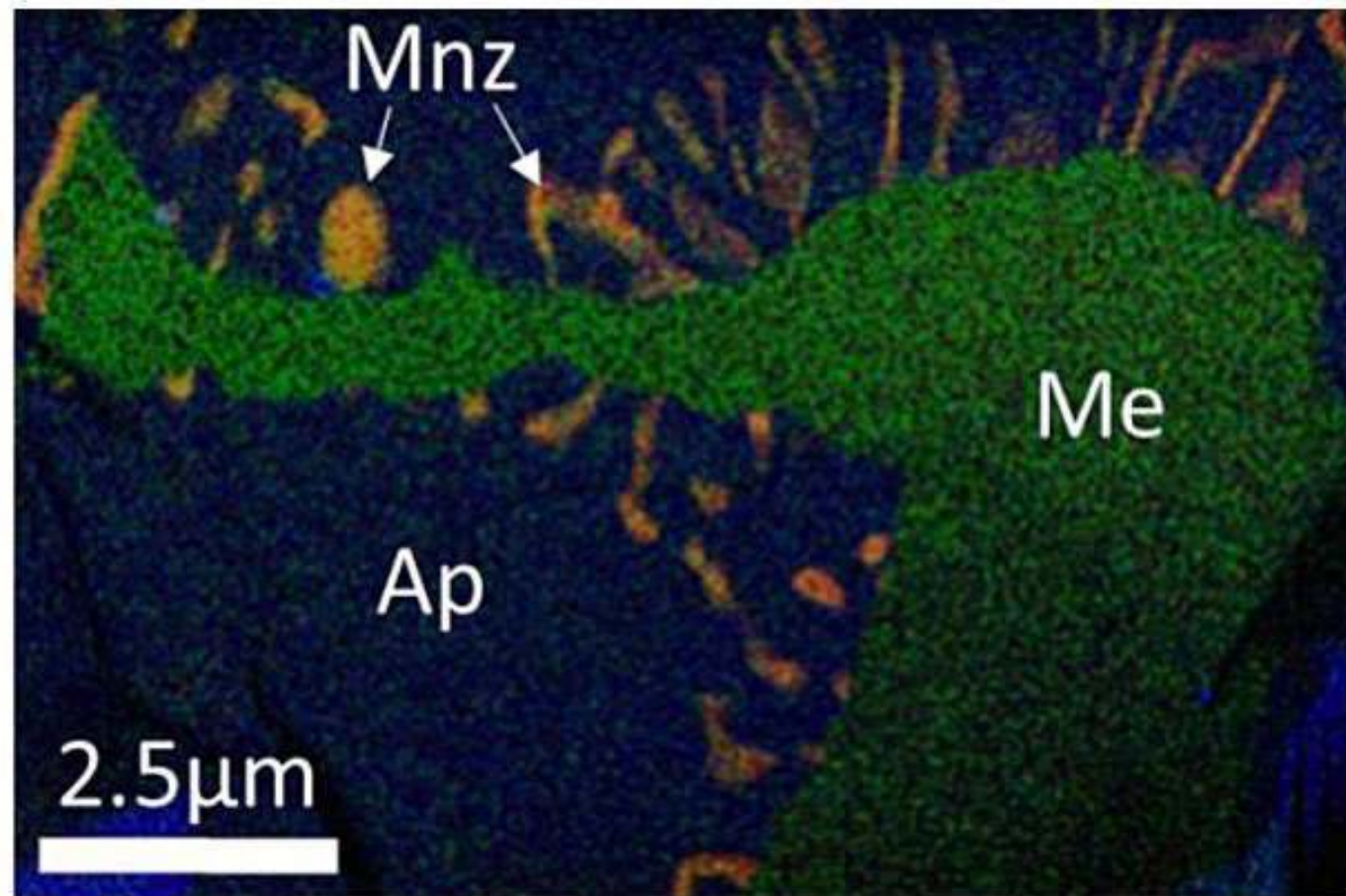
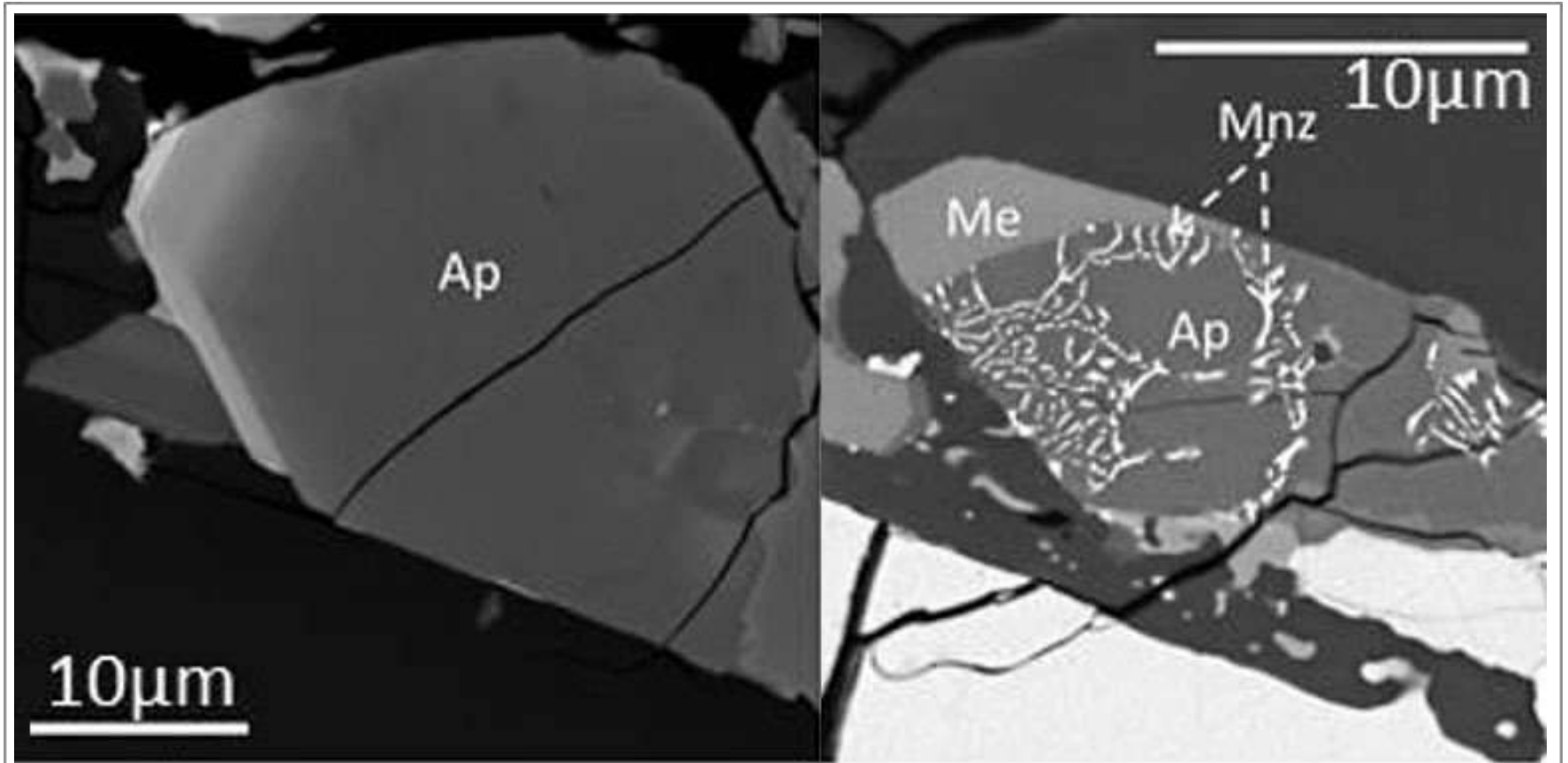
Backscattered electron image of monazite (Mon) in granitic fragment from Apollo 12 regolith sample 12023,147-10.

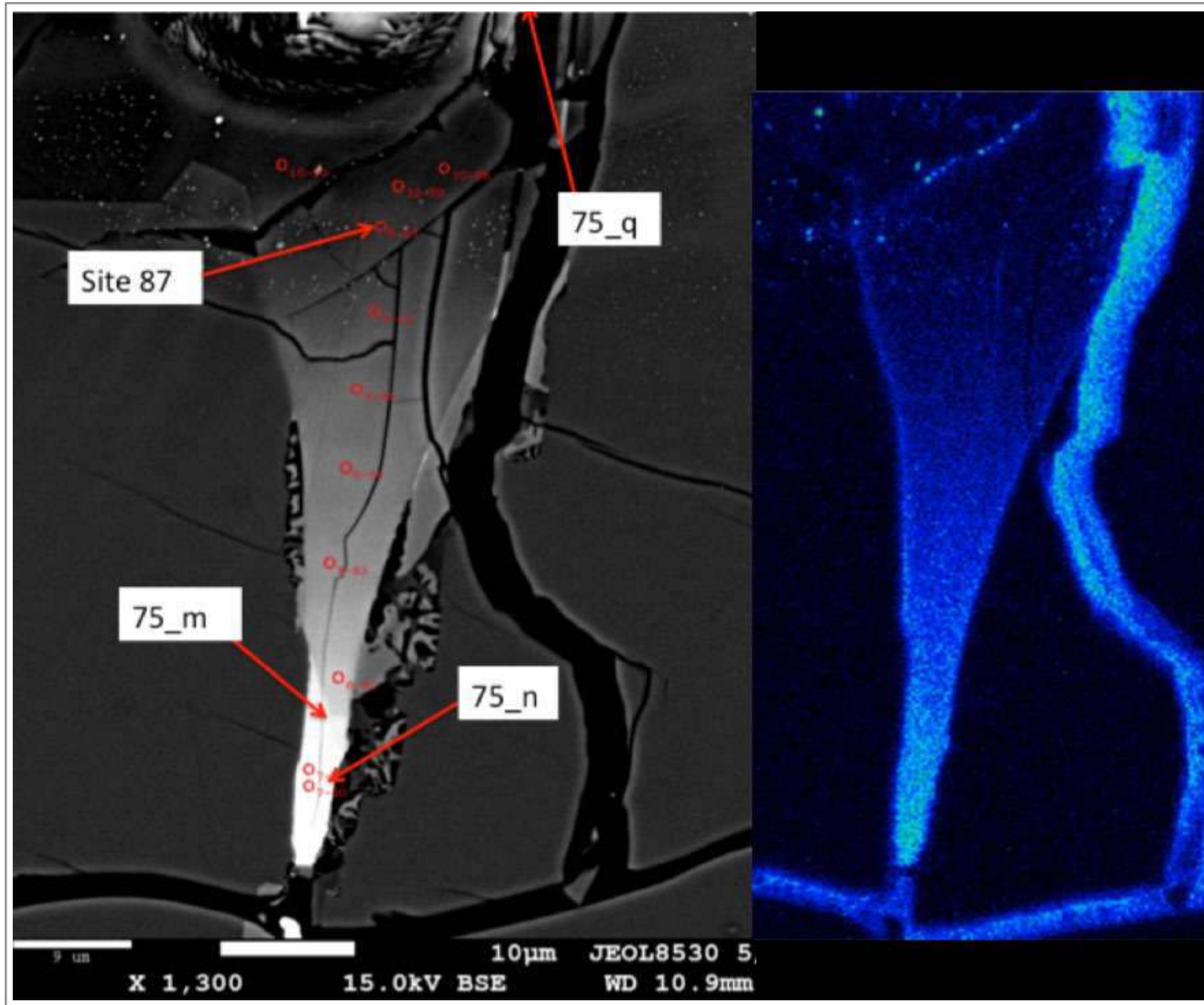
Backscattered electron images of phosphates in Apollo 11 High-Ti basalts.

Top left: zoned apatite (Ap) from low-K basalt 10029.

Top right: Symplectic assemblage of apatite (Ap), merrillite (Me) and monazite (Mnz) in high-K basalt 10024.

Bottom: false colour composite X-ray map of phosphates in high-K basalt 10024. (Green = Mg, Blue = F, Red = Ce).

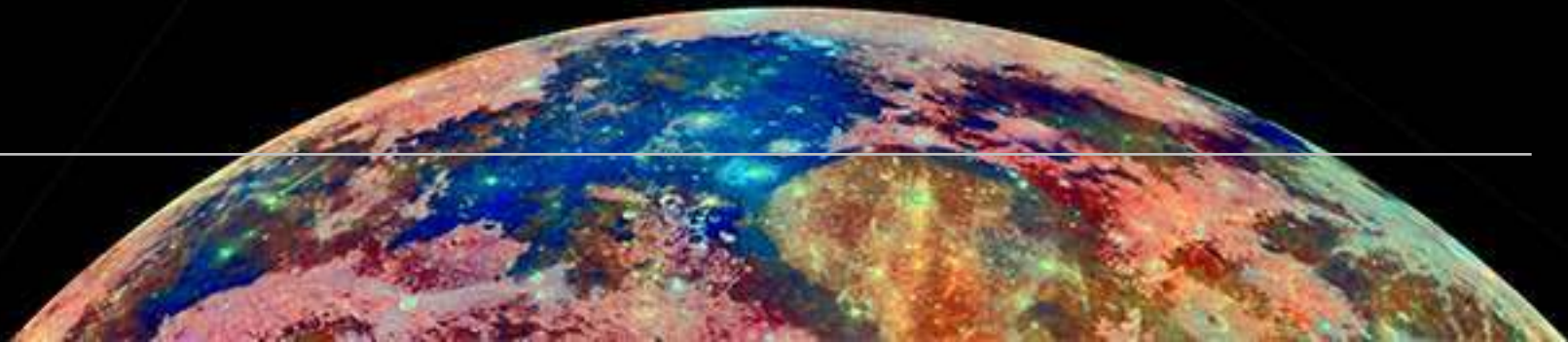




Taken From Lowe et al. (2016)

Backscattered electron image and chlorine elemental map showing Cl-rich britholite substitution in apatite from Apollo 17 high-titanium basalt 75055,50.

Chlorides



SPECIES

1. Akaganéite - $\text{Fe}_{7.6}\text{Ni}_{0.4}\text{O}_{6.35}(\text{OH})_{9.65}\text{Cl}_{1.25}$

2. Halite - NaCl

3. *Lawrencite?* - $\text{Fe}^{2+}\text{Cl}_2$

Rusty alteration in lunar rocks was first reported in Apollo 14 breccias and became more widely recognized in Apollo 16 breccias. The alteration is typically found in association with metal grains, and the best-studied sample is the “rusty rock” impact-melt 66095. In a thin section from 66095, the metallic iron grains are associated with thin grey margins and brown stains that extend into the adjacent silicates and have been interpreted as rusting in situ (Taylor et al., 1973; 1974). During the sample’s original examination considerable rust corresponding to the hydrous mineral akaganéite was found. Although many Apollo 16 rocks exhibit some rust around metallic iron grains, this sample is unusual in that it has abundant evidence of alteration. The presence of rust has been cited as evidence for water interaction on the Moon.

Hunter and Taylor (1981) summarize 66095 as a clast-laden impact-melt breccia - the most volatile-rich sample returned by the Apollo missions. The volatile nature shows as rust, schriebersite, and minor volatile-bearing compounds, usually associated with metallic iron and/or troilite. KREEP is considered to be the ultimate source of the volatiles which were incorporated into the breccia by hybridization and volatilization during impact processes.

Shearer et al. (2014) then suggested that the volatile enrichment in 66095 is due to degassing of an ejecta blanket (or far less likely, the degassing of a shallow basaltic intrusion). An ejecta-forming process was proposed. In this scenario,

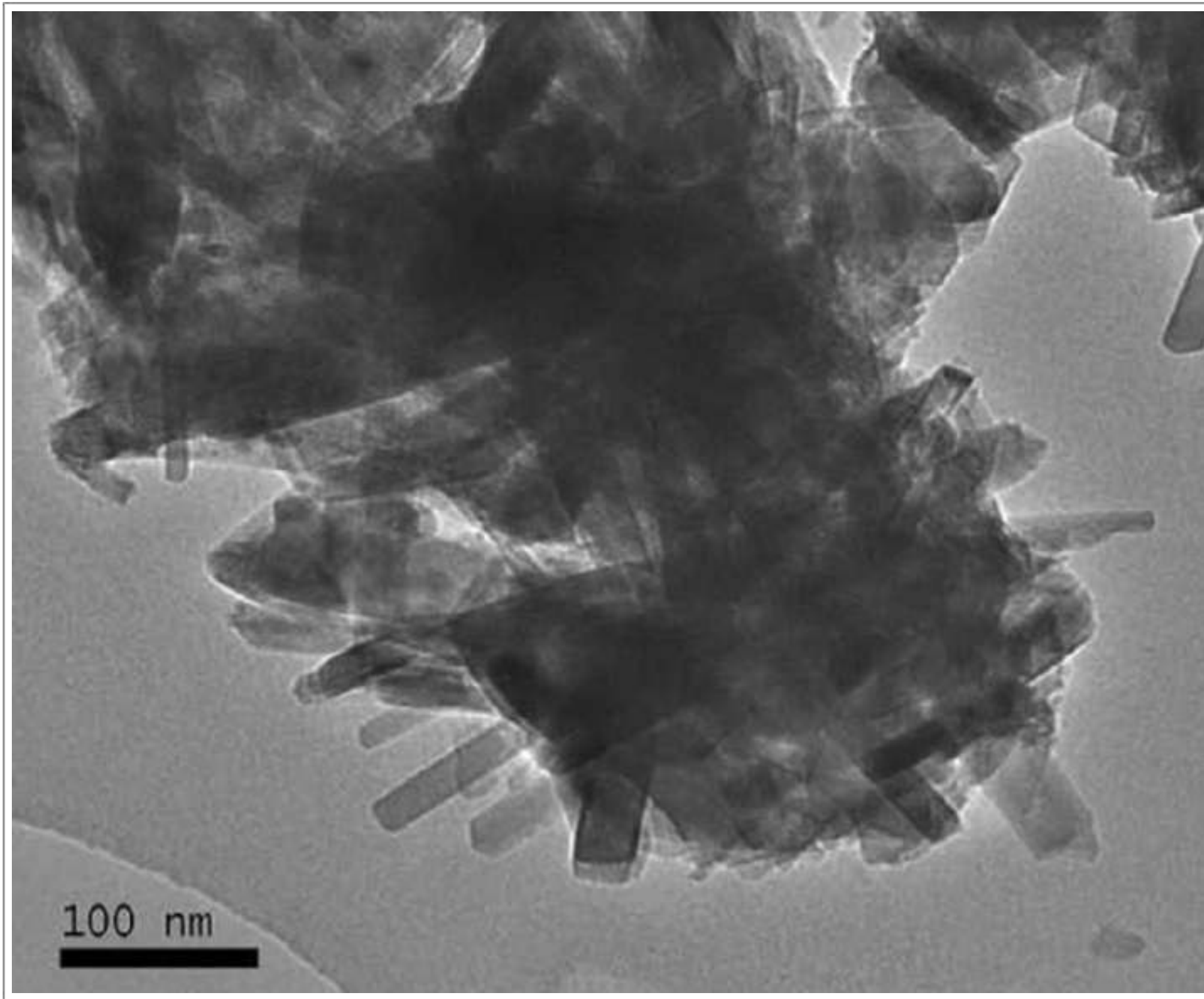
lawrencite was deposited on mineral surfaces at approximately 650°C to 570°C from a metal-chlorite-bearing and H-poor gas phase. The formation of akaganéite in 66095 is more problematic, as it could be solely attributed to terrestrial alteration of lawrencite - although there is some Cl isotope evidence to support a lunar origin for the species.

A further possibility was proposed by Jean et al. (2016) who noted that rust-coloured alteration is present in all Apollo 16 rocks. They attributed this to an association with meteorite fragments and proposed this was the source of Cl in Apollo 16 rocks/soils. The Cl had effectively reacted with the FeNi metal to form lawrencite, while still in the meteorite. Upon exposure to terrestrial air and water vapour, the lawrencite effectively reacted to $\beta\text{FeO}(\text{OH})$ and HCl, which further oxidized the minerals. The rust and its volatile components in the Apollo 16 rocks/soils are now considered to be exogenic, i.e., from meteorites and/or the Earth. See also McCubbin et al. (2015).

The metallic iron grains in lunar breccia meteorite Dhofar 025 typically have $\beta\text{-FeOOH}$ (akaganéite) rimming them, similar to many Apollo 16 highland rocks (Taylor et al., 1973). Akaganéite probably formed by terrestrial oxyhydration of lawrencite that was present in the meteorite as it left the Moon (Cahill et al., 2001).

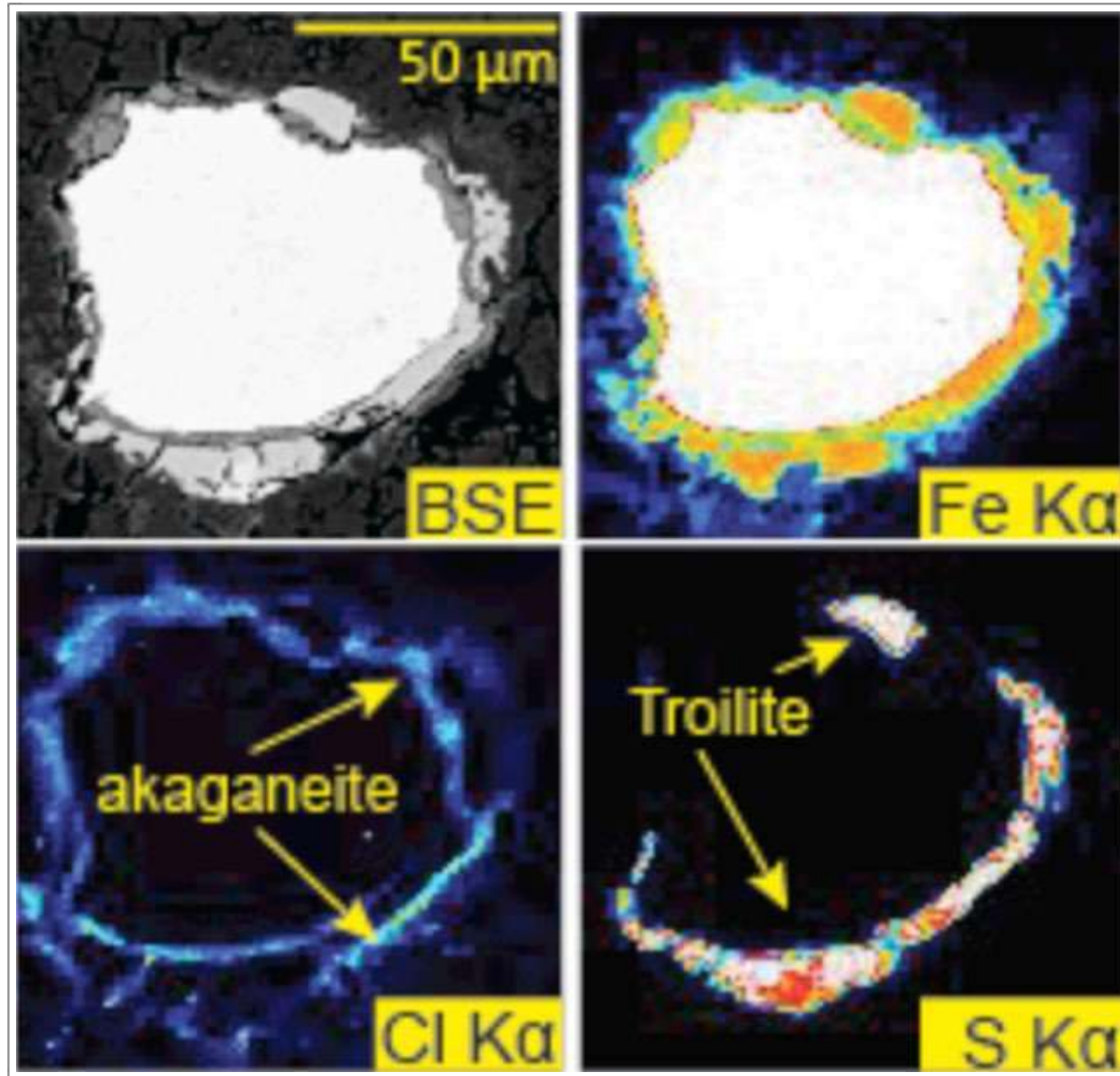
Halite has been observed by McKay and Wentworth (1992, 1993) as minute euhedral crystals associated with surface coatings on Apollo 17 orange volcanic glass beads (sample 74220). The

surface coatings are typically 20-150 nm thick and exhibit geochemical stratigraphy. Such surface coatings are considered to be condensates from later volatile phases.



Taken From Shearer et al. (2014)

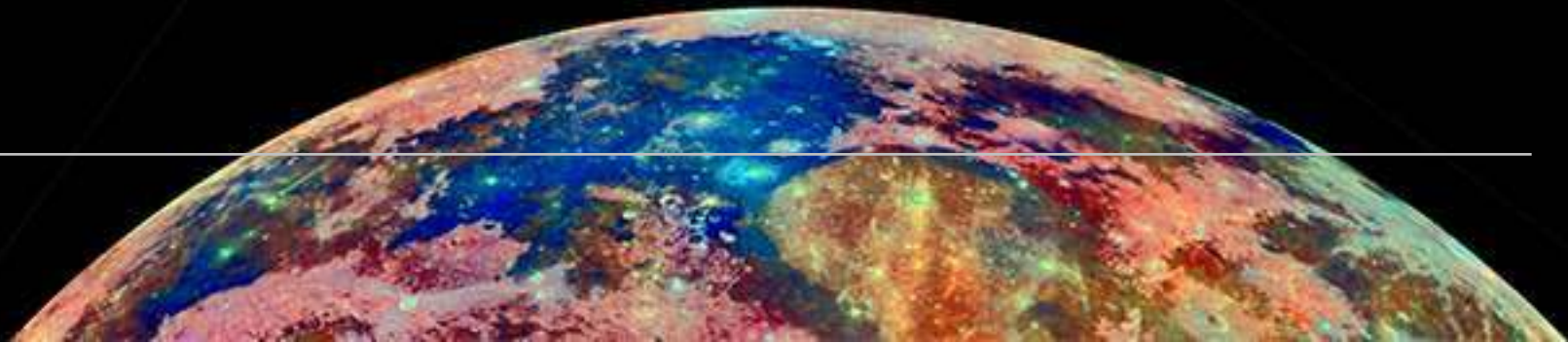
Akaganéite in Apollo 16 "rusty rock" impact-melt 66095.



Taken From Jean et al. (2016)

Akaganéite in Apollo 16 “rusty rock” impact-melt 66095.

Titanium Minerals



SPECIES

1. Armalcolite - $(\text{Mg}, \text{Fe}^{2+})\text{Ti}_2\text{O}_5$
2. Rutile (& Anatase) - TiO_2
3. Titanite - CaTiO_5
4. Yttrobetafite-(Y) - $\text{Y}(\text{Ti}, \text{Nb})_2\text{O}_6$
5. “Pyrochlore” - $(\text{Ca}, \text{Pb}, \text{Y}, \text{Th})_2(\text{Ti}, \text{Nb})_2\text{O}_6$
6. Chevkinite
- $(\text{Ce}, \text{Ca}, \text{Na}, \text{Th})_4(\text{Fe}^{2+}, \text{Mg})_2(\text{Ti}, \text{Fe}^{3+})_3\text{Si}_4\text{O}_{22}$
7. Perovskite (*dysanalyte*)? - $(\text{Ca}, \text{Fe})(\text{Ti}, \text{REE})\text{O}_3$

Note: ilmenite is the major titanium-rich mineral in lunar samples. It is not usually an accessory mineral so is discussed in Chapter 2, Section 4.

Tranquillityite is a titanium-zirconium species and is described in Section 9 of this Chapter.

Armalcolite

The occurrence of armalcolite is restricted to rocks with high TiO_2 content that have cooled rapidly. This rapid cooling (quenching) is essential to prevent early-formed armalcolite from reacting with the remaining liquid to form magnesian ilmenite (Haggerty, 1973a; Heiken et al., 1991).

Isolated grains of armalcolite have been identified in Apollo 11 crystalline rocks (samples 10022 and 10071) and in rock fragments within microbreccias (samples 10059, 10067, 10068 and 10084). In most cases armalcolite is mantled by a well defined overgrowth of ilmenite. It is opaque, grey and distinctly pleochroic (Anderson et al., 1970).

In Apollo 17 samples, armalcolite has been observed in pyroxenite and basaltic lithic fragments, usually in association with ilmenite and chromian ulvöspinel. On the basis of a large armalcolite dataset it has been possible to confirm that the two varieties (ortho-armalcolite and para-armalcolite) identified by earlier authors (Haggerty et al., 1973) are not distinct, rather they form a limited continuum of compositions with a spread of optical properties, probably resulting from fractional crystallization (Williams and Taylor, 1974).

Armalcolite is reported from the first lunar meteorite (ALHA81005) ever discovered. This polymict anorthositic breccia contains armalcolite crystallites in Ti-rich glass

(Marvin, 1983). Highland impact breccia meteorite Dhofar 303 is also reported to contain armalcolite, where it is found as an accessory mineral with Ti-rich chromite, ilmenite, rutile, troilite and metallic iron (Nazarov et al., 2002). The impact melted granulitic breccia lunar meteorite Dhofar 1766 contains rare euhedral armalcolite crystals up to 30 μm across (Wittmann et al., 2014).

A Zr-rich variety of armalcolite is reported from fragments of KREEP rock (basaltic, gabbro-noritic, gabbro-anorthositic, gabbro-troctolitic and anorthositic compositions) in lunar meteorites Dhofar 725, 760 and 761 - impact-melt breccias. K-Ba feldspar, whitlockite, apatite and baddeleyite are associated species (Demidova et al., 2005).

Rutile (& Anatase)

Rutile generally occurs in association with ilmenite. Lamellae of ilmenite indicate exsolution, whereas irregular intergrowths of Mg,Fe-rich rutile and Mg-ilmenite indicate breakdown of armalcolite (Haggerty, 1973b). Primary rutile tends to occur as twinned, randomly-oriented, euhedral crystals associated with ilmenite. Some analyses of primary rutile such as those from Apollo 12 microbreccia 12070 are rich in Nb (Smith and Steele, 1976). Probably all Nb-rich occurrences are in KREEP rocks (Heiken et al., 1991). One such example is the niobian rutile reported by

Hlava et al. (1972) in an Apollo 14 KREEP lithic fragment of basaltic texture. Coexisting minerals in the KREEP fragment are major amounts of plagioclase and orthopyroxene, and minor amounts of olivine, ilmenite, augite, barian K-feldspar, whitlockite, troilite, metallic iron, zirkelite and chromite.

Jedwab (1973) reports several types of rutile in lunar soils including a blue rutile with no detectable Nb or Zr. The blue rutile occurs as a 0.5 mm aggregate of micrometer grains, and may have resulted from condensation.

Rutile is associated with armalcolite, chromite, ilmenite and Ca phosphate in the accessory mineral assemblage of lunar meteorite Dhofar 733 - an anorthositic granulitic breccia (Foreman et al., 2008).

Anatase is reported to occur in association with rutile in the mesostasis areas of shocked lunar meteorite NWA 4734 - a mare basalt (Chen et al., 2018).

Titanite

Titanite, (alias sphene) occurs as anhedral, (5 μm grains associated with ilmenite and troilite in the basaltic mesostasis of Apollo 14 polymict breccia 14321 (Grieve et al., 1975).

Yttrobetafite-(Y) (now oxycalciobetafite)

A reclassification of the pyrochlore supergroup of minerals renamed yttrobetafite-(Y) as oxycalciobetafite (Atencio et al., 2010).

Yttrobetafite-(Y) has been identified in a coarse-grained granophyre (felsite) clast within Apollo 14 lunar breccia 14321,1494. The clast is partly brecciated with a high percentage of vesicular shock-melted glass. However, in some thin sections of this clast there is an un-melted igneous texture consisting of a coarse intergrowth of silica and potassium feldspar.

The origin of granophyric rock on the Moon is uncertain. Presumably, silicic lunar rocks are late-stage differentiates of a crystallizing magma ocean. The presence of rare, silica-rich glass particles ($\text{SiO}_2 > 72 \text{ wt}\%$) in the lunar soils indicates that granophyric rocks may be exposed on the lunar crust.

However, the great amount of cratering that has occurred on the lunar surface has obliterated much of the original mineralogy of lunar granophyre, so it is not certain if these silicic fragments were from plutonic igneous rocks. The relatively coarse grain size of this granophyre clast and the presence of yttrobetafite may indicate that some lunar granophyre could have been originally formed as pegmatite in the early lunar crust (Meyer and Yang, 1988).

However, the chemical characteristics of yttrobetafite (oxycalciobetafite) and zircon in the felsic clast within 14321 are more compatible with the crystallization of felsic melts on Earth and indicate crystallization from a relatively oxidized, low-T, incompatible element and possibly water or F- rich melt (Bellucci et al., 2018 & 2019). The implication being that the felsic clast is part of an Earth meteorite that had landed on the Moon.

Yttrobetafite has also been found in Apollo 12 sample 12023 - a small, monomict rock granitic fragment recovered from a regolith sample. The rock comprises graphic intergrowths of K-feldspar and quartz, and plagioclase and quartz, along with minor or accessory hedenbergite, fayalite, ilmenite, zircon, thorite, monazite and metallic iron (Seddio et al., 2014).

“Pyrochlore”

A single $\sim 5 \mu\text{m}$ grain of “pyrochlore” included in pyroxene reported by Dymek et al. (1975) from Apollo 17 troctolite 76535 contains a high concentration of radioelements ($\text{ThO}_2=16.2\%$, $\text{UO}_2=2.3\%$, $\text{PbO}=6.8\%$) and does not easily fit into the more recent classification scheme of the pyrochlore group (Atencio et al., 2010). It is found in the mesostasis area of the rock and is associated with metallic iron, baddeleyite, apatite, whitlockite and K-Ba feldspar.

Chevkinite-(Ce)

Rare chevkinite-(Ce) has been found in Apollo 11 mare basalt 10047 within angular pockets of late-stage mesostasis containing Si-Al-K glass and minerals rich in K, Ba, U, Th, Zr, REE, Nb, P, and Fe, including barian potassium feldspar, fayalite, pyroxferroite, troilite, metallic iron, apatite, britholite, monazite, zirconolite, tranquillityite and baddeleyite. One small crystal with elevated Fe content could be perrierite-(Ce) (Muhling et al., 2014).

Perovskite (variety Dysanalyte) ?

Apollo 11 ilmenite basalt 10047 contains ilmenite as a main component besides Al-bearing chromian ulvöspinel, a new Ti, Fe, Zr, Y, Ca silicate (later named tranquillityite), troilite, cobalt-rich metallic iron, minor hafnian baddeleyite and dysanalyte (Ramdohr and El Goresy, 1970).

Cadogan (1981) also reports perovskite (which although having the basic chemical formula CaTiO_3 may also incorporate zirconium). The author does not describe the rock type or occurrence.

Further confirmation of this species is desirable.



Reflected light images of armalcolite rimmed by ilmenite.

Apollo 17 ilmenite basalts: 71525 centre (width 1.3 mm), 71066 left (width 0.9 mm) and right (width 1.0 mm).

Credit: NASA (AGT Photographer).

Textural variation in armalcolite from Apollo 17 lunar soil 74242 (30).

a, ortho-armalcolite (A) mantled by ilmenite (I);

b, ortho-armalcolite (A) mantled by ilmenite (I), with subhedral grain of chromian ulvöspinel (S);

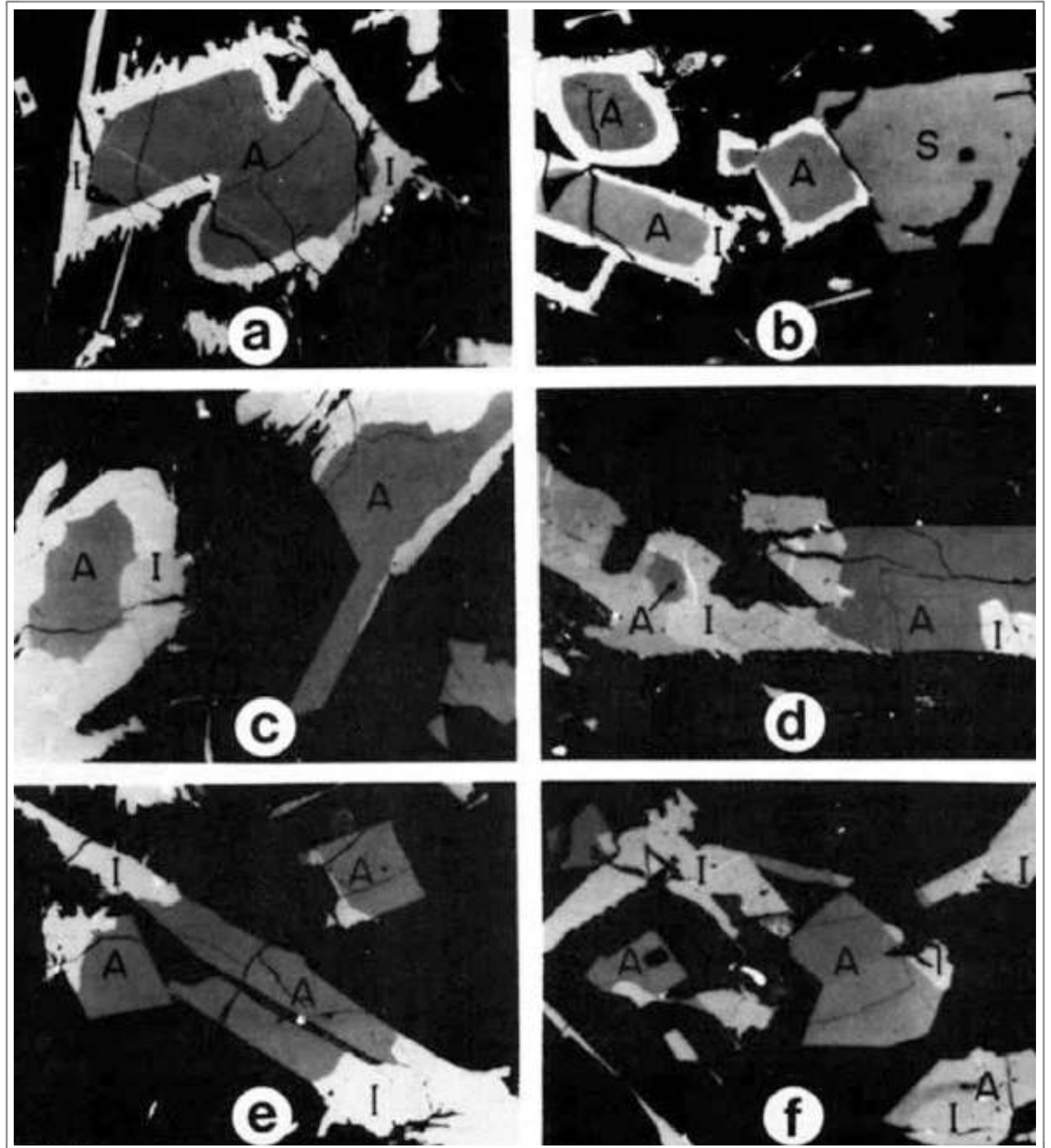
c, ortho-armalcolite (left) and para-armalcolite (right) with ilmenite;

d, small grain of ortho-armalcolite mantled by ilmenite, with larger area of para-armalcolite morphologically continuous with ilmenite;

e, para-armalcolite, morphologically continuous with ilmenite;

f, euhedral crystals of para-armalcolite, showing limited morphologic continuity with ilmenite. All photographs taken with 40X objective, oil immersion.

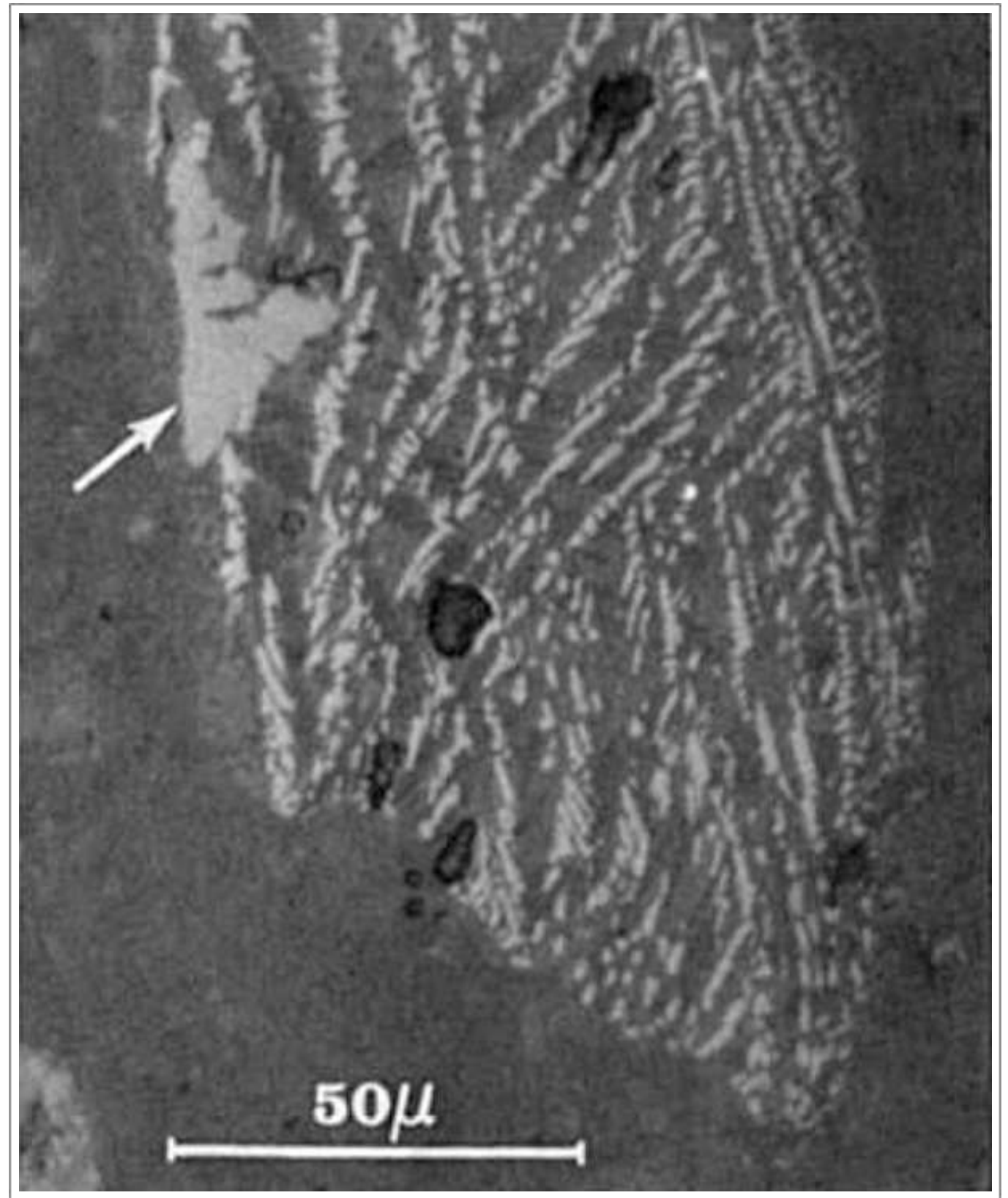
Note: optical and chemical data do not sustain the concept of two distinct varieties of armalcolite.

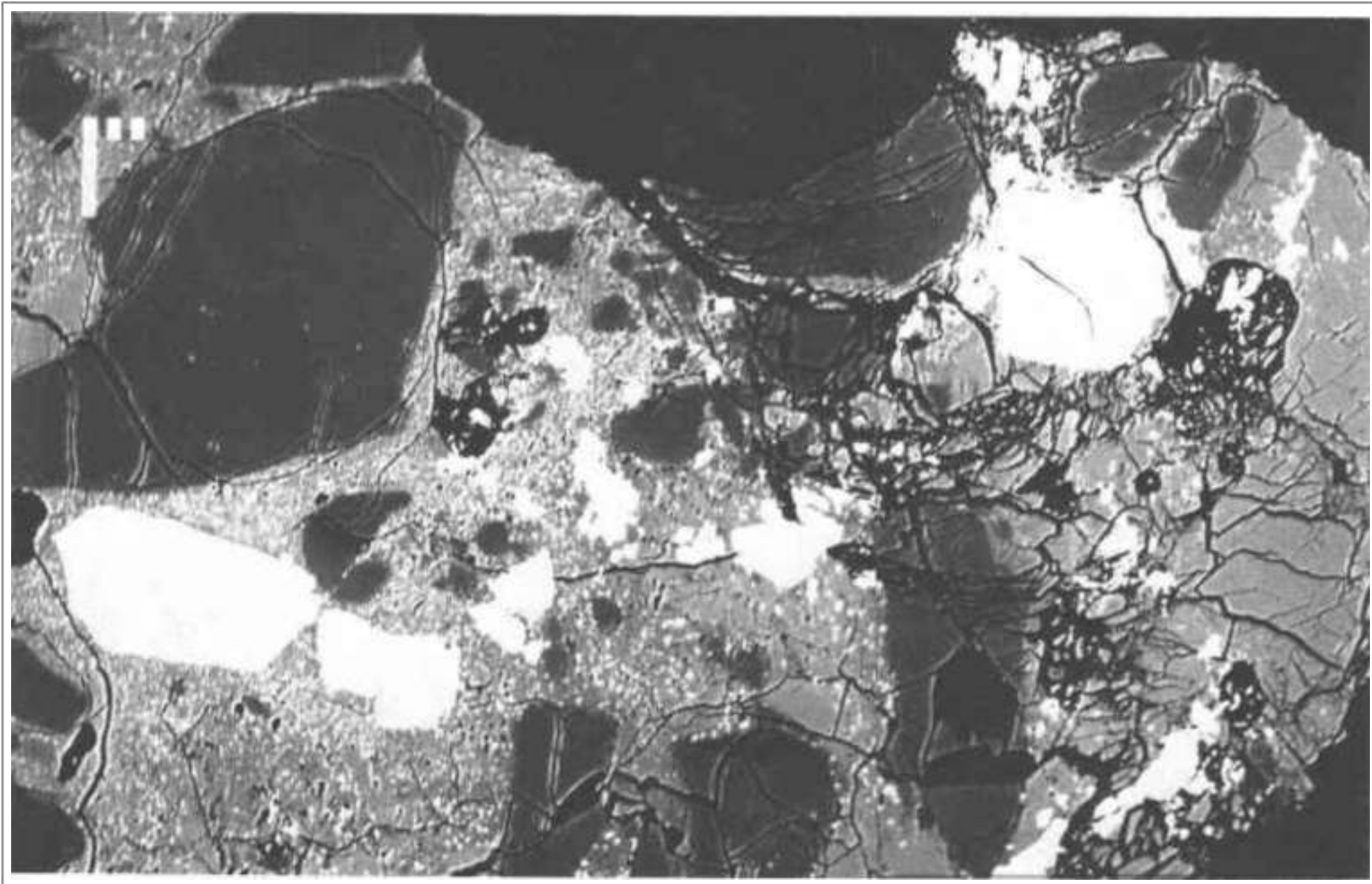


The first lunar meteorite ever discovered (ALHA81005) was found on January 18th, 1982 in the Allan Hills region of Victoria Land, Antarctica and is a polymict anorthositic breccia.

This reflected light image shows wavy rows of armalcolite crystallites associated with a larger grain of ulvöspinel (see arrow) within glass.

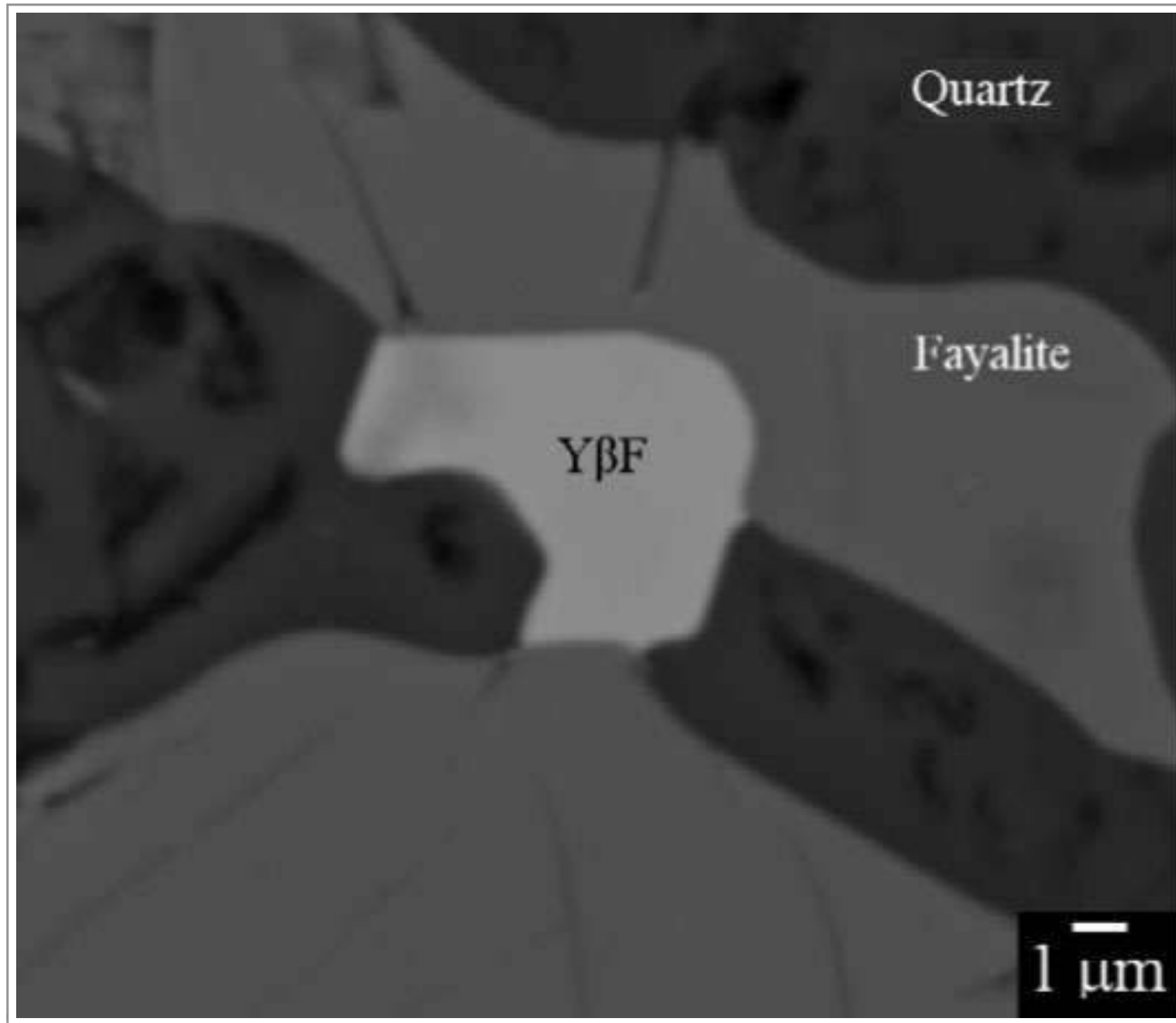
Lunar meteorite ALHA81005,22.





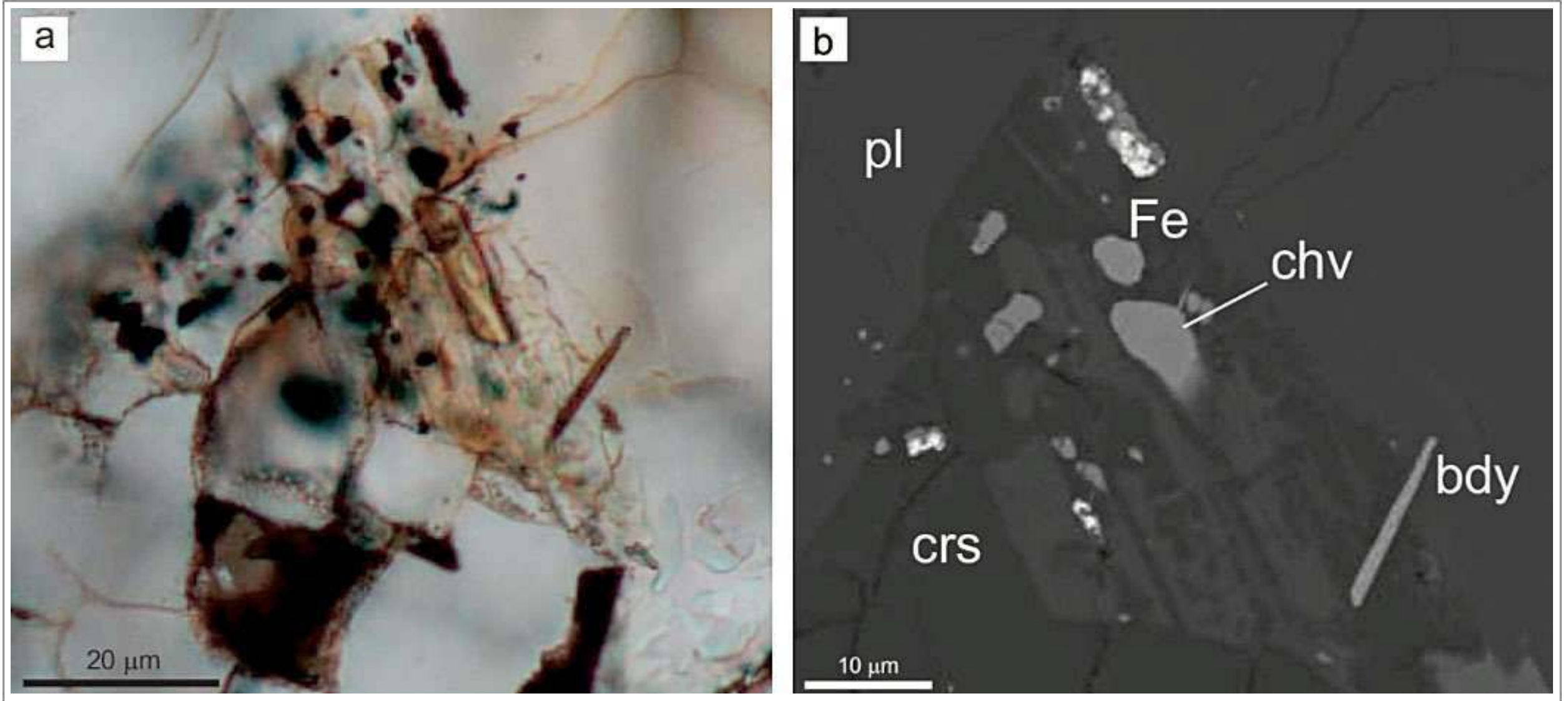
Taken From Meyer and Yang (1988)

Backscattered electron image of lunar granophyre in Apollo 14 sample 14321,1494. All the bright grains are yttrobetafite. The Ba-rich potassium feldspar is light grey, silica is dark, epoxy is black, and recrystallized glass is speckled. The large equant grain of yttrobetafite has vague hexagonal outline and is included in potassium feldspar. The scale bar is 100 μm .



Taken From Seddio et al. (2014)

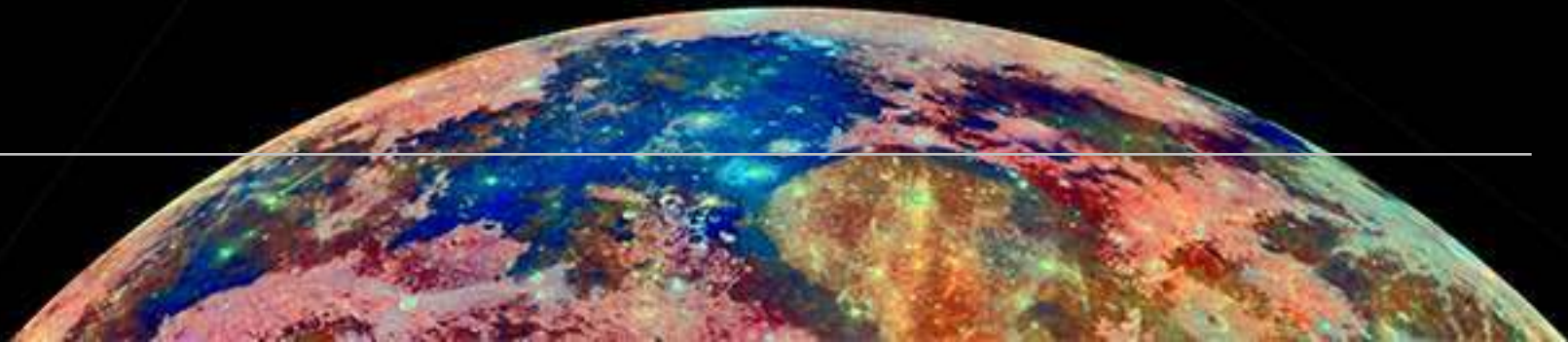
Backscattered electron image of yttrrobetafite ($Y\beta F$) in a granitic fragment from Apollo 12 regolith sample 12023.



Taken From Muhling et al. (2014)

Chevkinite-(Ce) in Apollo 11 ilmenite basalt 10047,227. (a) transmitted light (PPL) image. (b) backscattered electron image of the same grain showing a pocket of mesostasis between plagioclase (pl) and cristobalite (crs), with chevkinite (chv), baddeleyite (bdy), and metallic iron (Fe).

Zirconium Minerals



SPECIES

1. **Tranquillityite** - $\text{Fe}_8(\text{Zr,Y})_2\text{Ti}_3\text{Si}_3\text{O}_{24}$
2. **Baddeleyite** - ZrO_2
3. **Zircon** - ZrSiO_4
4. **Zirconolite** - $\text{CaZrTi}_2\text{O}_7$
5. **Zirkelite** - $(\text{Ti,Zr,Ca})\text{O}_{2-x}$ (where $x \sim 0.3$)

Zirconium mineral assemblages

Apollo 11 mare basalt 10047 contains numerous crystals of Zr-rich minerals (zirconolite, tranquillityite and baddeleyite), which are concentrated in pockets of late-stage mesostasis that comprises an intergrowth of silica, barian K-feldspar and Si-Al-K glass. The zirconolite and most of the baddeleyite are unaltered, however, tranquillityite is commonly replaced by a complex intergrowth of zirconolite, baddeleyite, ilmenite and fayalite, suggesting that the mineral became unstable and underwent isochemical alteration during cooling (Rasmussen et al., 2008).

Tranquillityite

Tranquillityite has been observed in crystalline basaltic rocks from Apollo 11 (10017, 10044, 10047, 10058) and Apollo 12 (12018, 12021, 12039, 12051) sites and from a lithic fragment in an Apollo 11 breccia (10073). It characteristically occurs as thin laths and sheaves of laths with overall dimensions usually much less than $100 \mu\text{m}$ (Lovering et al., 1971).

In sample 10047, tranquillityite typically occurs as laths ($<100 \mu\text{m}$ in length) or as intergrown clusters of crystals. It is commonly associated with zirconolite and

baddeleyite in late-stage mesostasis or adjacent to vermiform intergrowths in the margins of pyroxene. In transmitted light, it is dark foxy-red in colour and in reflected light is grey and less reflective than either zirconolite or baddeleyite. The conditions under which tranquillityite is stable are uncertain, however, in sample 10047 it must have been stable, or at least metastable during late-stage basalt crystallization, but became unstable, possibly during cooling, undergoing in-situ decomposition to zirconolite, baddeleyite, ilmenite and fayalite (Rasmussen et al., 2008).

Tranquillityite is also described from Apollo 17 ilmenite basalt 75035,76 where it occurs as thin laths or aggregates of lath-shaped crystals often associated with baddeleyite (Meyer and Boctor, 1974). Other reports include Apollo 12 basalt 12038,67 (Simpson and Bowie, 1971), Apollo 14 basalt 14276,13 (Gancarz et al., 1972), and Apollo 14 basalt 14310,101 (El Goresy et al., 1974).

Pb/Pb dating using a nanoSIMS 50 instrument has been carried out on tranquillityite in ilmenite basalts from Apollo 11 (sample 10044) and Apollo 17 (samples 75055 and 74255). The data indicate they were emplaced on the lunar surface at 3713 ± 8 Ma, 3769 ± 8 Ma and 3736 ± 10 Ma, respectively. These ages are consistent with crystallization ages determined previously using different chronometers, but provide tighter constraints on the

timing of eruption of three different types of high-Ti mare basalts (Tartèse et al., 2013a,b).

Tranquillityite is no longer an exclusively lunar species as it has since been found in dolerite dykes and sills in Western Australia (Rasmussen et al., 2012).

Baddeleyite

Baddeleyite has been found in Apollo 11 basalt 10047 where it typically occurs as tabular and bladed crystals <50 μ m long. It occurs as isolated crystals in pyroxene and ilmenite, but is more commonly associated with zirconolite and tranquillityite in late-stage mesostasis and vermiform margins on pyroxene crystals. It is commonly pale yellow-green in colour and more reflective than either tranquillityite or zirconolite (Rasmussen et al., 2008).

Baddeleyite is common in certain Apollo 14 clast-poor impact-melt rocks (e.g., 14310, 14073) where it is associated with schreibersite (El Goresy et al., 1971). Although these two minerals were originally thought to be indigenous to the Moon, it is now thought probable that the high Zr and P contents of these baddeleyite- and schreibersite-bearing rocks arise from meteoritic contamination that was incorporated into the original melts, which were produced by large meteoroid impact events (Heiken et al., 1991).

Impact-melt breccia 14310, in addition to having a somewhat KREEPY composition, contains one of the highest amounts of ZrO₂ (0.13%) in the Apollo 14 samples. This ZrO₂ content is contributed mainly by baddeleyite which occurs with ilmenite, troilite, and ulvöspinel, and the amount of this mineral is far greater than from Apollo 11 or 12 rocks (El Goresy and Ramdohr, 1972).

Baddeleyite is found only in association with fayalite in a granitic clast found in Apollo 12 sample 12032,366-19. Zirkelite, ilmenite, apatite and merrillite are the other accessory species present (Seddio et al., 2009).

Rare baddeleyite also occurs in Apollo 14 breccia sample 14063 (Christophe-Michel-Levy and Levy, 1972).

SIMS Pb/Pb dating of baddeleyite and zirconolite in Apollo 17 shocked norite 78235 confirm two significantly different ages at 4318 ±9 Ma and 4252 ±15 Ma, respectively. The older age is interpreted as the initial crystallization age, whereas the younger age reflects a significant impact event, consistent with the shock features observed in this rock (Zhang et al., 2012b).

In-situ U-Pb dating of baddeleyite was conducted by Shaulis et al. (2012) on gabbroic lunar meteorite NWA 6950 to give a ²⁰⁷Pb-²⁰⁶Pb age of 3100±16 Ma and ²⁰⁶Pb/²³⁸U age of 3110±22 Ma. These are interpreted as primary crystallization ages and link

the meteorite to other meteorites with olivine gabbro cumulate lithologies (NWA 733, NWA 2977 and NWA 3333).

Grange et al. (2009 and 2013) show that in Apollo 17 impact-melt breccia 73217,52 baddeleyite has reacted with surrounding silica-rich melt to create a corona of new granular zircon. The formation of zircon by reaction of baddeleyite with melt is summarised by: ZrO₂ (baddeleyite) + SiO₂ (silica) = ZrSiO₄ (zircon).

Sparse granophyric clasts in lunar meteorites NWA 4472 and NWA 4485 consist of “ribbon-like” subparallel intergrowths of silica and barian K-feldspar with accessory baddeleyite and rare tranquillityite (Kuehner et al., 2007).

In lunar meteorite Miller Range (MIL) 13317 - an anorthositic breccia, baddeleyite is found in four distinct petrologic contexts: (i) associated with symplectite regions, (ii) within pyroxene grains, (iii) isolated within the breccia matrix, and (iv) within a melt-vein (Shaulis et al., 2016).

Zhang et al. (2010) studied baddeleyite in an unbrecciated lunar basalt meteorite - LaPaz Icefield 02224. Two crystals were examined - one showed a large variation of Pb/Pb ages (3109±29 to 3547±21 Ma), whereas the second gave an age of 3005±17 Ma. The authors suggest the younger ages could reflect late thermal disturbance of the U-Pb system.

Zircon

Lunar zircons can be classified according to: (i) textural relationships between zircon and surrounding minerals in the host breccias, (ii) the internal microstructures of the zircon grains as identified by optical microscopy, cathodoluminescence (CL) imaging and electron backscattered diffraction (EBSD) mapping and (iii) results of in situ ion microprobe analyses of the Th–U–Pb isotopic systems. Primary zircon can occur as part of a cogenetic mineral assemblage (lithic clast) or as an individual mineral clast and is unzoned, or has sector and/or oscillatory zoning. The age of primary zircon is obtained when multiple ion microprobe analyses across the polished surface of the grain give reproducible and essentially concordant data. A secondary set of microstructures, superimposed on primary zircon, include localised recrystallized domains, localised amorphous domains, crystal–plastic deformation, planar deformation features and fractures, and are associated with impact processes. These secondary features can provide channels for Pb diffusion and result in partial resetting of the U–Pb isotopic systems (Grange et al., 2013).

Pomegranate is the name given by Smith et al. (1986) to an unusual cluster of zircon crystals in Apollo 17 cataclastic impact breccia 73235 (so called because the transmitted light image of the zircon assemblage resembles a cluster of pomegranate seeds). In thin section 82 a relatively large (500 μm) zircon

crystallized within a clast of Ca-rich plagioclase. It has been dated at 4.31 Ga. The zircon was fractured into numerous smaller crystals and was subsequently overgrown by a second generation of zircon at approximately 4.183 Ga. Both zircon and plagioclase were later emplaced within a melt sheet (breccia) around 4.0 Ga.

Pidgeon et al. (2007) used cathodoluminescence techniques to further examine the pomegranite cluster. They suggest the original zircon was subjected to a severe shock event at 4.18 b.y. which resulted in the fracturing of the zircon, the displacement and rotation of fragments, the compression of the aggregate to a lensoid shape, and the shock reduction of zircon to sub-micron-sized and amorphous granules in crush zones in the mosaic of fractures.

Granitic clasts in Apollo 12 mare breccia 12013 contain zircon grains that have been studied by ion-microprobe dating techniques. Most of the grains are angular fragments and range in size from 10 to 35 μm . Mineral phases around zircon usually contain radiating fractures from the boundaries between zircon and surrounding minerals. These fractures may be due to swelling caused by radioactive damage of the zircon.

The study revealed large age variations of zircon in 12013, among different grains and within individual grains, that were caused by post-crystallization impact events. Most ages are not original crystallization ages (Zhang et al., 2012a).

Zircons in breccia samples from the Apollo 14 and 17 landing sites were studied by Nemchin et al. (2008). They reported zircon crystals with rounded, irregular shaped, broken and rarely euhedral grains and as constituent minerals in a variety of lithic clasts ranging in composition from ultramafic and mafic rocks to highly evolved granophyres.

Apollo 17 aphanitic impact-melt breccia 73235 was the focus of a zircon study by Grange et al. (2011). They concluded that most zircon formed during multiple magmatic events between 4.37 and 4.31 Ga. In addition, zircons from the aphanitic breccias record several impact events prior to the ~3.9 Ga Late Heavy Bombardment.

Crow et al. (2017) present the results of a coordinated SIMS U-Pb, trace element, Ti-in-zircon thermometry, and microstructural study of 155 zircons separated from Apollo 14, 15, and 17 breccia and soil samples that help resolve discrepancies between the zircon data, the lunar whole rock history and lunar magma ocean crystallization models. The majority of lunar grains are detrital fragments that suggest crystallization in highly enriched KREEP magmas. The zircon age distributions for all three landing sites exhibit an abundance of ages at ~4.33 Ga. In sample 15455, two granular clusters of zircon with baddeleyite cores suggest at least one large impact is contemporaneous with the most common time of magmatic zircon formation on the Moon's crust.

Apollo 14 polymict breccia 14321 contains fragments of micronorite in which zircon typically occurs as poikiloblastic intergrowths with plagioclase feldspar (Greive et al., 1975). Zircon with a similar texture is also reported by Zhang et al. (2018) in Apollo 17 impact-melt breccia 73155,69 and U/Pb data from them is used as evidence to suggest that the Serenitatis basin was contaminated by Imbrium ejecta at ~3.9 Ga.

Apollo 16 impact-melt rock 67955,48 contains zircon with a blocky to subhedral shape. Some of the zircons show zoning in backscattered electron and cathodoluminescence images. Zones are either concentric, irregular or show different domains. A few zircons display inclusions (Vanderliek and Becker, 2017).

Polycrystalline zircon has been found in lunar meteorite Dhofar 458. The zircon contains small vesicles and rounded baddeleyite grains at its margin. The polycrystalline and porous texture of the zircon indicates high-pressure shock-induced melting and degassing. These features indicate that the shock pressure was greater than 60 GPa and the post-shock temperature greater than 1700°C (Zhang et al., 2011).

Lunar meteorite impact-melt breccia SaU 169 contains small zircon crystals with irregular shapes ranging from rounded, broadly tabular and indented grains to sieve-textured. Some form a poikilitic, branching, interstitial network, and are unlike any occurrence seen in terrestrial rocks. These are described as

“poikilitic impact-melt zircons” and formed during equilibrium crystallization of the impact-melt (Liu et al., 2012).

Demidova et al. (2014) note that zircon is a typical accessory mineral of KREEP rocks and used it to date KREEP fragments in one of the few KREEP lunar meteorites - Dhofar 1442. They used cathodoluminescence techniques to show compositional zoning in zircon and were able to discriminate between two populations - an old group (4309 ± 13 Ma) and a younger group (3951 ± 35 Ma). They suggest these age peaks could be related to major impact events, that resulted in the formation of Mare Imbrium.

Thiessen et al. (2018) note that impact-induced disturbance of the U-Pb system in zircon in a felsite clast from Apollo 12 breccia 12013 brings into question whether analysis of such grains can actually date any real magmatic or impact events. The implication is that previously published U-Pb data for zircon in highly shocked lithologies may be modified by undetected Pb loss and the ages produced could be ambiguous.

The microstructures of Apollo 17 zircon grains from breccia samples 72215, 73215, 73235 and 76295 have been characterized via optical microscopy, cathodoluminescence imaging, and electron backscatter diffraction mapping. Analysis show they contain planar deformation features (PDFs), nonplanar fractures, recrystallized domains with sharp, irregular interfaces, and localized annealing textures along fractures (Timms et al., 2012). These authors develop a conceptual model (or shock-

deformation mechanism map) to explain the relative timing, conditions, and complexity relationships between impact-related deformation microstructures in zircon.

Zirconolite

Zirconolite has been identified in Apollo 11 basalt 10047 and is commonly associated with other Zr- rich phases, including tranquillityite and baddeleyite. It is the most abundant Zr-rich phase in 10047,11. Zirconolite is a deep red brown colour and appears isotropic or weakly anisotropic between crossed polars. It is less reflective than ilmenite and co-existing baddeleyite and slightly more reflective than tranquillityite. Zirconolite ranges in shape from laths to tubular rods (Rasmussen et al., 2008).

Zirconolite is reported with baddeleyite in Apollo 17 ilmenite basalt 75035,76 where it occurs as very tiny grains. It shows remarkable enrichment in Y and Nb and the REEs (Meyer and Boctor, 1974).

A lunar granite from Apollo 12 (12032,366-19) was thought to contain two Zr-Ti-Fe phases, but Seddio et al. (2011) were able to confirm the presence of only one phase (zirconolite) using backscattered electron tomography. Most of the zirconolite grains are finely elongate (~ 3 μm wide, aspect ratio of ~ 30) although one grain of zirconolite is 100 μm long and 40 μm wide. Zirconolite in this sample was also described by Seddio et al. (2013b).

U–Pb isotopic compositions of zirconolite and apatite in coarse-grained Apollo 16 melt rock breccia 67955 date a basin-scale impact melting event on the Moon at 4.22 ± 0.01 Ga followed by entrainment of the melt rock in lower grade ejecta from a younger basin 300 million years later (Norman and Nemchin, 2014).

Zhang et al. (2010) studied zirconolite and baddeleyite in the unbrecciated lunar basalt meteorite - Miller Range 05035. A zirconolite Pb/Pb age of 3851 ± 8 Ma was obtained which corresponds to the late heavy impact bombardment of the Moon around 3.9 Ga.

Zirkelite

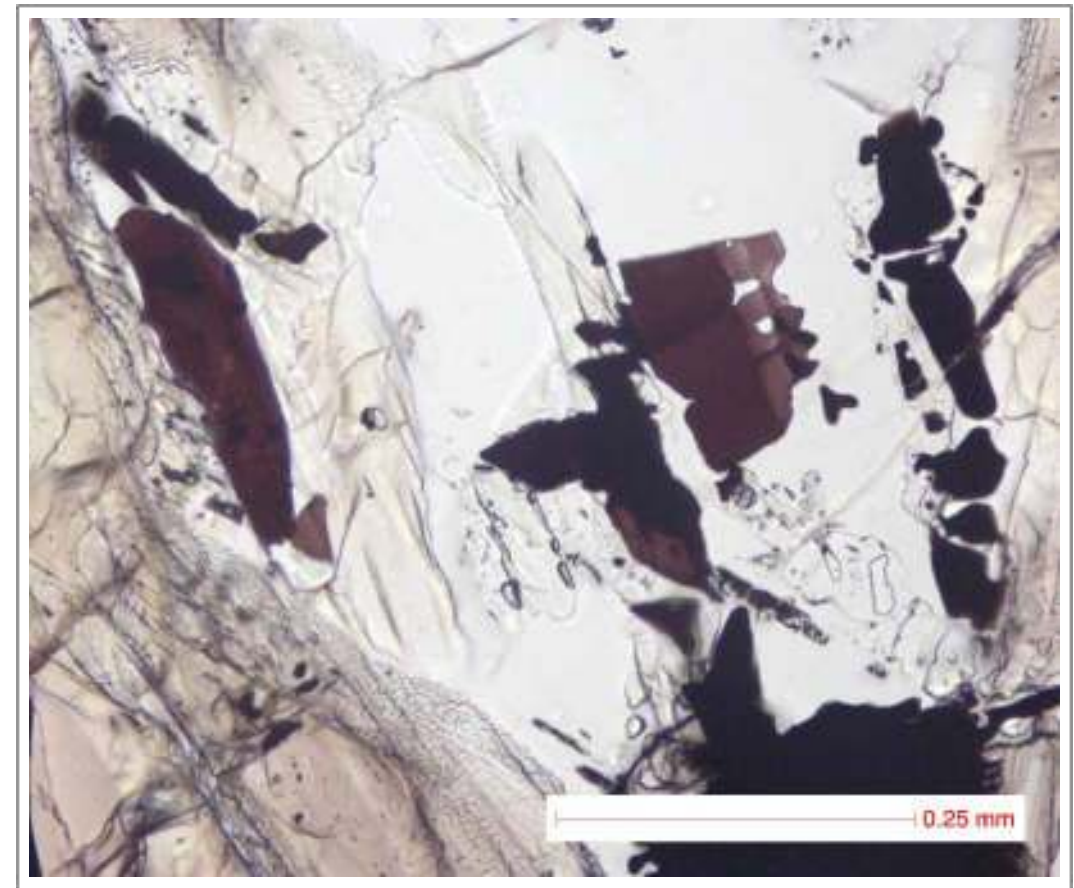
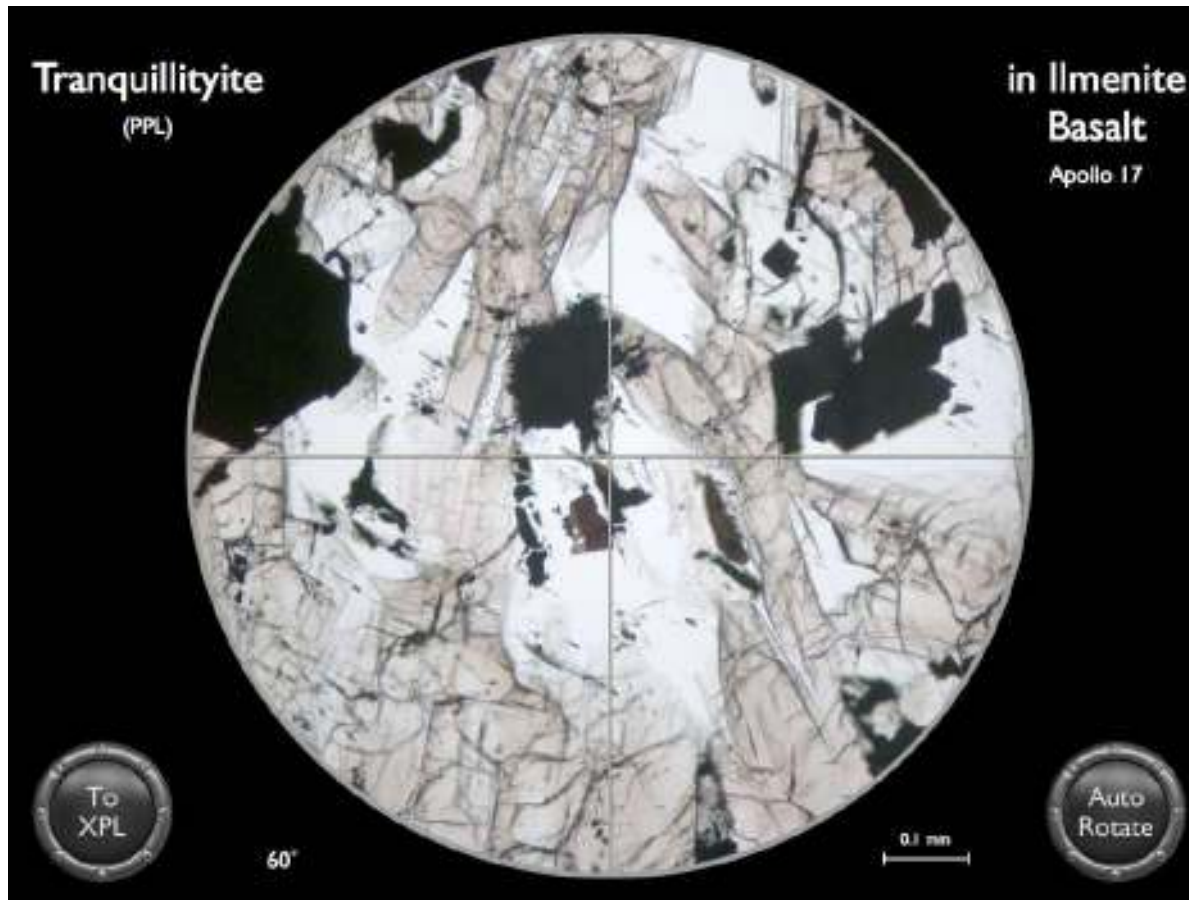
Zirkelite is opaque, or transparent in very thin fragments. Its colour is black or reddish brown to dark brown in transmitted light. It has been reported in Apollo 12 feldspathic peridotite 12036 and Apollo 14: in lithic fragments within 14163 and 14257 (Busch et al., 1972). However, there has been some confusion about its possible occurrence in lunar rocks and Wark et al. (1974) concluded that all previously reported zirkelite could instead be zirconolite. Bayliss et al. (1989) revised the nomenclature of these species and established zirconolite as the orthorhombic, monoclinic, trigonal and metamict variant and reserved zirkelite as the cubic variant.

Zirkelite, baddeleyite and tranquillityite are the three Zr-bearing minerals found in shocked lunar meteorite NWA 4734 (a mare

basalt). Other accessory species are fayalite, ilmenite, chromite, ulvöspinel, anatase, rutile, apatite, merrillite, quartz, coesite, tridymite and K-feldspar (Chen et al., 2018).

Moon Minerals: Titanium-Zirconium Minerals

Mineral Virtual Microscope: Tranquillityite

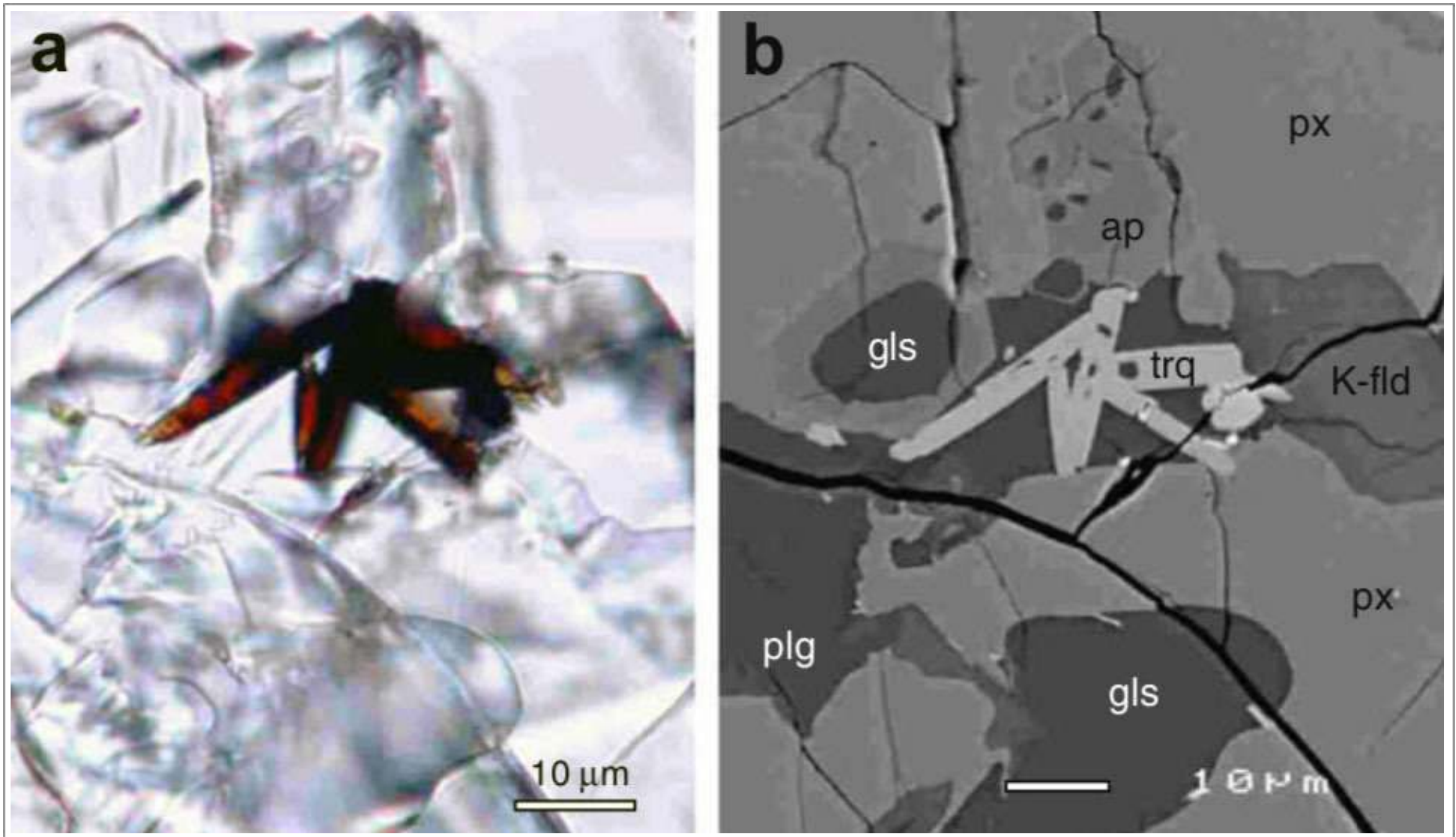


Tranquillityite (near centre) forms dark brown crystals in this medium-grained ilmenite basalt collected from the lunar regolith. Pyroxene and plagioclase feldspar are the major mineral species, although ilmenite is also in high abundance.

Apollo 17, Sample 78135.

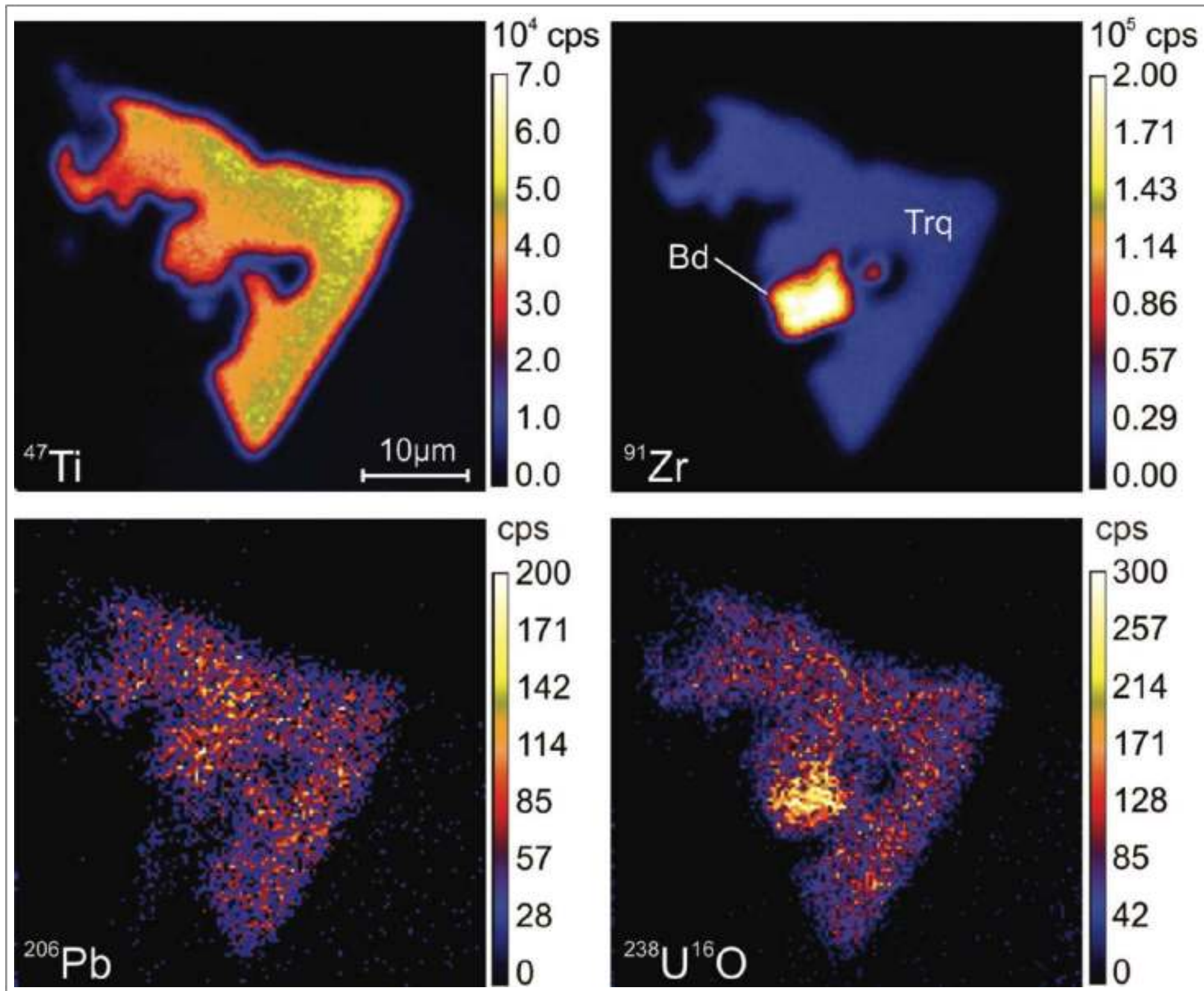
Credit: NASA (AGT Photographer)

Brown crystals of tranquillityite in Apollo 17 ilmenite basalt 78135.
Credit: NASA (AGT Photographer).



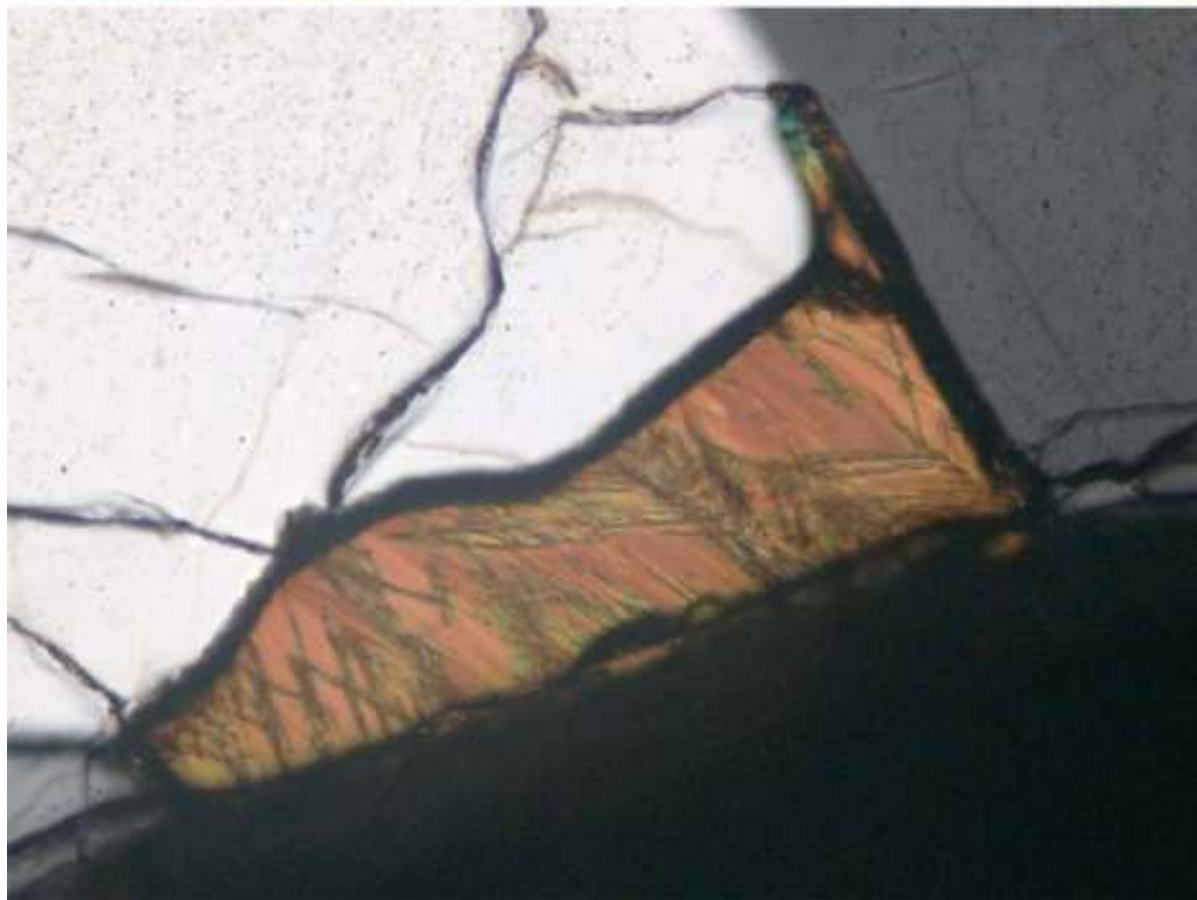
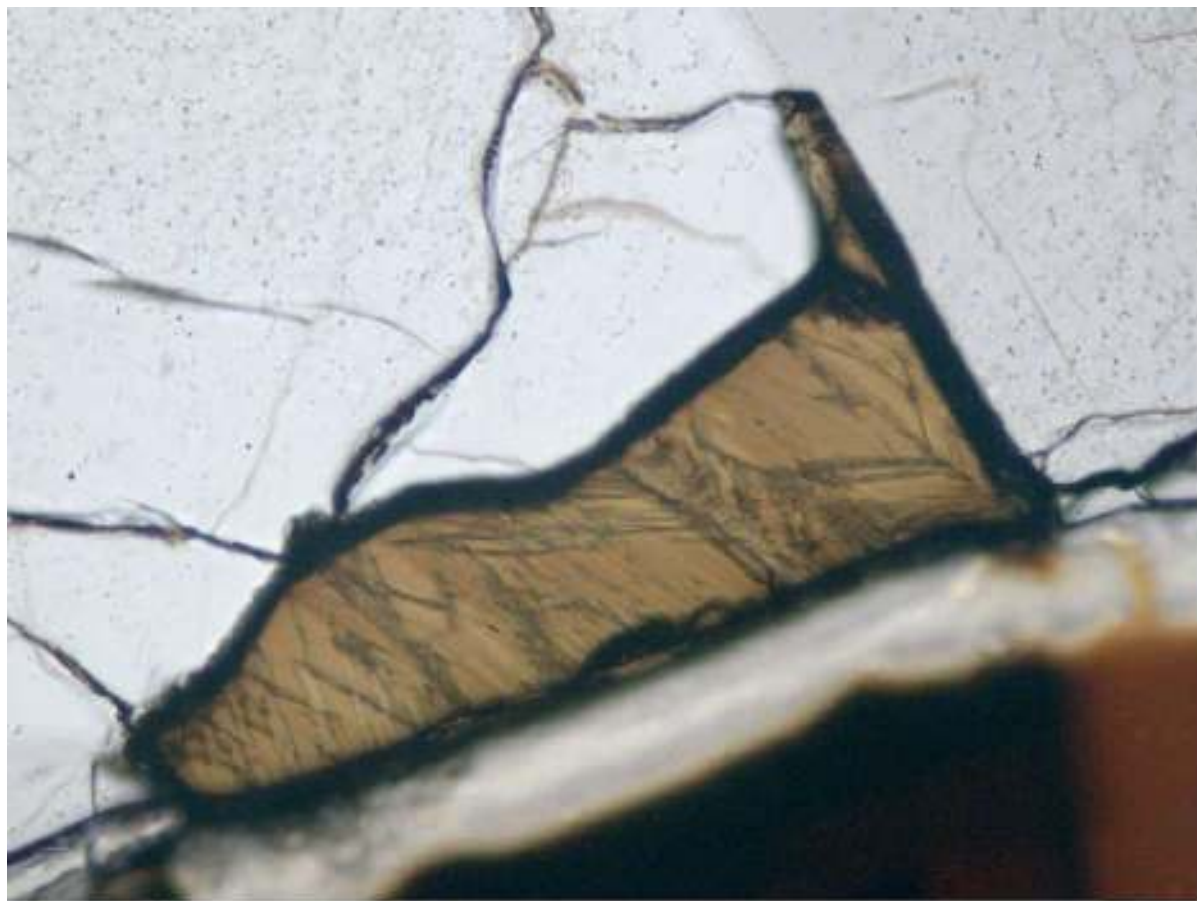
Taken From Rasmussen et al. (2008)

Apollo 11 basalt 10047,227: (a) Transmitted light photograph of foxy-red tranquillityite crystals. (b) Backscattered electron image of tranquillityite (trq) featured in (a). Adjacent minerals are pyroxene (px), apatite (ap), glass (gls), plagioclase (plg) and barian K-feldspar (K-fld).



Taken From Tartèse et al. (2013b)

Secondary ion images of ^{47}Ti , ^{91}Zr , ^{206}Pb , and $^{238}\text{U}^{16}\text{O}$ on an area enclosing tranquillityite and an associated baddeleyite grain in Apollo 11 high-Ti mare basalt 10044. UO intensity is higher and ^{206}Pb intensity is lower in baddeleyite compared to tranquillityite. This is related to the better Pb ionization efficiency in tranquillityite compared to baddeleyite.



Baddeleyite crystal in Apollo 17 troctolite 76535,51.
The crystal is 0.26 mm in length and exhibits complex twinning.

Top left: transmitted light, PPL

Bottom left: transmitted light, XPL

Top right: reflected light

Credit: NASA (AGT Photographer).

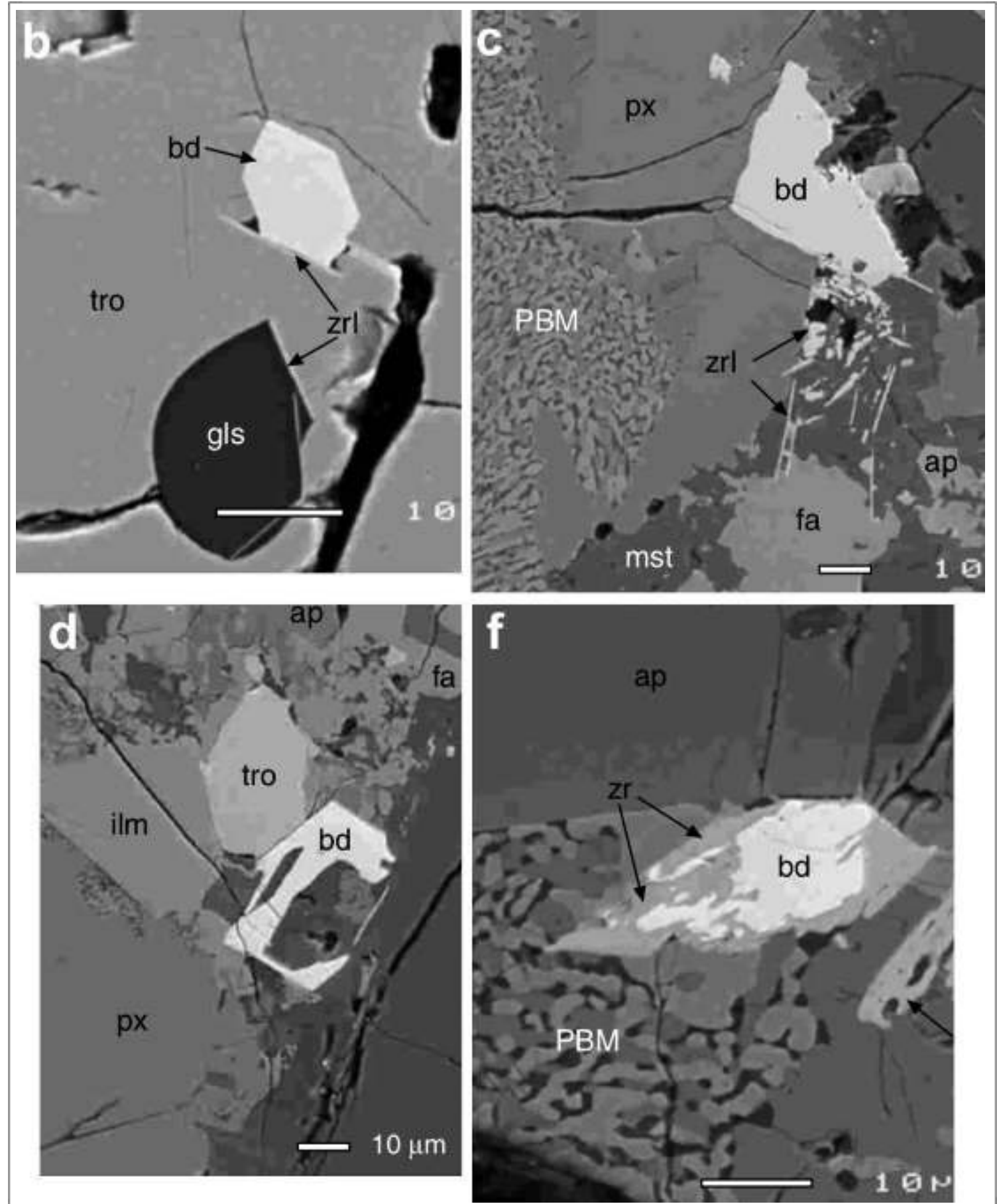
Backscattered electron images of baddeleyite in Apollo 11 ilmenite basalt 10047.

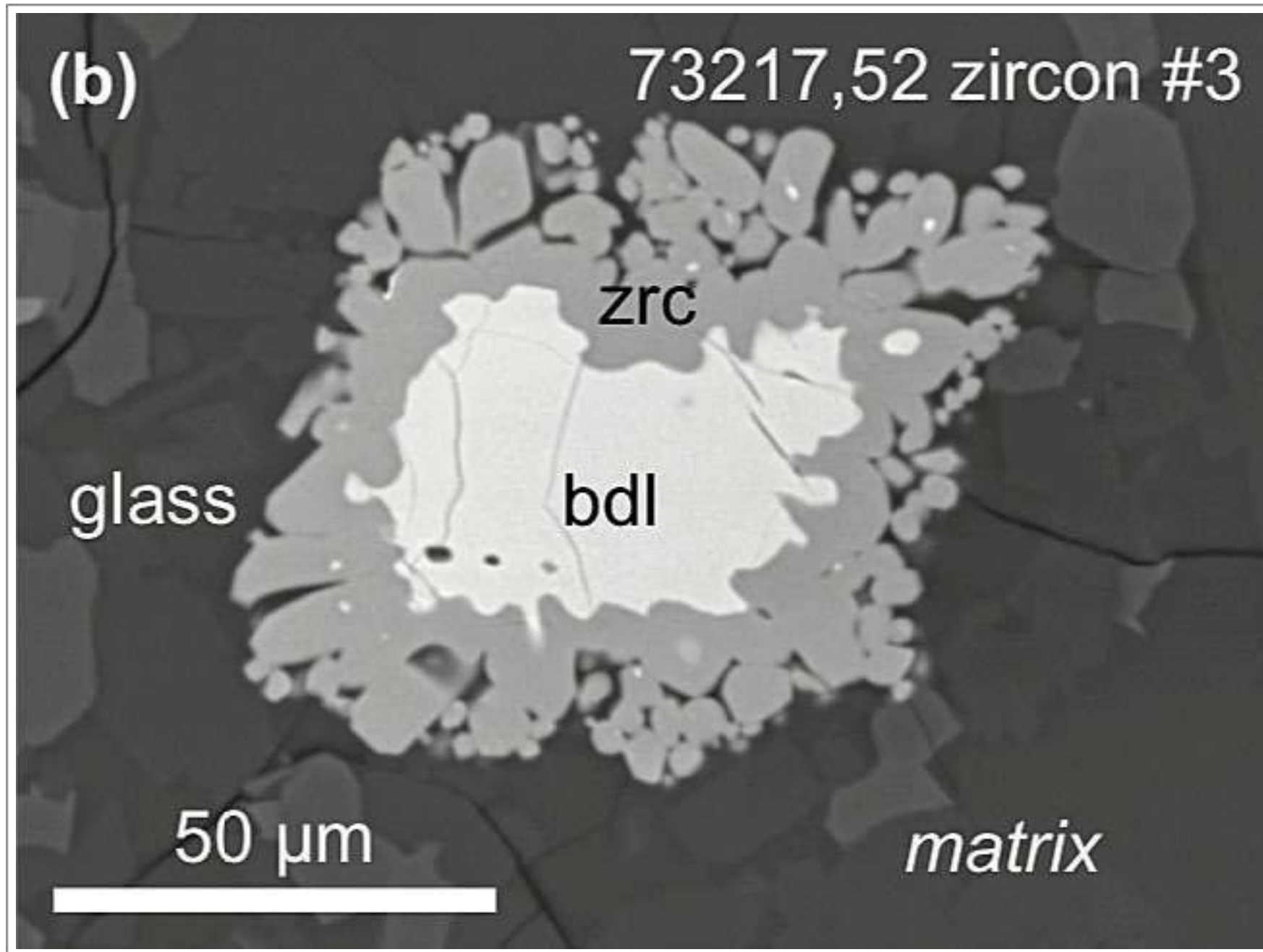
(b) Hexagonal baddeleyite crystal (bd) within troilite crystal (tro). Sample 10047,11.

(c) Coarse baddeleyite (bd) crystal partly embedded in pyroxene with vermiform intergrowth (PBM). Thin laths of zirconolite (zrl) occur immediately below, within mesostasis (mst). Sample 10047,11.

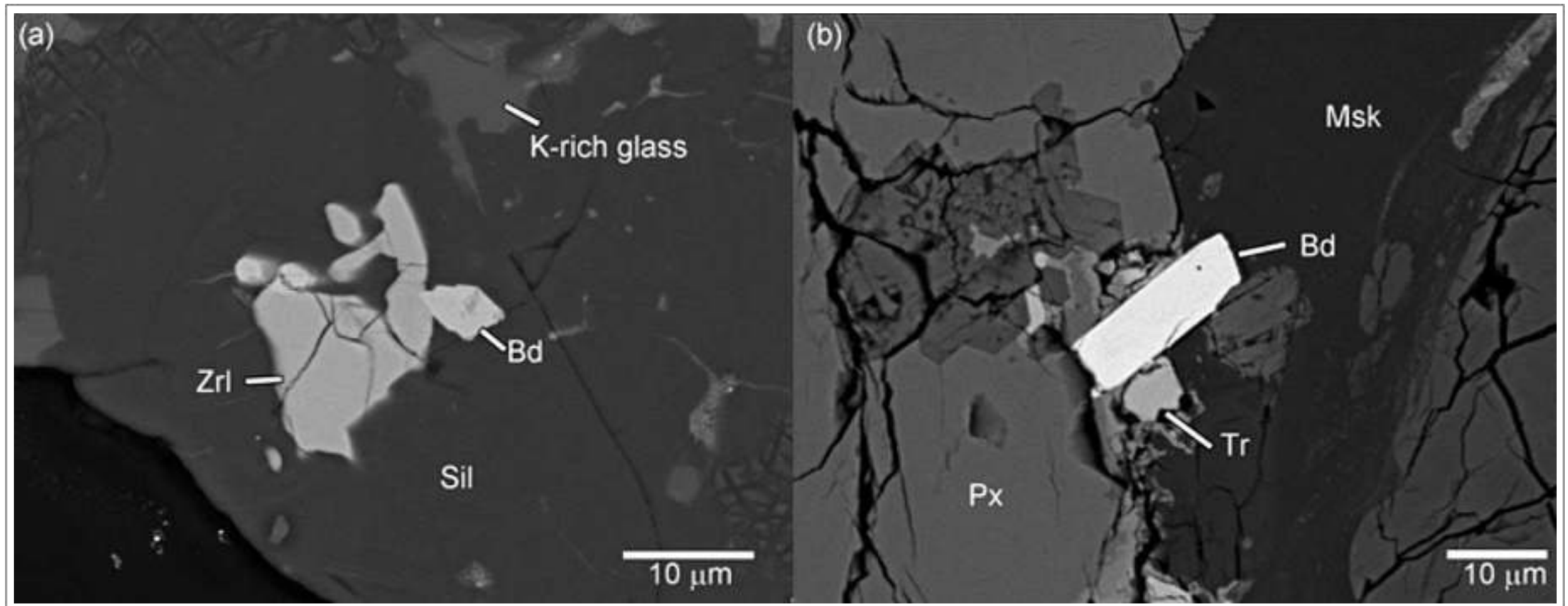
(d) Euhedral outline of baddeleyite crystal (bd) adjacent to troilite (tro), ilmenite (ilm), pyroxene (px) and plagioclase (plg). Sample 10047,227.

(f) Irregular baddeleyite (bd) core surrounded by secondary zircon (zr) in an area containing vermiform intergrowth (PBM) and apatite (ap). Sample 10047,11.





Backscattered electron image of a baddeleyite-zircon aggregate from Apollo 17 impact-melt breccia 73217,52. bdl = baddeleyite, zrc = zircon. It is interpreted to represent a reaction of baddeleyite with surrounding silica-rich melt to create new granular zircon.



Taken From Zhang et al. (2010)

Backscattered electron images of Zr-minerals in unbrecciated lunar basalt meteorites. (a) Zirconolite and baddeleyite are enclosed by a groundmass of silica and K-rich glass in Miller Range 05035. (b) A baddeleyite lath occurs between pyroxene and maskelynite in LaPaz Icefield 02224. Px, pyroxene; Msk, maskelynite; Sil, silica; Tr, troilite; Zrl, zirconolite; Bd, baddeleyite.

Internal structures of magmatic zircon in Apollo breccias.

Oscillatory zoning:

Zircon from Apollo 14 light matrix breccia 14083,35

(a) between crossed polars and (b) cathodoluminescence (CL) images - the insert shows details of the oscillatory zoning; the white arrow shows the sector zoning.

Zircon from Apollo 14 crystalline-matrix breccia 14303,49

(c) between crossed polars and (d) cathodoluminescence (CL) image.

Zircon extracted from Apollo 14 soil

(e) cathodoluminescence image.

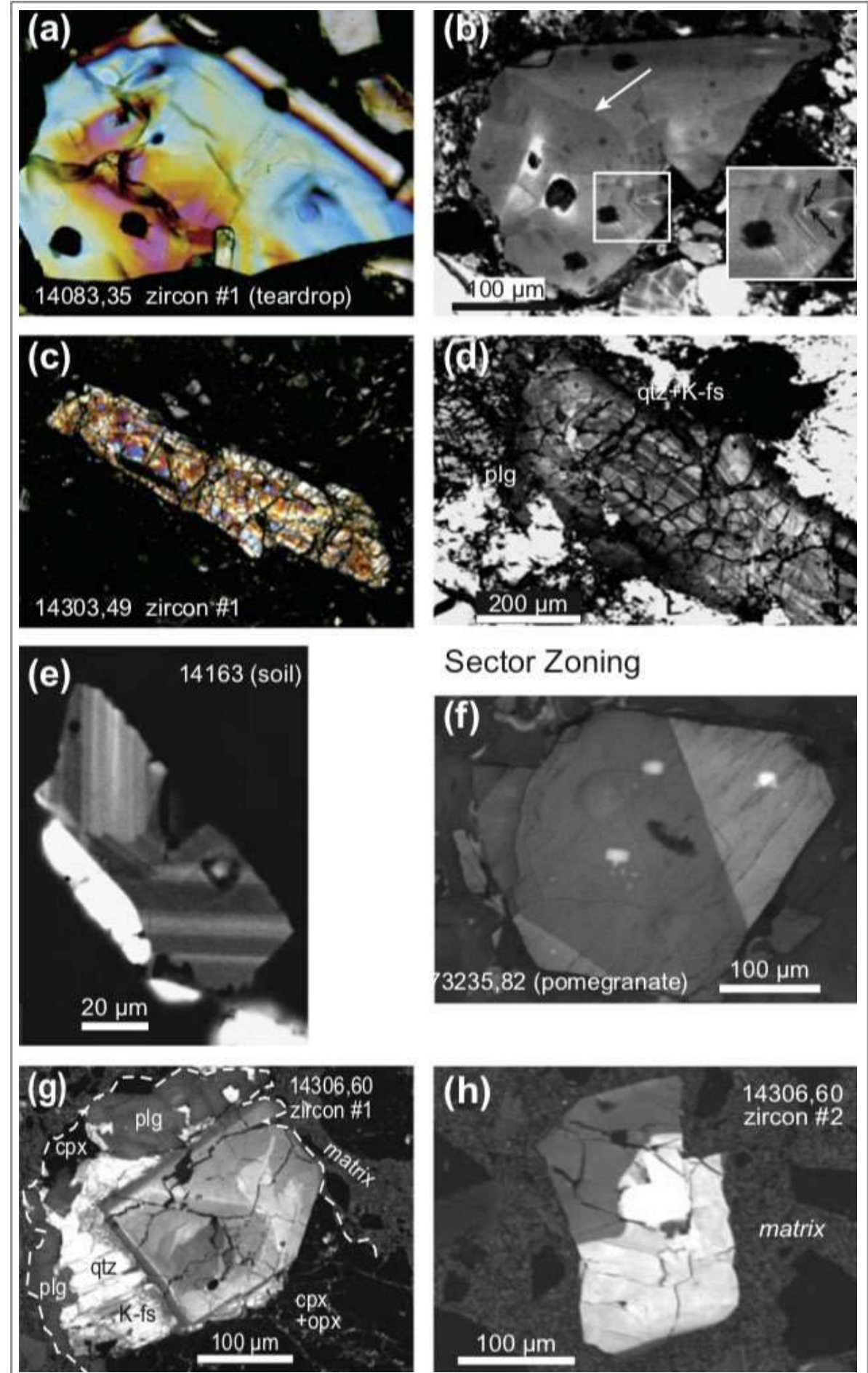
Sector zoning:

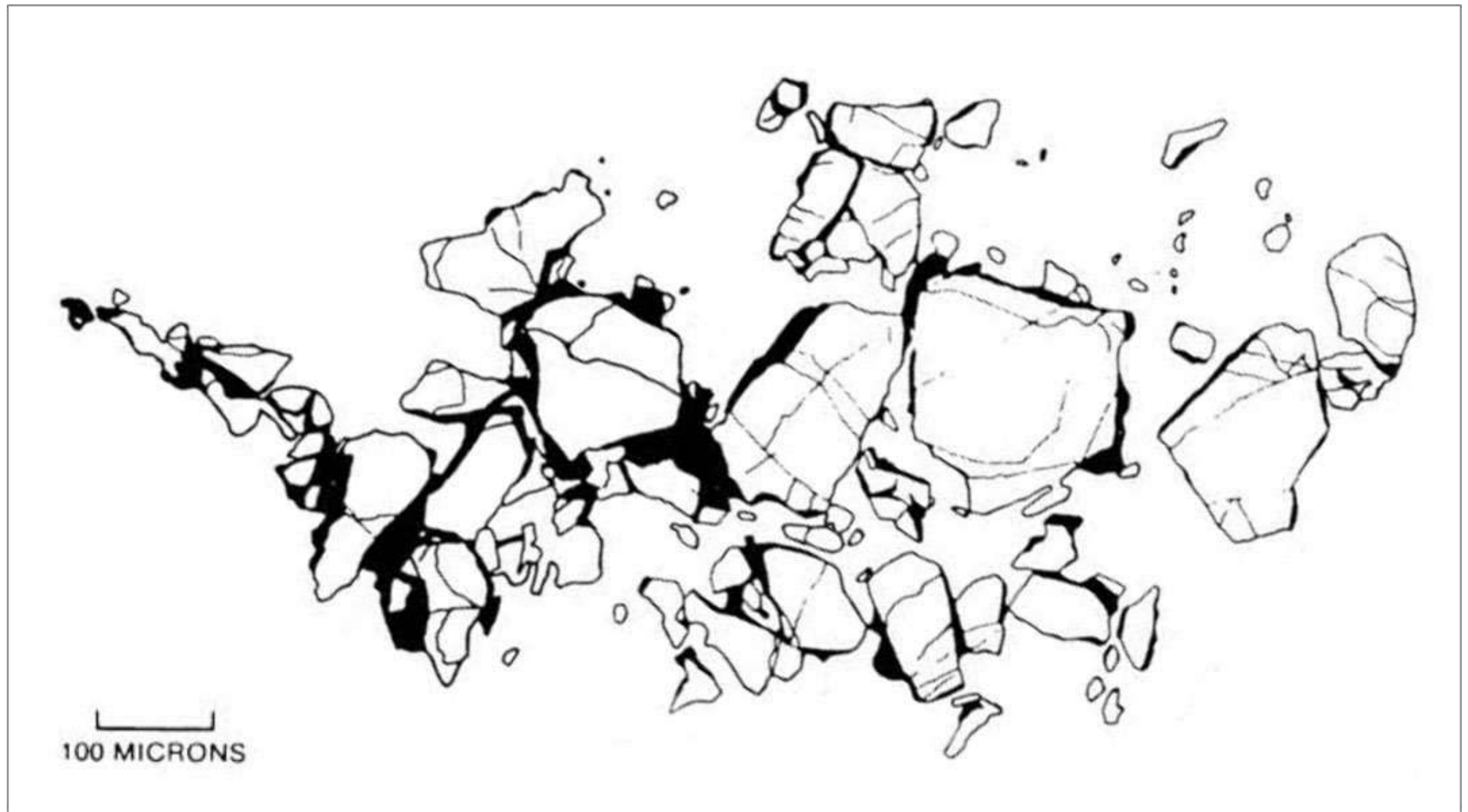
Zircon from Apollo 17 aphanitic impact-melt breccia 73235,82

(f) i cathodoluminescence (CL) image.

Zircon in Apollo 14 clast-rich impact breccia 14306,60

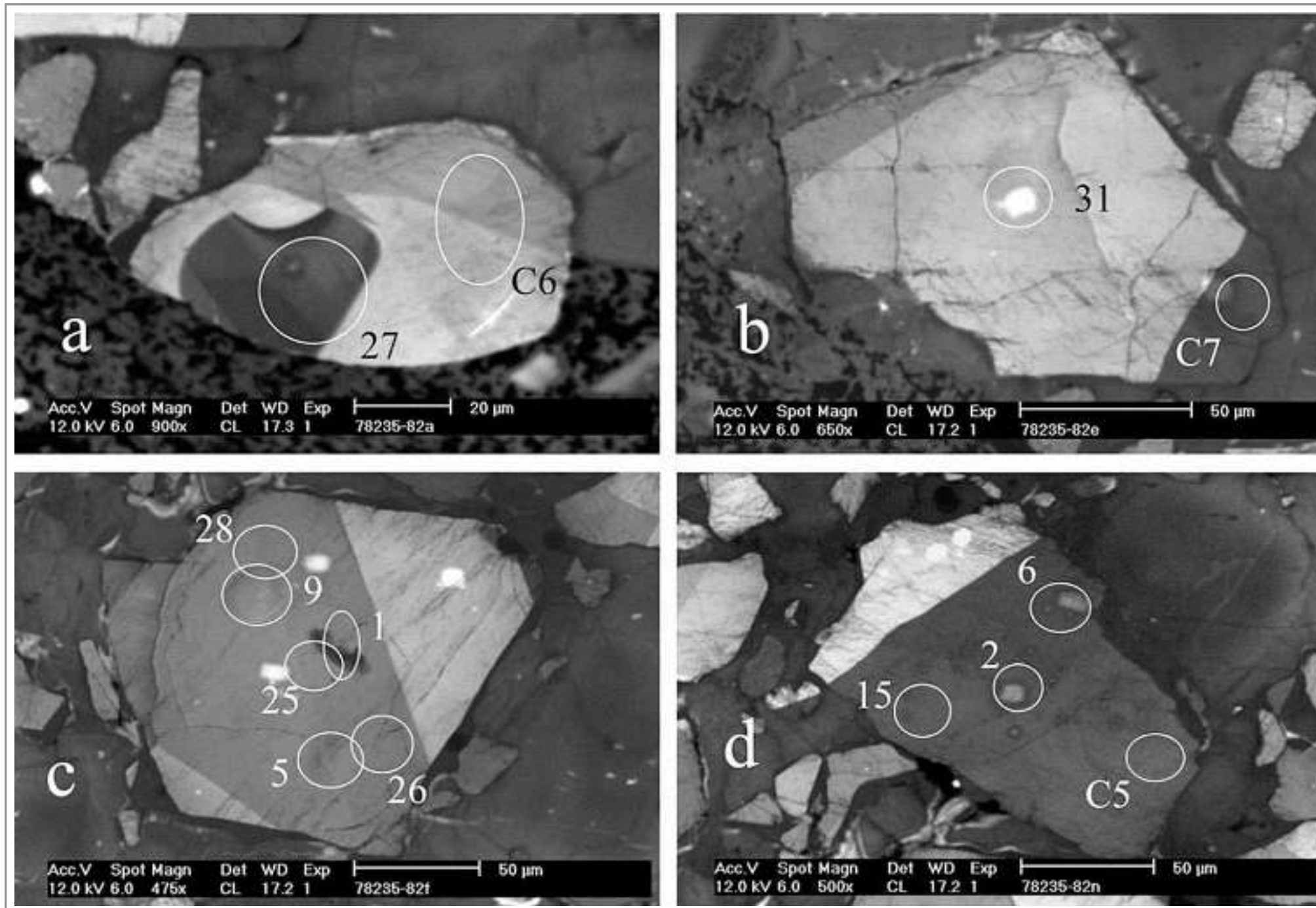
(g & h) cathodoluminescence (CL) image.





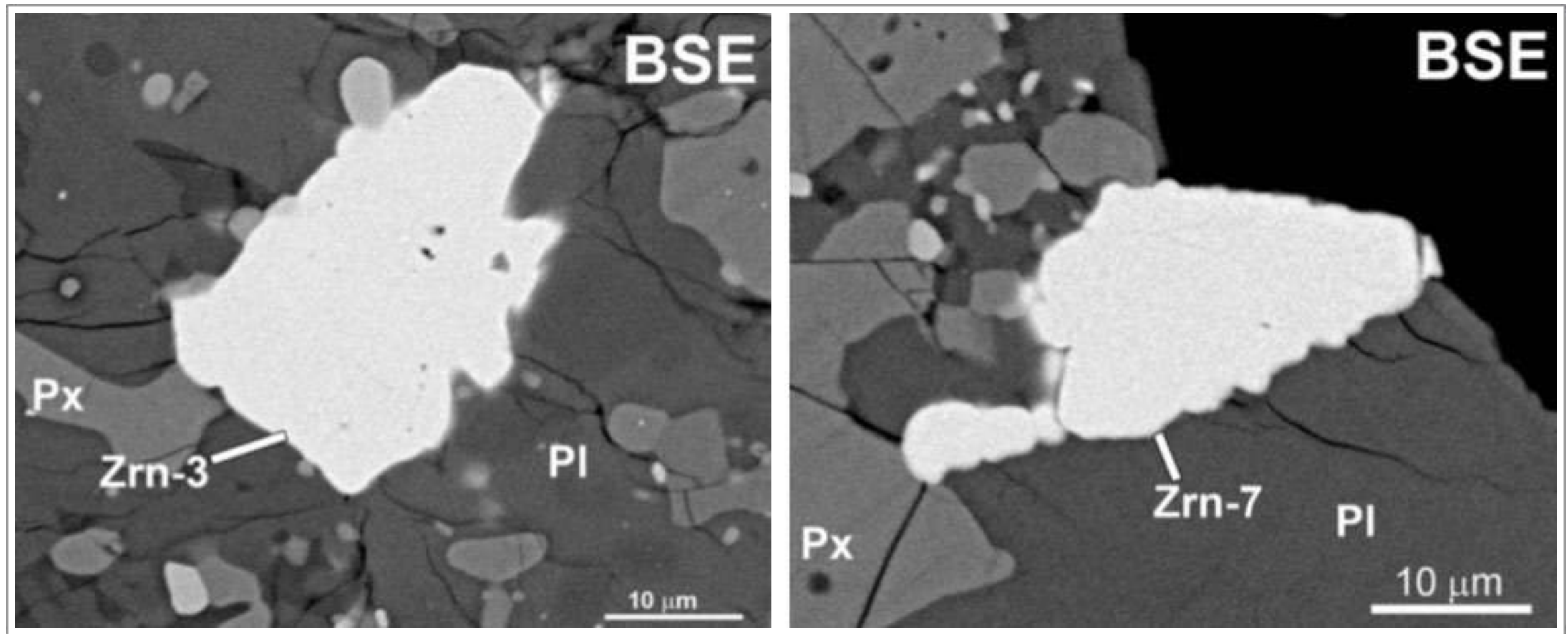
Taken From Smith et al. (1986)

Sketch of the "Pomegranate" cluster of zircon crystals in an anorthosite clast in Apollo 17 impact-melt breccia 73235,82. Second generation of zircon growth is shown in black.



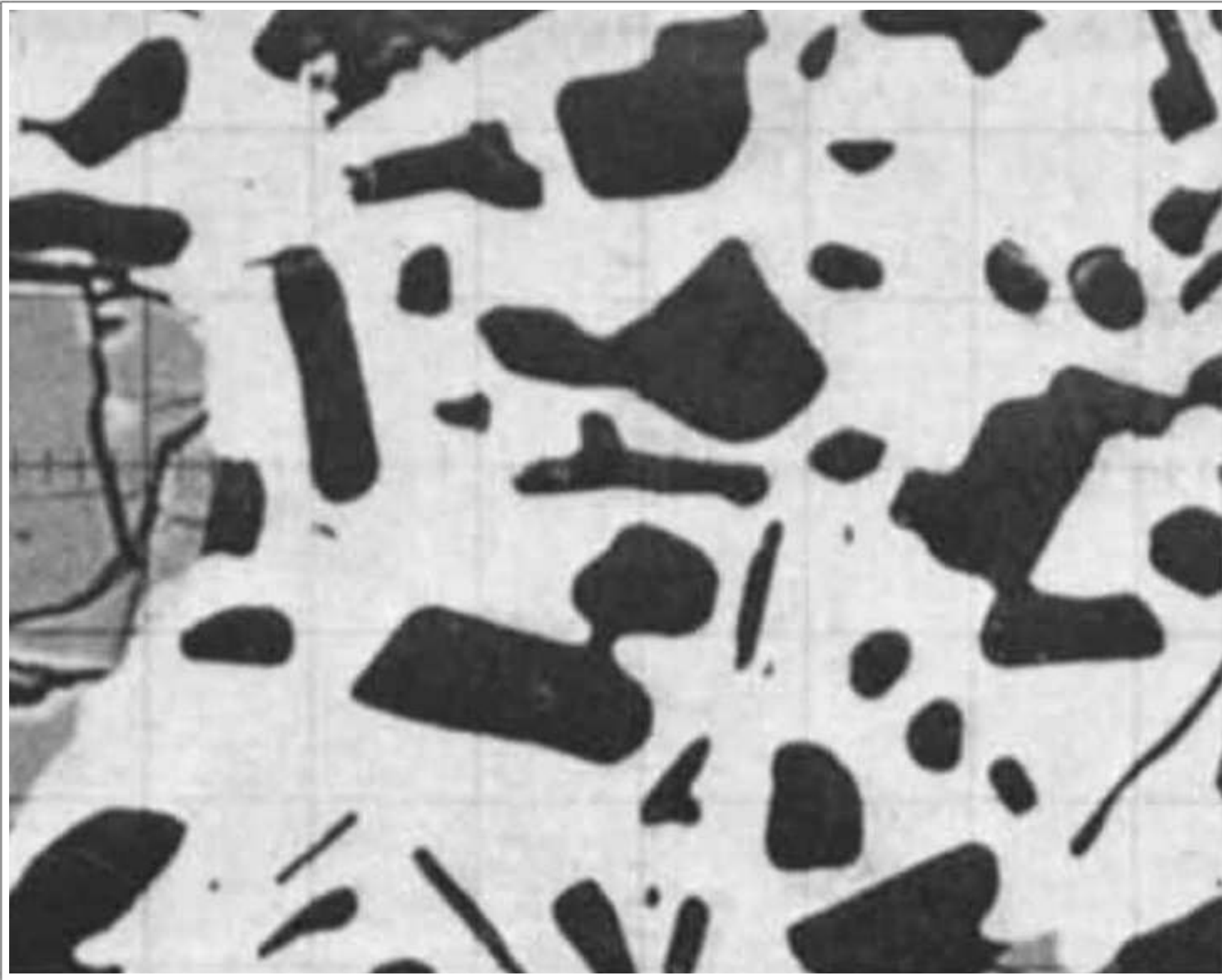
Taken From Pidgeon et al. (2007)

Cathodoluminescence (CL) images showing sector zoning patterns in four of the largest zircon fragments in an anorthosite clast in Apollo 17 impact-melt breccia 73235,82. (a) This fragment is situated on the outside of the anorthositic clast and its rounded surface is attributed to mechanical abrasion during formation of the breccia. It consists of light-grey CL, wedge-shaped sectors and a rounded, dark CL patch. (b–d) These fragments consist of dark-grey CL segments separated by straight-line borders from adjacent segments of lighter CL zircon. Fine sub-parallel hair-line fractures are evident in the fragments.



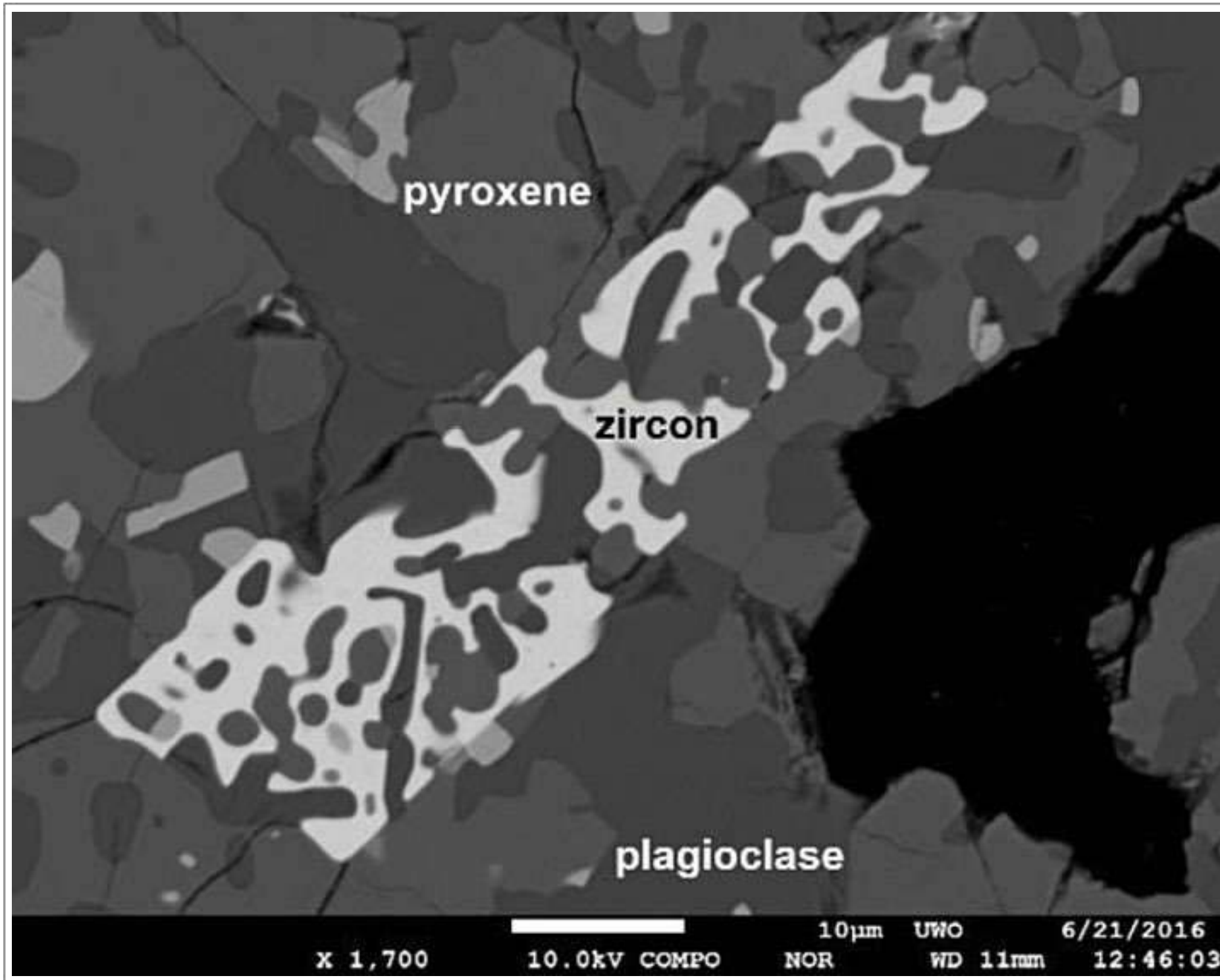
Taken From Zhang et al. (2012a)

Backscattered electron images of two representative zircon grains in granitic clasts from Apollo 12 breccia 12013.



Taken From Grieve et al. (1975)

Backscattered electron image of zircon crystals (black) in a fragment of micronorite within Apollo 14 polymict breccia 14321. Zircon typically occurs as poikiloblastic intergrowths with plagioclase feldspar. Width 100 μm .



Taken From Zhang et al. (2018)

Backscattered electron image of zircon with a poikilitic texture in Apollo 17 impact-melt breccia 73155,69.

Backscattered electron images of different morphological zircon types recognised in lunar breccias:

(A) Elongated prismatic zircon in Apollo 17 impact-melt breccia 73217;

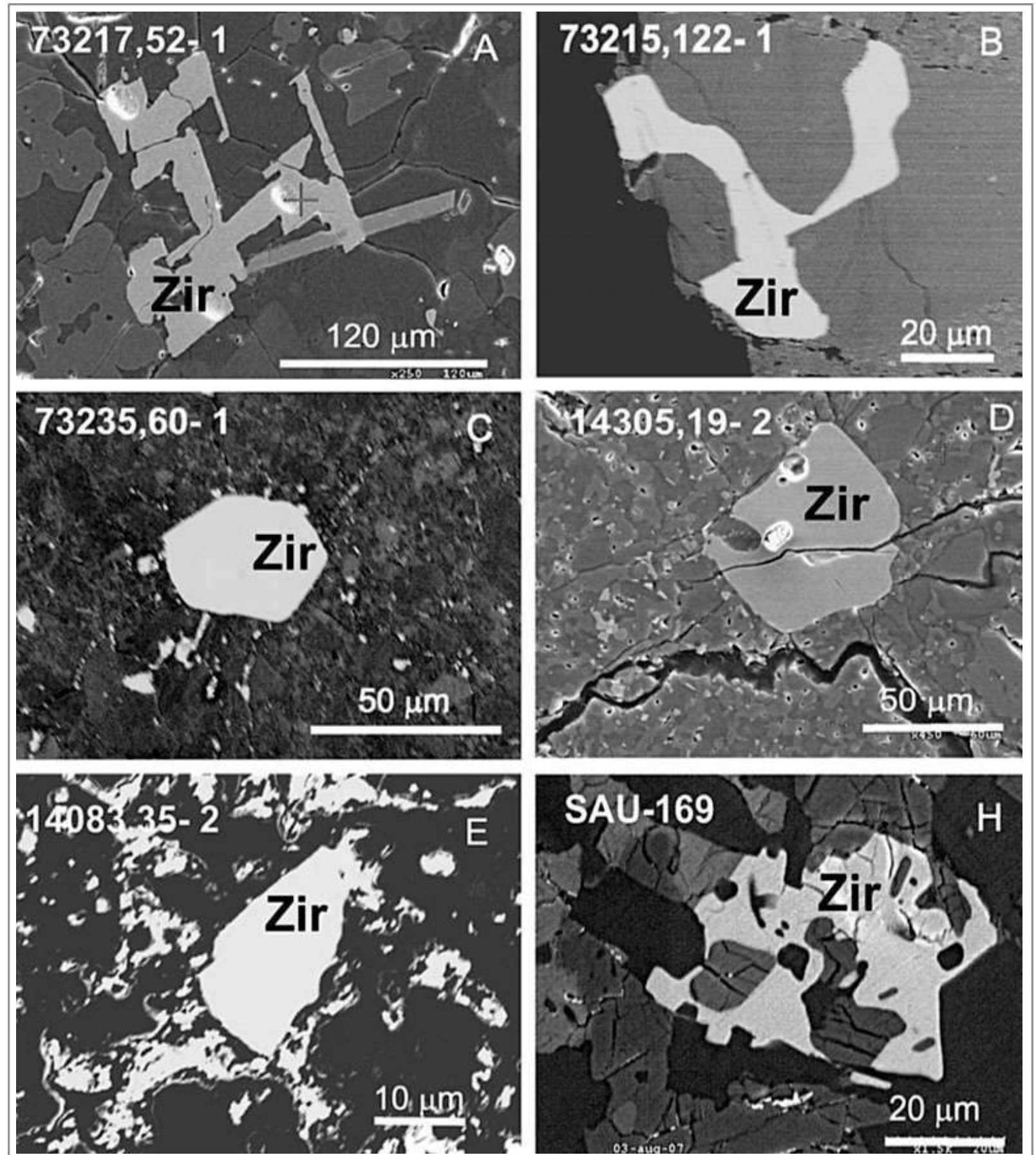
(B) Irregularly shaped zircon growing at the boundary of plagioclase grains in Apollo 17 aphanitic impact-melt breccia 73215;

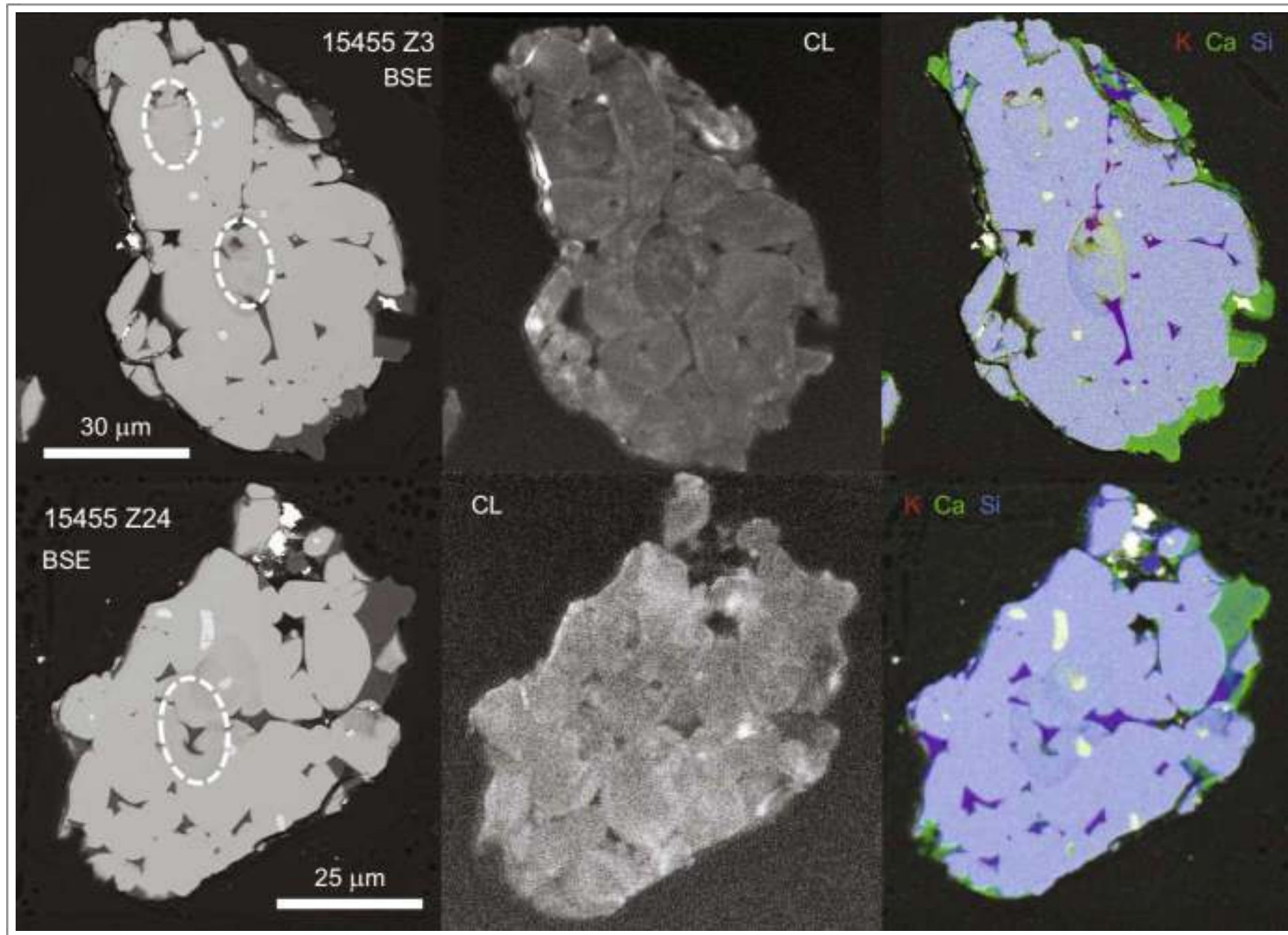
(C) Euhedral zircon with equal development of prism and pyramid faces in Apollo 17 aphanitic impact-melt breccia 73235;

(D) Fragmented grain with some of the original faces preserved in Apollo 14 polymict breccia 14305;

(E) Fragmented angular grain with none of the original faces visible in Apollo 14 light matrix breccia 14083;

(H) poikilitic impact-melt zircon from the lunar meteorite impact-melt breccia SaU 169.

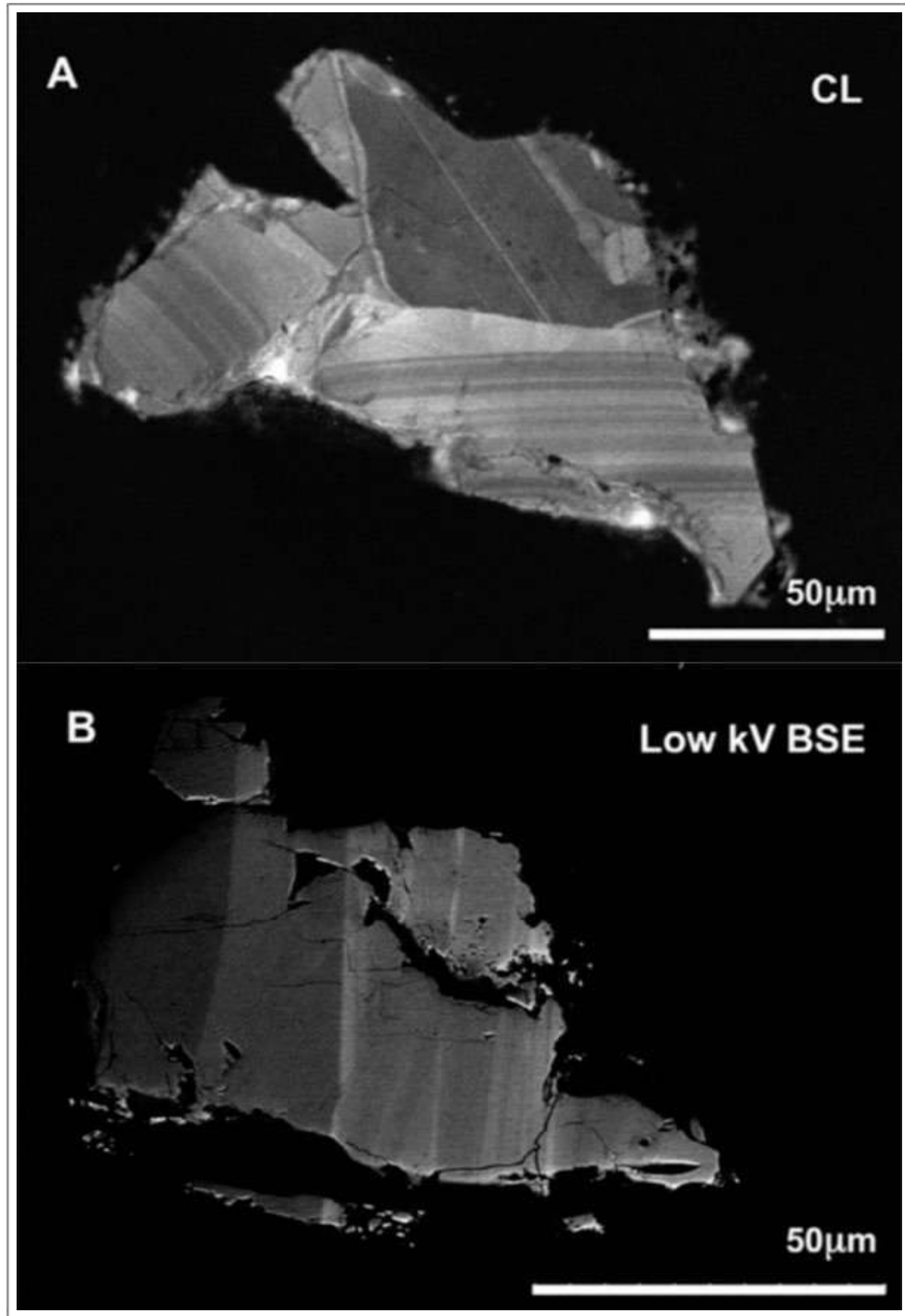


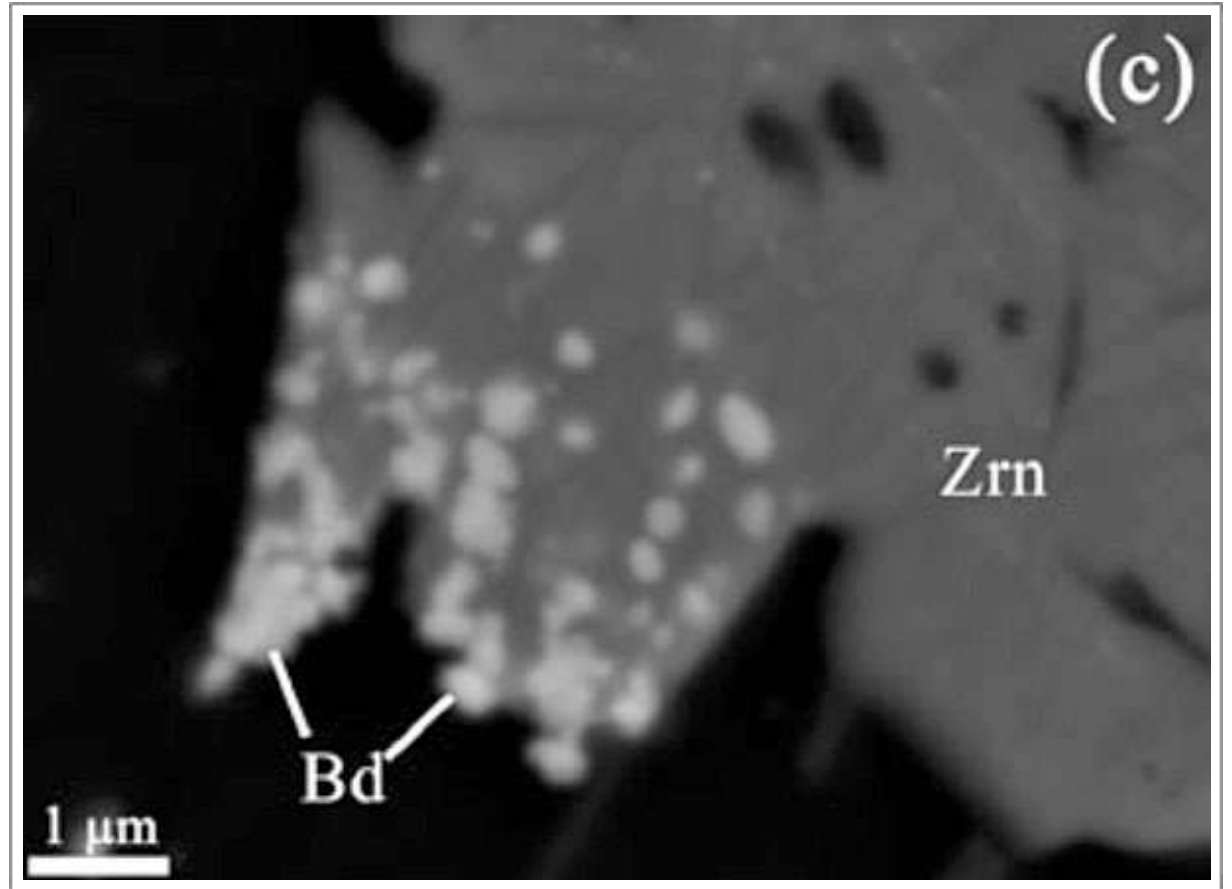
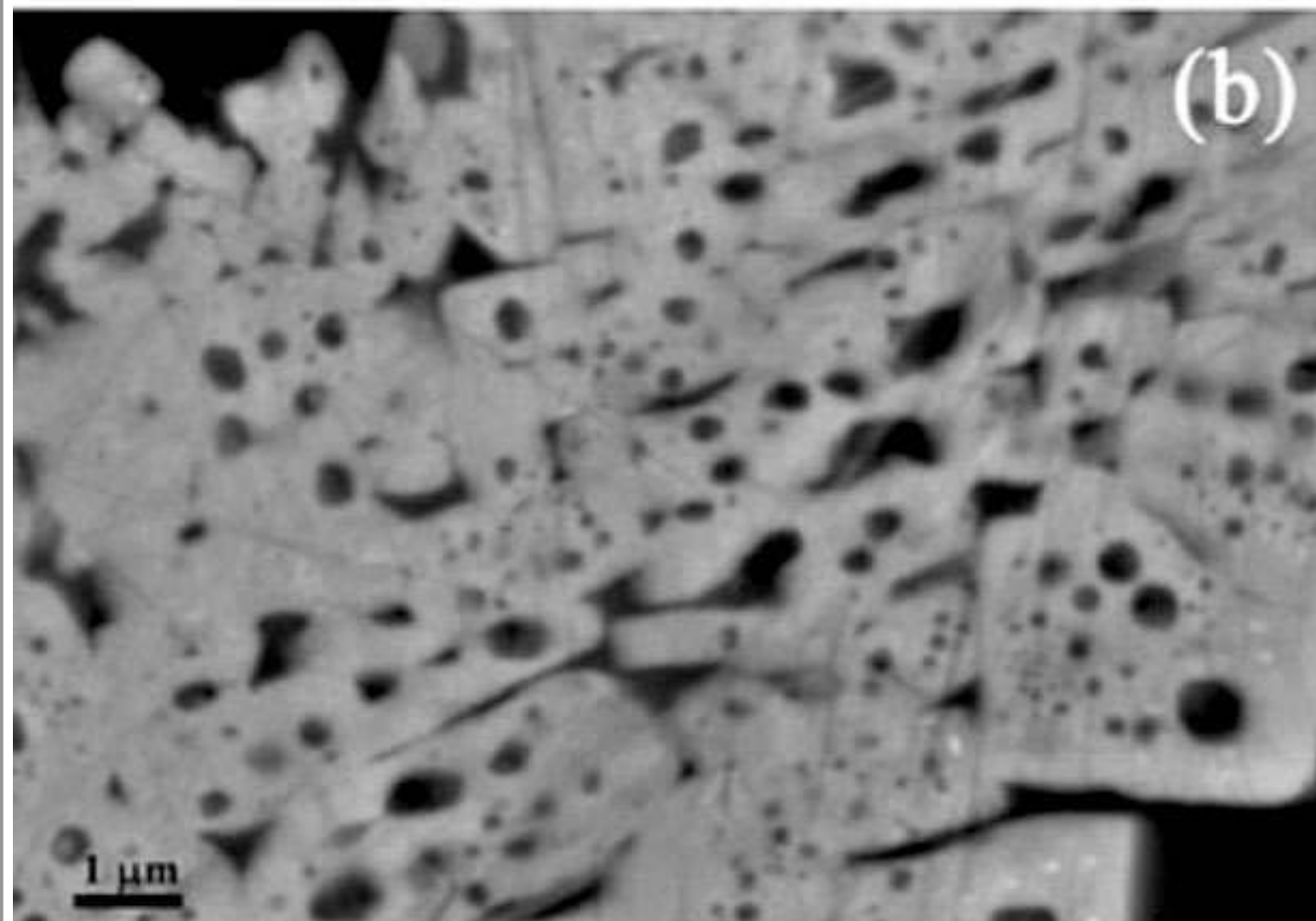
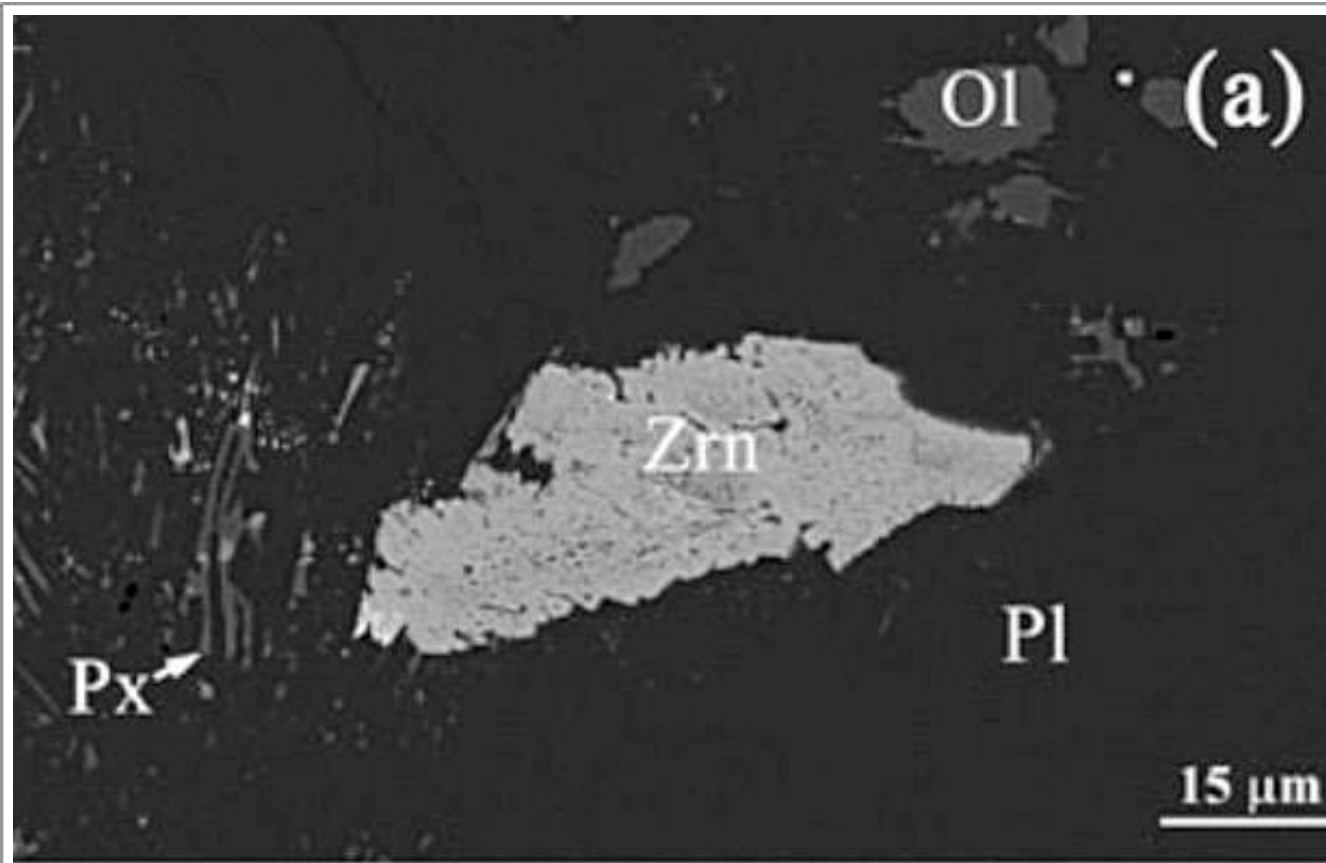


Taken From Crow et al. (2017)

Scanning electron microscope images of granular zircon clusters in an Apollo 15 breccia with a shocked norite clast - 15455. Both clusters contain multiple large granules with remnant baddeleyite cores that appear bright in the backscattered electron images and correlate with Si deficiencies in the X-ray maps (on the right). The interstitial material (purple in X-ray maps) is most likely a K-rich glass; plagioclase is green in the X-ray maps. The presence of baddeleyite and interstitial (impact) melt suggest these are impact grown zircons rather than being magmatic. Dashed circles in the BSE images show the position of secondary ion mass spectrometry (SIMS) analysis which give an age for the impact event at ~ 4.330 Ga. The central cathodoluminescence images show fine compositional variation in individual zircon granules.

Scanning electron microscope images of zircon from Apollo 14 polymict breccia 14305, showing both well-preserved primary oscillatory and sector growth zoning in the cathodoluminescence (A) and backscattered electron (B) images.

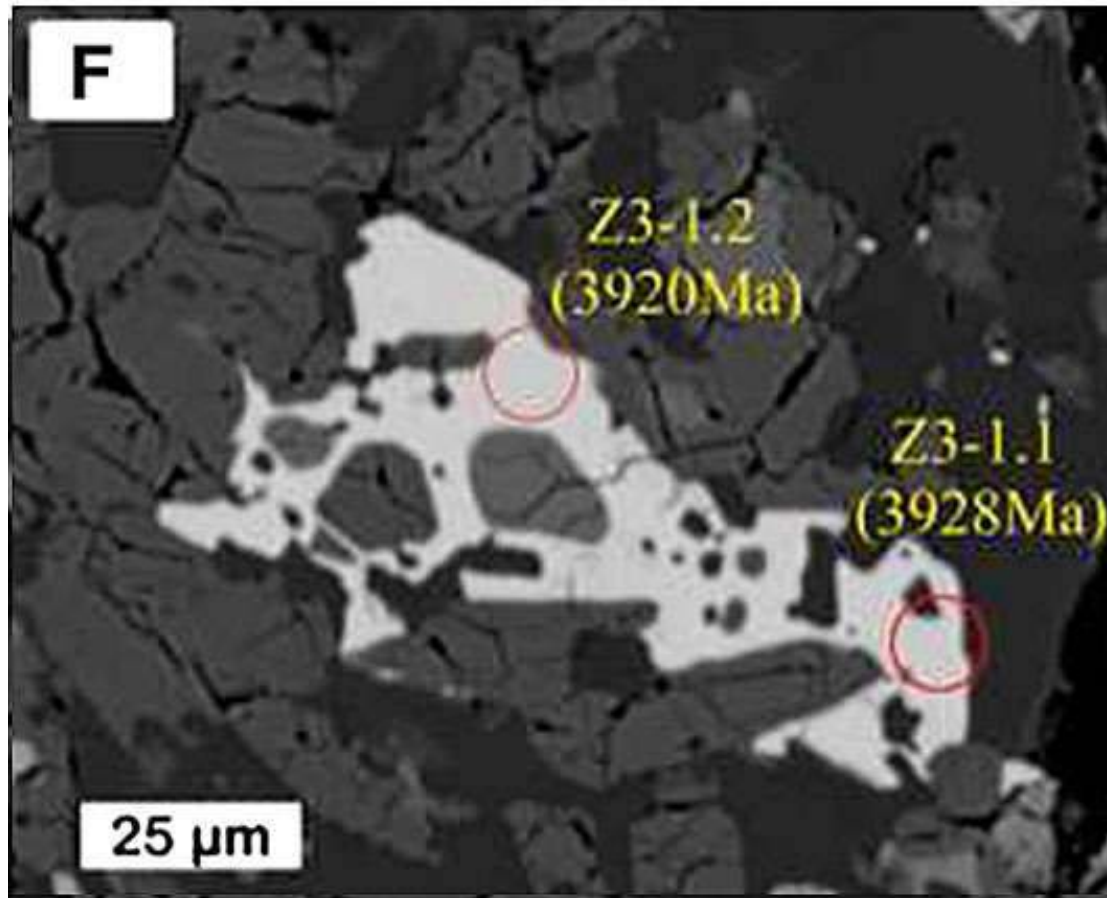
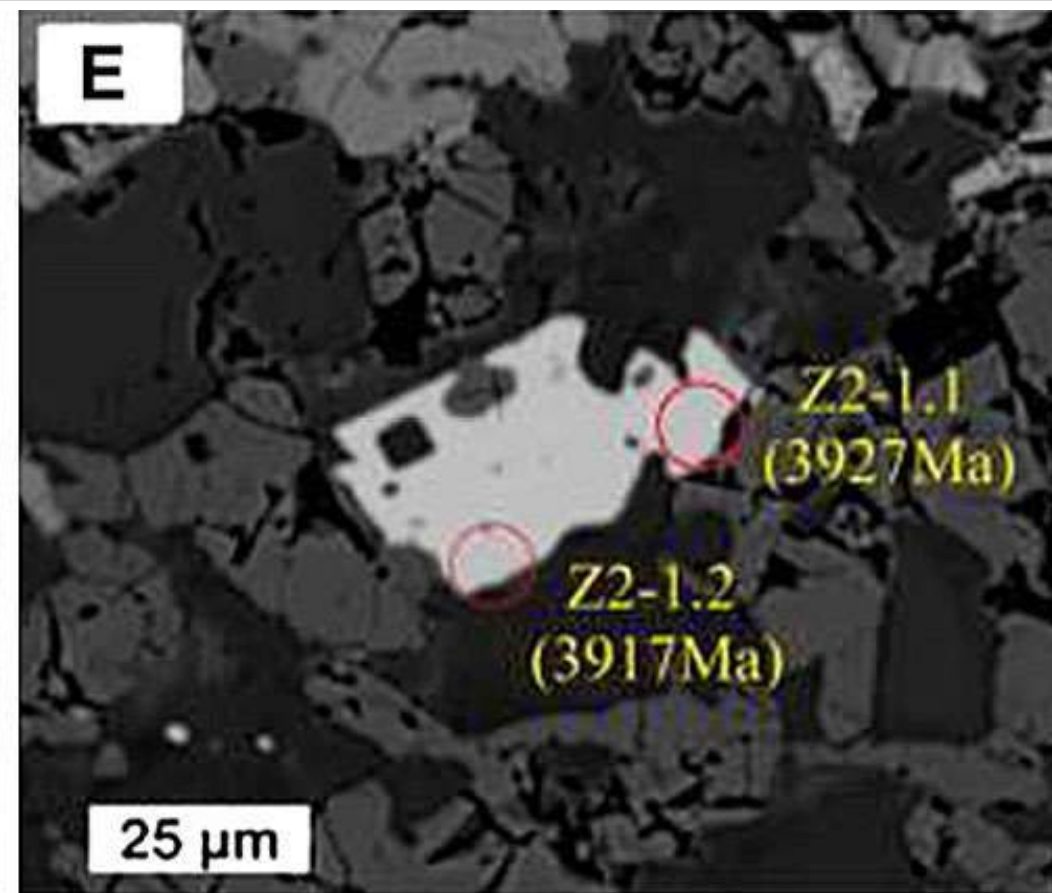
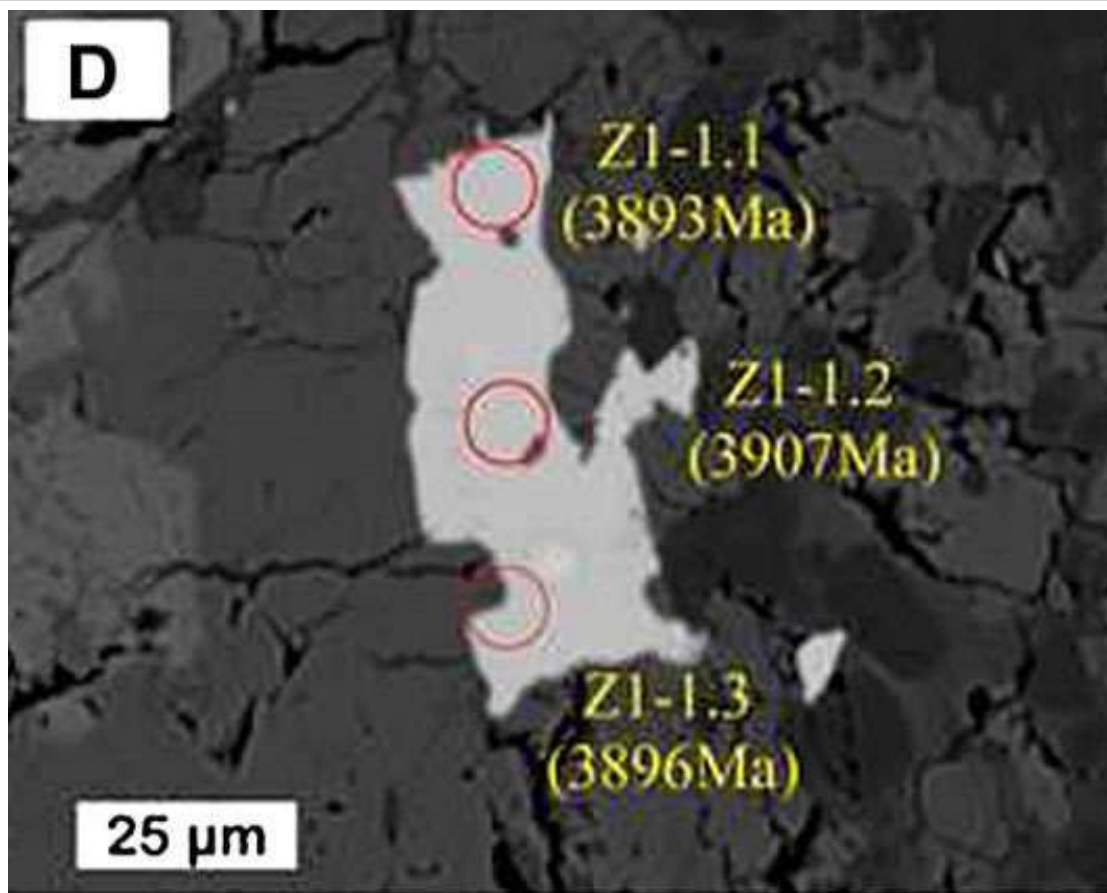




Taken From Zhang et al. (2011)

Backscattered electron image of polycrystalline zircon in lunar meteorite Dhofar 458.

- a) An irregular zircon grain entrained in plagioclase shows a polycrystalline texture.
- b) The zircon subgrains are porous, indicating a melting and degassing origin.
- c) A few fine-grained (less than 1 μm) baddeleyite grains occur at the margin of the zircon.

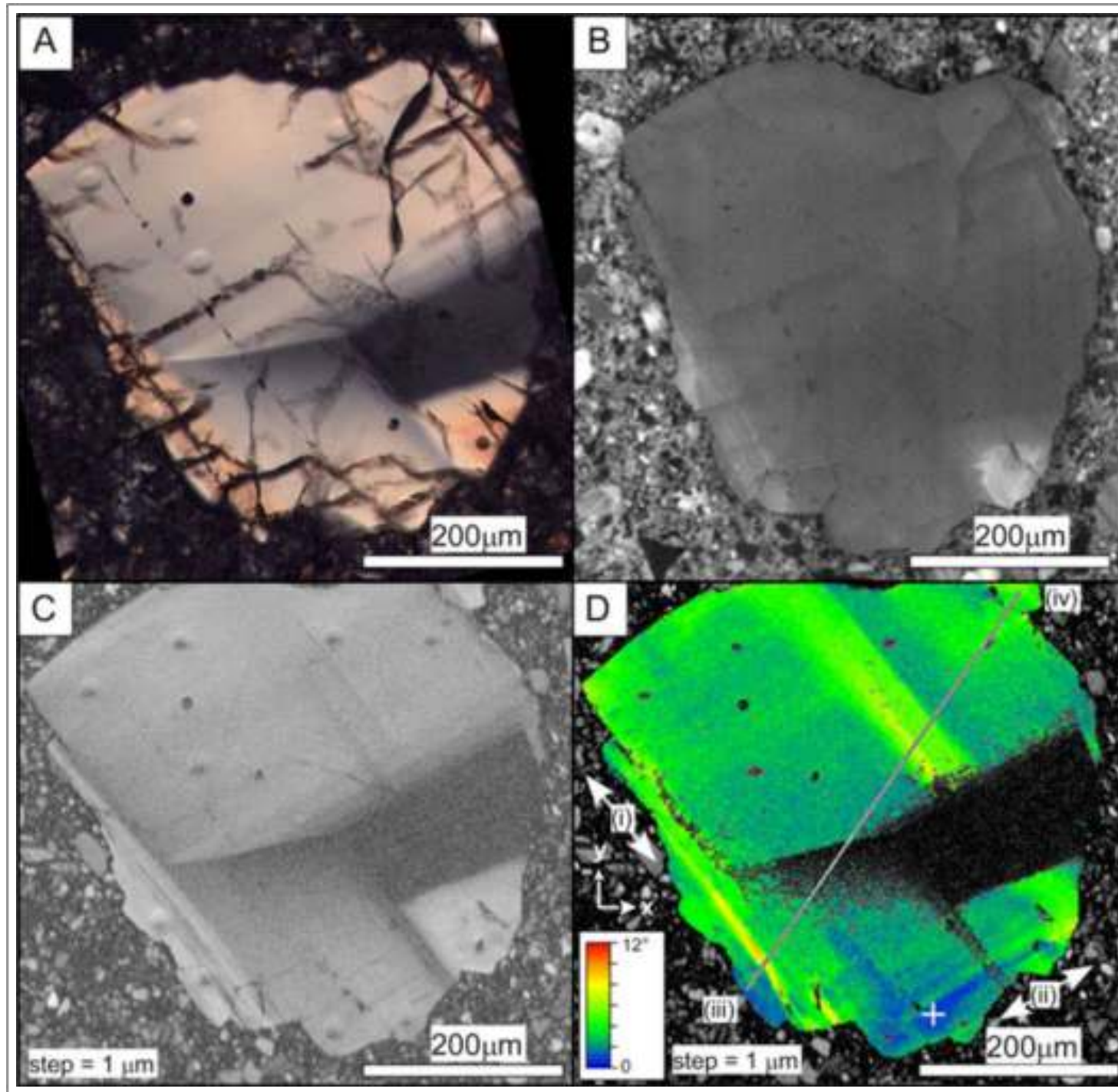


Backscattered electron images of zircon in lunar meteorite impact-melt breccia SaU 169 (plagioclase is dark grey; pyroxene, intermediate grey; and olivine, light grey).

(D) Approximately rectangular zircon grain intergrown with pyroxene.

(E) Rectangular grain with rounded, embayed and straight crystal-face boundaries with adjacent grains.

(F) Poikilitic zircon penetrating surrounding pyroxene and plagioclase, and enclosing small silicate mineral grains.



Taken From Timms et al. (2012)

Zircon from Apollo 17 aphanitic impact-melt breccia 72215,195. A) Transmitted light image showing sector zoning defined by variations in birefringence. Elliptical pits are from in situ ion microprobe analyses. B) Cathodoluminescence image. C) Electron backscatter diffraction (EBSD) band contrast map. D) Orientation map from EBSD data to show the intra-grain orientation variations. Each pixel is coloured from reference orientation (blue, indicated by white cross to a misorientation of 12° (red). Two sets of deformation bands are parallel to the trace of {100} planes, indicated by arrows (i) and (ii).

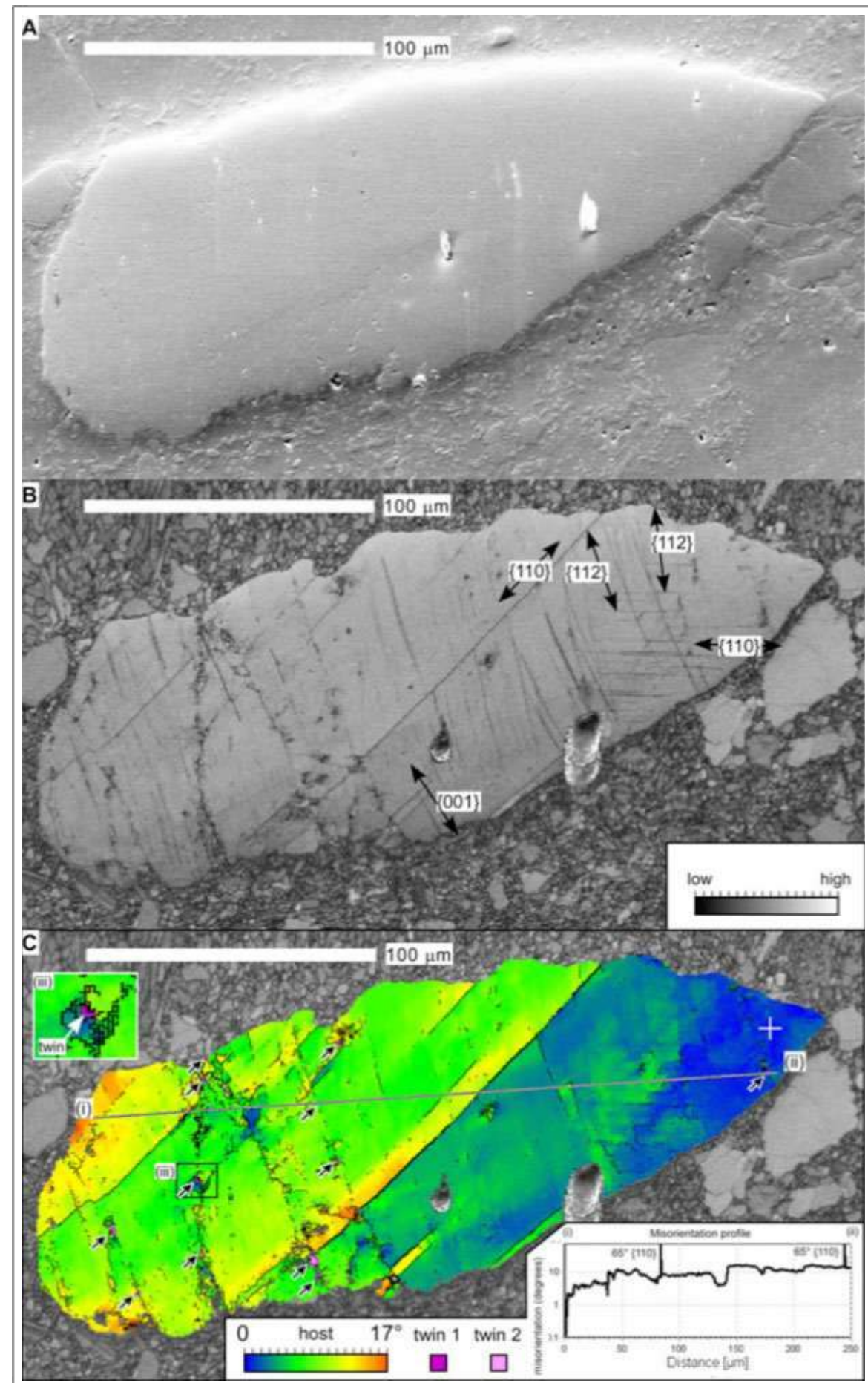
Zircon from Apollo 17 impact-melt breccia 76295,91.

A) Secondary electron image.

B) Electron backscatter diffraction (EBSD) band contrast map. Traces of crystallographic planes are indicated by arrows.

C) Orientation map from EBSD data to show intragrain crystallographic orientation variations from a reference point indicated by white cross (blue) to 17° misorientation (orange). Twin orientations 1 and 2 are colored purple and pink, respectively.

Misorientation profile along line (i)–(ii) is shown in lower right. iii) An example of a twin domain (inset)



Zircon from Apollo 17 aphanitic impact-melt breccia 73215,122.

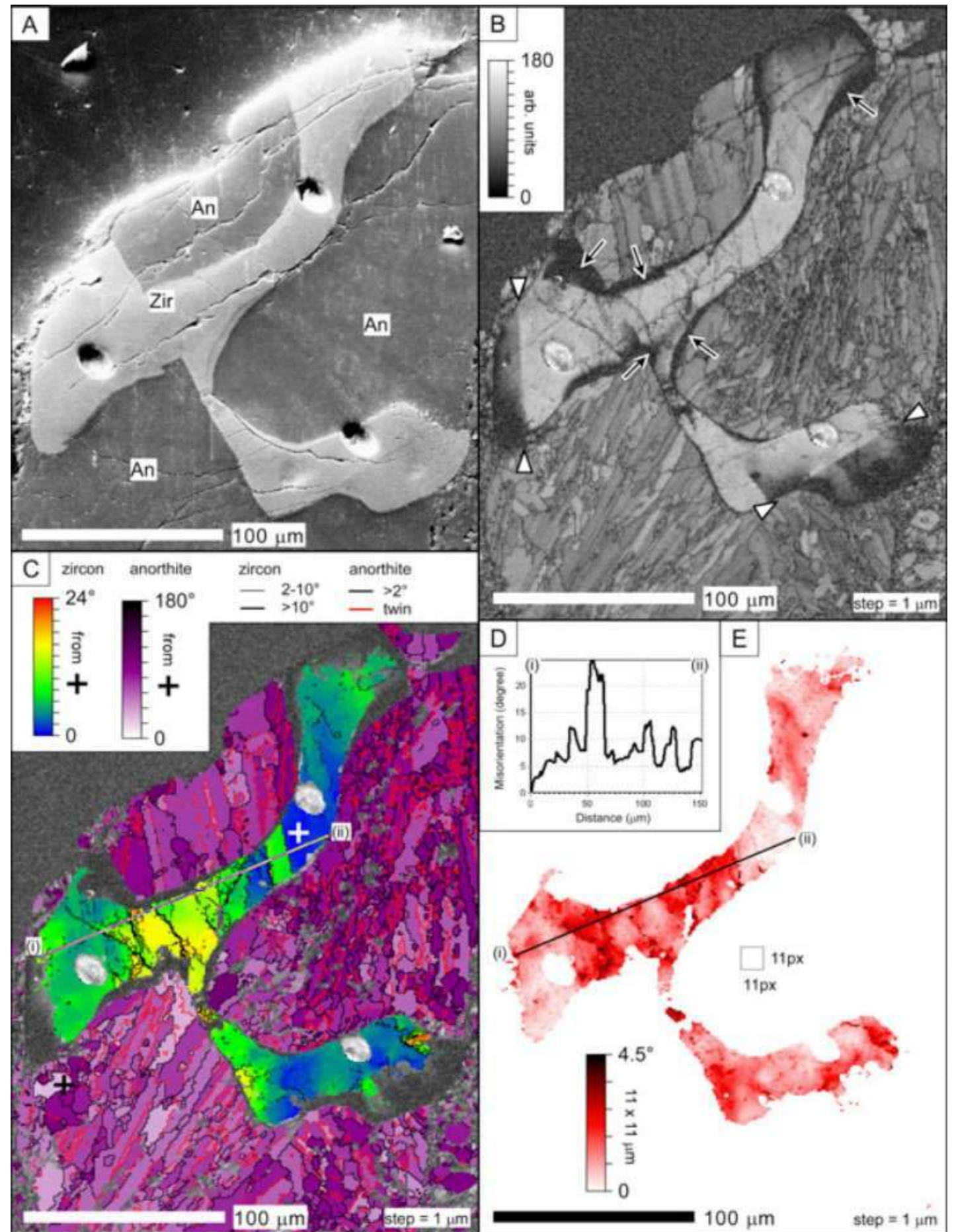
A) Secondary electron image showing the grain between three anorthite grains. Elliptical pits are from ion microprobe analyses.

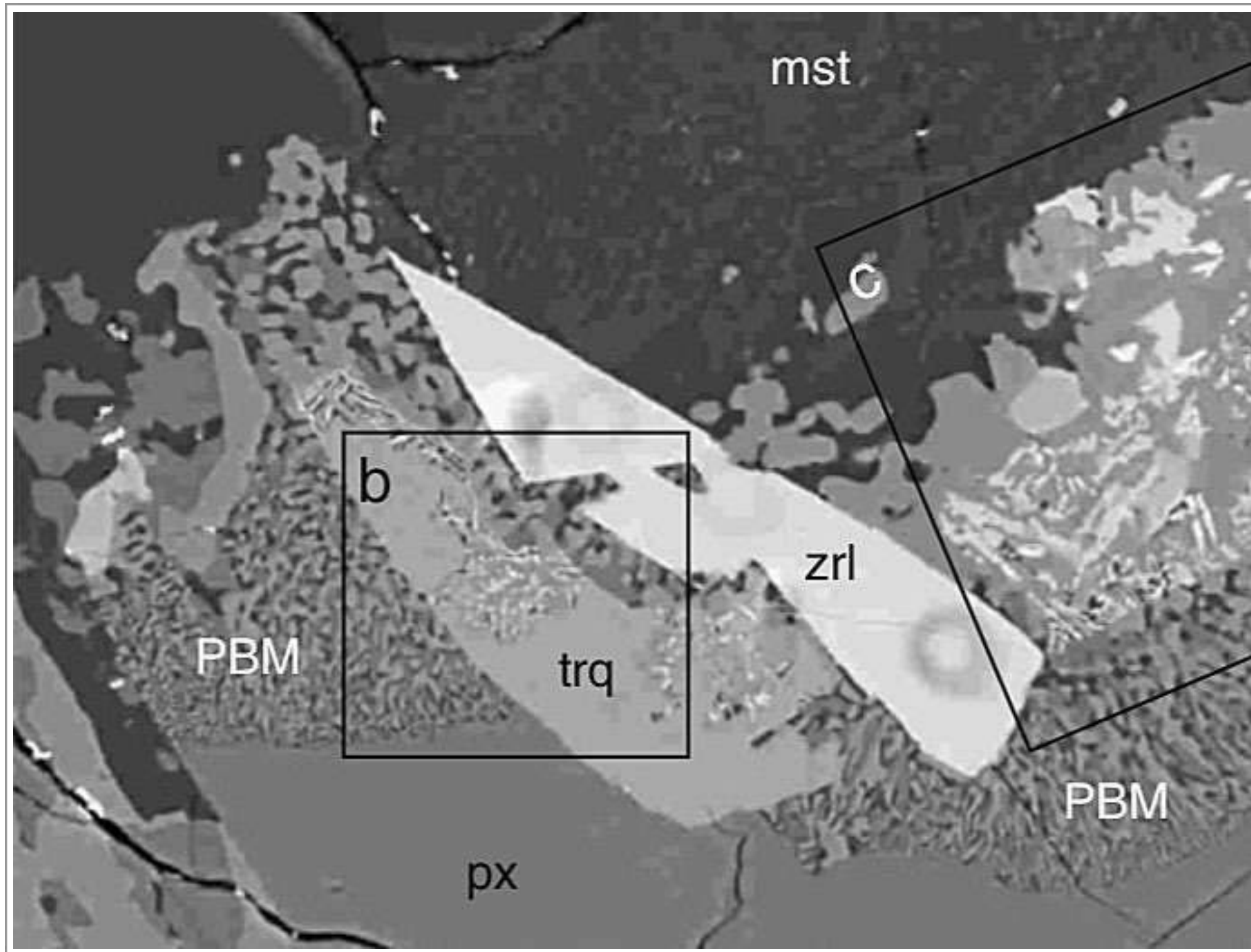
B) Electron backscatter diffraction (EBSD) band contrast map. Narrow domains at the grain interface indicated by the arrows yield low band contrast EBSD patterns. White arrows indicate sharp (100)-parallel boundaries to low band contrast domains.

C) Orientation map from EBSD data to show variations in the intra-grain orientation in the zircon and anorthite. Zircon is coloured from reference orientation (blue), indicated by white cross, to a misorientation of 24° (red). Anorthite is coloured for variations up to 180°. Boundaries between adjacent pixels with >2° misorientation are shown with solid lines (see legend).

D) Cumulative misorientation profile along line (i)–(ii) shown in (C).

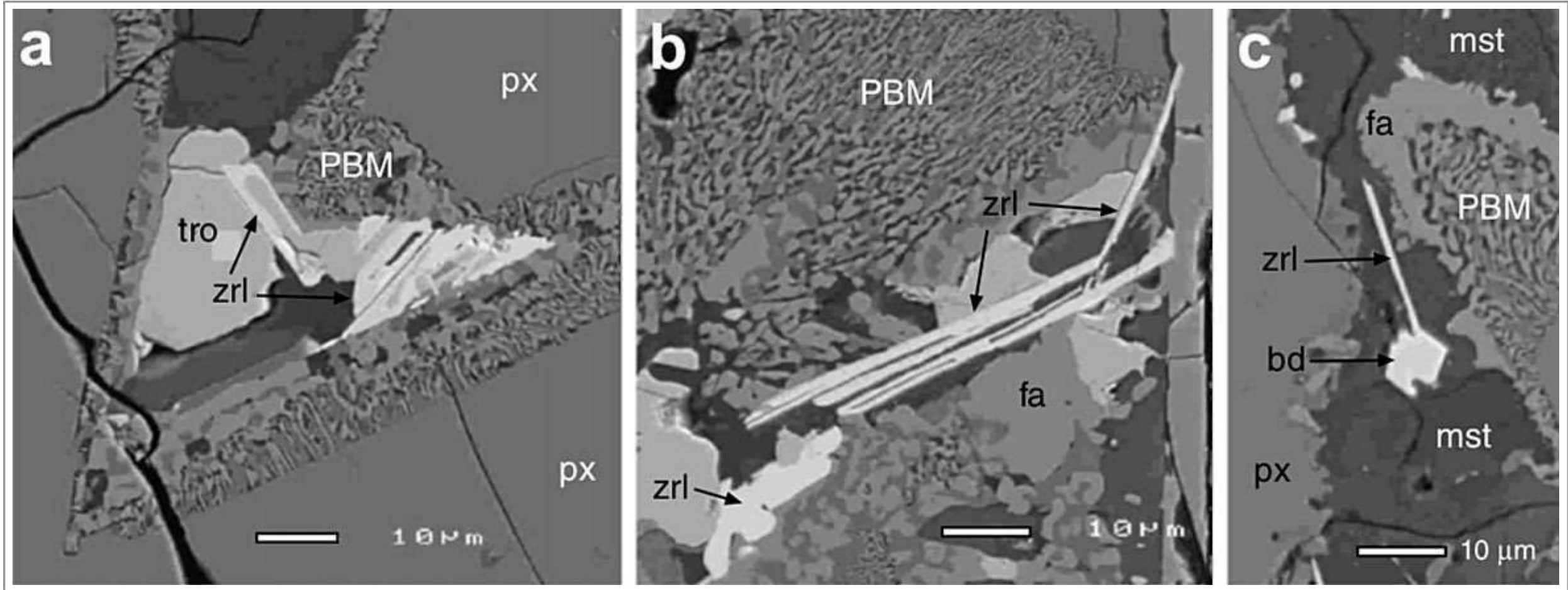
E) Local misorientation map to show orientation gradients within grains. Each pixel is coloured for mean misorientation (degrees) on a local 11x11 grid.





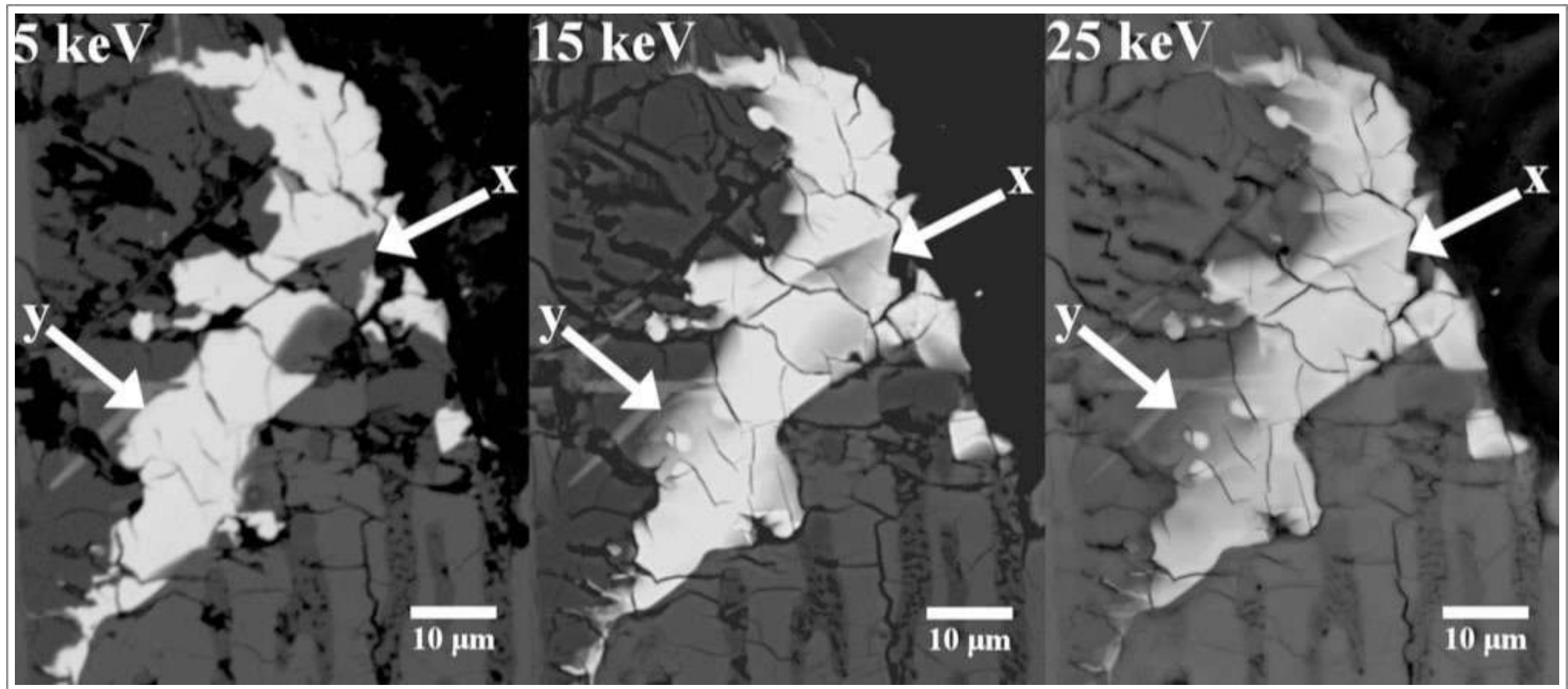
Taken From Rasmussen et al. (2008)

Apollo 11 ilmenite basalt 10047,11: Backscattered electron image of tranquillityite (trq) and zirconolite (zrl). The mesostasis area (mst) is juxtaposed against a region of vermiform fayalite-hedenbergite-silica intergrowth (PBM) mantling pyroxene (px). Baddeleyite and troilite are associated species.



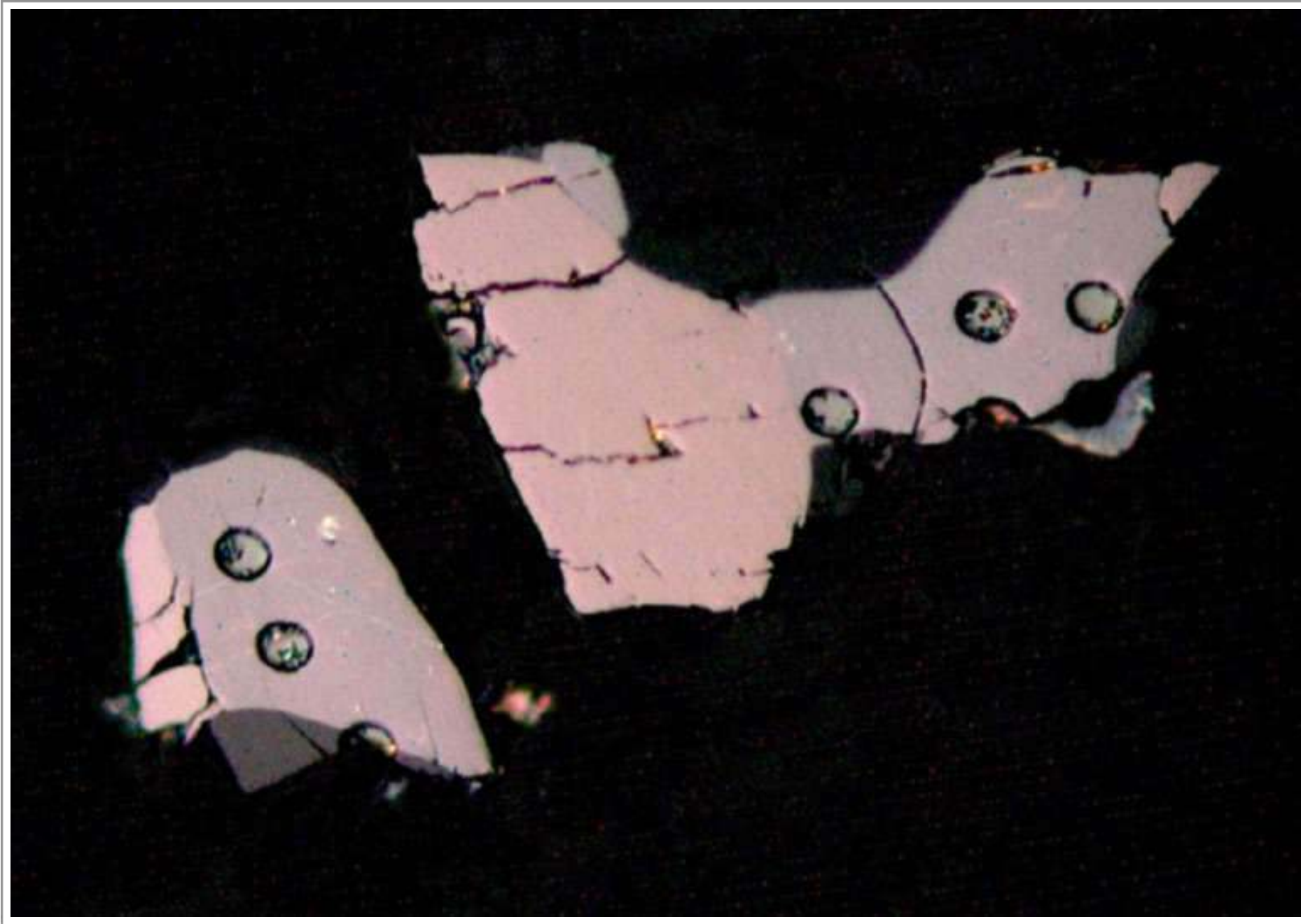
Taken From Rasmussen et al. (2008)

Apollo 11 ilmenite basalt 10047: (a) Zirconolite (zrl) intergrown with baddeleyite and tranquillityite in the interstices between pyroxene. Adjacent minerals are troilite (tro) and cristobalite (cst). The margin of the pyroxene is lined by a symplectitic intergrowth comprising hedenbergite, fayalite and silica (PBM). Sample 10047,227. (b) Elongate, straw-like zirconolite (zrl) crystals adjacent to vermiform hedenbergite-fayalite-silica intergrowth (PBM). Sample 10047,11. (c) Equant baddeleyite crystal with straw-like zirconolite projection within mesostasis (mst) comprising silica and barian K-feldspar. Sample 10047,11.



Taken From Seddio et al. (2013b)

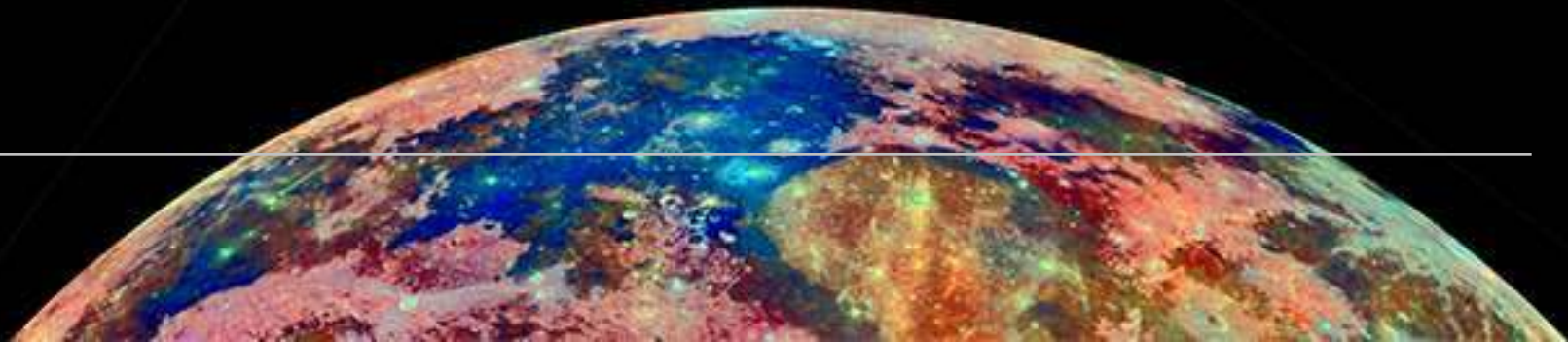
Apollo 12 granite fragment 12032,366-19: three backscattered electron images of a zirconolite grain taken at various accelerating voltages of 5, 15, and 25 kV. Arrow “x” points to a region that is covered by a thin layer of K-feldspar. Arrow “y” points to a region where the zirconolite is thin. The thin layers become transparent in the images taken at higher accelerating voltages because backscattered electrons can come from greater depths in the sample at higher accelerating voltages.



Taken From Norman and Nemchin (2014)

Reflected light view of zirconolite associated with ilmenite (pink) in Apollo 16 impact-melt breccia. Circular ion microprobe spots are visible on the zirconolite grains. In the original publication a bright residual gold coating from the ion microprobe analysis mantled the mineral cluster and has been digitally removed here. Width approx. 100 μm .

Silica Minerals



SPECIES

1. Quartz - SiO_2
2. Cristobalite - SiO_2
3. Tridymite - SiO_2
4. Coesite - SiO_2
5. Stishovite - SiO_2
6. Moganite - SiO_2
7. Seifertite - SiO_2

Silica minerals include several structurally different minerals, all of which have the simple formula SiO_2 . These minerals are generally rare on the Moon. This rarity is one of the major mineralogic differences between the Moon and the Earth, where silica minerals are abundant in such common rocks as granite, sandstone, and chert. The relative absence of silica minerals on the Moon is a result of several factors. For one thing, the Moon has apparently not evolved chemically beyond the formation of a low-silica, high-alumina anorthositic crust, so that high-silica granitic rocks are rare. For another, the Moon lacks hydrous and hydrothermal systems like those that can crystallize silica on Earth (Heiken et al., 1991).

Quartz occurs in a few granite-like (felsite) clasts (e.g., Apollo 12; sample 12013) as needle-shaped crystals that probably represent structural transformation (inversion) of original tridymite (Quick et al., 1981). Some tridymite is preserved in these felsite clasts. Quartz is also abundant in the rare fragments of coarse-grained lunar granite. The largest lunar granite clast yet found, from Apollo 14 breccia 14321, weighs 1.8 g and contains 40 vol.% quartz. A smaller granite clast from sample 14303 was estimated to have 23 vol.% quartz (Warren et al., 1983).

Granite and rhyolitic clasts in lunar breccias are also reported from Apollo 14 samples 14306 and 14270 (Smith and Steele, 1976). These authors note that quartz is usually intergrown with barian sanidine.

Microcrystals of coesite and stishovite were discovered as inclusions in amorphous silica grains in shocked melt pockets of lunar breccia meteorite Asuka 881757 and indicate that the meteorite experienced an equilibrium shock-pressure of at least 8-30 GPa. Secondary quartz grains are also observed in separate amorphous silica grains in the meteorite. Observation of coesite and stishovite formed in lunar breccias suggests that high-pressure impact metamorphism and formation of high-pressure minerals are common phenomena in brecciated lunar surface altered by the heavy meteoritic bombardment (Ohtani et al., 2011; Miyahara et al., 2016).

Silica polymorphs in Apollo 12 lunar granite and felsite samples (found as granophyric intergrowths of silica and K-feldspar) have been examined using laser-Raman spectroscopy (Seddio et al., 2013a). They found quartz with a hackle fracture pattern and silica glass if not fractured in 12001,909-14; quartz with a hackle fracture pattern in 12023,147-10; 12033,634-30 and 12033,634-34; and cristobalite in 12032,367-16. Tridymite has only been reported in granitic breccia 12013. The hackle fracture pattern of quartz in lunar samples is attributed to inversion from cristobalite or tridymite and most is best referred to as inverted cristobalite. The preservation of high-temperature silica polymorphs (before inversion at some point later) and the fine-grained textures of most granitic lunar samples indicate that the samples experienced relatively rapid cooling (e.g., rhyolitic volcanism).

Several quartz, tridymite, and cristobalite grains measuring 10-100 μm across occur in the mafic impact-melt breccia part of Apollo15 regolith breccia 15299. Vesicular melt veins of less than $\sim 200 \mu\text{m}$ wide cut across the mafic melt breccia matrix and mineral fragments. Some silica grains are entrained in the melt veins and one of the silica grains entrained consists of stishovite along with tridymite and silica glass (Kaneko et al., 2015; Miyahara, 2016).

Moganite, a monoclinic SiO_2 phase, has been discovered in lunar meteorite NWA 2727. Silica micrograins occur as nanocrystalline aggregates of mostly moganite and occasionally coesite and stishovite in this KREEP-like gabbroic-basaltic breccia. It is thought that these grains developed when alkaline water was delivered to the Moon via carbonaceous chondrite collisions followed by fluid capture during impact-induced brecciation. Moganite precipitated from the captured H_2O when the meteorite was ejected from the Moon during a later impact. On the subsurface, this captured H_2O may still remain as ice at estimated bulk content of >0.6 weight %. This indicates the possibility of the presence of abundant available water resources underneath local sites of the host bodies within the Procellarum KREEP and South Pole Aitken terranes (Kayama et al., 2018).

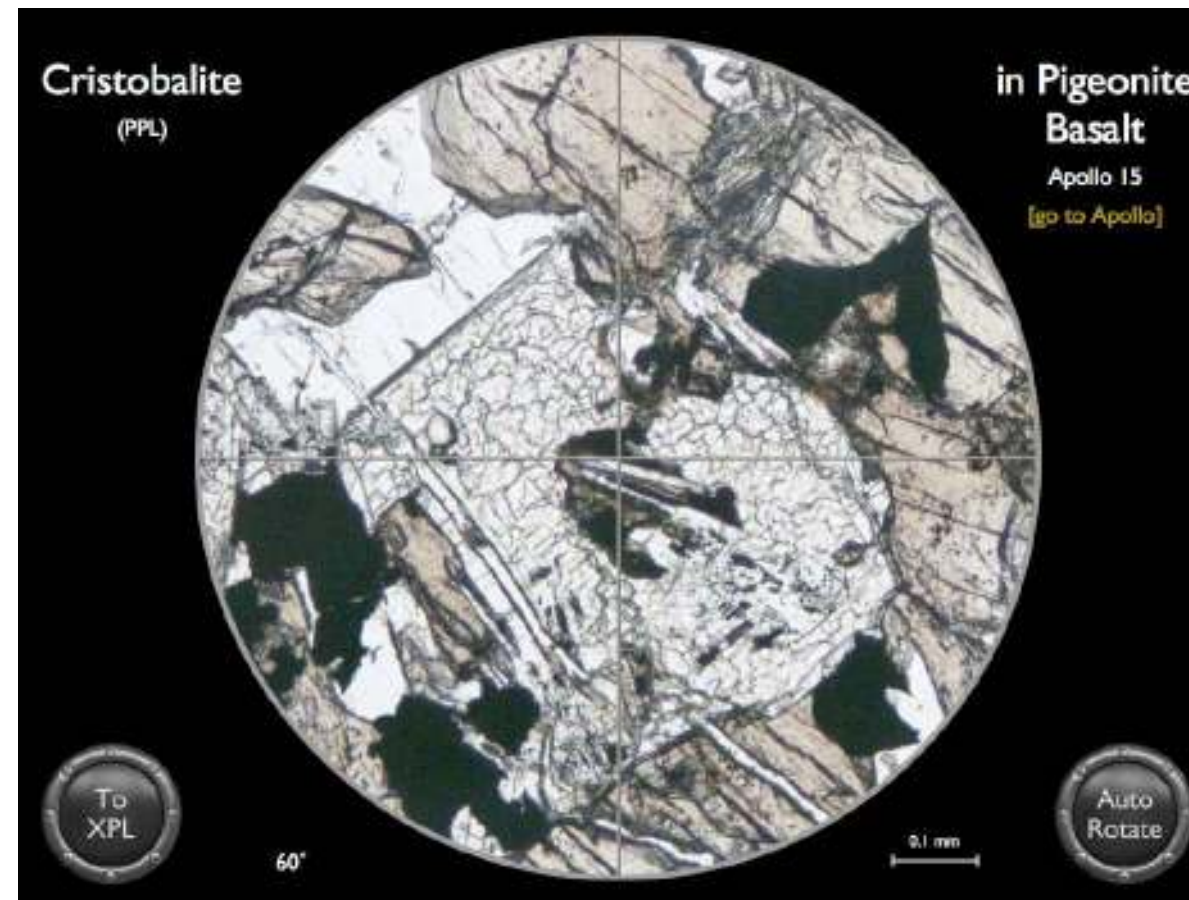
The ultra high pressure silica polymorph seifertite has been found in shocked lunar meteorite NWA 4734 - a mare basalt. Cristobalite transforms to seifertite under ultra-high pressures and

temperatures. Coesite and cristobalite-stishovite reactions are noted by Miyahara et al., (2013 and 2016). The existence of seifertite, coesite and stishovite infers that intense planetary collisions (like the late heavy bombardment scenario) occurred on the Moon until at least about 2.7 Ga ago.

Chen et al. (2018) also studied NWA 4734 and noted shocked tridymite and quartz grains intergrown with K-feldspar. Coesite grains were observed within the silica glass along regions of shock melt.

Moon Minerals: Silica Minerals

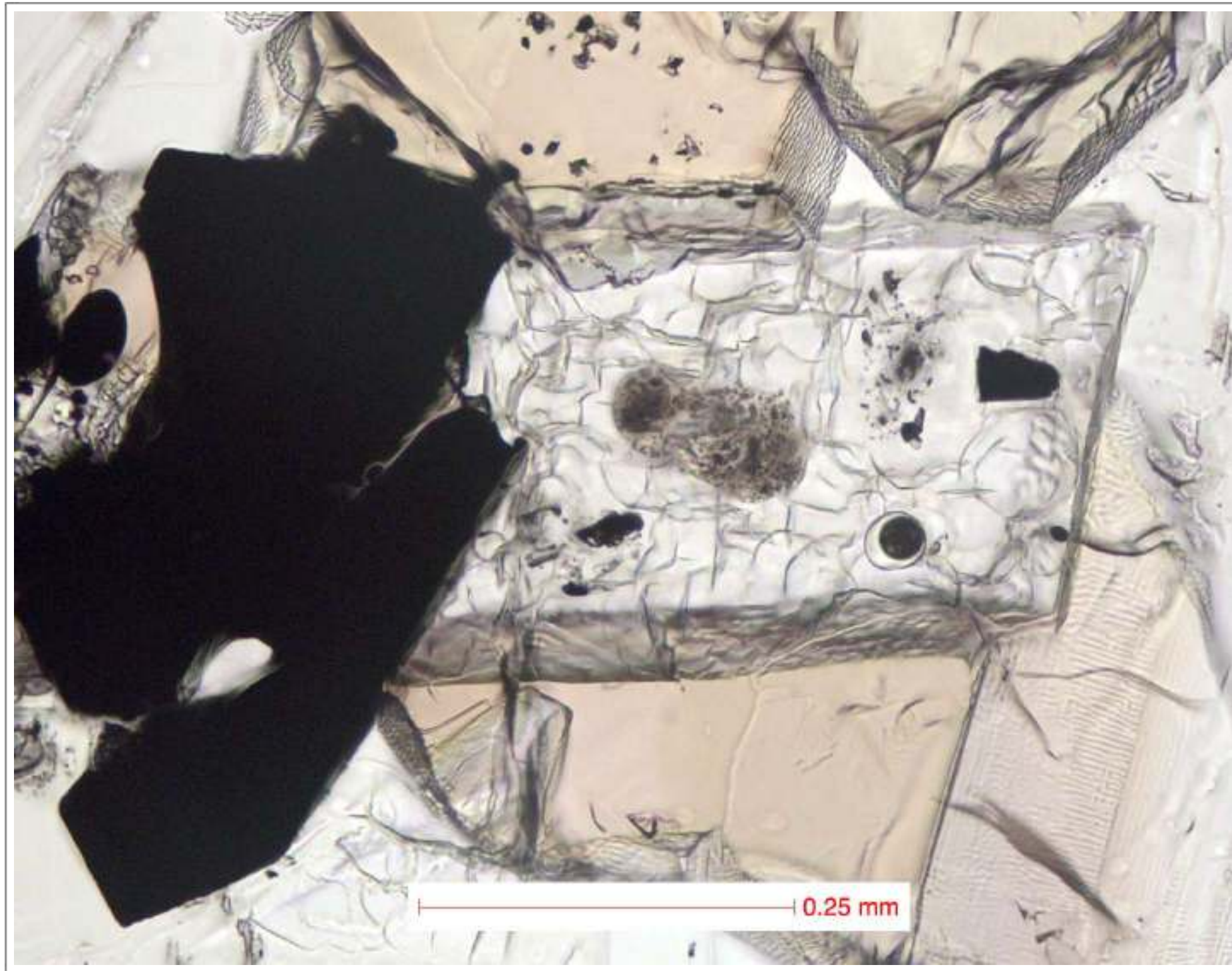
Mineral Virtual Microscope: Cristobalite



Rectangular cristobalite crystal showing typical hackled texture in PPL. Pyroxene (pigeonite), plagioclase feldspar and ilmenite mantle the cristobalite.

Apollo 15, Sample 15058.

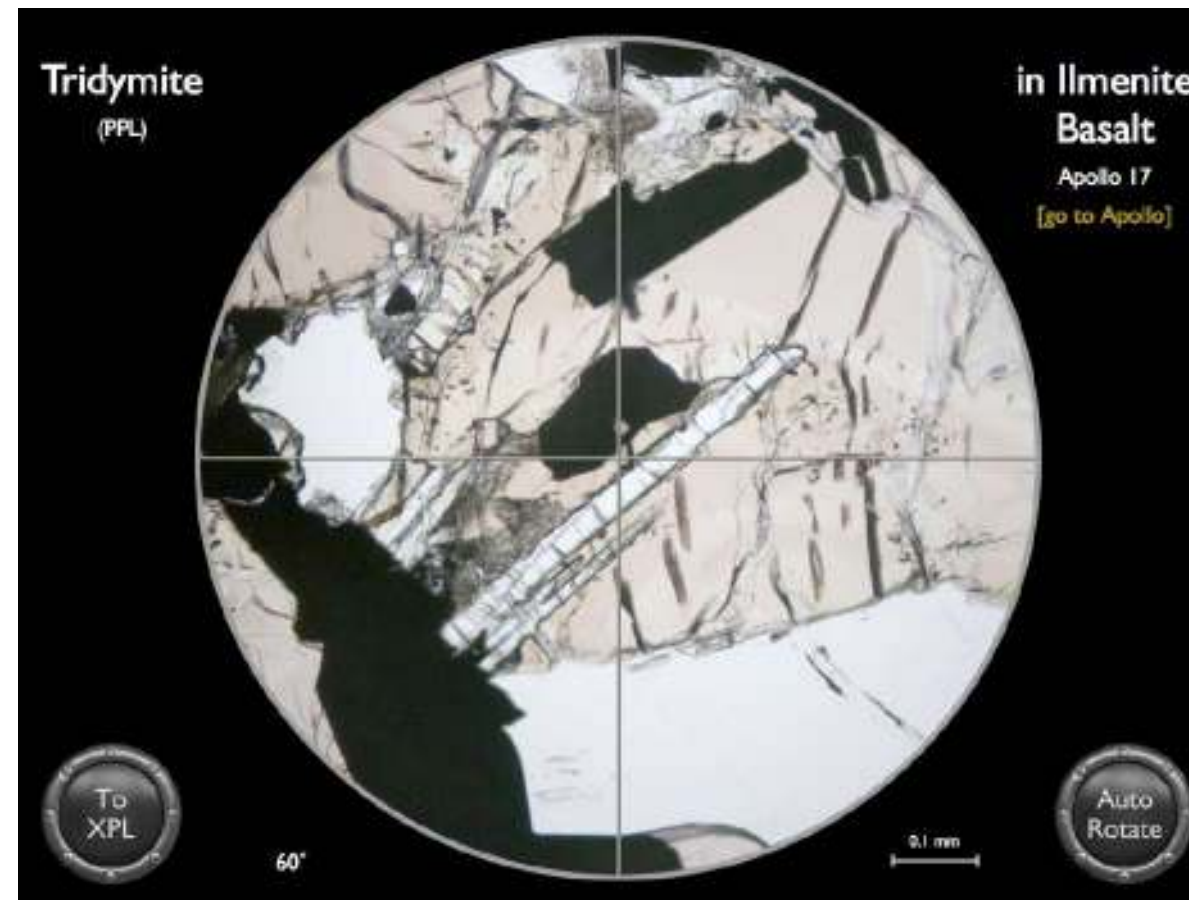
Credit: NASA (AGT Photographer)



Plane polarised light image of cristobalite in Apollo 17 ilmenite basalt 78135. Note the hackled texture of the cristobalite and the variety of inclusions. The ripples in the surrounding pyroxene are artifacts caused by the processing of this multi-layer stacked image. Credit: NASA (AGT Photographer).

Moon Minerals: Silica Minerals

Mineral Virtual Microscope: Tridymite



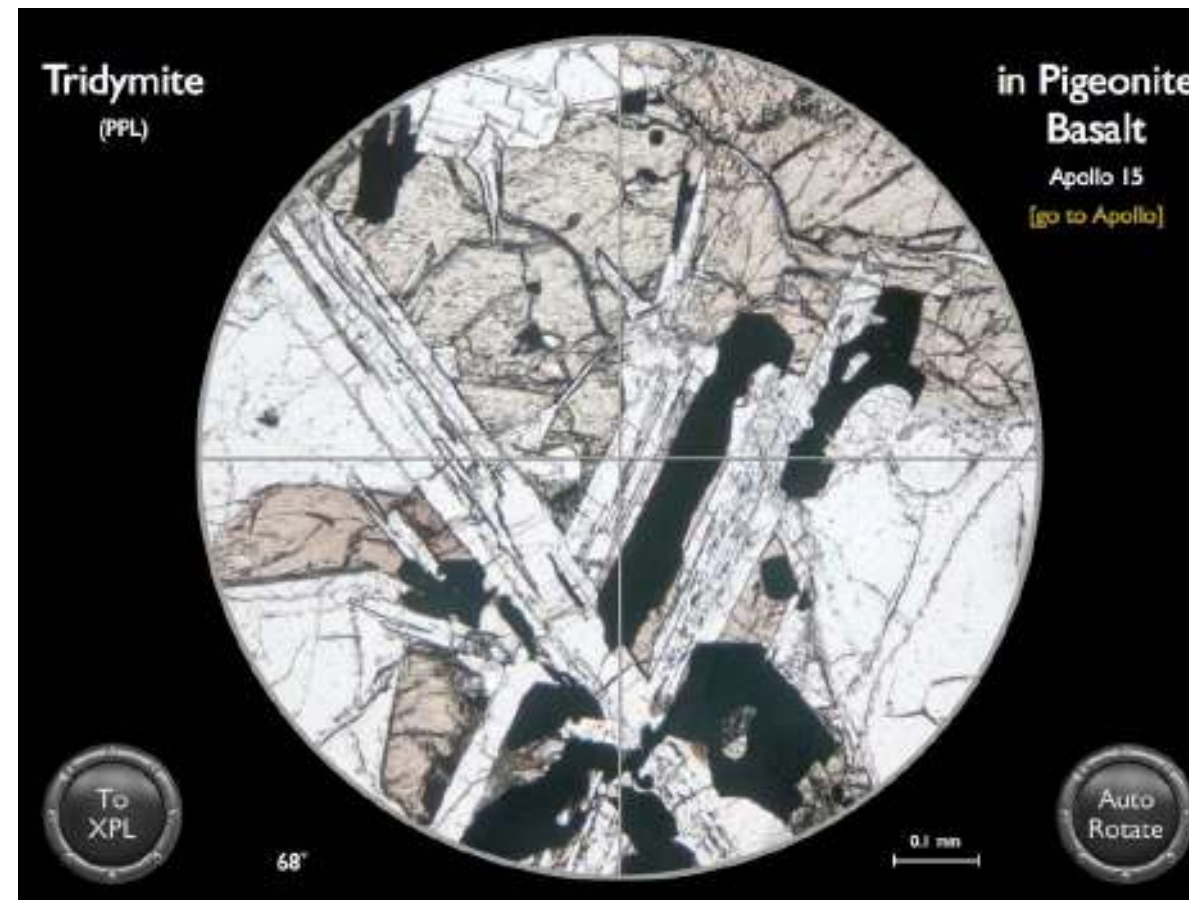
Needle-like crystals of tridymite enclosed in pyroxene and associated with plagioclase feldspar and ilmenite.

Apollo 17, Sample 75015.

Credit: NASA (AGT Photographer)

Moon Minerals: Silica Minerals

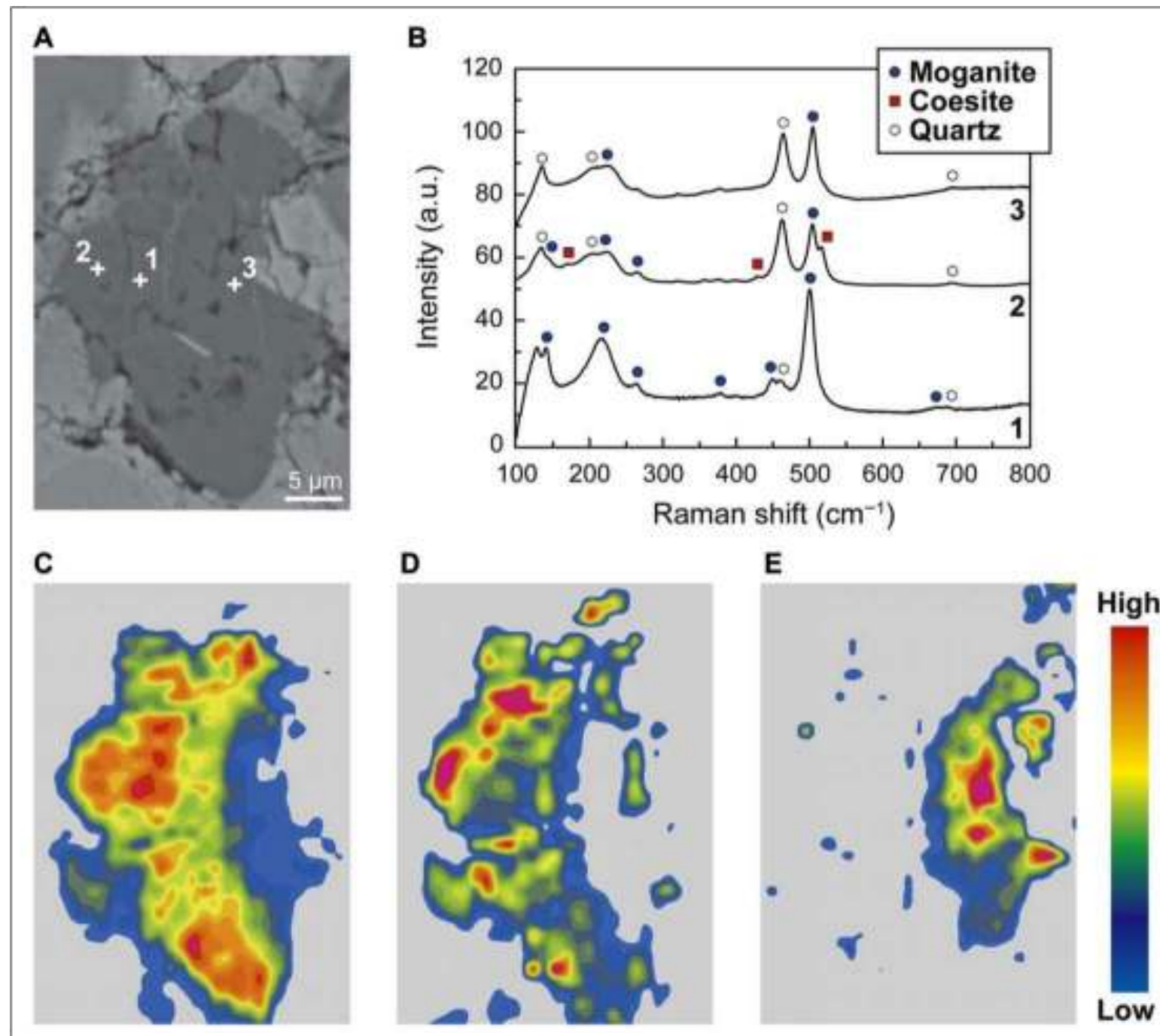
Mineral Virtual Microscope: Tridymite



Blades of tridymite associated with olivine, pyroxene (pigeonite), plagioclase feldspar and ilmenite. A small crystal of cristobalite partially mantled by ilmenite appears on the right (at 68°).

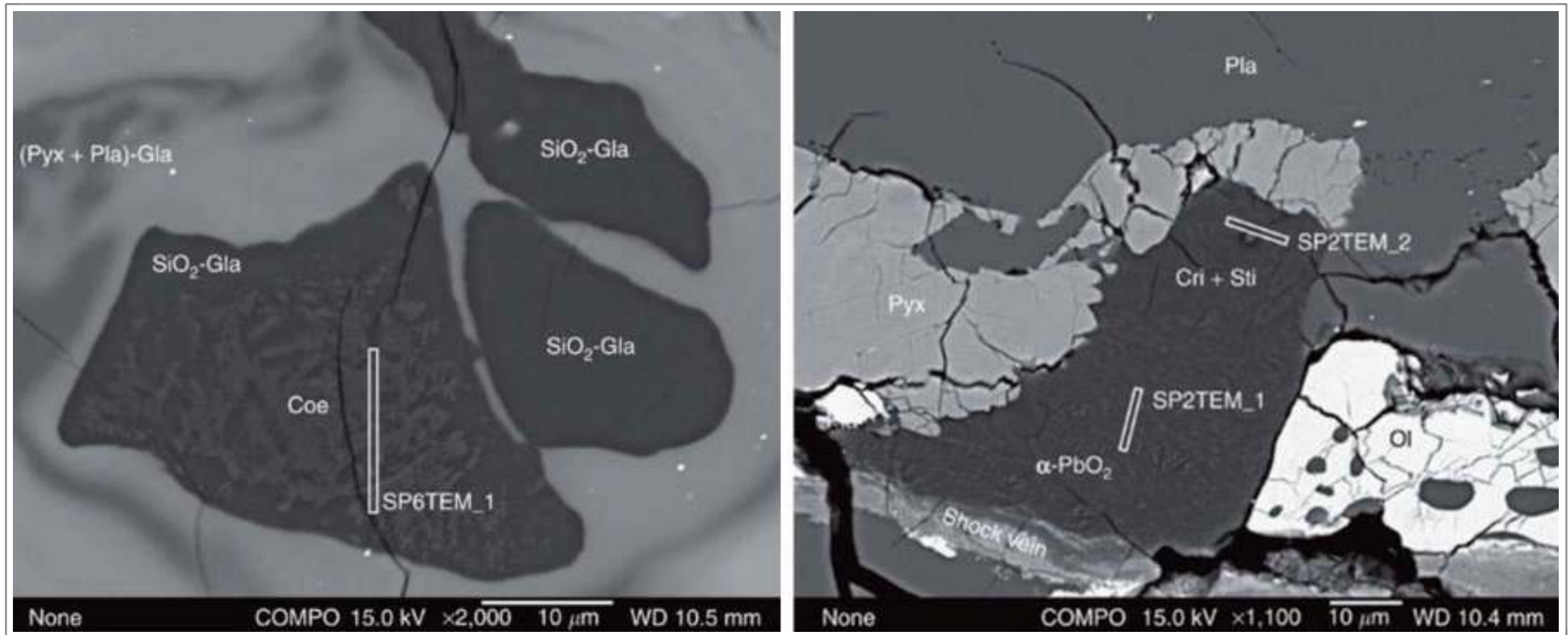
Apollo 15, Sample 15065.

Credit: NASA (AGT Photographer)



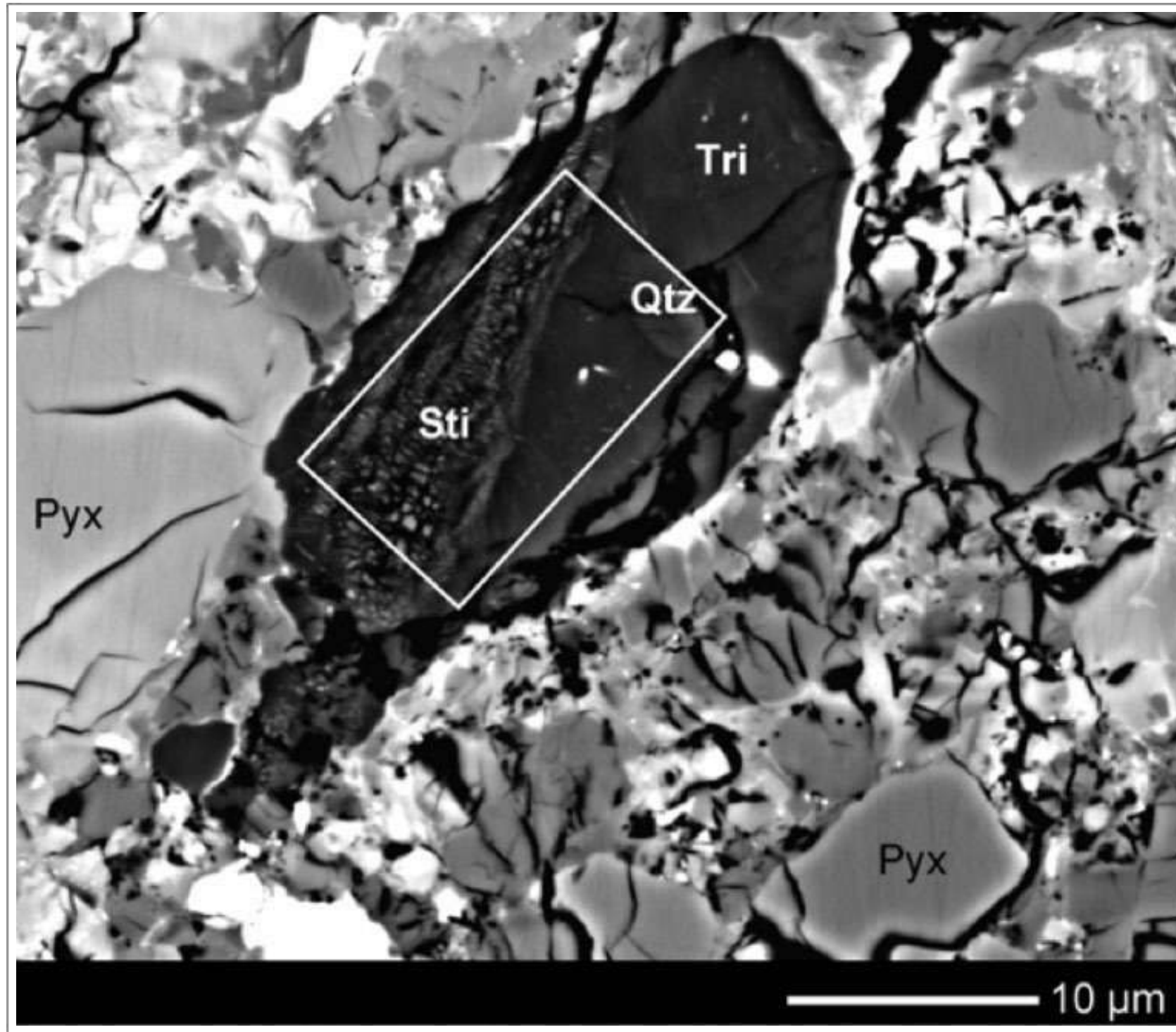
Taken From Kayama et al. (2018)

Micro-Raman spectroscopy and mapping of an amygdaloidal silica micrograin in the breccia matrix of lunar meteorite NWA 2727. (A) High-magnification BSE image of an amygdaloidal silica micrograin. White crosses indicate the analytical points for Raman spectroscopy. (B) Raman spectra of the silica micrograin. Obvious coesite bands are present together with the moganite signature in the rim of the silica micrograin (area 2). a.u., arbitrary units. (C to E) Raman intensity maps of the moganite (C), coesite (D), and quartz (E) bands. Red and blue denote the high- and low-relative Raman intensities of each silica band, respectively. Moganite becomes dominant at the left part of the silica micrograin, whereas quartz is abundant in the right part. Coesite coexists with moganite and occurs in the outermost rim on the left, as indicated by the areas of overlap in the spectra.



Taken From Miyahara et al. (2013)

Backscattered electron images of silica in shock veins in lunar meteorite NWA 4734 showing intergrowths of coesite, cristobalite, stishovite and seifertite. Coe, coesite; Cri, cristobalite; Sti, stishovite; α -PbO₂, seifertite; Ol, olivine; Pyx, pyroxene; SiO₂-Gla, silica glass; Pla, plagioclase glass. TEM slices prepared using a FIB are indicated by the white boxes labelled SP2TEM and SP6TEM.



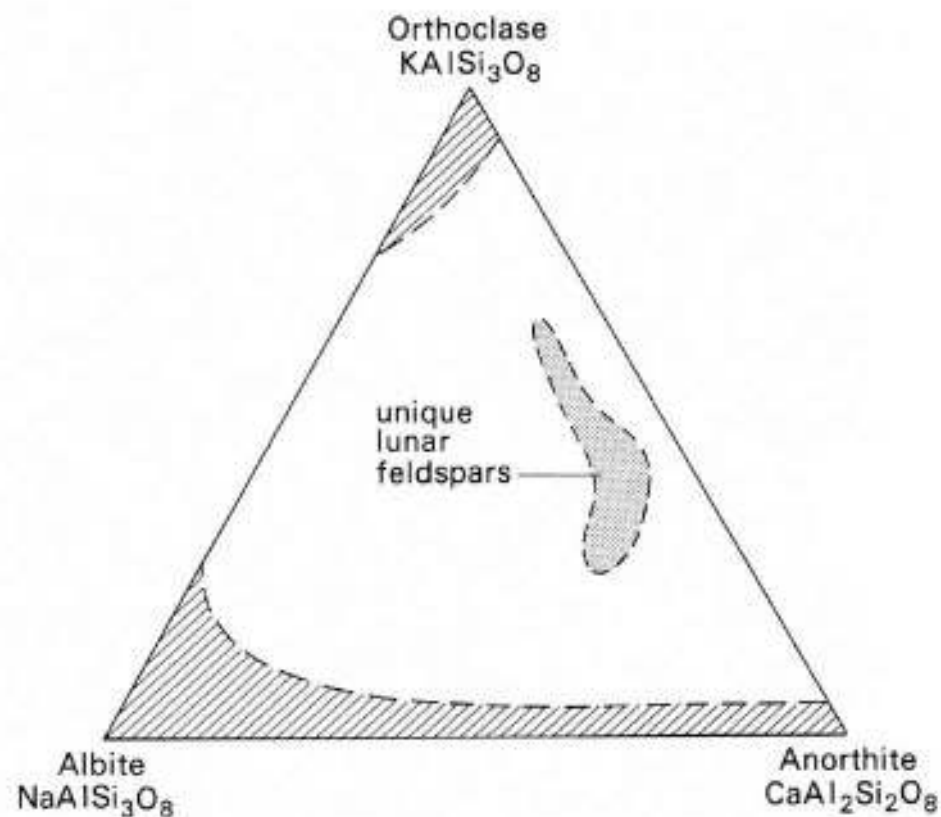
Taken From Kaneko et al. (2015)

Backscattered electron image of a silica grain in Apollo 15 regolith breccia 15299. Qtz = quartz, St= stishovite, Tr = tridymite, Pyx = pyroxene. A rectangular piece excavated for XRD analysis is shown by the white box.

K-Feldspar

SPECIES

1. K-Feldspar - KAlSi_3O_8
2. Hyalophane - $(\text{K,Ba})\text{AlSi}_3\text{O}_8$
3. Barian Sanidine - $(\text{K,Ba})\text{AlSi}_3\text{O}_8$



Feldspar compositions (from Cadogan, 1981).

K-feldspar is a late-stage mineral found in lunar basalts. Because the other basalt minerals (e.g., pyroxene, olivine, and plagioclase feldspar) accept very little of the relatively large K^+ ion into their structures, it becomes concentrated in the residual melt that remains after most minerals have crystallized.

In high-silica highland rocks, which have granitic or so-called “KREEPy” compositions, potassium feldspar is commonly neither minor nor fine-grained. In Apollo 12 sample 12013 (a KREEPy polymict breccia) there are abundant patches of fine-grained granitic material (felsite) that contain 50% potassium feldspar, 40% silica minerals, 5% Fe-rich augite, and 5% other phases (Quick et al., 1981a).

K-feldspar is also found in an unusual K-rich mare basalt type (very high-K basalt), which has been discovered as clasts in two Apollo 14 breccias (14305 and 14168). These clasts contain several percent K-feldspar, which has formed as a late-crystallizing phase with Fe-rich olivine, oxides, and mesostasis glass. It varies in shape from anhedral and interstitial to blocky, subhedral prisms, and in size from 10 to 400 μm . More rarely, oriented glass inclusions in Fe-rich olivine contain tiny (10-15 μm) inclusions of K-feldspar.

Shervais et al. (1985) conclude that these basalts have most likely been produced by the partial assimilation of lunar granite crust by a normal low-Ti mare basalt magma on its way to the surface.

Sample 12023,147-10 is a granitic lithic fragment from the Apollo 12 regolith. It consists of ~80% granophyric intergrowths of K-feldspar and silica and ~15% granophyric intergrowths of plagioclase and silica. A second granite clast contains 35% K-feldspar, 34% silica, 23% plagioclase, 4.2% high-Ca pyroxene, 2.5% low-Ca pyroxene, 1.2% ilmenite, and ~1% zircon and is petrographically dominated by granophyric intergrowths of K-feldspar and silica (Seddio et al., 2012a). A third clast (12032,366-19) is a granite which is primarily composed of graphic intergrowths of Ba-rich K-feldspar (~55%) and silica. It is considered to be a pristine granite that does not contain impact-generated glass or brecciated material (Seddio et al., 2009; 2013b). This sample and granite clasts in polymict breccia 12013 were also examined by Seddio et al. (2011) who suggest they were probably derived from the impact melting of granitic source rocks.

Nemchin et al. (2017) studied felsic clasts in Apollo 14 impact-melt breccias 14083 and 14303. In 14083,35 one clast is composed mostly of fine intergrowths of K-feldspar and silica, although larger elongated crystals (200-500 μm in length) of silica, as well as similar sized crystals of ilmenite and plagioclase, are present on one side of the clast. Pb-Pb analyses of K-feldspar in these clasts indicate a profound resetting of the U-Pb system and homogenisation of Pb at least on a thin section scale during a 3.92 Ga event, interpreted to be the impact that formed the Imbrium basin.

Northwest Africa 773 and related lunar meteorites contain olivine cumulate gabbro and clasts enriched in K,Ba-feldspar. Coarse-grained olivine \pm pyroxene occur with K,Ba-feldspar, feldspathic glass and silica. BaO-content in feldspar ranges up to 8.5 wt%. Ca-phosphates, ilmenite, troilite, \pm baddeleyite are also present. K,Ba-feldspar also occurs in intercumulus domains of the olivine cumulate gabbro. These domains are bordered by olivine and pyroxenes with compositions typical of the gabbro. Calcium phosphates, troilite and ilmenite coexist with the K,Ba-feldspar (range of 1 to 4 wt% BaO) in these domains.

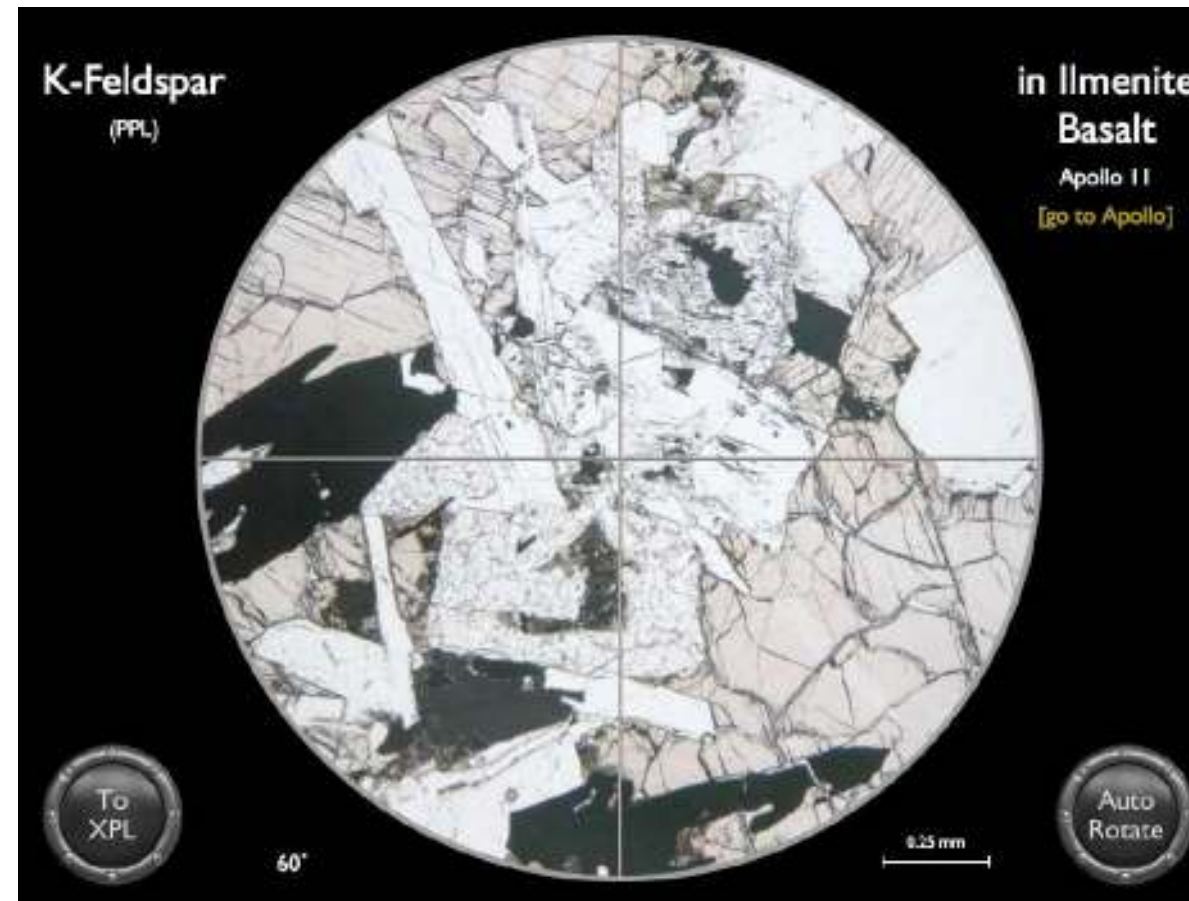
Fractional crystallization of olivine and pyroxene led to enrichments in incompatible K and Ba, among other elements, in inter-cumulate domains of the olivine cumulate gabbro. The residual intercumulus pockets were isolated from the main body of liquid, which subsequently fractionated to form liquid high in K_2O , BaO and $\text{Fe}/(\text{Fe}+\text{Mg})$. Crystallization of this liquid formed the K,Ba-feldspar-bearing clasts (Fagan et al., 2008).

Sparse granophyric clasts in lunar meteorites NWA4472 and NWA4485 consist of “ribbon-like” subparallel intergrowths of silica and barian K-feldspar with accessory baddeleyite and rare tranquillityite. They appear to represent silicic liquids enriched in K, Zr, P and other incompatible elements that were generated by protracted fractional crystallisation of mafic magmas (Kuehner et al., 2007).

Hyalophane is reported in Apollo 14 breccia sample 14063
(Christophe-Michel-Levy and Levy, 1972).

Moon Minerals: K-Feldspar

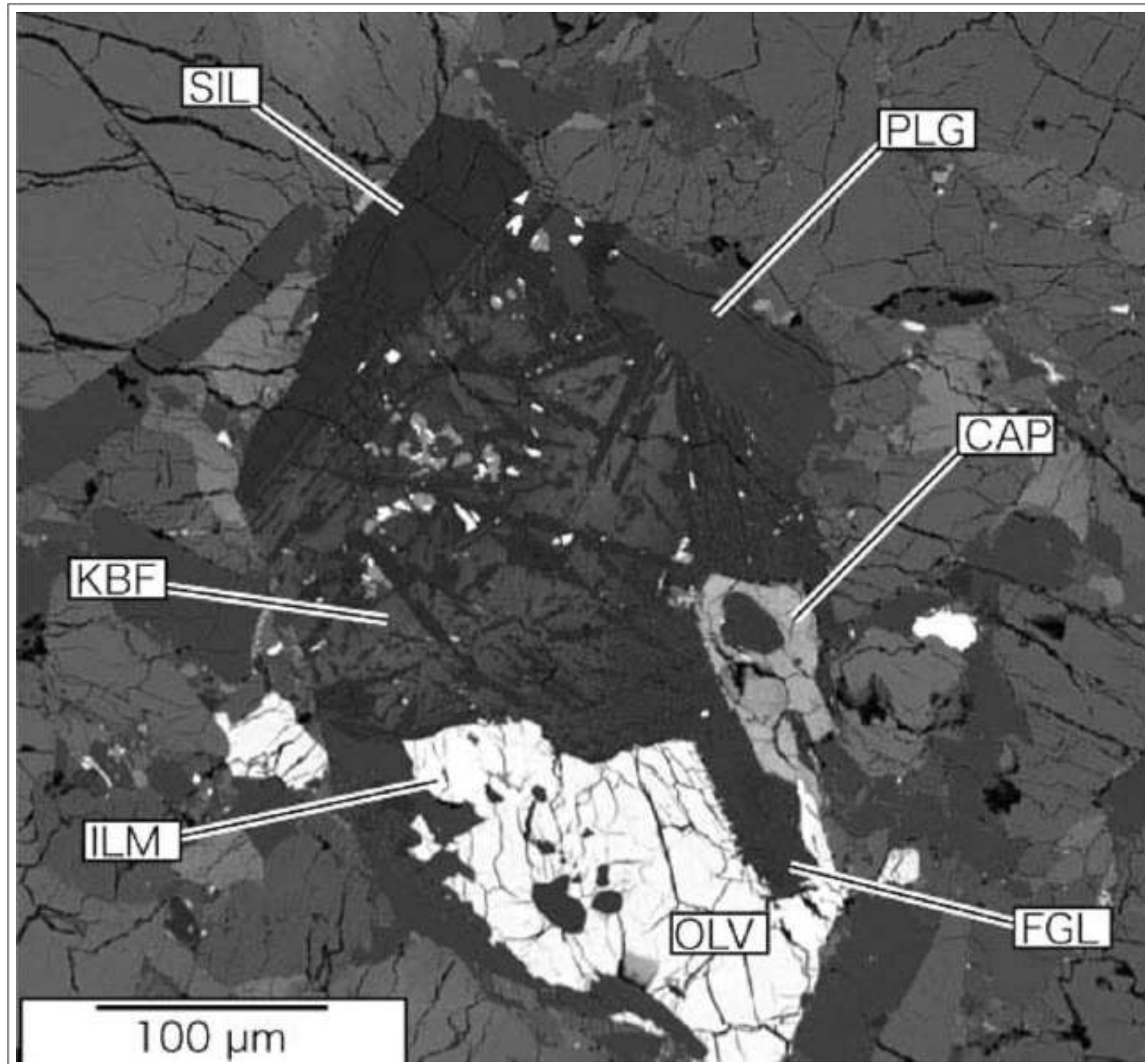
Mineral Virtual Microscope: K-Feldspar



10047 is a relatively coarse-grained, vuggy, ilmenite basalt with an ophitic texture consisting of pyroxene enclosing earlier-formed plagioclase feldspar and ilmenite. Associated with these major species are lower abundances of olivine, pyroxferroite, zirconolite, baddeleyite, phosphate, cristobalite, ulvospinel, troilite and a K-rich glass. This field of view centres on a vuggy area containing cristobalite (crinkly texture) and an untwinned feldspar - possibly K-feldspar.

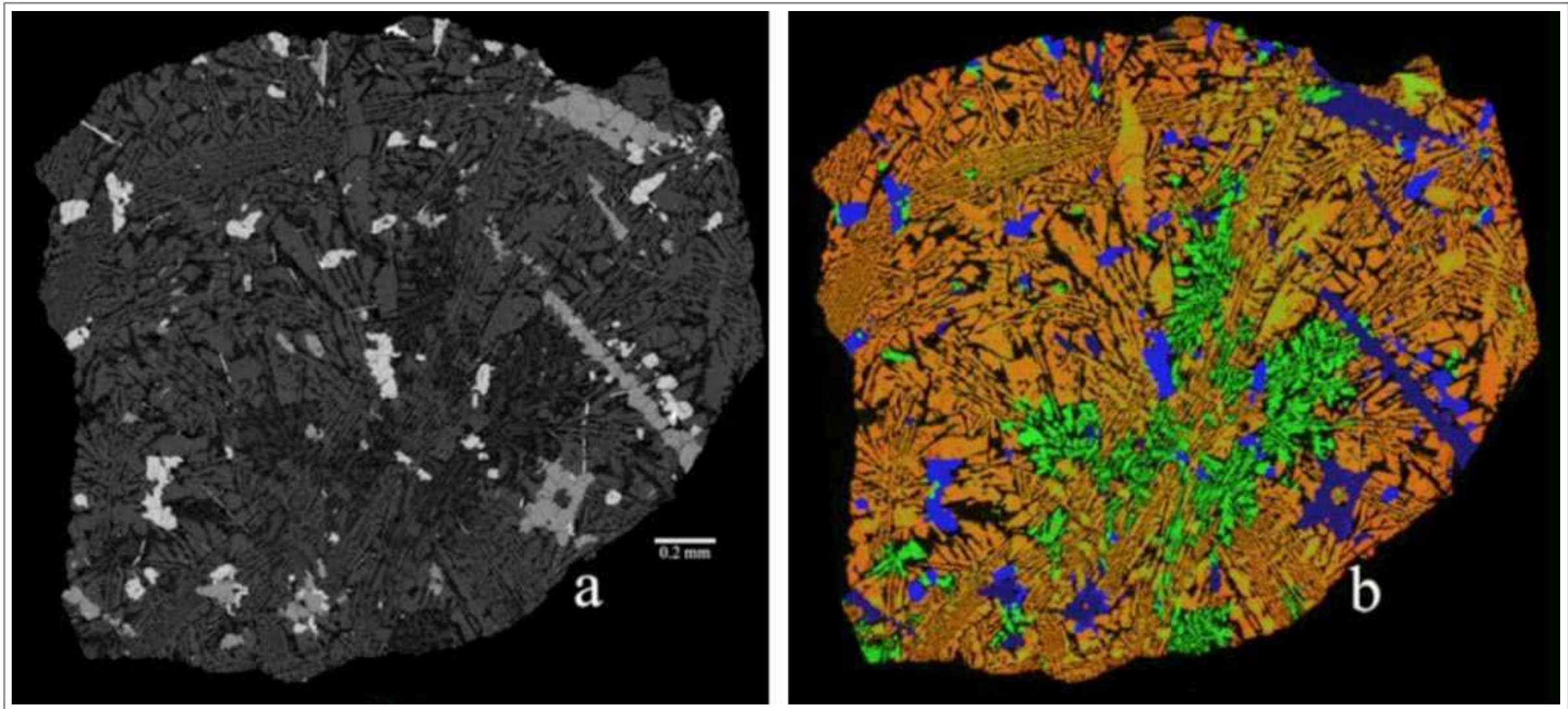
Apollo 11, Sample 10047.

Credit: NASA (AGT Photographer)



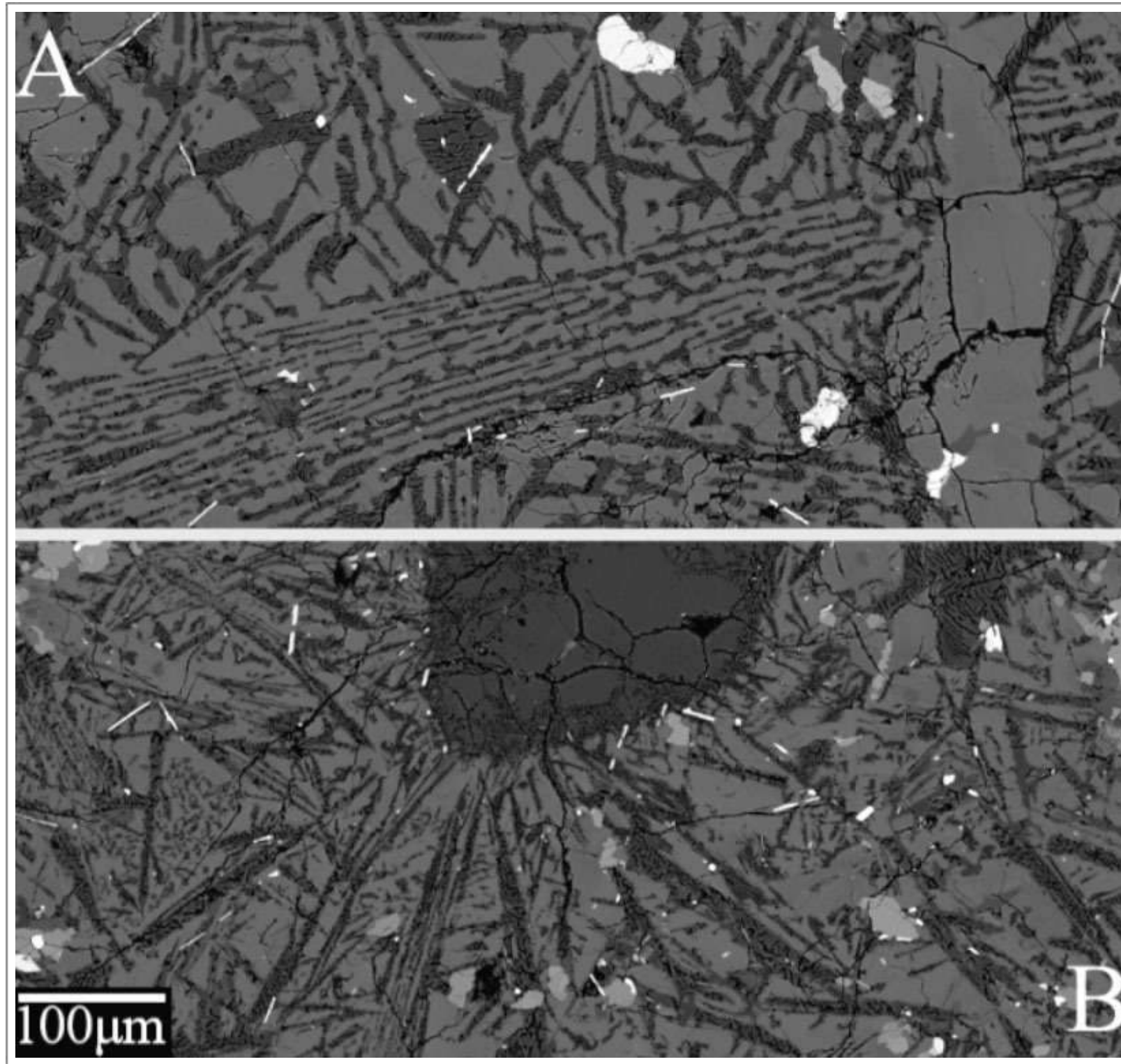
Taken From Fagan et al. (2005)

Backscattered electron image of K,Ba-feldspar clast in NWA 773 group lunar meteorite (either NWA 773 or NWA 2727).
SIL = silica, PLG = plagioclase, KBF = K,Ba-feldspar, ILM = ilmenite, OLV = olivine, CAP = calcium phosphate, FGL = feldspathic glass.



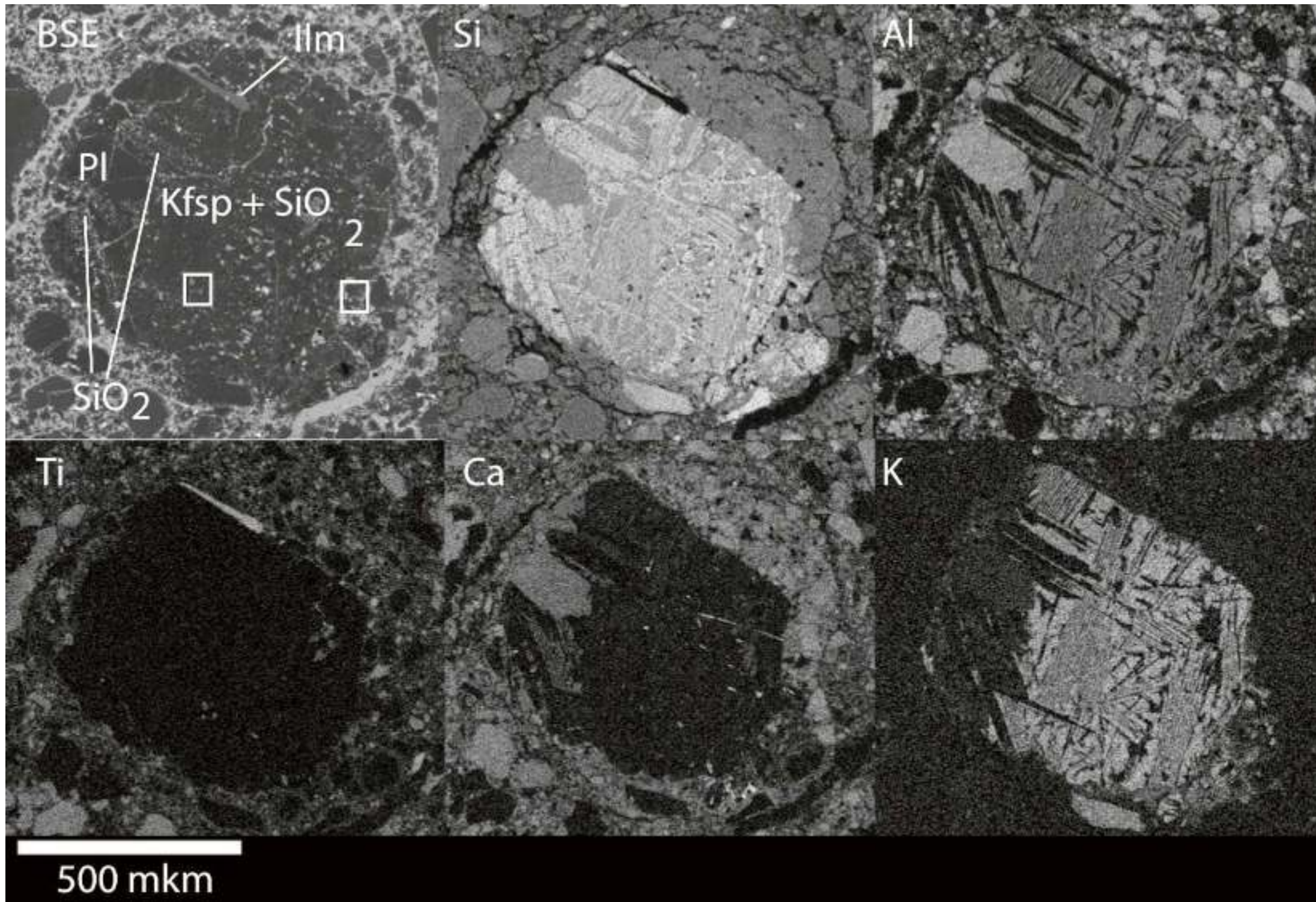
Taken From Seddio et al. (2009)

Apollo 12 regolith granitic lithic fragment 12032,366-19. a. Backscattered electron image. b. Combination X-ray map of K, Na, and Fe converted into an RGB image. Orange is K-feldspar (the lighter orange is K-feldspar with a higher Na content). Bright green is plagioclase feldspar. Bright blue is olivine, and navy blue is pyroxene. Silica is represented as black.



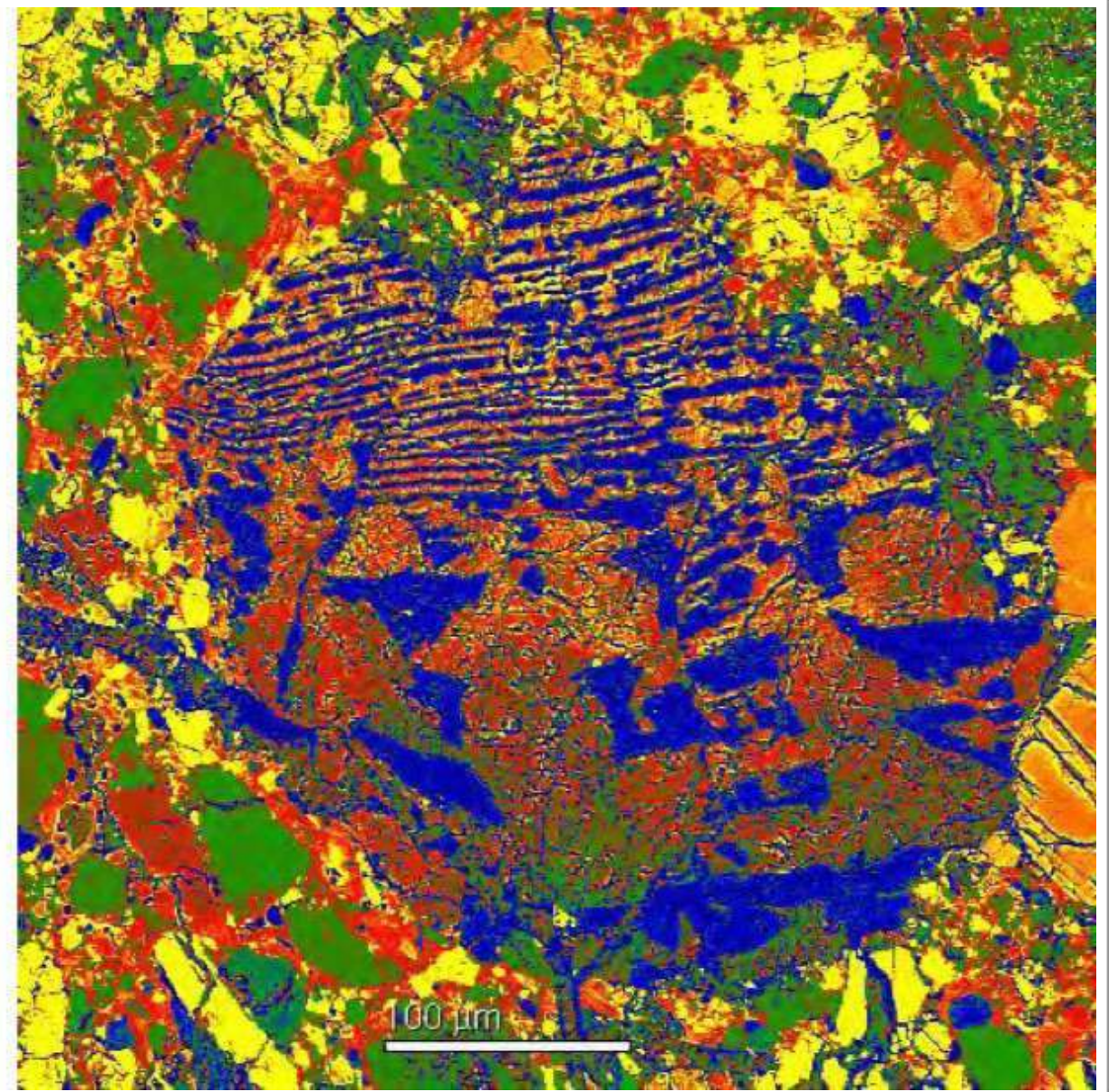
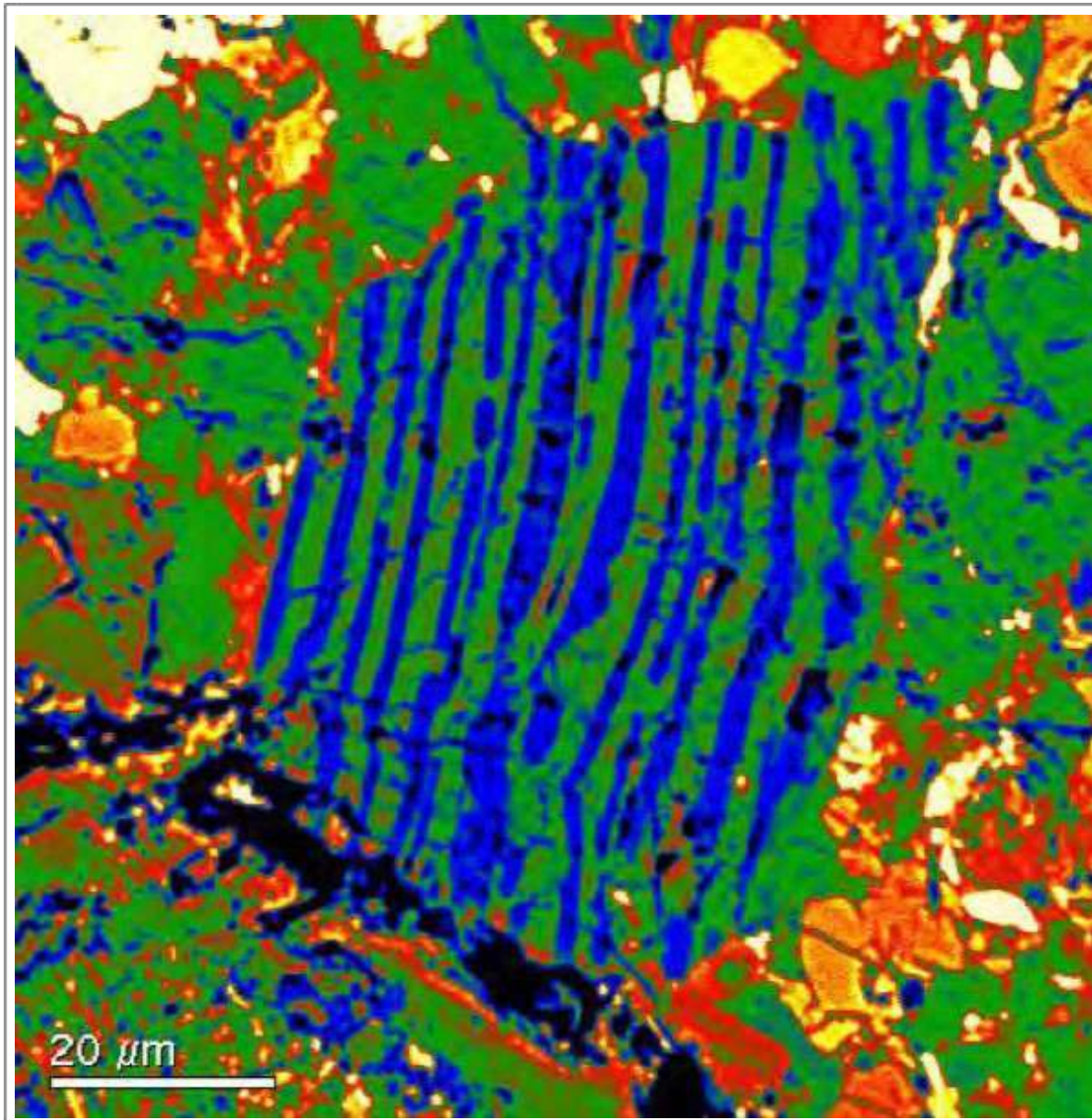
Taken From Seddio et al. (2011)

Backscattered electron images. A: K-feldspar (light grey) and silica (darker grey) intergrowth in Apollo 12 granitic lithic fragment 12032,366-19. B: K-feldspar and silica intergrowth in Apollo 12 granitic lithic fragment 12013,13. A silica bleb is partially visible at top-centre (dark, sub-rounded crystal).



Taken From Nemchin et al. (2017)

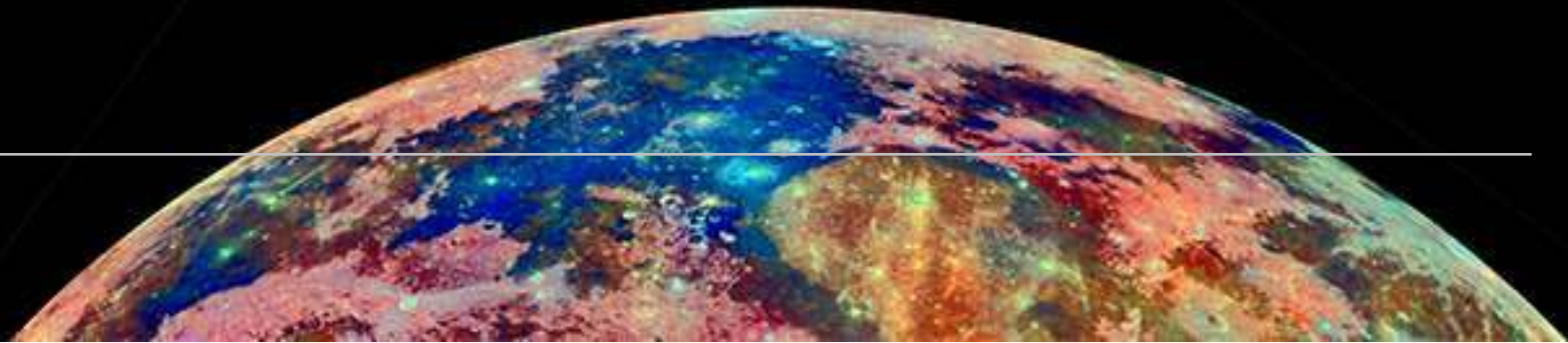
Backscattered electron image and element maps of felsite clast in a felsite clast within Apollo 14 impact-melt breccia 14083, 35. The clast comprises intergrown K-feldspar (Kfsp) and silica (SiO_2) with minor plagioclase (PI) and ilmenite (Ilm).



Taken From Kuehner et al. (2007)

Backscattered electron images of lamellar intergrowth clasts in lunar meteorites NWA 4472 (left) and NWA 4485 (right) - silica (blue), K-feldspar (green to red).

Pyroxferroite



SPECIES

1. Pyroxferroite - $(\text{Ca,Fe})(\text{Fe}^{2+}\text{Mn})_6(\text{Si}_7\text{O}_{21})$

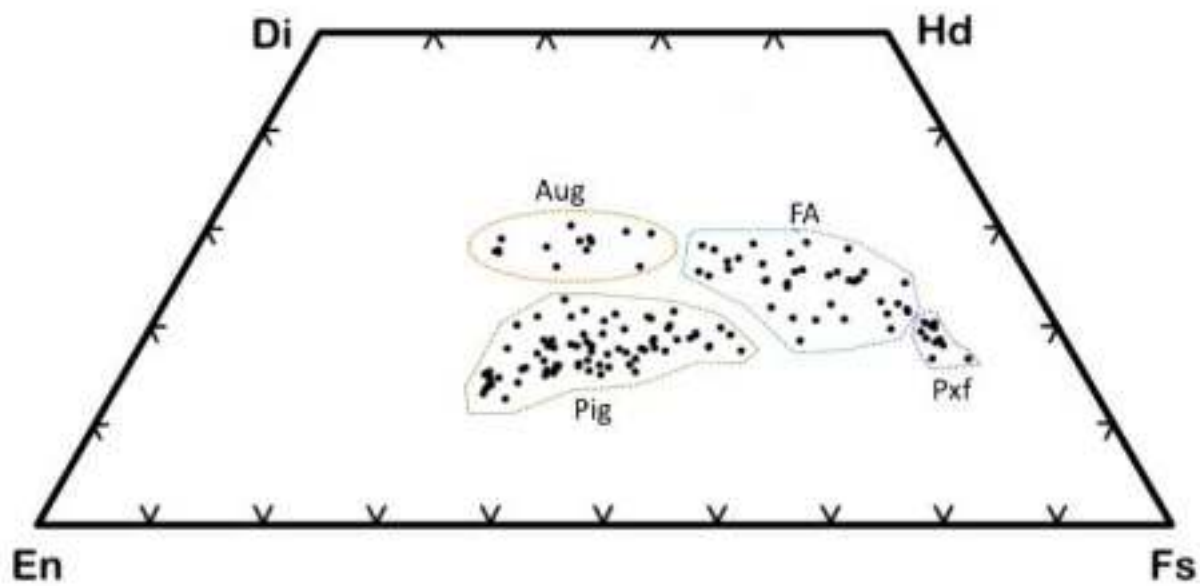
Pyroxferroite, a pyroxenoid with a seven-repeat silicate chain, commonly crystallized instead of pyroxene from the late residua of mare basalts and is associated with cristobalite, tridymite and glass. It has been suggested that pyroxferroite crystallized metastably and was then cooled so rapidly that a more stable assemblage was unable to form. Samples from Apollo 12 olivine basalt 12021 and two Apollo 14 basaltic soils (14163 and 14168) were used in heating and Mössbauer experiments (Lindsley et al., 1972). Their results indicate that such lunar basalts cooled to below 900°C within three days after crystallization of pyroxferroite. If they had remained above this temperature for a longer time, the pyroxferroite would have broken down to the three stable minerals - Ca-rich pyroxene + fayalite (Fe_2SiO_4) + tridymite (SiO_2).

Pyroxferroite was first recognized in 1969 as an unidentified yellow mineral that seemed to be concentrated in vuggy areas of microgabbro and diabase samples such as Apollo 11 ilmenite basalt 10047. The principal minerals are sub-calcic augite, ilmenite and calcic plagioclase (Chao et al., 1970).

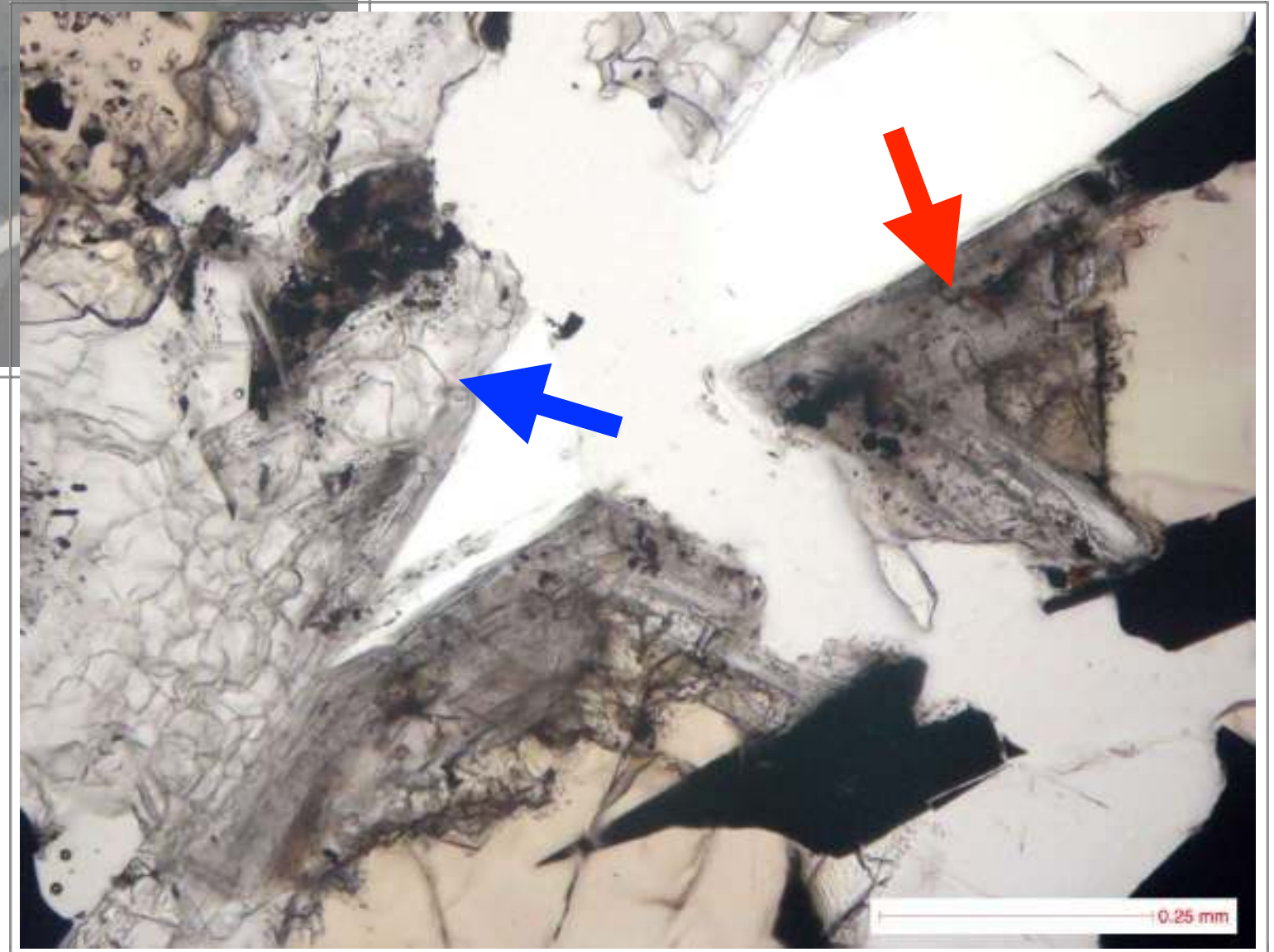
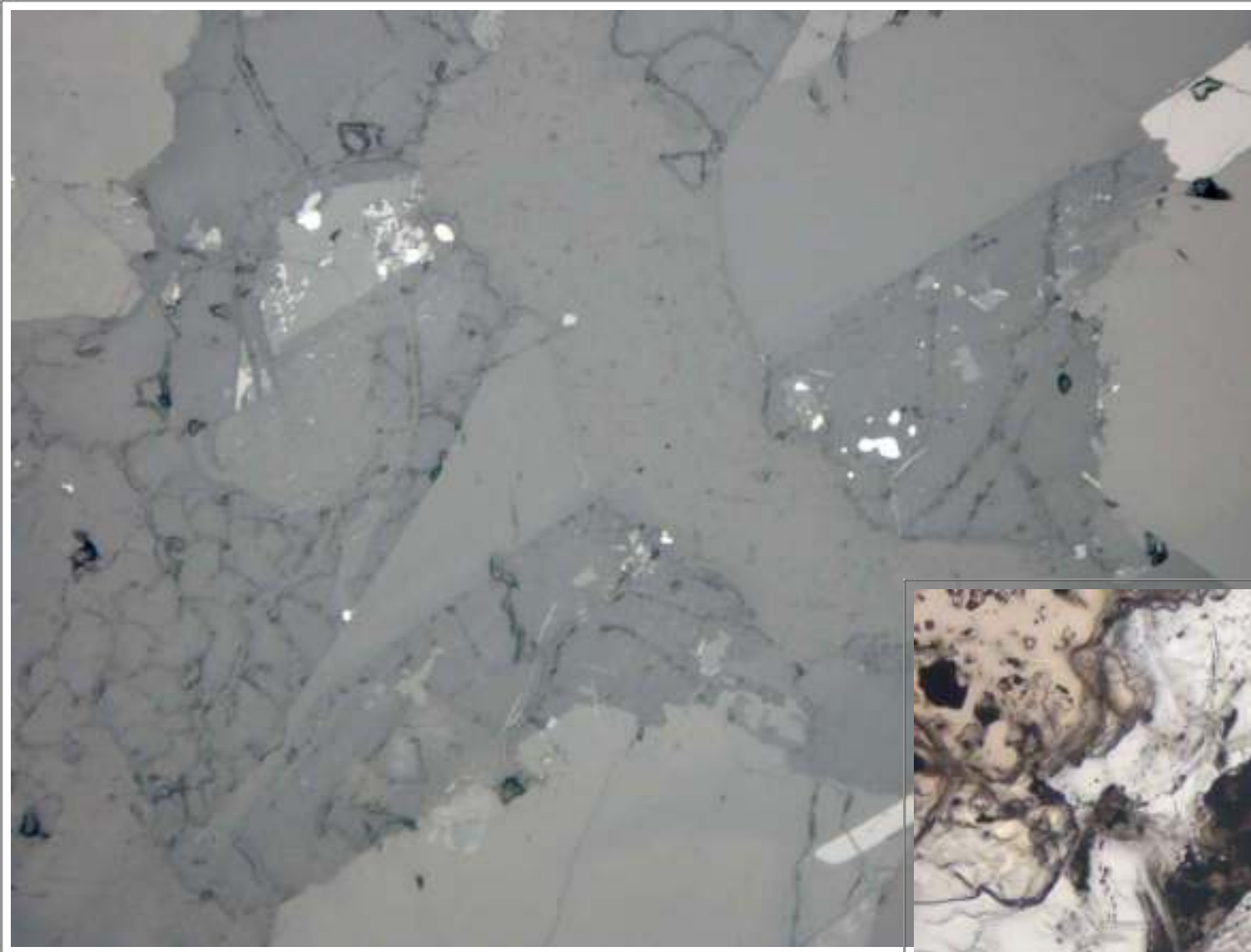
Apollo 11 ilmenite basalt 10044 hosts Fe-rich, Mn-poor yellow pyroxferroite containing euhedral inclusions of fluorapatite (Fuchs, 1970).

Pyroxferroite has also been reported in lunar meteorites, such as Dhofar 925, 960 and 961 - all impact-melt breccias. Here it is associated with the pyroxenes pigeonite and augite (Demidova et al., 2005).

North et al. (2013) report the presence of pyroxferroite in a ferroan gabbro clast within lunar meteorite NWA 2727 and imply that the grain must have crystallized relatively rapidly, perhaps in a shallow intrusive, in order to preserve a composition within a metastable “forbidden zone” and to not form separate grains of hedenbergite, fayalite and silica.

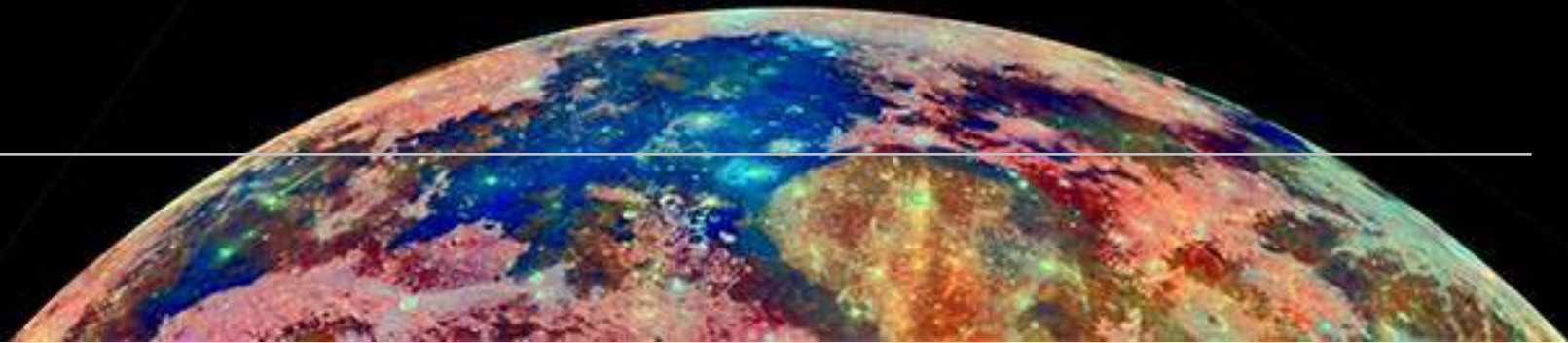


Pyroxene quadrilateral of the ferroan gabbro clast in lunar meteorite NWA 2727 (North et al., 2013). All measurements fall in the ranges of pigeonite (Pig), augite (Aug), ferroaugite (FA) and pyroxferroite (Pxf).



Plane polarised (right) and reflected light (top) images of a melt pocket in Apollo 17 ilmenite basalt 78135. Pyroxferroite (red arrow) appears as a zoned overgrowth on earlier formed pyroxene. Cristobalite (blue arrow) is an associated species. Width 0.5 mm. Credit: NASA (AGT Photographer).

Cordierite



SPECIES

1. Cordierite - $\text{Mg}_2\text{Al}_4\text{Si}_5\text{O}_{18}$

A single grain of cordierite is reported from an Apollo 17 spinel troctolite clast within a polymict breccia (72435,8). It contains olivine and plagioclase along with Mg-rich spinel grains (Herzberg and Baker, 1980; Shearer et al., 2015b).

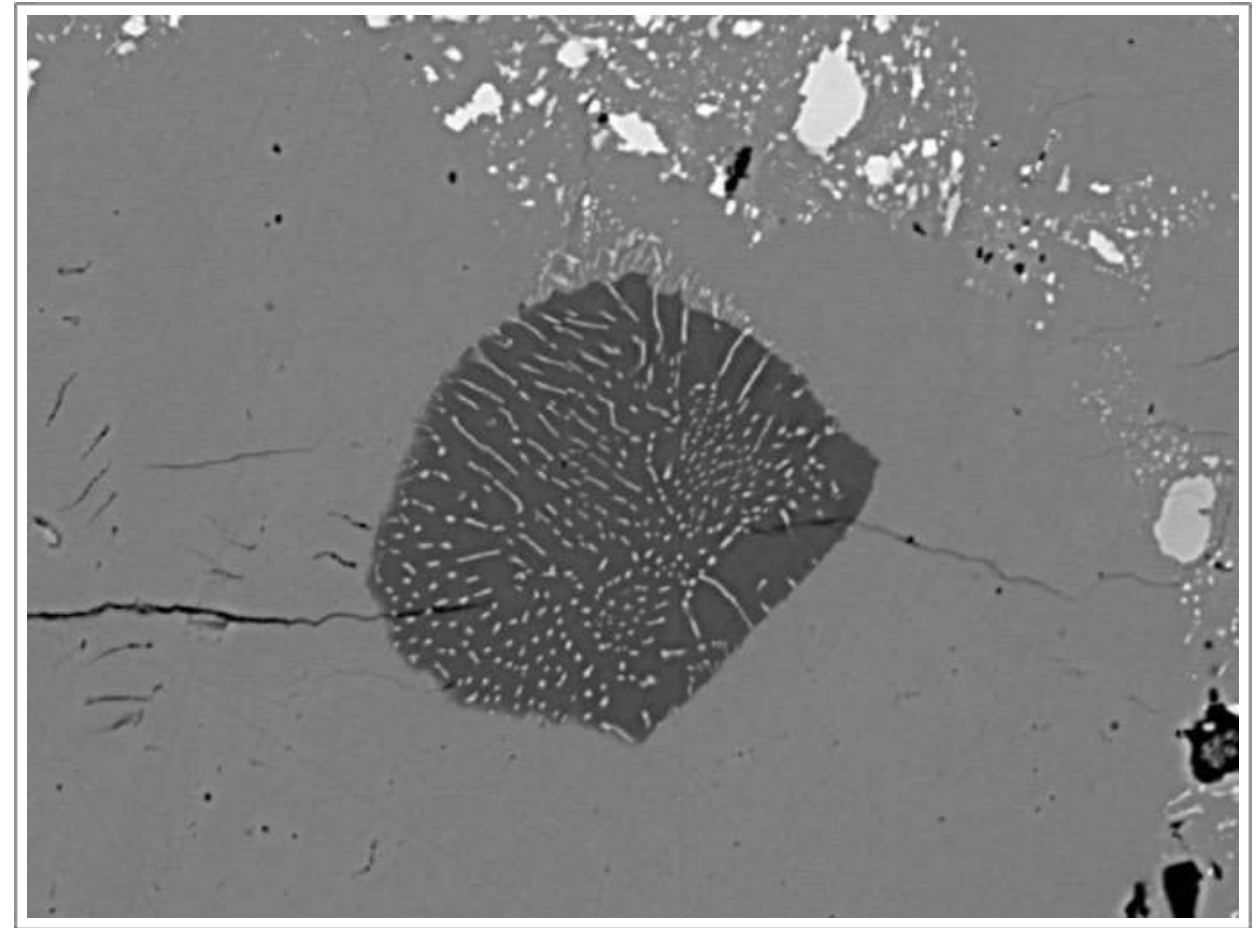
A clast of spinel troctolite containing 8 percent cordierite has been identified among the constituents of Apollo 15 regolith breccia 15295. The cordierite and associated anorthite, forsteritic olivine, ilmenite and pink pleonaste spinel represent a new, Mg-rich lunar highlands lithology that formed by metamorphism of an igneous spinel cumulate. The cordierite-forsterite pair in the assemblage is stable at a maximum pressure of 2.5 kilobars, equivalent to a depth of 50 kilometres, or 10 kilometers above the lunar crust-mantle boundary. The occurrence of the clast indicates that spinel cumulates are a more important constituent of the lower lunar crust than has been recognized. The rarity of cordierite-spinel troctolite among lunar rock samples suggests that it is excavated only by large impact events, such as the one that formed the adjacent Imbrium Basin (Marvin et al., 1989).

Tremain et al. (2012) add that spinel-rich rocks may be widespread in the lunar crust where picritic magmas assimilated anorthositic rock. If a spinel-rich mesocumulate rock were in the target of a significant impact, heat of the impact and pressure release (as from central peak uplift) could have partially melted the cumulate, and that partial melt could have been drawn off into an intrusion or into

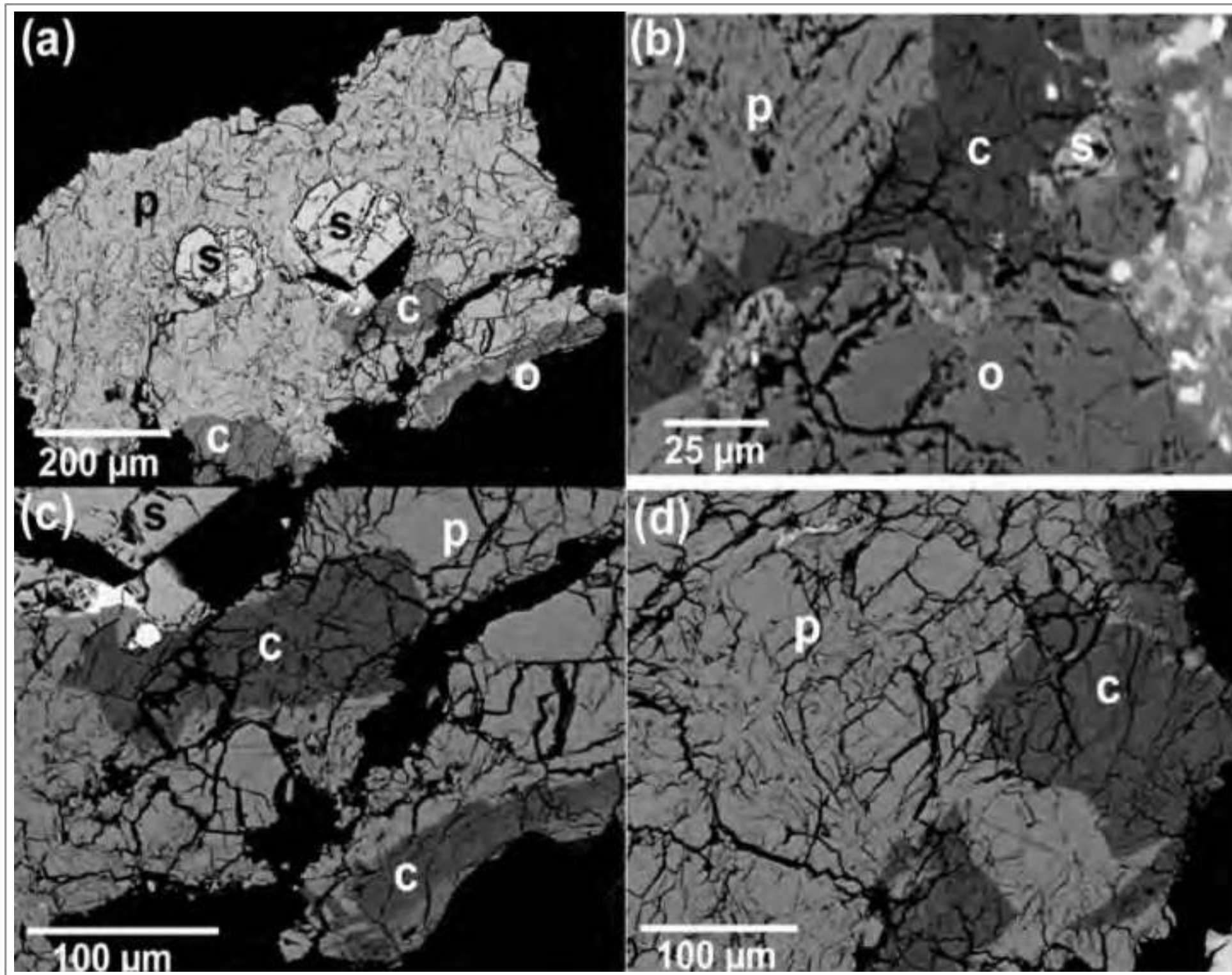
impact melt. This partial melt could then crystallize to rocks like the cordierite-spinel-troctolite.

Cordierite is also present in the Dhofar 025 lunar feldspathic meteorite - an anorthositic impact melt breccia containing mineral and lithic fragments set within a glassy impact melt matrix. One grain of plagioclase (150 x 280 μm in size) set within the impact-melt matrix of the meteorite contains an inclusion of polygonal shape (43 x 50 μm in size). The inclusion has mostly a sharp boundary with the host plagioclase. One side of the inclusion contacts with the impact-melt matrix of the meteorite. The inclusion consists of symplectite intergrowths cordierite and an Al-rich phase (<1 of μm in size) that is too small for a precise analysis but appears to be pleonaste (Demidova et al., 2015).

Wittmann et al. (2018) suggest that the cordierite crystals found in vitric melt lunar meteorite Dhofar 1528 formed from reactions of spinel with impact melt at low pressures, although they note it is possible they may represent assemblages that re-equilibrated at shallower depths than ~30-50 km.

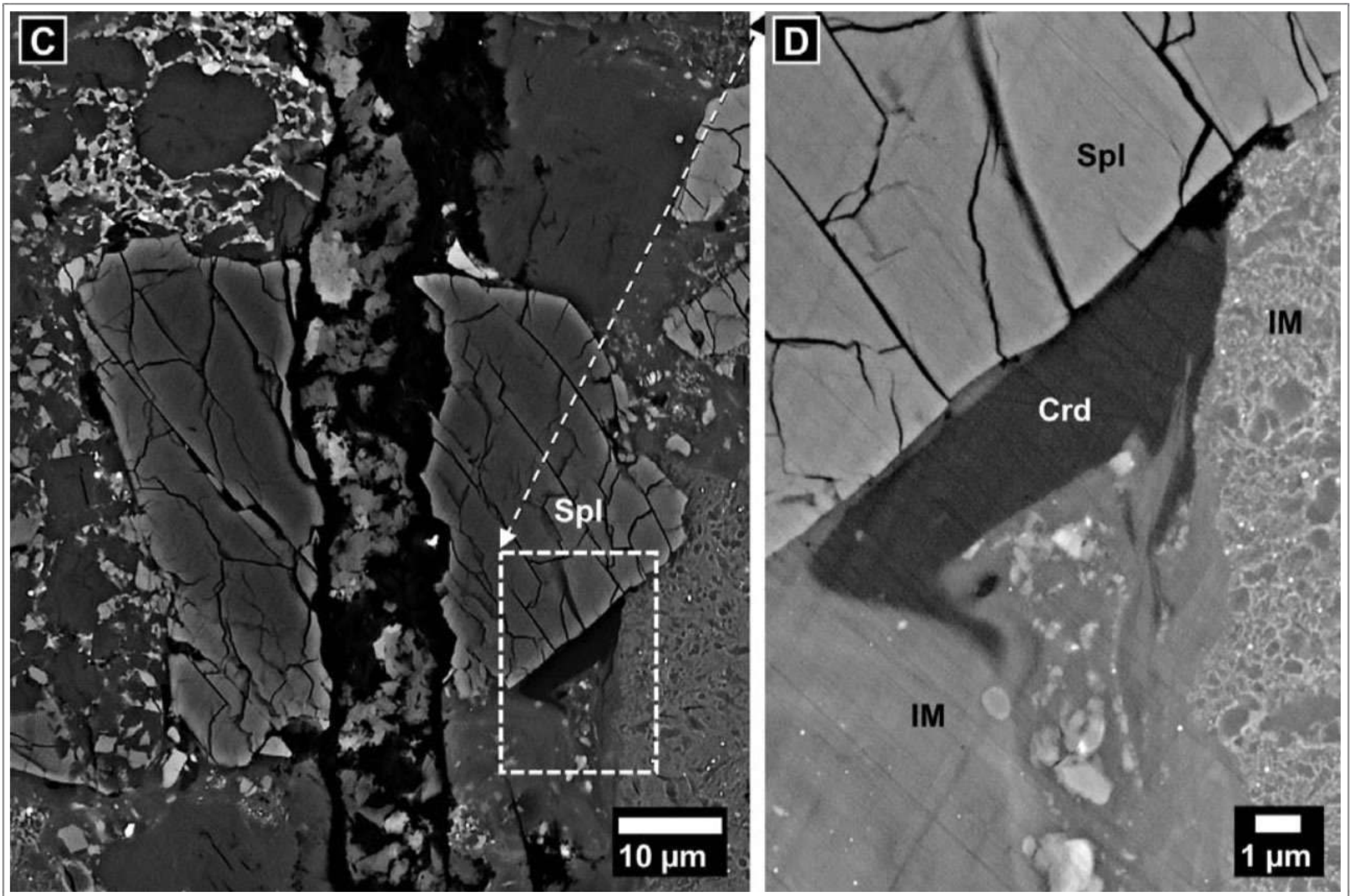


Backscattered electron image of the cordierite-pleonaste inclusion found in lunar feldspathic meteorite Dhofar 025. cordierite - dark grey; pleonaste spinel - light grey filaments (Demidova et al., 2015). Width of cordierite grain 50 μm .



Taken From Treiman et al. (2012)

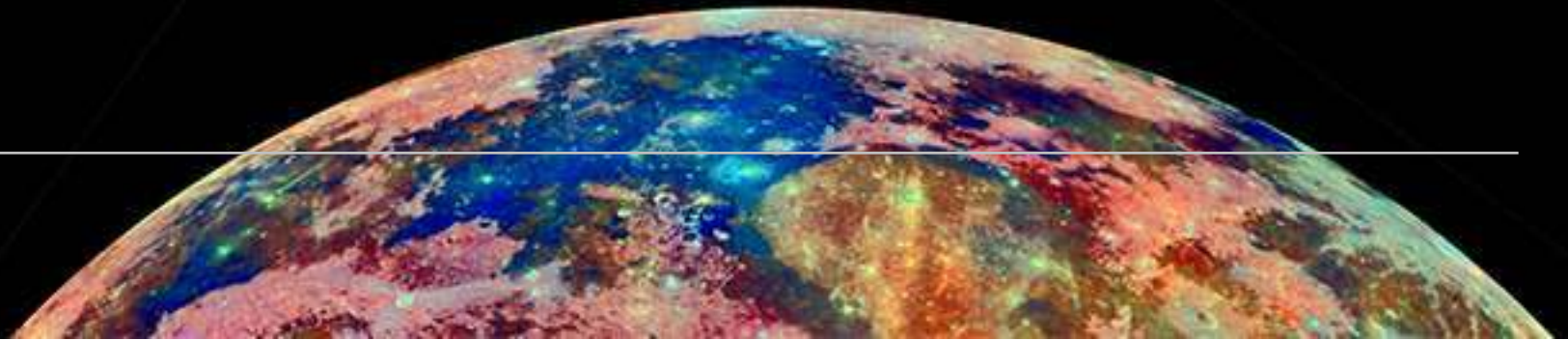
Backscattered electron images of cordierite troctolite in Apollo 15 sample 15295. (a) Two spinel euhedra and many cordierite anhedral grains in plagioclase. Brightest-tone grains are ilmenite and rutile. (b) Cordierite and spinel on a grain boundary between plagioclase and olivine. (c) Detail of a, showing anhedral, rounded cordierite in plagioclase. (d) Cordierite grains with linear boundaries in plagioclase. Minerals are: c, cordierite; p, plagioclase; s, spinel; o, olivine.



Taken From Wittmann et al. (2018)

Backscattered electron images of cordierite assemblages in vitric breccia lunar meteorite Dhofar 1528. Angular spinel clast (Spl) with planar fractures and cordierite (Crd) intergrowth. IM-impact-melt clasts.

Almandine

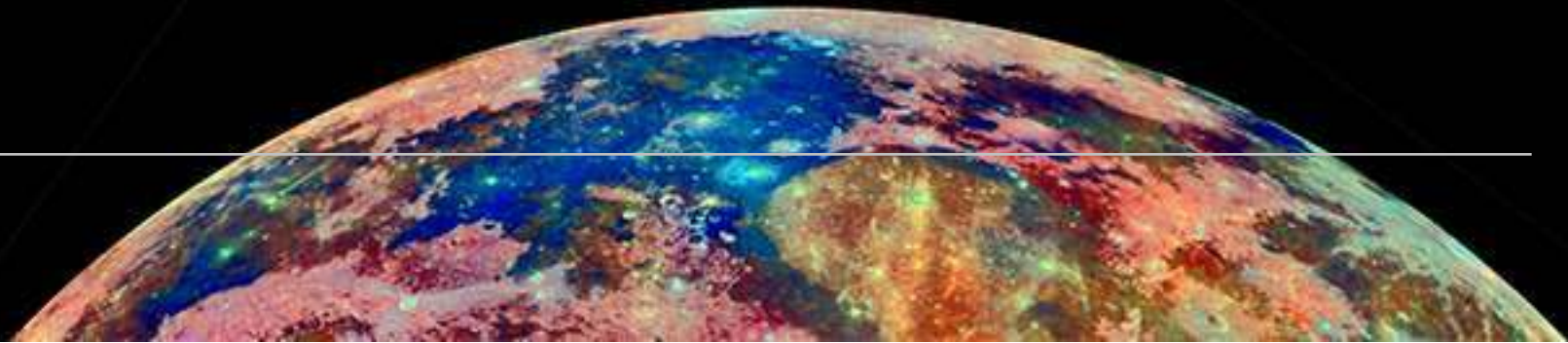


SPECIES

1. Almandine - $\text{Fe}_3\text{Al}_2\text{Si}_3\text{O}_{12}$

Loose grains of almandine-rich garnet from Apollo 12 mare basalt 12021 were interpreted as rare constituents of late differentiates (Traill et al., 1970). Of more general interest is the speculation that a garnet precursor was involved in the generation of Apollo 15 ol-opx-plag cataclasite 15445 (Ridley et al., 1973). For all models of the Moon which involve compositions dominated by olivine, pyroxene, and plagioclase, garnet must be considered as a possible constituent at depth (Smith and Steele, 1976).

Yoshiokaite



SPECIES

1. Yoshiokaite - $\text{Ca}(\text{Al},\text{Si})_2\text{O}_4$

Yoshiokaite has been found at the Fra Mauro Base (Apollo 14) in regolith breccia 14076. The 2 gm sample is in two parts, separated by a sharp contact. The first part is typical Apollo 14 regolith, whereas the other part is exotic and contains yoshiokaite. It is thought to represent an old and previously unknown regolith. The exotic portion has no agglutinates (vesicular glass-bonded soil) and very few glass spheres. Yoshiokaite occurs as single crystal grains and as small intergrown crystals within devitrified glasses. Most abundant (12 of the 18 particles studied) are fragments of devitrified glass. Six of the 18 yoshiokaite particles are single crystals ranging in size from 45 to 235 μm . These crystals are generally fractured and have patchy to undulatory extinction. Lamellae that may be shock-induced occur in most of the crystals. Crystals larger than 50 μm are severely fractured.

Although yoshiokaite is hexagonal, most of the crystals in regolith breccia 14076 have anomalous optical properties due to strain. All grains are optically positive. Birefringence is -0.02 or less, and single crystals generally have undulatory or patchy extinction. In devitrified glasses with 30 wt% SiO_2 , crystals of yoshiokaite are interlocking, angular, and anhedral, with no preferred orientation. The devitrified glasses with 34 wt% SiO_2 , have spherulites and plumose crystals with inclined extinction.

The melting and cooling conditions for this mode of formation are readily produced by impact melting (Vaniman and Bish, 1990).

Apollo 14 regolith breccia 14076.

(A) plumose to spherulitic relatively high-silica glass (34 wt%SiO₂) of uncertain mineral content.

(B) granular devitrified silica-poor (22 wt%SiO₂) glass with anhedral interlocking crystals of yoshiokaite; note gradation from relatively coarse (5-15 μm) grains to finer (1-2 μm) grains at the rim of the devitrified glass (crossed polarizers).

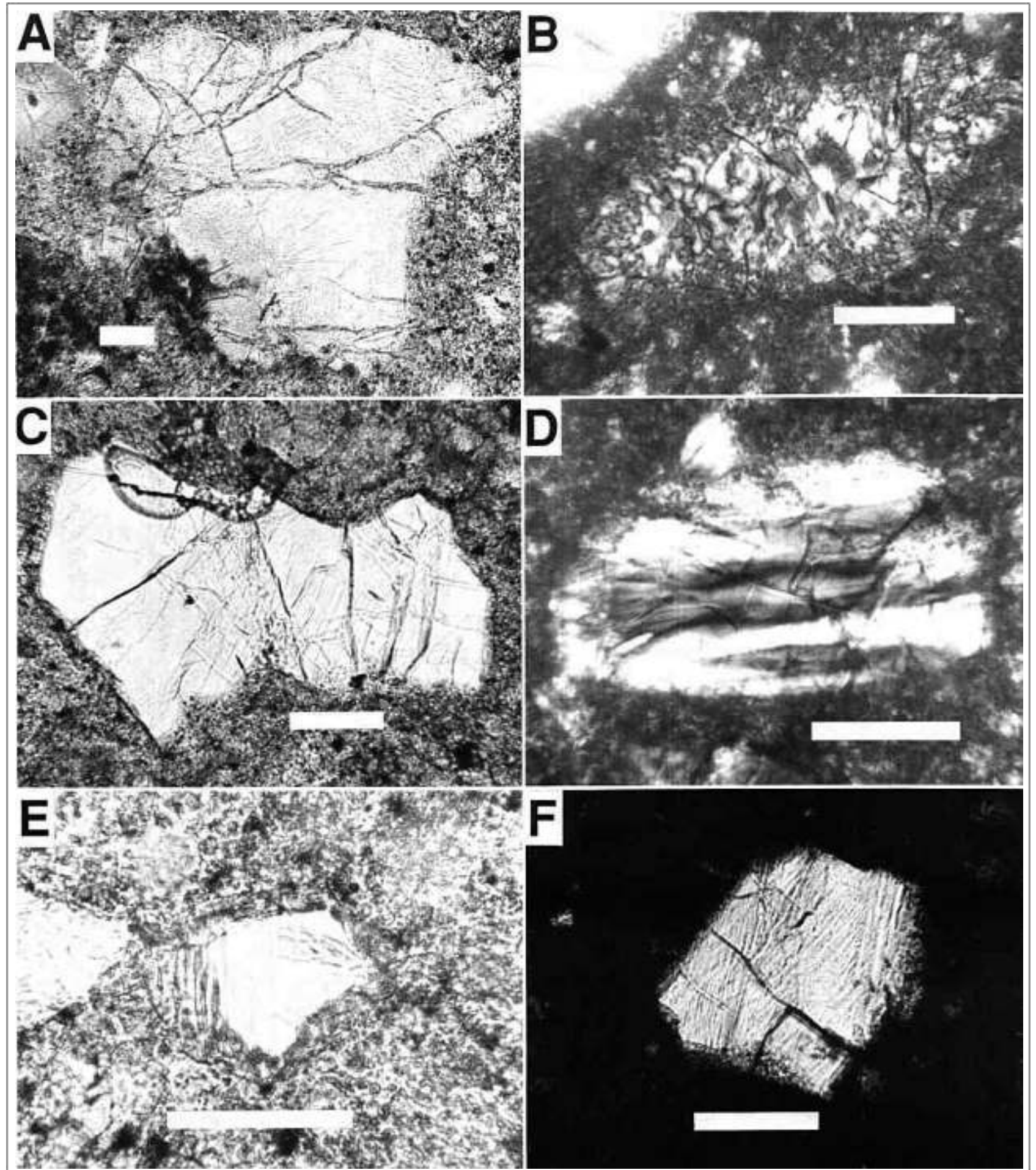
(C) largest yoshiokaite crystal yet found; note fracturing probably caused by shock deformation.

(D) streaked and patchy birefringence in shocked yoshiokaite crystal (crossed polarizers).

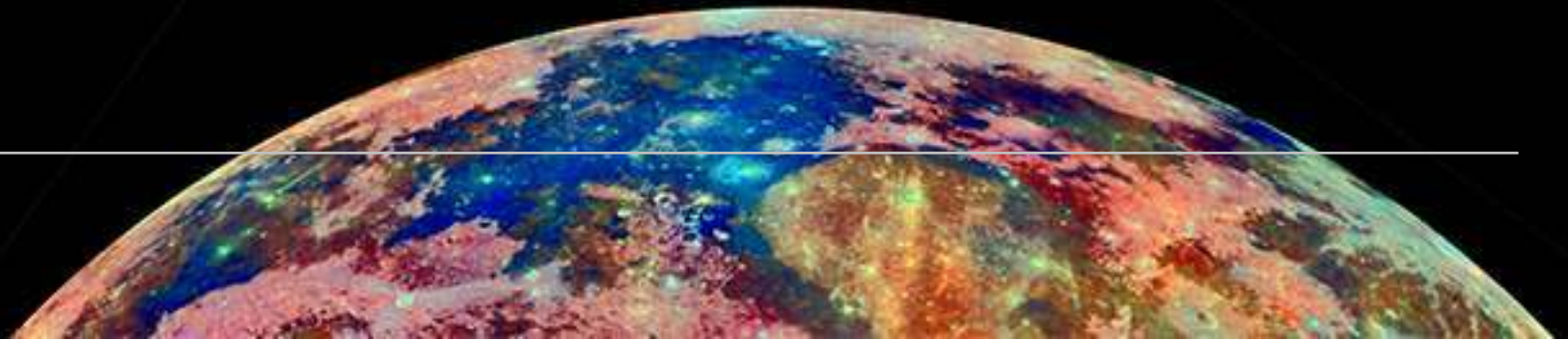
(E) shock lamellae in small yoshiokaite crystal

(F) sets of shock lamellae in yoshiokaite, crossed by poorly developed cleavage (dark fractures trending NW; crossed polarizers).

White scale bar in each photomicrograph is 50 μm long.



Rhönite



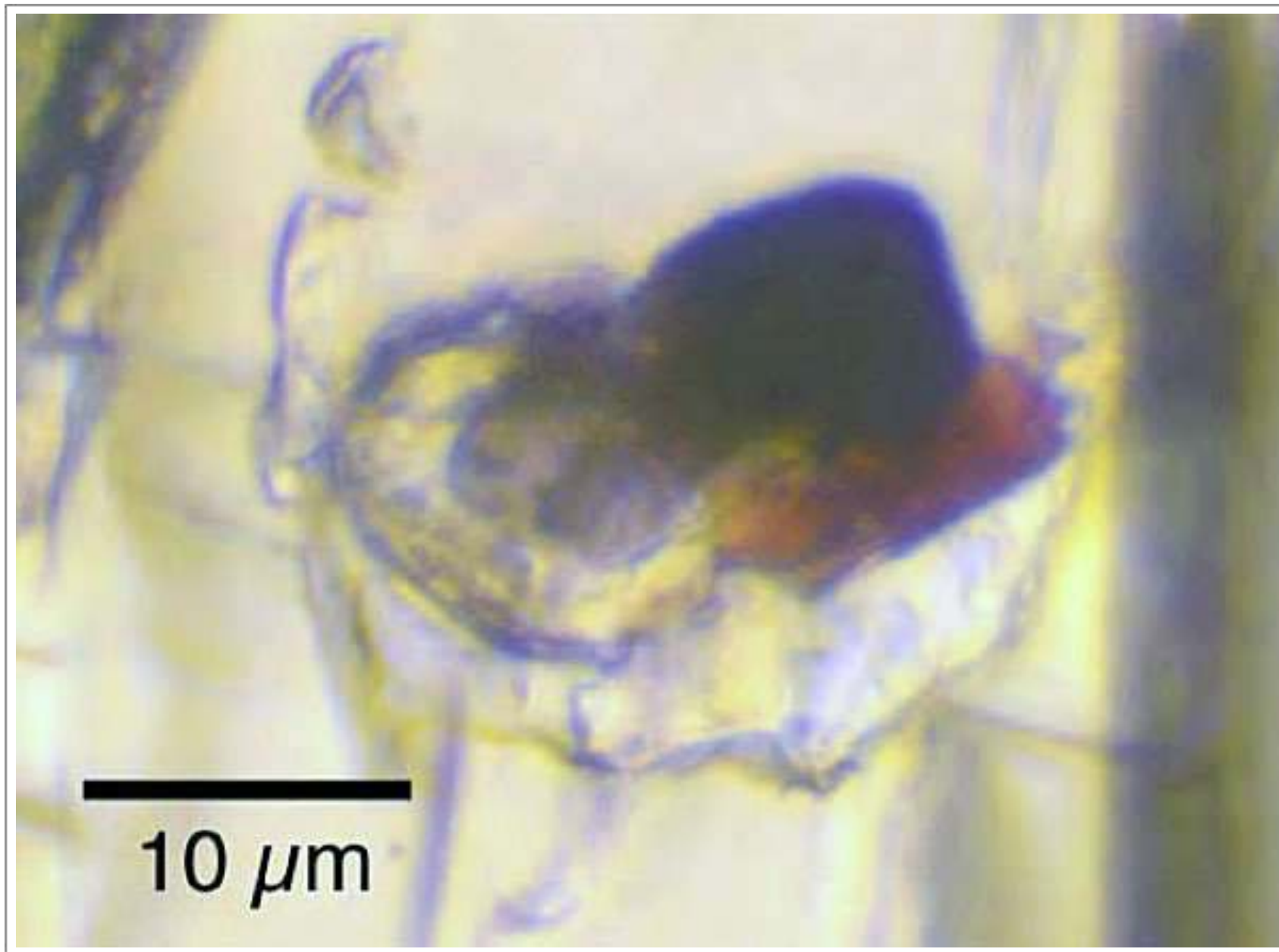
SPECIES

1. Rhönite - $\text{Ca}_2(\text{Mg}, \text{Fe}^{2+}, \text{Fe}^{3+}, \text{Ti})_6(\text{Si}, \text{Al})_6\text{O}_{20}$

Rhönite has a composition similar to that of kaersutite amphibole. It has been found in magmatic inclusions in pyroxene from the regolith sample collected in 1976 during the Luna 24 mission. The Luna 24 regolith contains mineral fragments, rock fragments, and glasses. Most mineral fragments are pyroxene (pigeonite and augite), and most of them contain glassy inclusions with or without crystalline phases. These inclusions are interpreted as magmatic inclusions - remnant of magma trapped in growing crystals.

Magmatic inclusions in several pyroxenes contain tabular brown crystals which are optically anisotropic, pleochroic from pale greenish brown to reddish brown, and with inclined extinction. Ulvöspinel is an associated species.

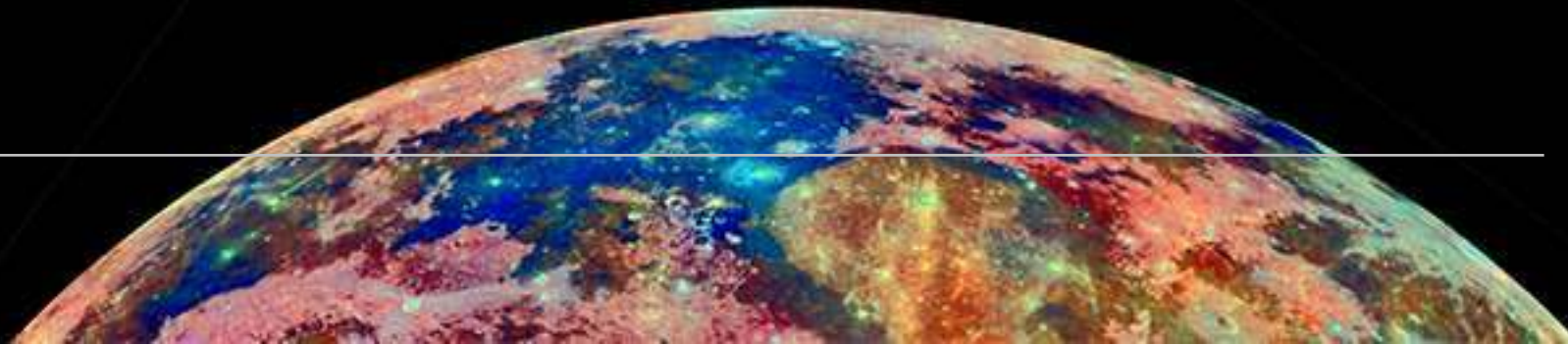
The significance of rhönite is in its implication for volatiles in planetary magmas, specifically in comparison with kaersutite amphibole. Kaersutite decomposes to rhönite (and other phases) in heating and/or dehydration, so volatile-poor lunar magmas would be expected to produce rhönite, not kaersutite (Treiman, 2007).



Taken From Treiman (2007)

Transmitted light image of rhönite (brown) associated with ulvöspinel (black) in lunar regolith collected during the Luna 24 mission. Both species are inclusions within pyroxene.

Keiviite-(Y)



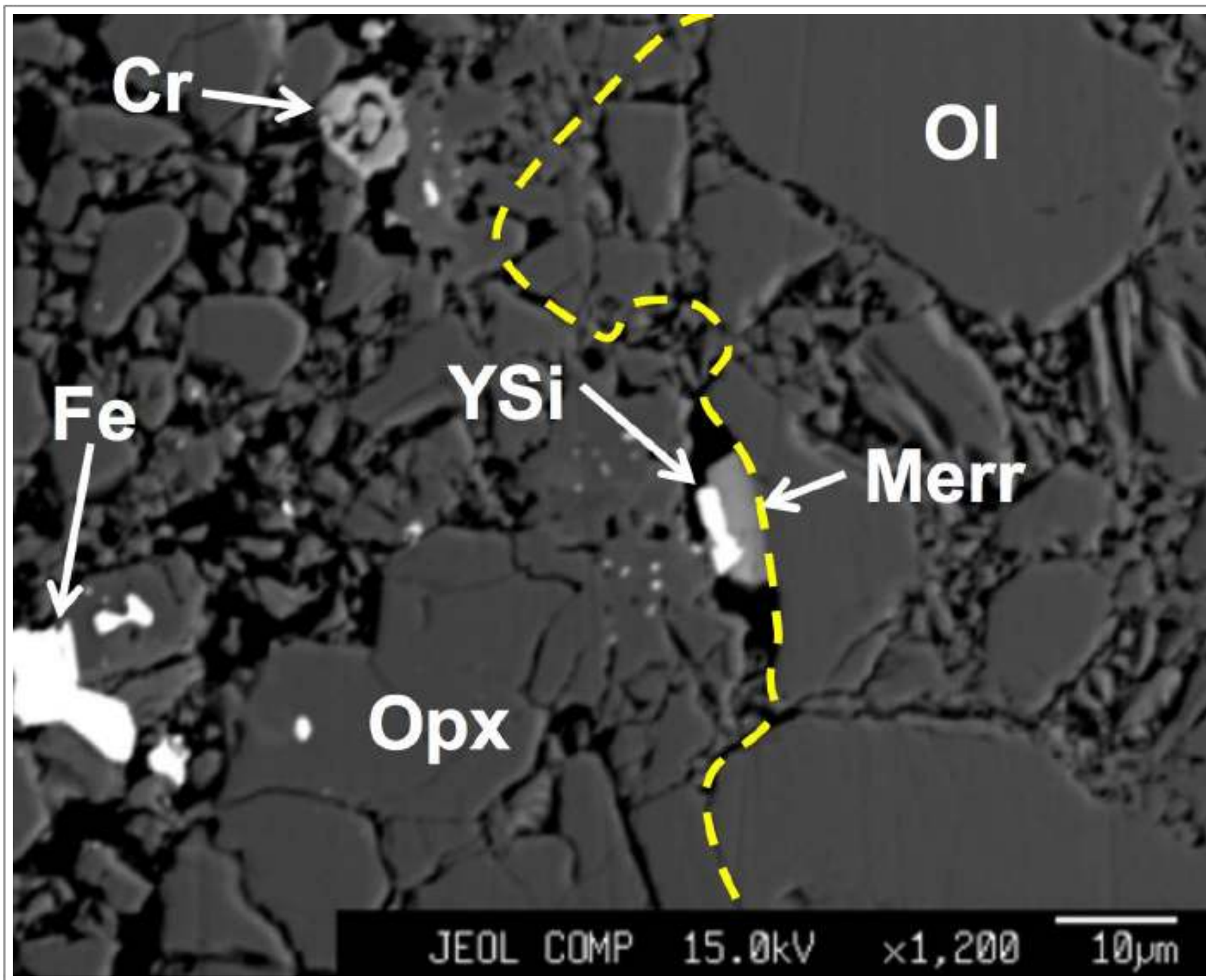
SPECIES

1. Keiviite-(Y) - $(Y,REE)_2Si_2O_7$

Keiviite-(Y)

In terrestrial environments, keiviite-(Y) occurs in rocks subjected to high Y activity with readily available Si. These conditions are reported from the Kola peninsula of Russia, within the quartz and fluorite vein-fill of amazonitic pegmatites. Here Y and heavy REE-rich species are mostly found in rocks exhibiting extensive metasomatism.

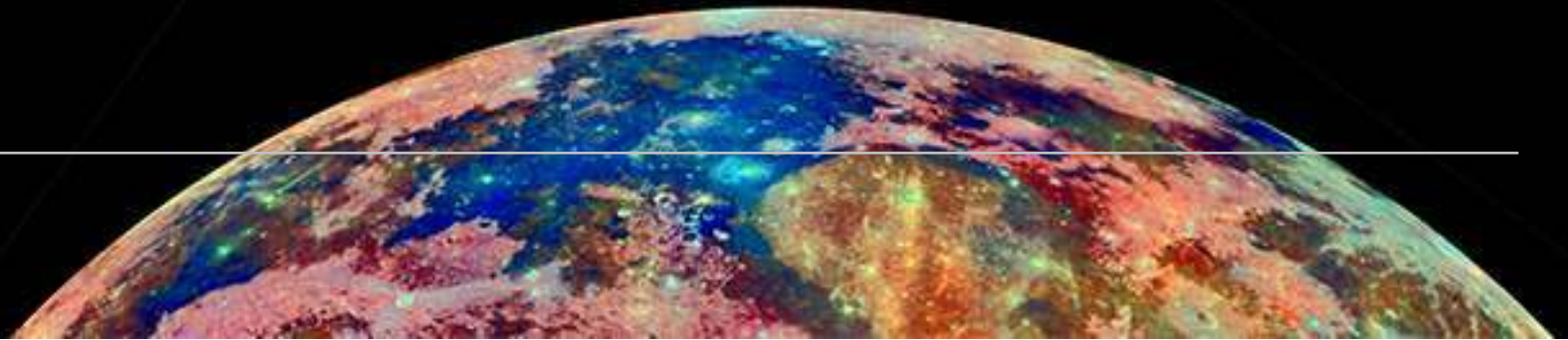
Keiviite-(Y) was found during a routine electron microprobe investigation of Apollo 17 troctolitic anorthosite 76335. The occurrence of lunar keiviite-(Y) at the lithologic boundary between orthopyroxene and olivine-dominated assemblages, in what appears to be a void with associated merrillite, suggests that metasomatic processes and possible vapour-phase deposition are important to keiviite-(Y) formation on the Moon (Carpenter et al., 2011). This discovery was also described by Edmunson et al. (2010). Lacking structural data, these authors could not distinguish between yttrialite ($Y_2Si_2O_7$) and keiviite.



Taken From Carpenter et al. (2011)

Keiviite-(Y) was found during a routine electron microprobe investigation of Apollo 17 troctolitic anorthosite 76335. In this backscattered electron image keiviite-(Y) occurs closely associated with merrillite in a small cavity between olivine and orthopyroxene crystals. Key: YSi - keiviite-(Y), Merr - merrillite, Opx - orthopyroxene, Fe - metallic iron, Cr - chromite.

Thorite

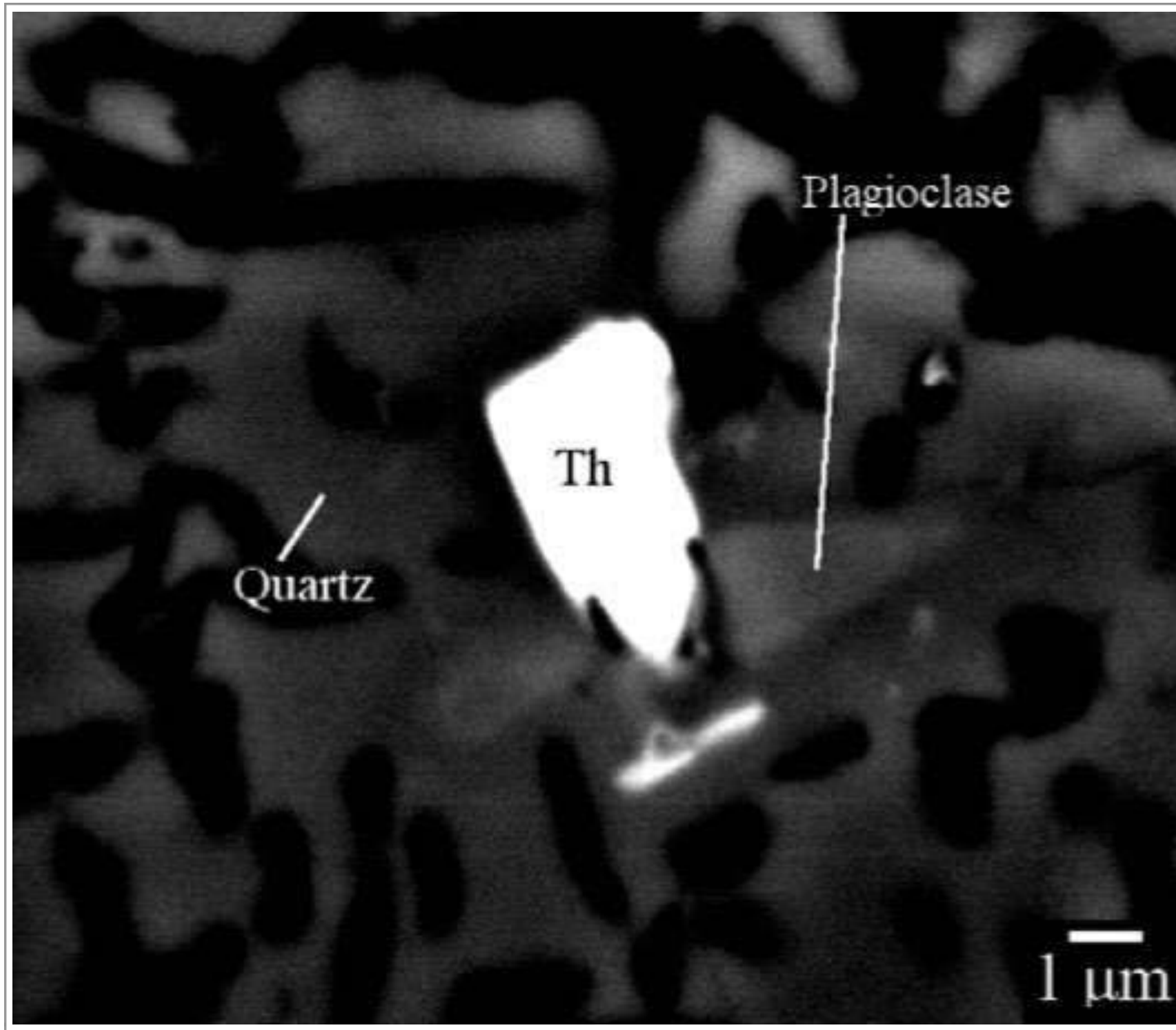


SPECIES

1. Thorite - ThSiO_4

Thorite has been found in Apollo 12 sample 12023,147-10 - in a small, monomict rock granitic fragment recovered from a regolith sample. The rock comprises graphic intergrowths of K-feldspar and quartz, and plagioclase and quartz, along with minor or accessory hedenbergite, fayalite, ilmenite, zircon, yttrrobetafite, thorite, monazite and metallic iron. Thorite occurs in the assemblage adjacent to quartz and plagioclase grains and is in solid solution with end-member xenotime $(\text{Y,HREE})\text{PO}_4$, and comprises 88% thorite and 12% xenotime (Seddio et al., 2012b, 2014).

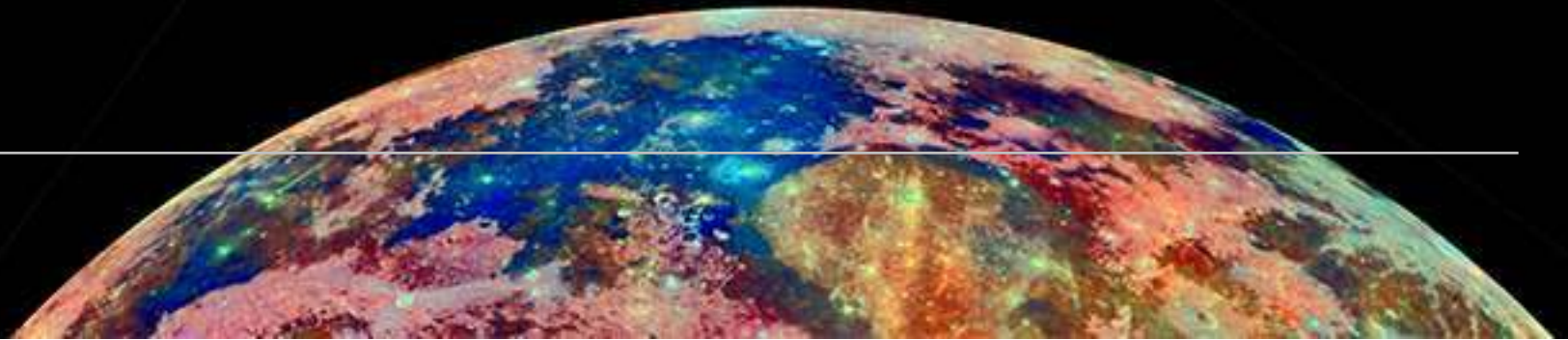
Haines et al. (1972) previously reported a single grain of thorite in Apollo 14 soil sample 14259, however, no analyses (qualitative or quantitative) were included with their description.



Taken From Seddio et al. (2012)

Backscattered electron image of thorite in a granitic fragment from Apollo 12 regolith 12023.

Corundum



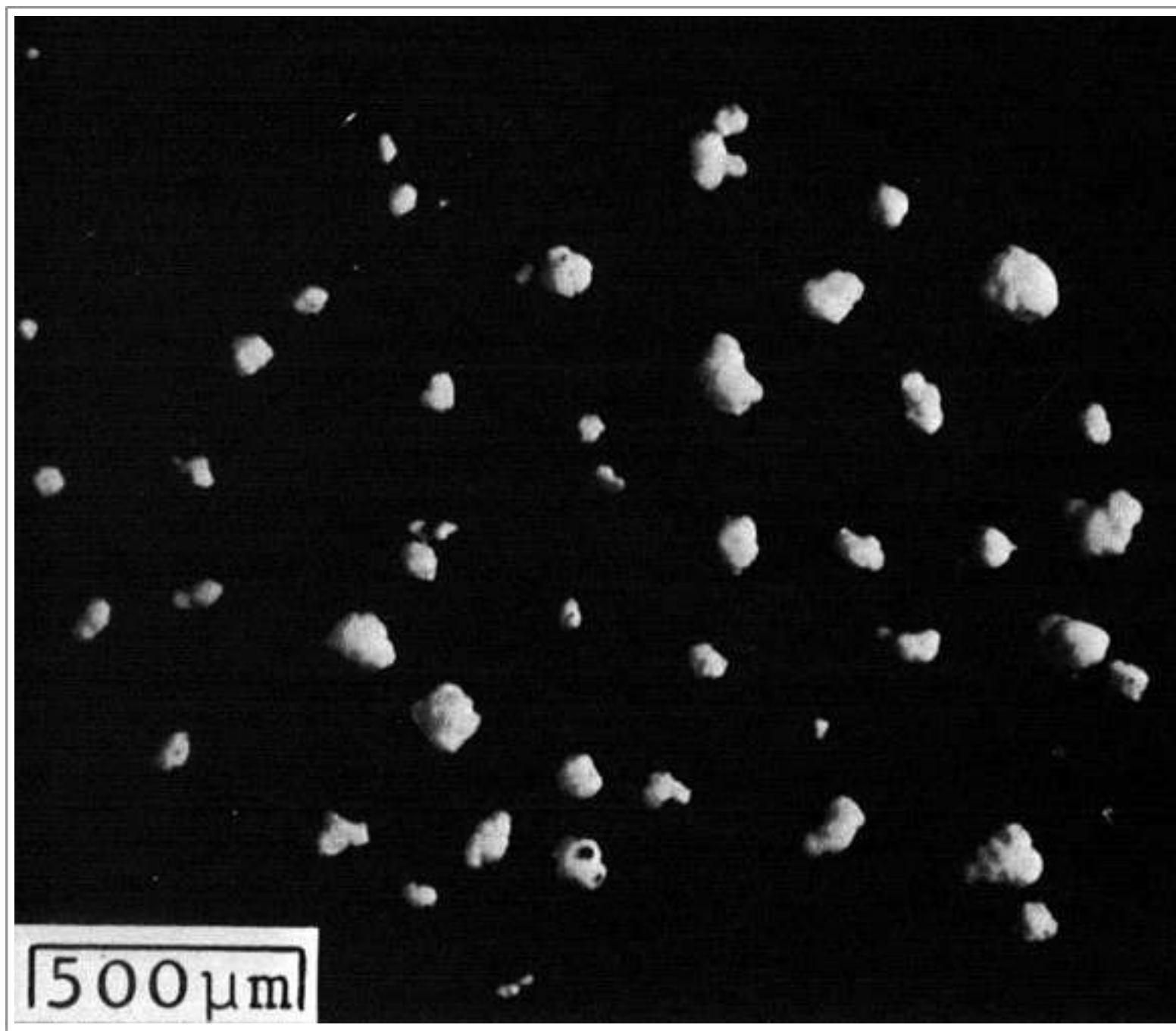
SPECIES

1. Corundum - Al_2O_3



Corundum aggregates from Apollo 11 regolith soil sample 10004 fines were interpreted as condensates of impact-derived vapour (Kleinmann and Ramdohr, 1971). A 200 μm crystal was found in Apollo 14 sample 14163 fines (Christophe-Michel-Levy et al., 1972), but no corundum has been reported in lunar rocks (Smith and Steele, 1976).

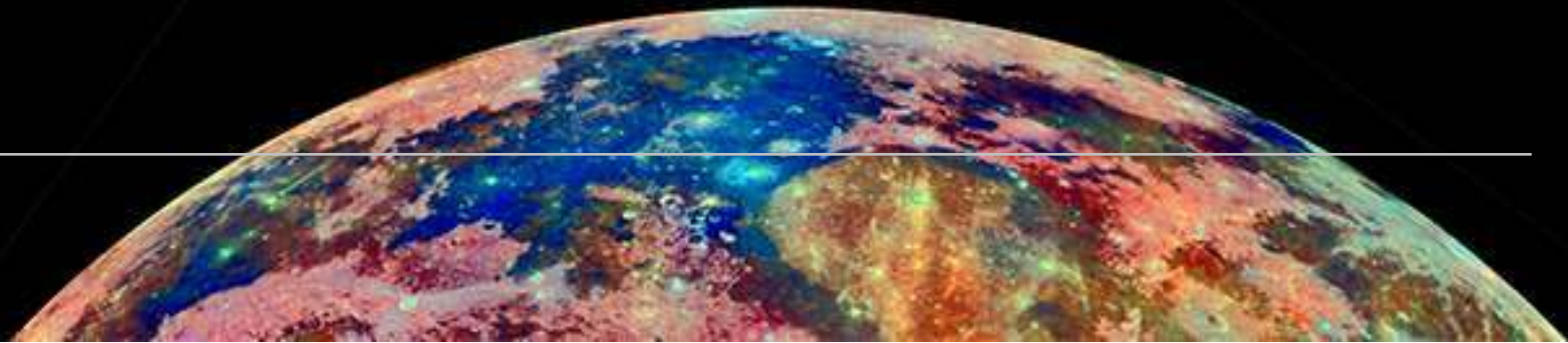
Drive tube used to collect regolith soil samples - in this example Apollo 12 astronaut Al Bean collects soil near Halo Crater.
Courtesy of NASA.



Taken From Kleinmann and Ramdohr (1971)

White grains of corundum from the Apollo 11 fines.

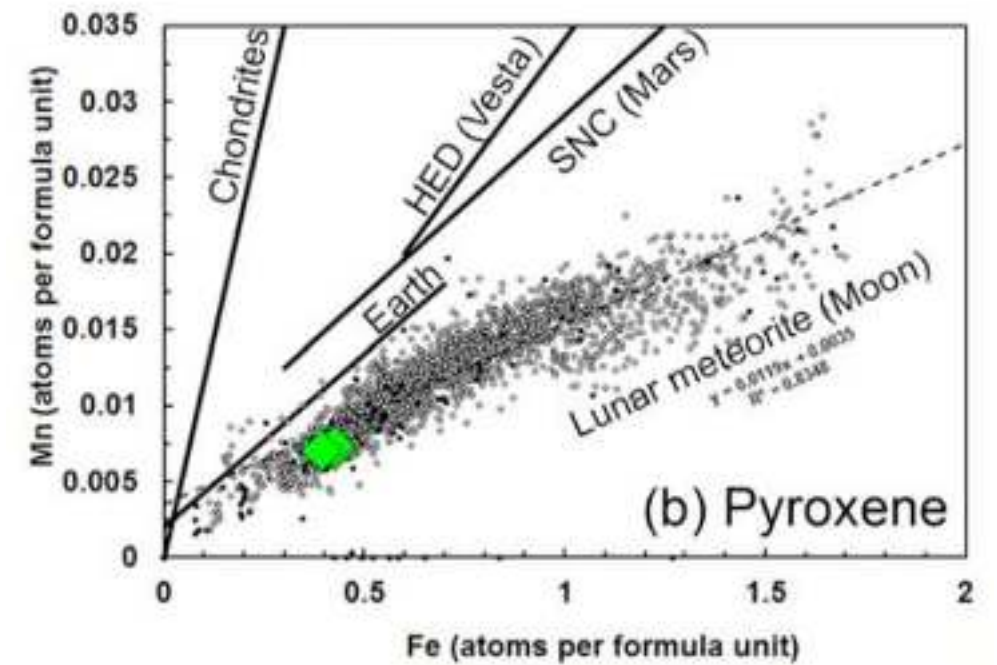
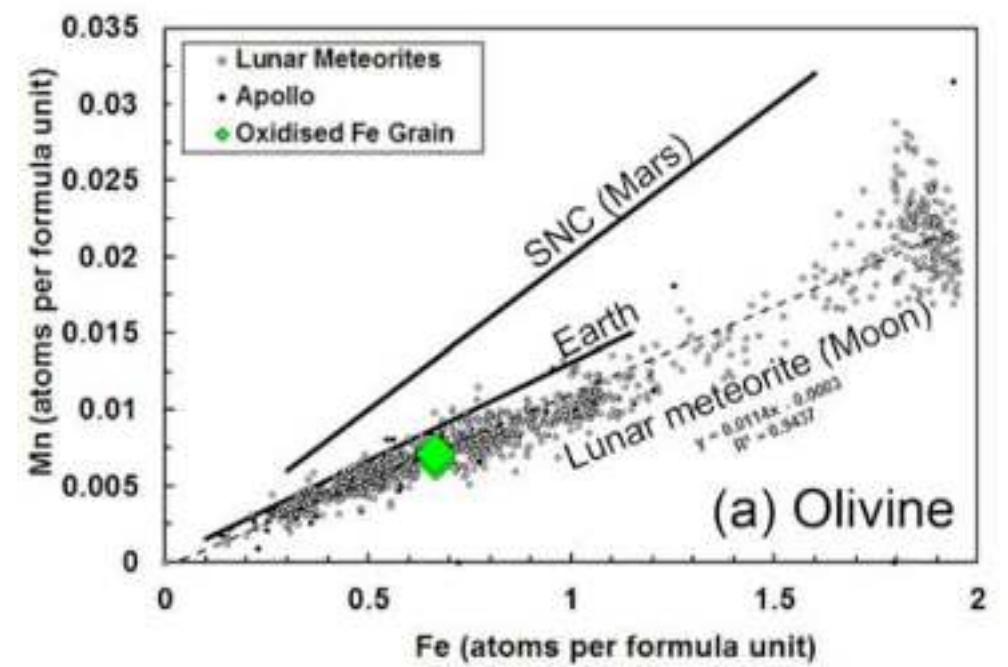
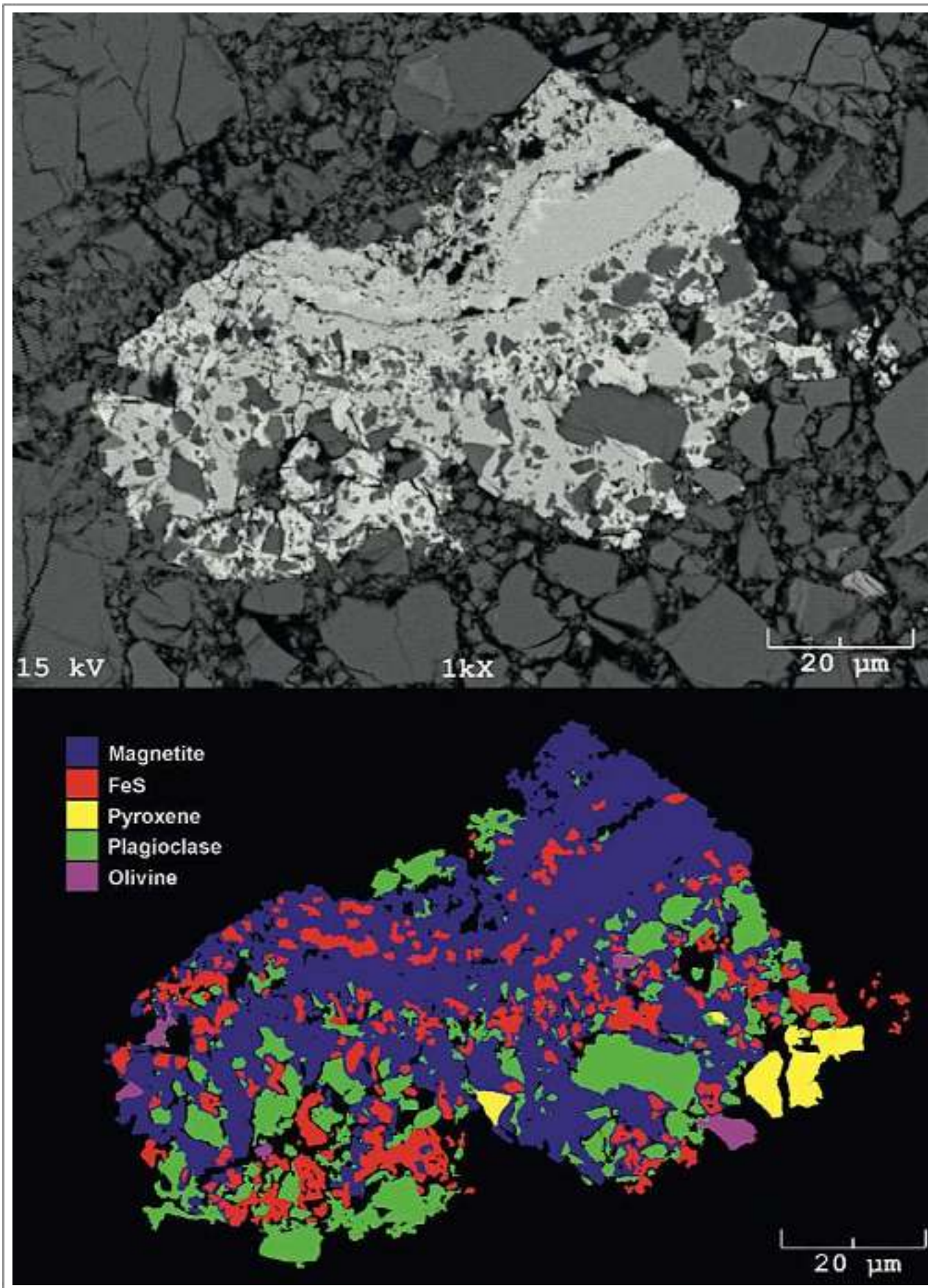
Magnetite



SPECIES

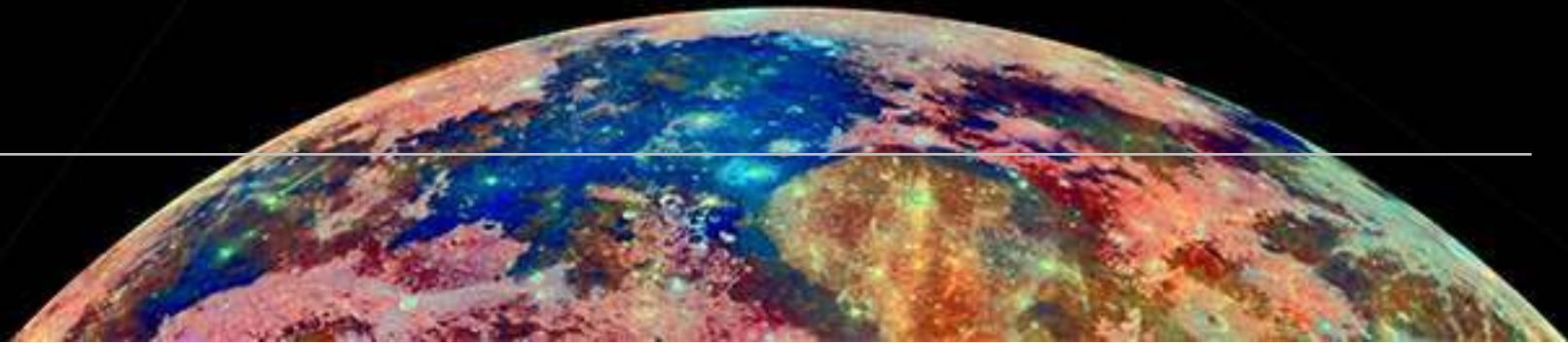
1. Magnetite - $\text{Fe}^{2+}\text{Fe}^{3+}_2\text{O}_4$

Magnetite has been discovered in Apollo 16 sample 60016 - an “ancient” feldspathic regolith breccia that was converted from a soil to a rock around 3.8 billion years ago. The breccia contains a small ($70 \times 50 \mu\text{m}$) rock fragment composed dominantly of an Fe-oxide phase with disseminated domains of troilite. Fragments of plagioclase, pyroxene, and olivine are distributed in and adjacent to the magnetite. The silicate minerals have lunar compositions that are similar to anorthosites. This discovery provides direct evidence for oxidized conditions on the Moon. Thermodynamic modelling shows that magnetite could have been formed from oxidization-driven mineral replacement of metallic iron or desulphurisation from Fe-sulphide (troilite) at low temperatures ($<570^\circ\text{C}$). Oxidizing conditions may have arisen from vapour transport during degassing of a magmatic source region, or from a hybrid endogenic-exogenic process when gases were released during an impacting asteroid or comet impact (Joy et al., 2015).



Magnetite-rich fragment in Apollo 16 “ancient” feldspathic regolith breccia sample 60016,83. Backscattered electron image of (top left); Minerals phases identified in the fragment. FeS is troilite. Black areas represent pores, fractures or phases that were not be identified (bottom left). 60016 (green diamonds) on olivine and pyroxene plots (right) (Joy et al., 2015).

Carbonates



SPECIES

1. Calcite - CaCO_3
2. Siderite - FeCO_3

Calcite

Calcite has been found in a clast of granitic rock composition from a lunar regolith sample that was returned by the Luna 20 space mission. It occurs as inclusions in quartz, intergrown with K-feldspar and displays an undamaged igneous texture.

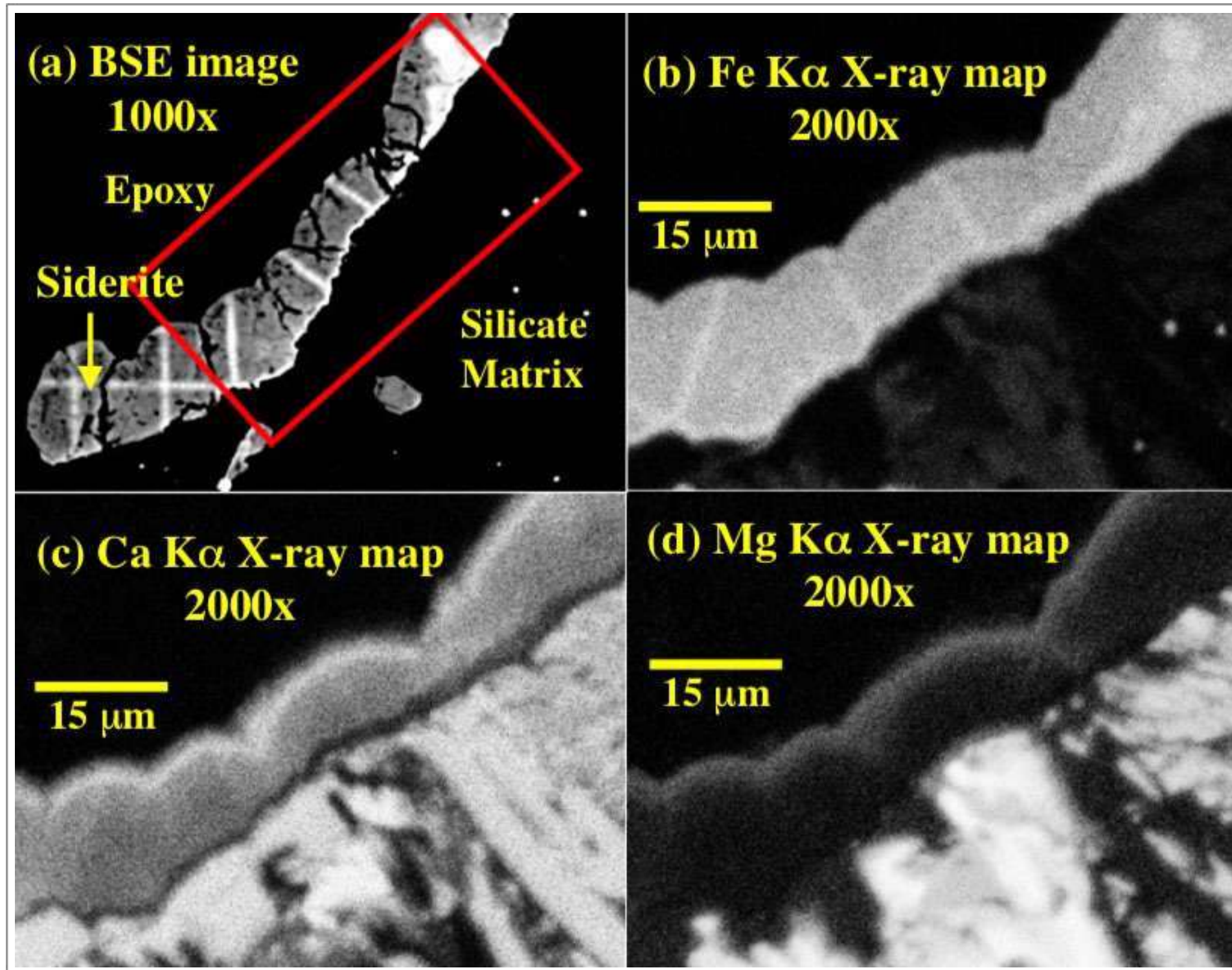
One possible scenario is that the granite crystallized during fractionation from a KREEP-rich melt and the carbonate inclusion represents a residue of immiscible CO_2 -rich parts (carbonatite?) of this melt. The presence of calcite in the Luna 20 sample provides evidence for the presence of volatiles during lunar crust formation (Götze et al., 2011).

Calcite, along with gypsum, celestite, baryte and Fe hydroxide are all reported from lunar meteorite Dhofar 730 - an anorthositic impact- melt breccia. However, these species are not lunar species. They represent terrestrial contamination and formed after the meteorite landed in the Oman desert (Nazarov et al., 2004).

Siderite

Siderite ($\text{Fe}_{0.81}\text{Mg}_{0.05}\text{Mn}_{0.01}\text{Ca}_{0.14}$) CO_3 has been found in sample 65903,16-7 - a 2-4 mm (16.7 mg) rocklet from an Apollo 16 rake sample. It is a slightly vesicular

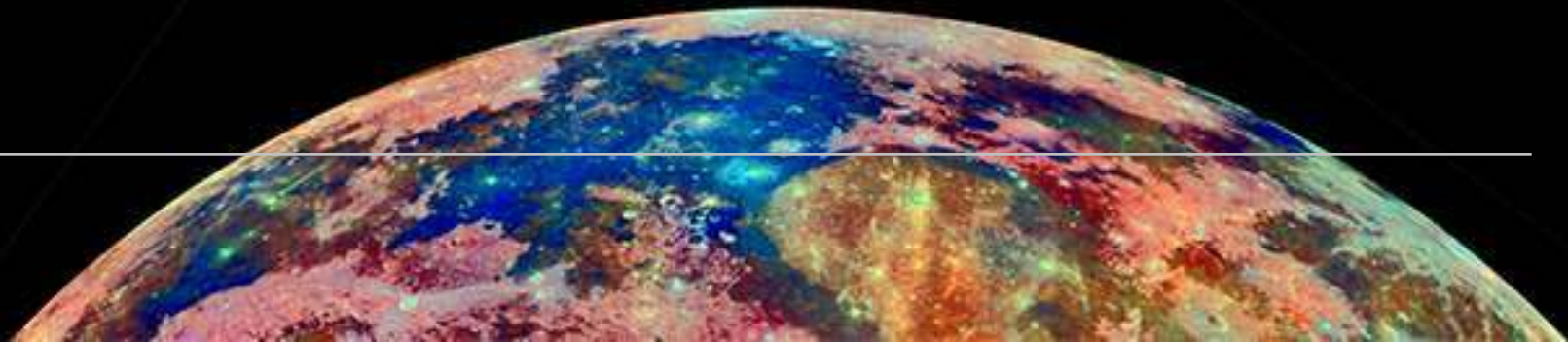
impact-melt breccia, with clasts of anorthite, grains of forsteritic olivine, and metal-phosphide intergrowths in a very-fine-grained matrix of magnesian augite, sodic plagioclase, and ternary feldspar-like glass. On the basis of textural evidence, siderite formed on the Moon from a fluid derived from the vapourisation of a volatile-rich impactor (Zeigler et al., 2001).



Taken From Zeigler et al. (2001)

Backscattered electron image of an exterior siderite grain in Apollo 16 impact-melt breccia 65903,16-7. Bright areas in the grain are electron microprobe damage. Field of view is $\sim 90 \mu\text{m}$. Red box is enlarged and rotated in (b), (c), and (d).

Goethite



SPECIES

1. Goethite - αFeOOH

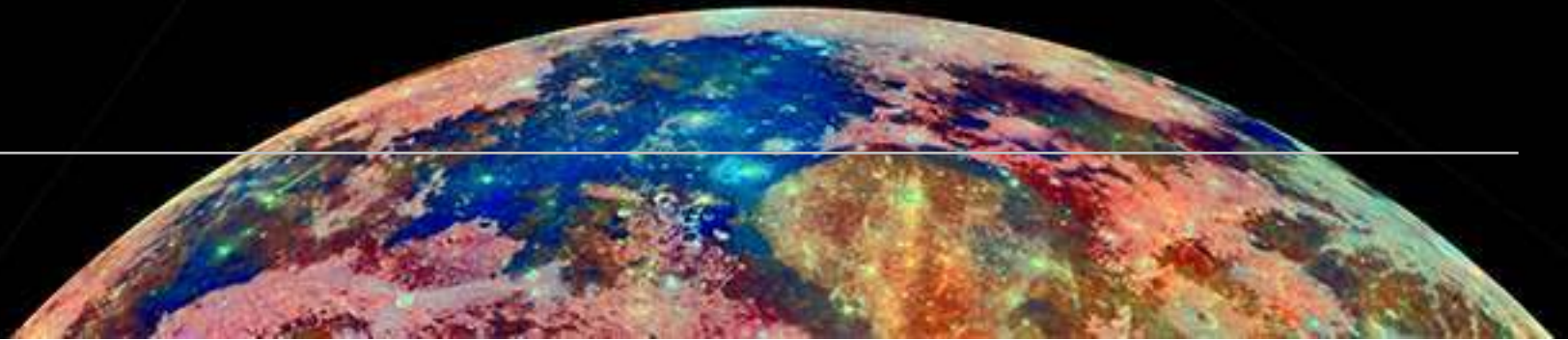
Goethite is reported by Agrell et al. (1972) from Apollo 14 regolith breccia 14301. This dominantly microritic rock contains some metallic iron fragments surrounded by a narrow red-brown halo with the reddish internal reflections suggestive of goethite. A discrete origin for the small amount of water required to produce goethite could not be determined, but both internal and external sources were discussed.

Goethite has also been found in Apollo 16 impact-melt breccia 65903,16-7 - a 2-4 mm (16.7 mg) aliquot taken from a rake sample. It contains clasts of anorthite, grains of forsteritic olivine, and metal-phosphide intergrowths in a very-fine-grained matrix of magnesian augite, sodic plagioclase, and ternary feldspar-like glass.

Goethite occurs in veins as sub-micron rims of uniform thickness between siderite and matrix silicates. Some of the smallest veins appear to consist entirely of goethite. Whether or not the goethite formed on the Moon is less clear. Although goethite is a common alteration product of siderite, during the preparation of the polished section it was subjected to hot water rinsing, however, the overall evidence suggests goethite did not form in this manner. Goethite is not observed on any exterior surface of the sample, but is found throughout the veinlets.

On the basis of textural evidence, siderite, and possibly goethite, formed on the Moon from a fluid derived from the vaporization of a volatile-rich impactor (Zeigler et al., 2001).

Nepheline Group



SPECIES

1. Nepheline - $(\text{Na,K})\text{AlSiO}_4$

Cadogan (1981) states that basalts (presumably lunar basalts) which are highly deficient in silica may crystallize nepheline. No further details are provided. It is uncertain if this is a confirmed lunar species.

Silica-depleted alkali-rich domains analyzed remotely by the Chandrayaan-1 X-ray Spectrometer have been identified at and near Tyco crater, located at the southern highland of the nearside of the Moon. Nepheline is considered to be the major feldspathoid in these alkaline rocks which can be best classified as nepheline troctolite (Basu Sarbadhikari, et al., 2018). However, nepheline remains to be observed.

Amphibole Group

SPECIES

1. Arfvedsonite - $\text{NaNa}_2(\text{Mg}_4\text{Fe}^{3+})\text{Si}_8\text{O}_{22}(\text{OH})_2$
2. Tschermakite - $\text{Ca}_2(\text{Mg}_3\text{Al}_2)(\text{Si}_6\text{Al}_2)\text{O}_{22}(\text{OH})_2$
3. Richterite - $\text{Na}(\text{NaCa})\text{Mg}_5\text{Si}_8\text{O}_{22}(\text{OH})_2$
4. Kaersutite - $\text{NaCa}_2(\text{Mg}_3\text{Ti}^{4+}\text{Al})\text{Si}_8\text{O}_{22}(\text{OH})_2$

Amphiboles are extremely rare in lunar samples because of the absence or near-absence of hydrous fluids on the Moon. However, Gay et al. (1970a) chipped a small grain from a vug in Apollo 11 mare basalt 10058. Its magnesioarfvedsonite composition is surprisingly high in Na and low in Ca with respect to other lunar minerals.

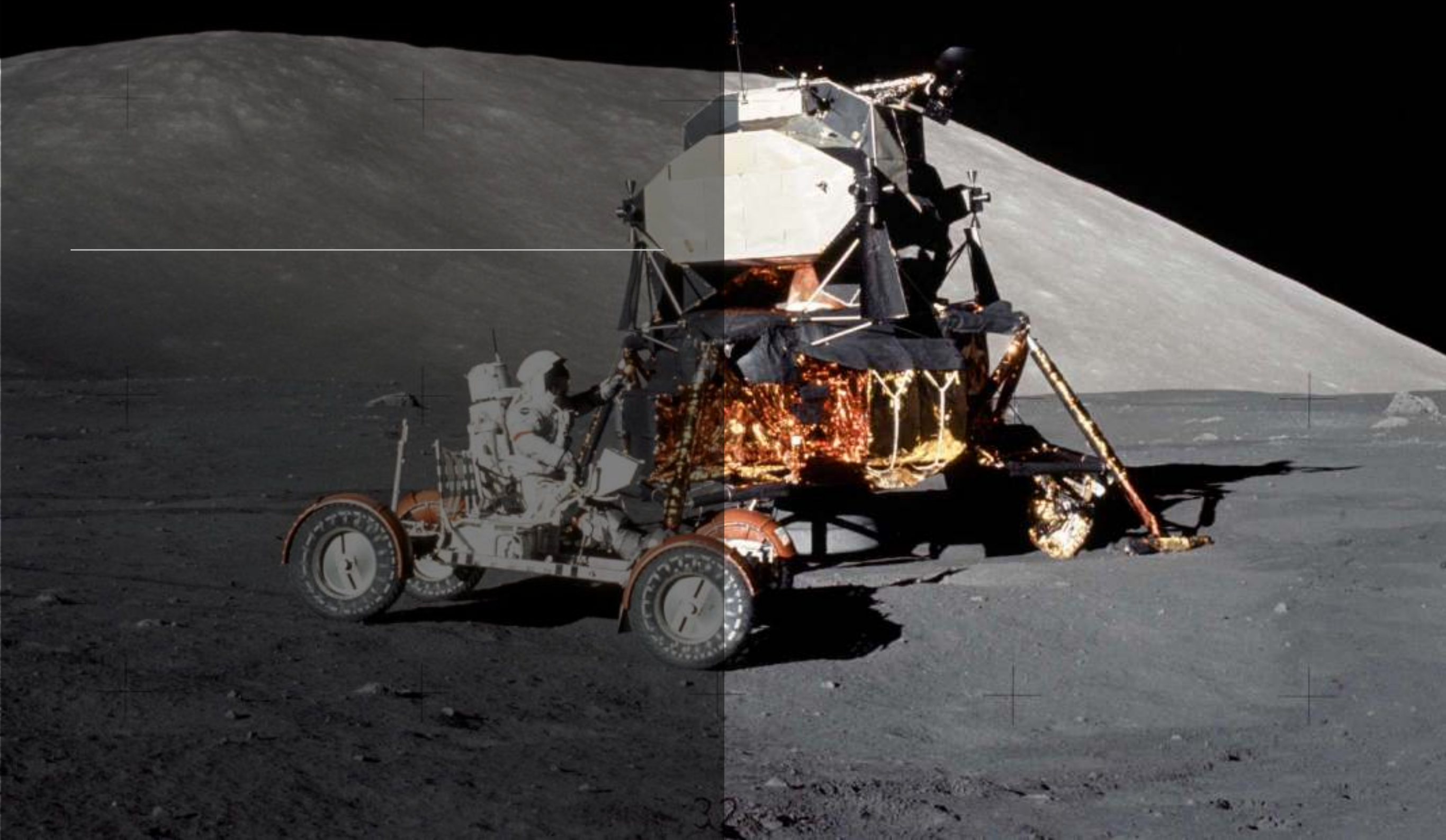
Douglas et al. (1971) reported aluminotschermakite grains from a bag containing Apollo 12 mare basalt 12021 and suggested that the amphibole together with garnet crystallized metastably. The electron microprobe analysis shows low but significant alkalies, low F and Cl, and near-equal CaO, MgO, and FeO.

Mason et al. (1972) observed loose grains of amphibole in Apollo 14 sample 14163 fines, with chemical and optical properties indicative of Fe-rich richterite and argued against it being a terrestrial contaminant.

Referring to Mason's work, Frondel (1975) describe dark brown, non-pleochroic and isotropic hornblende in Apollo 14 breccia 14319,13 and in the fines of sample 14163,42A as being kaersutite.

Apparently these early "finds" have not been verified (Treiman, 2007).

References



References

Adcock, C.T. and Hausrath, E.M. (2017) Synthesis of Na-bearing whitlockite and implications for interpretation of extraterrestrial phosphate minerals. Proc 48th Lunar & Planetary Science Conf., Abstract 2237. ([pdf](#))

Adler, I., Halter, L.S., Lowman, P.D., Glass, P.D., Heinrich, K.J.F. and Goldstein, J.I. (1970) Electron microprobe analysis of Lunar Samples. Proc. of the Apollo 11 Lunar Science Conf., 152-153.

Agrell, S.O., Scoon, J.H., Long, J.V.P., and Coles, J.N. (1972) The occurrence of goethite in a microbreccia from the Fra Mauro Formation. Proc. of the 3rd Lunar Science Conf., 7-9.

Al-Kathiri, A., Gnos, E. and Hoffman, B.A. (2007) The regolith portion of the lunar meteorite Sayh al Uhaymir 169. Meteoritics & Planetary Science, 42, 2137-2152. ([pdf](#))

Anand, M., Taylor, L.A., Nazarov, M.A., Shu, J., Mao, H.K. and Hemley, R.J. (2003a) New lunar mineral hapkeite: Product of impact-induced vapour-phase deposition in the regolith? Proc. 34th Lunar & Planetary Science Conf., Abstract 1818. ([pdf](#))

Anand, M., Taylor, L.A., Neal, C.R., Snyder, G.A., Patchen, A., Sano, Y. and Terada, K. (2003b) Petrogenesis of lunar meteorite EET 96008. Geochimica et Cosmochimica Acta, 67, 3499-3518.

Anand, M., Taylor, L.A., Nazarov, M.A., Shu, J., Mao, H.K. and Hemley, R.J. (2004) Space weathering on airless planetary bodies: Clues from the lunar mineral hapkeite. Proc. of the National Academy of Sciences, 101, 6847-6851. ([pdf](#))

Anand, M., Taylor, L.A., Floss, C., Shu, J., Neal, C.R., Terada, K. and Tanikawa, S. (2006) Petrology and geochemistry of LaPaz Icefield 02205: A new unique low-Ti mare-basalt meteorite. Geochimica et Cosmochimica Acta, 70, 246-264.

Anand, M., Tartese, R. and Barnes, J.J. (2014) Understanding the origin and evolution of water in the Moon through lunar sample studies. Phil. Trans. Roy. Soc. A, 372, 1-33. ([pdf](#))

Anderson A.T., Bunch T.E., Cameron E.N., Haggerty S.E., Boyd F.R., Finger L.W., James O.B., Keil K., Prinz M., Ramdohr P. and El Goresy A. (1970) Armalcolite: a new mineral from the Apollo 11 samples. Geochimica et Cosmochimica Acta Supplement, Proc. of the Apollo 11 Lunar Science Conf., 1, 55-63.

Arai, T., Takeda, H. and Warren, P.H. (1996) Four lunar mare lunar meteorites: crystallization trends of pyroxenes and spinels. *Meteoritics & Planetary Science*, 31, 877-892. ([pdf](#))

Arai, T., Ishi, T. and Otsuki, M. (2002) Mineralogy of a new lunar meteorite Yamato 918031. *Proc. 33rd Lunar & Planetary Science Conf.*, Abstract 2064. ([pdf](#))

Arai, T., Otsuki, M., Ishii, T., Mikouchi, T. and Miyamoto, M. (2005) Mineralogy of Yamato 983885 lunar polymict breccia with a KREEP basalt, a high-Al basalt, a very low-Ti basalt and Mg-rich rocks. *Antarctic Meteorite Research*, 18, 17-45. ([pdf](#))

Arai, T., Takeda, H. and Miyamoto, M. (2006) Experimental petrology of ancient lunar mare basalt Asuka-881757: Spinel crystallization as a petrologic indicator. *Antarctic Meteorite Research*, 19, 1-19. ([pdf](#))

Arai, T., Hawke, B.R., Giguere, T.A., Misawa, K., Miyamoto, M. and Kojima, H. (2010) Antarctic lunar meteorites Yamato-793169, Asuka-881757, MIL 05035, and MET 01210 (YAMM): Launch pairing and possible cryptomare origin. *Geochimica et Cosmochimica Acta*, 74, 2231-2248.

Arndt, J. and von Engelhardt, W. (1987) Formation of Apollo 17 orange and black glass beads. *Journal of Geophysical Research; Solid Earth*, 92, E372-E376.

Atencio, D., Andrade, M.B., Christy, A.G., Gieré, R. and Kartashov, P.M. (2010) The pyrochlore supergroup of minerals: nomenclature. *Canadian Mineralogist*, 48, 673-698. ([pdf](#))

Baker, M.B. and Herzberg, C.T. (1980) Spinel cataclasites in 15445 and 72435: Petrology and criteria for equilibrium. *Conference on the Lunar Highlands Crust*, Houston, Tex., November 14-16, 1979, Proceedings. (A81-26201, 10-91) New York and Oxford, Pergamon Press, 113-132. ([pdf](#))

Baldrige, W.S., Beaty, D.W., Hill, S.M.R. and Albee, A.L. (1979) The petrology of the Apollo 12 pigeonite basalt suite. *Proc. 10th Lunar & Planetary Science Conf.*, 141-179. ([pdf](#))

Barnes, J.J., Franchi, I.A., Anand, M., Tartèse, R., Starkey, N.A., Koike, M., Sano, Y., and Russell, S.S. (2013) Accurate and precise measurements of the D/H ratio and hydroxyl content in lunar apatites using NanoSIMS. *Chemical Geology*, 337-338, 48-55.

Barnes, J.J., Tartèse, R., Anand, M., McCubbin, F.M., Franchi, I.A., Starkey, N.A. and Russell, S.S. (2014) The origin of water in the primitive Moon as revealed by the lunar highlands samples. *Earth and Planetary Science Letters*, 390, 244-252.

Barnes, J.J., Tartèse, R., Anand, M., McCubbin, F.M., Neal, C.R. and Franchi, I.A. (2016a) The chlorine isotopic composition of lunar urKREEP. *Proc. 46th Lunar & Planetary Science Conf.*, Abstract 1439. ([pdf](#))

Barnes, J.J., Tartèse, R., Anand, M., McCubbin, F.M., Neal, C.R. and Franchi, I.A. (2016b) Early degassing of lunar urKREEP by crust-breaching impact(s). *Earth and Planetary Science Letters*, 447, 84-94. ([pdf](#))

Barnes, J.J., Thompson, M.S., McCubbin, F.M., Howe, J.Y., Rahman, Z., Messenger, S. and Zega, T. (2018) Coordinated microanalysis of phosphates in Apollo 11 high-titanium basalts. *Proc. 49th Lunar & Planetary Science Conf.*, Abstract 2667. ([pdf](#))

Barnes J. J., Franchi, I.A., McCubbin, F.M. and Anand, M. (2019) Multiple reservoirs of volatiles in the Moon revealed by the isotopic composition of chlorine in lunar basalts. *Geochimica Cosmochimica Acta*, in press ([pdf](#))

Barrat, J.A., Chaussidon, M., Bohn, M., Gillet, P., Göpel, C. and Lesourd, M. (2005) Lithium behavior during cooling of a dry basalt: An ion-microprobe study of the lunar meteorite Northwest Africa 479 (NWA 479). *Geochimica et Cosmochimica Acta*, 69, 23, 5597-5609.

Basu Sarbadhikari, A., Ghosh, J. and Narendranath, S. (2018) Alkali-rich rocks at and near Tycho crater of the Moon. *Proc. 49th Lunar & Planetary Science Conf.*, Abstract 1439. ([pdf](#))

Bayliss, P., Mazzi, F., Munno, R. and White, T.J. (1989) Mineral nomenclature: zirconolite. *Mineralogical Magazine*, 53, 565-569.

Bellucci, J.J., Grange, M.L., Collins, G., Whitehouse, M.J., Snape, J.F., Norman, M.D., Kring, D.A., Robinson, K. and Nemchin, A.A. (2018) Can “granite” clast from an Apollo 14 breccia be a fragment of a terrestrial meteorite? *Bombardment: Shaping Planetary Surfaces and Their Environments Conf.*, Abstract 2032. ([pdf](#))

Bellucci, J.J., Nemchin, A.A., Grange, M.L., Robinson, K., Collins, G., Whitehouse, M.J., Snape, J.F., Norman, M.D., Kring, D.A. (2019) Terrestrial-like zircon in a clast from an Apollo 14 breccia. *Earth and Planetary Science Letters*, 510, 173-185.

Bouvier, A., Gattacceca, J., Agree, C., Grossman, J. and Metzler, K. (2017) *The Meteoritical Bulletin*, No. 104. *Meteoritics & Planetary Science* 1. ([pdf](#))

Boyce, J.W., Liu, Y., Rossman, G.R., Guan, Y., Eiler, J.M., Stolper, E.M. and Taylor, L.A. (2010) Lunar apatite with terrestrial volatile abundances. *Nature*, 466, 466-469.

Brett, R., Gooley, R.C., Dowty, E., Prinz, M. and Keil, K. (1973) Oxide minerals in lithic fragments from Luna 20 fines. *Geochimica et Cosmochimica Acta*, 37, 761-773.

Burger, P.V., Shearer C.K. and Papike J.J. (2009) The multi-stage cooling history of lunar meteorite NWA 032 as recorded by phenocrystic olivine and pyroxene. *Proc. 40th Lunar & Planetary Science Conf.*, Abstract 2043. ([pdf](#))

Busch, F.D., Prinz, M., Keil, K. and Kurat, G. (1972) Lunar zirkelite: a uranium-bearing phase. *Earth and Planetary Science Letters*, 14, 313-321.

Cadogan, P.H. (1981) *The Moon our Sister Planet*. Cambridge University Press.

Cahill, J., Cohen, B.A., Taylor, L.A. and Nazarov, M.A. (2001) Mineralogy and petrology of Dhofar 025. *Proc. 32nd Lunar & Planetary Science Conf.*, Abstract 1840. ([pdf](#))

Cameron, E.N. (1970) Opaque minerals in certain lunar rocks from Apollo 11. *Proc. of the Apollo 11 Lunar Science Conf.*, 1, 221-245. ([pdf](#))

Carpenter, P., Edmunson J., Cohen B.A., Zeigler R.A., and Jolliff B.L. (2011) First lunar occurrence of keiviite-(Y) in troctolitic anorthosite 76335. *Proc. 42nd Lunar & Planetary Science Conf.*, Abstract 2767. ([pdf](#))

Carter, J.L., Clanton, U.S., Fuhrman, R., Laughton, R.B., McKay, D.S. and Usselman, T.M. (1975) Morphology and composition of chalcopyrite, chromite, Cu, Ni-Fe, pentandite, and troilite in vugs of 76015 and 76215. *Proc. 6th Lunar Science Conf.*, 719-728. ([pdf](#))

Cernok, A., White, L.F., Darling, J., Dunlop, J. and Anand, M. (2019) Shock-induced microtextures in lunar apatite and merrillite. *Meteoritics & Planetary Science*, 1-21.

Chao E.C.T., Minkin J.A., Frondel C., Klein C., Drake J.C., Fuchs L., Tani B., Smith J.V., Anderson A.T., Moore P.B., Zechman G.R., Traill R.J., Plant A.G., Douglas J.A.V. and Dence M.R. (1970) Pyroxferroite, a new calcium-bearing iron silicate from Tranquillity Base. *Geochimica et Cosmochimica Acta, Supplemental Proc. of the Apollo 11 Lunar Science Conf.*, 1, 65-79. ([pdf](#))

Chen, J., A. Wang, A., Jolliff, B.L., Korotev, R.L., Ling, Z.C., Fu, X.H. and Ni, Y.H. (2018) Petrogenetic and shock history of mare basaltic lunar meteorite Northwest Africa 4734. *Proc. 49th Lunar & Planetary Science Conf.*, Abstract 2976. ([pdf](#))

Chen, J., A., Jolliff, B.L., Korotev, R.L., Wang, K., Wang, A., Carpenter, P.K., Chen, H. and Ling, Z.C. (2019) Northwest Africa 10985: a new lunar gabbro? *Proc. 50th Lunar & Planetary Science Conf.*, Abstract 2463. ([pdf](#))

Christophe-Michel-Levy, M., Levy, R., Caye, R. and Pierrot, R. (1972) The magnesian spinel-bearing rocks from the Fra Mauro formation. *Proc. 3rd Lunar Science Conf.*, 887-894. ([pdf](#))

Cohen, B.A., James, O.B., Taylor, L.A., Nazarov, M.A. and Barsukova, L.D. (2004) Lunar highland meteorite Dhofar 026 and Apollo sample 15418: Two strongly shocked, partially melted, granulitic breccias. *Meteoritics & Planetary Science*, 39, 1419-1447. ([pdf](#))

Cohen, M.E., Kuehner, S.M., Tepper, J.H., Burney, D.C., Neal, C.R., Irving, A.J., Korotev, R.L. and Hoefnagels, B. (2019)

Mineralogy and bulk composition of lunar mare basalt Northwest Africa 12008. Proc. 50th Lunar & Planetary Sciences Conf., Abstract 2508. ([pdf](#))

Connolly, H.C., Smith, C., Benedix, G., Folco, L., Richter, K., Zipfel, J., Yamaguchi, A. and Chennaoui Aoudjehane, H. (2007) The Meteoritical Bulletin, No. 93, 2008 March. Meteoritics & Planetary Science, 43, 571-632. ([pdf](#))

Cronberger, K. and Neal, C.R. (2018) Origin(s) and Evolution of KREEP Basalts. Proc. 49th Lunar & Planetary Science Conf., Abstract 1305. ([pdf](#))

Crow, C.A., McKeegan, K.D. and Moser, D.E. (2017) Coordinated U–Pb geochronology, trace element, Ti-in-zircon thermometry and microstructural analysis of Apollo zircons. Geochimica et Cosmochimica Acta, 202, 264-284.

Dalton, J., Hollister, L., Kulick, C. and Hargraves, R. (1974) The nature of the chromite to ulvospinel transition in mare basalt 15555. Proc. 5th Lunar & Planetary Science Conf., 5, 160-162. ([pdf](#))

Day, J.M.D., Taylor, L.A., Floss, C., Patche, A.D., Schnare, D.W., Pearson, D.G. (2006) Comparative petrology, geochemistry, and petrogenesis of evolved, low-Ti lunar mare basalt meteorites from the LaPaz Icefield, Antarctica. Geochimica et Cosmochimica Acta, 70, 1581-1600.

Delano, J.W. (1996) Compositional range of primary magmas observed among the Apollo 127 orange volcanic glasses (74220). Proc. 27th Lunar & Planetary Sciences Conf., Abstract 303-304. ([pdf](#))

Demidova, S.I., Nazarov, M.A., Kurat, G., Brandstätter, F. and Ntaflou, T. (2005) New lunar meteorites from Oman: Dhofar 925, 960 and 961. Proc. 36th Lunar & Planetary Science Conf. Abstract 1607. ([pdf](#))

Demidova, S.I., Nazarov, M.A., Ryazantsev, K.M., Brandstätter, F. and Ntaflou, T. (2015) Cordierite from the Dhofar 025 lunar feldspathic meteorite. Proc. 46th Lunar & Planetary Science Conf. Abstract 1772. ([pdf](#))

Dikov, Y.P., Ivanov, A.V., Wlotzka, F., Galimov, E.M., Wänke, H. (1998) High enrichment of carbon and volatile elements in the surface layers of Luna 16 soil sample 1635: Result of comet or meteorite impact? Earth and Planetary Science Letters, 155, 197-204.

Dikov, Y.P., Wlotzka, F. and Ivanov, A.V., (1998) XPS evidence for SiC on the surface of Luna-16 regolith particles. Proc. 30th Lunar & Planetary Sciences Conf., Abstract 1012. ([pdf](#))

Dikov, Y.P., Gorshkov, A.I., Sivtsov, A.I., Wlotzka, F., and Ivanov, A.V. (2002) SiC and graphite in the sublimate layer of lunar glass spherules. Proc. 33rd Lunar & Planetary Sciences Conf., Abstract 1186. ([pdf](#))

Drever, H.I., Butler, P., Gibb, F.G.F. and Whitley, J.E. (1972) Some textures in lunar igneous rocks and terrestrial analogs. Proc. 3rd Lunar Science Conf., 189-191. ([pdf](#))

Douglas, J.A.V., Dence, M.R., Plant, A.G. and Traill, R.J (1971) Mineralogy and petrology of some Apollo 12 samples. Proc. 2nd Lunar Science Conf., 285-299. ([pdf](#))

Dowty, E., Keil, K., and Prinz, M. (1974) Igneous rocks from Apollo 16 rake samples. Proc. 5th Lunar Science Conf., Vol. 2, 431-445. ([pdf](#))

Dowty, E. (1977) Phosphate in Angra dos Reis: Structure and composition of the $\text{Ca}_3(\text{PO}_4)_2$ minerals. Earth and Planetary Science Letters, 35, 347-351.

Dungan, M.A., Brown, R.W. and Myers, R.M. (1977) The petrology of the Apollo 12 ilmenite basalt suite. Proceedings of the 8th Lunar Science Conference, 1339-1381. ([pdf](#))

Dygert, N., Hirth, G. and Liang, Y. (2015) Rheology of ilmenite and ilmenite-olivine aggregates: implications for lunar cumulate mantle overturn. Proc. 46th Lunar Science Conf., Abstract 2058. ([pdf](#))

Dymek R.F., Albee A.L., and Chodos A.A. (1975) Comparative petrology of lunar cumulate rocks of possible primary origin: Dunite 72415, troctolite 76535, norite 78235, and anorthosite 62237. Proc. 6th Lunar Science Conf., 301-341. ([pdf](#))

Elardo, S.M., McCubbin, F.M. and Shearer, C.K. (2012) Chromite symplectites in Mg-suite troctolite 76535 as evidence for infiltration metasomatism of a lunar layered intrusion. *Geochimica et Cosmochimica Acta*, 87, 154-177.

Edmunson J., Cohen B.A., Carpenter P., Zeigler R.A. and Jolliff B.L. (2010) Yttrium silicate in lunar troctolitic anorthosite 76335. Proc. 41st Lunar & Planetary Science Conf., Abstract 2627. ([pdf](#))

El Goresy, A., Ramdohr, P. and Taylor, L. (1971a) The geochemistry of the opaque minerals in Apollo 14 crystalline rocks. *Earth & Planetary Science Letters*, 13, 121-129. ([abstract online](#))

El Goresy, A., Ramdohr, P. and Taylor, L. (1971b) The opaque minerals in the lunar rocks from Oceanus Procellarum. Proc. 2nd Lunar Science Conf., 1, 219-235. ([pdf](#))

El Goresy, A. and Ramdohr, P. (1972) Fra Mauro crystalline rocks: petrology, geochemistry, and subsolidus reduction of the opaque minerals. Proc. 3rd Lunar Science Conf., 224. ([pdf](#))

El Goresy, A., Ramdohr, P., Pavicevic, M., Medenbach, O., Muller, O., and Gentner, W. (1973) Zinc, lead, chlorine and FeOOH-bearing assemblages in the Apollo 16 sample 66095: Origin by impact of a comet or a carbonaceous chondrite? *Earth and Planetary Science Letters*, 18, 411-419.

El Goresy, A., Ramdohr, P., Medenbach, O. and Bernhardt, H.-J. (1974) Taurus-Littrow crystalline rocks: Opaque mineralogy and geochemistry. Proc. 5th Lunar and Planetary Science Conf., 209-211. ([pdf](#))

Elikns-Tanton, L.T., Chatterjee, N. and Grove, T.L. (2003) Experimental and petrological constraints on lunar differentiation from the Apollo 15 green picritic glasses. Meteoritics and Planetary Science, 38, 515-527. ([pdf](#))

Evans, H.T. (1970) The crystallography of lunar troilite. Proc. 1st Lunar Science Conf., 399-408. ([pdf](#))

Fagan, T.J., Hayakawa, S., Kodama, S., Kataoka, Y. and Sasamoto, A. (2008) Late-stage crystallization products in NWA 773 group lunar meteorites. Proc. 39th Lunar and Planetary Science Conf., Abstract 1854. ([pdf](#))

Fagan, T.J., Gross, J., Ramsey, S. and Turrin, B. (2018) Northwest Africa 8632 - recording young lunar volcanism. Proc. 49th Lunar and Planetary Science Conf., Abstract 2584. ([pdf](#))

Foreman, A.B., Korotev, R.L., Jolliff, B.L. and Zeigler, R.A. (2008) Petrography and geochemistry of Dhofar 733 - an unusually sodic, feldspathic lunar meteorite. Proc. 39th Lunar and Planetary Science Conf., Abstract 1853. ([pdf](#))

Fron del, J.W. (1975) Lunar Mineralogy; Wiley-Interscience: New York, USA.

Fuchs, L.H. (1970) Fluorapatite and other accessory minerals in Apollo 11 rocks. Proc. 1st Lunar Science Conf., 475-479. ([pdf](#))

Fuchs, L.H. (1971) Orthopyroxene and orthopyroxene-bearing rock fragments rich in K, REE, and P in Apollo 14 soil sample 14163. Earth and Planetary Science Letters, 12, 170-174.

Gancarz, A.J., Albee, A.L., and Chodos, A.A. (1972) Comparative petrology of Apollo 16 sample 68415 and Apollo 14 samples 14276 and 14310: Earth and Planetary Science Letters, 16, 307-330.

Gay, P., Bancroft, G.M. and Brown, M.G. (1970a) Diffraction and Mössbauer studies of minerals from lunar soils and rocks. Geochimica et Cosmochimica Acta Supplement, Volume 1. Proc. of the Apollo 11 Lunar Science Conf., 481-497. ([pdf](#))

Gay, P., Brown, M.G., and Rickson, K.O. (1970b) Mineralogical studies of lunar rock 12023,10. Earth and Planetary Science Letters, 9, 124-126.

Goldstein, J.I., Axon, H.J. and Yen, C.F. (1972) Metallic particles in the Apollo 14 lunar soil. Proc. 3rd Lunar Science Conf., 1037-1064. ([pdf](#))

Goldstein, J.I., Hewins, R.H. and Romig, A.D. (1976) Carbides in lunar soils and rocks. Proc. 7th Lunar Science Conf., 807-818. ([pdf](#))

Gooley, R. C., Brett, R. and Warner, J.L. (1973) Crystallization history of metal particles in Apollo 16 rake samples. Proc. 4th Lunar Science Conf., 799-810. ([pdf](#))

Götze, J., Gucsik, A., Kempe, U., Ott, U., Hoppe, P., Nagy, Sz., Bérczi, Sz. and Veres, M. (2011) Magmatic origin of calcite from the Luna-20 Regolith sample. 74th Annual Meteoritical Society Meeting, Abstract 5123. ([pdf](#))

Grange, M.L., Nemchin, A.A., Timms, N., Pidgeon, R.T. and Meyer, C. (2011) Complex magmatic and impact history prior to 4.1 Ga recorded in zircon from Apollo 17 South Massif aphanitic breccia 73235. *Geochimica et Cosmochimica Acta*, 75, 2213-2232.

Grange, M.L., Nemchin, A.A., Pidgeon, R.T., Timms, N., Muhling, J.R. and Kennedy, A.K. (2009) Thermal history recorded by the Apollo 17 impact melt breccia 73217. *Geochimica et Cosmochimica Acta*, 73, 3093-3107.

Grange, M.L., Pidgeon, R.T., Nemchin, A.A., Timms, N. and Meyer, C. (2013) Interpreting U–Pb data from primary and secondary features in lunar zircon. *Geochimica et Cosmochimica Acta*, 101, 112-132.

Grieve, R.A., McKay, F.G.A., Smith, H.D. and Weill, D.F. (1975) Lunar polymict breccia 14321: a petrographic study. *Geochimica et Cosmochimica Acta*, 39, 229-245.

Griffin, W.L., Amlı, R. and Heier, K.S. (1972) Whitlockite and apatite from lunar rock 14310 and from Ödegarden, Norway. *Earth and Planetary Science Letters*, 15, 53-58.

Griffiths, A.A., Barnes, J.J., Tartèse, R., Potts, N.J. and Anand, M. (2014) Characterization of mesostasis areas in mare basalts: petrography and mineral chemistry. Proc. 45th Lunar & Planetary Science Conf., Abstract 1905. ([pdf](#))

Gross, J. and Treiman, A. (2011) Unique spinel-rich lithology in lunar meteorite ALHA 81005: Origin and possible connection to M3 observations of the farside highlands. *Journal of Geophysical Research Atmospheres*, 116, E10009, 1-9. ([pdf](#))

Gross, J., Isaacson, P.J., Treiman, A., Le, L. and Gorman, J.K. (2014) Spinel-rich lithologies in the lunar highland crust: Linking lunar samples with crystallization experiments and remote sensing. *American Mineralogist*, 99, 1849-1859.

Gross, J., Prissel, T.C., Korotev, R.L. and Parman, S.W. (2017) Unique pink spinel symplectite assemblage in Northwest Africa (NWA) 10401: breakdown reaction through solid-state diffusion and potential relation to Apollo 17 samples. Proc. 48th Lunar & Planetary Science Conf., Abstract 2589. ([pdf](#))

Haggerty S.E. (1973a) Armalcolite and genetically associated opaque minerals in the lunar samples. Proc. 4th Lunar Science Conf., 777-797. ([pdf](#))

Haggerty, S.E. (1973b) Luna 20: Mineral chemistry of spinel, pleonaste, chromite, ulvöspinel, ilmenite and rutile. *Geochimica Cosmochimica Acta*, 37, 857-867.

Haines, E.L., Albee, A.L., Chodos, A.A. and Wasserburg, G.J. (1971) Uranium-bearing minerals of lunar rock 12013. *Earth and Planetary Science Letters*, 12, 145-154.

Haines, E.L., Gancarz, A.J. and Wasserburg, G.J. (1972) The uranium distribution in lunar soils and rocks 12013 and 14310. *Proc. 3rd Lunar Science Conf.*, 350. ([pdf](#))

Haloda, J., Tycova, P., Korotev, R.L., Fernandes, V.A., Burgess, R., Thöni, M., Jelenc, M., Jakes, P., Gabzdyl, P. and Kosler, J. (2009) Petrology, geochemistry, and age of low-Ti mare-basalt meteorite Northeast Africa 003-A: A possible member of the Apollo 15 mare basaltic suite. *Geochimica Cosmochimica Acta*, 73, 3450-3470.

Hauri, E.K., Saal, A.E., Nakajima, M., Anand, M., Rutherford, M.J., Van Orman, J.A. and Le Voyer, M. (2017) Origin and Evolution of Water in the Moon's Interior. *Annual Rev. Earth Planet. Sci.*, 45, 89-111. ([pdf](#))

Heiken, G.H., Vaniman, D.T. and French, B.M., Eds.; (1991) *Lunar Sourcebook*. Cambridge University Press: Cambridge, UK. pp. 736. ([available online](#))

Herzberg, C.T. and Baker, M.B. (1980) The cordierite- to spinel-cataclasite transition: structure of the lunar crust. *Conference on*

the Lunar Highlands Crust, Houston, Tex., November 14-16, 1979, *Proceedings*. (A81-26201, 10-91) New York and Oxford, Pergamon Press, 113-132. ([pdf](#))

Hidaka, Y., Yamaguchi, A. and Ebihara, M. (2014) Lunar meteorite, Dhofar 1428: Feldspathic breccia containing KREEP and meteoritic components. *Meteoritics & Planetary Science*, 49, 921-928. ([pdf](#))

Hlava, P.F., Prinz, M. and Keil, K. (1972) Niobian rutile in an Apollo KREEP fragment. *Meteoritics and Planetary Science*, 7, 479-485. ([pdf](#))

Hudgins, J.A., Walton, E.L. and Spray, J.G. (2007) Mineralogy, petrology, and shock history of lunar meteorite Sayh al Uhaymir 300: A crystalline impact-melt breccia. *Meteoritics & Planetary Science* 42, 1763-1779. ([pdf](#))

Hunter and Taylor (1981) Rusty rock 66095: a paradigm for volatile-element mobility in highland rocks. *Proc. Lunar & Planetary Science Conf.*, 12B, 261-280. ([pdf](#))

Jean, M.M., Bodnar, B., Farley, C., and Taylor, L.A. (2016) 'Rusty Rocks' from the Moon: Volatile-element contributions from meteorites. *Proc. 47th Lunar & Planetary Science Conf.*, Abstract 2498. ([pdf](#))

Jedwab, J. (1973) Surface morphology of free-growing ilmenites and chromites from vuggy rocks 10072,31 and 12036,2. Proc. 2nd Lunar Science Conf., 923-935. ([pdf](#))

Jolliff, B.L (1993) A monazite-bearing clast in Apollo 17 melt breccia. Proc. 24th Lunar & Planetary Science Conf., 725-726. ([pdf](#))

Jolliff, B.L., Haskin, L.A., Colson, R.O. and Wadhwa, M. (1993) Partitioning in REE-saturated minerals: theory, experiment, and modelling of whitlockite, apatite, and evolution of lunar residual magmas. *Geochimica et Cosmochimica Acta*, 57, 4069-4094.

Jolliff, B.L., Floss, C., McCallum, I.S. and Schwartz, J.M. (1999) Geochemistry, petrology, and cooling history of 14161,7373: A plutonic lunar sample with textural evidence of granitic-fraction separation by silicate-liquid immiscibility. *American Mineralogist*, 84, 821-837.

Jolliff, B.L., Korotev, R.L., Zeigler, R.A. and Floss, C. (2003) Northwest Africa 773: Lunar mare breccia with a shallow-formed olivine-cumulate component, inferred very-low-Ti (VLT) heritage, and a KREEP connection. *Geochimica et Cosmochimica Acta*, 67, 4857-4879.

Jolliff, B.L., Hughes, J.M., Freeman, J.J. and Zeigler, R.A. (2006) Crystal chemistry of lunar merrillite and comparison to other meteoritic and planetary suites of whitlockite and merrillite. *American Mineralogist*, 91, 1583-1595.

Joy, K.H., Crawford, I.A., Downes, H., Russell, S.S. and Kearsley, A.T. (2006) A petrological, mineralogical, and chemical analysis of the lunar mare basalt meteorite LaPaz Icefield 02205, 02224, and 02226. *Meteoritics & Planetary Science*, 41, 1003-1025. ([pdf](#))

Joy, K.H., Crawford, I.A., Anand, M., Greenwood, R.C., Franchi, I.A., and Russell, S.S. (2008) The petrology and geochemistry of Miller Range 05035: A new lunar gabbroic meteorite. *Geochimica et Cosmochimica Acta*, 72, 3822-3844.

Joy, K.H., Burgess, R., Hinton, R., Fernandes, V.A., Crawford, I.A., Kearsley, A.T. and Irving, A.J. (2009) U-Pb and Ar-Ar chronology of lunar meteorite Northwest Africa 4472. Proc. 40th Lunar & Planetary Science Conf., Abstract 1708. ([pdf](#))

Joy, K.H., Burgess, R., Hinton, R., Fernandes, V.A., Crawford, I.A., Kearsley, A.T. and Irving, A.J. (2011) Petrogenesis and chronology of lunar meteorite Northwest Africa 4472: A KREEPy regolith breccia from the Moon. *Geochimica et Cosmochimica Acta*, 75, 2420-2452.

Joy, K.H., Nemchin, A., Grange, M., Lapen, T.J., Peslier, A.H., Ross, D.K., Zolensky, M.E. and Kring, D.A. (2014) Petrography, geochronology and source terrain characteristics of lunar meteorites Dhofar 925, 961 and Sayh al Uhaymir 449. *Geochimica et Cosmochimica Acta*, 144, 299-325.

Joy, K.H., Visscher, C., Zolensky, E., Mikouchi, T., Hagiya, K., Ohsumi, K. and Kring, D.A. (2015) Identification of magnetite in

lunar regolith breccia 60016: Evidence for oxidized conditions at the lunar surface. *Meteoritics & Planetary Science*, 50, 1157-1172. ([pdf](#))

Kaneko, S., Miyahara, M., Ohtani, E., Arai, T., Hirao, N. and Sato, K. (2015) Discovery of stishovite in Apollo 15299 sample. *American Mineralogist*, 100, 1308–1311.

Kayama, M., Tomioka, N., Ohtani, E., Seto, Y., Nagaoka, H., Götze, J., Miyake, A., Ozawa, S., Sekine, T., Miyahara, M., Tomeoka, K., Matsumoto, M., Shoda, N., Hirao, N. and Kobayashi, T. (2018) Discovery of moganite in a lunar meteorite as a trace of H₂O ice in the Moon's regolith. *Science Advances*, 4, EAAR4378, 1-11. ([pdf](#))

Kartashov, P.M., Bogatikov, O.A., Mokhov, A.V., Gorshkov, A.I., Ashikhmina, N.A., Magazina, L.O. and Koporulina, E.V. (2006) Lunar Monazites. In *Doklady Earth Sciences; MAIK Nauka/Interperiodica*, 407A, 498-502. ([abstract online](#))

Keprta, T., Clemett, S.J., Berger, E. L., Rahman, Z., McKay, D.S., Gibson, E.K. and Wentworth, S. J. (2014) Vesicles in Apollo 15 green glass: the nature of ancient lunar gases. *Proc. 45th Lunar & Planetary Science Conf.*, Abstract 2507 ([pdf](#))

Kleinmann, B. and Ramdohr, P. (1971) Alpha corundum from the lunar dust. *Earth & Planetary Science Letters*, 13, 19-22.

Koeberl, C., Kurat, G. and Branstatter, F. (1991) Lunar meteorite Yamato-793274: Mixture of Mare and Highland components and barringerite from the Moon. *Proc. NIPR Symp. Antarct. Meteorites*, 4, 33-55. ([pdf](#))

Kuehner, S.M., Irving, A. J., Korotev, R. L., Hupé, G. M. and Ralew, S. (2007) Zircon-baddeleyite-bearing silica+K-feldspar granophyric clasts in KREEP-rich lunar breccias Northwest Africa 4472 and 4485. *Proc. 38th Lunar Planetary Science Conf.*, Abstract 1516. ([pdf](#))

Kuehner, S.M., Irving, A. J. and Korotev, R. L. (2014) Petrology and composition of lunar felsic granulitic breccia Northwest Africa 8022 and occurrence of forsterite in lunar breccia NWA8001. *Proc. 45th Lunar Planetary Science Conf.*, Abstract 2495. ([pdf](#))

Kuehner, S.M., Wittmann, A., Korotev, R. L., Carpenter, P., Macke, R.J., Britt, D.T. and Irving, A. J. (2016) Petrologic, chemical and physical characterization of unique lunar vitric regolith breccia Northwest Africa 10404. *Proc. 47th Lunar Planetary Science Conf.*, Abstract 2246. ([pdf](#))

Li, G., Bai, W., Shi, N., Fang, Q., Xiong, M., Yang, J., Ma, Z. and Rong, H. (2012) Linzhiite, FeSi₂, a redefined and revalidated mineral species from Luobusha, Tibet, China. *European Journal of Mineralogy*, 24, 1047-1052.

Lindsley, D.H., Papike, J.J. and Bence, A.E. (1972) Pyroxferroite breakdown at low pressure and high temperature. Proc. 3rd Lunar Science Conf., 483. ([pdf](#))

Lui, Y., Floss, C., Day, J.M., Hill, E. and Taylor, L.A. (2009) Petrogenesis of lunar mare basalt meteorite Miller Range 05035. Meteoritics & Planetary Science, 44, 261-284. ([pdf](#))

Lui, Y., Jolliff, B.J., Zeigler, R.A., Korotev, R.L., Wan, Y., Xie, H., Zhang, Y., Dong, C. and Wang, W. (2012) Comparative zircon U-Pb geochronology of impact-melt breccias from Apollo 12 and lunar meteorite SaU 169, and implications for the age of the Imbrium impact. Earth and Planetary Science Letters, 319-320, 277-286.

Lovering, J.F., Wark, D.A., Reid, A.F., Ware, N.G., Keil, K., Prinz, M., Bunch, T.E., El Goresy, A., Ramdohr, P., Brown, G.M., Peckett, A., Phillips, R., Cameron, E.M., Douglas, J.A.V. and Plant, A.G. (1971). Tranquillityite: A new silicate mineral from Apollo 11 and Apollo 12 basaltic rocks. Proc. 2nd Lunar Science Conf., 39-45. ([pdf](#))

Lowe, M., Mahmood, S., McKeeby, B., and Greenwood, J. P. (2016) Cl-rich britholite substitution in apatite of high-titanium basalt 75055: A chlorine and REE-enriched phase of lunar phosphates. Proc. 47th Lunar & Planetary Science Conf. Abstract 1285. ([pdf](#))

Ma, M.-S., Schmitt, R.A., Taylor, G.J., Warner, R.D., and Keil, K. (1981) Chemical and petrographic study of spinel troctolite in 67435: Implications for the origin of Mg-rich plutonic rocks. Proc. 12th Lunar & Planetary Science Conf., 640-642. ([pdf](#))

Martin, D.J.P., Pernet-Fisher, J.F., Joy, K.H., Wogelius, R.A., Morlok, A. and Hiesinger, H. (2017) Investigating the shock histories of lunar meteorites Miller Range 090034, 090070, and 090075 using petrography, geochemistry, and micro-FTIR spectroscopy. Meteoritics & Planetary Science, 52, 1103-1124. ([pdf](#))

Marvin, U.B. (1983) The discovery and initial characterization of Allan Hills 81005: the first lunar meteorite. Geophysical Research Letters, 10, 775-778.

Marvin, U.B., and Walker, D. (1985) A transient heating event in the history of a highlands troctolite from Apollo 12 soil 12033. Proc. 15th Lunar and Planetary Science Conf., Journal of Geophysical Research, 90, C421-C429. ([pdf](#))

Marvin, U.B., Carey, JW. and Lindstrom, M.M. (1989) Cordierite-spinel troctolite, a new magnesium-rich lithology from the lunar highlands. Lunar and Planetary Exploration, 243, 925-928. ([abstract online](#))

McCallum, I.S. and Schwartz, J.M. (2001) Lunar Mg suite: Thermobarometry and petrogenesis of parental magmas. Journal of Geophysical Research, 106, 27,969-27,983. ([pdf](#))

McCallum, I.S., Domeneghetti, M.C., Schwartz, J.M., Mullen, E.K., Zema, M., Cámara, F., McCammon, C. and Ganguly, J. (2006) Cooling history of lunar Mg-suite gabbro-norite 76255, troctolite 76535 and Stillwater pyroxenite SC-936: The record in exsolution and ordering in pyroxenes. *Geochimica et Cosmochimica Acta*, 70, 6068-6078.

McCanta, M.C., Darby Dyar, M., Rutherford, M.J. Lanzirotti, A., Sutton, S.R. and Thomson, B.J. (2017) In situ measurement of ferric iron in lunar glass beads using Fe-XAS. *Icarus*, 285, 95-102.

McCubbin, F.M., Nekvasil, H., Jolliff, B.L., Carpenter, P.K. and Zeigler, R.A. (2008) A survey of lunar apatite volatile contents for determining bulk lunar water: how dry is “bone dry”? *Proc. 39th Lunar & Planetary Sciences Conf.*, Abstract 1788. ([pdf](#))

McCubbin, F.M., Steele, A., Haun, E.H., Nekvasil, H., Yamashita, S. and Hemley, R.J. (2010) Nominally hydrous magmatism on the Moon. *Proc. National Academy of Science USA*, 107, 11223-11228. ([pdf](#))

McCubbin, F.M., Jolliff, B.L., Nekvasil, H., Carpenter, P.K., Zeigler, R.A., Steele, A., Elardo, S.M., and Lindsley, D.H. (2011) Fluorine and chlorine abundances in lunar apatite: Implications for heterogeneous distributions of magmatic volatiles in the lunar interior. *Geochimica et Cosmochimica Acta*, 75, 5073-5093.

McCubbin, F.M. and 13 others (2015) Magmatic volatiles (H, C, N, F, S, Cl) in the lunar mantle, crust, and regolith: Abundances,

distributions, processes, and reservoirs. *American Mineralogist*, 100, 1668-1707. ([pdf](#))

McKay D.S. and Williams R.J. (1979) A geologic assessment of potential lunar ores. In: *Space Resources and Space Settlements* (J. Billingham et al., eds.), pp. 243-256. NASA SP-428.

McKay, D.S., and Wentworth, S.J. (1992) Morphology and composition of condensates on Apollo 17 orange and black glass. In *Lunar Science Institution, Workshop on Geology of the Apollo 17 Landing Site*, 31-36.

McKay, D.S., and Wentworth, S.J. (1993) Grain surface features of Apollo 17 orange and black glass. *Proc. 24th Lunar & Planetary Sciences Conf.*, Part 2: G-M961–962. ([pdf](#))

McLeod, C.L. and Krekeler, M.P.S. (2017) Sources of Extraterrestrial Rare Earth Elements: To the Moon and Beyond. *Resources*, 6, 1-28. ([pdf](#))

Meyer, C. (2003) The Lunar Petrographic Educational Thin Section Set. ([pdf](#))

Meyer, H.O.A. and Boctor N.Z. (1974) Opaque mineralogy: Apollo 17 rock 75035. *Proc. 5th Lunar Science Conf.*, 707-716. ([pdf](#))

Meyer, C. and Yang, S.V. (1988) Tungsten-bearing yttrobetafite in lunar granophyre. *American Mineralogist*, 73, 1420-1425.

Miyahara, M., Kaneko, S., Sakai, T., Nagase, T., Kayama, M., Nishido, H. and Hirao, N. (2013) Discovery of seifertite in a shocked lunar meteorite. *Nature Communications*, 4, Article 1737, 1-7. ([pdf](#))

Miyahara, M., Ohtani, E., Yamaguchi, A. and Ozawa, S. (2016) Discovery of coesite, stishovite and seifertite in shocked meteorites and its implication. *Proc. 79th Meeting of the Meteorite Society*, Abstract 6026. ([pdf](#))

Molly, C., McCanta, M.C., Dyar, M.D., Rutherford, M.J., Lanzirotti, A., Sutton, S.R. and Thomson, B.J. (2017) In situ measurement of ferric iron in lunar glass beads using Fe-XAS. *Icarus*, 285, 95-102.

Morland, Z.S., Joy, K.H., Gholinia, A. and Degli Alessandrini, G. (2019) Metal in lunar meteorite Northwest Africa 10989: Insight into survivability of impactor material delivered to the Moon. *Proc. 50th Lunar & Planetary Sciences Conf.*, Abstract 1275. ([pdf](#))

Muhling, J.R., Suvorova, A.A. and Rasmussen, B. (2014) The occurrence and composition of chevkinite-(Ce) and perrierite-(Ce) in tholeiitic intrusive rocks and lunar mare basalt. *American Mineralogist*, 99, 1911-1921.

Nagaoka, H., Karouji, Y., Arai, T., Ebihara, M. and Hasebe, N. (2013) Geochemistry and mineralogy of a feldspathic lunar meteorite (regolith breccia), Northwest Africa 2200. *Polar Science*, 7, 241-259. ([pdf](#))

Nagaoka, H., Takeda, H., Karouji, Y., Ohtake, M., Yamaguchi, A., Yoneda, S. and Hasebe, N. (2014) Implications for the origins of pure anorthosites found in the feldspathic lunar meteorites, Dhofar 489 group. *Earth, Planets and Space*, 66, 1-15. ([pdf](#))

Nagaoka, H., Takeda, H., Karouji, Y., Ohtake, M., Yamaguchi, A., Yoneda, S. and Hasebe, N. (2015) Mineralogy and petrology of lunar meteorite Northwest Africa 2977 consisting of olivine cumulate gabbro including inverted pigeonite. *Earth, Planets and Space*, 67, 1-8. ([pdf](#))

Nazarov, M.A., Demidova, S.I., Patchen, A. and Taylor, L.A. (2002) Dhofar 301. 302. 303: three new lunar highland meteorites from Oman. *Proc. 33rd Lunar & Planetary Sciences Conf.*, Abstract 1186. ([pdf](#))

Nazarov, M.A., Demidova, S.I., Patchen, A. and Taylor, L.A. (2004) Dhofar 311, 730 and 731: New lunar meteorites from Oman. *Proc. 35th Lunar & Planetary Sciences Conf.*, Abstract 1233. ([pdf](#))

Nazarov, N.A., Aranovich, L.Ya., Demidova, S.I., Ntaflos, T. and Brandstätter, F. (2011) Aluminous enstatites of lunar meteorites and deep-seated lunar rocks. *Petrology*, 19, 13-25.

Nazarov, N.A., Demidova, S.I., Ntaflos, T. and Brandstätter, F. (2012a) Native silicon, Fe-silicides and a condensate lithology in the Dhofar 280 lunar meteorite. *Proc. 43rd Lunar & Planetary Science Conf.*, Abstract 1073. ([pdf](#))

Nazarov, N.A., Demidova, S.I., Anosova, M.O., Kostitsyn, Y.A., Ntaflos, T. and Brandstätter, F. (2012b) Native silicon and iron silicides in the Dhofar 280 lunar meteorite. *Petrology*, 20, 506-519.

Nazarov, N.A., Shornikov, S.I. and Demidova, S.I. (2015) Origin of native silicon and iron silicides in the Dhofar 280 lunar meteorite. *Petrology*, 23, 168-175.

Neal, C.R. and Taylor, L.A. (1991) Evidence for metasomatism of the lunar highlands and the origin of whitlockite. *Geochimica et Cosmochimica Acta*, 55, 2965-2980.

Neal, C.R., Hacker, M.D., Snyder, G.A., Taylor, L.A., Liu, Y.-G. and Schmitt, R.A. (1994) Basalt generation at the Apollo 12 site, Part 2: Source heterogeneity, multiple melts, and crustal contamination. *Meteoritics*, 29, 349-361.

Nemchin, A.A., Pidgeon, R.T., Whitehouse, M.J., Vaughan, J.P. and Meyer, C. (2008) SIMS U–Pb study of zircon from Apollo 14 and 17 breccias: Implications for the evolution of lunar KREEP. *Geochimica et Cosmochimica Acta*, 72, 668-689.

Nemchin, A.A., Pidgeon, R.T., Healy, D., Grange, M.L., Whitehouse, M.J. and Vaughan, J.P. (2009) The comparative behavior of apatite-zircon U-Pb systems in Apollo 14 breccias: Implications for the thermal history of the Fra Mauro Formation. *Meteoritics & Planetary Science*, 44, 1717-1734. ([pdf](#))

Nemchin, A.A., Jeon, H., Bellucci, J.J., Timms, N.E., Snape, J.F., Kilburn, M.R. and Whitehouse, M.J. (2017) Pb-Pb ages of feldspathic clasts in two Apollo 14 breccia samples. *Geochimica et Cosmochimica Acta*, 217, 441-461.

Ni, P., Zhang, Y. and Gan, Y. (2017) Volatile loss during homogenization of lunar melt inclusions. *Earth and Planetary Science Letters*, 478, 214-224.

Norman, M.D., Borg, L.E., Nyquist, L.E. and Bogard, D.D. (2003) Chronology, geochemistry, and petrology of a ferroan noritic anorthosite clast from Descartes breccia 67215: Clues to the age, origin, structure, and impact history of the lunar crust. *Meteoritics & Planetary Science*, 38, 645-661.

Norman, M.D. and Nemchin, A.A. (2014) A 4.2 billion year old impact basin on the Moon: U–Pb dating of zirconolite and apatite in lunar melt rock 67955. *Earth and Planetary Science Letters*, 388, 387-398.

North, S.N., Jolliff, B.L. and Korotev, R.L. (2013) Pyroxene composition in lunar meteorite NWA 727 and comparison to NWA 7007. *Proc. 44th Lunar & Planetary Science Conf.*, Abstract 3013. ([pdf](#))

Ohtani, E., Ozawa, S., Miyahara, M., Ito, Y., Mikouchi, T., Kimura, M., Arai, T., Sato, K. and Hiraga, K. (2011) Coesite and stishovite in a shocked lunar meteorite, Asuka-881757, and impact events in lunar surface. *PNAS*, 108, 463-466.

Papike, J.J. and Bence, A.E. (1972) Apollo 14 inverted pigeonites: possible samples of lunar plutonic rocks. *Earth & Planetary Science Letters*, 14, 176-182.

Papike J.J., Karner J.M., and Shearer C.K. (2003) Determination of planetary basalt parentage: A simple technique using the electron microprobe. *American Mineralogist*, 88, 469-472.

Papike, J.J., Shearer, C.K., Burger, P.V. and Bell, A.S. (2014) The REE (Moon) and sodium (Mars) crystal chemistry of merrillite: an important discriminant of Moon-Mars differences and evolution. *Proc. 8th Mars Conf.*, Abstract 1300. ([pdf](#))

Patchen, A.P. (2004) The most reduced rock from the Moon - Apollo 14 basalt 14053: extreme reduction entirely from a re-heating event. *Proc. 35th Lunar & Planetary Science Conf.*, Abstract 1762. ([pdf](#))

Pernet-Fisher, J.F., Joy, K.H. and Martin, D.J.P. (2016) Plagioclase in regolith breccias: critical tools for deciphering the shock history of the lunar highlands. *Proc. 47th Lunar & Planetary Science Conf.*, Abstract 1499. ([pdf](#))

Pidgeon, R.T., Nemchin, A.A., van Bronswijk, W., Geisler, T., Meyer, C., Compston, W. and Williams, I.S. (2007) Complex history of a zircon aggregate from lunar breccia 73235. *Geochimica et Cosmochimica Acta*, 71, 1370-1381.

Pieters, C.M., Besse, S., Boardman, J., Buratti, B., Cheek, L., Clark, R.N., Combe, J.P., Dhingra, D., Goswami, J.N., Green, R.O. and others. (2011) Mg-spinel lithology: A new rock type on the lunar farside. *Journal of Geophysical Research*, 116, E00G08 ([pdf](#))

Potts, N.J., Tartèse, R., Anand, M., van Westrenen, W., Griffiths, A.A., Barrett, T.J. and Franchi, I.A. (2016) Characterization of mesostasis regions in lunar basalts: Understanding late-stage melt evolution and its influence on apatite formation. *Meteoritics & Planetary Science*, 51, 1555-1575.

Prinz, M., Dowty, E., Keil, K., and Bunch, T.E. (1973) Spinel troctolite and anorthosite in Apollo 16 samples. *Science*, 179, 74-76.

Prissel, T.C., Parman, S.W., Jackson, C.R.M., Rutherford, M.J., Hess, P.C., Head, J.W., Cheek, L., Dhingra, D. and Pieters, C.M. (2014) Pink Moon: The petrogenesis of pink spinel anorthosites and implications concerning Mg-suite magmatism. *Earth and Planetary Science Letters*, 403, 144-156.

Prissel, T.C., Parman, S.W. and Head, J.W. (2016) Formation of the lunar highlands Mg-suite as told by spinel. *American Mineralogist*, 101, 1624-1635. ([pdf](#))

Provincio, P., Bell, A.S., Shearer, C. and Burger, P. (2015) A TEM study of the sulfide replacement assemblages in lunar breccia.

Proc. 46th Lunar and Planetary Science Conf., Abstract 2812.
(pdf)

Quick J.E., James O.B., and Albee A.L. (1981) Petrology and petrogenesis of lunar breccia 12013. Proc. 12th Lunar and Planetary Science Conf., 117-172. (pdf)

Ramhdor, P. (1972) Lunar pentlandite and sulfidization reactions in microbreccia 14315,9. Earth and Planetary Science Letters, 15, 113-115.

Ramdohr, P. and El Goresy, A. (1970) Opaque minerals of the lunar Rocks and dust from Mare Tranquillitatis. Science, 167, 615-618. (abstract online)

Rasmussen, B., Fletcher, I.R. and Muhling, J.R. (2008) Pb/Pb geochronology, petrography and chemistry of Zr-rich accessory minerals (zirconolite, tranquillityite and baddeleyite) in mare basalt 10047. Geochimica et Cosmochimica Acta, 72, 5799-5818.

Rasmussen, B., Fletcher, I.R. Gregory, C.J., Muhling, J.R. and Suvorova, A.A. (2012) Tranquillityite: The last lunar mineral comes down to Earth. Geology, 40, 83-86. (pdf)

Rhodes, J.M., Brannon, J.C., Rodgers, K.V., Blanchard, D.P. and Dungan, M.A. (1977) Chemistry of Apollo 12 mare basalts: Magma types and fractionation processes. Proc. 8th Lunar Science Conference, 1305-1338. (pdf)

Ridley, W.I., Hubbard, N.J., Rhodes, J.M., Weismann, H. and Bansal, B. (1973) The petrology of lunar breccia 15445 and petrogenetic implications. Journal of Geology, 81, 621-631.

Roberts, S.E., Jean, M.M., Sueilem, M.B., and L.A.Taylor, L.A. (2017) Northwest Africa 10986: An impact-melt breccia from the lunar highlands. Proc. 48th Lunar & Planetary Science Conf., Abstract 2220. (pdf)

Robinson, K.L., Barnes, J.J., Anand, M., Taylor, G.J., and Franchi, I.A. (2016) Volatiles in evolved lunar rocks: Connecting water and chlorine. New Views of the Moon 2 meeting, Article 6081.

Robinson, K.L. and Kring, D.A. (2018) The Northwest Africa 5744 group: a glimpse into Schrödinger-like lithologies? Proc. 49th Lunar & Planetary Science Conf., Abstract 1635. (pdf)

Rubin, A.E. (2015) Maskelynite in asteroidal, lunar and planetary basaltic meteorites: An indicator of shock pressure during impact ejection from their parent bodies. Icarus, 257, 221-229.

Ryder, G. (1985) Catalog of Apollo 15 Rocks Part 2. 15306-15468. Curatorial Branch Publication, 72, 443 pp. NASA.

Ryder, G. and Bower, J.F. (1977) Petrology of Apollo 15 black-and-white rocks 15445 and 15455 - fragments of the Imbrium impact melt sheet? Proc. 8th Lunar Science Conf., 1895-1923. (pdf)

Saal, A.E., Hauri, E.K., Lo Cascio, M., Van Orman, J.A., Rutherford, M.J. and Cooper, R.F. (2008) Volatile content of lunar volcanic glasses and the presence of water in the Moon's interior. *Nature*, 254, 192-195. ([pdf](#))

Saal, A.E., Hauri, E.K., Van Orman, J.A. and Rutherford, M.J. (2013) Hydrogen Isotopes in lunar volcanic glasses and melt inclusions reveal a carbonaceous chondrite heritage. *Science*, 340, 1317-1320.

Sack, R.O. and Ghiorso, M.S. (1991): Chromian spinels as petrogenetic indicators: Thermodynamic and petrological applications. *American Mineralogist*, 76, 827-847.

Seddio, S.M., Jolliff, B.L., Korotev, R.L. and Zeigler, R.A. (2009) A newly characterized granite from the Apollo 12 regolith. Proc. 40th Lunar & Planetary Science Conf., Abstract 2704. ([pdf](#))

Seddio, S.M., Jolliff, B.L., Korotev, R.L. and Zeigler, R.A. (2011) Fragments of granite in Apollo 12 regolith: Pieces of 12013? Proc. 42nd Lunar & Planetary Science Conf., Abstract 2381. ([pdf](#))

Seddio, S.M., Jolliff, B.L., Korotev, R.L. and Carpenter, P.K. (2011) Back-scattered Electron Tomography and X-Ray Microanalysis of Zirconolite in Lunar Granite 12032,366-19. *Microscopy Microanalysis*, 17 (Suppl. 2), 570-571.

Seddio, S.M., Korotev, R.L. and Jolliff, B.L. (2012a) Two Apollo granite rock fragments: evidence for the proximal coexistence of

high-Ti impact-melt breccia and granite. Proc. 43rd Lunar & Planetary Science Conf., Abstract 1006. ([pdf](#))

Seddio, S.M., Jolliff, B.L., Korotev, R.L. and Carpenter, P.K. (2012b) Thorite in an Apollo 12 granite fragment and age determination using the electron microprobe. Proc. 43rd Lunar & Planetary Science Conf., Abstract 2704. ([pdf](#))

Seddio, S.M., Wang, A., Korotev, R.L. and Jolliff, B.L. (2013a) Silica polymorphs in lunar granite. Proc. 44th Lunar & Planetary Science Conf., Abstract 2660. ([pdf](#))

Seddio, S.M., Jolliff, B.L., Korotev, R.L. and Zeigler, R.A. (2013b) Petrology and geochemistry of lunar granite 12032,366-19 and implications for lunar granite petrogenesis. *American Mineralogist*, 98, 1697-1713.

Seddio, S.M., Jolliff, B.L., Korotev, R.L. and Carpenter, P.K. (2014) Thorite in an Apollo 12 granite fragment and age determination using the electron microprobe. *Geochimica et Cosmochimica Acta*, 135, 307-320.

Shaulis, B.J., Righter, M., Lapen, T.J., Korotev, R.L., Irving, A.J. and Kuehner, S.M. Baddeleyite chronology of Northwest Africa 6950: a 3.1 Ga lunar olivine gabbro paired with NWA 2977 and the cumulate mare gabbro lithology in NWA 773. Proc. 43rd Lunar & Planetary Science Conf., Abstract 2236. ([pdf](#))

Shaulis, B.J., Kring, D.A., Lapen, T.J. and Righter, M. (2016) Petrology and distribution of U-Pb ages in lunar meteorite breccia Miller Range (MIL) 13317. Proc. 47th Lunar & Planetary Science Conf., Abstract 2027. ([pdf](#))

Shearer, C.K., Papike, J.J. and Spilde, M.N. (2001) Trace-element partitioning between immiscible lunar melts: An example from naturally occurring lunar melt inclusions. *American Mineralogist*, 86, 238-246.

Shearer, C.K., Burger, P.V., Sutton, S.R., Papike, J.J. and McCubbin, F. (2011) REE crystal chemistry of phosphates in extraterrestrial basalts at different oxygen fugacities. Direct determination of europium valence state in merrillite-whitlockite. Proc. 42nd Lunar & Planetary Science Conf., Abstract 1143. ([pdf](#))

Shearer, C.K., Burger, P.V., Guan, Y., Papike, J.J., Sutton, S.R. and Atudorei, N.-V. (2012) Origin of sulfide replacement textures in lunar breccias. Implications for vapor element transport in the lunar crust. *Geochimica et Cosmochimica Acta*, 83, 138-158.

Shearer, C.K., Sharp, Z.D., Burger, P.V., McCubbin, F.M., Provencio, P.P., Brearley, A.J. and Steele, A. (2014) Chlorine distribution and its isotopic composition in “rusty rock” 66095. Implications for volatile element enrichments of “rusty rock” and lunar soils, origin of “rusty” alteration, and volatile element behaviour on the Moon. *Geochimica et Cosmochimica Acta*, 139, 411-433.

Shearer, C.K., Burger, P.V., Bell, A.S., Guan, Y. and Neal, C.R. (2015a) Exploring the Moon’s surface for remnants of the lunar mantle 1. Dunite xenoliths in mare basalts. A crustal or mantle origin? Proc. 46th Lunar & Planetary Science Conf., Abstract 1426. ([pdf](#))

Shearer, C.K., Elardo, S.M., Petro, N.E., Borg, L.E. and McCubbin, F.M. (2015b) Origin of the lunar highlands Mg-suite: An integrated petrology, geochemistry, chronology, and remote sensing perspective. *American Mineralogist*, 100, 294-325.

Shervais, J.W., Taylor, L.A., Laul, J.C., Shih, C.-Y., and Nyquist, L. E. (1985) Very high potassium (VHK) basalt: Complications in mare basalt petrogenesis. Proc. 16th Lunar & Planetary Sci. Conf. in *J. Geophys. Res.*, 90, D3-D18. ([pdf](#))

Shi, N., Li, G., Bai, W., Xiong, M., Yang, J., Fang, Q., Ma, Z., Rong, H. (2012) Naquite, FeSi, a new mineral species from Luobusha, Tibet, Western China. *Acta Geologica Sinica*, 86, 533-538.

Simon, S.B., Papike, J.J. and Shearer, C.K. (1983) Petrology of ALHA81005, the first lunar meteorite. *Geophysical Research Letters*, 10, 787-790.

Simpson, P.R. and Bowie, S.H.U. (1970) Quantitative optical and electron-probe studies of opaque phases in Apollo 11 samples. Proc. Apollo 11 Lunar Science Conf., 1, 873-890. ([pdf of all abstracts from the 1st Lunar Conference](#))

Skinner, B.J. (1970) High crystallization temperatures indicated for igneous rocks from Tranquillity Base. *Science*, 167, 652-654.

Smith, J.H., Meyer, C., Compston, W. and Williams, I.S. (1986) 73235,82 (Pomegranate): an assemblage of lunar zircon with unique overgrowth. *Proc. 17th Lunar & Planetary Science Conf.*, 805-806. ([pdf](#))

Smith, J.V. and Steele, I.M. (1976) Lunar Mineralogy: a heavenly story. Part II. *American Mineralogist*, 61, 1059-1116. ([pdf](#))

Snyder, G.A. and Taylor, L.A. (1991) Whitlockite-rich basalts from 4-10 mm boulders at Apollo 14: Mineralogy and petrology. *Proc. 22nd Lunar & Planetary Science Conf.*, Abstract 1641. ([pdf](#))

Spicuzza, M.J., Valley, J.W., Fournelle, J., Huberty, J.M., and Treiman, A. (2011) Native silicon and Fe-silicides from the Apollo 16 lunar regolith: extreme reduction, metal-silicate immiscibility, and shock melting. *Proc. 42nd Lunar & Planetary Science Conf.*, Abstract 2231. ([pdf](#))

Sugihara, T., Ohtake, O., Owada, A., Ishii, T., Otsuki, M. and Takeda, H. (2004) Petrology and reflectance spectroscopy of lunar meteorite Yamato 981031: Implications for the source region of the meteorite and remote-sensing spectroscopy. *Antarct. Meteorite Research*, 17, 209-230. ([pdf](#))

Stöffler D., Knöll H.-D., Marvin U. B., Simonds C. H., and Warren P. H. (1980) Recommended classification and nomenclature of

lunar highland rocks - a committee report. *Proceedings of the Conference on the Lunar Highlands Crust* (J. J. Papike and R. B. Merrill, eds.), pp. 51-70. Pergamon, New York.

Takeda, H. and Miyamoto, M. (1977) Inverted pigeonites from lunar breccia 76255 and pyroxene-crystallization trends in lunar and achondritic crusts. In *Proc. 8th Lunar Science Conf.*, 2617-2626. ([pdf](#))

Takeda, H., Nagaoka, H., Ohtake, M., Kobayashi, S., Yamaguchi, A., Morota, T., Karouji, Y., Haruyama, J., Katou, M., Hiroi, T. and Nyquist, L.E. (2012) Comparisons of mineralogy of lunar meteorites possibly from the Farside and the Kaguya remote sensing data to reconstruct the earliest anorthositic crust of the Moon. *Proc. 43rd Lunar & Planetary Science Conf.*, Abstract 1379. ([pdf](#))

Tartèse, R., Anand, M. and Delhaye, T. (2013a) NanoSIMS Pb/Pb dating of tranquillityite in high-Ti lunar basalts: constraints on ages and duration of high-Ti volcanism on the Moon. *Proc. 44th Lunar & Planetary Science Conf.*, Abstract 1274. ([pdf](#))

Tartèse, R., Anand, M. and Delhaye, T. (2013b) NanoSIMS Pb/Pb dating of tranquillityite in high-Ti lunar basalts: Implications for the chronology of high-Ti volcanism on the Moon. *American Mineralogist*, 98, 1477-1486. ([pdf](#))

Tartèse, R., Anand, M., Barnes, J.J., Starkey, N.A., Franchi, I.A. and Sano, Y. (2013c) The abundance, distribution, and isotopic

composition of Hydrogen in the Moon as revealed by basaltic lunar samples: Implications for the volatile inventory of the Moon. *Geochimica et Cosmochimica Acta*, 122, 58-74. ([pdf](#))

Tartèse, R., Anand, M., Joy, K.H. and Franchi, I.A. (2014a) H and Cl isotope systematics of apatite in brecciated lunar meteorites Northwest Africa 4472, Northwest Africa 773, Sayh al Uhaymir 169, and Kalahari 009. *Meteoritics and Planetary Science*, 49, 2266-2289. ([pdf](#))

Tartèse, R., Anand, M., McCubbin, F.M., Elardo, S.M., Shearer, C.K. and Franchi, I.A. (2014b) Apatites in lunar KREEP basalts: The missing link to understanding the H isotope systematics of the Moon. *Geology*, 42, 363-366. ([pdf](#))

Taylor, L.A. and Williams, K.L. (1973) Cu-Fe-S Phases in Lunar Rocks. *American Mineralogist*, 58, 952-954. ([pdf](#))

Taylor, L.A., Mao, H.K. and Bell, P.M. (1973) "Rust" in the Apollo 16 rocks. *Proc. 4th Lunar Science Conf.*, 829-839. ([pdf](#))

Taylor, L.A., Mao, H.K. and Bell, P.M. (1974) Identification of the hydrated iron oxide mineral akaganéite in Apollo 16 lunar rocks. *Geology*, 2, 429-432.

Taylor, L.A., Shervais, J.W., Hunter, R.H., Shih, C.-Y., Bansal, B.M., Wooden, J.L., Nyquist, L.E. and Laul, L.C. (1983) Pre-4.2 AE mare-basalt volcanism in the lunar highlands. *Earth and Planetary Science Letters*, 66, 33-47.

Taylor, S.R. (1975) *Lunar Science: a post-Apollo view: Scientific results and insights from the lunar samples*. Pergamon Press, New York, USA.

Thiessen, F., Nemchin, A.A., Snape, J.F., Bellucci, J.J. and Whitehouse, M.J. (2018) Apollo 12 breccia 12013: Impact-induced partial Pb loss in zircon and its implications for lunar geochronology. *Geochimica et Cosmochimica Acta*, 230, 94-111.

Timms, N.E., Reddy, S.M., Healy, D., Nemchin, A.A., Grange, M.L., Pidgeon, R.T., and Hart, R. (2012) Resolution of impact-related microstructures in lunar zircon: A shock-deformation mechanism map. *Meteoritics and Planetary Science*, 47, 120-141. ([pdf](#))

Trill, R.J., Plant, A.G. and Douglas, J.A.V. (1970) Garnet: first occurrence in the lunar rocks. *Science*, 169, 981-982.

Treiman, A.H. (2007) Rhönite in Luna 24 pyroxenes: first find from the Moon, and implications for water in planetary magmas. *Proc. 38th Lunar & Planetary Science Conf.*, Abstract 1244. ([pdf](#))

Treiman, A.H., and Gross, J. (2012) Lunar cordierite-spinel troctolite: Igneous history and volatiles. *Proc. 43rd Lunar & Planetary Science Conf.*, Abstract 1196. ([pdf](#))

Treiman, A.H., Boyce, J.W., Gross, J., Guan, Y., Eiler, J. and Stolper, E.M. (2014) Phosphate-halogen metasomatism of granulite 79215: Impact-induced fractionation of lunar volatiles

and incompatible elements. *American Mineralogist*, 99, 1860-1870.

Treiman, A.H., and Semprich, J. (2019) Dunite in lunar meteorite Northwest Africa 11421: Petrology and Origin. Proc. 50th Lunar & Planetary Science Conf., Abstract 1225. ([pdf](#))

Treiman, A.H., Kulis, M.J. and Glazner, A.F. (2019) Spinel-anorthosites on the Moon: Impact melt origins suggested by enthalpy constraints. *American Mineralogist*, 104, 370-384.

Vanderliek, D.M. and Becker, H. (2017) Petrologic context of Zr phases in lunar impactites. Proc. 48th Lunar & Planetary Science Conf., Abstract 2991 ([pdf](#))

Vaniman, D.T. and Bish, D.L. (1990) Yoshiokaite, a new CaAl-silicate mineral from the Moon. *American Mineralogist*, 75, 676-486.

Walter, L.S., French, B.M. and Dian, A.S. (1972) Petrographic analysis of lunar samples 14171 and 14305 (Breccias) and 14310 (Melt rock). Proc. 3rd Lunar Science Conf., Abstract 1286. ([pdf](#))

Wang, Y., Hsu, W., Guan, Y., Li, X., Li, Q., Liu, Y. and Tang, G. (2012a) Petrogenesis of the Northwest Africa 4734 basaltic lunar meteorite. *Geochimica et Cosmochimica Acta*, 92, 329-344.

Wang, Y., Guan, Y., Hsu, W. and Eiler, J.M. (2012b) Water content, chlorine and hydrogen isotope compositions of lunar apatite.

Proc. 75th Annual Meteoritical Society Meeting, Abstract 5170 ([pdf](#))

Wang, Y. and Hsu, W. (2016) Shock-induced metamorphism in the lunar meteorite Northwest Africa 4734. Proc. 79th Annual Meteoritical Society Meeting, Abstract 6337. ([pdf](#))

Wang, Y., Hsu, W. and Guan, Y. (2019) An extremely heavy chlorine reservoir in the Moon: Insights from the apatite in lunar meteorites. *Nature Scientific Report*, 9, 5727. ([pdf](#))

Wark, D.A., Reid, A.F., Lovering, J.F. and El Goresy, A. (1973) Zirconolite (vs zirkelite) in lunar rocks. Proc. 4th Lunar Science Conf., 764-766. ([pdf](#))

Warner, R.D., Taylor, G.J., Keil, K., Planner, H.N., Nehru, C.E., Ma, M.-S. and Schmitt, R.A. (1978) Green glass vitrophyre 78526: an impact melt of very low-Ti mare basalt composition. Proc. 9th Lunar & Planetary Science Conf., 547-563. ([pdf](#))

Warren P.H., Taylor G.J., Keil K., Shirley D.N., and Wasson J.T. (1983a) Petrology and chemistry of two "large" granite clasts from the Moon. *Earth & Planetary Science Letters*, 64, 175-185.

Warren P.H., Taylor G.J., Keil K., Kallemeyn, G.W. Shirley D.N., and Wasson J.T. (1983b) Seventh Foray: Whitlockite-rich lithologies, a diopside-bearing troctolitic anorthosite, ferroan anorthosites, and KREEP. Proc. 14th Lunar and Planetary Science

Conf., Part 1 Journal of Geophysical Research, 88, Supplement, B151-164. ([pdf](#))

Wenkui, G. (1988) The problems of tin metallogeny. In Geology of Tin Deposits in Asia and the Pacific. Hutchinson, C.S. (ed.), Publ. Springer-Verlag, Berlin, 50-58.

Williams K.L. and Taylor L.A. (1974) Optical properties and chemical compositions of Apollo 17 armalcolites. *Geology*, 2, 5-8.

Wittmann, A., Korotev, R.L., and Jolliff, B.L. (2014) Third of a kind - impact melted lunar granulitic breccia meteorite Dhofar 1766. Proc. 45th Lunar & Planetary Science Conf., Abstract 1182. ([pdf](#))

Wittmann, A., Korotev, R.L., Jolliff, B.L., and Carpenter, P.K. (2018) Spinel assemblages in lunar meteorites Graves Nunataks 06157 and Dhofar 1528: Implications for impact melting and equilibration in the Moon's upper mantle. *Meteoritics & Planetary Science*, 54, 379-394.

Zeigler, R.A., Jolliff, B.L., Wang, A., Korotev, R.L., Kremser, D.T. and Haskin, L.A. (2001) Formation of carbonate and oxyhydroxide minerals by impact of a volatile-rich body. Proc. 32nd Lunar & Planetary Science Conf., Abstract 1243. ([pdf](#))

Zeigler R.A., Korotev R.L., Jolliff B.L. and Haskin L.A. (2005a) Petrography and geochemistry of the LaPaz Icefield basaltic lunar meteorite and source crater pairing with Northwest Africa 032. *Meteoritics & Planetary Science*, 40, 1073-1101. ([pdf](#))

Zeigler R.A., Korotev R.L., Jolliff B.L. and Haskin L.A. (2005b) Petrography of lunar meteorite MET 01210, a new basaltic regolith breccia. Proc. 36th Lunar & Planetary Science Conf., Abstract 2385. ([pdf](#))

Zhang, A.C. and Hsu, W-B. (2009) Petrography, mineralogy, and trace element geochemistry of lunar meteorite Dhofar 1180. *Meteoritics & Planetary Science*, 44, 1265-1286. ([pdf](#))

Zhang, A.C., Hsu, W-B., Li, X.H., Jiang, Y. and Tang, G-Q (2011) SIMS Pb/Pb dating of Zr-rich minerals in lunar meteorites Miller Range 05035 and LaPaz Icefield 02224: Implications for the petrogenesis of mare basalt. *Science China: Earth Sciences*, 53, 327-334. ([pdf](#))

Zhang, A.C., Hsu, W-B., Li, X.H., Ming H-L., Li, Q-L., Liu, Y. and Liu, Y. (2011) Impact melting of lunar meteorite Dhofar 458: Evidence from polycrystalline texture and decomposition of zircon. *Meteoritics & Planetary Science*, 46, 103-115. ([pdf](#))

Zhang, A.C., Taylor, L.A., Wang, R.C., Li, Q.L., Li, X.H., Patchen, A.D. and Liu, Y. (2012a) Thermal history of Apollo 12 granite and KREEP-rich rock: Clues from Pb/Pb ages of zircon in lunar breccia 12013. *Geochimica et Cosmochimica Acta*, 95, 1-14.

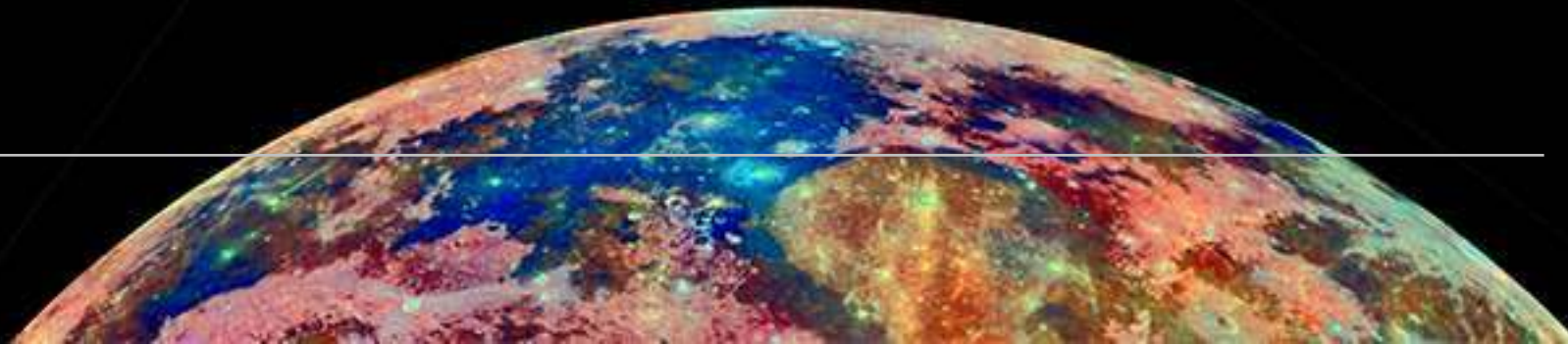
Zhang, A.C., Taylor, L.A., Wang, R.C., Li, Q.L., Li, X.H., Patchen, A.D. and Liu, Y. (2012b) SIMS Pb/Pb ages of baddeleyite and zirconolite in Apollo 17 norite 78235: implications for shock

histories of extraterrestrial rocks. Proc. 43rd Lunar & Planetary Science Conf., Abstract 1036. ([pdf](#))

Zhang, B., Lin, Y., Moser, D.E., Schieh, S.R. and Bouvier, A. (2018) Imbrium Zircon Age for Apollo 73155 Serenitatis Impact Melt Breccia: Implications for the Lunar Bombardment History. Bombardment: Shaping Planetary Surfaces and Their Environments Conf., Abstract 2021. ([pdf](#))

Zhou, Q., Yin, Q.Z., Zeigler, R., Korotev, R., Jolliff, B., Wu, F.Y., Li, Q.L., Tang, G.Q. and Li, C.L. (2015) U-Pb dating of phosphates in lunar meteorite Dhofar 1442. Proc. 46th Lunar & Planetary Science Conf., Abstract 1771. ([pdf](#))

Appendix



Requires further investigation

The following native metals and other species reported (mainly) from the Russian Luna missions have also been described:

Native Metals

Aluminium (Luna 20)
Antimony (Luna 16)
Boron (Luna 24)
Cerium (Luna 24 - Bogatikov et al., 2002)
Chromium (Luna 24)
Cobalt (Luna 24)
Hafnium (Luna 20)
Indium (Luna 16 & 24)
Gold (Luna 16)
Lead (Luna 16)
Molybdenum (Luna 16 & 24)
Nickel (Luna 24 & Apollo 12)
Niobium (Luna 24)
Platinum (Luna 16)
Rhenium (Luna 24 - Bogatikov et al., 2002)
Silver (Luna 16)
Tantalum (Luna 24)
Tin (Luna 16 & 24 - Bogatikov et al., 2002)
Tungsten (Luna 16 & 24)

Ytterbium (Luna 24)

Zinc (Luna 24 - Bogatikov et al., 2002)

Perhaps there is confusion between reports of native metals and bulk rock analyses of Luna rocks?

Other Species

Acanthite (Luna 24)
Anhydrite (Luna 24 - Mokhov et al., 2008)
Baryte (Luna 16, 20 & 24)
Bastnasite-(Ce) (Luna 24 - Mokhov et al., 2008)
Celestine (Luna 16)
Dolomite (Luna 24)
Eskolaite (Luna 24)
Fluorite (Luna 24 - Mokhov et al., 2008)
Greenockite (Luna 16)
Magnesite (Luna 24)
Oldhamite (Luna 24)
Oxycalciopyrochlore (Luna 24 - Mokhov et al., 2008)
Pyrite (Luna 20)
Scheelite (Luna 16 & 20)
Sylvite (Luna 24)

Wurtzite (Luna 24)

Zhanghengite (Luna 24)

Zincite (Luna 24)

Taylor (1975) suggests the three minerals below have been tentatively identified, but does not elaborate on their occurrence:

Ansovite

Hematite

Wustite

Gay et al. (1970a) examined soil and rocks from Apollo 11 and reported:

Aragonite in 10058

Mica in 10084

Tin in 10084

FrondeL (1975) in her Lunar Mineralogy book mentions:

Talnakhite

Wustite

Other problematic identifications (in this book) include:

Chapter 2 Section 3 Sulphides

Chapter 2 Section 7 Chlorides

Chapter 2 Sections 8&9 Titanium & Zirconium Minerals

Chapter 2 Section 21 Goethite

Chapter 2 Section 22 Nepheline Group

Chapter 2 Section 23 Amphibole Group

Selected Russian References

Bogatikov, O.A., Gorshkov, A.I., Mokhov, A.V., Kartashov, P.M., Ashikhmina, N.A. and Magazina, L.O. (2002) New Finds of Native Metals in a Lunar Regolith from the Crises Sea. *Doklady Earth Sciences*, 382, 83-85.

Gornostaeva, T.A., Mokhov, A.V., Kartashov, P.M. and Bogatikov, O.A. (2014): Native Hafnium from the Continental Regolith Probe. *Doklady Earth Sciences*, 456, 545-547.

Kartashov, P.M., Bogatikov, O.A., Mokhov, A.V., Gorshkov, A.I., Ashikhmina, N.A., Magazina, L.O. and Koporulina, E.V. (2006) Lunar monazites. *Doklady Earth Sciences*, 407A, 498-502.

Mokhov A.V., Kartashov P.M., Bogatikov, O.A. (2006) Rhenium oxide, potassium perrhenate, hydroxychlorides of iron and aluminium, baryte and celestine in Lunar regolith. *Doklady RAN*, 407, 654-659 (in Russian).

Mokhov, A.V., Kartashov, P.M. and Bogatikov, O.A. (2007) Moon under a microscope. Moscow, Nauka (in Russian).

Mokhov, A.V., Kartashov, P.M., Bogatikov, O.A., Ashikhmina, N.A., Magazina, L.O. and Koporulina, E.V. (2008) Fluorite, hatchettolite, calcium sulphate, and bastnasite-(Ce) in the lunar regolith from Mare Crisium. *Doklady Earth Sciences*, 422, 1178-1180.

Acknowledgements

This iBook includes many photographs and virtual microscopes created by the authors from samples supplied by NASA. Further thanks to NASA for images provided from their public websites. We also gratefully acknowledge the UK Science and Technology Facilities Council (STFC), the European Commission and the UK Space Agency (UKSA) that has supported our lunar research at the Open University, the outputs of which has contributed to this book. In addition, we would like to thank and acknowledge Kurt Hollocher, Sam Faircloth and the following sources for the use of images in this publication:

Al-Kathiri, A., Gnos, E. and Hoffman, B.A. (2007) The regolith portion of the lunar meteorite Sayh al Uhaymir 169. *Meteoritics & Planetary Science* 42, 2137-2152., Anand, M., Taylor, L.A., Nazarov, M.A., Shu, J., Mao, H.K. and Hemley, R.J. (2003a) New lunar mineral hapkeite: Product of impact-induced vapour-phase deposition in the regolith? *Proc 34th Lunar & Planetary Science Conf.*, Abstract 1818., Anand, M., Taylor, L.A., Floss, C., Shu, J., Neal, C.R., Terada, K. and Tanikawa, S. (2006) Petrology and geochemistry of LaPaz Icefield 02205: A new unique low-Ti mare-basalt meteorite. *Geochimica et Cosmochimica Acta*, 70, 246-264., Anand, M., Tartese, R. and Barnes, J.J. (2014) Understanding the origin and evolution of water in the Moon through lunar sample studies. *Phil. Trans. Roy. Soc. A*, 372., Arai, T., Takeda, H. and Warren, P.H. (1996) Four lunar mare lunar meteorites: crystallization trends of pyroxenes and spinels. *Meteoritics & Planetary Science*, 31, 877-892., Arai, T., Otsuki, M., Ishii, T., Mikouchi, T. and Miyamoto, M. (2005) Mineralogy of Yamato 983885 lunar polymict breccia with a KREEP basalt, a high-Al basalt, a very low-Ti basalt and Mg-rich rocks. *Antarctic Meteorite Research*, 18, 17-45., Arai, T., Takeda, H. and Warren, P.H. (2010) Antarctic lunar meteorites Yamato-793169, Asuka-881757, MIL 05035, and MET

01210 (YAMM): Launch pairing and possible cryptomare origin. *Geochimica et Cosmochimica Acta*, 74, 2231-2248., Barnes, J.J., Thompson, M.S., McCubbin, F.M., Howe, J.Y., Rahman, Z., Messenger, S. and Zega, T. (2018) Coordinated microanalysis of phosphates in Apollo 11 high-titanium basalts. *Proc. 49th Lunar & Planetary Science Conf.*, Abstract 2667., Barnes J. J., Franchi, I.A., McCubbin, F.M. and Anand, M. (2019) Multiple reservoirs of volatiles in the Moon revealed by the isotopic composition of chlorine in lunar basalts. *Geochimica Cosmochimica Acta*, in press., Boyce, J.W., Liu, Y., Rossman, G.R., Guan, Y., Eiler, J.M., Stolper, E.M. and Taylor, L.A. (2010) Lunar apatite with terrestrial volatile abundances. *Nature*, 466, 466-469., Burger, P.V., Shearer C.K. and Papike J.J. (2009) The multi-stage cooling history of lunar meteorite NWA 032 as recorded by phenocrystic olivine and pyroxene. *Proc. 40th Lunar & Planetary Science Conf.*, Abstract 2043., Cadogan, P.H. (1981) *The Moon our Sister Planet*. Cambridge University Press., Carpenter P., Edmunson J., Cohen B.A., Zeigler R.A., and Jolliff B.L. (2011) First lunar occurrence of keiviite-(Y) in troctolitic anorthosite 76335. *Proc. 42nd Lunar & Planetary Science Conf.*, Abstract 2767., Cernok, A., White, L.F., Darling, J., Dunlop, J. and Anand, M. (2019) Shock-induced microtextures in lunar apatite and merrillite. *Meteoritics & Planetary Science*, 1-21., Chen, J., A., Jolliff, B.L., Korotev, R.L., Wang, K., Wang, A., Carpenter, P.K., Chen, H. and Ling, Z.C. (2019) Northwest Africa 10985: a new lunar gabbro?. *Proc. 50th Lunar & Planetary Science Conf.*, Abstract 2463., Cohen, M.E., Kuehner, S.M., Tepper, J.H., Burney, D.C., Neal, C.R., Irving, A.J., Korotev, R.L. and Hoefnagels, B. (2019) Mineralogy and bulk composition of lunar mare basalt Northwest Africa 12008. *Proc. 50th Lunar & Planetary Sciences Conf.*, Abstract 2508., Cronberger, K. and Neal, C.R. (2018) Origin(s) and Evolution of KREEP Basalts. *Proc. 49th Lunar & Planetary Science Conf.*, Abstract 1305., Crow, C.A., McKeegan, K.D.

and Moser, D.E. (2017) Coordinated U–Pb geochronology, trace element, Ti-in-zircon thermometry and microstructural analysis of Apollo zircons. *Geochimica et Cosmochimica Acta*, 202, 264-284., Demidova, S.I., Nazarov, M.A., Ryazantsev, K.M., Brandstätter, F. and Ntaflos, Th. (2015) Cordierite from the Dhofar 025 lunar feldspathic meteorite. *Proc. 46th Lunar & Planetary Science Conf. Abstract 1772.*, Dikov, Y.P., Gorshkov, A.I., Sivtsov, A.I., Wlotzka, F., and Ivanov, A.V. (2002) SiC and graphite in the sublimate layer of lunar glass spherules. *Proc. 33rd Lunar & Planetary Sciences Conf.*, Abstract 1186., Elardo, S.M., McCubbin, F.M. and Shearer, C.K. (2012) Chromite symplectites in Mg-suite troctolite 76535 as evidence for infiltration metasomatism of a lunar layered intrusion. *Geochimica et Cosmochimica Acta*, 87, 154-177., Evans, H.T. (1970) The crystallography of lunar troilite. *Proc. 1st Lunar Science Conf.*, 399-408., Fagan, T.J., Hayakawa, S., Kodama, S., Kataoka, Y. and Sasamoto, A. (2008) Late-stage crystallization products in NWA 773 group lunar meteorites. *Proc. 39th Lunar and Planetary Science Conf.*, Abstract 1854., Fagan, T.J., Gross, J., Ramsey, S. and Turrin, B. (2018) Northwest Africa 8632 - recording young lunar volcanism. *Proc. 49th Lunar and Planetary Science Conf.*, Abstract 2584., Grange, M.L., Pidgeon, R.T., Nemchin, A.A., Timms, N. and Meyer, C. (2013) Interpreting U–Pb data from primary and secondary features in lunar zircon. *Geochimica et Cosmochimica Acta*, 101, 112-132., Grieve, R.A., McKay, F.G.A., Smith, H.D. and Weill, D.F. (1975) Lunar polymict breccia 14321: a petrographic study. *Geochimica et Cosmochimica Acta*, 39, 229-245., Griffiths, A.A., Barnes, J.J., Tartèse, R., Potts, N.J. and Anand, M. (2014) Characterization of mesostasis areas in mare basalts: petrography and mineral chemistry. *Proc. 45th Lunar & Planetary Science Conf.*, Abstract 1905., Gross, J. and Treiman, A. (2011) Unique spinel-rich lithology in lunar meteorite ALHA 81005: Origin and possible connection to M3 observations of the farside highlands. *Journal of Geophysical Research Atmospheres*, 116, E10009., Haines, E.L., Albee, A.L., Chodos, A.A. and Wasserburg, G.J. (1971) Uranium-bearing minerals of lunar rock 12013. *Earth and Planetary Science Letters*, 12, 145-154., Hauri, E.K., Saal, A.E., Nakajima, M., Anand, M., Rutherford, M.J., Van Orman, J.A. and Le Voyer, M. (2017) Origin and Evolution of Water in the Moon's Interior. *Annual Rev. Earth Planet. Sci.*, 45, 89-111., Lunar Sourcebook: A

User's Guide to the Moon (1991, Cambridge University Press). Republished with permission of the Lunar and Planetary Institute, Houston., Hidaka, Y., Yamaguchi, A. and Ebihara, M. (2014) Lunar meteorite, Dhofar 1428: Feldspathic breccia containing KREEP and meteoritic components. *Meteoritics & Planetary Science*, 49, 921-928., Hudgins, J.A., Walton, E.L. and Spray, J.G. (2007) Mineralogy, petrology, and shock history of lunar meteorite Sayh al Uhaymir 300: A crystalline impact-melt breccia. *Meteoritics & Planetary Science* 42, 1763-1779., Jean, M.M., Bodnar, B., Farley, C., and Taylor, L.A. (2016) 'Rusty Rocks' from the Moon: Volatile-element contributions from meteorites. *Proc. 47th Lunar & Planetary Science Conf.*, Abstract 2498., Jolliff, B.L., Haskin, L.A., Colson, R.O. and Wadhwa, M. (1993) Partitioning in REE-saturated minerals: theory, experiment, and modelling of whitlockite, apatite, and evolution of lunar residual magmas. *Geochimica et Cosmochimica Acta*, 57, 4069-4094., Jolliff, B.L., Korotev, R.L., Zeigler, R.A. and Floss, C. (2003) Northwest Africa 773: Lunar mare breccia with a shallow-formed olivine-cumulate component, inferred very-low-Ti (VLT) heritage, and a KREEP connection. *Geochimica et Cosmochimica Acta*, 67, 4857-4879., Joy, K.H., Crawford, I.A., Downes, H., Russell, S.S. and Kearsley, A.T. (2006) A petrological, mineralogical, and chemical analysis of the lunar mare basalt meteorite LaPaz Icefield 02205, 02224, and 02226. *Meteoritics & Planetary Science*, 41, 1003-1025., Joy, K.H., Burgess, R., Hinton, R., Fernandes, V.A., Crawford, I.A., Kearsley, A.T. and Irving, A.J. (2009) U-Pb and Ar-Ar chronology of lunar meteorite Northwest Africa 4472. *Proc. 40th Lunar & Planetary Science Conf.*, Abstract 1708., Joy, K.H., Nemchin, A., Grange, M., Lapen, T.J., Peslier, A.H., Ross, D.K., Zolensky, M.E. and Kring, D.A. (2014) Petrography, geochronology and source terrain characteristics of lunar meteorites Dhofar 925, 961 and Sayh al Uhaymir 449. *Geochimica et Cosmochimica Acta*, 144, 299-325., Joy, K.H., Visscher, C., Zolensky, E., Mikouchi, T., Hagiya, K., Ohsumi, K. and Kring, D.A. (2015) Identification of magnetite in lunar regolith breccia 60016: Evidence for oxidized conditions at the lunar surface. *Meteoritics & Planetary Science*, 50, 1157-1172., Kaneko, S., Miyahara, M., Ohtani, E., Arai, T., Hirao, N. and Sato, K. (2015) Discovery of stishovite in Apollo 15299 sample. *American Mineralogist*, 100, 1308-1311., Kayama, M., Tomioka, N., Ohtani, E., Seto, Y.,

Nagaoka, H., Götze, J., Miyake, A., Ozawa, S., Sekine, T., Miyahara, M., Tomeoka, K., Matsumoto, M., Shoda, N., Hirao, N. and Kobayashi, T. (2018) Discovery of moganite in a lunar meteorite as a trace of H₂O ice in the Moon's regolith. *Science Advances*, 4, EAAR4378, 1-11., Kleinmann, B. and Ramdohr, P. (1971) Alpha corundum from the lunar dust., Koeberl, C., Kurat, G. and Branstatter, F. (1991) Lunar meteorite Yamato-793274: Mixture of Mare and Highland components and barringerite from the Moon. *Proc. NIPR Symp. Antarct. Meteorites*, 4, 33-55., Kuehner, S.M., Irving, A. J., Korotev, R. L., Hupé, G. M. and Ralew, S. (2007) Zircon-baddeleyite-bearing silica+K-feldspar granophyric clasts in KREEP-rich lunar breccias Northwest Africa 4472 and 4485. *Proc. 38th Lunar Planetary Science Conf.*, Abstract 1516., Kuehner, S.M., Wittmann, A., Korotev, R. L., Carpenter, P., Macke, R.J., Britt, D.T. and Irving, A. J. (2016) Petrologic, chemical and physical characterization of unique lunar vitric regolith breccia Northwest Africa 10404. *Proc. 47th Lunar Planetary Science Conf.*, Abstract 2246., Lui, Y., Floss, C., Day, J.M., Hill, E. and Taylor, L.A. (2009) Petrogenesis of lunar mare basalt meteorite Miller Range 05035. *Meteoritics & Planetary Science*, 44, 261-284., Lui, Y., Jolliff, B.J., Zeigler, R.A., Korotev, R.L., Wan, Y., Xie, H., Zhang, Y., Dong, C. and Wang, W. (2012) Comparative zircon U-Pb geochronology of impact melt breccias from Apollo 12 and lunar meteorite SaU 169, and implications for the age of the Imbrium impact. *Earth and Planetary Science Letters*, 319-320, 277-286., Lowe, M., Mahmood, S., McKeeby, B., and Greenwood, J. P. (2016) Cl-rich britholite substitution in apatite of high-titanium basalt 75055: A chlorine and REE-enriched phase of lunar phosphates. *Proc. 47th Lunar & Planetary Science Conf.* Abstract 1285., Marvin, U.B. (1983) The discovery and initial characterization of Allan Hills 81005: the first lunar meteorite. *Geophysical Research Letters*, 10, 775-778., McCallum, I.S. and Schwartz, J.M. (2001) Lunar Mg suite: Thermobarometry and petrogenesis of parental magmas. *Journal of Geophysical Research*, 106, 27,969-27,983., McCallum, I.S., Domeneghetti, M.C., Schwartz, J.M., Mullen, E.K., Zema, M., Cámara, F., McCammon, C. and Ganguly, J. (2006) Cooling history of lunar Mg-suite gabbro 76255, troctolite 76535 and Stillwater pyroxenite SC-936: The record in exsolution and ordering in pyroxenes. *Geochimica et Cosmochimica Acta*, 70, 6068-6078., McCanta, M.C., Darby Dyar, M., Rutherford, M.J. Lanzirotti, A., Sutton, S.R. and Thomson, B.J. (2017) In situ measurement of ferric iron in lunar glass beads using Fe-XAS. *Icarus*, 285, 95-102., McCubbin, F.M., Nekvasil, H., Jolliff, B.L., Carpenter, P.K. and Zeigler, R.A. (2008) A survey of lunar apatite volatile contents for determining bulk lunar water: how dry is "bone dry"? *Proc. 39th Lunar & Planetary Sciences Conf.*, Abstract 1788., McCubbin, F.M., Steele, A., Haun, E.H., Nekvasil, H., Yamashita, S. and Hemley, R.J. (2010) Nominally hydrous magmatism on the Moon. *Proc. National Academy of Sciences*, 107, 11223-11228., McCubbin, F.M. and 13 others (2015) Magmatic volatiles (H, C, N, F, S, Cl) in the lunar mantle, crust, and regolith: Abundances, distributions, processes, and reservoirs. *American Mineralogist*, 100, 1668-1707., McLeod, C.L. and Krekeler, M.P.S. (2017) Sources of Extraterrestrial Rare Earth Elements: To the Moon and Beyond. *Resources*, 6, 1-28., Meyer, C. (2003) The Lunar Petrographic Educational Thin Section Set., Meyer, C. and Yang, S.V. (1988) Tungsten-bearing yttrobetafite in lunar granophyre. *American Mineralogist*, 73, 1420-1425., Miyahara, M., Kaneko, S., Sakai, T., Nagase, T., Kayama, M., Nishido, H. and Hirao, N. (2013) Discovery of seifertite in a shocked lunar meteorite. *Nature Communications*, 4, Article 1737, 1-7., Morland, Z.S., Joy, K.H., Gholinia, A. and Degli Alessandrini, G. (2019) Metal in lunar meteorite Northwest Africa 10989: Insight into survivability of impactor material delivered to the Moon. *Proc. 50th Lunar & Planetary Sciences Conf.*, Abstract 1275., Muhling, J.R., Suvorova, A.A. and Rasmussen, B. (2014) The occurrence and composition of chevkinite-(Ce) and perrierite-(Ce) in tholeiitic intrusive rocks and lunar mare basalt. *American Mineralogist*, 99, 1911-1921., Nagaoka, H., Karouji, Y., Arai, T., Ebihara, M. and Hasebe, N. (2013) Geochemistry and mineralogy of a feldspathic lunar meteorite (regolith breccia), Northwest Africa 2200. *Polar Science*, 7, 241-259., Nagaoka, H., Takeda, H., Karouji, Y., Ohtake, M., Yamaguchi, A., Yoneda, S. and Hasebe, N. (2015) Mineralogy and petrology of lunar meteorite Northwest Africa 2977 consisting of olivine cumulate gabbro including inverted pigeonite. *Earth, Planets and Space*, 67, 1-8., Nemchin, A.A., Pidgeon, R.T., Whitehouse, M.J., Vaughan, J.P. and Meyer, C. (2008) SIMS U-Pb study of zircon from Apollo 14 and 17 breccias: Implications for the evolution of lunar KREEP. *Geochimica et*

Cosmochimica Acta, 72, 668-689., Nemchin, A.A., Jeon, H., Bellucci, J.J., Timms, N.E., Snape, J.F., Kilburn, M.R. and Whitehouse, M.J. (2017) Pb-Pb ages of feldspathic clasts in two Apollo 14 breccia samples. *Geochimica et Cosmochimica Acta*, 217, 441-461., Ni, P., Zhang, Y. and Gan, Y. (2017) Volatile loss during homogenization of lunar melt inclusions. *Earth and Planetary Science Letters*, 478, 214-224., Norman, M.D. and Nemchin, A.A. (2014) A 4.2 billion year old impact basin on the Moon: U-Pb dating of zirconolite and apatite in lunar melt rock 67955. *Earth and Planetary Science Letters*, 388, 387-398., Norman, M.D., Borg, L.E., Nyquist, L.E. and Bogard, D.D. (2003) Chronology, geochemistry, and petrology of a ferroan noritic anorthosite clast from Descartes breccia 67215: Clues to the age, origin, structure, and impact history of the lunar crust. *Meteoritics & Planetary Science*, 38, 645-661., North, S.N., Jolliff, B.L. and Korotev, R.L. (2013) Pyroxene composition in lunar meteorite NWA 727 and comparison to NWA 7007. *Proc. 44th Lunar & Planetary Science Conf.*, Abstract 3013., Patchen, A.P. (2004) The most reduced rock from the Moon - Apollo 14 basalt 14053: extreme reduction entirely from a re-heating event. *Proc. 35th Lunar & Planetary Science Conf.*, Abstract 1762., Pernet-Fisher, J.F., Joy, K.H. and Martin, D.J.P. (2016) Plagioclase in regolith breccias: critical tools for deciphering the shock history of the lunar highlands. *Proc. 47th Lunar & Planetary Science Conf.*, Abstract 1499., Pidgeon, R.T., Nemchin, A.A., van Bronswijk, W., Geisler, T., Meyer, C., Compston, W. and Williams, I.S. (2007) Complex history of a zircon aggregate from lunar breccia 73235. *Geochimica et Cosmochimica Acta*, 71, 1370-1381., Potts, N.J., Tartèse, R., Anand, M., van Westrenen, W., Griffiths, A.A., Barrett, T.J. and Franchi, I.A. (2016) Characterization of mesostasis regions in lunar basalts: Understanding late-stage melt evolution and its influence on apatite formation. *Meteoritics & Planetary Science*, 51, 1555-1575., Provencio, P., Bell, A.S., Shearer, C. and Burger, P. (2015) A TEM study of the sulfide replacement assemblages in lunar breccia. *Proc. 46th Lunar and Planetary Science Conf.*, Abstract 2812., Rasmussen, B., Fletcher, I.R. and Muhling, J.R. (2008) Pb/Pb geochronology, petrography and chemistry of Zr-rich accessory minerals (zirconolite, tranquillityite and baddeleyite) in mare basalt 10047. *Geochimica et Cosmochimica Acta*, 72, 5799-5818., Roberts, S.E., Jean, M.M., Sueilem, M.B.,

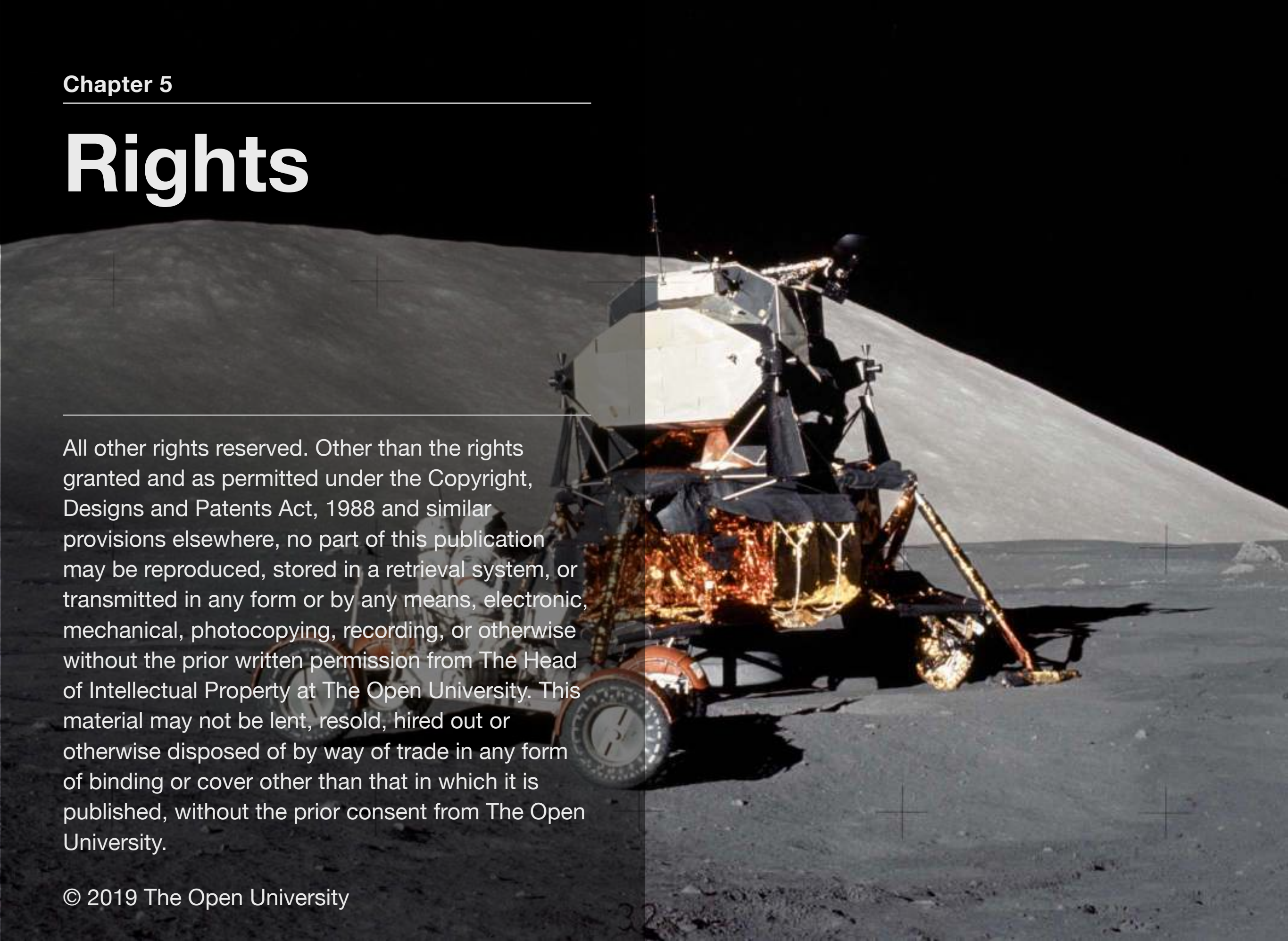
and L.A.Taylor, L.A. (2017) Northwest Africa 10986: An impact-melt breccia from the lunar highlands. *Proc. 48th Lunar & Planetary Science Conf.*, Abstract 2220., Robinson, K.L. and Kring, D.A. (2018) The Northwest Africa 5744 group: a glimpse into Schrödinger-like lithologies? *Proc. 49th Lunar & Planetary Science Conf.*, Abstract 1635., Seddio, S.M., Jolliff, B.L., Korotev, R.L. and Zeigler, R.A., P.K. (2009) A newly characterized granite from the Apollo 12 regolith. *Proc. 40th Lunar & Planetary Science Conf.*, Abstract 2704., Seddio, S.M., Jolliff, B.L., Korotev, R.L. and Zeigler, R.A. (2011) Fragments of granite in Apollo 12 regolith: Pieces of 12013? *Proc. 42nd Lunar & Planetary Science Conf.*, Abstract 2381., Seddio, S.M., Jolliff, B.L., Korotev, R.L. and Carpenter, P.K. (2012b) Thorite in an Apollo 12 granite fragment and age determination using the electron microprobe. *Proc. 43rd Lunar & Planetary Science Conf.*, Abstract 2704., Seddio, S.M., Jolliff, B.L., Korotev, R.L. and Zeigler, R.A. (2013b) Petrology and geochemistry of lunar granite 12032,366-19 and implications for lunar granite petrogenesis. *American Mineralogist*, 98, 1697-1713., Seddio, S.M., Jolliff, B.L., Korotev, R.L. and Carpenter, P.K. (2014) Thorite in an Apollo 12 granite fragment and age determination using the electron microprobe. *Geochimica et Cosmochimica Acta*, 135, 307-320., Shearer, C.K., Papike, J.J. and Spilde, M.N. (2001) Trace-element partitioning between immiscible lunar melts: An example from naturally occurring lunar melt inclusions. *American Mineralogist*, 86, 238-246., Shearer, C.K., Burger, P.V., Guan, Y., Papike, J.J., Sutton, S.R. and Atudorei, N.-V. (2012) Origin of sulfide replacement textures in lunar breccias. Implications for vapor element transport in the lunar crust. *Geochimica et Cosmochimica Acta*, 83, 138-158., Shearer, C.K., Sharp, Z.D., Burger, P.V., McCubbin, F.M., Provencio, P.P., Brearley, A.J. and Steele, A. (2014) Chlorine distribution and its isotopic composition in "rusty rock" 66095. Implications for volatile element enrichments of "rusty rock" and lunar soils, origin of "rusty" alteration, and volatile element behaviour on the Moon. *Geochimica et Cosmochimica Acta*, 139, 411-433., Smith, J.H., Meyer, C., Compston, W. and Williams, I.S. (1986) 73235,82 (Pomegranate): an assemblage of lunar zircon with unique overgrowth. *Proc. 17th Lunar & Planetary Science Conf.*, 805-806., Spicuzza, M.J., Valley, J.W., Fournelle, J., Huberty, J.M., and Treiman, A. (2011) Native silicon and Fe-silicides from the Apollo 16 lunar regolith:

extreme reduction, metal-silicate immiscibility, and shock melting. Proc. 42nd Lunar & Planetary Science Conf., Abstract 2231., Tartèse, R., Anand, M. and Delhaye, T. (2013b) NanoSIMS Pb/Pb dating of tranquillityite in high-Ti lunar basalts: Implications for the chronology of high-Ti volcanism on the Moon. *American Mineralogist*, 98, 1477-1486., Tartèse, R., Anand, M., McCubbin, F.M., Elardo, S.M., Shearer, C.K. and Franchi, I.A. (2014b) Apatites in lunar KREEP basalts: The missing link to understanding the H isotope systematics of the Moon. *Geology*, 42, 363-366., Timms, N.E., Reddy, S.M., Healy, D., Nemchin, A.A., Grange, M.L., Pidgeon, R.T., and Hart, R. (2012) Resolution of impact-related microstructures in lunar zircon: A shock-deformation mechanism map., Treiman, A.H. (2007) Rhönite in Luna 24 pyroxenes: first find from the Moon, and implications for water in planetary magmas. Proc. 38th Lunar & Planetary Science Conf., Abstract 1244., Treiman, A.H., and Semprich, J. (2019) Dunite in lunar meteorite Northwest Africa 11421: Petrology and Origin. Proc. 50th Lunar & Planetary Science Conf., Abstract 1225., Treiman, A.H., and Gross, J. (2012) Lunar cordierite-spinel troctolite: Igneous history and volatiles. Proc. 43rd Lunar & Planetary Science Conf., Abstract 1196., Treiman, A.H., Kulis, M.J. and Glazner, A.F. (2019) Spinel-anorthosites on the Moon: Impact melt origins suggested by enthalpy constraints. *American Mineralogist*, 104, 370-384., Vaniman, D.T. and Bish, D.L. (1990) Yoshiokaite, a new CaAl-silicate mineral from the Moon. *American Mineralogist*, 75, 676-486., Wang, Y., Hsu, W., Guan, Y., Li, X., Li, Q., Liu, Y and Tang, G. (2012) Petrogenesis of the Northwest Africa 4734 basaltic lunar meteorite. *Geochimica et Cosmochimica Acta*, 92, 329-344., Williams, K.L. and Taylor, L.A. (1974) Optical Properties and Chemical Compositions of Apollo 17 Armalcolites. *Geology*, 2, 5-8., Wittmann, A., Korotev, R.L., and Jolliff, B.L. (2014) Third of a kind - impact melted lunar granulitic breccia meteorite Dhofar 1766. Proc. 45th Lunar & Planetary Science Conf., Abstract 1182., Wittmann, A., Korotev, R.L., Jolliff, B.L., and Carpenter, P.K. (2018) Spinel assemblages in lunar meteorites Graves Nunataks 06157 and Dhofar 1528: Implications for impact melting and equilibration in the Moon's upper mantle. *Meteoritics & Planetary Science*, 54, 379-394., Zeigler, R.A., Jolliff, B.L., Wang, A., Korotev, R.L., Kremser, D.T. and Haskin, L.A. (2001) Formation of carbonate and oxyhydroxide minerals by

impact of a volatile-rich body. Proc. 32nd Lunar & Planetary Science Conf., Abstract 1243., Zeigler R.A., Korotev R.L., Jolliff B.L. and Haskin L.A. (2005b) Petrography of lunar meteorite MET 01210, a new basaltic regolith breccia. Proc. 36th Lunar & Planetary Science Conf., Abstract 2385., Zhang, A.C. and Hsu, W. (2009) Petrography, mineralogy, and trace element geochemistry of lunar meteorite Dhofar 1180. *Meteoritics & Planetary Science*, 44, 1265-1286., Zhang, A.C., Hsu, W-B., Li, X.H., Jiang, Y. and Tang, G-Q (2011) SIMS Pb/Pb dating of Zr-rich minerals in lunar meteorites Miller Range 05035 and LaPaz Icefield 02224: Implications for the petrogenesis of mare basalt. *Science China: Earth Sciences*, 53, 327-334., Zhang, A.C., Hsu, W-B., Li, X.H., Ming H-L., Li, Q-L., Liu, Y. and Liu, Y. (2011) Impact melting of lunar meteorite Dhofar 458: Evidence from polycrystalline texture and decomposition of zircon. *Meteoritics & Planetary Science*, 46, 103-115., Zhang, A.C., Taylor, L.A., Wang, R.C., L, Q.L., L, X.H., Patchen, and Liu, Y. (2012) Thermal history of Apollo 12 granite and KREEP-rich rock: Clues from Pb/Pb ages of zircon in lunar breccia 12013. *Geochimica et Cosmochimica Acta*, 95, 1-14., Zhang, B., Lin, Y., Moser, D.E., Schieh, S.R. and Bouvier, A. (2018) Imbrium Zircon Age for Apollo 73155 Serenitatis Impact Melt Breccia: Implications for the Lunar Bombardment History. *Bombardment: Shaping Planetary Surfaces and Their Environments Conf.*, Abstract 2021.

Rights

All other rights reserved. Other than the rights granted and as permitted under the Copyright, Designs and Patents Act, 1988 and similar provisions elsewhere, no part of this publication may be reproduced, stored in a retrieval system, or transmitted in any form or by any means, electronic, mechanical, photocopying, recording, or otherwise without the prior written permission from The Head of Intellectual Property at The Open University. This material may not be lent, resold, hired out or otherwise disposed of by way of trade in any form of binding or cover other than that in which it is published, without the prior consent from The Open University.



Agglutinate

Agglutinates are small glassy breccias formed when a micrometeorite strikes the lunar regolith. Micrometeorites are a millimetre or less in size. Millions of micrometeorites strike the Moon every day. When a micrometeorite strikes the lunar surface, some of the impacted regolith melts and some doesn't, so the product is a glass with mineral and rock fragments entrained. The glass often shows flow features. Agglutinates are typically tens of micrometres to a few millimetres in size.

Related Glossary Terms

Drag related terms here

Index

Find Term

Anhedral

Anhedral is the name given to mineral grains that have no well-formed crystal faces or cross-section shape in thin section. Anhedral crystal growth occurs in a competitive environment with no free space for the formation of crystal faces.

Related Glossary Terms

Drag related terms here

Index

Find Term

Anorthosite

Anorthosite is an intrusive igneous rock type mostly composed of plagioclase feldspar (90-100%), with a minimal mafic component (0-10%).

Related Glossary Terms

Drag related terms here

Index

Find Term

Breccia

Lunar breccias are the lithified aggregates of clastic debris and melt generated by meteorite bombardment of the lunar surface. Most of the breccias returned by the Apollo missions were formed in the ancient lunar highlands about 3900 to 4000 million years ago.

Related Glossary Terms

Drag related terms here

Index

Find Term

Carbonaceous Chondrites

Carbonaceous chondrites are primitive and undifferentiated meteorites that formed in oxygen-rich regions of the early solar system so that most of their metal content is not found in its free form but as silicates, oxides, or sulphides. Most of them contain water or minerals that have been altered in the presence of water, and some of them contain larger amounts of carbon as well as organic compounds. They represent less than 5% of all meteorite falls.

Related Glossary Terms

Drag related terms here

Index

Find Term

Carbonatite

Carbonatite is a type of igneous rock consisting of greater than 50% carbonate minerals such as calcite or dolomite.

Related Glossary Terms

Drag related terms here

Index

Find Term

Cathodoluminescence

Cathodoluminescence (CL) is the emission of photons of characteristic wavelengths from a material that is under high-energy electron bombardment. The electron beam is typically produced in an electron microprobe, a scanning electron microscope or a cathodoluminescence microscopy attachment to a petrographic microscope. The nature of CL in a material is a complex function of composition, lattice structure and superimposed strain or damage on the structure of the material.

Related Glossary Terms

Drag related terms here

Index

Find Term

Devitrification

Devitrification is the growth of crystalline structures within or on the surface of glass.

Related Glossary Terms

Drag related terms here

Index

Find Term

Euhedral

Euhedral crystals are those that are well-formed, with sharp, easily recognised faces.

Related Glossary Terms

Drag related terms here

Index

Find Term

Exsolution

Exsolution is a process by which a solid solution phase unmixes into two separate phases in the solid state. Exsolution occurs only in minerals whose compositions vary between two or more pure end-member compositions.

Related Glossary Terms

Drag related terms here

Index

Find Term

FTIR

Fourier transform infrared (FTIR) spectroscopy is a technique which acquires broadband Near InfraRed (NIR) to Far InfraRed (FIR) spectra. Unlike a dispersive instrument, i.e. a grating monochromator or spectrograph, FTIR spectrometers collect all wavelengths simultaneously.

The term Fourier-transform infrared spectroscopy originates from the fact that a Fourier transform (a mathematical process) is required to convert the raw data into the actual spectrum.

Related Glossary Terms

Drag related terms here

Index

Find Term

Gabbro

Gabbro is a coarse-grained, dark-coloured, intrusive igneous rock. It is composed mainly of calcic plagioclase feldspar and clinopyroxene (augite). Olivine gabbro is a common variant.

Related Glossary Terms

Drag related terms here

Index

Find Term

Granophyre

Normally a granitic rock consisting of intergrown feldspar and quartz crystals in a medium- to fine-grained groundmass. Granophyre can also occur within layered igneous intrusions dominated by rocks with compositions like that of gabbro. In such occurrences, the granophyre may form as an end product of fractional crystallization of a parent mafic magma, or by melting of rocks into which the mafic magma was emplaced.

Related Glossary Terms

Drag related terms here

Index

Find Term

Highlands

The lunar highlands are lighter in colour than the lunar mare. They represent the earliest crust on the Moon. Anorthosite is a major component of the lunar highlands.

Related Glossary Terms

Drag related terms here

Index

Find Term

Holohyaline

A rarely used textural term usually referring to igneous rocks or parts of igneous rocks which are composed entirely of glass. In a lunar context the term has been applied to clasts within breccias which are of unaltered glass - i.e. have not devitrified.

Related Glossary Terms

Drag related terms here

Index

Find Term

Impactite

Impactite (or impact glass) is rock created or modified by the impact of a meteorite. Impactites have been physically altered by the tremendous heat, pressure and shock waves associated with meteorite impact and have a vesicular, glassy to finely crystalline texture produced by fusion or partial fusion of the target rock (or regolith soil).

Related Glossary Terms

Drag related terms here

Index

Find Term

Intrafasciculate

A textural term introduced by Drever et al. (1972) to denote a characteristic tendency for elongate pyroxene crystals to develop within hollow plagioclase feldspar crystals.

Related Glossary Terms

Drag related terms here

Index

Find Term

KREEP

KREEP is an acronym built from the letters K (the atomic symbol for potassium), REE (Rare Earth Elements) and P (for phosphorus). It is a geochemical component of some lunar impact breccias from non-mare regions and some basalts. These rocks have a common petrologic link with Mg-suite rocks and evolved plutonic rocks, including the alkali suite and a range of siliceous plutonic rocks referred to as granites. Impact induced emplacement of KREEP magma from a primary mantle source, followed by transportation into the crust by an unspecified possibly plume-like process has been proposed.

According to the giant impact hypothesis the lunar KREEP component is thought to have been produced by the crystallization of a lunar magma ocean and represents the last ~0.5% of liquid.

Related Glossary Terms

Drag related terms here

Index

Find Term

Late Heavy Bombardment

The Late Heavy Bombardment (or lunar cataclysm) is an event thought to have occurred approximately 4.1 to 3.8 billion years (Ga) ago. It was a time when the Earth suffered constant attack from leftover planet-building material at a time when the giant planets were moving in their orbits.

Related Glossary Terms

Drag related terms here

Index

Find Term

Mare

The lunar maria (singular: mare) are large, dark, basaltic plains on the Moon, formed by ancient volcanic eruptions. They were dubbed maria, Latin for "seas", by early astronomers who mistook them for actual seas.

Related Glossary Terms

Drag related terms here

Index

Find Term

Mesocumulate

Mesocumulates are rocks with between 93 and 85% accumulated minerals in a groundmass. Cumulate rocks are igneous rocks formed by the accumulation of crystals from a magma either by settling or floating. Cumulate rocks are the typical product of precipitation of solid crystals from a fractionating magma chamber.

Related Glossary Terms

Drag related terms here

Index

Find Term

Mesostasis

Mesostasis describes the last-formed interstitial material between larger mineral grains in an igneous rock or in a microcrystalline groundmass. In lunar basalts the mesostasis is often the location for accessory minerals such as apatite, baddeleyite, tranquillityite and zircon.

Related Glossary Terms

Drag related terms here

Index

Find Term

Metasomatism

Metasomatism is a chemical process by which the composition of a rock is altered in a pervasive manner and which involves the introduction and/or removal of chemical components as a result of the interaction of the rock with later fluids.

Related Glossary Terms

Drag related terms here

Index

Find Term

Mössbauer

Mössbauer spectroscopy is a versatile technique that can be used to provide information in many areas of science such as Physics, Chemistry, Biology and Metallurgy. It can give very precise information about the chemical, structural, magnetic and time-dependent properties of a material.

The Mössbauer effect was discovered by Rudolf Mössbauer in 1958 and consists of nearly recoil-free, resonant absorption and emission of gamma rays in solids.

Related Glossary Terms

Drag related terms here

Index

Find Term

NanoSIMS

Nanoscale secondary ion mass spectrometry (nanoSIMS) is a nanoscopic scale resolution chemical imaging mass spectrometer based on secondary ion mass spectrometry.

Related Glossary Terms

Drag related terms here

Index

Find Term

Norite

Norite is a mafic intrusive igneous rock composed largely of the calcic plagioclase feldspar, and orthopyroxene (hypersthene).

Related Glossary Terms

Drag related terms here

Index

Find Term

Pleochroism

Pleochroism is the change in colour evident as a mineral is rotated under plane-polarised light. The primary cause of pleochroism in minerals is due to adsorption of particular wavelengths of light.

Related Glossary Terms

Drag related terms here

Index

Find Term

Poikilitic

Describes the texture of an igneous rock in which small crystals of one mineral species occur within crystals of another.

Related Glossary Terms

Drag related terms here

Index

Find Term

Polymict

Polymict - (of a breccia) consisting of fragments of several different rock types.

In a lunar context, a polymict impact breccia is a breccia with a crystalline or glassy matrix (derived from the crystallization of impact melt) containing lithic and mineral clasts excavated by an impact and showing different degree of shock metamorphism.

Related Glossary Terms

Drag related terms here

Index

Find Term

REE

An abbreviation of “rare-earth element”. The rare-earth elements include 15 lanthanide elements - cerium (Ce), dysprosium (Dy), erbium (Er), europium (Eu), gadolinium (Gd), holmium (Ho), lanthanum (La), lutetium (Lu), neodymium (Nd), praseodymium (Pr), promethium (Pm), samarium (Sm), terbium (Tb), thulium (Tm), ytterbium (Yb), as well as scandium (Sc) and yttrium (Y).

In lunar rocks the REE’s are concentrated in the accessory mineral merrillite/whitlockite.

Related Glossary Terms

Drag related terms here

Index

Find Term

Regolith

Regolith is a layer of unconsolidated debris on the lunar surface. The thickness of the regolith varies from about 5 metres on mare surfaces to about 10 metres on highland surfaces. The bulk of the regolith is a fine grey soil, but the regolith also includes breccia and rock fragments from the local bedrock.

Related Glossary Terms

Drag related terms here

Index

Find Term

SIMS

Secondary-ion mass spectrometry (SIMS) is a technique used to analyze the composition of solid surfaces and thin films by sputtering the surface of the specimen with a focused primary ion beam and collecting and analyzing ejected secondary ions.

Related Glossary Terms

Drag related terms here

Index

Find Term

Subhedral

Subhedral is a crystal shape intermediate between euhedral (well formed) and anhedral (poorly formed) crystals.

Related Glossary Terms

Drag related terms here

Index

Find Term

Subsolidus

That part of a phase diagram that lies below the solidus, thus representing a system that is wholly solid. In geological terms subsolidus describes the various reactions and readjustments that occurs in rocks during cooling at the post-magmatic stage.

Related Glossary Terms

Drag related terms here

Index

Find Term

Troctolite

Troctolite is a mafic intrusive rock type. It consists essentially of major but variable amounts of olivine and calcic plagioclase (sometimes with minor pyroxene). It is an olivine-rich anorthosite, or a pyroxene-depleted relative of gabbro.

Related Glossary Terms

Drag related terms here

Index

Find Term